

# METHODS IN MOLECULAR BIOLOGY

*Series Editor*  
**John M. Walker**  
**School of Life Sciences**  
**University of Hertfordshire**  
**Hatfield, Hertfordshire, AL10 9AB, UK**

For further volumes:  
<http://www.springer.com/series/7651>



# Plasmodesmata

## Methods and Protocols

Edited by

**Manfred Heinlein**

*Institut de Biologie Moléculaire des Plantes (IBMP-CNRS), Strasbourg, France*

 **Humana Press**

*Editor*

Manfred Heinlein  
Institut de Biologie Moléculaire des Plantes (IBMP-CNRS)  
Strasbourg, France

Additional material to this book can be downloaded from <http://extras.springer.com>

ISBN 978-1-4939-4643-3      ISBN 978-1-4939-1523-1 (eBook)  
DOI 10.1007/978-1-4939-1523-1  
Springer New York Heidelberg Dordrecht London

© Springer Science+Business Media New York 2015

Softcover reprint of the hardcover 1st edition 2015

This work is subject to copyright. All rights are reserved by the Publisher, whether the whole or part of the material is concerned, specifically the rights of translation, reprinting, reuse of illustrations, recitation, broadcasting, reproduction on microfilms or in any other physical way, and transmission or information storage and retrieval, electronic adaptation, computer software, or by similar or dissimilar methodology now known or hereafter developed. Exempted from this legal reservation are brief excerpts in connection with reviews or scholarly analysis or material supplied specifically for the purpose of being entered and executed on a computer system, for exclusive use by the purchaser of the work. Duplication of this publication or parts thereof is permitted only under the provisions of the Copyright Law of the Publisher's location, in its current version, and permission for use must always be obtained from Springer. Permissions for use may be obtained through RightsLink at the Copyright Clearance Center. Violations are liable to prosecution under the respective Copyright Law.

The use of general descriptive names, registered names, trademarks, service marks, etc. in this publication does not imply, even in the absence of a specific statement, that such names are exempt from the relevant protective laws and regulations and therefore free for general use.

While the advice and information in this book are believed to be true and accurate at the date of publication, neither the authors nor the editors nor the publisher can accept any legal responsibility for any errors or omissions that may be made. The publisher makes no warranty, express or implied, with respect to the material contained herein.

Printed on acid-free paper

Humana Press is a brand of Springer  
Springer is part of Springer Science+Business Media ([www.springer.com](http://www.springer.com))

---

## Preface

Intercellular communication is an essential biological process during the coordination of development in multicellular organisms. Plants are sessile organisms that require communication between cells and tissues also for facing the constant challenges from the environment. To enable direct cell-to-cell communication, plants have evolved plasmodesmata (PD), plasma membrane-lined, gated cell wall microchannels that provide cytoplasmic continuity between cells. The system of PD forms a tightly regulated symplasmic communication network by which plants exert cell-to-cell and systemic control over cell fates, epigenetic states, and defenses against biotic and abiotic stresses. Communication through PD involves both selective and nonselective movement of various molecules that function in diverse biological processes. A continuously expanding range of non-cell-autonomous proteins and RNA molecules is known to move from cell to cell through PD to play crucial roles in developmental and defense signaling. Moreover, viruses exploit PD for intercellular and systemic spread, which often results in serious crop diseases. Given these diverse and important implications of PD-mediated macromolecular trafficking, an increasing number of researchers are interested to further explore the structure and regulation of PD as well as the molecular and cellular mechanisms by which informational macromolecules are targeted to PD, move through the channel, and act in recipient cells.

This book aims to provide a unique compendium of currently applied methods to address these important questions. The two chapters in Part I present overviews about current knowledge regarding (1) PD structure and their function during development and (2) the role of viruses as models for addressing cellular mechanisms in macromolecular trafficking and movement through PD. This introductory part is followed by 19 chapters that provide detailed experimental protocols for imaging PD (Part II), the isolation and structural analysis of PD (Part III), the analysis of PD conductivity and regulation (Part IV), and studying cellular mechanisms by which macromolecules are targeted to PD and transported through the channel (Part V). The experimental protocols are written by leading experts with hands-on experience in the respective method. The major goal of this book is to deliver detailed information about the specific practical procedures and thus to enable their reproduction and application in PD-related research in other laboratories. I hope that the growing research community interested in PD will accept this book as a useful reference for the coming years.

I greatly acknowledge the contribution of all the authors who contributed to this book and shared their laboratory secrets and useful hints in the Notes sections. I also thank the series editor, John M. Walker, for his continuous support in developing this volume.

*Strasbourg, France*

*Manfred Heinlein*



---

# Contents

<i>Preface</i> . . . . .	<i>v</i>
<i>Contributors</i> . . . . .	<i>ix</i>
PART I OVERVIEW	
1 Plasmodesmata: Channels for Intercellular Signaling During Plant Growth and Development . . . . .	3
<i>Iris Sevillem, Shri Ram Yadav, and Ykä Helariutta</i>	
2 Plasmodesmata: Channels for Viruses on the Move . . . . .	25
<i>Manfred Heinlein</i>	
PART II IMAGING OF PLASMODESMATA	
3 Imaging Plasmodesmata with High-Resolution Scanning Electron Microscopy . . . . .	55
<i>Deborah A. Barton and Robyn L. Overall</i>	
4 Preparative Methods for Imaging Plasmodesmata at Super-resolution . . . . .	67
<i>Karen Bell and Karl Oparka</i>	
PART III STRUCTURAL ANALYSIS OF PLASMODESMATA	
5 Isolation of Plasmodesmata from Arabidopsis Suspension Culture Cells . . . . .	83
<i>Magali S. Grison, Lourdes Fernandez-Calvino, Sébastien Mongrand, and Emmanuelle M.F. Bayer</i>	
6 Immunofluorescence Detection of Callose Deposition Around Plasmodesmata Sites . . . . .	95
<i>Ali Pendle and Yoselin Benitez-Alfonso</i>	
7 Imaging Callose at Plasmodesmata Using Aniline Blue: Quantitative Confocal Microscopy . . . . .	105
<i>Raul Zavaliev and Bernard L. Epel</i>	
8 Localization of Fluorescently Tagged Protein to Plasmodesmata by Correlative Light and Electron Microscopy . . . . .	121
<i>Shannon Modla, Jeffrey L. Caplan, Kirk J. Czymmek, and Jung-Youn Lee</i>	
PART IV ANALYSIS OF PLASMODESMATA CONDUCTIVITY AND REGULATION	
9 Quantification of Plant Cell Coupling with Live-Cell Microscopy . . . . .	137
<i>Johannes Liesche and Alexander Schulz</i>	
10 Drop-ANd-Sec: A Simple, Real-Time, and Noninvasive Technique for Assaying Plasmodesmal Permeability . . . . .	149
<i>Weier Cui, Xu Wang, and Jung-Youn Lee</i>	

11	Mapping Symplasmic Fields at the Shoot Apical Meristem Using Iontophoresis and Membrane Potential Measurements . . . . .	157
	<i>Christiaan van der Schoot and Päivi L.H. Rinne</i>	
12	Analysis of the Conductivity of Plasmodesmata by Microinjection . . . . .	173
	<i>Friedrich Kragler</i>	
13	Investigating Plasmodesmata Genetics with Virus-Induced Gene Silencing and an Agrobacterium-Mediated GFP Movement Assay . . . . .	185
	<i>Jacob O. Brunkard, Tessa M. Burch-Smith, Anne M. Runkel, and Patricia Zambryski</i>	
14	Probing Plasmodesmata Function with Biochemical Inhibitors . . . . .	199
	<i>Rosemary G. White</i>	
 PART V STUDYING MACROMOLECULAR TRAFFICKING		
15	GAL4 Transactivation-Based Assay for the Detection of Selective Intercellular Protein Movement . . . . .	231
	<i>Dhinesh Kumar, Huan Chen, Yeonggil Rim, and Jae-Yean Kim</i>	
16	Techniques for Assessing the Effects of Pharmacological Inhibitors on Intercellular Protein Movement . . . . .	245
	<i>Shuang Wu and Kimberly L. Gallagher</i>	
17	Probing Protein Targeting to Plasmodesmata Using Fluorescence Recovery After Photo-Bleaching . . . . .	259
	<i>Kathryn M. Wright and Katrin M. MacKenzie</i>	
18	The Tracking of Intercellular Small RNA Movement . . . . .	275
	<i>Christophe Himber and Patrice Dunoyer</i>	
19	Analysis of the Role of Myosins in Targeting Proteins to Plasmodesmata . . . . .	283
	<i>Martin Di Donato and Khalid Amari</i>	
20	Pumilio-Based RNA In Vivo Imaging . . . . .	295
	<i>Jens Tilsner</i>	
21	In Vivo RNA Labeling Using MS2 . . . . .	329
	<i>Eduardo Peña, Manfred Heinlein, and Adrian Sambade</i>	
	<i>Index</i> . . . . .	343

---

## Contributors

- KHALID AMARI • *Institut de Biologie Moléculaire des Plantes (IBMP, CNRS-UPR2357), Université de Strasbourg, Centre National de la Recherche Scientifique (CNRS), Strasbourg, France; Zürich-Basel Plant Science Center, Botany, Department of Environmental Sciences, University of Basel, Basel, Switzerland*
- DEBORAH A. BARTON • *School of Biological Sciences, University of Sydney, Sydney, NSW, Australia*
- EMMANUELLE M.F. BAYER • *Laboratory of Membrane Biogenesis, CNRS UMR5200, University of Bordeaux, Bordeaux, France*
- KAREN BELL • *Institute of Molecular Plant Sciences, University of Edinburgh, Edinburgh, UK*
- YOSELIN BENITEZ-ALFONSO • *Centre for Plant Sciences, School of Biology, University of Leeds, Leeds, UK*
- JACOB O. BRUNKARD • *Department of Plant and Microbial Biology, University of California, Berkeley, CA, USA*
- TESSA M. BURCH-SMITH • *Department of Biochemistry, Cellular, and Molecular Biology, University of Tennessee, Knoxville, TN, USA*
- JEFFREY L. CAPLAN • *Delaware Biotechnology Institute, University of Delaware, Newark, DE, USA*
- HUAN CHEN • *Division of Applied Life Science, Plant Molecular Biology & Biotechnology Research Center, Gyeongsang National University, Gyeongsangnam-do, Korea*
- WEIER CUI • *Department of Plant and Soil Sciences, University of Delaware, Newark, DE, USA; Delaware Biotechnology Institute, University of Delaware, Newark, DE, USA*
- KIRK J. CZYMMEK • *Delaware Biotechnology Institute, University of Delaware, Newark, DE, USA; Carl Zeiss Microscopy, Thornwood, NY, USA*
- MARTIN DI DONATO • *Department of Biology-Plant Biology, University of Fribourg, Fribourg, Switzerland*
- PATRICE DUNOYER • *Institut de Biologie Moléculaire des Plantes (IBMP-CNRS), Strasbourg, France*
- BERNARD L. EPEL • *Department of Molecular Biology and Ecology of Plants, George S. Wise Faculty of Life Sciences, Tel Aviv University, Tel Aviv, Israel*
- LOURDES FERNANDEZ-CALVINO • *Centre for Plant Biotechnology and Genomics (UPM-INIA), Madrid, Spain*
- KIMBERLY L. GALLAGHER • *University of Pennsylvania, Philadelphia, PA, USA*
- MAGALI S. GRISON • *Laboratory of Membrane Biogenesis, CNRS UMR5200, University of Bordeaux, Bordeaux, France*
- MANFRED HEINLEIN • *Institut de Biologie Moléculaire des Plantes (IBMP-CNRS), Strasbourg, France; Department of Environmental Sciences, University of Basel, Basel, Switzerland*
- YKÄ HELARIUTTA • *Department of Bio and Environmental Sciences, Institute of Biotechnology, University of Helsinki, Helsinki, Finland*
- CHRISTOPHE HIMBER • *Institut de Biologie Moléculaire des Plantes (IBMP-CNRS), Strasbourg, France*
- JAE-YEAN KIM • *Division of Applied Life Science, Plant Molecular Biology & Biotechnology Research Center, Gyeongsang National University, Gyeongsangnam-do, Korea*

- FRIEDRICH KRAGLER • *Max Planck Institute of Molecular Plant Physiology, Golm, Germany*
- DHINESH KUMAR • *Division of Applied Life Science, Plant Molecular Biology & Biotechnology Research Center, Gyeongsang National University, Gyeongsangnam-do, Korea*
- JUNG-YOUN LEE • *Department of Plant and Soil Sciences, University of Delaware, Newark, DE, USA; Delaware Biotechnology Institute, University of Delaware, Newark, DE, USA*
- JOHANNES LIESCHE • *Department of Plant and Environmental Sciences, University of Copenhagen, Copenhagen, Denmark*
- KATRIN M. MACKENZIE • *Biomathematics and Statistics Scotland, Dundee Unit, Invergowrie, UK*
- SHANNON MODLA • *Delaware Biotechnology Institute, University of Delaware, Newark, DE, USA*
- SÉBASTIEN MONGRAND • *Laboratory of Membrane Biogenesis, CNRS UMR5200, University of Bordeaux, Bordeaux, France*
- KARL OPARKA • *Institute of Molecular Plant Sciences, University of Edinburgh, Edinburgh, UK*
- ROBYN L. OVERALL • *School of Biological Sciences, University of Sydney, Sydney, NSW, Australia*
- EDUARDO PEÑA • *Institut de Biologie Moléculaire des Plantes (IBMP-CNRS-UPR2357), Centre National de la Recherche Scientifique (CNRS), Strasbourg, France*
- ALI PENDLE • *John Innes Centre, Norwich, UK*
- YEONGGIL RIM • *Division of Applied Life Science, Plant Molecular Biology & Biotechnology Research Center, Gyeongsang National University, Gyeongsangnam-do, Korea*
- PAIVI L.H. RINNE • *Norwegian University of Life Sciences, Aas, Norway*
- ANNE M. RUNKEL • *Department of Plant and Microbial Biology, University of California, Berkeley, CA, USA*
- ADRIAN SAMBADE • *Instituto Cavanilles de Biodiversidad y Biología Evolutiva, Universidad de Valencia, Valencia, Spain*
- CHRISTIAAN VAN DER SCHOOT • *Norwegian University of Life Sciences, Aas, Norway*
- ALEXANDER SCHULZ • *Department of Plant and Environmental Sciences, University of Copenhagen, Copenhagen, Denmark*
- IRIS SEVILEM • *Department of Bio and Environmental Sciences, Institute of Biotechnology, University of Helsinki, Helsinki, Finland*
- JENS TILSNER • *Biomedical Sciences Research Complex, University of St. Andrews, St. Andrews, Fife, UK; Cell & Molecular Sciences, The James Hutton Institute, Invergowrie, UK*
- XU WANG • *Department of Plant and Soil Sciences, University of Delaware, Newark, DE, USA; Delaware Biotechnology Institute, University of Delaware, Newark, DE, USA*
- ROSEMARY G. WHITE • *CSIRO Plant Industry, Canberra, ACT, Australia*
- KATHRYN M. WRIGHT • *Cell and Molecular Sciences Group, The James Hutton Institute, Invergowrie, UK*
- SHUANG WU • *University of Pennsylvania, Philadelphia, PA, USA*
- SHRI RAM YADAV • *Department of Bio and Environmental Sciences, Institute of Biotechnology, University of Helsinki, Helsinki, Finland*
- PATRICIA ZAMBRYSKI • *Department of Plant and Microbial Biology, University of California, Berkeley, CA, USA*
- RAUL ZAVALIEV • *Department of Molecular Biology and Ecology of Plants, George S. Wise Faculty of Life Sciences, Tel Aviv University, Tel Aviv, Israel*

# Part I

## Overview



# Chapter 1

## Plasmodesmata: Channels for Intercellular Signaling During Plant Growth and Development

Iris Sevillem, Shri Ram Yadav, and Ykä Helariutta

### Abstract

Plants have evolved strategies for short- and long-distance communication to coordinate plant development and to adapt to changing environmental conditions. Plasmodesmata (PD) are intercellular nano-channels that provide an effective pathway for both selective and nonselective movement of various molecules that function in diverse biological processes. Numerous non-cell-autonomous proteins (NCAP) and small RNAs have been identified that have crucial roles in cell fate determination and organ patterning during development. Both the density and aperture size of PD are developmentally regulated, allowing formation of spatial symplastic domains for establishment of tissue-specific developmental programs. The PD size exclusion limit (SEL) is controlled by reversible deposition of callose, as well as by some PD-associated proteins. Although a large number of PD-associated proteins have been identified, many of their functions remain unknown. Despite the fact that PD are primarily membranous structures, surprisingly very little is known about their lipid composition. Thus, future studies in PD biology will provide deeper insights into the high-resolution structure and tightly regulated functions of PD and the evolution of PD-mediated cell-to-cell communication in plants.

**Key words** Plasmodesmata (PD), Non-cell-autonomous proteins (NCAP), Plant development, Callose, Rafts

---

### 1 Introduction

Plants are multicellular organisms that, unlike animals, continue to grow and develop throughout their life-spans. Positional signals transmitted between cells, tissues, and organs specify patterning in plants. Consequently, plants are able to grow in a highly plastic manner, and adapt to changing environmental conditions despite their sessile lifestyles. The cytoplasm of nearly all plant cells are connected via plant-specific channels, called plasmodesmata (PD). Various molecules move via PD, either by diffusion or in a targeted manner. PD can regulate diffusion by modifying their inner diameter. On the other hand, PD can be temporarily dilated by some mobile proteins that move in a so-called targeted manner. PD are known to transmit mobile signals such as transcription factors and

RNA molecules, which provide crucial information for plant development [1–3]. Here, we discuss PD and the role of symplastic communication during various developmental processes.

---

## 2 Structure of PD

PD enable cytoplasmic continuity by crossing cell walls of neighboring cells. In addition to water and small molecules, large molecules such as proteins, RNA, and some pathogens move via PD. PD are lined with plasma membrane and a tube of compressed endoplasmic reticulum (ER), called the desmotubule, runs across the pore. Molecules move from cell to cell through the cytoplasmic sleeve, which is the space between the desmotubule and plasma membrane. Inside the cytoplasmic sleeve, proteins are located on the surface of both membranes to regulate molecule movement (Fig. 1) [1–3]. Additionally, molecules are known to traffic along the membranes of the ER [4], and small molecules up to 10.4 kDa can also move between the ER lumen via the desmotubule lumen [5]. Biochemical and proteomic analyses of PD-enriched cell wall fractions have identified a large number of different kinds of proteins associated with PD [6–13]. These proteins can either be uniformly distributed along the plasma membrane or specifically localized to some regional membrane microdomains, called membrane rafts. For example, the PD-located protein, PDLPI, is targeted along the length of plasma membrane [8] whereas glycosylphosphatidylinositol (GPI)-anchored PD callose-binding (PDCBs) proteins are only localized to the neck region of PD [9]. Plant-specific proteins, remorins, which are highly enriched in sterol/sphingolipid-rich detergent-insoluble membrane fractions of PM, are also associated with PD [14, 15]. Thus, the raft-like nature of PD may be important for its function, such as in sorting and recruiting associated proteins [16–19]. The plant cytoskeleton proteins, actin and myosin, have also been immunolocalized to PD and may have a role in symplastic transport [20]. PD can be classified according to their origin into primary PD that arise during cell division and secondary PD that arise after cell division. Both primary and secondary PD are structurally diverse, having a simple, twinned, or branched type. Simple PD connect neighboring cells with a single linear channel, whereas branched ones have multiple channels. Young tissues contain mainly simple PD, and twinned and branched predominate in mature tissues [21]. The number of PD and the state of their dilation are developmentally regulated. The SEL, which is the upper size limit of molecules that can diffuse through PD, is defined by the degree of dilation of the PD aperture. Closed PD inhibit all traffic, whereas open PD enable movement of solutes less than 1 kDa, and dilated PD are permeable to larger molecules, such as proteins. In growing tissues the SELs are

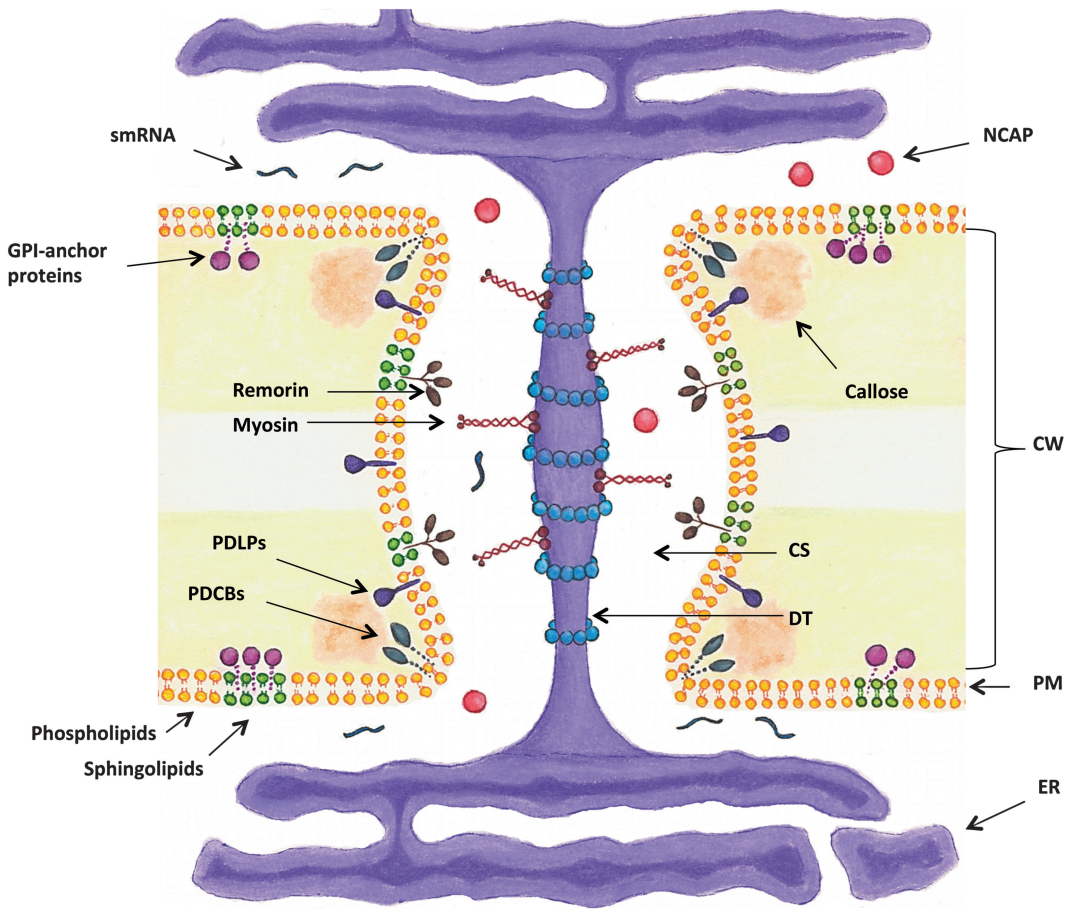


**Fig. 1** Plasmodesmata. Plasma membrane-lined pores called plasmodesmata (PD) penetrate cell walls (CW) of neighboring cells. Compressed endoplasmic reticulum (ER), called desmotubule (DT), runs through the pore. Molecules such as non-cell-autonomous proteins (NCAPs) and small RNAs (smRNAs) can move from cell to cell via the cytoplasmic sleeve (CS) or along the ER membrane. Small molecules can also move via the DT lumen. Callose turnover at the neck region of PD regulates the channel aperture. Various PD-localized proteins have been identified, including remorins, myosin, GPI-anchor proteins, callose-binding proteins (PDCBs), and PD-localized proteins (PDLs). Remorins and GPI-anchor proteins may be associated with sphingolipid-containing microdomains of PM

generally between 30 and 50 kDa [22, 23]. In *Arabidopsis* root, experiments with freely moving 27 kDa RFP expressed from the ground tissue (*J0571*; *UAS::RFP*) suggested that PD interconnecting the majority of root cells have SELs that are greater than 27 kDa. Stele/endodermis and cortex/epidermis boundaries likely have an SEL of ~60 kDa. The SEL of PD from the cortex and the quiescent center (QC) up to the distal root cap cells is between 27 and 54 kDa. Thus, all proteins below 60 kDa could potentially move in a non-targeted fashion in the radial direction [24]. However, the SEL cannot be expressed precisely in kDa, since it is not the weight but rather the size and shape (Stokes radius) of a

molecule that determine its permeability. Therefore, molecules of the same weight can have significant differences in their capacity to diffuse via PD [25, 26].

---

### 3 PD Interconnections Form Symplastic Domains

The plant embryo is morphologically different to an adult plant, since many new parts develop postembryonically. The embryo develops meristems with totipotent stem cells, which are responsible for producing new organs in an adult plant. Growth from the meristems occurs in a modular fashion, producing repeated structural units from the apices. When the cytoplasm of a group of cells are shared through open PD interconnections, they are said to form symplastic domains. Symplastic domains are important for the development of different cell types, tissues, and organs by establishing spatial domains that allow localized signaling to take place. These domains are thought to have a reduced SEL at their borders, which restricts communication with surrounding cells, thus enabling the activation of developmental programs in restricted areas. During early embryogenesis, all cells are connected in the suspensor and the embryo, forming a single symplast. As development proceeds, PD apertures are downregulated to form distinct symplastic domains. The first boundary forms between the suspensor and the embryo hypophysis. During later stages, symplastic domains are formed corresponding to the shoot apex, cotyledons, hypocotyl, and root along the longitudinal axis. As further differentiation occurs, additional tissue-specific sub-domains are known to be formed [3, 27, 28]. Analyzing the movement of different size green fluorescent protein (GFP) molecules (1×, 2×, and 3×-GFP) have shown differential molecular trafficking in these sub-domains [23].

Studies with *Arabidopsis* root have shown that PD distribution and their permeability is tissue specific. As the cells mature, the tissue-specific distribution of PD remains unchanged but their density reduces dramatically [29]. Transverse cell walls have generally higher number of primary PD whereas secondary PD are mostly distributed along the longitudinal cell walls [30]. In the meristem, the initial cells have more symplastic connections with their derivative immature cells through transverse walls. Therefore, primary PD appear to be the main route for molecular traffic within tissues [29]. Symplastic connectivity between the sieve elements (SE) and companion cells (CC) of the phloem is especially extensive, since the PD connecting these two cell types is much higher (>67 kDa) compared to the PD connecting SE with other neighboring cells [31]. This is critical since the enucleated SE is physiologically dependent on the CC.

## 4 Symplastic Signaling Pathways Coordinate Development

### 4.1 Maintenance of the SAM Involves Mobile Homeobox Factors

The SAM at the shoot apex contains self-renewing stem cells that contribute to continuous growth and development of above-ground parts of a plant. The size of the SAM stays remarkably stable throughout development, although cell flux from the meristem to developing lateral organs and underlying stem is continuous. Stem cell maintenance to ensure constant SAM size and controlled differentiation of certain cells into primordial founder cells are two distinct but simultaneously happening processes, which are controlled by complex intercellular signaling [32, 33].

The L1 and L2 cell layers of the vegetative SAM and the inflorescence meristem (IM) are connected through secondary PD [34], which allow passage of several critical developmental regulators. Maize *KNOTTED1* (KN1), a KNOX homeodomain transcription factor essential for SAM formation and maintenance, was the first regulator shown to be mobile [35, 36]. Subsequently, *Arabidopsis* homologs of KN1, *KNOTTED 1*-like homeobox protein 1/*BREVIPEDICELLUS* (KNAT1/BP), and *SHOOT MERISTEMLESS* (STM) were shown to move from L1 to L2/L3 layers of the SAM. The movement of these factors is required for SAM initiation and maintenance, as well as epidermis differentiation and plant architecture [37].

Additionally, stem cell maintenance in the SAM is crucially dependent on a homeobox transcription factor, *WUSCHEL* (WUS), which is transcribed in a few cells of the L3 layer of the organizing center (OC), just beneath the central zone (CZ) (Fig. 2a) [38–40]. WUS is mainly regulated by *CLAVATA 3* (CLV3), which acts as a signal to repress WUS expression and forms a negative feedback loop with WUS to maintain a constant size of the SAM [41]. A recent study has shown that the WUS protein moves through PD to adjacent cells [42]. It moves from L3 to L2/L1 layers of SAM and from L2 to L1 layer of floral meristem and activates transcription of *CLV3* by directly binding to its regulatory elements in its promoter. Interestingly, by restricting the movement of WUS protein either by increasing its molecular size by fusing tandem repeats of GFP or through targeting the fusion protein to the nucleus, WUS failed to rescue SAM phenotypes of *wus-1* mutants, demonstrating that movement of WUS protein is required for its shoot meristem functions [42].

### 4.2 Lateral Inhibition Coordinates Trichome and Root Hair Patterning

Leaf trichomes and root hairs both differentiate from epidermal cells, and appear in regular intervals. These patterning events have similarities also in their regulatory mechanism, as they both depend on cell-to-cell communication, and involve the same regulators [43, 44]. A WD40 protein *TRANSPARENT TESTA GLABRA 1* (TTG1), a bHLH-like transcription factor *GLABRA3* (GL3), the

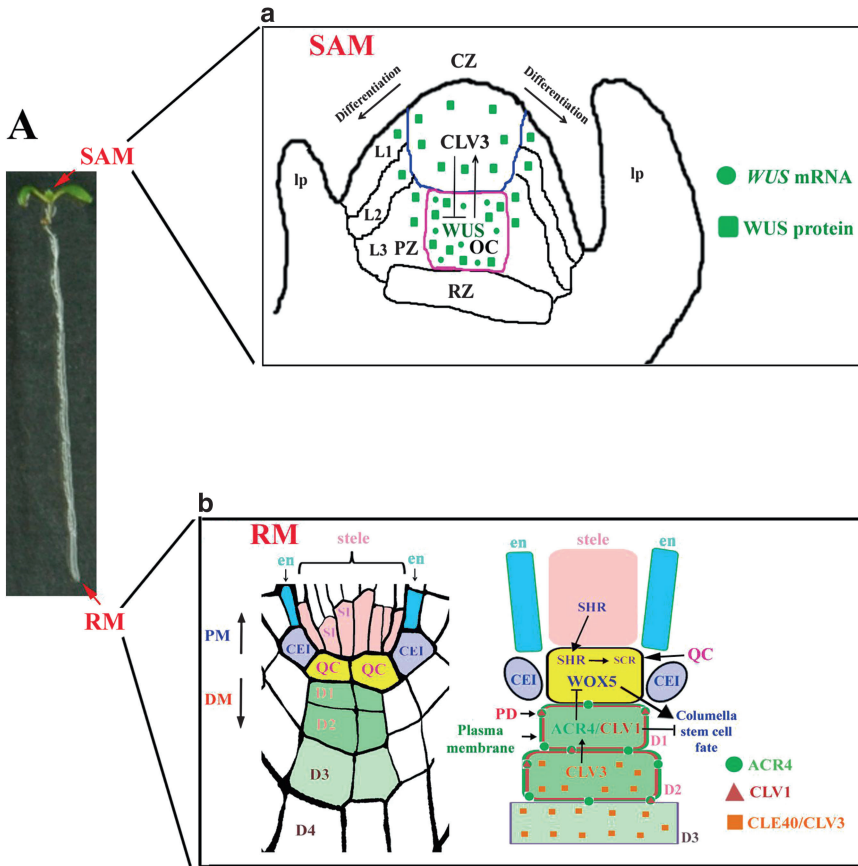


**Fig. 2** Cell-to-cell communication during stem cell niche maintenance in *Arabidopsis*. (A) The positions of the shoot apical meristem (SAM) and the root meristem (RM) in *Arabidopsis* seedling are pointed with red arrows. (a) Organization of the SAM: Three tissue layers (L1–L3) and various functional zones are shown in the schematic diagram. The undifferentiated stem cells are maintained in the central zone (CZ) of the meristem, positioned just above the rib zone (RZ). The daughter cells derived from stem cell divisions enter the peripheral zone (PZ) to undergo differentiation during shoot organ development. The CLV3-CLV1-WUS signaling pathway controls SAM function. WUS mRNA is restricted to the organizing center (OC), but WUS protein moves to the CZ and PZ. *lp* Leaf primordia. (b) Organization of the RM (*left panel*): Proximal meristem (PM), distal meristem (DM), distal cell layers (D1–D4), stele initials (SI), quiescent center (QC), endodermis (en), cortex/endodermis initial (CEI). The *right panel* shows regulatory mechanisms controlling stem cell maintenance in the RM. SHORT ROOT (SHR) proteins move from stele to QC where it activates SCARECROW (SCR). The CLV3/CLE40-CLV1/ACR4-WOX5 module controls the DM. CLV1 and ACR4 proteins are localized to the plasma membrane and plasmodesmata (PD)

ENHANCER OF GLABRA3 (EGL3), and GLABRA2 (GL2) promote trichome and non-hair cell differentiation [45, 46]. During trichome development, TTG1 is expressed in all epidermal cells and can freely move between cells. In trichome precursors, the TTG1 protein is captured to the nucleus by GL3. Consequently, trichome promoting TTG1 is depleted from the surroundings, inhibiting trichome development in the adjacent cells [47, 48].

Moreover, TTG1 with other trichome-promoting factors upregulates the expression of trichome inhibiting R3 MYB proteins, including TRYPTICHON (TRY) and CAPRICE (CPC), and ENHANCER OF TRY AND CPC 3 (ETC3). TRY, CPC, and ETC3 have been shown to move to the surrounding cells to inhibit trichome development [49]. Additionally, similar lateral inhibition by R3 MYB proteins occurs as in trichome development. TRY and CPC are known to move from non-hair cells to the neighboring cells to promote hair cell fate [50–53]. Root hair development also involves bHLH-like transcription factors GL3 and EGL3, which promote non-hair cell development [54]. However, unlike in trichome patterning, the GL3 protein is mobile in the root, and moves from the hair cells to the non-hair cells, which is the opposite direction of CPC movement [55].

### **4.3 Symplastic Isolation During Phase Changes**

During postembryonic development, the shoot undergoes a juvenile vegetative phase, an adult vegetative phase, and a reproductive phase. Vegetative and reproductive phases are controlled by interactive, but temporally relatively independent regulatory networks [56]. Only after the transition to the adult vegetative phase can floral induction begin [57]. *FLOWERING LOCUS T* (FT) is a mobile protein that transmits the signal of inductive photoperiod via phloem from the leaves to the shoot apex where flowering is initiated [58–60]. In the shoot apex, FT interacts with bZIP transcription factor FD, and the FT/FD complex activates genes that promote transition to flowering [61, 62]. A link between reduced symplastic traffic from the leaf to the SAM during flowering induction has been observed in *Arabidopsis* [63]. Similarly, through microinjection of fluorescent dyes, symplastic isolation has been observed in Birch apical meristem, where the central undifferentiated zone of tunica and surrounding peripheral zone form distinct symplastic domains, and which is broken down by short photoperiod [64]. These results suggest that PD may play an important role in transition from vegetative to reproductive development.

Research in poplar further suggests that PD may coordinate dormancy in perennial plants. The meristem is symplastically isolated during dormancy, and PD are re-opened after chilling, leading to reactivation of the meristem. Since FT functions as a negative regulator of dormancy, it is possible that this temporary PD closure induced by short days serves to inhibit FT entrance to the meristem, which allows dormancy to begin. Opening of the PD after chilling lets FT to re-enter the meristem and induce vegetative and generative growth [65].

### **4.4 Transcription Factors on the Move During Floral Meristem Identity and Floral Organ Patterning**

In *Arabidopsis*, an important floral meristem identity gene is LEAFY (LFY), which exhibits a non-cell-autonomous function through its movement to adjacent cells where it can activate downstream target genes [66]. The mobility of LFY is different between the lateral cells within a layer and the cells of underlying layers,

since it moves more readily from L1 to underlying cells than to laterally adjacent cells [67]. During floral organ patterning, MADS box-containing B-function factors, DEFICIENS (DEF) and GLOBOSA (GLO), control together as a heterodimer petal and stamen identities in *Antirrhinum* flowers [68]. Using somatically stable periclinal chimeras [69], it was shown that both of these factors exhibit regulated mobility, whereby the movement of DEF is polar, following a track from inner layers to the epidermal cell layer [69]. In *Arabidopsis*, the C-function MADS-box gene AGAMOUS (AG) controls stamen and carpel identities as well as floral meristem determinacy [70, 71]. AG can move from the epidermal cell layer to the subepidermal cell layer of the floral meristem through secondary PD and this movement of AG into subepidermal layers fully complements *ag* phenotypes, demonstrating its non-cell-autonomous functions in floral organ patterning and floral determinacy [72].

#### **4.5 Mobile TMO7 Specifies the Hypophysis to Initiate Root Growth**

During embryogenesis of *Arabidopsis*, the first division of the zygote is asymmetric and results in the formation of an apical cell and a larger basal cell. In the globular stage, the apical cell divides to form an eight-cell embryo proper and the basal cell divides to form the suspensor and the uppermost cell, called the hypophysis. The root quiescent center (QC) and columella cells originate from the hypophysis, whereas the remaining cells that will form the root derive from the embryo proper [73]. Extensive signaling occurs during specification of the hypophysis. MONOPTEROS (MP) is an auxin response factor required for root formation that promotes auxin flow from the embryonic cells to the hypophysis precursor [74]. In addition, it has been recently discovered that direct cell-to-cell communication also occurs. MP directly activates transcription of *TARGET OF MONOPTEROS 7 (TMO7)* in the embryonic cells, and the TMO7 protein moves to the hypophysis precursor to promote asymmetric division of the hypophysis, which is essential for the initiation of root growth. Division of the hypophysis produces an apical daughter cell that gives rise to the columella root cap and basally the QC cells, which give rise to the initials. TMO7 is thought to act as a cofactor for other cell-autonomous bHLH transcription factors. Hypophysis defects in *mp* loss-of-function mutants can be partially rescued by expressing *TMO7* in the mutant suspensor cells, demonstrating that TMO7 movement to the hypophysis participates in MP-dependent root formation [75].

#### **4.6 Extensive Signaling Maintains the Root Stem Cell Niche**

During postembryonic development, continuous growth and development of the root are crucially dependent on signaling events that balance cell division and cell differentiation rates in the root. *SHR* and *SCARECROW (SCR)*, another member of GRAS (GAI, RGA, SCR) family of transcription factors, are essential for maintenance of the stem cell niche by promoting QC and stem cell

identities. *SHR* is transcribed only in a certain part of the vascular tissue including xylem precursors and procambium, but not in phloem precursors and adjacent pericycle. The *SHR* protein moves into the endodermis, QC, and cortex/endodermal initial cell (CEI), where *SHR* and *SCR* physically interact and form a complex, which confines it to the nucleus, and activates the expression of *SCR* [76, 77]. *SHR* movement to the QC and subsequent activation of *SCR* are required to specify QC identity as well as to maintain surrounding initials (Fig. 2b). In *shr* loss-of-function mutants the QC is disorganized, the activity of the initials is lost, and root growth is inhibited. In *scr* mutants QC specification is abolished and initials have undergone differentiation. This can be observed in columella initials, which in *scr* mutants produce gravity-sensing starch granules called amyloplasts prematurely. In wild-type plants these amyloplasts only occur in differentiated columella cells. *shr* mutants have also defects in QC and stem cell identity, which are not restored when *SCR* is re-expressed in the QC. Therefore, activation of other components by *SHR* in addition to *SCR* is needed. *SCR* expression in the QC is required for initial identity, as *SCR* expression in the QC but not in columella or vascular cells can restore QC identity and initials in *scr* mutants [78].

To the best of our knowledge, the identity of the signals from QC to initials is still unknown. It is likely that the *WUSCHEL-RELATED HOMEBOX 5 (WOX5)* gene is involved. *WOX5* is a homeobox transcription factor related to *WUSCHEL (WUS)*, which is involved in shoot apical meristem maintenance. *WOX5* is expressed in the QC and is required non-cell-autonomously for the maintenance of columella initials (Fig. 2b). In *wox-5* loss-of-function mutants, QC cells are enlarged and columella stem cells accumulate starch granules, while the rest of the stem cells remain normal. *WOX5* also takes part in the maintenance of proximal stem cells redundantly with other factors. *WOX5* expression is reduced or completely lacking in *shr* and *scr* mutants, as well as in *mp* mutants. Thus, MP as well as *SCR/SHR* maintain *WOX5* expression. Whether *WOX5* itself or a downstream component moves to the initials remains to be discovered. Interestingly, *WUS* can replace *WOX5* in the maintenance of the root initials, indicating related mechanism in the maintenance of both meristems [79]. Moreover, *WUS* protein has been shown to be mobile in the shoot apical meristem [42].

Besides these factors, the members of CLV signaling pathway have a critical role in controlling distal meristem activity [79–81]. In spite of the similarities between the stem cell regulation in shoot and root, the molecular mechanisms are distinct in these tissues. In the shoot, CLV3-CLV1-WUS module controls stem cell niche, whereas in the root this module has an additional player to control the distal root meristem, a receptor kinase ARABIDOPSIS CRINKLY4 (ACR4) [80, 81]. The ACR4-CLV1 complex perceives the

CLE40/CLV3 signal, which restricts the expression of WOX5 (Fig. 2b). Interestingly, both CLV1 and ACR4 are localized to PD, suggesting their role in regulating trafficking through PD [81].

#### **4.7 Asymmetric Divisions: The Cortex/Endodermal Initial Cell**

Asymmetric cell division is an essential mechanism for the creation of different cell types and tissues during embryonic and postembryonic development. In addition to maintaining the stem cell niche, *SHR* functions as a positional signal that instructs the establishment of adjacent ground tissue by moving from the stele to the CEI cell layer. There it controls *SCR* transcription, which leads to asymmetric division of the initial to produce cortex and endodermal cell layers as well as differentiation of endodermal attributes. In both *shr* and *scr* mutants CEI gives rise to only a single cell layer instead of two. In *scr* mutants this cell layer contains attributes of both cortex and endodermal cells, but in *shr* mutants only cortex attributes are present [76, 77], indicating that SHR and SCR proteins control together asymmetric division of the CEI cell, whereas differentiation of endodermal attributes requires only SHR. Interestingly, SHR/SCR regulation of asymmetric division of the CEI cell has been directly linked to cell-cycle control. *CYCLIN D6;1*, a component of the cell-cycle machinery, has been identified as an SHR/SCR downstream target. It is transcribed in the CEI and is required for the correct asymmetric division to occur [82]. Thus, SHR/SCR provides the instructive signal that aligns the asymmetry and mediates it directly to specific genes regulating the cell cycle.

#### **4.8 Radial Patterning of the Root Relies on Bidirectional Signaling**

The patterning of stele and endodermis is coordinated by a reciprocal signaling cascade between the tissue layers. Protoxylem and metaxylem establishment requires localization of SHR and SCR in the endodermis, where they promote transcription of *MIR165A* and *MIR166B*. miR165/166 promote protoxylem development by moving inwards to the stele periphery, and cleave the mRNAs of *class III homeodomain leucine zipper* transcription factors, such as *PHABULOSA (PHB)*. Thus, PHB translational domain is confined to the central stele by SHR and SCR, which promote miR165/166 transcription (Fig. 3). Expansion of PHB domain, such as in *shr* and *scr* knockout mutants and *phb-7d* gain-of-function mutant, leads to ectopic metaxylem formation [83].

The miRNAs are additionally required for proper ground tissue and pericycle development. miRNA-dependent restriction of *PHB* expression promotes expression of a C2H2 zinc finger protein *JACKDAW (JKD)* in the ground tissue, which is necessary to restrict SHR movement. In *phb-1d* roots with ectopic *PHB* expression SHR movement is not inhibited by *JKD*, leading to the development of an extra cortex layer. In addition, *PHB* restriction mediated by the miRNAs is necessary for pericycle differentiation, as in both *phb-1d* and *scr-3* the expression of two pericycle identity markers, *AHP6* and *SKOR*, is reduced in the pericycle domain [84].

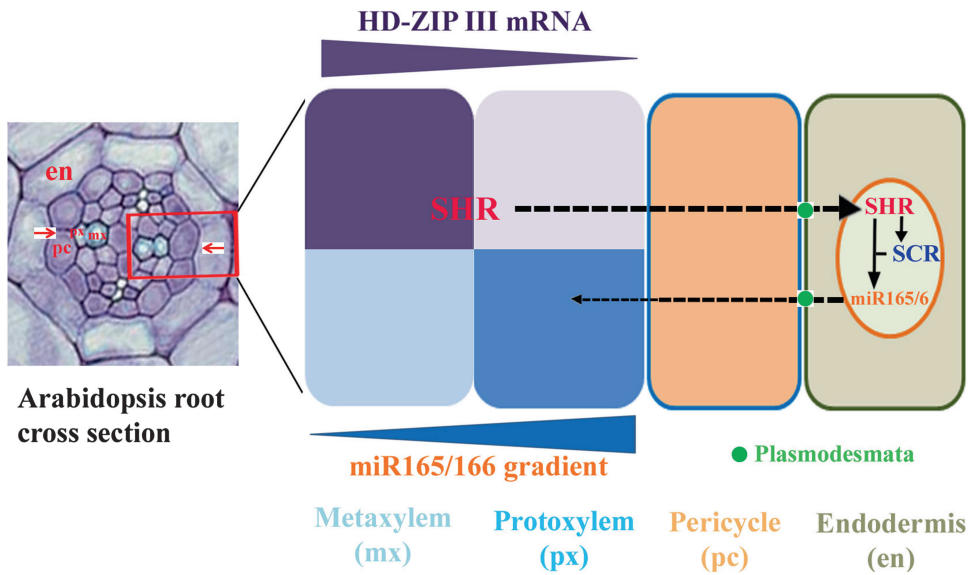


**Fig. 3** Bi-directional signaling mediated by SHR and miRNA165/166 controls xylem cell identity. SHR is synthesized in stele tissues but the protein moves to endodermis (en) through PD and activates SCR and miR165/166. The miRNAs move back to vascular tissues via PD, forming a concentration gradient that generates an opposite gradient for its target genes, HD ZIP III factors, which specify xylem cell identity in a dose-dependent manner. The cells with low HD ZIP III levels develop as protoxylem, and the cells with high HD ZIP III levels acquire metaxylem identity

## 5 Mechanisms Regulating Traffic via PD

### 5.1 The SEL of PD Is Regulated by Callose

Callose is a  $\beta$ -1,3 glucan polymer derived from UDP-glucose that plays crucial roles in plant development and physiological and stress responses [85–87]. It is dynamically deposited at PD, in cell plates during cell division, in developing pollen, and at phloem sieve plates. The critical level of callose is therefore regulated by a balance between  $\beta$ -1,3-glucan synthases (also called callose synthase) and  $\beta$ -1,3-glucanases that degrade callose [87, 88]. At PD, callose turnover regulates the permeability of the pore by functioning as a physical barrier at the neck region of PD that inhibits the passage of molecules by reducing the SEL (Figs. 1 and 4) [88, 89].

During birch and poplar development, PD are closed temporarily by callose deposition in the SAM during the dormancy period, and  $\beta$ -1,3-glucanases are thought to mediate the restoration of symplastic organization of the SAM after dormancy. Chilling, which releases the dormancy, restores symplastic communication by causing elevation in  $\beta$ -1,3-glucanase levels leading to removal of callose from PD [65, 90]. A PD-associated  $\beta$ -1,3-glucanase has been identified in *Arabidopsis* that controls trafficking through PD. This protein contains a GPI anchor motif, which links the protein to the extracellular face of the plasma membrane.

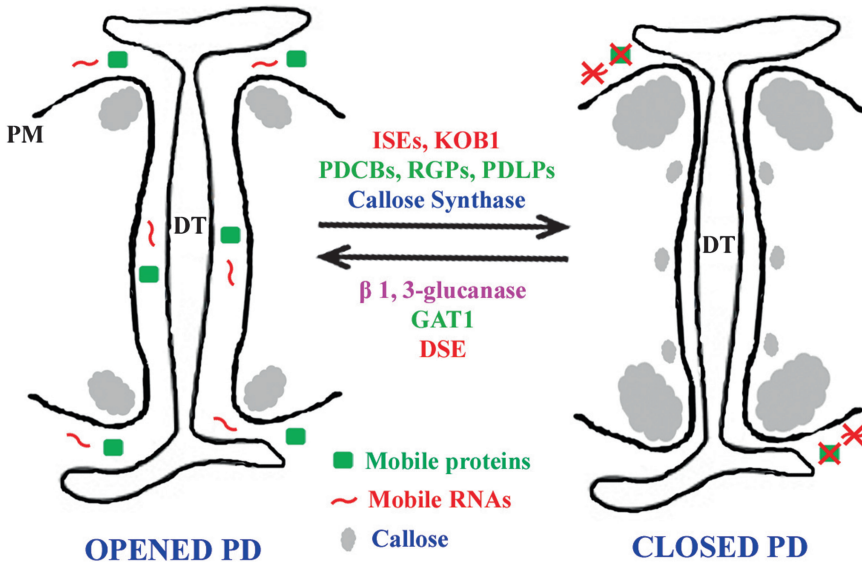


**Fig. 4** Schematic diagram showing regulation of molecular trafficking through PD. PD are opened and closed in a reversible manner by the activities of various regulators. Callose turnover is a well-studied mechanism for control of PD-mediated trafficking

It is thought that  $\beta$ -1,3-glucanase degrades callose in the extracellular wall region. Mutant plants accumulating less  $\beta$ -1,3-glucanase accumulate more callose and have lowered SEL, which was demonstrated by reduced diffusion of GFP through PD [7, 91]. Recently, Benitez-Alfonso et al. [92] showed that spatiotemporal control of callose deposition and symplastic connectivity regulated by two  $\beta$ -1,3-glucanases, plasmodesmal-localized  $\beta$ -1,3-glucanase 1 and 2 (PdBG1 and PdBG2), are required for lateral root development. In wild-type roots, callose deposition at PD increases and symplastic transport decreases progressively during the development of a lateral root primordium (LRP), isolating it from the surrounding cells. In *pdbg1,2* double mutants callose levels are elevated and increased number of LRPs is observed. Similarly, the number of LRPs increases when the *icals3m* system is expressed in the lateral root-competent xylem pole pericycle cells. Thus, symplastic domain formation by callose plays an essential role in LRP initiation and their spatial positioning [92].

The *Arabidopsis* genome contains 12 callose synthase (CalS) genes [93], several of which are known to function in symplastic communication in various tissues. *CalS10* (*GSL8*) is required for callose deposition at cell wall, cell plate, and PD and has a role in regulating cytokinesis, cell-cell connectivity, stomata patterning, and ploidy consistency in gametes [94]. *calS10* loss-of-function mutants have increased symplastic connectivity between epidermal cells, leading to enhanced movement of the stomata identity factor

SPEECHLESS (SPCH), resulting in defective stomata patterning [95]. *CalS7* (*GSL7*) is responsible for callose deposition at PD and sieve plates of developing phloem sieve elements [96, 97]. Callose levels are greatly reduced in the sieve elements in *cals7* loss-of-function mutants, resulting in sieve plates with fewer pores. These mutants also have various growth defects such as shorter stems and roots and reduced phloem transport capacity [96, 97]. *CalS3* (*GSL12*) is expressed in the stele and in and around the stem cell niche in *Arabidopsis* root, and promotes callose deposition at PD [98]. *cals3-d* gain-of-function mutations cause reversible over accumulation of callose at PD, leading to reduced SEL. The phloem unloading of GFP driven by the companion cell-specific promoter *pSUC2* is reduced in *cals3-1d* mutants compared to wild type. Moreover, the mutants phenocopy *phb-7d* and other mutants with a disturbed *SHR*-miRNA pathway [98]. Recently, a maize callose synthase mutant, *Tie-dyed2* (*tdy2*), was shown to be affected in leaf vein development and symplastic trafficking in phloem tissues [99]. Collectively, these results suggest that callose deposition and removal can be an important mechanism to regulate movement of signaling molecules during development that can overcome some other regulatory mechanisms controlling the SEL.

## **5.2 Callose-Associated Proteins Regulate Intercellular Trafficking**

In addition to callose synthases and glucanases, several other proteins have been described that may function in regulation of callose deposition at PD (Figs. 1 and 4). A group of proteins called PD callose-binding proteins (PDCBs) belonging to a family of small GPI-linked proteins have been identified that may be involved in callose-mediated regulation of cell-to-cell movement. PDCBs can bind to callose in vitro and YFP-PDCB1 was found to localize to the neck region of PD. Increased expression of PDCB1 led to an increase in callose accumulation and a reduction of GFP movement. Thus, PDCBs might function to recruit and stabilize callose to the PD neck region [9]. Reversibly glycosylated polypeptides (RGPs) are plant-specific proteins consisting of class 1 and class 2 RGPs, of which class 1 members have been found to associate with PD [100]. They are soluble proteins that are actively delivered at PD by Golgi vesicles and may regulate PD flux. Transgenic tobacco plants expressing *Arabidopsis* RGP2-GFP have reduced PD permeability, which may be related to callose deposition as the overexpressor mutants also have excessive callose at PD. However, the underlying mechanisms are still unclear [101]. Members of the PDLPI (plasmodesmata-located proteins) family consist of type I membrane receptor-like proteins, which are targeted to PD. One of them, PDLPIa, has been shown to affect cell-to-cell communication in a GFP diffusion assay. Transgenic lines overexpressing *PDLPI* showed a dramatic reduction in GFP movement, whereas in combined knockout lines of several clade members GFP movement was increased [8]. Like RGPs, they are delivered by the secretory

pathway, but unlike RGP are membrane proteins. Interestingly, PDL1 contains a single transmembrane domain, which is necessary and sufficient for the protein to be PD targeted, and can be used to target other proteins to PD and perhaps in the future to manipulate PD function [8]. Recently, PDLs were shown to mediate virus spread by binding MPs encoded by certain viruses. These viruses are dependent on this interaction as their spread is significantly reduced in *pdlp* loss-of-function mutants. This makes the PDLs a unique class, since in contrast to the inhibition of virus spread, GFP movement is increased in *pdlp* mutants [102]. Investigating whether these proteins are necessary for targeted movement of endogenous proteins would be highly valuable. Additionally, PDL5 also localizes to PD and acts as an inhibitor of PD trafficking likely by enhancing callose deposition at PD. In contrast with PDL1, downregulation of PDL5 alone is sufficient to enhance PD permeability [103].

### **5.3 PD Are Regulated by Redox Homeostasis**

From several recent studies, redox homeostasis has been shown to control molecular trafficking through PD. There is also evidence that callose deposition is regulated by redox homeostasis, since accumulation of reactive oxygen species (ROS) is associated with the production of callose [104]. GFP ARRESTED TRAFFICKING1 (GAT1) is an m-type thioredoxin functioning in redox homeostasis in plastids of sink tissues, and has been shown to affect PD transport [104]. The *gat1* mutants have reduced symplastic transport capacity of GFP especially in meristems. Both callose and H<sub>2</sub>O<sub>2</sub> were found to be increased in the *gat1* mutant, and therefore it has been proposed to function in redox regulation of callose deposition. Additionally, *gat1* mutants have an increased proportion of complex PD. GAT1:TRX-m3 does not target to PD specifically, which supports the view that accumulation of ROS in *gat1* mutants is responsible for callose accumulation [104]. This finding further supports the importance of callose in regulation of PD permeability.

*INCREASED SIZE EXCLUSION LIMIT (ISE)1* and *2* were identified in a screen for mutants with defects in the regulation of symplastic domain size. *ISE1* encodes a mitochondrial DEAD-box RNA helicase and controls mitochondrial functions and cell-to-cell transport through PD [105]. On the other hand, *ISE2* encodes a chloroplast-localized putative DEVH box RNA helicase and has a role in PD functions through controlling RNA metabolism [21, 106]. Additionally, both the genes are involved in plastid development by controlling expression of a common set of genes whose products are directly involved in plastid function, providing evidence for organelle–nucleus cross talk during PD-mediated intercellular communication [21]. Similarly to *gat1*, *ise1* and *ise2* have more complex PD. The mutants have, however, an opposite effect on transport. Interestingly, a recent study shows that redox

state of plastids and mitochondria differentially regulate PD-mediated intercellular transport [107]. The mitochondria are more oxidized in *ISE1*-silenced leaves whereas plastids are more reduced in both *ISE1*- and *ISE2*-silenced leaves. Thus, oxidative shift in plastids and mitochondria have opposite effects on intercellular transport. This study also provides evidence for the role of plastids and mitochondria in controlling molecular trafficking via PD [107].

#### 5.4 Other Regulators of PD

A plasma membrane-localized glycotransferase-like protein, KOBITO1 (KOB1), controls stomata patterning by regulating PD permeability, without affecting callose level at PD in *Arabidopsis* [108]. KOB1 is necessary for normal cellulose biosynthesis during cell expansion [109] and also mediates response to ABA and sugar [110]. *kob1-3* mutants develop clustered stomata in *erl1*, *erl2* background but not in wild type due to increased diffusion of stomata cell fate-specifying factor, SPCH [108]. Importantly, defect in cellulose biosynthesis associated with *kob* mutants is not a major cause for permeability defects of PD. Very recently, *LYSIN MOTIF DOMAIN-CONTAINING GLYCOSYLPHOSPHATIDYLINOSITOL-ANCHORED PROTEIN 2* (LYM2), which encodes the *Arabidopsis* homolog of rice chitin receptor-like protein, is shown to control molecular flux through PD in the presence of chitin [111]. LYM2 protein is localized to the plasma membrane and PD. LYM2 functions as a pathogen recognition receptor (PRR) that in the presence of chitin decreases molecular flux through PD. This signaling is important in chitin-triggered immunity in *Arabidopsis* [111]. An effect of reduced PD and molecular trafficking is also observed in the *Arabidopsis* embryo-lethal mutant *decreased size exclusion limit1* (*dse1*) during embryogenesis [112]. *dse1* mutants have a reduced number of X, Y-shaped and twinned PD. *AtDSE1* encodes for a WD-repeat protein required for morphogenesis and reproduction [112, 113].

---

## 6 Movement via PD: Targeted or Non-targeted

The terms “targeted” and “non-targeted” movement are used to describe the mechanisms by which molecular traffic occurs through PD [22]. In non-targeted movement, molecules move through PD by diffusion without interacting with PD or associated components; therefore their movement is restricted by the size of the molecules which must be smaller than the SEL of PD. Metabolites, such as sugars and amino acids, as well as GFP and LFY proteins are thought to move by a non-targeted mechanism [67]. PD are designed to allow controlled passage of certain proteins. These often large proteins overcome the SEL by temporarily dilating the PD aperture. Therefore, this pathway is not dependent on the

physiological state of the aperture/SEL, but instead on the molecular characteristics of the protein. Viruses have evolved to spread through plants using this pathway. Movement proteins (MPs) encoded by viruses facilitate the spread of virus particles or viral ribonuclear protein complexes by modifying the SEL of PD using a variety of mechanisms [114]. As illustrated in experiments with tobacco leaves, GFP fused to viral MPs can, despite its larger size, move much more efficiently compared to GFP alone even in mature tissues [115]. Since this mechanism involves interaction with the PD, a crucial characteristic of targeted molecules is that they contain a specific movement sequence that gives them competence to move by mediating this interaction. Such a sequence has been discovered in KNOTTED1 (KN1), which is the first endogenous plant protein found to traffic via PD in a targeted manner [36]. The protein contains a nuclear localization sequence located within its homeodomain (HD), which is an essential region for transport. When the KN1 HD was fused to a cell-autonomous MYB transcription factor, *GLABROUS1*, the protein gained the capacity to move from cell to cell, indicating that this specific region is necessary and sufficient for proteins to be targeted and transported via PD [116]. Also, in *CAPRICE* two sequences have been identified that are necessary and sufficient for transport; one in the N-terminus and the other in the MYB domain [53]. In contrast, there is no requirement for movement sequences in proteins that move nonselectively between cells. For example in *LEAFY*, deletion experiments have not been able to abolish movement of the protein, and therefore it is considered to move by diffusion [67]. While most transcription factors are thought to move in a targeted manner, no universal trafficking sequences have been found. For example in *SHR* not a single movement sequence has been identified that is necessary and sufficient for movement. Multiple regions in the GRAS domain are required for *SHR* movement, most of which are also required for activity [117]. Recently, an endosome-associated protein, *SHORT-ROOT INTERACTING EMBRYONIC LETHAL* (SIEL), has been shown to interact with *SHR*, *CPC*, and *TMO7* and to promote *SHR* movement [118]. Intriguingly, both the SIEL protein localization and *SHR* movement require intact microtubules, suggesting a role for PD-associated microtubules in facilitating cell-to-cell movement of endogenous proteins [119].

A recent study on KN1 suggests that a chaperonin complex is necessary for targeted movement of some transcription factors. The authors identified a chaperonin, CCT8 (for chaperonin containing TCP1, subunit 8), that directly interacts with KN1 protein and is essential for its trafficking from cell to cell [120]. CCT8 is a subunit of the type II chaperonin complex, which assists in protein folding. Surprisingly, the authors showed that CCT8 was required specifically in the destination cells for proper KN1 trafficking,

and therefore suggest that the chaperonin complex functions in refolding of the KN1 proteins. This mechanism is likely conserved, since it is also required for trafficking of STM, although not universally applicable, as, e.g., SHR movement was found not to depend on CCT8 [120]. Most mobile transcription factors identified are thought to move in a targeted manner, and this ability to move seems to be tissue specific. An interesting example is CPC, which moves strictly between hair cells and non-hair cells in wild-type *Arabidopsis* and was found not to move when expressed in the stele [53], whereas expression from the ground tissue leads to extensive movement in a non-targeted manner. These results do not correlate with the SEL of PD, suggesting that there is some mechanism regulating specifically targeted movement in a tissue-specific manner [24]. Thus, there are still unknown mechanisms that regulate movement patterns, and more research is therefore needed to bring further understanding to how the symplastic pathways are controlled.

---

## 7 Conclusions

The majority of the cell types in the plant body are connected to the cytoplasmic network formed by PD connections. Trafficking via PD seems to be controlled by PD abundance, their aperture size, and selectivity towards transported molecules. Proteomics-based analyses have identified a large number of candidate proteins which are likely associated with PD, supporting the hypothesis that transport through PD is highly regulated. However, our understanding of PD structure, dynamics, and mechanisms regulating PD-mediated molecular trafficking is not yet comprehensive. A recent study has shown that microtubules are required for SHR movement [119], raising strong possibility of direct role of cytoskeleton components in symplastic communication. Additionally, a potential physiological role of lipid rafts at PD is emerging. The PM is now considered to be composed of various heterogeneous membrane rafts enriched in sphingolipids and sterols, and some of the raft-associated proteins are also present at PD, suggesting that PD might have similar properties to rafts [16]. Therefore, analyzing the PD-associated lipid composition will further provide greater insights into PD structure. Importantly, further research is necessary to uncover how the various components participate in PD-related functions, such as sorting and targeting cargo to PD. Transport through PD is selectively variable depending on the tissue type and its developmental stage, and various developmentally significant molecules are known to move through PD. The number of symplastically mediated developmental pathways is extremely high. In this work, we have discussed the breadth of these pathways using diverse examples, which demonstrate the vital nature of PD in all aspects of development.

## Acknowledgements

This work was funded by Tekes funds, Academy of Finland, and ERC Grant (Y.H.). I.S. was also funded by Viikki Doctoral Program in Molecular Biosciences.

## References

1. Cilia ML, Jackson D (2004) Plasmodesmata form and function. *Curr Opin Cell Biol* 16:500–506
2. Lucas WJ, Lee JY (2004) Plasmodesmata as a supracellular control network in plants. *Nat Rev Mol Cell Biol* 5:712–726
3. Lucas WJ, Ham BK, Kim JY (2009) Plasmodesmata - bridging the gap between neighboring plant cells. *Trends Cell Biol* 19:495–503
4. Guenoune-Gelbart D, Elbaum M, Sagi G et al (2008) *Tobacco* mosaic virus (TMV) replicase and movement protein function synergistically in facilitating TMV spread by lateral diffusion in the plasmodesmal desmotubule of *Nicotiana benthamiana*. *Mol Plant Microbe Interact* 21:335–345
5. Barton DA, Cole L, Collings DA et al (2011) Cell-to-cell transport via the lumen of the endoplasmic reticulum. *Plant J* 66:806–817
6. Bayer EM, Bottrill AR, Walshaw J et al (2006) *Arabidopsis* cell wall proteome defined using multidimensional protein identification technology. *Proteomics* 6:301–311
7. Levy A, Erlanger M, Rosenthal M et al (2007) A plasmodesmata-associated beta-1,3-glucanase in *Arabidopsis*. *Plant J* 49:669–682
8. Thomas CL, Bayer EM, Ritzenthaler C et al (2008) Specific targeting of a plasmodesmal protein affecting cell-to-cell communication. *PLoS Biol* 6:e7
9. Simpson C, Thomas C, Findlay K et al (2009) An *Arabidopsis* GPI-anchor plasmodesmal neck protein with callose binding activity and potential to regulate cell-to-cell trafficking. *Plant Cell* 21:581–594
10. Fernandez-Calvino L, Faulkner C, Walshaw J et al (2011) *Arabidopsis* plasmodesmal proteome. *PLoS One* 6:e18880
11. Ham BK, Li G, Kang BH et al (2012) Overexpression of *Arabidopsis* plasmodesmata germin-like proteins disrupts root growth and development. *Plant Cell* 24:3630–3648
12. Salmon MS, Bayer EM (2013) Dissecting plasmodesmata molecular composition by mass spectrometry-based proteomics. *Front Plant Sci* 3:307
13. Zalepa-King L, Citovsky V (2013) A plasmodesmal glycosyltransferase-like protein. *PLoS One* 8:e58025
14. Raffaele S, Bayer E, Lafarge D et al (2009) Remorin, a solanaceae protein resident in membrane rafts and plasmodesmata, impairs *Potato virus X* movement. *Plant Cell* 21:1541–1555
15. Raffaele S, Bayer E, Mongrand S (2009) Upregulation of the plant protein remorin correlates with dehiscence and cell maturation: a link with the maturation of plasmodesmata? *Plant Signal Behav* 4:915–919
16. Mongrand S, Stanislas T, Bayer EM et al (2010) Membrane rafts in plant cells. *Trends Plant Sci* 15:656–663
17. Keinath NF, Kierszniowska S, Lorek J et al (2010) PAMP (pathogen-associated molecular pattern)-induced changes in plasma membrane compartmentalization reveal novel components of plant immunity. *J Biol Chem* 285:39140–39149
18. Simon-Plas F, Perraki A, Bayer E et al (2011) An update on plant membrane rafts. *Curr Opin Plant Biol* 14:642–649
19. Tilsner J, Amari K, Torrance L (2011) Plasmodesmata viewed as specialised membrane adhesion sites. *Protoplasma* 248:39–60
20. White RG, Barton DA (2011) The cytoskeleton in plasmodesmata: a role in intercellular transport? *J Exp Bot* 62:5249–5266
21. Burch-Smith TM, Stonebloom S, Xu M et al (2011) Plasmodesmata during development: re-examination of the importance of primary, secondary, and branched plasmodesmata structure versus function. *Protoplasma* 248:61–74
22. Crawford KM, Zambryski PC (2000) Subcellular localization determines the availability of non-targeted proteins to plasmodesmata transport. *Curr Biol* 10:1032–1040
23. Kim I, Cho E, Crawford K et al (2005) Cell-to-cell movement of GFP during embryogenesis and early seedling development in *Arabidopsis*. *Proc Natl Acad Sci U S A* 102:2227–2231
24. Rim Y, Huang L, Chu H et al (2011) Analysis of *Arabidopsis* transcription factor families revealed extensive capacity for cell-to-cell movement as well as discrete trafficking patterns. *Mol Cells* 32:519–526
25. Terry Terry BR, Robards AW (1987) Hydrodynamic radius alone governs the mobility of molecules through plasmodesmata. *Planta* 171:145–157

26. Dashevskaya S, Kopito RB, Friedman R et al (2008) Diffusion of anionic and neutral GFP derivatives through plasmodesmata in epidermal cells of *Nicotiana benthamiana*. *Protoplasma* 234:13–23
27. Kim I, Kobayashi K, Cho E et al (2005) Subdomains for transport via plasmodesmata corresponding to the apical-basal axis are established during *Arabidopsis* embryogenesis. *Proc Natl Acad Sci U S A* 102:11945–11950
28. Kim I, Zambryski PC (2005) Cell-to-cell communication via plasmodesmata during *Arabidopsis* embryogenesis. *Curr Opin Plant Biol* 8:593–599
29. Zhu T, Lucas WJ, Rost TL (1998) Directional cell-to-cell communication in the *Arabidopsis* root apical meristem I. An ultrastructural and functional analysis. *Protoplasma* 203:35–47
30. Zhu T, O'Quinn RL, Lucas WJ et al (1998) Directional cell-to-cell communication in the *Arabidopsis* root apical meristem II. Dynamics of plasmodesmatal formation. *Protoplasma* 204:84–93
31. Stadler R, Lauterbach C, Sauer N (2005) Cell-to-cell movement of green fluorescent protein reveals post-phloem transport in the outer integument and identifies symplastic domains in *Arabidopsis* seeds and embryos. *Plant Physiol* 139:701–712
32. Reddy GV, Heisler MG, Ehrhardt DW et al (2004) Real-time lineage analysis reveals oriented cell divisions associated with morphogenesis at the shoot apex of *Arabidopsis thaliana*. *Development* 131:4225–4237
33. Williams L, Fletcher JC (2005) Stem cell regulation in the *Arabidopsis* shoot apical meristem. *Curr Opin Plant Biol* 8:582–586
34. Marcotrigiano M (2001) Genetic mosaics and the analysis of leaf development. *Int J Plant Sci* 162:513–525
35. Jackson D, Veit B, Hake S (1994) Expression of maize KNOTTED1 related homeobox genes in the shoot apical meristem predicts patterns of morphogenesis in the vegetative shoot. *Development* 120:405–413
36. Lucas WJ, Bouché-Pillon S, Jackson DP et al (1995) Selective trafficking of KNOTTED1 homeodomain protein and its mRNA through plasmodesmata. *Science* 270:1980–1983
37. Kim JY, Yuan Z, Jackson D (2003) Developmental regulation and significance of KNOX protein trafficking in *Arabidopsis*. *Development* 130:4351–4362
38. Laux T, Mayer KF, Berger J et al (1996) The WUSCHEL gene is required for shoot and floral meristem integrity in *Arabidopsis*. *Development* 122:87–96
39. Mayer KF, Schoof H, Haecker A et al (1998) Role of WUSCHEL in regulating stem cell fate in the *Arabidopsis* shoot meristem. *Cell* 95:805–815
40. Tucker MR, Laux T (2007) Connecting the paths in plant stem cell regulation. *Trends Cell Biol* 17:403–410
41. Schoof H, Lenhard M, Haecker A et al (2000) The stem cell population of *Arabidopsis* shoot meristems is maintained by a regulatory loop between the CLAVATA and WUSCHEL genes. *Cell* 100:635–644
42. Yadav RK, Perales M, Gruel J et al (2011) WUSCHEL protein movement mediates stem cell homeostasis in the *Arabidopsis* shoot apex. *Genes Dev* 25:2025–2030
43. Ishida T, Kurata T, Okada K et al (2008) A genetic regulatory network in the development of trichomes and root hairs. *Annu Rev Plant Biol* 59:365–386
44. Schiefelbein J, Kwak SH, Wiecekowsky Y et al (2009) The gene regulatory network for root epidermal cell-type pattern formation in *Arabidopsis*. *J Exp Bot* 60:1515–1521
45. Pesch M, Hülskamp M (2009) One, two, three...models for trichome patterning in *Arabidopsis*? *Curr Opin Plant Biol* 12: 587–592
46. Balkunde R, Pesch M, Hülskamp M (2010) Trichome patterning in *Arabidopsis thaliana*: from genetic to molecular models. *Curr Top Dev Biol* 91:299–321
47. Bouyer D, Geier F, Kragler F et al (2008) Two-dimensional patterning by a trapping/depletion mechanism: the role of TTG1 and GL3 in *Arabidopsis* trichome formation. *PLoS Biol* 6:e141
48. Balkunde R, Bouyer D, Hülskamp M (2011) Nuclear trapping by GL3 controls intercellular transport and redistribution of TTG1 protein in *Arabidopsis*. *Development* 138:5039–5048
49. Wester K, Digiuni S, Geier F et al (2009) Functional diversity of R3 single-repeat genes in trichome development. *Development* 136:1487–1496
50. Wada T, Tachibana T (1997) Epidermal cell differentiation in *Arabidopsis* determined by a Myb homolog, CPC. *Science* 277:1113–1116
51. Wada T, Kurata T, Tominaga R et al (2002) Role of a positive regulator of root hair development, CAPRICE, in *Arabidopsis* root epidermal cell differentiation. *Development* 129:5409–5419
52. Schellmann S, Schnittger A, Kirik V et al (2002) TRIPTYCHON and CAPRICE mediate lateral inhibition during trichome and root hair patterning in *Arabidopsis*. *EMBO J* 21:5036–5046
53. Kurata T, Ishida T, Kawabata-Awai C et al (2005) Cell-to-cell movement of the CAPRICE protein

- in *Arabidopsis* root epidermal cell differentiation. *Development* 132:5387–5398
54. Bernhardt C, Lee MM, Gonzalez A et al (2003) The bHLH genes GLABRA3 (GL3) and ENHANCER OF GLABRA3 (EGL3) specify epidermal cell fate in the *Arabidopsis* root. *Development* 130:6431–6439
  55. Bernhardt C, Zhao M, Gonzalez A et al (2005) The bHLH genes GL3 and EGL3 participate in an intercellular regulatory circuit that controls cell patterning in the *Arabidopsis* root epidermis. *Development* 132:291–298
  56. Putterill J, Laurie R, Macknight R (2004) It's time to flower: the genetic control of flowering time. *Bioessays* 26:363–373
  57. Imaizumi T, Kay S (2006) Photoperiodic control of flowering: not only by coincidence. *Trends Plant Sci* 11:550–558
  58. Corbesier L, Vincent C, Jang S et al (2007) FT protein movement contributes to long-distance signaling in floral induction of *Arabidopsis*. *Science* 316:1030–1033
  59. Jaeger K, Wigge P (2007) FT protein acts as a long-range signal in *Arabidopsis*. *Curr Biol* 17:1050–1054
  60. Mathieu J, Warthmann N, Kuttner F et al (2007) Export of FT protein from phloem companion cells is sufficient for floral induction in *Arabidopsis*. *Curr Biol* 17:1055–1060
  61. Abe M, Kobayashi Y, Yamamoto S et al (2005) FD, a bZIP protein mediating signals from the floral pathway integrator FT at the shoot apex. *Science* 309:1052–1056
  62. Wigge P, Kim M, Jaeger K et al (2005) Integration of spatial and temporal information during floral induction in *Arabidopsis*. *Science* 309:1056–1059
  63. Gisel A, Barella S, Hempel FD et al (1999) Temporal and spatial regulation of symplastic trafficking during development in *Arabidopsis thaliana* apices. *Development* 126:1879–1889
  64. Rinne PL, van der Schoot C (1998) Symplasmic fields in the tunica of the shoot apical meristem coordinate morphogenetic events. *Development* 125:1477–1485
  65. Rinne PL, Welling A, Vahala J et al (2011) Chilling of dormant buds hyperinduces FLOWERING LOCUS T and recruits GA-inducible 1,3-beta glucanases to reopen signal conduits and release dormancy in *Populus*. *Plant Cell* 23:130–146
  66. Sessions A, Yanofsky MF, Weigel D (2000) Cell-cell signaling and movement by the floral transcription factors LEAFY and APETALA1. *Science* 289:779–782
  67. Wu X, Dinneny JR, Crawford KM et al (2003) Modes of intercellular transcription factor movement in the *Arabidopsis* apex. *Development* 130:3735–3745
  68. Tröbner W, Ramirez L, Motte P et al (1992) GLOBOSA: a homeotic gene which interacts with DEFICIENS in the control of *Antirrhinum* floral organogenesis. *EMBO J* 11:4693–4704
  69. Perbal MC, Haughn G, Saedler H et al (1996) Non-cell-autonomous function of the *Antirrhinum* floral homeotic proteins DEFICIENS and GLOBOSA is exerted by their polar cell-to-cell trafficking. *Development* 122:3433–3441
  70. Bowman JL, Smyth DR, Meyerowitz EM (1989) Genes directing flower development in *Arabidopsis*. *Plant Cell* 1:37–52
  71. Lenhard M, Bohnert A, Jürgens G et al (2001) Termination of stem cell maintenance in *Arabidopsis* floral meristems by interactions between WUSCHEL and AGAMOUS. *Cell* 105:805–814
  72. Urbanus SL, Martinelli AP, Dinh QD et al (2010) Intercellular transport of epidermis-expressed MADS domain transcription factors and their effect on plant morphology and floral transition. *Plant J* 63:60–72
  73. Dolan L, Janmaat K, Willemsen V et al (1993) Cellular organisation of the *Arabidopsis thaliana* root. *Development* 119:71–84
  74. Weijers D, Schlereth A, Ehrismann JS et al (2006) Auxin triggers transient local signaling for cell specification in *Arabidopsis* embryogenesis. *Dev Cell* 10:265–270
  75. Schlereth A, Möller B, Liu W et al (2010) MONOPTEROS controls embryonic root initiation by regulating a mobile transcription factor. *Nature* 464:913–916
  76. Helariutta Y, Fukaki H, Wysocka-Diller J et al (2000) The SHORT-ROOT gene controls radial patterning of the *Arabidopsis* root through radial signaling. *Cell* 101:555–567
  77. Nakajima K, Sena G, Nawy T et al (2001) Intercellular movement of the putative transcription factor SHR in root patterning. *Nature* 413:307–311
  78. Sabatini S, Heidstra R, Wildwater M et al (2003) SCARECROW is involved in positioning the stem cell niche in the *Arabidopsis* root meristem. *Genes Dev* 17:354–358
  79. Sarkar AK, Luijten M, Miyashima S et al (2007) Conserved factors regulate signalling in *Arabidopsis thaliana* shoot and root stem cell organizers. *Nature* 446:811–814
  80. Stahl Y, Wink RH, Ingram GC et al (2009) A signaling module controlling the stem cell niche in *Arabidopsis* root meristems. *Curr Biol* 19:909–914
  81. Stahl Y, Grabowski S, Bleckmann A et al (2013) Moderation of *Arabidopsis* root stemness by CLAVATA1 and ARABIDOPSIS

- CRINKLY4 receptor kinase Complexes. *Curr Biol* 23:362–371
82. Sozzani R, Cui H, Moreno-Risueno MA et al (2010) Spatiotemporal regulation of cell-cycle genes by SHORTROOT links patterning and growth. *Nature* 466:128–132
  83. Carlsbecker A, Lee JY, Roberts CJ et al (2010) Cell signalling by microRNA165/6 directs gene dose-dependent root cell fate. *Nature* 465:316–321
  84. Miyashima S, Koi S, Hashimoto T et al (2011) Non-cell-autonomous microRNA165 acts in a dose-dependent manner to regulate multiple differentiation status in the *Arabidopsis* root. *Development* 138:2303–2313
  85. Samuels AL, Giddings TH Jr, Staehelin LA (1995) Cytokinesis in tobacco BY-2 and root tip cells: a new model of cell plate formation in higher plants. *J Cell Biol* 130:1345–1357
  86. Parre E, Geitmann A (2005) More than a leak sealant. The mechanical properties of callose in pollen tubes. *Plant Physiol* 137:274–286
  87. Chen XY, Kim JY (2009) Callose synthesis in higher plants. *Plant Signal Behav* 4:489–492
  88. Zavaliev R, Ueki S, Epel BL et al (2011) Biology of callose (beta-1,3-glucan) turnover at plasmodesmata. *Protoplasma* 248:117–130
  89. Bucher GL, Tarina C, Heinlein M et al (2001) Local expression of enzymatically active class I beta-1, 3-glucanase enhances symptoms of TMV infection in tobacco. *Plant J* 28:361–369
  90. Rinne PL, Kaikuranta PM, van der Schoot C (2001) The shoot apical meristem restores its symplasmic organization during chilling-induced release from dormancy. *Plant J* 26:249–264
  91. Levy A, Guenoune-Gelbart D, Epel BL (2007) beta-1,3-Glucanases: plasmodesmal gate keepers for intercellular communication. *Plant Signal Behav* 2:404–407
  92. Benitez-Alfonso Y, Faulkner C, Pendle A et al (2013) Symplastic intercellular connectivity regulates lateral root patterning. *Dev Cell* 26:136–147
  93. Verma DP, Hong Z (2001) Plant callose synthase complexes. *Plant Mol Biol* 47:693–701
  94. Chen XY, Liu L, Lee E et al (2009) The *Arabidopsis* callose synthase gene GSL8 is required for cytokinesis and cell patterning. *Plant Physiol* 150:105–113
  95. Guseman JM, Lee JS, Bogenschutz NL et al (2010) Dysregulation of cell-to-cell connectivity and stomatal patterning by loss-of-function mutation in *Arabidopsis* chorus (glucan synthase-like 8). *Development* 137:1731–1741
  96. Barratt DH, Kölling K, Graf A et al (2011) Callose synthase GSL7 is necessary for normal phloem transport and inflorescence growth in *Arabidopsis*. *Plant Physiol* 155:328–341
  97. Xie B, Wang X, Zhu M et al (2011) CalS7 encodes a callose synthase responsible for callose deposition in the phloem. *Plant J* 65:1–14
  98. Vatén A, Dettmer J, Wu S et al (2011) Callose biosynthesis regulates symplastic trafficking during root development. *Dev Cell* 21:1144–1155
  99. Slewinski TL, Baker RF, Stubert A et al (2012) Tie-dyed2 encodes a callose synthase that functions in vein development and affects symplastic trafficking within the phloem of maize leaves. *Plant Physiol* 160:1540–1550
  100. Sagi G, Katz A, Guenoune-Gelbart D et al (2005) Class I reversibly glycosylated polypeptides are plasmodesmal-associated proteins delivered to plasmodesmata via the Golgi apparatus. *Plant Cell* 17:1788–1800
  101. Zavaliev R, Sagi G, Gera A et al (2010) The constitutive expression of *Arabidopsis* plasmodesmal-associated class I reversibly glycosylated polypeptide impairs plant development and virus spread. *J Exp Bot* 61:131–142
  102. Amari K, Boutant E, Hofmann C et al (2010) A family of plasmodesmal proteins with receptor-like properties for plant viral movement proteins. *PLoS Pathog* 6:e1001119
  103. Lee JY, Wang X, Cui W et al (2011) A Plasmodesmata-Localized Protein Mediates Crosstalk between Cell-to-Cell Communication and Innate Immunity in *Arabidopsis*. *Plant Cell* 23:3353–3373
  104. Benitez-Alfonso Y, Cilia M, San Roman A et al (2009) Control of *Arabidopsis* meristem development by thioredoxin-dependent regulation of intercellular transport. *Proc Natl Acad Sci U S A* 106:3615–3620
  105. Stonebloom S, Burch-Smith T, Kim I et al (2009) Loss of the plant DEAD-box protein ISE1 leads to defective mitochondria and increased cell-to-cell transport via plasmodesmata. *Proc Natl Acad Sci U S A* 106:17229–17234
  106. Kobayashi K, Otegui MS, Krishnakumar S et al (2007) INCREASED SIZE EXCLUSION LIMIT 2 encodes a putative DEVH box RNA helicase involved in plasmodesmata function during *Arabidopsis* embryogenesis. *Plant Cell* 19:1885–1897
  107. Stonebloom S, Brunkard JO, Cheung AC et al (2012) Redox states of plastids and mitochondria differentially regulate intercellular transport via plasmodesmata. *Plant Physiol* 158:190–199
  108. Kong D, Karve R, Willet A et al (2012) Regulation of plasmodesmatal permeability and stomatal patterning by the glycosyltransferase-like protein KOBITO1. *Plant Physiol* 159:156–168

109. Pagant S, Bichet A, Sugimoto K et al (2002) KOBITO1 encodes a novel plasma membrane protein necessary for normal synthesis of cellulose during cell expansion in *Arabidopsis*. *Plant Cell* 14:2001–2013
110. Brocard-Gifford I, Lynch TJ, Garcia ME et al (2004) The *Arabidopsis thaliana* ABSCISIC ACID-INSENSITIVE8 encodes a novel protein mediating abscisic acid and sugar responses essential for growth. *Plant Cell* 16:406–421
111. Faulkner C, Petutschnig E, Benitez-Alfonso Y et al (2013) LYM2-dependent chitin perception limits molecular flux via plasmodesmata. *Proc Natl Acad Sci U S A* 110:9166–9170
112. Xu M, Cho E, Burch-Smith TM et al (2012) Plasmodesmata formation and cell-to-cell transport are reduced in decreased size exclusion limit 1 during embryogenesis in *Arabidopsis*. *Proc Natl Acad Sci U S A* 109:5098–5103
113. Yamagishi K, Nagata N, Yee KM et al (2005) TANMEI/EMB2757 encodes a WD repeat protein required for embryo development in *Arabidopsis*. *Plant Physiol* 139:163–173
114. Benitez-Alfonso Y, Faulkner C, Ritzenthaler C et al (2010) Plasmodesmata: gateways to local and systemic virus infection. *Mol. Plant Microbe Interact* 23:1403–1412
115. Crawford KM, Zambryski PC (2001) Non-targeted and targeted protein movement through plasmodesmata in leaves in different developmental and physiological states. *Plant Physiol* 125:1802–1812
116. Kim JY, Rim Y, Wang J et al (2005) A novel cell-to-cell trafficking assay indicates that the KNOX homeodomain is necessary and sufficient for intercellular protein and mRNA trafficking. *Genes Dev* 19:788–793
117. Gallagher KL, Benfey PN (2009) Both the conserved GRAS domain and nuclear localization are required for SHORT-ROOT movement. *Plant J* 57:785–797
118. Koizumi K, Wu S, MacRae-Crerar A et al (2011) An essential protein that interacts with endosomes and promotes movement of the SHORT-ROOT transcription factor. *Curr Biol* 21:1559–1564
119. Wu S, Gallagher KL (2013) Intact microtubules are required for the intercellular movement of the SHORT-ROOT transcription factor. *Plant J* 74:148–159
120. Xu XM, Wang J, Xuan Z et al (2011) Chaperonins facilitate KNOTTED1 cell-to-cell trafficking and stem cell function. *Science* 333:1141–1144

# Chapter 2

## Plasmodesmata: Channels for Viruses on the Move

Manfred Heinlein

### Abstract

The symplastic communication network established by plasmodesmata (PD) and connected phloem provides an essential pathway for spatiotemporal intercellular signaling in plant development but is also exploited by viruses for moving their genomes between cells in order to infect plants systemically. Virus movement depends on virus-encoded movement proteins (MPs) that target PD and therefore represent important keys to the cellular mechanisms underlying the intercellular trafficking of viruses and other macromolecules. Viruses and their MPs have evolved different mechanisms for intracellular transport and interaction with PD. Some viruses move from cell to cell by interacting with cellular mechanisms that control the size exclusion limit of PD whereas other viruses alter the PD architecture through assembly of specialized transport structures within the channel. Some viruses move between cells in the form of assembled virus particles whereas other viruses may interact with nucleic acid transport mechanisms to move their genomes in a non-encapsidated form. Moreover, whereas several viruses rely on the secretory pathway to target PD, other viruses interact with the cortical endoplasmic reticulum and associated cytoskeleton to spread infection. This chapter provides an introduction into viruses and their role in studying the diverse cellular mechanisms involved in intercellular PD-mediated macromolecular trafficking.

**Key words** Plasmodesmata, Plant virus, Movement protein, Membrane, Cytoskeleton, RNA silencing

---

### 1 Interaction of Viral Movement Proteins with PD

The trafficking of viruses and other macromolecules through PD depends on intracellular transport mechanisms and is restricted by the size of the PD aperture. The size exclusion limit (SEL) of PD, thus the upper limit of the size of molecules transported by PD, is under tight control and changes during plant growth and development. Younger leaves that act as physiological sinks for photo-assimilates have PD with an overall larger SEL than the PD in mature source tissues. Leaf maturation and the corresponding overall decrease in the SEL of PD have been correlated with a change in PD structure from “simple” to “branched” [1]. Nevertheless, despite the restricted SEL of PD in mature leaves, cells in both mature and immature leaves interact with neighboring

cells and can have PD in various states of aperture (closed, open, dilated), thus indicating that the PD aperture of cells is individually regulated and able to respond to specific signals [2].

A hallmark feature of viral MPs is their ability to manipulate the mechanism that determines the SEL and increase the aperture of PD even in mature leaves. This ability of MPs to “gate” PD was first discovered for the MP of *Tobacco mosaic virus* (TMV). Microinjection of fluorescent, membrane-impermeable size-specific dextran probes into the cytoplasm revealed that transgenic tobacco plants constitutively expressing the MP allowed the cell-to-cell diffusion of probes with an approximate size of 10 kDa whereas diffusion was restricted to a molecular size of 0.8 kDa in control plants [3]. The protein was then shown to spread itself between cells upon injection [4] or upon transient expression from a plasmid (introduced into tissue by microprojectile bombardment [2] or agroinfiltration [5]). Experiments using microprojectile bombardment have shown that only 2 % of the cells in mature leaves allowed the cell-to-cell diffusion of 2 × GFP (two fused copies of green fluorescent protein, 54 kDa) whereas 52 % of the cells allowed the trafficking of GFP fused to MP (MP:GFP; 58 kDa) [2]. The ability of MP to alter PD aperture is usually correlated with the accumulation of the protein at PD. Several studies indicated that MP accumulates preferentially to the complex, branched PD in mature tissues [6–9]. However, more recent studies have shown that MP also accumulates in simple PD of immature cells [2, 10]. Moreover, the presence of accumulated MP in PD does not necessarily indicate that the PD are gated. Microinjection of cytoplasmic probes into cells within different radial zones of spreading TMV infection sites has demonstrated that the gating of PD by MP is restricted to cells at the infection front although the MP resides in PD throughout the infection site [11]. Accumulation of MP in PD and gating may even represent independent functions of MP, since TMV was shown to spread through PD without MP being trapped in PD [10] and certain transiently expressed mutants of MP moved between cells in the absence of any accumulation in the channel [5]. Plants that express the MP and are able to complement the movement function of movement-deficient TMV mutants do not show obvious growth defects, suggesting the existence of mechanisms that tightly control the ability of MP to modify PD aperture and thus prevent the continuous trafficking of signaling macromolecules between cells. The nature of these mechanisms remains to be elucidated. However, the MP has several amino acids that are phosphorylated *in vivo* [12–16] and that may play a role in regulating MP functions. The C-terminus of MP is dispensable for function in virus movement but carries phosphorylation sites that if phosphorylated downregulate the ability of MP to move from cell to cell and to gate PD in a host-dependent manner [17, 18]. Consistent with this type of posttranslational control, PD are associated with several kinases [19–23]

and a specific kinase, plasmodesmal associated kinase (PAPK), was shown to specifically phosphorylate the C-terminal phosphorylation sites of MP in vitro and also to be active on a subset of other MPs and non-cell-autonomous plant transcription factors [22]. Another hallmark of MP function is the ability of the protein to bind single-stranded nucleic acids in a sequence-independent manner in vitro [24]. Since TMV does not require its coat protein (CP) for intercellular movement [25], the MP is believed to form an MP:RNA complex with viral RNA (vRNA) and to support viral movement in the form of a non-encapsidated viral ribonucleoprotein complex (vRNP). This non-virion mode of movement by TMV has strong potential for providing insights into the cellular mechanisms by which cells support the intercellular trafficking of protein and RNA molecules.

Although TMV and its MP continue to play a major role in pioneering work addressing virus movement, many more viruses and their MPs have also been studied in the meantime. These studies revealed that viruses may encode more than one protein required for movement and that viral MPs may use different mechanisms for targeting PD and for facilitating virus movement through the channel. Thus, dependent on the virus species, intercellular virus movement occurs in virion or non-virion form and often depends on viral coat protein (CP) in addition to MP. The following paragraphs describe different MP-mediated mechanisms by which viruses target and move through PD. Since the movement of different viruses has been recently reviewed [26, 27], only selected virus models are described here.

---

## 2 Virion Movement of Tubule-Forming Viruses

Viruses that move from cell to cell in the form of encapsidated virions encounter the problem that the size of the virion particles (>10 nm) exceeds the cytoplasmic channel diameter in PD (the cytoplasmic sleeve is at most 10 nm in diameter). As a result, the viruses must have adopted drastic strategies to allow the particles to pass through the pore. Several viruses known to move between cells in the form of assembled virions encode MPs able to assemble a large tubular transport structure inside PD [28–30] (Fig. 1). The desmotubule is absent from such modified PD and the overall diameter of the PD can be dilated [31]. The molecular mechanism of tubule-guided transport of viral particles through the pore is not known. However, some MPs of tubule-forming viruses interact with the CP of the respective virus, usually at the C-terminus of the MP. The C-terminus of the MP of *Compea mosaic virus* (CPMV) is located on the inside of the tubule [30], thus in close proximity to the virus particle passing through the tubule. Consistent with a requirement of MP:CP interactions between the inner tubule wall

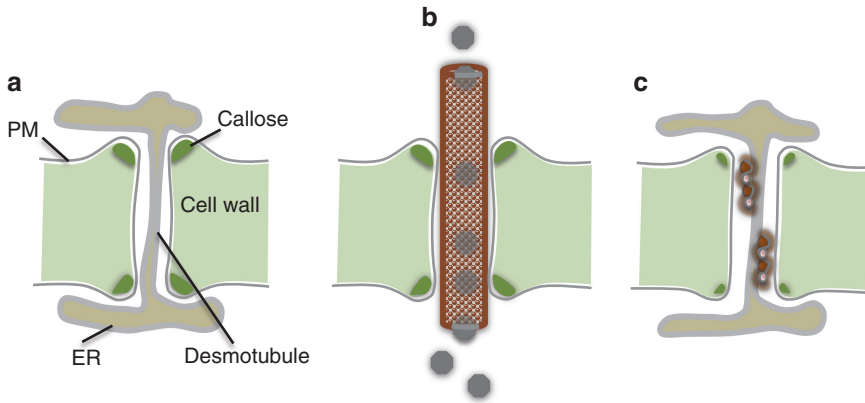


**Fig. 1** PD structure and modification by viruses. **(a)** General structure of primary PD. The PD pore maintains plasma membrane (PM) and endoplasmic reticulum (ER) continuity between cells. The ER traverses the pore as a thin tube known as the desmotubule. Callose deposits in the cell wall around the PD neck regions play an important role in controlling macromolecular transport through the channel. **(b)** Modification of PD by tubule-forming viruses. The tubule is assembled from viral MP and permits the movement of whole virion particles between cells. Since the tubule replaces the desmotubule, this type of movement disrupts ER continuity between cells. **(c)** Modification of PD by viruses that move from cell to cell in a non-encapsidated form. The MPs of these viruses cause an increase in PD SEL. An increased SEL is often linked to the degradation of PD-associated callose but may also involve a role of PD-associated actin. The viral ribonucleoprotein complexes traverse the PD channel likely in association with the fluid ER/desmotubule membrane

and CPMV particles for transport, only “empty” tubules were observed, when the C-terminus of the MP was deleted [32]. Specific interactions between tubules and virions mediated by the C-terminus of MP have also been observed for the *Grapevine fan-leaf nepovirus* (GFLV) [33]. The interaction between the tubule-forming MPs and the CPs of the respective tubule-forming viruses represents an important determinant for movement specificity. For example, the MP of CPMV does not interact with particles of other tested virus species [34] and the MP of the GFLV-related *Arabidopsis mosaic virus* failed to support GFLV movement unless the nine C-terminal amino acids of the MP were replaced by the nine C-terminal amino acids of the GFLV MP [33]. The interactions of tubule-forming MPs with the CP of the respective virus may suggest that virus transport may occur through polar assembly/disassembly of MP tubules that may propel MP-bound viral particles in a mechanism analogous to microtubule treadmilling [26]. Such a mechanism would depend on continuous delivery of MP to the base of the tubule within the infected cell.

As shown for GFLV and *Cauliflower mosaic virus* (CaMV), efficient tubule assembly and virus infection depend on interaction of the tubule-forming MP with PD-localized proteins (PDL), a multigene protein family that localizes to PD via the ER-Golgi

secretory pathway [35] (Fig. 2a). The MPs interact with PDLP at PD and not earlier within the secretory pathway, since the treatment with the secretory pathway inhibitor Brefeldin A (BFA) resulted in the accumulation of the MPs in the cytosol [36–38] and not, as would be expected, in BFA bodies, as seen for PDLP [35, 39]. The secretory pathway consists of interacting and highly dynamic organelles that move intracellularly with support of the actin cytoskeleton ([40] and citations herein). Thus, consistent with the role of the secretory pathway in the targeting of PDLP to PD, intracellular transport of PDLP as well as of Golgi bodies is strongly affected by the treatment with Latrunculin B (LatB: inhibitor of actin polymerization) and 2,3-butanedione monoxime (BDM, myosin ATPase inhibitor), both of which inhibit the actomyosin system in Golgi trafficking along the ER required for secretory cargo uptake [41, 42]. In agreement with these findings the PD targeting of PDLP as well as of GFLV MP, tubule formation, and virus movement depend on the activity of specific myosin XI classes (particularly myosin XI-2 and XI-K) [43] that are known to play important roles in cell dynamics, including F-actin organization, ER motility, and organelle trafficking [44–48]. The inhibition of myosin XI-K did not alter the subcellular distribution of cellular markers of the plasma membrane (PM), of lipid raft subdomains within the PM and PD, of the PD neck, or the vacuolar membrane, thus indicating that the XI-K-dependent PD targeting by PDLP follows a specific route [43].

Given these insights into the PD targeting of PDLP it now remains to determine how the MP and the viral particles of GFLV (and of other PDLP-dependent viruses) are targeted to PD. Previous studies indicated that the application of inhibitors that interfere with microtubule polymerization causes GFLV tubules to form at ectopic cortical sites rather than at PD [37]. This may be consistent with the recent proposal that cortical, ER-intersecting microtubules form specific cortical ER-associated landmarks for the proper positioning of organelles and membrane transport pathways in the cell cortex [49, 50]. Therefore, it is conceivable that the MP interacts with the ER and/or microtubules and that the lack of microtubules causes the disappearance of important positional information required for PD targeting. Since GFLV and CPMV replicate in perinuclear aggregates of recruited ER membranes [51, 52], the route by which the MP reaches PD may be via trafficking along the ER membrane, thus similar to the route taken by several other RNA viruses, like TMV (see below). The CP of GFLV has been localized to viroplasms and to the tips of MP tubules in the cell periphery [51]. However, how the CP or the assembled virions are targeted from viroplasms to PD remains to be studied.

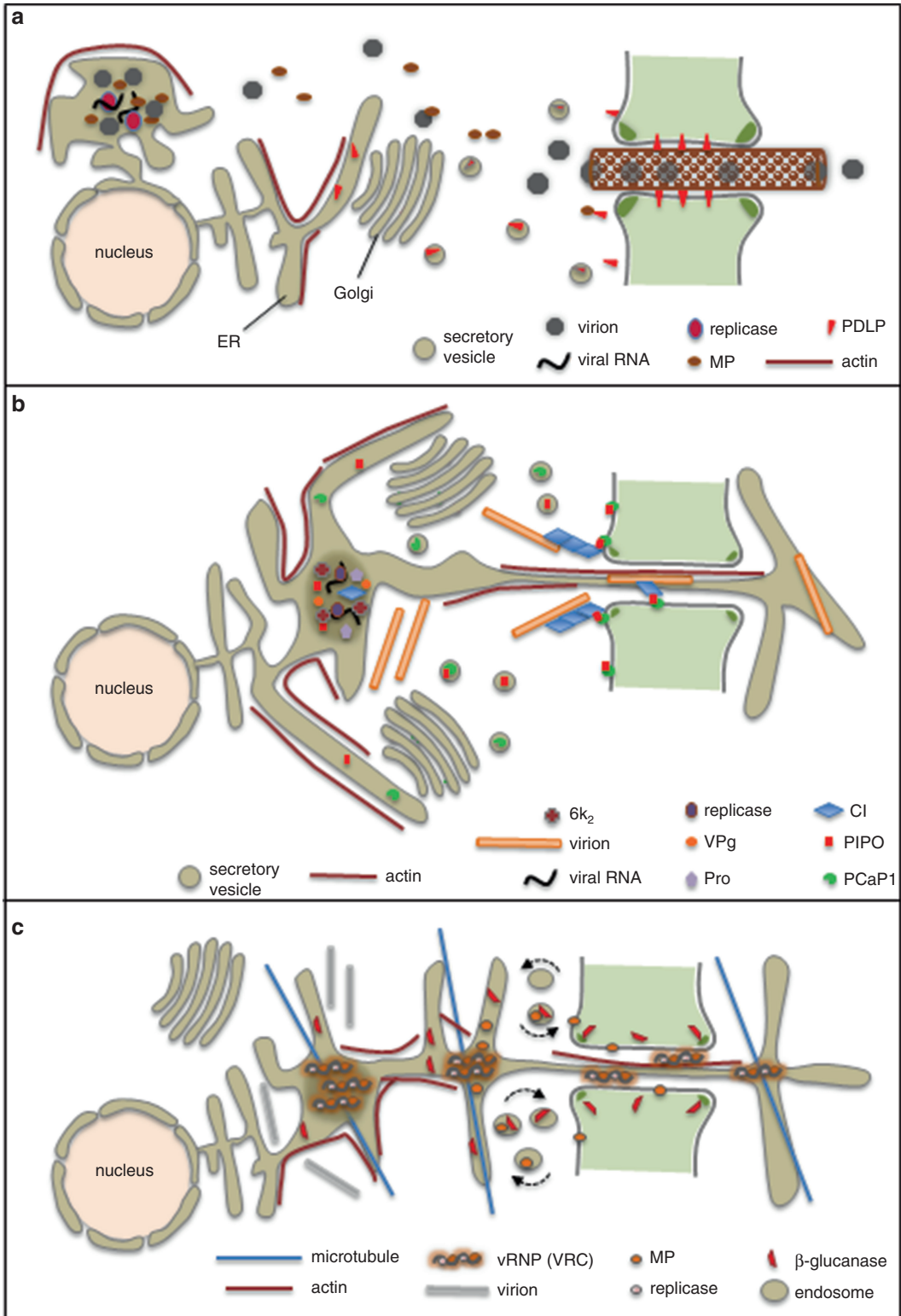


**Fig. 2** Cellular mechanisms that target viruses to PD. **(a)** PD targeting by tubule-forming viruses, e.g., GFLV. This virus replicates in aggregates of recruited ER membrane near the nucleus and requires the secretory pathway

### 3 Tubule-Independent Virion Movement

In contrast to the tubule-forming viruses, most plant viruses move through PD without inducing major structural changes in channel architecture. This mode of virus movement must be associated with infectious particles and movement mechanisms that are adapted to PD structure and function and likely relies on existing cellular mechanisms for the transport of macromolecules. As a consequence of such adaptation the majority of the viruses not relying on a tubule-forming MP evolved mechanisms to move from cell to cell in a non-encapsidated form. These are described further below (*see* Subheading 4). Here, I first mention examples of viruses proposed to move through PD in the form of encapsidated virions despite that they have not been reported to form MP tubules (*see* Subheadings 3.1 and 3.2).

#### 3.1 Movement of Closteroviruses

Closteroviruses represent a first example for viruses apparently moving from cell to cell as virions through PD without tubule formation. These viruses have particularly large RNA genomes and form very long and flexible virions. Their movement involves four structural proteins and one ER-localized MP, which is required for virus movement but is not an integral virion component [53]. Three of the four structural components form a narrow tail that functions in virion movement [54]. One of these components, the Hsp70 homolog (HSP70h), localizes to PD in a manner dependent on myosin VIII and thus might be involved in targeting the virion to PD or in transporting the virion through the pore [55]. It has been proposed that the latter may be facilitated by the ATPase function of Hsp70h, which may generate mechanical force required for translocation [56].

**Fig. 2** (continued) as well as the actin cytoskeleton and associated myosin motors for intercellular movement. The mechanism that targets the MP and virions to PD is not known. However, efficient tubule formation and virus movement depend on the interaction of MP with PD-localized PDLP, which requires the secretory pathway to reach PD. **(b)** PD targeting of potyviruses, e.g., TuMV. Movement is thought to occur in the form of virions and involves the virus-encoded proteins CI and P3N-PIPO, as well as host-encoded PCaP1. Virions produced in membrane-associated replication complexes associate with CI, which targets PD through interaction with P3N-PIPO and the PM-associated protein PCaP1. The CI protein accumulates at PD where it forms characteristic inclusions that may direct the virions into the PD pore. Given that P3N-PIPO moves between cells, the PCaP1-bound P3N-PIPO may facilitate the movement of the virion through the PD into the neighboring cell. **(c)** PD targeting of non-encapsidated virus, e.g., TMV. This virus replicates in association with the ER and uses the ER-actin network for PD targeting and the transport of replication complexes (VRCs) into the neighboring cell. The MP interacts with microtubules to assist in the assembly and controlled release of VRCs from cortical microtubule-associated ER sites (c-MERs). VRCs that remain anchored at these sites continue replication and form viral factories that produce virions. The MP interacts with, or induces the recruitment of,  $\beta$ -glucanase to facilitate intercellular movement of the VRC by degradation of PD-associated callose. Both proteins may reach the PD neck region with support of an endosomal cycling pathway

### 3.2 Movement of Potyviruses

Another virus family potentially moving through PD in the form of virions without tubule formation may be represented by potyviruses, the largest group of plant viruses (Fig. 2b). Evidence for movement in the form of encapsidated virions comes from mutations in the conserved core region of the *Tobacco etch virus* (TEV) CP that abolished both virion assembly and cell-to-cell movement [57, 58]. Virus movement is facilitated by the cylindrical inclusion (CI) protein, which forms cone-shaped cylindrical structures at PD. The CI protein of *Potato virus A* (PVA) binds and copurifies with virions [59] and the *Turnip mosaic virus* (TuMV) CP, which is required for TuMV movement, co-localizes to PD-associated CI cones [60]. The localization of the TuMV CI protein to PD depends on a more recently identified potyviral protein termed P3N-PIPO, which targets PD via the ER-Golgi secretory pathway [60] and interacts with host factors that facilitate its own movement [61]. P3N-PIPO may function as the core MP of the virus by facilitating the transport of the CI with bound virus particles from ER-associated viral replication complexes (VRCs) to PD. The PIPO domain of P3N-PIPO interacts with a plasma membrane-associated cation-binding protein, PCaP1. Virus accumulation, movement, and disease symptoms were reduced in an Arabidopsis PCaP1 knockout and it has been suggested that this protein may provide a membrane-binding function that may be required for potyviral movement through PD [61]. A recent study using specific inhibitors, dominant negative mutants, and virus-induced gene silencing to target different host cell transport systems led to the conclusion that TuMV movement depends on intact pre- and post-Golgi transport as well as on myosin XI-2 and XI-K but is independent of endosomes [62]. However, it may still be unclear whether all potyviruses indeed move between cells in the form of encapsidated virions. Although potyviruses have a flexuous filamentous virion morphology, the longitudinal and lateral dimensions (680–900 nm long and 11–15 nm wide) of the particles may be incompatible with the native structure of PD. Moreover, the CI protein of *Plum pox virus* (PPV) is an RNA helicase [63] and microinjection studies with proteins encoded by *Lettuce mosaic potyvirus* (LMV) and *Bean common mosaic necrotic potyvirus* (BCMNV) indicated that the CP and HC-Pro (helper component-protease) of these potyviruses are able to modify the SEL of PD, move from cell to cell, and facilitate the movement of viral RNA [64], which are hallmark features of the widespread non-virion mode of virus movement exemplified by TMV. Indeed, recent in vivo studies provide evidence supporting the conclusion that TuMV infection spreads between cells in the form of membrane-bound VRCs [65].

## 4 Virion-Independent Virus Movement (as vRNP)

Most non-tubule-forming viruses encode MPs that form vRNPs with vRNA and facilitate the intercellular spread of the vRNPs by interacting with the cellular machinery that transports macromolecules and regulates the SEL of PD. The prototype virus exemplifying this type of movement is TMV [3, 24, 66]. This type of movement can be independent of CP, as in the case of TMV [25], or may require CP as, for example, in the case of the bromoviruses *Brome mosaic virus* (BMV) and *Cucumber mosaic virus* (CMV) [67–69] or the potexviruses [70]. However, although the CP of TMV is dispensable for local movement of the virus, it is required for long-distance movement through the phloem [25]. As for many other viruses, this requirement of CP for long-distance movement may not necessarily reflect a requirement of virion formation but may indicate the requirement of additional stabilization of the vRNP for either entry or movement through the vasculature [71].

### 4.1 Movement of TMV

TMV may still be the best studied virus with regard to movement (Fig. 2c). Cell biological observations and mutational studies suggest that the vRNPs of TMV are associated with viral replication complexes (VRCs) that in addition to vRNA and MP also contain the viral 126 and 186 kDa replicase proteins and produce CP [72–75]. According to microscopical *in vivo* observations the VRCs assemble at sites in the cortical ER-actin network that coincide with cortical microtubules [50, 76–79]. These microtubule-associated ER sites (c-MERs) may represent important “cortical landmarks” at which various endomembrane and motor-driven organelle trafficking pathways are proposed to convene to catalyze the encounter and molecular exchange between organelles and macromolecular trafficking and signaling pathways [49, 50, 78]. The MP exhibits strong binding affinity to tubulin and microtubules [72, 80, 81], and therefore may assist in the anchorage, formation, and maturation of the ER-associated VRCs by an aggresomal mechanism that recruits host factors and membranes with support of the cytoskeleton and associated motor proteins [50, 78]. In addition to binding to microtubules, the MP also interacts with important regulators of the microtubule cytoskeleton, such as  $\gamma$ -tubulin [77] and microtubule END-BINDING 1 (EB1) [82], which may explain the observation of microtubule nucleation events at VRCs during early maturation stages and the occurrence of multiple microtubules joined together in the center of larger, more mature VRCs at later stages [50, 78]. Expression of MP in mammalian cells causes the displacement microtubule nucleation activity from the centrosome to ectopic sites in the cytoplasm [83], thus suggesting that the MP may subvert the plant

microtubule nucleation machinery to support VRC formation and growth. The MP may interact with a common mechanism recently reported for microtubule reorientation in plants [84]. This mechanism consists in the recruitment of  $\gamma$ -tubulin and the nucleation of new microtubules at existing microtubules and thus to the formation of microtubule crossovers, which act as templates for the production of additional microtubules with support of the microtubule-severing protein katanin. It seems possible that the MP interacts with  $\gamma$ -tubulin to recruit this mechanism to the site of the VRC and thus to support VRC maturation and growth with the help of nucleated microtubules.

In time-lapse movies monitoring the behavior of fluorescent protein-tagged MP, the MP-associated VRCs/MP particles are first visualized as very small cortical particles that either remain attached to c-MERs or get detached to move in a directional stop-and-go fashion along the ER-actin network between c-MERs, in a manner depending on a dynamic actin and microtubule cytoskeleton [50, 77]. Consistent with their VRC nature, the ability of MP to interact with microtubules and the formation of the mobile MP particles is correlated with MP function in virus movement [76, 77, 85]. Moreover, in agreement with the association of the spread of infection with VRC movement along the ER-actin network between c-MERs, the efficiency by which infection spreads between cells is independent of the secretory pathway [86] but depends on dynamic microtubules [87], on the integrity of actin filaments, and on the expression or activity of specific myosin motors [74, 88–90].

VRCs that do not move but remain anchored at c-MERs in the infected cell may grow into virus factories [50, 78]. Thus, as infection spreads forward into yet uninfected cells, the cells behind the infection front develop factories (or “X-bodies”) that accumulate high levels of replicase, coat protein, and viral RNA in addition to MP [72, 73, 91]. At this stage, highly expressed MP can show profound accumulation of MP in viral factories and along microtubules to which the virus factories are aligned [72, 81]. Subsequently, thus soon after accumulation along microtubules, the MP is degraded except for MP localized to PD. The process of degradation may be triggered by ER stress caused by the accumulation of unfolded or aggregated MP, which induces the AAA ATPase CDC48. This protein extracts the MP from the ER, and thus allows the ER to recover, and the delivery of MP to the cytoplasm where it first decorates the microtubule cytoskeleton and is then degraded by the 26S proteasome [92].

It is curious why TMV infection is associated with such high overaccumulating levels of MP. Indeed, only a small fraction (2 %) of the amount of MP produced during TMV infection is required for the spread of infection [93]. Consistently, virus variants that produce lower amounts of MP spread normally and MP

localization is restricted to small cortical MP particles/VRCs and to PD in these cases [72, 94]. It appears possible that the accumulating levels of MP during late stages of infection play a regulatory role. Accumulation of MP along microtubules, as seen during late stages of TMV infection, was shown to interfere with kinesin-mediated motility [80], with the movement of MP particles [76], and with virus movement [95, 96]. Thus, by producing high levels of MP the virus may be able to prevent the further PD targeting and spread of infection between cells that are already behind the infection front. Moreover, in agreement with the inhibition of MP targeting to PD during late infection stages, the ability of MP to alter the SEL is limited to cells at the infection front [11]. The inhibition of virus movement and MP trafficking between cells behind the infection front may facilitate a phase change from mechanisms that support virus movement towards mechanisms that rather support VRC growth and virion progeny production.

Further studies might reveal how the various functions of MP are regulated. Apart from the already mentioned C-terminal phosphorylation, the MP is regulated by ubiquitinylation [80, 97]. Moreover, the MP may assume different folds. The MP is a hydrophobic protein with two hydrophobic regions involved in ER association [98]. A structural model predicted that the hydrophobic regions act as transmembrane domains [99, 100]. In this model the MP domains required for RNA binding [101] and interaction with microtubules [85], chaperones [102], and cell wall-associated proteins [103] are buried in the membrane suggesting that either this model is not correct or additional protein folds must exist [104]. Assuming that the model is correct and supported by the observation that MP oligomerizes *in vivo* [105], we proposed that MP may form higher order complexes with monomers carrying different folds and thus combine different MP functions within the complex [50, 78]. However, according to a recent report the protein does not form transmembrane helices but rather localizes to the cytoplasmic face of the membrane [104]. In contrast to the transmembrane insertion model, the latter model allows cytoplasmic accessibility of the MP domains required for function.

## **4.2 Movement of “Triple-Gene-Block” Viruses**

Membrane-associated replication and transport of VRCs are documented for a diverse range of viruses [106–108] and, unlike for TMV, often involve more than one MP. The rod-shaped hordei-like (hordei-, pomo-, peclu-, and beny-) viruses and potexviruses encode three MPs in overlapping ORFs, the triple gene block (TGB). The mode of action of these proteins has been intensely studied [70, 109–111] and led to the proposal of somewhat varied movement strategies of the TGB-encoding viruses [110]. The general model for movement of these viruses involves the binding of viral RNA by TGB1 and the targeting of the TGB1:RNA complex to PD with the help of TGB2 and TGB3, transmembrane

proteins that are localized to the ER. Unlike for hordeiviruses, the movement of potexviruses and, presumably, of other viruses with potex-like TGB proteins depends on the CP in addition to the TGB proteins. However, whether potexviruses move in the form of virions or rather in a non-encapsidated form is unclear. Electron micrographs showing fibrillar material that appears to resemble PVX virions located within PD of infected leaves and the reaction of this material with antibody able to bind to PVX virus particles but not to isolated CP subunits led to the proposal that PVX moves between cells in the form of encapsidated virions [112]. In contrast, the results of microinjection experiments and the mutational analysis of CP indicating that virion formation is not sufficient for virus movement rather favored the proposal that potexvirus transport occurs in the form of a TGB1-CP-RNA complex [113]. The latter model was supported by the observation that potexvirus CP mutants capable of virion formation but not capable to move between cells could be functionally complemented by the CP of unrelated viruses such as the potyviruses *Potato virus A* or *Potato virus Y* or the sobemovirus *Cocksfoot mottle virus*, and even by the MP of TMV [114, 115]. The currently prevailing model proposes that PVX movement occurs in the form of a partially encapsidated viral RNA with a 5' associated TGB1 [110]. The requirement for CP in TGB virus movement may depend on the size and domain structure of TGB1. Whereas potexviruses have small TGB1 proteins and require CP for movement the viruses of the hordei-like group have TGB1 proteins with extended N-terminal domains and do not require CP for movement. The extended N-terminal domain may thus act as a chaperone able to sufficiently protect the viral RNA during movement and thus neutralize a need of CP for such function [116]. Recent studies on movement of the potexvirus *Bamboo mosaic virus* (BaMV) confirmed the role of the TGB2/TGB3 complex in the targeting of TGB1 to PD. Interestingly, the same complex was shown to be stably associated with virions, thus suggesting that BaMV targets PD in the form of virions [117]. Future research may show whether this virus moves through PD in virion form.

Many experiments have provided important insights into the host components involved in the targeting of TGB-containing viruses to PD. Several observations indicated that the TGB2 and TGB3 proteins associate with the ER and with ER-derived, TGB2-induced motile granules that are visualized along actin filaments, whereas the TGB1 protein localizes to the cytoplasm and requires TGB2 and TGB3 for PD targeting [117–135]. The TGB-RNA complexes (TGB-virion complexes in the case of BaMV, [117]) thus reach the cell wall by trafficking along the ER-actin network and once at PD facilitate transport of viral RNA (or virions) through the pore, presumably by increasing the PD SEL by mechanisms that involve TGB1 [136–138] and TGB2 [118, 139].

Studies with the pomovirus *Potato mop-top virus* (PMTV) indicated that the TGB2 and TGB3 proteins remain in the infected cell and are recycled by endosomal membrane trafficking for further rounds of transport [118].

The TGB complex that targets PD may be associated with viral replication or may itself represent a VRC. Indeed, the virion-associated TGB3-containing ER membrane complex of BaMV also contains viral replicase [117] and interactions between the CP and the helicase domain of the replicase are essential for virus movement [140]. PVX replicates in association with the ER [141] and the TGB2-induced motile ER-derived and TGB3-containing granules are associated with replicase, as well as with ribosomes and virions [119, 124], thus suggesting that these granules contain replication complexes (VRCs). At later stages of infection, the TGB proteins also colocalize with non-encapsidated viral RNA to replication factories (X-bodies) that are formed by TGB1-mediated ER membrane recruitment and produce virions [142, 143]. The vicinity of the TGB proteins and CP to viral RNA or replicase in the motile granules and factories suggests that the proteins are locally translated near VRCs and remain associated with them through their network interactions in motile granules and X-bodies during early and later stages of infection. Taken together, these observations suggest the model that during the course of infection TGB2/3-associated VRCs form along the ER. Initially motile along the dynamic ER-actin network, they soon encounter PD, where the TGB2 and TGB3 proteins interact with TGB1 to insert CP into the channel, probably in the form of a movement complex with viral RNA. This insertion process may be supported by continuous replication within the PD-associated VRC. At later stages of infection, the PD-associated VRCs and also the VRCs that remained along the ER network grow into ER-associated granules that finally accumulate in a perinuclear TGB1 aggregate (X-body) that acts as a viral factory and produces viral progeny [144].

The process by which PVX targets PD may be facilitated by the affinity of the potexvirus TGB3 protein to highly curved ER membrane domains enriched with reticulon-like proteins [145, 146]. It has been suggested that this affinity may target TGB3-containing complexes to the desmotubule, which may require reticulons for structural stabilization [147]. The PD targeting of PVX or its anchorage near the channel may also involve an interaction with specific PM domains since PVX movement was inhibited by expression of Remorin, a protein proposed to localize PD via plasma membrane (PM) rafts. Since Remorin was shown to interact with TGB1 it may inhibit virus movement by titrating TGB1 away from PD [148].

PD targeting and movement of TGB viruses may also involve a function of microtubules. The CP of PVX was shown to interact with microtubules and to interfere with MAP2 binding in vitro

[149]. Moreover, PVX movement was inhibited by overexpression of the microtubule-binding protein MPB2C [150]. The TGB1 protein of PMTV was shown to interact with microtubules *in vivo* and to form cortical particles along them [151, 152]. Deletion mutation analysis demonstrated a correlation between the microtubule association of TGB1 and its accumulation in PD. Microtubule disruption by colchicine treatment abolished the accumulation of TGB1 at PD as well as the formation of TGB1 particles, leading to accumulation of the protein along the ER network. These findings suggest a role of microtubules in the localized interaction of TGB1 with the membrane proteins TGB2 and TGB3. Since TGB1 interacts with viral RNA, these microtubule-associated processes may reflect the localized formation and transport of VRCs. Further studies may reveal whether or not the formation and transport of TGB virus VRCs along the ER occur in analogy to the formation and transport pathway proposed for TMV VRCs, thus involving c-MERs [50] (Fig. 2c).

---

## **5 The Use of Biochemical Inhibitors May Be of Limited Value in the Analysis of the Cellular Components Involved in Virus Movement**

Although there is accumulating evidence for a role of microtubules in macromolecular and viral trafficking and particularly in the formation and guided intracellular trafficking of VRCs and other macromolecules to PD [50, 78, 153], the spread of viruses is usually not affected by the presence of microtubule inhibitors [74, 80, 154]. This interesting feature has led to disagreements in the earlier literature but may be explained simply by inhibitors not being fully effective, either because they do not reach all cellular targets or because microtubules are stabilized. The treatment of plant cells with microtubule inhibitors can indeed fail to disrupt parts of the microtubule cytoskeleton as was demonstrated, for example, by antibody labeling and by showing that the MP of TMV still labels microtubules during infection in inhibitor-treated tissues [155]. In the case of TMV, resistance against microtubule inhibitors may be partly explained also by the ability of MP to manipulate the microtubule nucleation machinery and to confer superstability to microtubules [80, 83, 85]. Moreover, microtubule-associated cortical landmarks (c-MERs) are stable structures that require microtubules for their formation but not for their functional maintenance, at least over certain periods of time [49]. Thus, upon inhibition of microtubules, TMV may still be able to interact with c-MERs and the connecting ER-actin network for spread.

The lack of an effect on TMV spread is not limited to inhibitors of microtubules but may also be observed for inhibitors of the actin cytoskeleton. Although the virus moves along the ER-actin network, infection continued to spread during 24 h of treatment

with actin inhibitor [90]. While the latter finding could argue against a role of actin filaments in TMV movement, the same study showed that TMV movement was dominantly inhibited upon expression of an actin-binding protein that also inhibited the motor-dependent trafficking of Golgi complexes along the ER, thus clearly indicating a role of myosin-mediated trafficking along the ER membrane in TMV movement [90]. Moreover, inhibition of TMV movement by actin inhibitors was observed upon prolonged treatments with actin inhibitor and in plants silenced for actin or myosin motors [74, 89, 156]. Actin inhibition was also shown not to affect the accumulation of MP to PD [157], although FRAP experiments clearly indicated that the efficient targeting of PD by MP requires an intact ER-actin network [158]. The careful application of biochemical inhibitors may not be able to inhibit virus movement because inhibition is rarely complete and virus spread depends on the successful cell-to-cell movement of only few virus genomes [159]. Thus, even if the inhibitor is effective to some degree and induces a strong bottleneck for virus movement, infection may continue to spread normally. Similarly, MP can accumulate in PD over time although actin inhibitors interfere with the efficient functioning of the PD targeting pathway to some extent. Given these considerations, it is important that experiments applying biochemical inhibitors to the analysis of virus movement are carefully designed and cautiously interpreted.

---

## 6 Viral Mechanisms to Control PD Aperture

Upon arrival at PD, the VRCs could, in principle, continue to diffuse along the ER membrane to pass along the desmotubule and into the adjacent cell. ER membrane-intrinsic and luminal probes readily diffuse between cells [160, 161], thus supporting the fluidity of the desmotubular membrane [162, 163] and the ability of the desmotubule to transport macromolecules. However, due to the large size of the viral complex, additional mechanisms that expand the PD aperture are necessary.

### 6.1 Interference with PD-Associated Actin

Several studies indicate that the aperture of PD is directly or indirectly controlled by actin filaments [164, 165] and structural models depict the PD channel with actin filaments wrapped around the desmotubule [166, 167]. Consistent with a role of actin in controlling PD aperture, the MPs of TMV and of *Cucumber mosaic virus* were shown to exhibit actin-severing activity in vitro. Moreover, the stabilization of actin filaments by treatment with phalloidin prevented the ability of MP to increase PD SEL in vivo [164]. Nevertheless, although these findings suggest that MPs manipulate actin to control the PD aperture, it remains to be

shown whether the actin-severing activity of these MPs occurs at PD or elsewhere in the cell. It is also yet unclear whether these MPs indeed interact with actin *in vivo*.

## 6.2 Interference with Callose Deposition

Another important mechanism that restricts PD aperture and that is indeed likely to be modified by the infecting virus is the deposition of callose in the cell walls surrounding the PD neck regions (Fig. 1). Callose is a  $\beta$ -glucan polysaccharide that is deposited at the PD neck region during different stresses, including wounding and pathogen attack [168]. The deposition of callose at PD has been linked to the salicylic acid (SA) defense signaling pathway that induces callose synthase activity [169] and leads to callose deposition at PD by a pathway involving EDS1, NPR1, and the PD-associated protein PDL5 [170, 171]. Experimental evidence indicates that the MP of TMV allows VRC movement through the PD by preventing the deposition of callose induced by infection. To account for this effect it has been proposed that the MP may recruit  $\beta$ -1,3 glucanases to degrade stress-induced callose at PD [160, 172] (Fig. 2c). This hypothesis is based on previous reports indicating a positive correlation between  $\beta$ -1,3-glucanase expression and viral spread [173–175]. A glucanase isoform that may be targeted to PD during TMV infection is AtBG<sub>pap</sub>. Similar to several recently isolated PD proteins, this protein is predicted to be a glycosylphosphatidylinositol (GPI)-anchored protein. This protein was localized to the ER, the cell periphery, and PD, and mutation of the protein-encoding gene by a T-DNA insertion led to a reduction in GFP cell-to-cell movement and stress-induced callose deposition at PD [176]. Moreover, the cell-to-cell movement of GFP-tagged *Turnip vein clearing virus* (TVCV), a TMV-related tobamovirus, was reduced in *Arabidopsis athg<sub>pap</sub>* mutants. The same mutants showed highly increased PD-associated callose levels, thus confirming the role of AtBG<sub>pap</sub>-mediated callose degradation during virus movement [177]. While a direct role of this or another glucanase in the degradation of callose deposits during virus movement awaits to be demonstrated, the ability of MP to inhibit callose deposition at PD was shown to involve an ankyrin-repeat-containing protein (ANK), which facilitates TMV spread and interacts with MP [178]. The regulation of callose deposition at PD during infection may also involve the viral replicase. Evidence comes from the analysis of MP-transgenic *Nicotiana benthamiana* plants in which MP facilitated the non-cell-autonomous diffusion of ER-localized, GFP-tagged probes in the presence but not in the absence of infection and/or replicase [160]. This finding supports virus movement in the form of a VRC and is also consistent with a role of the replicase-encoding region of TMV in virus movement [75].

A role of callose deposition in restricting virus movement was also established for PVX [175] and a two-hybrid screen led to the

isolation of TGB2-interacting proteins (TIP1, TIP2, TIP3) that interact with  $\beta$ -1,3, glucanase and may play a role in regulating PD SEL [179].

A number of observations indicate that the callose deposition at PD and the regulation of PD SEL are regulated by redox homeostasis [180–182] and calcium [183–185]. Thus, it is conceivable that MPs may alter the PD SEL and facilitate virus movement also through interaction with pathways that influence the redox and calcium states of the infected cell.

---

## 7 Requirement of Structural Unfolding for Movement Through PD

In addition to the modification of PD SEL, viral movement through PD may also require the structural modification of the transported complex. The observation that in vitro-assembled MP:RNA complexes have a thin and elongated appearance raised the proposal that the MP chaperones the vRNA through the dilated PD [101]. The hordevirus TGB1 proteins have three RNA-binding domains and the interaction of these domains may play a role in VRC remodeling during movement [116]. Consistent with a requirement for structural unfolding for movement, the cell-to-cell movement of the non-cell-autonomous protein (NCAP) KN1 (see below) was inhibited by chemical cross-linking [186]. Moreover several chaperone proteins have been associated with macromolecular trafficking through PD [102, 187–190].

---

## 8 Plant Viruses Use Existing Mechanisms for Macromolecular Transport

The MP of TMV was the first protein shown to alter the SEL of PD and to support its own spread between cells [3]. Later, it was demonstrated that this is a hallmark property of many viral MPs as well as of a special class of endogenous proteins commonly referred to as non-cell-autonomous proteins (NCAPs). Many NCAPs act as transcription factors playing important non-cell-autonomous roles in cell-type specification and differentiation [191–193]. NCAPs may also be involved in the cell-to-cell and long-distance transport of various RNA molecules, including mRNAs [193–197] and small RNAs [198–202]. It is likely that the ability of viruses to target and spread through PD evolved as an adaptation to essential mechanisms that also contribute to the transport of endogenous macromolecules. This hypothesis is supported by several observations. For example, expression of a dominant-negative form of the NON-CELL AUTONOMOUS PATHWAY PROTEIN 1 (NCAPP1) blocked the cell-to-cell trafficking of the MP of TMV as well as of the *Cucurbita maxima* PHLOEM PROTEIN 16 (CmPP16) [187]. Moreover, expression of the microtubule-associated protein

MPBP2C interfered with the cell-to-cell movement of TMV [96], PVX [150], as well as the *Zea mays* homeobox protein KNOTTED 1 (KN1) [203]. In addition, the intercellular trafficking of both KN1 and TMV was shown to be sensitive to mutations in CCT8, a chaperonin complex believed to act in the post-translocational refolding of transported proteins [188]. Also, the MP of TMV facilitated the spread of silencing signal [5] which may suggest that small RNAs and viral RNAs share a common pathway or mechanism for spread.

---

## 9 Virus Movement and Defense Responses

The efficiency of virus movement through PD is affected by plant defense responses that cause a reduction of the PD SEL, reduce viral replication, or lead to degradation of the viral proteins or genome. As already mentioned above, virus infection triggers the salicylic acid (SA) signaling pathway that involves the deterrence of pathogens through increasing callose deposition at PD and viruses may have evolved a recruitment of glucanase enzymes to degrade callose and thus to reverse this defense-induced constriction of PD.

The efficiency of virus infection is also determined by the interaction of viruses with posttranscriptional RNA silencing that targets viral and host RNAs for cleavage or translational repression. As a counter strategy against this important defense response, plant viruses have evolved proteins able to suppress RNA silencing by interfering with different components of the RNA silencing pathway [204, 205]. The silencing suppressor of TMV resides in the 126 kDa small replicase subunit and likely acts through sequestration of virus-derived small RNAs [206, 207]. The ability of the viral MP to facilitate the spread of silencing [5] suggests that TMV and potentially also other viruses may facilitate their movement not only by suppression but also by exploitation of the host RNA silencing machinery. It is conceivable that MP enhances host cell susceptibility for the incoming virus by facilitating the PD-mediated intercellular spreading of virus- and host-derived small RNAs that may act as RNA-based effectors to downregulate defense-related genes in cells at the virus front, whereas the silencing suppressor may act only after virus movement, i.e., in cells containing replication factories and producing virions [208]. Pathogen-encoded small RNA effectors that target host defense genes are well known for several mammalian viruses [209] and have been recently reported also for the plant pathogenic fungus *Botrytis cinerea* [210]. However, whether motile, small RNA-based effectors spreading through PD indeed play a role in facilitating the cell-to-cell propagation of virus infection remains to be investigated. Recent observations indicate that Arabidopsis plants are able to sense virus infection by pathogen-recognition receptors (PRR) and to mount pathogen-associated

molecular pattern (PAMP)-triggered immunity (PTI) through the PAMP co-receptor BAK1 (for BRASSINOSTEROID INSENSITIVE1 (BRI1)-ASSOCIATED RECEPTOR KINASE1) [211]. It will be interesting to see whether this response, or its potential signaling propagation between cells, involves PD.

---

## 10 Conclusions

Viruses transport their genomes between cells to spread infection and thus are convenient systems to study the cellular pathways by which macromolecules are targeted and transported through PD. As pathogens, viruses are also excellent systems to determine the manifold mechanisms by which cells defend themselves at PD against invaders. Although numerous viral systems suitable to address these questions are available, only few could be mentioned here. Plant viruses illuminate different pathways by which viruses and other macromolecules can be transported to and through PD. TMV exemplifies a mechanism that involves the viral manipulation of the PD SEL and depends on the ER-actin network that in coordination with specific microtubule system activities supports both the replication and the movement of the virus in a non-encapsidated form. Tubule-forming viruses are systems that depend on the secretory ER-Golgi-plasma membrane pathway for movement. The tubules formed by these viruses replace the desmotubule in PD and thus disrupt the ER connectivity between cells used by other viruses like TMV. Cytoplasmic plant viruses provide important insights into the structural and functional organization of the cortical cytoplasm. Studies with TMV suggest a role of specialized microtubule-associated ER sites (c-MERs) in the assembly of VRCs for either movement (early infection) or growth into viral factories (late infection). It will be interesting to see whether the same sites play a role also in the assembly of complexes of other viruses or in the intercellular movement of cellular proteins and RNAs [50]. Viruses also continue to provide important information with regard to the role of callose in the regulation of the PD SEL. However, since viruses are pathogens, many events occurring in the infected cells may be related to replication, defense, and degradation processes rather than to macromolecular movement through PD. Thus, it is important to dissect the *in vivo* observations with respect to their functional significance in movement. Future research can make use of an excellent panel of novel helpful *in vivo* techniques, such as superresolution microscopy [212]; fluorescent *in vivo* detection of RNA and RNA spread, e.g., [62, 77, 91, 213, 214]; *in vivo* analysis of complexes by FLIM-FRET and BiFC, e.g., [35, 61, 82, 105]; dominant-negative inhibition of cellular processes, e.g., [43, 62]; and novel dye

loading methods to measure PD conductivity, e.g., [171], to just name a few. In combination with genetic and novel next-generation sequencing-based approaches these will lead to a new era of understanding about the mechanisms of PD-mediated intercellular communication in plant development and disease.

---

## Acknowledgements

The author acknowledges support by the University of Strasbourg Institute of Advanced Study (USIAS), the Zürich-Basel Plant Science Center, and the Swiss National Science Foundation.

## References

- Oparka KJ, Roberts AG, Boevink P et al (1999) Simple, but not branched, plasmodesmata allow the nonspecific trafficking of proteins in developing tobacco leaves. *Cell* 97: 743–754
- Crawford KM, Zambryski PC (2001) Non-targeted and targeted protein movement through plasmodesmata in leaves in different developmental and physiological states. *Plant Physiol* 125:1802–1812
- Wolf S, Deom CM, Beachy RN et al (1989) Movement protein of *Tobacco mosaic virus* modifies plasmodesmatal size exclusion limit. *Science* 246:377–379
- Waigmann E, Lucas W, Citovsky V et al (1994) Direct functional assay for *Tobacco mosaic virus* cell-to-cell movement protein and identification of a domain involved in increasing plasmodesmal permeability. *Proc Natl Acad Sci U S A* 91:1433–1437
- Vogler H, Kwon MO, Dang V et al (2008) *Tobacco mosaic virus* movement protein enhances the spread of RNA silencing. *PLoS Pathog* 4:e1000038
- Ding B, Haudenschild JS, Hull RJ et al (1992) Secondary plasmodesmata are specific sites of localization of the *Tobacco mosaic virus* movement protein in transgenic tobacco plants. *Plant Cell* 4:915–928
- Epel B (1994) Plasmodesmata: composition, structure and trafficking. *Plant Mol Biol* 26:1343–1356
- Hofius D, Herbers K, Melzer M et al (2001) Evidence for expression level-dependent modulation of carbohydrate status and viral resistance by a *Potato leafroll virus* movement protein in transgenic tobacco plants. *Plant J* 28:529–543
- Roberts IM, Boevink P, Roberts AG et al (2001) Dynamic changes in the frequency and architecture of plasmodesmata during the sink-source transition in tobacco leaves. *Protoplasma* 218:31–44
- Kim I, Kobayashi K, Cho E et al (2005) Subdomains for transport via plasmodesmata corresponding to the apical-basal axis are established during Arabidopsis embryogenesis. *Proc Natl Acad Sci U S A* 102:11945–11950
- Oparka KJ, Prior DAM, Santa Cruz S et al (1997) Gating of epidermal plasmodesmata is restricted to the leading edge of expanding infection sites of *Tobacco mosaic virus*. *Plant J* 12:781–789
- Haley A, Hunter T, Kiberstis P et al (1995) Multiple serine phosphorylation sites on the 30 kDa TMV cell-to-cell movement protein synthesized in tobacco protoplasts. *Plant J* 8:715–724
- Tyulkina LG, Karger EM, Sheveleva AA et al (2010) Binding of monoclonal antibodies to the movement protein (MP) of *Tobacco mosaic virus*: influence of subcellular MP localization and phosphorylation. *J Gen Virol* 91: 1621–1628
- Kawakami S, Padgett HS, Hosokawa D et al (1999) Phosphorylation and/or presence of serine 37 in the movement protein of *Tomato mosaic tobamovirus* is essential for intracellular localization and stability in vivo. *J Virol* 73:6831–6840
- Watanabe Y, Meshi T, Okada Y (1992) *In vivo* phosphorylation of the 30-kDa protein of *Tobacco mosaic virus*. *FEBS Lett* 313: 181–184
- Citovsky V, McLean BG, Zupan JR et al (1993) Phosphorylation of *Tobacco mosaic*

- virus* cell-to-cell movement protein by a developmentally regulated plant cell wall-associated protein kinase. *Genes Dev* 7:904–910
17. Trutnyeva K, Bachmaier R, Waigmann E (2005) Mimicking carboxyterminal phosphorylation differentially effects subcellular distribution and cell-to-cell movement of *Tobacco mosaic virus* movement protein. *Virology* 332:563–577
  18. Waigmann E, Chen M-H, Bachmeier R et al (2000) Regulation of plasmodesmal transport by phosphorylation of *Tobacco mosaic virus* cell-to-cell movement protein. *EMBO J* 19: 4875–4884
  19. Fernandez-Calvino L, Faulkner C, Walshaw J et al (2011) Arabidopsis plasmodesmal proteome. *PLoS One* 6:e18880
  20. Salmon MS, Bayer EM (2012) Dissecting plasmodesmata molecular composition by mass spectrometry-based proteomics. *Front Plant Sci* 3:307
  21. Jo Y, Cho WK, Rim Y et al (2011) Plasmodesmal receptor-like kinases identified through analysis of rice cell wall extracted proteins. *Protoplasma* 248:191–203
  22. Lee JY, Taoka K, Yoo BC et al (2005) Plasmodesmal-associated protein kinase in tobacco and Arabidopsis recognizes a subset of non-cell-autonomous proteins. *Plant Cell* 17:2817–2831
  23. Yaholom A, Lando R, Katz A et al (1998) A calcium-dependent protein kinase is associated with maize mesocotyl plasmodesmata. *J Plant Physiol* 153:354–362
  24. Citovsky V, Knorr D, Schuster G et al (1990) The P30 movement protein of *Tobacco mosaic virus* is a single-strand nucleic acid binding protein. *Cell* 60:637–647
  25. Holt CA, Beachy RN (1991) In vivo complementation of infectious transcripts from mutant *Tobacco mosaic virus* cDNAs in transgenic plants. *Virology* 181:109–117
  26. Niehl A, Heinlein M (2011) Cellular pathways for viral transport through plasmodesmata. *Protoplasma* 248:75–99
  27. Schoelz JE, Harries PA, Nelson RS (2011) Intracellular transport of plant viruses: finding the door out of the cell. *Mol Plant* 4:813–831
  28. Kasteel DTJ, Perbal M-C, Boyer J-C et al (1996) The movement proteins of *Cowpea mosaic virus* and *Cauliflower mosaic virus* induce tubular structures in plant and insect cells. *J Gen Virol* 77:2857–2864
  29. van Lent JWM, Schmitt-Keichinger C (2006) Viral movement proteins induce tubule formation in plant and insect cells. In: Baluska F, Volkmann D, Barlow PW (eds) *Cell-cell channels*. Springer, New York, NY
  30. van Lent J, Storms M, van der Meer F et al (1991) Tubular structures involved in movement of *Cowpea mosaic virus* are also formed in infected cowpea protoplasts. *J Gen Virol* 72:2615–2623
  31. van der Wel NN, Goldbach R, van Lent J (1998) The movement protein and coat protein of *Alfalfa mosaic virus* accumulate in structurally modified plasmodesmata. *Virology* 244:322–329
  32. Lekkerkerker A, Wellink J, Yuan P et al (1996) Distinct functional domains in the *Cowpea mosaic virus* movement protein. *J Virol* 70: 5658–5661
  33. Belin C, Schmitt C, Gaire F et al (1999) The nine C-terminal residues of the *Grapevine fanleaf nepovirus* movement protein are critical for systemic virus spread. *J Gen Virol* 80:1347–1356
  34. Carvalho CM, Wellink J, Ribeiro SG et al (2003) The C-terminal region of the movement protein of *Cowpea mosaic virus* is involved in binding to the large but not to the small coat protein. *J Gen Virol* 84:2271–2277
  35. Amari K, Boutant E, Hofmann C et al (2010) A family of plasmodesmal proteins with receptor-like properties for plant viral movement proteins. *PLoS Pathog* 6:e1001119
  36. Pouwels J, Van Der Krogt GN, Van Lent J et al (2002) The cytoskeleton and the secretory pathway are not involved in targeting the *Cowpea mosaic virus* movement protein to the cell periphery. *Virology* 297:48–56
  37. Laporte C, Vetter G, Loudes AM et al (2003) Involvement of the secretory pathway and the cytoskeleton in intracellular targeting and tubule assembly of *Grapevine fanleaf virus* movement protein in tobacco BY-2 cells. *Plant Cell* 15:2058–2075
  38. Huang Z, Han Y, Howell SH (2000) Formation of surface tubules and fluorescent foci in *Arabidopsis thaliana* protoplasts expressing a fusion between the green fluorescent protein and the *Cauliflower mosaic virus* movement protein. *Virology* 271:58–64
  39. Thomas CL, Bayer EM, Ritzenthaler C et al (2008) Specific targeting of a plasmodesmal protein affecting cell-to-cell communication. *PLoS Biol* 6:e7
  40. Brandizzi F, Wasteney GO (2013) Cytoskeleton-dependent endomembrane organization in plant cells: an emerging role for microtubules. *Plant J* 75:339–349
  41. Nebenführ A, Gallagher LA, Dunahay TG et al (1999) Stop-and-go movements of plant

- Golgi stacks are mediated by the acto-myosin system. *Plant Physiol* 121:1127–1142
42. Tominaga M, Yokota E, Sonobe S et al (2000) Mechanism of inhibition of cytoplasmic streaming by a myosin inhibitor, 2,3-butanedione monoxime. *Protoplasma* 213:46–54
  43. Amari K, Lerich A, Schmitt-Keichinger C et al (2011) Tubule-guided cell-to-cell movement of a plant virus requires class XI myosin motors. *PLoS Pathog* 7:e1002327
  44. Avisar D, Prokhnevsky AI, Makarova KS et al (2008) Myosin XI-K Is required for rapid trafficking of Golgi stacks, peroxisomes, and mitochondria in leaf cells of *Nicotiana benthamiana*. *Plant Physiol* 146:1098–1108
  45. Ueda H, Yokota E, Kutsuna N et al (2010) Myosin-dependent endoplasmic reticulum motility and F-actin organization in plant cells. *Proc Natl Acad Sci U S A* 107:6894–6899
  46. Prokhnevsky AI, Peremyslov VV, Dolja VV (2008) Overlapping functions of the four class XI myosins in Arabidopsis growth, root hair elongation, and organelle motility. *Proc Natl Acad Sci U S A* 105:19744–19749
  47. Peremyslov VV, Prokhnevsky AI, Avisar D et al (2008) Two class XI myosins function in organelle trafficking and root hair development in Arabidopsis. *Plant Physiol* 146:1109–1116
  48. Peremyslov VV, Prokhnevsky AI, Dolja VV (2010) Class XI myosins are required for development, cell expansion, and F-Actin organization in Arabidopsis. *Plant Cell* 22:1883–1897
  49. Hamada T, Tominaga M, Fukaya T et al (2012) RNA processing bodies, peroxisomes, Golgi bodies, mitochondria, and endoplasmic reticulum tubule junctions frequently pause at cortical microtubules. *Plant Cell Physiol* 53:699–708
  50. Peña EJ, Heinlein M (2013) Cortical microtubule-associated ER sites: organization centers of cell polarity and communication. *Curr Opin Plant Biol* 16:764–773
  51. Ritzenthaler C, Laporte C, Gaire F et al (2002) *Grapevine fanleaf virus* replication occurs on endoplasmic reticulum-derived membranes. *J Virol* 76:8808–8819
  52. Carette JE, van Lent J, MacFarlane SA et al (2002) *Cowpea mosaic virus* 32- and 60-kilodalton replication proteins target and change the morphology of endoplasmic reticulum membranes. *J Virol* 76:6293–6301
  53. Peremyslov VV, Pan YW, Dolja VV (2004) Movement protein of a closterovirus is a type III integral transmembrane protein localized to the endoplasmic reticulum. *J Virol* 78:3704–3709
  54. Dolja VV, Kreuze JF, Valkonen JPT (2006) Comparative and functional genomics of closteroviruses. *Virus Res* 117:38–51
  55. Avisar D, Prokhnevsky AI, Dolja VV (2008) Class VIII myosins are required for plasmodesmata localization of a closterovirus Hsp70 homolog. *J Virol* 82:2836–2843
  56. Peremyslov VV, Hagiwara Y, Dolja VV (1999) HSP70 homolog functions in cell-to-cell movement of a plant virus. *Proc Natl Acad Sci U S A* 96:14771–14776
  57. Dolja VV, Haldeman R, Robertson NL et al (1994) Distinct functions of capsid protein in assembly and movement of *Tobacco etch virus*. *EMBO J* 13:1482–1491
  58. Dolja VV, Haldeman-Cahill R, Montgomery AE et al (1995) Capsid protein determinants involved in cell-to-cell and long distance movement of *Tobacco etch potyvirus*. *Virology* 206:1007–1016
  59. Gabrenaite-Verkhovskaya R, Andreev IA, Kalinina NO et al (2008) Cylindrical inclusion protein of *Potato virus A* is associated with a subpopulation of particles isolated from infected plants. *J Gen Virol* 89:829–838
  60. Wei T, Zhang C, Hong J et al (2010) Formation of complexes at plasmodesmata for potyvirus intercellular movement is mediated by the viral protein P3N-PIPO. *PLoS Pathog* 6:e1000962
  61. Vijayapalani P, Maeshima M, Nagasaki-Takekuchi N et al (2012) Interaction of the trans-frame potyvirus protein P3N-PIPO with host protein PCaP1 facilitates potyvirus movement. *PLoS Pathog* 8:e1002639
  62. Agbeci M, Grangeon R, Nelson RS et al (2013) Contribution of host intracellular transport machineries to intercellular movement of *Turnip mosaic virus*. *PLoS Pathog* 9:e1003683
  63. Lain S, Riechmann JL, Garcia JA (1990) RNA helicase: a novel activity associated with a protein encoded by a positive strand RNA virus. *Nucl Acids Res* 18:7003–7006
  64. Rojas MR, Zerbini M, Allison RF et al (1997) Capsid protein and helper component-proteinase function as potyvirus cell-to-cell movement proteins. *Virology* 237:283–295
  65. Grangeon R, Jiang J, Wan J et al (2013) 6 K2-induced vesicles can move cell to cell during *Turnip mosaic virus* infection. *Front Microbiol* 4:351
  66. Deom CM, Oliver MJ, Beachy RN (1987) The 30-kilodalton gene product of *Tobacco mosaic virus* potentiates virus movement. *Science* 237:384–389

67. Kim SH, Kalinina NO, Andreev I et al (2004) The C-terminal 33 amino acids of the *Cucumber mosaic virus* 3a protein affect virus movement, RNA binding and inhibition of infection and translation. *J Gen Virol* 85: 221–230
68. Nagano H, Mise K, Furusawa I et al (2001) Conversion in the requirement of coat protein in cell-to-cell movement mediated by the *Cucumber mosaic virus* movement protein. *J Virol* 75:8045–8053
69. Sasaki N, Kaido M, Okuno T et al (2005) Coat protein-independent cell-to-cell movement of bromoviruses expressing *Brome mosaic virus* movement protein with an adaptation-related amino acid change in the central region. *Arch Virol* 150:1231–1240
70. Verchot-Lubicz J, Ye CM, Bamunusinghe D (2007) Molecular biology of potexviruses: recent advances. *J Gen Virol* 88:1643–1655
71. Hipper C, Brault V, Ziegler-Graff V et al (2013) Viral and cellular factors involved in phloem transport of plant viruses. *Front Plant Sci* 4:154
72. Heinlein M, Padgett HS, Gens JS et al (1998) Changing patterns of localization of the *Tobacco mosaic virus* movement protein and replicase to the endoplasmic reticulum and microtubules during infection. *Plant Cell* 10:1107–1120
73. Asurmendi S, Berg RH, Koo JC et al (2004) Coat protein regulates formation of replication complexes during *Tobacco mosaic virus* infection. *Proc Natl Acad Sci U S A* 101: 1415–1420
74. Kawakami S, Watanabe Y, Beachy RN (2004) *Tobacco mosaic virus* infection spreads cell to cell as intact replication complexes. *Proc Natl Acad Sci U S A* 101:6291–6296
75. Hirashima K, Watanabe Y (2001) Tobamovirus replicase coding region is involved in cell-to-cell movement. *J Virol* 75: 8831–8836
76. Boyko V, Hu Q, Seemanpillai M et al (2007) Validation of microtubule-associated *Tobacco mosaic virus* RNA movement and involvement of microtubule-aligned particle trafficking. *Plant J* 51:589–603
77. Sambade A, Brandner K, Hofmann C et al (2008) Transport of TMV movement protein particles associated with the targeting of RNA to plasmodesmata. *Traffic* 9:2073–2088
78. Niehl A, Peña EJ, Amari K et al (2013) Microtubules in viral replication and transport. *Plant J* 75:290–308
79. Peña EJ, Heinlein M (2012) RNA transport during TMV cell-to-cell movement. *Front Plant Sci* 3:193
80. Ashby J, Boutant E, Seemanpillai M et al (2006) *Tobacco mosaic virus* movement protein functions as a structural microtubule-associated protein. *J Virol* 80:8329–8344
81. Heinlein M, Epel BL, Padgett HS et al (1995) Interaction of tobamovirus movement proteins with the plant cytoskeleton. *Science* 270:1983–1985
82. Brandner K, Sambade A, Boutant E et al (2008) *Tobacco mosaic virus* movement protein interacts with green fluorescent protein-tagged microtubule end-binding protein 1. *Plant Physiol* 147:611–623
83. Ferralli J, Ashby J, Fasler M et al (2006) Disruption of microtubule organization and centrosome function by expression of *Tobacco mosaic virus* movement protein. *J Virol* 80: 5807–5821
84. Lindeboom JJ, Nakamura M, Hibbel A et al (2013) A mechanism for reorientation of cortical microtubule arrays driven by microtubule severing. *Science* 342:1245533
85. Boyko V, Ferralli J, Ashby J et al (2000) Function of microtubules in intercellular transport of plant virus RNA. *Nat Cell Biol* 2:826–832
86. Tagami Y, Watanabe Y (2007) Effects of brefeldin A on the localization of tobamovirus movement protein and cell-to-cell movement of the virus. *Virology* 361:133–140
87. Ouko MO, Sambade A, Brandner K et al (2010) Tobacco mutants with reduced microtubule dynamics are less susceptible to TMV. *Plant J* 62:829–839
88. Harries PA, Schoelz JE, Nelson RS (2009) Covering common ground: F-actin-dependent transport of plant viral protein inclusions reveals a novel mechanism for movement utilized by unrelated viral proteins. *Plant Signal Behav* 4:454–456
89. Liu J-Z, Blancaflor EB, Nelson RS (2005) The *Tobacco mosaic virus* 126-kilodalton protein, a constituent of the virus replication complex, alone or within the complex aligns with and traffics along microfilaments. *Plant Physiol* 138:1877–1895
90. Hofmann C, Niehl A, Sambade A et al (2009) Inhibition of *Tobacco mosaic virus* movement by expression of an actin-binding protein. *Plant Physiol* 149:1810–1823
91. Tilsner J, Linnik O, Christensen NM et al (2009) Live-cell imaging of viral RNA genomes using a Pumilio-based reporter. *Plant J* 57:758–770
92. Niehl A, Amari K, Gereige D et al (2012) Control of *Tobacco mosaic virus* movement protein fate by CELL-DIVISION-CYCLE

- protein 48 (CDC48). *Plant Physiol* 160: 2093–2108
93. Arce-Johnson P, Kahn TW, Reimann-Philipp U et al (1995) The amount of movement protein produced in transgenic plants influences the establishment, local movement, and systemic spread of infection by movement protein-deficient *Tobacco mosaic virus*. *Mol Plant Microbe Interact* 3:415–423
  94. Szécsi J, Ding XS, Lim CO et al (1999) Development of *Tobacco mosaic virus* infection sites in *Nicotiana benthamiana*. *Mol Plant Microbe Interact* 2:143–152
  95. Chen MH, Tian GW, Gafni Y et al (2005) Effects of calreticulin on viral cell-to-cell movement. *Plant Physiol* 138:1866–1876
  96. Kragler F, Curin M, Trutnyeva K et al (2003) MPB2C, a microtubule-associated plant protein binds to and interferes with cell-to-cell transport of *Tobacco mosaic virus* movement protein. *Plant Physiol* 132:1870–1883
  97. Reichel C, Beachy RN (2000) Degradation of the *Tobacco mosaic virus* movement protein by the 26S proteasome. *J Virol* 74:3330–3337
  98. Fujiki M, Kawakami S, Kim RW et al (2006) Domains of *Tobacco mosaic virus* movement protein essential for its membrane association. *J Gen Virol* 87:2699–2707
  99. Brill LM, Dechongkit S, DeLaBarre B et al (2004) Dimerization of recombinant *Tobacco mosaic virus* movement protein. *J Virol* 78:3372–3377
  100. Brill LM, Nunn RS, Kahn TW et al (2000) Recombinant *Tobacco mosaic virus* movement protein is an RNA-binding,  $\alpha$ -helical membrane protein. *Proc Natl Acad Sci U S A* 97:7112–7117
  101. Citovsky V, Wong ML, Shaw AL et al (1992) Visualization and characterization of *Tobacco mosaic virus* movement protein binding to single-stranded nucleic acids. *Plant Cell* 4:397–411
  102. Shimizu T, Yoshii A, Sakurai K et al (2009) Identification of a novel tobacco DnaJ-like protein that interacts with the movement protein of *Tobacco mosaic virus*. *Arch Virol* 154:959–967
  103. Chen M-H, Citovsky V (2003) Systemic movement of a tobamovirus requires host cells pectin methylesterase. *Plant J* 35:386–392
  104. Peiroa A, Martinez-Gil L, Tamborero S et al (2014) The *Tobacco mosaic virus* movement protein associates with but does not integrate into biological membranes. *J Virol* 88: 3016–3026
  105. Boutant E, Didier P, Niehl A et al (2010) Fluorescent protein recruitment assay for demonstration and analysis of in vivo protein interactions in plant cells and its application to *Tobacco mosaic virus* movement protein. *Plant J* 62:171–177
  106. Verchot J (2011) Wrapping membranes around plant virus infection. *Curr Opin Virol* 1:388–395
  107. Laliberté JF, Sanfaçon H (2010) Cellular remodeling during plant virus infection. *Annu Rev Phytopathol* 48:69–91
  108. Grangeon R, Jiang J, Laliberté JF (2012) Host endomembrane recruitment for plant RNA virus replication. *Curr Opin Virol* 2: 683–690
  109. Morozov SY, Solovyev AG (2003) Triple gene block: modular design of a multifunctional machine for plant virus movement. *J Gen Virol* 84:1351–1366
  110. Verchot-Lubicz J, Torrance L, Solovyev AG et al (2010) Varied movement strategies employed by triple gene block-encoding viruses. *Mol Plant Microbe Interact* 23:1231–1247
  111. Solovyev AG, Kalinina NO, Morozov SY (2012) Recent advances in research of plant virus movement mediated by triple gene block. *Front Plant Sci* 3:276
  112. Cruz SS, Roberts AG, Prior DAM et al (1998) Cell-to-cell and phloem-mediated transport of *Potato virus X*: the role of virions. *Plant Cell* 10:495–510
  113. Lough TJ, Netzler NE, Emerson SJ et al (2000) Cell-to-cell movement of potexviruses: evidence for a ribonucleoprotein complex involving the coat protein and first triple gene block protein. *Mol Plant Microbe Interact* 13:962–974
  114. Fedorkin ON, Merits A, Lucchesi J et al (2000) Complementation of the movement-deficient mutations in *Potato virus X*: potyvirus coat protein mediates cell-to-cell trafficking of C-terminal truncation but not deletion mutant of potexvirus coat protein. *Virology* 270:31–42
  115. Fedorkin O, Solovyev A, Yelina N et al (2001) Cell-to-cell movement of *Potato virus X* involves distinct functions of the coat protein. *J Gen Virol* 82:449–458
  116. Makarov VV, Rybakova EN, Efimov AV et al (2009) Domain organization of the N-terminal portion of hordeivirus movement protein TGBp1. *J Gen Virol* 90:3022–3032
  117. Chou YL, Hung YJ, Tseng YH et al (2013) The stable association of virion with the triple-gene-block protein 3-based complex of *Bamboo mosaic virus*. *PLoS Pathog* 9:e1003405
  118. Haupt S, Cowan GH, Ziegler A et al (2005) Two plant-viral movement proteins traffic in the endocytic recycling pathway. *Plant Cell* 17:164–181

119. Ju HJ, Samuels TD, Wang YS et al (2005) The *Potato virus X* TGBp2 movement protein associates with endoplasmic reticulum-derived vesicles during virus infection. *Plant Physiol* 138:1877–1895
120. Lauber E, Janssens L, Weyens G et al (2001) Rapid screening for dominant negative mutations in the *Beet necrotic yellow vein virus* triple gene block proteins P13 and P15 using a viral replicon. *Transgenic Res* 10:293–302
121. Mitra R, Krishnamurthy K, Blancaflor E et al (2003) The *Potato virus X* TGBp2 protein association with the endoplasmic reticulum plays a role in but is not sufficient for viral cell-to-cell movement. *Virology* 312:35–48
122. Samuels TD, Ju HJ, Ye CM et al (2007) Subcellular targeting and interactions among the *Potato virus X* TGB proteins. *Virology* 367:375–389
123. Solovyev AG, Stroganova TA, Zamyatin AA Jr (2000) Subcellular sorting of small membrane-associated triple gene block proteins: TGBp3-assisted targeting of TGBp2. *Virology* 269:113–127
124. Bamunusinghe D, Hemenway CL, Nelson RS et al (2009) Analysis of *Potato virus X* replicase and TGBp3 subcellular locations. *Virology* 393:272–285
125. Chang BY, Lin NS, Liou DY et al (1997) Subcellular localization of the 28 kDa protein of the triple-gene-block of *Bamboo mosaic potexvirus*. *J Gen Virol* 78:1175–1179
126. Davies C, Hills G, Baulcombe DC (1993) Sub-cellular localization of the 25-kDa protein encoded in the triple gene block of *Potato virus X*. *Virology* 197:166–175
127. Zamyatin AA Jr, Solovyev AG, Savenkov EI et al (2004) Transient coexpression of individual genes encoded by the triple gene block of *Potato mop-top virus* reveals requirements for TGBp1 trafficking. *Mol Plant Microbe Interact* 17:921–930
128. Erhardt M, Vetter G, Gilmer D et al (2005) Subcellular localization of the Triple Gene Block movement proteins of *Beet necrotic yellow vein virus* by electron microscopy. *Virology* 340:155–166
129. Lim HS, Bragg JN, Ganesan U et al (2008) Triple gene block protein interactions involved in movement of *Barley stripe mosaic virus*. *J Virol* 82:4991–5006
130. Lim HS, Bragg JN, Ganesan U et al (2009) Subcellular localization of the *Barley stripe mosaic virus* triple gene block proteins. *J Virol* 83:9432–9448
131. Schepetilnikov MV, Solovyev AG, Gorshkova EN et al (2008) Intracellular targeting of a hordeiviral membrane-spanning movement protein: sequence requirements and involvement of an unconventional mechanism. *J Virol* 82:1284–1293
132. Tilsner J, Cowan GH, Roberts AG et al (2010) Plasmodesmal targeting and intercellular movement of *Potato mop-top pomovirus* is mediated by a membrane anchored tyrosine-based motif on the luminal side of the endoplasmic reticulum and the C-terminal transmembrane domain in the TGB3 movement protein. *Virology* 402:41–51
133. Cowan GH, Lioliopoulou F, Ziegler A et al (2002) Subcellular localization, protein interactions, and RNA binding activity of *Potato mop-top virus* triple gene block proteins. *Virology* 298:106–115
134. Krishnamurthy K, Mitra R, Payton ME et al (2002) Cell-to-cell movement of the PVX 12 K, 8 K, or coat proteins may depend on the host, leaf developmental stage, and the PVX 25 K protein. *Virology* 300:269–281
135. Krishnamurthy K, Heppler M, Mitra R et al (2003) The *Potato virus X* TGBp3 protein associates with the ER network for virus cell-to-cell movement. *Virology* 309:135–151
136. Angell SM, Davies C, Baulcombe DC (1996) Cell-to-cell movement of *Potato virus X* is associated with a change in the size-exclusion limit of plasmodesmata in trichome cells of *Nicotiana clevelandii*. *Virology* 216:197–201
137. Lough TJ, Shash K, Xoconostle-Cazares B et al (1998) Molecular dissection of the mechanism by which potexvirus triple gene block proteins mediate cell-to-cell transport of infectious RNA. *Mol Plant Microbe Interact* 11:801–814
138. Howard AR, Heppler ML, Ju HJ et al (2004) *Potato virus X* TGBp1 induces plasmodesmata gating and moves between cells in several host species whereas CP moves only in *N. benthamiana* leaves. *Virology* 328:185–197
139. Tamai A, Meshi T (2001) Cell-to-cell movement of *Potato virus X*: the role of p12 and p8 encoded by the second and third open reading frames of the triple gene block. *Mol Plant Microbe Interact* 10:1158–1167
140. Lee CC, Ho YN, Hu RH et al (2011) The interaction between *Bamboo mosaic virus* replication protein and coat protein is critical for virus movement in plant hosts. *J Virol* 85:12022–12031
141. Doronin SV, Hemenway C (1996) Synthesis of *Potato virus X* RNAs by membrane-containing extracts. *J Virol* 70:4795–4799
142. Linnik O, Liesche J, Tilsner J et al (2013) Unraveling the structure of viral replication complexes at super-resolution. *Front Plant Sci* 4:6

143. Tilsner J, Linnik O, Wright KM et al (2012) The TGB1 movement protein of *Potato virus X* reorganizes actin and endomembranes into the X-body, a viral replication factory. *Plant Physiol* 158:1359–1370
144. Tilsner J, Linnik O, Louveau M et al (2013) Replication and trafficking of a plant virus are coupled at the entrances of plasmodesmata. *J Cell Biol* 201:981–995
145. Lee SC, Wu CH, Wang CW (2010) Traffic of a viral movement protein complex to the highly curved tubules of the cortical endoplasmic reticulum. *Traffic* 11:912–930
146. Wu CH, Lee SC, Wang CW (2011) Viral protein targeting to the cortical endoplasmic reticulum is required for cell-cell spreading in plants. *J Cell Biol* 193:521–535
147. Tilsner J, Amari K, Torrance L (2011) Plasmodesmata viewed as specialised membrane adhesion sites. *Protoplasma* 248:39–60
148. Raffaele S, Bayer E, Lafarge D et al (2009) Remorin, a solanaceae protein resident in membrane rafts and plasmodesmata, impairs *Potato virus X* movement. *Plant Cell* 21:1541–1555
149. Serazev TV, Nadezhkina ES, Shanina NA et al (2003) Virions and membrane proteins of the potato X virus interact with microtubules and enables tubulin polymerization in vitro. *Mol Biol* 37:919–925
150. Cho SY, Cho WK, Choi HS et al (2012) Cis-acting element (SL1) of *Potato virus X* controls viral movement by interacting with the NbMPB2Cb and viral proteins. *Virology* 427:166–176
151. Wright KM, Cowan GH, Lukhovitskaya NI et al (2010) The N-terminal domain of PMTV TGB1 movement protein is required for nucleolar localization, microtubule association, and long-distance movement. *Mol Plant Microbe Interact* 23:1486–1497
152. Shemyakina EA, Solov'yev AG, Leonova OG et al (2011) The role of microtubule association in plasmodesmal targeting of *Potato mop-top virus* movement protein TGBp1. *Open Virol J* 5:1–11
153. Heinlein M (2008) Microtubules and viral movement. In: Nick P (ed) *Plant microtubules*. Springer, Berlin, pp 141–173
154. Gillespie T, Boevink P, Haupt S et al (2002) Functional analysis of a DNA shuffled movement protein reveals that microtubules are dispensable for the cell-to-cell movement of *Tobacco mosaic virus*. *Plant Cell* 14:1207–1222
155. Seemanpillai M, Elamawi R, Ritzenthaler C et al (2006) Challenging the role of microtubules in *Tobacco mosaic virus* movement by drug treatments is disputable. *J Virol* 80: 6712–6715
156. Harries PA, Park JW, Sasaki N et al (2009) Differing requirements for actin and myosin by plant viruses for sustained intercellular movement. *Proc Natl Acad Sci U S A* 106: 17594–17599
157. Prokhnevsky AI, Peremyslov VV, Dolja VV (2005) Actin cytoskeleton is involved in targeting of a viral Hsp70 homolog to the cell periphery. *J Virol* 79:14421–14428
158. Wright KM, Wood NT, Roberts AG et al (2007) Targeting of TMV movement protein to plasmodesmata requires the actin/ER network: evidence from FRAP. *Traffic* 8:21–31
159. Gutierrez S, Yvon M, Thebaud G et al (2010) Dynamics of the multiplicity of cellular infection in a plant virus. *PLoS Pathog* 6:e1001113
160. Guenoune-Gelbart D, Elbaum M, Sagi G et al (2008) *Tobacco mosaic virus* (TMV) replicase and movement protein function synergistically in facilitating TMV spread by lateral diffusion in the plasmodesmal desmotubule of *Nicotiana benthamiana*. *Mol Plant Microbe Interact* 21:335–345
161. Barton DA, Cole L, Collings DA et al (2011) Cell-to-cell transport via the lumen of the endoplasmic reticulum. *Plant J* 66:806–817
162. Cantrill LC, Overall RL, Goodwin PB (1999) Cell-to-cell communication via plant endomembranes. *Cell Biol Int* 23:653–661
163. Grabski S, de Feijter AW, Schindler M (1993) Endoplasmic reticulum forms a dynamic continuum for lipid diffusion between contiguous soybean root cells. *Plant Cell* 5:25–38
164. Su S, Liu Z, Chen C et al (2010) *Cucumber mosaic virus* movement protein severs actin filaments to increase the plasmodesmal size exclusion limit in tobacco. *Plant Cell* 22: 1373–1387
165. White RG, Barton DA (2011) The cytoskeleton in plasmodesmata: a role in intercellular transport? *J Exp Bot* 62:5249–5266
166. Overall RL, Blackman LM (1996) A model of the macromolecular structure of plasmodesmata. *Trends Plant Sci* 1:307–311
167. Maule AJ (2008) Plasmodesmata: structure, function and biogenesis. *Curr Opin Plant Biol* 11:680–686
168. Zavaliev R, Ueki S, Epel BL et al (2011) Biology of callose (beta-1,3-glucan) turnover at plasmodesmata. *Protoplasma* 248:117–130
169. Dong X, Hong Z, Chatterjee J et al (2008) Expression of callose synthase genes and its connection with *Npr1* signaling pathway during pathogen infection. *Planta* 229:87–98

170. Lee JY, Wang X, Cui W et al (2011) A plasmodesmata-localized protein mediates crosstalk between cell-to-cell communication and innate immunity in Arabidopsis. *Plant Cell* 23:3353–3373
171. Wang X, Sager R, Cui W et al (2013) Salicylic acid regulates plasmodesmata closure during innate immune responses in Arabidopsis. *Plant Cell* 25:2315–2329
172. Epel BL (2009) Plant viruses spread by diffusion on ER-associated movement-protein-rafts through plasmodesmata gated by viral induced host  $\beta$ -1,3-glucanases. *Semin Cell Dev Biol* 20:1074–1081
173. Beffa RS, Hofer RM, Thomas M et al (1996) Decreased susceptibility to viral disease of  $\beta$ -1,3-glucanase-deficient plants generated by antisense transformation. *Plant Cell* 8:1001–1011
174. Bucher GL, Tarina C, Heinlein M et al (2001) Local expression of enzymatically active class 1  $\beta$ -1,3-glucanase enhances symptoms of TMV infection in tobacco. *Plant J* 28:361–369
175. Iglesias VA, Meins F Jr (2000) Movement of plant viruses is delayed in a  $\beta$ -1,3-glucanase-deficient mutant showing a reduced plasmodesmatal size exclusion limit and enhanced callose deposition. *Plant J* 21:157–166
176. Levy A, Erlanger M, Rosenthal M et al (2007) A plasmodesmata-associated  $\beta$ -1,3-glucanase in Arabidopsis. *Plant J* 49:669–682
177. Zavaliev R, Levy A, Gera A et al (2013) Subcellular dynamics and role of Arabidopsis  $\beta$ -1,3-glucanases in cell-to-cell movement of tobamoviruses. *Mol Plant Microbe Interact* 26:1016–1030
178. Ueki S, Spektor R, Natale DM et al (2010) ANK, a host cytoplasmic receptor for the *Tobacco mosaic virus* cell-to-cell movement protein, facilitates intercellular transport through plasmodesmata. *PLoS Pathog* 6:e1001201
179. Fridborg I, Grainger J, Page A et al (2003) TIP, a novel host factor linking callose degradation with the cell-to-cell movement of *Potato virus X*. *Mol Plant Microbe Interact* 16:132–140
180. Benitez-Alfonso Y, Jackson D (2009) Redox homeostasis regulates plasmodesmal communication in Arabidopsis meristems. *Plant Signal Behav* 4:655–659
181. Benitez-Alfonso Y, Jackson D, Maule A (2011) Redox regulation of intercellular transport. *Protoplasma* 248:131–140
182. Stonebloom S, Brunkard JO, Cheung AC et al (2012) Redox states of plastids and mitochondria differentially regulate intercellular transport via plasmodesmata. *Plant Physiol* 158:190–199
183. Tucker EB (1990) Calcium-loaded 1,2-bis(2-aminophenoxy)ethane-N,N,N',N'-tetraacetic acid blocks cell-to-cell diffusion of carboxyfluorescein in staminal hairs of *Setcreasea purpurea*. *Planta* 182:34–38
184. Tucker EB, Boss WF (1996) Mastoparan induced intracellular  $\text{Ca}^{2+}$  fluxes may regulate cell-to-cell communication in plants. *Plant Physiol* 111:459–467
185. Holdaway-Clarke TL, Walker NA, Hepler PK et al (2000) Physiological elevations in cytoplasmic free calcium by cold or ion injection result in transient closure of higher plant plasmodesmata. *Planta* 210:329–335
186. Kragler F, Monzer J, Shash K et al (1998) Cell-to-cell transport of proteins: requirement for unfolding and characterization of binding to a putative plasmodesmal receptor. *Plant J* 15:367–381
187. Lee J-Y, Yoo B-C, Rojas MR et al (2003) Selective trafficking of non-cell-autonomous proteins mediated by NtNCAPP1. *Science* 299:392–396
188. Fichtenbauer D, Xu XM, Jackson D et al (2012) The chaperonin CCT8 facilitates spread of tobamovirus infection. *Plant Signal Behav* 7:318–321
189. Aoki K, Kragler F, Xoconostle-Cazares B et al (2002) A subclass of plant heat shock cognate 70 chaperones carries a motif that facilitates trafficking through plasmodesmata. *Proc Natl Acad Sci U S A* 99:16342–16347
190. Xu XM, Wang J, Xuan Z et al (2011) Chaperonins facilitate KNOTTED1 cell-to-cell trafficking and stem cell function. *Science* 333:1141–1144
191. Wu S, Gallagher KL (2012) Transcription factors on the move. *Curr Opin Plant Biol* 15:645–651
192. Haywood V, Kragler F, Lucas WJ (2002) Plasmodesmata: pathways for protein and ribonucleoprotein signaling. *Plant Cell* 14(Suppl):S303–S325
193. Lucas WJ, Lee JY (2004) Plasmodesmata as a supracellular control network in plants. *Nat Rev Mol Cell Biol* 5:712–726
194. Lucas WJ, Yoo B-C, Kragler F (2001) RNA as a long-distance information macromolecule in plants. *Nat Rev Mol Cell Biol* 2:849–857
195. Hannapel DJ, Sharma P, Lin T (2013) Phloem-mobile messenger RNAs and root development. *Front Plant Sci* 4:257
196. Kim M, Canio W, Kessler S et al (2001) Developmental changes due to long-distance

- movement of a homeobox fusion transcript in tomato. *Science* 293:287–289
197. Kehr J, Buhtz A (2008) Long distance transport and movement of RNA through the phloem. *J Exp Bot* 59:85–92
  198. Yoo BC, Kragler F, Varkonyi-Gasic E et al (2004) A systemic small RNA signaling system in plants. *Plant Cell* 16:1979–2000
  199. Furuta K, Lichtenberger R, Helariutta Y (2012) The role of mobile small RNA species during root growth and development. *Curr Opin Cell Biol* 24:211–216
  200. Brosnan CA, Voinnet O (2011) Cell-to-cell and long-distance siRNA movement in plants: mechanisms and biological implications. *Curr Opin Plant Biol* 14:580–587
  201. Skopelitis DS, Husbands AY, Timmermans MC (2012) Plant small RNAs as morphogens. *Curr Opin Cell Biol* 24:217–224
  202. Melnyk CW, Molnar A, Baulcombe DC (2011) Intercellular and systemic movement of RNA silencing signals. *EMBO J* 30:3553–3563
  203. Winter N, Kollwig G, Zhang S et al (2007) MPB2C, a microtubule-associated protein, regulates non-cell-autonomy of the homeodomain protein KNOTTED1. *Plant Cell* 19:3001–3018
  204. Wu Q, Wang X, Ding SW (2010) Viral suppressors of RNA-based viral immunity: host targets. *Cell Host Microbe* 8:12–15
  205. Burgyan J, Havelda Z (2011) Viral suppressors of RNA silencing. *Trends Plant Sci* 16:265–272
  206. Csorba T, Bovi A, Dalmay T et al (2007) The p122 subunit of *Tobacco Mosaic Virus* replicase is a potent silencing suppressor and compromises both small interfering RNA- and microRNA-mediated pathways. *J Virol* 81:11768–11780
  207. Vogler H, Akbergenov R, Shivaprasad PV et al (2007) Modification of small RNAs associated with suppression of RNA silencing by tobamovirus replicase protein. *J Virol* 81:10379–10388
  208. Amari K, Vazquez F, Heinlein M (2012) Manipulation of plant host susceptibility: an emerging role for viral movement proteins? *Front Plant Sci* 3:10
  209. Umbach JL, Cullen BR (2009) The role of RNAi and microRNAs in animal virus replication and antiviral immunity. *Genes Dev* 23:1151–1164
  210. Weiberg A, Wang M, Lin FM et al (2013) Fungal small RNAs suppress plant immunity by hijacking host RNA interference pathways. *Science* 342:118–123
  211. Kørner CJ, Klauser D, Niehl A et al (2013) The immunity regulator BAK1 contributes to resistance against diverse RNA viruses. *Mol Plant Microbe Interact* 26:1271–1280
  212. Fitzgibbon J, Bell K, King E et al (2010) Super-resolution imaging of plasmodesmata using three-dimensional structured illumination microscopy. *Plant Physiol* 153:1453–1463
  213. Tilsner J, Oparka KJ (2010) Tracking the green invaders: advances in imaging virus infection in plants. *Biochem J* 430:21–37
  214. Dunoyer P, Schott G, Himber C et al (2010) Small RNA duplexes function as mobile silencing signals between plant cells. *Science* 328:912–916

## **Part II**

### **Imaging of Plasmodesmata**



## Imaging Plasmodesmata with High-Resolution Scanning Electron Microscopy

Deborah A. Barton and Robyn L. Overall

### Abstract

High-resolution scanning electron microscopy (HRSEM) is an effective tool to investigate the distribution of plasmodesmata within plant cell walls as well as to probe their complex, three-dimensional architecture. It is a useful alternative to traditional transmission electron microscopy (TEM) in which plasmodesmata are sectioned to reveal their internal substructures. Benefits of adopting an HRSEM approach to studies of plasmodesmata are that the specimen preparation methods are less complex and time consuming than for TEM, many plasmodesmata within a large region of tissue can be imaged in a single session, and three-dimensional information is readily available without the need for reconstructing TEM serial sections or employing transmission electron tomography, both of which are lengthy processes. Here we describe methods to prepare plant samples for HRSEM using pre- or postfixation extraction of cellular material in order to visualize plasmodesmata embedded within plant cell walls.

**Key words** Cell wall, Detergent extraction, Freeze cracking, High-resolution scanning electron microscopy, Immunogold labeling, Plasmodesmata

---

### 1 Introduction

Imaging plasmodesmata, the plasma membrane-lined channels linking plant cells across the cell wall, is challenging because, at approximately 50 nm in diameter, they cannot be resolved distinctly using conventional fluorescence or confocal microscopy [1]. While there is a huge potential for super-resolution microscopy to reveal the precise locations of fluorescently tagged proteins at plasmodesmata [2, 3], electron microscopy remains the only technology to elucidate plasmodesmatal ultrastructure. Transmission electron microscopy has been traditionally employed in studies of plasmodesmata substructure [4] or to immunolocalize proteins such as actin [5] and myosin [6] or carbohydrates such as callose [6] to plasmodesmata. However, it is difficult to obtain three-dimensional information about plasmodesmata from TEM ultrathin sections and while electron tomography has the capability

to reveal three-dimensional plasmodesmatal structures [7], as yet, this technology has not been extensively applied to plasmodesmata.

High-resolution scanning electron microscopy (HRSEM), through use of scanning electron microscopes fitted with field emission guns, has similar resolution capabilities to TEM, and there are advantages of using it to study plasmodesmata. It is the ideal way to determine the frequency of plasmodesmata within plant cell walls [8, 9], it can provide three-dimensional information about the internal and external surfaces of plasmodesmata [9], and specimen preparation is faster and less onerous than for TEM. However, to view the distribution of plasmodesmata in cell walls with HRSEM, all cellular contents must first be removed to reveal the surface of the cell wall and the holes in it through which plasmodesmata pass. This can be achieved through several approaches including using detergents, such as saponin, to strip cells of membrane and cytosolic material before fixation [9, 10], or freeze-cracking frozen samples, such as tobacco leaf trichomes, with a cooled blade to expose plasmodesmata in the cell wall [8].

These specimen preparation approaches can be modified to view specific plasmodesmatal features. For example, to reveal external surfaces of plasmodesmata we used pectinase enzymes to digest pectin within the specialized cell wall sleeve of plasmodesmata prior to fixation or even completely removed the wall during cryo-sectioning [9]. Alternatively, examination of the cell wall sleeve would require complete removal of plasmodesmatal membranes and proteins. Sodium hypochlorite treatment, which removed cellular contents of root cells and exposed cellulose microfibrils within cell walls after fixation [11], could be useful here. To image internal substructures with HRSEM, plasmodesmata need to be cut open in the correct orientation while frozen. We have found that this can be difficult using rudimentary freeze-cracking methods and sometimes a large number of cells were examined before we found plasmodesmata that were broken open in the correct plane. Preparing cryosections [9] or cutting samples open in a cryo-preparation unit [8] could alleviate some of the randomness of this procedure.

While immunolabeling of plasmodesmatal proteins or cell wall components has not been attempted yet for HRSEM, it should be possible given the successful immunolabeling of microtubules and microtubule-associated proteins within the cortical cytoplasm of leaf epidermal cells [12] or callose at Hechtian strands within plasmolyzed cells [13]. In our experience, colloidal gold secondary antibodies do not penetrate through large SEM samples as effectively as the smaller nanogold-conjugated secondary antibodies. Here we describe methods to prepare plant samples for HRSEM, including pre- and post-extraction techniques to expose plasmodesmata in cell walls, as well as steps for immunolabeling proteins at plasmodesmata.

## 2 Materials

All chemicals can be sourced from commercial suppliers. Prepare all solutions in milli-Q ultrapure water. Chemicals used to fix plant samples are toxic and should be handled with care. Dispose of toxic chemicals according to hazardous waste guidelines.

### 2.1 Specialized SEM Equipment

1. Field emission scanning electron microscope with an in-lens secondary electron detector and a backscattered electron detector.
2. Critical point dryer.
3. Sputter coater with a platinum target.

### 2.2 Buffers

1. Phosphate buffer: 0.1 M  $\text{NaH}_2\text{PO}_4$ , 0.1 M  $\text{Na}_2\text{HPO}_4 \cdot 7\text{H}_2\text{O}$ , pH 6.9.

Prepare stock solutions of 0.2 M  $\text{NaH}_2\text{PO}_4$  (2.78 g in 100 mL water) and 0.2 M  $\text{Na}_2\text{HPO}_4 \cdot 7\text{H}_2\text{O}$  (5.365 g in 100 mL water). To make 0.1 M phosphate buffer at pH 6.9, add 4.5 mL of 0.2 M  $\text{NaH}_2\text{PO}_4$  to 5.5 mL of 0.2 M  $\text{Na}_2\text{HPO}_4 \cdot 7\text{H}_2\text{O}$  and add 10 mL water.

2. PME: 50 mM PIPES, 5 mM  $\text{MgSO}_4$ , 5 mM EGTA, pH 6.9 (*see Note 1*).

Dissolve 4.73 g PIPES dipotassium salt (*see Note 2*), 0.308 g  $\text{MgSO}_4$ , and 0.475 g EGTA in 250 mL water and pH the solution to 6.9.

3. Phosphate-buffered saline (PBS): 3.3 mM  $\text{Na}_2\text{HPO}_4 \cdot 7\text{H}_2\text{O}$ , 1.6 mM  $\text{NaH}_2\text{PO}_4$ , 145 mM NaCl, pH 6.9. Dissolve 0.885 g  $\text{Na}_2\text{HPO}_4 \cdot 7\text{H}_2\text{O}$ , 0.249 g  $\text{NaH}_2\text{PO}_4$ , and 8.5 g NaCl in 1 L water.

### 2.3 Preparing Plant Samples for Fixation

1. Fresh plant material.
2. Razor blades, single and/or double sided.
3. Two pairs of forceps, one with blunt tips, the other with fine tips.
4. Polyethylenimine-coated 22 mm  $\times$  22 mm cover slips (*see Note 3*):

Prepare a solution of 0.1 % (v/v) polyethylenimine. Dip a cotton bud into the solution and wipe the wet bud over the surface of a cover slip. Let the solution dry before using the cover slip.

5. 1% (w/v) low-melting-point agarose (e.g., Type VII from Sigma-Aldrich):

Weigh out 0.5 g of low-melting-point agarose and place it in a conical flask. Add 50 mL water and heat in a microwave until the solution boils and the agarose dissolves. Wearing a heat-resistant glove, swirl the solution, let it cool a little, and then

aliquot it out into 1.5 mL microcentrifuge tubes. Use immediately, or if the agarose sets, insert a tube into a microcentrifuge floating rack and place this in a hot water bath to melt the agarose.

6. Filter paper cut into small arcs (*see* **Note 4**).

#### **2.4 Extraction, Fixation, and Freeze-Cracking Plant Samples**

1. Saponin, 5 % (w/v) stock solution.
2. Sodium hypochlorite (bleach).
3. 16 % Paraformaldehyde, EM-grade stock solution.
4. 25 % Glutaraldehyde, EM-grade stock solution.
5. DMSO (dimethyl sulfoxide).
6. Liquid nitrogen.
7. Polystyrene box, approximately 30 × 20 × 15 cm.
8. Double-sided razor blades mounted onto wooden sticks for freeze cracking: Break a double-sided razor blade in half, and then break each half into small segments using a pair of pliers. Create a small crack in the end of a 20 cm long wooden stick by cutting it with a single-sided razor blade. Gently insert the blunt end of the double-sided razor blade segment into the crack of the wooden stick and secure it by wrapping the end of the stick with electrical tape. Alternatively, use superglue to secure the razor blade to the stick before wrapping the end of the stick with electrical tape.

#### **2.5 Immunolabeling**

1. Normal goat serum.
2. Bovine serum albumin (protease free).
3. Primary antibody of choice, e.g., anti- $\beta$ -1,3-glucan raised in mouse.
4. Gold-conjugated secondary antibody of choice, e.g., 10 nm colloidal gold-conjugated anti-mouse IgG or FluoroNanogold-conjugated anti-mouse Fab' fragment.
5. Goldenhance kit (Nanoprobes, USA).

#### **2.6 Postfixation, Dehydration, Drying, and Mounting onto SEM Stubs**

1. Osmium tetroxide, 2 % stock solution.
2. 30, 50, 70, 100, and 100 % (anhydrous) ethanol solutions.
3. Specimen holders for critical point drying (Fig. 1).
4. SEM stubs.
5. Double-sided carbon tape.
6. Carbon paint.
7. Wooden toothpicks.

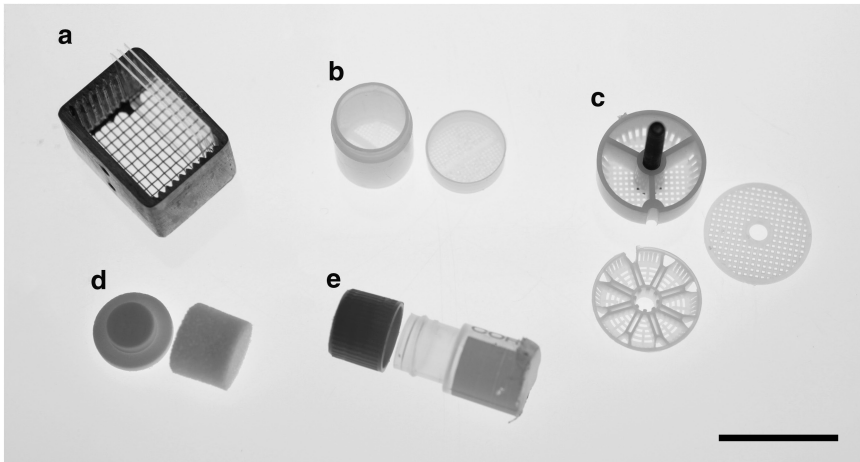


**Fig. 1** Specimen holders for a critical point dryer. **(a)** A custom-made coverslip holder that holds 20 cover slips, **(b–d)** Disposable specimen holders available from commercial electron microscope suppliers such as ProSciTech, Australia. **(b)** A plastic specimen holder with perforated lid and base, **(c)** specimen baskets and lid, and **(d)** a microporous specimen capsule. **(e)** Custom-made plastic specimen holder consisting of a small plastic tube with one end removed and re-sealed with 11  $\mu\text{m}$  nylon mesh. Scale bar represents 2 cm

### 3 Methods

#### 3.1 Preparing Plant Tissue (See Note 5)

1. Dissect a plant sample in phosphate buffer or PME using a sharp razor blade. Wear gloves and use fine forceps to hold the sample gently in place.
2. When the sample is a few mm or so in several dimensions (*see Note 6*), place it in a microcentrifuge tube containing buffer and proceed to Subheading 3.2.
3. If the specimen is smaller than a few mm and could be easily lost through multiple rinsing steps, secure it to a 22 mm  $\times$  22 mm cover slip coated with 0.1 % (v/v) polyethylenimine.
4. Transfer the specimen to the cover slip. Dip the tapered end of a piece of filter paper into molten 1 % (w/v) low-melting-point agarose, remove it, and wait a few seconds for the agarose to cool. Trace around the edge of the specimen with the tapered end of the filter paper. A ring of warm agarose should surround and fix the specimen on the cover slip. Wait for the agarose to dry and then bathe the specimen in buffer (*see Note 7*).

#### 3.2 Pre-extraction: Optional

1. Prepare a 0.04 % (v/v) saponin solution in buffer by diluting 80  $\mu\text{L}$  of 5 % stock solution into 9.920 mL buffer (*see Note 8*).
2. Apply it to the specimen for 30–120 min depending on the size of the specimen: smaller/thinner specimens require shorter extraction times than larger specimens.
3. Rinse the specimen thoroughly with the buffer to remove excess cytosol, e.g., 4  $\times$  5 min.

**3.3 Fixation**

1. Prepare 0.5 % (v/v) paraformaldehyde and 0.1 % (v/v) glutaraldehyde in buffer (*see Note 9*). These chemicals are toxic, so work in a fume hood and wear appropriate protective clothing.
2. Apply this fixation solution to the specimens for 15–30 min.
3. Rinse three times in buffer, usually for 5–10 min each.

**3.4 Cracking Specimens Open**

1. OPTIONAL: Cryoprotect specimens in 25 % (v/v) DMSO, and then 50 % (v/v) DMSO diluted in buffer, each for 20 min.
2. Wearing protective gloves and glasses, half-fill a sturdy polystyrene box with liquid nitrogen. Grasping the specimen or cover slip with a pair of forceps, plunge it quickly into liquid nitrogen. Cool a double-sided razor blade attached to a wooden stick by placing the blade into liquid nitrogen and then crack the specimen open. Either break the specimen into smaller pieces, provided the smaller pieces can be captured quickly, or shave the edge off the specimen by repeatedly running the blade over the surface of the specimen (*see Note 10*).
3. Thaw the specimen either in 50 % (v/v) DMSO (if using cryoprotection) or in buffer.
4. Rinse the specimen thoroughly in buffer (*see Note 11*).

**3.5 Post-extraction: Optional**

1. Prepare a 0.04 % (v/v) saponin solution in buffer by diluting 80  $\mu$ L of 5 % stock solution into 9.920 mL buffer.
2. Apply it to the specimen for 30–60 min depending on the size of the specimen and degree of extraction required.
3. Alternatively, prepare 0.1 % (v/v) sodium hypochlorite and apply it to the specimen for 10 min [11].
4. Rinse the specimen thoroughly with the buffer to remove excess cytosol, e.g., 4  $\times$  5 min.

**3.6 Immunolabeling for Callose at Plasmodesmata: Optional**

1. Block the specimens against nonspecific antibody binding with 10 % (v/v) normal goat serum and 3 % (w/v) bovine serum albumin in PBS.
2. Dilute the primary antibody, e.g., anti-1,3- $\beta$ -glucan (Biosupplies Australia), 1:20 in PBS [13], and apply it to the specimen, either for 2 h at 37 °C or overnight at 4 °C (*see Note 12*).
3. Rinse the specimen thoroughly in PBS.
4. Apply a secondary antibody to the specimen, e.g., goat anti-mouse IgG conjugated to a 10 nm colloidal gold particle diluted 1:25 in PBS for 1 h at room temperature [10], or FluoroNanogold-conjugated anti-mouse diluted 1:25 in PBS [12] for 1.5 h at 37 °C.
5. Rinse the specimens thoroughly in PBS.

6. If using FluoroNanogold secondary antibodies, increase the size of the Nanogold particles using a Goldenhance kit (Nanoprobes); apply the Goldenhance solution for 10 min for large samples, or for 2–3 min for thin, flat samples.
7. Rinse the specimens thoroughly.

### **3.7 Post-fixation and Drying the Specimen**

1. Prepare a 0.5 % (v/v) solution of OsO<sub>4</sub> in PBS and apply it to the specimens for 10 min at 4 °C (*see Note 13*). OsO<sub>4</sub> is toxic, so use protective clothing and work in a fume hood. Dispose of waste appropriately.
2. Rinse thoroughly in PBS.
3. Select an appropriate specimen carrier for critical point drying (Fig. 1) and place the specimens or cover slips in it.
4. Dehydrate the specimens through a graded series of ethanol dilutions, for example, 30, 50, 70, 100, and 100 % anhydrous (v/v) ethanol each for 30 min (*see Note 14*). If the samples are large and thick, increase the number of dehydration concentrations and number of times they are applied.
5. Critical point drying (*see Note 15*): Transfer your specimen in 100 % anhydrous ethanol to a critical point dryer and follow the instructions for drying it. During the process liquid carbon dioxide will replace the ethanol and the pressure inside the chamber will increase until the carbon dioxide passes through its critical point and becomes a gas. More frequent rinses in liquid carbon dioxide will be necessary for larger and denser samples. If the dehydration and drying steps are not optimized samples can become distorted (Fig. 2).

### **3.8 Mounting Specimens/Cover Slips onto Stubs**

1. Identify stubs that are suitable for the field emission scanning electron microscope that you will use.
2. Place a piece of double-sided carbon sticky tape onto the stub and mount your specimen or cover slip onto it. Dip a toothpick into carbon paint and trace around the edges of your specimen with the carbon paint, being careful not to cover cells of interest (*see Note 16*).
3. Coat your specimen with 2.5 nm platinum in a sputter coater. It is now ready for imaging.

### **3.9 Imaging with a Field Emission Scanning Electron Microscope**

1. Image your sample initially with a low-voltage electron beam (<5 kV) as this will provide detailed surface information about the cellular structures (Fig. 2) without causing damage to the sample. Collect secondary electrons using an in-lens secondary electron detector.
2. Visualize immunogold labeling through capturing high-energy backscattered electrons. It may be necessary to increase the voltage of the electron beam to approximately 10 kV to produce

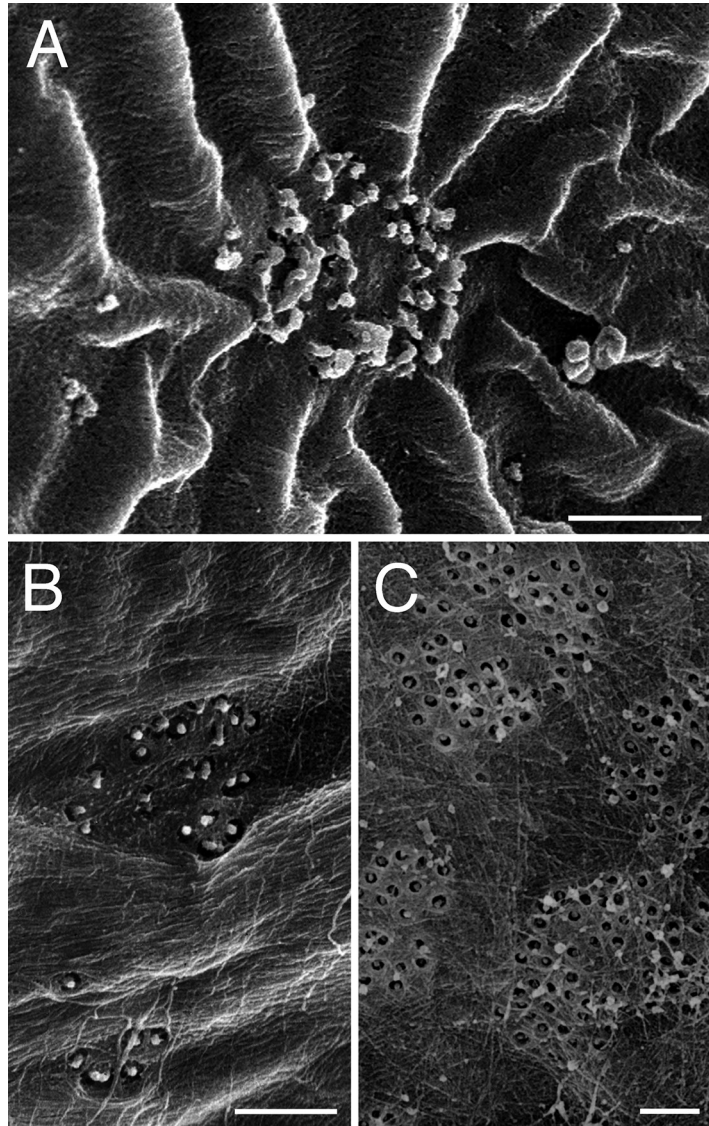


**Fig. 2** Effects of critical point drying on groups of plasmodesmata within plant cell walls. **(a)** A large group of plasmodesmata in an *Arabidopsis* cotyledon epidermal cell wall. Note that the cell wall is wrinkled and folded, an artefact of poor dehydration and critical point drying. **(b)** Groups of plasmodesmata in an onion root tip cell. There are several minor folds of the cell wall. **(c)** Discrete groups of plasmodesmata in cell walls of *Chara corallina* nodal cells. The walls are flat, have been dried well, and **(b, c)** have been reproduced with slight modifications from Brecknock et al. [9] with kind permission from Springer Science and Business Media. Scale bars represent 500 nm

enough electrons of high enough energy to be captured in a backscattered electron detector.

3. Although structures in SEM images appear three-dimensional, collecting stereo images provides extra three-dimensional

information. After collecting an image of the structure, rotate the stage by approximately  $8\text{--}10^\circ$  and collect another image. These can then be examined together as a stereo pair.

---

## 4 Notes

1. PME is a microtubule-stabilizing buffer but has been used in generic HRSEM specimen preparation protocols [10].
2. The dipotassium salt of PIPES is easier to dissolve than other PIPES salts.
3. Polyethylenimine creates a sticky film on cover slips and plant cells adhere to it.
4. Cut a piece of filter paper, 9 cm in diameter, into half. Then fold each half into two. Cut small segments of the filter paper from the round, outer edge to the point where the fold meets the diameter. This should result in small pieces of filter paper, each with a tapered point, which can be inserted into a microcentrifuge tube containing molten 1 % agarose.
5. Before commencing sample preparation it is important to consider how the specimen will be held throughout the critical point drying step. The sample needs to be secured within a specialized CPD holder (Fig. 1), which allows easy infiltration of liquid carbon dioxide into the sample. The sample should be small enough to fit within a holder but large enough that it could not escape through holes in the holder. Alternatively specimens can be secured to cover slips and these can be inserted into a coverslip holder (Fig. 1).
6. It is also important to consider how large to make the sample. Larger samples that are densely packed with cells will take a longer time to dehydrate and infiltrate with liquid carbon dioxide than smaller samples. Consequently, they may not dry as well as smaller and/or thinner samples.
7. It is essential that the agarose dries completely before bathing the specimen in buffer, particularly if the specimen is to be plunged into liquid nitrogen in later steps. If the agarose does not dry completely, the specimen could float off the cover slip during rinsing steps.
8. If it is necessary to retain microtubules in the sample, add  $10\text{ }\mu\text{M}$  taxol to the extraction solution [14].
9. Low concentrations of paraformaldehyde and glutaraldehyde improve HRSEM specimen preparation because extraneous cellular material can be extracted more easily in later steps. If fixation needs to be improved, increase the concentration of paraformaldehyde to 0.75 or 1 % (v/v) and increase the concentration of glutaraldehyde to 0.5 % (v/v). However, it is important to note

that increasing the concentration of glutaraldehyde during fixation will reduce the antigenicity of the sample.

10. Cracking the sample open requires substantial force and if the blade is not strong enough try using a single-sided blade grasped with a pair of blunt-edged forceps.
11. It is very important to remove all DMSO from cryoprotected specimens as it can react with the osmium tetroxide used in later steps.
12. Each primary antibody binds to its antigen with a different efficiency, so it is important to optimize the antibody concentration to use for a sample. Generally, the concentration of a primary antibody should be higher for immunogold labeling than for immunofluorescence labeling.
13.  $\text{OsO}_4$  treatment preserves membranes and can add conductivity to a sample.
14. Fixed specimens can be stored in 70 % ethanol overnight, or for a few days but prolonged storage is not advisable.
15. Critical point drying is the optimal method to use to dry plant samples for HRSEM, particularly those that are delicate [15]. Do not attempt to air-dry your samples, as they will appear distorted when imaged with HRSEM.
16. The carbon provides a path for electrons to travel off the sample whilst in the electron microscope and so reduces damage from the electron beam.

## References

1. Jahn KA, Barton DA, Kobayashi K et al (2011) Correlative microscopy: providing new understanding in the biomedical and plant sciences. *Micron* 43:565–582
2. Fitzgibbon J, Bell K, King E et al (2010) Super-resolution imaging of plasmodesmata using three-dimensional structured illumination microscopy. *Plant Physiol* 153:1453–1463
3. Bell K, Oparka K (2011) Imaging plasmodesmata. *Protoplasma* 248:9–25
4. Overall RL, Wolfe J, Gunning BES (1982) Intercellular communication in *Azolla* roots: I. Ultrastructure of plasmodesmata. *Protoplasma* 111:134–150
5. White RG, Badelt K, Overall RL et al (1994) Actin associated with plasmodesmata. *Protoplasma* 180:169–184
6. Radford JE, Veski M, Overall RL (1998) Callose deposition at plasmodesmata. *Protoplasma* 201:30–37
7. Biliska A, Sowinski P (2010) Closure of plasmodesmata in maize (*Zea mays*) at low temperature: a new mechanism for inhibition of photosynthesis. *Ann Bot* 106:675–686
8. Faulkner C, Akman OE, Bell K et al (2008) Peeking into pit fields: a multiple twinning model of secondary plasmodesmata formation in tobacco. *Plant Cell* 20:1504–1518
9. Brecknock S, Dibbayawan TP, Veski M et al (2011) High resolution scanning electron microscopy of plasmodesmata. *Planta* 234:749–758
10. Veski M, Dibbayawan TP, Veski PA et al (2000) Field emission scanning electron microscopy of plant cells. *Protoplasma* 210:138–155
11. Sugimoto K, Williamson RE, Wasteneys GO (2000) New techniques enable comparative analysis of microtubule orientation, wall texture, and growth rate in intact roots of *Arabidopsis*. *Plant Physiol* 124:1493–1506

12. Barton DA, Vantard M, Overall RL (2008) Analysis of cortical arrays from *Tradescantia virginiana* at high resolution reveals discrete microtubule subpopulations and demonstrates that confocal images of arrays can be misleading. *Plant Cell* 20:982–994
13. Lang I, Barton DA, Overall RL (2004) Membrane-wall attachments in plasmolysed plant cells. *Protoplasma* 224:231–243
14. Vesik PA, Vesik M, Gunning BES (1996) Field emission scanning electron microscopy of microtubule arrays in higher plant cells. *Protoplasma* 195:168–182
15. Bray D (2000) Critical point drying of biological specimens for scanning electron microscopy. *Method Biotechnol* 13:235–243



## Preparative Methods for Imaging Plasmodesmata at Super-resolution

Karen Bell and Karl Oparka

### Abstract

Much of our knowledge of plasmodesmata has come from the ability to visualize them. Light microscopy is a popular tool for exploring subcellular structures but is limited in its resolving power due to the diffractive properties of light. At 50 nm in diameter plasmodesmata are below this limit and so cannot be resolved. Super-resolution microscopy operates beyond the limits of conventional light microscopy affording a more detailed view. Although lacking the ultrastructural resolving power of the electron microscope (EM), super-resolution microscopy helps to bridge the gap between conventional light microscopy and EM.

Here we present three preparative methods for studying plasmodesmata at super-resolution using 3D-structured illumination microscopy (3D-SIM).

**Key words** Plasmodesmata, Super-resolution microscopy, Immunofluorescence, 3D-SIM, Electron microscopy, Correlative microscopy

---

### 1 Introduction

Due to its compatibility with many molecular methods, light microscopy remains a powerful tool for the plant-cell biologist. Light microscopy has enabled the imaging of live cells, the study of dynamic processes, and the genetic labelling of multiple targets using the ever-expanding pallet of fluorescent proteins. However, conventional light microscopy is still limited by a comparative lack of resolution compared to electron microscopy. This is due to the diffraction limit of light which dictates that, in an ideal system, objects closer together than approximately 200 nm laterally ( $x$ - $y$ ) and 500 nm axially (in  $z$ ) cannot be resolved but instead appear blurred (for brief discussion *see* [1] and references therein). The point scanning and optical sectioning capacity of confocal laser scanning microscopy (CSLM) has allowed researchers to work close to this limit. This has brought many cellular components in sharper focus but, at 50 nm in diameter, plasmodesmata (PD)

cannot be resolved. Proteomic approaches have identified new PD-associated proteins [2, 3] but their location at or within the PD pore remains speculative due to the lack of detail afforded by CSLM. Recent innovations in biological imaging have broken the diffraction limit and promise to offer new views of structures and cellular processes. One example we have used to image PD is structured illumination microscopy (SIM). SIM uses spatially patterned excitation to extend resolution. This involves introducing a defined patterned structure to the incident light which when it interacts with the sample structure, as represented by the distribution of the dye/fluorescent protein, produces emitted light that contains interference fringes. This is best explained in terms of the moiré effect [4] that dictates that if two fine patterns are superimposed multiplicatively, a moiré fringe will result in the product. This fringe may be coarser than either of the original patterns and so may be more readily observable in the microscope. As the illumination pattern is known, this can be readily accounted for within the moiré fringe, allowing additional information about the unknown sample structure to be determined. As the patterning of the incident light is directional, it is necessary to shift and rotate the phase over  $360^\circ$  resulting in multiple images, each taken 125 nm apart in Z [5]. The images are then processed to produce the final super-resolution image. Currently the resolution achievable with 3D-SIM is 100 nm in xy direction and 200 nm in z direction [6]. This increased resolution is of obvious benefit to PD researchers but equally so is the increased optical sectioning capacity (125 nm steps). The typical plant cell is 700 nm thick and 3D-SIM allows up to five images to be taken in this volume (c.f. approximately only once every 500 nm with CSLM). This allows different components of PD to be spatially resolved (Fig. 1).

3D-SIM has been commercialized by Applied Precision Inc. (Washington, USA) and released with the title Optical Microscope eXperimental (OMX). The OMX design seeks to maximize the photon budget (number of photons transmitted through the microscope) by optimizing the efficiency of light transmission, and by the suppression of stray light and noise [5]. The illumination and imaging systems are placed in an acoustically isolated, thermally controlled room. A dedicated auxiliary microscope, with transmission and epi-fluorescence illumination, is used for sample location and mapping. The high-precision motorized stage is cross-linked with that of the OMX to allow coordinate sharing. A tile scan is performed of the sample before it is mounted on the OMX stage, which is then used as a high-resolution location map for finding specific features/locations, preserving the sample from further illumination prior to imaging.

3D-SIM is compatible with standard fluorochromes and sample preparation techniques. The utility of 3D-SIM in PD and phloem research has already been established [8, 9] and detailed preparative methods for its use are described in this chapter.

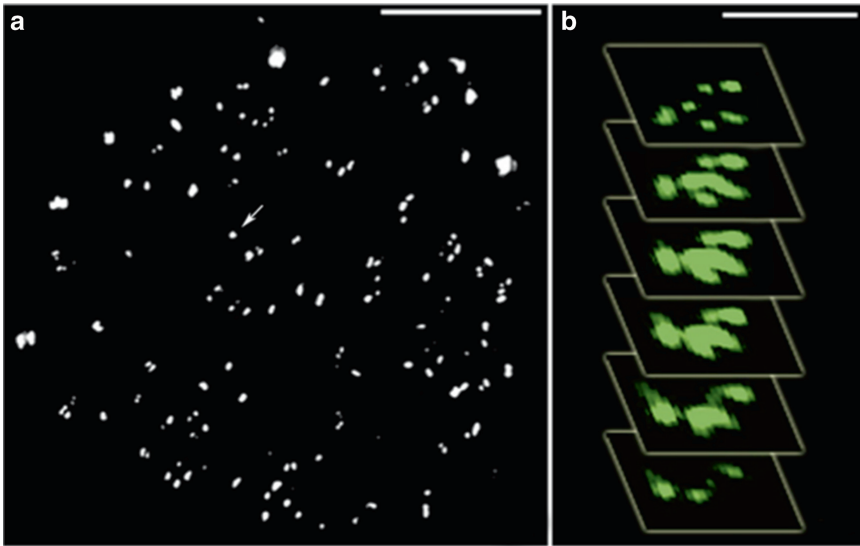


**Fig. 1** 3D-SIM images of branched plasmodesmata. (a) A volume projection showing all the branched plasmodesmata at the trichome-epidermis interface (as highlighted by TMV MP-GFP; [7]). Scale bar 5  $\mu\text{m}$ . (b) Optical sections (125 nm apart) of a single branched PD (arrowed in a). Note that six branches can be detected at the trichome face with only three emerging in the epidermis. Pores fuse in the middle lamella region of the wall. Scale bar 1  $\mu\text{m}$ . Figure (a) and (b) reproduced from Fitzgibbon, J., Bell, K., King, E., and Oparka, K. (2010) Super-resolution imaging of plasmodesmata using three-dimensional structured illumination microscopy. *Plant Physiol* 153, 1453–1463. [www.plantphysiol.org](http://www.plantphysiol.org) Copyright American Society of Plant Biologists

Although super-resolution microscopy offers a bridge between conventional light microscopy and electron microscopy, it would be desirable to confirm that observations made using this technology are robust and that they can be readily confirmed using the transmission electron microscope (TEM). It is, however, a considerable challenge to produce material that has been adequately fixed and processed so that it can withstand the rigors of imaging with the electron microscope while still retaining fluorescence and antigenicity. London Resin (LR) is an acrylic-based resin that is compatible with light and electron microscopy. The resin is hardened by free radical chain polymerization that shows no affinity for proteins or nucleic acids in the sample. In this chapter we mention the use of LR to embed material while retaining fluorescence and antigenicity, allowing the same cells to be imaged using light and transmission electron microscopy. This approach generates complementary structural information beyond that possible using a single imaging technique [9].

Many of the new super-resolution approaches currently suffer from a comparative lack of “user friendliness” that is taken for granted with conventional imaging. Live-cell imaging, for instance, has been done at super-resolution [10–12] but is by no means routine, and has yet to be conducted in plants. Currently, super-resolution techniques

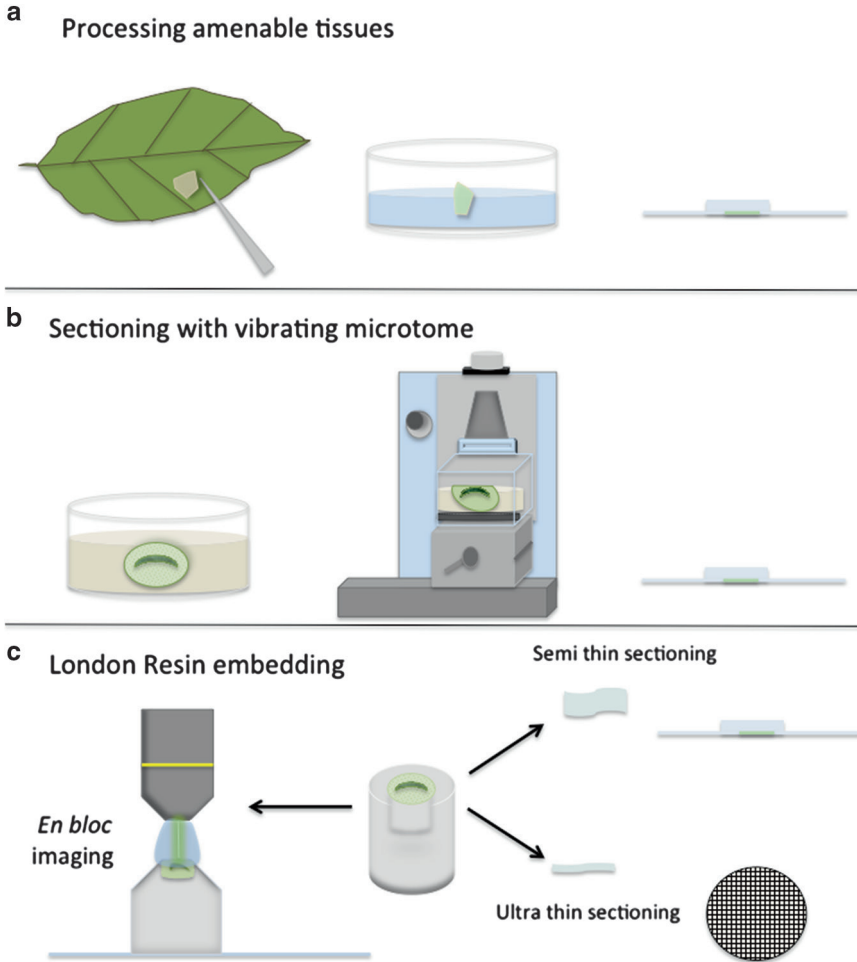


**Fig. 2** Three methods for preparing materials for 3D-SIM. **(a)** Processing amenable tissues or preparing epidermal peels. Tissues and peels are processed in a petri dish and then mounted on a slide under a number 1.5 cover slip for fluorescence and SIM imaging. **(b)** Sectioning with a vibrating microtome. Samples are first fixed and then stabilized with phytoagar in a petri dish ahead of sectioning with a vibrating microtome. Sections are then processed essentially as in **(a)**, ahead of mounting and imaging for fluorescence and SIM. **(c)** Embedding in London Resin. Samples are fixed and dehydrated ahead of embedding in London Resin. The sample can then be viewed *en bloc* using a confocal microscope ahead of cutting semi-thin sections for fluorescence, immunofluorescence, or SIM imaging. Ultrathin sections can also be cut for transmission electron microscopy (TEM). This method allows the same cells to be imaged using fluorescence, SIM, and TEM, allowing a direct comparison of these imaging technologies

offer the greatest, and most readily achievable, advantages when using fixed, thin, or sectioned samples. In this chapter we present three methods for preparing material for 3D-SIM (Fig. 2). The first is direct processing of amenable plant tissues, e.g., fine roots, hypocotyls, or epidermal leaf peels that can be readily mounted under a cover slip (Fig. 2a). The second is a method suitable for imaging the vasculature (Fig. 2b). Vascular tissues generally lie deep within plant organs, exceeding the working distance of conventional lenses.

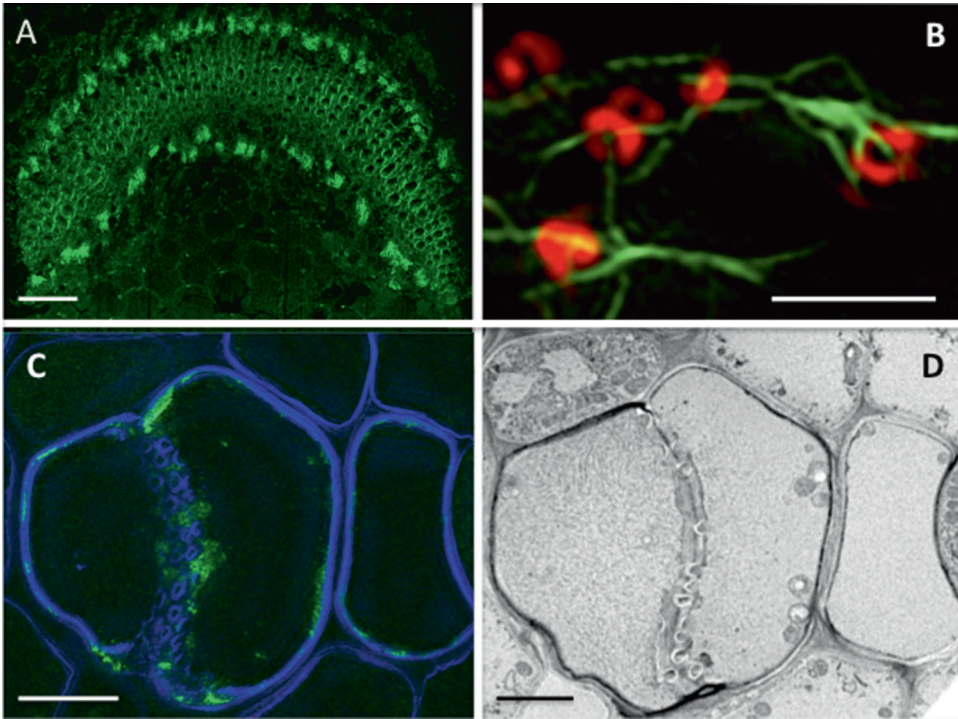


**Fig. 3** Images of processed material. (a) *En bloc* image of a London Resin-embedded tobacco petiole expressing pSE02:HDEL:GFP (shown in *green*; [13]), which highlights the sieve element reticulum and making the sieve elements clearly visible. Scale 600  $\mu\text{m}$ . (b) 3D-SIM image showing tobacco mosaic virus movement protein fused to GFP (TMV MP-GFP) expressed from the CaMV 35S promoter. TMV MP-GFP is associated with the pore plasmodesma units (PPUs) at the sieve element-companion cell interface. 3D-SIM image reveals that individual strands of MP connect many PPUs. Scale 5  $\mu\text{m}$ . (c) 3D-SIM image of phloem expressing pSE02:HDEL:GFP and counterstained with calcofluor white to highlight the cell wall and sieve-plate callose. The image was reconstructed from 20 serial Z sections and reveals callose collars in the sieve plate as well as the intricate nature of the sieve-element reticulum. Scale 5  $\mu\text{m}$ . (d) TEM image of the same field of view shown in (c). Greater ultrastructural detail is revealed than in (c) but the image lacks the 3D context afforded by SIM. Scale 3  $\mu\text{m}$ . Figure (a), (c), and (d), reproduced from Bell, K., Mitchell, S., Paultre, D., Posch, M., and Oparka, K. (2013) Correlative imaging of fluorescent proteins in resin-embedded plant material. *Plant Physiology*, 161: 1595–1603. [www.plantphysiol.org](http://www.plantphysiol.org) Copyright American Society of Plant Biologists. Figure (b) reproduced from Fitzgibbon, J., Bell, K., King, E., and Oparka, K., (2010) Super-resolution imaging of plasmodesmata using three-dimensional structured illumination microscopy. *Plant Physiology* 153, 1453–1463. [www.plantphysiol.org](http://www.plantphysiol.org) Copyright American Society of Plant Biologists

By stabilizing the material and sectioning with a vibrating microtome it is possible to produce 50  $\mu\text{m}$  sections. The vibrations of the blade ensure that the cut is made with less pressure than with a static blade, which is desirable when cutting tissues that have not first been reinforced with resin. The final method uses London Resin to infiltrate the tissue, allowing semi-thin (0.5–2  $\mu\text{m}$ ) and ultrathin (60 nm) sections to be obtained from the block (Fig. 2c). All three methods preserve fluorescence and antigenicity (*see* Fig. 3 for a panel of representative images). However, the method selected will depend on the

specific question being addressed. Making epidermal peels may be sufficient to analyze cells for transient assays, while investing time in embedding tissue in London Resin has more flexibility and allows long-term storage (>1 year at 4 °C).

## 2 Materials

### 2.1 Processing Epidermal Peels for Antibody Labelling

1. Fixative: 50 mM 1,4-piperazinediethanesulfonic acid (PIPES) pH 6.9, 2 mM EGTA, 1 % (w/v) bovine serum albumin (BSA) in distilled H<sub>2</sub>O (dH<sub>2</sub>O). Add 4 % (v/v) formaldehyde and 0.25 % (v/v) glutaraldehyde. Prepare fresh (*see Note 1*).
2. Wash buffer: 2 mM EGTA, 1 % (w/v) BSA, 50 mM PIPES pH 6.9 in dH<sub>2</sub>O.
3. PBS: Phosphate-buffered saline: 1 mM KH<sub>2</sub>PO<sub>4</sub>, 155 mM NaCl, and Na<sub>2</sub>HPO<sub>4</sub>·7H<sub>2</sub>O in dH<sub>2</sub>O, pH 7.4.
4. Blocking solution: 3 % (w/v) BSA and 50 mM glycine in PBS.
5. Antibody solution: Pertinent antibody diluted in PBS containing 1 % (w/v) BSA and 0.02 % (v/v) Tween-20.
6. Mount: Use a number 1.5 cover slip (0.17 mm thick) and anti-fade mountant, such as Citifluor AF1 (Citifluor Ltd. Leicester, UK). Seal cover slips on a slide using nail varnish.

### 2.2 Producing Sections Using a Vibrating Microtome

1. Stabilizer: 5 % (w/v) phytoagar in dH<sub>2</sub>O (*see Note 2*).
2. Enzyme solution: 2 % (w/v) driselase (w/v) in PBS with 1 % (w/v) BSA and 5 mM EDTA (*see Note 3*).
3. Rinse buffer: 50 mM PIPES, 2 mM EGTA, 1 % (w/v) BSA in dH<sub>2</sub>O with 10 % (v/v) glycerol, and 0.2 % (v/v) Triton X-100.

Otherwise the same solutions are used as in Subheading 2.1.

### 2.3 Embedding in London Resin for Retention of Fluorescent Proteins [9]

*Green and yellow fluorescent protein fluorescence has been retained in tobacco and Arabidopsis leaves, stems, petioles, and roots using this method [9].*

1. Fixative: 50 mM PIPES (pH 6.9) and 1 mM CaCl<sub>2</sub> in dH<sub>2</sub>O. Add formaldehyde to 4 % (v/v) and glutaraldehyde to 2 % (v/v). Make fresh (*see Note 4*).
2. Wash buffer: 50 mM PIPES (pH 6.9) and 1 mM CaCl<sub>2</sub> in dH<sub>2</sub>O.
3. Dehydration solutions: 50, 70, and 90 % (v/v) ethanol diluted with dH<sub>2</sub>O and supplemented with 1 mM dithiothreitol (DTT) (*see Note 5*). Store at 4 °C.
4. Infiltration solutions: 90 % (v/v) ethanol with 1 mM DTT (as prepared above) and London Resin Medium Grade (LR; Agar Scientific, Essex, UK) in a 1:1, 1:2, 1:3 (90 % ethanol:LR) ratio. Store components at 4 °C and use while chilled.

5. Staining solutions: (a) 1 µg/mL propidium iodide in dH<sub>2</sub>O; (b) 10 µg/mL calcofluor white in dH<sub>2</sub>O.
6. Poly-L-lys-coated glass slides: Immerse slides into poly-L-lys diluted 1:10 with dH<sub>2</sub>O and agitate for 5 min. Drain and then dry the slides at 60 °C for 60 min or at room temperature (18–26 °C) overnight.
7. Ultrathin section stains: (a) 1 % uranyl acetate in double-distilled H<sub>2</sub>O (ddH<sub>2</sub>O) (*see Note 6*); (b) lead citrate staining solution: 40 nM lead nitrate, 61 nM sodium citrate in ddH<sub>2</sub>O: mix to a uniform milky suspension. To this add 0.2 M sodium hydroxide, and mix by inversion until suspension clears completely (*see Note 7*).

Otherwise the same solutions are used as in Subheading 2.1.

---

### 3 Methods

#### 3.1 Processing Epidermal Peels for Imaging PD

*This method is compatible with fluorescence microscopy immunofluorescence labelling and 3D-SIM.*

1. Make an abaxial leaf peel and float it immediately on the fixative at room temperature for 45 min (*see Note 8*).

*From now on all processing should occur at room temperature with gentle agitation unless stated otherwise.*

2. Replace the fixative with wash buffer and incubate for 10 min. Make a further two changes of wash buffer, changing the solution every 10 min as before.

*Samples can now be mounted (*see* Subheading 3.1, **step 7**) or processing can continue for antibody labelling:*

3. Replace with the blocking solution and incubate as above for 20 min.
4. Replace with the antibody solution with primary antibody diluted as appropriate. Incubate for 16 h at 37 °C without agitation (*see Note 9*).
5. Rinse by replacing the primary antibody solution with the blocking solution. Change the solution three times, once every 10 min.
6. Replace with the antibody solution, with secondary antibody diluted as appropriate, and incubate for 3 h at 37 °C without agitation.
7. Rinse with PBS twice for 5 min each before mounting directly upon a number 1.5 cover slip. Add a drop of Citifluor AF1 antifade medium (Citifluor Ltd., Leicester, UK) to the slide and then press gently to spread the mountant (*see Note 10*).

### 3.2 Producing Sections Using a Vibrating Microtome

*This method is compatible with fluorescence microscopy, immunofluorescence labelling, and 3D-SIM, and is best accomplished using a vibrating microtome.*

1. Vascular tissues can be fixed effectively by allowing the fixative to transpire in the xylem from where it moves laterally to other tissues, including the phloem. This method allows delivery of fixative to delicate cells (e.g., sieve elements), avoiding the need for cutting live tissues. To achieve this, immediately submerge the cut petiole or stem in the fixative solution and then trim the bottom 5 mm from the submerged tissue to eliminate any potential airlocks. Leave to transpire in an illuminated fume hood for 60 min.
2. Pour cooled (40 °C) molten stabilizer into a petri dish and add trimmed tissue on top. Push down gently with a blunt implement to submerge. Take care to remove any surrounding air bubbles and orientate the sample to reflect the direction of sectioning desired, e.g., lying flat at 180° to the surface to produce longitudinal sections or at 90° to the surface to cut transversely. Once set, trim any extra stabilizer from the surface and section with the vibrating microtome (we use a Vibroslice HA752 from Campden Instruments, Leicestershire, UK) at a medium-fast setting to produce 100 µm sections.

*All further processing occurs at room temperature with gentle agitation unless stated otherwise.*

3. Transfer sections to a 5 mL petri dish filled with wash buffer. Replace every 10 min three times.

*Samples can now be counterstained (Subheading 3.2, **step 9**) and mounted (Subheading 3.2, **step 10**) for imaging or processed further for immunofluorescence:*

4. Optional driselase digestion: Replace wash buffer with enzyme solution and incubate for 15 min at 37 °C without agitation. Using rinse buffer wash three times replacing every 10 min. Then wash with PBS three times, changing every 5 min.
5. Replace with the blocking solution and incubate for 20 min.
6. Remove the blocking solution and replace with the antibody solution, with the primary antibody diluted as appropriate. Incubate for 16 h at 37 °C without agitation.
7. Rinse the sections using the blocking solution. Change the solution three times, once every 10 min.
8. Dilute the secondary antibody in the antibody solution and incubate the sections in this solution for 3 h at 37 °C without agitation.
9. *Optional counterstaining:* Rinse the sections with PBS, twice for 5 min each time. Stain briefly for 1 min by replacing the

PBS with stain (e.g., Calcofluor White at 10 µg/mL to highlight cellulose in cell walls) prior to rinsing with dH<sub>2</sub>O.

10. Rinse with PBS, twice for 5 min each time (*unless following Subheading 3.2, step 9, above*), and then mount sections directly on a number 1.5 cover slip. Add a drop of Citifluor AFI antifade medium (Citifluor Ltd. Leicester, UK) to the slide and then press gently to spread the mountant. Seal with nail varnish to facilitate long-term storage.

### **3.3 Correlative Imaging of Fluorescent Proteins in Material Embedded in London Resin**

#### **3.3.1 Tissue Processing**

*This method is compatible with en bloc imaging, fluorescence microscopy, immunofluorescence, 3D-SIM, and TEM.*

1. Fix the sample using the fixative described in Subheading 2.3 and in the manner described in Subheading 3.1, **step 1**, if using peels or seedlings, or as in Subheading 3.2, **step 1**, if fixing vasculature tissues. Following the initial 60-min fixation, peels and seedlings are fixed further by incubating on a rolling-bed platform in the dark at 8 °C for 16 h. To ensure that the dense vasculature is well fixed after the 60-min xylem irrigation of fixative, the petiole or stem is trimmed into approximately 2 mm segments using a double-sided razor blade and fixed for a further 16 h on a rolling-bed platform in the dark at 8 °C.

*From now on processing is done at 8°C in the dark, with constant gentle agitation using a rolling-bed platform unless otherwise stated.*

2. Remove the fixative and rinse the tissues three times in wash buffer, changing every 10 min.
3. Dehydrate the tissue using a series of dehydration solutions (each for 15 min) that contain increasing concentrations of ethanol. Use the 90 % ethanol-containing solution twice.
4. Infiltrate the tissue sections with infiltration solutions (containing increasing concentrations of the LR resin) for 45 min each followed by two 60-min changes in 100 % LR, the final one of which is incubated at room temperature.
5. Transfer the samples to gelatine capsules and fill to overflowing with 100 % resin at room temperature. Close the lid tightly (*see Note 11*). Polymerize the resin for 24 h at 50 °C (*see Note 12*).
6. Remove the gelatine capsule with a razor blade. Trim the block top carefully to a trapezoid with the section area being as small as possible to include the part(s) of the specimen of interest.

*The specimen may now be viewed directly en bloc, or sections can be taken using an ultramicrotome for fluorescence microscopy, antibody labelling, or ultrastructural observation in the transmission electron microscope.*

### 3.3.2 *En Bloc* Imaging and Staining

*This is a simple way to check the quality and orientation of the specimen ahead of further sectioning.*

1. Stick the base of the polymerized block to a slide with adhesive tack and then carefully lower the objective lens in place (*see Note 13*). The optical sectioning properties of a confocal microscope should allow imaging up to 40  $\mu\text{m}$  into the block where, if present, the fluorescent protein should still be visible [9] which is useful for identifying structures of interest and to allow targeted sectioning.
2. The cell-wall stains propidium iodide or calcofluor white penetrate the resin block well and provide a useful reference point for imaging cell walls. Add a drop of either staining solution to the trimmed block face and allow the stain to penetrate into the tissue for 20 min at room temperature. The remaining dye can then be rinsed from the block face by immersing it in distilled water for 2 min and gently agitating the block using a rolling-bed platform.
3. Stained or unstained, the blocks may be stored for up to 1 year in the dark at 4 °C (*see Note 14*).

### 3.3.3 *Dye Staining of Semi-thin Sections for Fluorescence Microscopy*

1. Cut semi-thin sections (1–2  $\mu\text{m}$ ) using a glass knife and, if not already stained *en bloc*, stain these briefly as in Subheading 3.2, **step 9**, prior to rinsing in  $\text{dH}_2\text{O}$  and mounting with Citifluor antifade agent under a number 1.5 cover slip. Seal the cover slip to the slide with nail varnish.

### 3.3.4 *Labeling Semi-thin Sections with Antibodies for Fluorescence Microscopy*

1. Affix semi-thin sections to poly-l-lys-coated slides by heating briefly (1–2 min) on a slide warmer.
2. Incubate the sections in blocking solution for 10 min and rinse three times for 1 min with PBS.
3. Dilute primary antibody as appropriate in the antibody solution and incubate the sections for 90 min at 37 °C in this solution.
4. Rinse sections three times for 1 min with blocking solution.
5. Dilute the secondary antibody in the antibody solution and incubate the sections in this solution at 37 °C for 60 min.
6. Mount and counterstain, if desired, as in Subheading 3.2, **steps 9 and 10**.

### 3.3.5 *Preparing Sections for TEM*

1. Cut ultrathin (60 nm) sections using a glass or diamond knife and mount on an EM grid. To do this, have sections floating on water and touch the dull side of the grid to the center of the section briefly taking care not to break the surface tension of the water. If the grids are clean the sections should readily transfer from the water to the grid.

2. To stain, first quickly wet the grids in ddH<sub>2</sub>O (*see Note 15*) and then float section side down, on a drop (*see Note 16*) of uranyl acetate for 45 min. Using forceps grasp the grid by its edge and wash by dipping it rapidly in ddH<sub>2</sub>O for 1 min and then repeat for a further 1 min in a fresh pool of ddH<sub>2</sub>O. Counterstain with lead citrate by inverting the grid section side down onto a drop and leaving for 10 min. Wash again, as above, and then allow to air-dry prior to imaging with the TEM.

---

## 4 Notes

1. While it is advisable to prepare the fixative solution on the day of use, the stocks (PIPES, EGTA, BSA) may be prepared ahead of time and autoclaved to facilitate long-term storage. Use fixatives supplied in single-use glass ampules. Use EM-grade glutaraldehyde and a methanol-free preparation of formaldehyde. Decant into screw-cap glass bottle (store glutaraldehyde at 4 °C and formaldehyde at RT) and use within 1 month.
2. It is necessary to support the tissue during sectioning. Phytoagar is a plant tissue culture agar with a high gel strength and can be used at a minimal concentration of 5.0 g/L to obtain a solid gel. This concentration matches the mechanical properties of a young petiole well and so adequately supports sectioning. However, it will be necessary to vary the concentration of phytoagar when handling other tissues (e.g., leaves) so that the agar does not buckle or break away from the tissue.
3. Driselase is useful when processing vasculature as it allows the sectioned material to separate slightly, affording a better view of phloem strands.
4. In order to preserve fine structure at the TEM level it is necessary to increase the concentration of glutaraldehyde. We found 2 % to be sufficient to preserve ultrastructure while retaining fluorescence and antigenicity, at least for callose labelling [9].
5. When dehydrating before London Resin embedding it is necessary to use ethanol because acetone can act as a free radical scavenger that interferes with the polymerization of the resin. To limit aldehyde-induced autofluorescence, DTT is included during dehydration and infiltration. When used in combination with low-temperature processing, DTT reduces background autofluorescence [14], preserves antigenicity during chemical fixation [15, 16], and may prevent quenching of fluorescent proteins [17].
6. 1 % uranyl acetate takes between 1 and 2 h to dissolve in ddH<sub>2</sub>O on a rotary mixer. Filter through a syringe-driven 33 mm gage filter unit prior to use.

7. It is necessary to shake the constituents of the lead citrate stain vigorously intermittently for up to 30 min to ensure adequate mixing to a uniform milky suspension. This should clear following addition of 0.2 M sodium hydroxide and mixing by inversion. The solution can be stored at 4 °C in a tightly capped bottle for up to 1 month.
8. Peeling the lower rather than the upper leaf surface is advantageous as in some species it avoids trichomes that can be auto-fluorescent. Use ultrafine forceps to peel tissue. Thickness will vary along the length of the peel but trim any extraneous tissue prior to mounting.
9. It is necessary to empirically determine the concentration and duration of incubation necessary for each primary antibody.
10. Add the tissue directly to the cover slip to ensure that it is as close as possible to the lens. A thick layer of mountant can be difficult to image through and for 3D-SIM best results are achieved when material is within 16 µm of the cover slip.
11. Although it is reported that LR will not polymerize in the presence of oxygen [18], we have found that blocks will polymerize well if a small air bubble remains after capping.
12. If the blocks still seem soft, yield when squeezed, or are tacky when handled, they can be hardened up by incubating them at 50 °C for a further 8 h. Further incubation may also aid in the cutting of ultrathin sections for TEM.
13. This method is suitable for water-dipping lenses that have a working distance of up to 0.5 cm. Low-magnification (5×, 10×) dry lenses also image the block well. Take care when imaging the blocks and ensure that there are no hanging or rough edges to that might catch and damage the lenses.
14. 14 months is currently the longest time we have stored blocks. There has been no obvious deterioration in fluorescence or structure in this time.
15. Wetting the grids briefly prior to staining prevents extensive air-stain contact, thereby reducing contamination [19].
16. It is necessary to spot stain onto a plastic rather than glass petri dish to achieve a drop with the desired size and shape. Cover the petri dish during staining to protect from dust, evaporation, and CO<sub>2</sub> from expelled air. Protection from CO<sub>2</sub> is particularly pertinent when staining with lead citrate.

---

## Acknowledgements

We would like to thank Steve Mitchell for help when developing the LR method and Dr. Alison Roberts for advice in using the vibrating microtome.

## References

1. Bell K, Oparka K (2010) Imaging plasmodesmata. *Protoplasma* 248:9–25
2. Thomas CL, Bayer EM, Ritzenthaler C et al (2008) Specific targeting of a plasmodesmal protein affecting cell-to-cell communication. *PLoS Biol* 6:180–190
3. Simpson C, Thomas C, Findlay K et al (2009) An Arabidopsis GPI-anchor plasmodesmal neck protein with callose binding activity and potential to regulate cell-to-cell trafficking. *Plant Cell* 21:581–594
4. Gustafsson MGL (2000) Surpassing the lateral resolution limit by a factor of two using structured illumination microscopy. *J Microsc* 198: 82–87
5. Dobbie IM, King E, Parton RM et al (2011) OMX: a new platform for multimodal, multi-channel wide-field imaging. *Cold Spring Harb Protoc* 8:899–909
6. Schermelleh L, Carlton PM, Haase S et al (2008) Subdiffraction multicolor imaging of the nuclear periphery with 3D structured illumination microscopy. *Science* 320:1332–1336
7. Roberts IM, Boevink P, Roberts AG et al (2001) Dynamic changes in the frequency and architecture of plasmodesmata during the sink-source transition in tobacco leaves. *Protoplasma* 218:31–44
8. Fitzgibbon J, Bell K, King E et al (2010) Super-resolution imaging of plasmodesmata using three-dimensional structured illumination microscopy. *Plant Physiol* 153:1453–1463
9. Bell K, Mitchell S, Paultre D et al (2013) Correlative imaging of fluorescent proteins in resin-embedded plant material. *Plant Physiol* 161:1595–1603
10. Kner P, Chhun BB, Griffis ER et al (2009) Super-resolution video microscopy of live cells by structured illumination. *Nat Methods* 6: 339–342
11. Wombacher R, Heidbreder M, van de Linde S et al (2010) Live-cell super-resolution imaging with trimethoprim conjugates. *Nat Methods* 7:717–719
12. Balint S, Verdeny Vilanova I, Sandoval Alvarez A et al (2013) Correlative live-cell and super-resolution microscopy reveals cargo transport dynamics at microtubule intersections. *Proc Natl Acad Sci U S A* 110:3375–3380
13. Knoblauch M, Peters WS (2010) Münch, morphology, microfluidics: our structural problem with the phloem. *Plant Cell Environ* 33: 1439–1452
14. Brown R, Lemmon B, Mullinax J (1992) Immunofluorescent staining of microtubules in plant tissues: improved embedding and sectioning techniques using polyethylene glycol (PEG) and Steedman's wax. *Bot Acta* 102: 54–61
15. Baskin TI, Busby CH, Fowke LC et al (1992) Improvements in immunostaining samples embedded in methacrylate: localisation of microtubules and other antigens throughout developing organs in plants. *Planta* 187: 405–413
16. Baskin TI, Miller DD, Vos JW et al (1996) Cryofixing single cells and multicellular specimens enhances structure and immunocytochemistry for light microscopy. *J Microsc* 182: 149–161
17. Thompson MV, Wolniak SM (2008) A plasma membrane-anchored fluorescent protein fusion illuminates sieve element plasma membranes in Arabidopsis and Tobacco. *Plant Physiol* 146:1599–1610
18. Keene DR, Tufa SF, Lunstrum GP et al (2008) Confocal/TEM overlay microscopy: a simple method for correlating confocal and electron microscopy of cells expressing GFP/YFP fusion proteins. *Microsc Microanal* 14: 342–348
19. Hayat MA (1968) The principles and techniques of electron microscopy, vol 1. Van Nostand Reinhold Company, New York, NY



## **Part III**

### **Structural Analysis of Plasmodesmata**



## Isolation of Plasmodesmata from *Arabidopsis* Suspension Culture Cells

Magali S. Grison, Lourdes Fernandez-Calvino,  
Sébastien Mongrand, and Emmanuelle M.F. Bayer

### Abstract

Due to their position firmly anchored within the plant cell wall, plasmodesmata (PD) are notoriously difficult to isolate from plant tissue. Yet, getting access to isolated PD represents the most straightforward strategy for the identification of their molecular components. Proteomic and lipidomic analyses of such PD fractions have provided and will continue to provide critical information on the functional and structural elements that define these membranous nano-pores. Here, we describe a two-step simple purification procedure that allows isolation of pure PD-derived membranes from *Arabidopsis* suspension cells. The first step of this procedure consists in isolating cell wall fragments containing intact PD while free of contamination from other cellular compartments. The second step relies on an enzymatic degradation of the wall matrix and the subsequent release of “free” PD. Isolated PD membranes provide a suitable starting material for the analysis of PD-associated proteins and lipids.

**Key words** Plasmodesmata, Membrane, Cell wall, Cellulase, Suspension cell, Proteomic, Lipidomic, *Arabidopsis thaliana*

---

### 1 Introduction

Plasmodesmata (PD) are plant-specific nano-pores spanning the adjoining wall of most cells, thereby providing a conduit for intercellular communication. They contain specialized membrane domains derived from the endoplasmic reticulum (ER; called the desmotubule) and from the plasma membrane (PM; called PD-PM). Both domains carry specific sets of proteins and lipids that differ from the surrounding bulk membranes. This unique molecular composition plays a role in PD function and considerable efforts have been devoted to defining structural and functional PD components [1, 2]. Access to pure PD fractions is a prerequisite to establishing the proteomic and lipidomic profiles of these membranous structures. Data collected from such approaches have

and will continue to provide valuable information on the molecular mechanisms that govern PD function.

PD are known to be refractory to simple biochemical isolation owing to their tight association with the complex cell wall matrix and to the small contribution they make to the total plant tissue mass. For a long time, commonly used subcellular fractionation approaches were based on the rigorous purification of cell wall fractions from various plant tissues. As PD are firmly lodged within the extracellular matrix, this procedure has proven to be an effective way of getting subcellular fractions enriched for PD. Although this has led to the successful identification of a number of PD proteins [3–8], the physical contribution of PD to the cell wall mass is still relatively small. Further refinement to the cell fractionation approaches originated from the work of Bernard L. Epel and his team [9, 10]. Using an enzymatic degradation of the walls, they first reported the recovery of free intact PD from plant tissues. The crucial advance was that PD-derived membranes were released from their position embedded in the wall by treatment with cellulase. Working with *Arabidopsis thaliana* suspension culture cells, the Maule group adapted the cellulase-based approach to purify PD from wall fractions. Combined with proteomic analyses, this approach has spawned the identification of an unprecedented number of proteins that show stable physical association with the PD pores [11–13]. The main difficulty in getting pure PD fractions lies in the effective disruption of cells. Differentiated plant tissues are often resistant to breakage due to the presence of secondary cell wall and lignin. *A. thaliana* suspension cells offer an attractive alternative to complex plant tissues as they comprise a friable population of relatively uniform large cells, from which clean wall fractions and therefore PD fractions can be obtained [1, 14]. The cells have abundant simple PD within division walls resembling in their basic structure the primary PD found in intact tissues. Cultured cells also represent an abundant source of biological material allowing the preparation of relatively large quantities of PD-derived membranes suitable for biochemical analysis.

The purpose of this chapter is to provide a detailed PD purification protocol that is simple and efficient. The procedure relies on the use of *A. thaliana* suspension cells as starting plant material. The first step of the purification procedure consists in isolating wall fragments containing intact PD. Cell disruption and release of organelles are achieved by N<sub>2</sub> decompression coupled to grinding steps in liquid nitrogen. Wall fragments are recovered by low-speed centrifugation. In a second step, “free” PD are released from their trapped position in the pectocellulosic matrix by using the cell wall-degrading enzyme cellulase. Subsequently, the PD are recovered by high-speed centrifugation.

## 2 Materials

Prepare all solutions with ultrapure water (sensitivity 18 M $\Omega$  at 25 °C) and analytical grade reagents. All buffers and reagents should be kept at 4 °C. For a longer conservation, buffers can be sterilized at 110 °C for 30 min before storage at 4 °C.

### 2.1 Plant Material

*A. thaliana* liquid-cultured cells (ecotype *Landsberg erecta*) should be grown in Murashige and Skoog medium containing vitamins and supplemented with 2.5  $\mu$ M  $\alpha$ -naphthalene acetic acid (NAA), 0.25  $\mu$ M kinetin, 87 mM sucrose, and 2.5 mM 2(*N*-morpholino)-ethane sulfonic acid (MES). Adjust the pH to 5.8 with 1 M KOH solution and sterilize at 110 °C for 30 min. Subculture the cells once a week (transfer 20 mL of the cultured cells into 200 mL fresh medium) under a laminar flow hood and keep on a shaker set to 220 rpm, at 24 °C, with constant light.

### 2.2 Purification of Cell Wall Fragments from *Arabidopsis thaliana* Suspension Cells

1. Cell wall preparation (CWP) buffer: 100 mM Tris-HCl, 100 mM KCl, 10 mM EDTA, 0.45 M d-mannitol, and 10 % glycerol. Adjust the pH to 8.0 with 1 M KOH. Keep the solution at 4 °C. Before use, add one tablet of EDTA-free complete protease inhibitor cocktail (Roche Diagnostic) per 50 mL of buffer.
2. Cell wall washing (CWW) buffer: 10 mM Tris-HCl, 100 mM NaCl, 10 mM EDTA, and 10 % glycerol. Adjust the pH to 8.0 with 1 M KOH. Keep the solution at 4 °C.
3. N<sub>2</sub> decompression-based cell disruption: We use a Parr Cell Disruption Device (Parr Instruments Co., Moline, Illinois, USA). The total volume of the vessel is about 900 mL; however, samples to be processed are adjusted to a volume of 50 mL. To reduce the volume capacity of the cell disruption vessel, a zinc cylinder with a hole that can contain a 50 mL Falcon tube has to be engineered by a local workshop facility (Fig. 1a).
4. Refrigerated centrifuge allowing centrifugation of 50 mL tubes at low speed in a swinging-bucket rotor.
5. 50 mL Falcon tubes
6. Pipettes (25 mL) and a pipetboy.
7. Ice and ice bucket.
8. Mortar (diameter 20 cm) and pestle.
9. N<sub>2</sub> liquid and N<sub>2</sub> liquid container.

### 2.3 Cell Wall Digestion with Cellulase

1. Digestion buffer: 10 mM 2(*N*-morpholino)-ethane sulfonic acid (MES), 240 mM d-mannitol. Adjust pH to 5.5 with 1 M KOH. Immediately before use add 1  $\mu$ M phenylmethylsulfonyl fluoride (PMSF) and complete protease inhibitor cocktail (Roche Diagnostic).

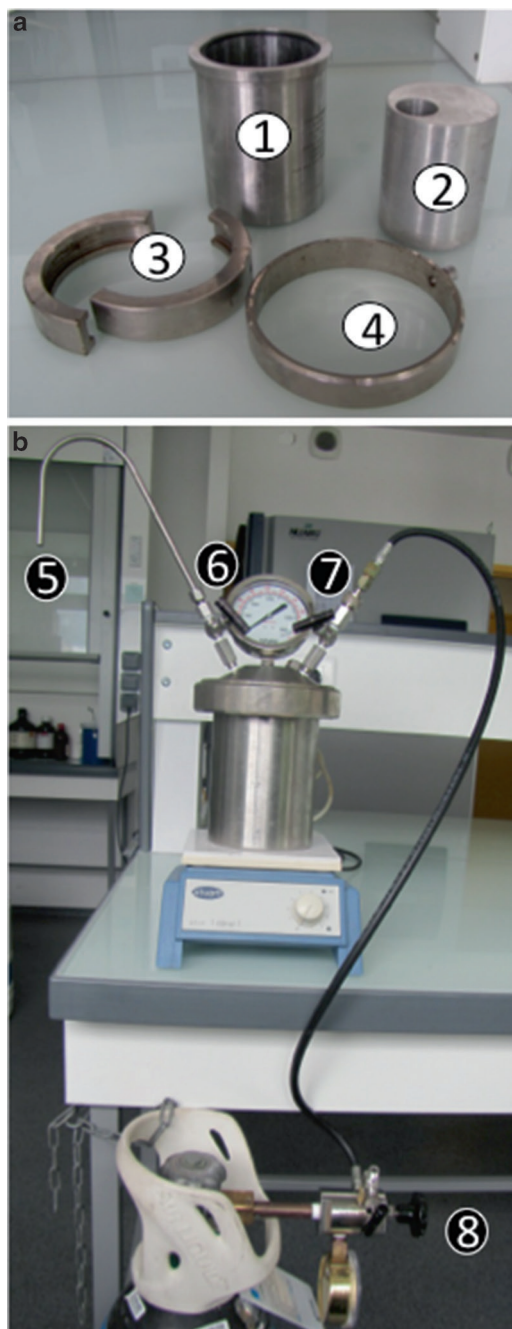


**Fig. 1** Description of the  $N_2$  decompression-based cell disruption device. (a) The parts of the disassembled cell disruption device. (b) Cell disruption device ready for use with loaded sample. (1) Vessel. (2) Zinc cylinder (that is going inside the vessel). (3) Split ring. (4) Cover ring. (5) Exit sample collection. (6) Discharging valve. (7) Charging valve. (8). Valve connecting the cell disruption vessel with the gas cylinder

2. Cellulase R10 (Karlan) (store at  $-20^{\circ}\text{C}$ ).
3. Tris-buffered saline buffer (TBS 1 $\times$ ): 20 mM Tris-HCl, 0.14 M NaCl, and 2.5 mM KCl, pH 7.4, containing 1 tablet per 25 mL complete protease inhibitor cocktail (Roche Diagnostic) added before use.
4. 50 mL Falcon tubes.
5. 20 mL syringe without needle.
6. Syringe filter (0.2  $\mu\text{m}$ ) with support membrane.
7. Water bath.
8. Orbital shaking incubator ( $37^{\circ}\text{C}$ ).
9. Refrigerated centrifuge for rotation of 30 mL Corex centrifuge tube at  $6,000\times g$ .
10. 30 mL Corex centrifuge tubes.
11. Ultraspeed refrigerated centrifuge for swinging bucket rotation of 30 mL centrifuge tubes at  $100,000\times g$ .
12. 30 mL ultracentrifugation tubes.
13. 1.5 mL microcentrifuge tubes.

## **2.4 Purity Assessment of the PD Fraction**

1. Antibodies:
  - (a) Against PD proteins PDL1 [7] and PDCB1 [6].
  - (b) Against potential contaminants; examples are BiP (ER marker) [15], Membrin 11 (Golgi marker; we used an antibody provided by A. Hocquellet, L. Maneta-Peyret, and P. Moreau, Bordeaux, France), P16 (thylakoid marker) [16], and PMA2 (PM marker) [17].
2. Protein quantification:
  - (a) Bicinchoninic acid (BCA) protein assay kit.
  - (b) 1.5 mL microcentrifuge tubes.
  - (c) Spectrophotometer.
3. SDS PAGE protein electrophoresis:
  - (a) Laemmli buffer 2 $\times$ : 4 % (w/v) sodium dodecyl sulfate (SDS), 16 % (w/w) glycerol, 20 mM Tris-HCl (pH 6.8) and 0.02 % (w/w) bromophenol blue.
  - (b) Protein electrophoresis device.
  - (c) Power supply.
  - (d) Solution for resolving gel: 10 % acrylamide/bis-acrylamide mix (37.5:1), 375 mM Tris-HCl buffer, pH 8.8, 0.5 % (w/v) SDS, 0.07 % (w/v) of ammonium persulfate, 0.06 % (v/v) *N,N,N'*-tetramethylethylenediamine (TEMED).
  - (e) Solution for stacking gel: 3 % (w/v) acrylamide-bisacrylamide mix (37.5:1), 125 mM Tris-HCl buffer, pH 7, 0.15 % ammonium persulfate, and 0.05 % TEMED.

- (f) Running buffer: 25 mM Tris-HCl, 192 mM glycine, 0.1 % SDS.
  - (g) SDS-PAGE molecular weight standards.
4. Western blot analysis.
- (a) Trans-Blot cell system.
  - (b) Transfer buffer: 25 mM Tris-HCl, 192 mM glycine, and 20 % (v/v) ethanol.
  - (c) Nitrocellulose or polyvinylidene difluoride (PVDF) membrane.
  - (d) Blotting paper.
  - (e) TBS buffer (10×): 200 mM Tris-HCl, 1.4 M NaCl, and 25 mM KCl, pH 7.4.
  - (f) Washing buffer: 1× TBS 0.1 % (v/v) Tween 20.
  - (g) Blocking buffer: 5 % (w/v) nonfat dry milk in 1× TBS.
  - (h) Secondary antibodies: Horseradish peroxidase-coupled goat anti-rabbit.
  - (i) Enhanced chemiluminescence (ECL) system for the visualization of immunodecorated proteins.

---

### 3 Methods

PD purification takes place in two main steps (Fig. 2): (1) The purification of cell wall fragments containing PD followed by (2) the enzymatic digestion of the cell wall fraction allowing the release of “free” PD. Each step (about 4–5 h of work for each) can be performed independently during different days, usually during two consecutive days. All steps should be carried out at 4 °C unless otherwise specified.

#### 3.1 Cell Wall Purification

The procedure starts with the disruption of *A. thaliana* suspension cells using a nitrogen decompression-based cell disruption device and recovery of the cell walls by low-speed centrifugation. In order to remove any trapped subcellular debris and organelles, the sample is then ground in liquid nitrogen using a mortar and pestle.

##### 3.1.1 Cell Disruption Using a N<sub>2</sub> Decompression-Based Device

1. Divide 200 mL of 5–6-day-old cultured cells (*see* **Notes 1** and **2**) into 4×50 mL Falcon tubes and centrifuge the suspension cells at 400×*g* for 5 min, at RT.
2. Meanwhile, place the cell disruption device (precooled at 4 °C) on a magnetic stirrer and open the valve connecting the disruption vessel and the gas nitrogen cylinder so that the device is ready to use (Fig. 1b).
3. Discard the supernatant by inverting the tubes and resuspend the cell pellet (about 20 mL) with an equal volume of ice-cold

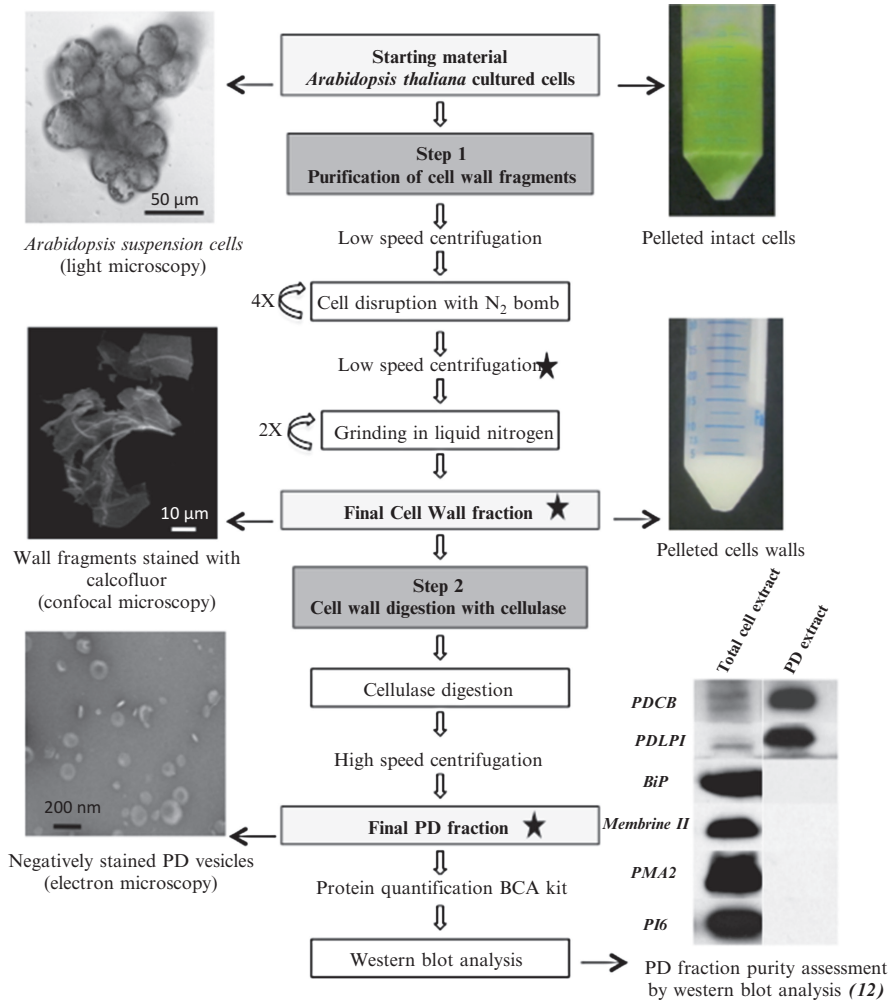


**Fig. 2** The different steps of the PD purification protocol. Stars indicate steps where the purification process can be interrupted

CWP buffer containing protease inhibitors (total volume should be around 50 mL). Place a magnet bar into the Falcon tube.

- Position the sample inside the cell disruption device; set the head on the vessel with the dip tube extending into the sample and attach the split ring cover clamp (Fig. 1a). Make sure that the magnetic bar is stirring the sample before closing (*see Note 3*). Close the discharge valve (Fig. 1b) before pressurizing the vessel to 120 bars (*see Note 4*) by opening the charging valve (Fig. 1b). When the appropriate pressure is reached, close the charging valve and wait for 3 min for the pressure to equilibrate.

5. To disrupt the cells, slowly open the releasing valve (Fig. 1b) to obtain a thin stream (*see Note 5*) and collect the disrupted cells in a 50 mL Falcon tube. Proceed until only gas is left to exit the cell disruption device (*see Note 6*). Leave the discharging valve opened until the pressure in the vessel is zero.
6. Collect an aliquot (total cell extract) for western blot analysis (Subheading 3.3). Store at  $-20^{\circ}\text{C}$ .
7. Divide the solution containing disrupted cells (about 40–50 mL) into two new 50 mL Falcon tubes and adjust the volume to 40 mL with ice-cold CWW buffer. Centrifuge the solution at  $400\times g$  for 5 min at  $4^{\circ}\text{C}$ . Cell walls will sediment while the cytosolic content stays in the supernatant.
8. Carefully remove the supernatant using 25 mL pipettes and resuspend the sedimented walls in ice-cold CWW buffer. Adjust the volume to 50 mL.
9. Repeat **steps 4–8** three more times (omit **step 6**).
10. The cell wall sediment can be stored at  $-20^{\circ}\text{C}$ .

### 3.1.2 Cell Wall Grinding in Liquid Nitrogen

1. Harvest the frozen pellet of cell walls from Subheading 3.1.1 by using a spatula. Place it in a mortar and grind the sample with a pestle in liquid  $\text{N}_2$  to a fine powder.
2. Use the spatula to load the frozen powder into a 50 mL Falcon tube and fill with ice-cold CWW buffer. Mix by vortexing.
3. Spin the suspension at  $400\times g$  for 5 min at  $4^{\circ}\text{C}$ .
4. Carefully remove the supernatant using a 25 mL pipette. Freeze the wall pellet by immersing the 50 mL tube into liquid  $\text{N}_2$ .
5. Repeat the grinding steps (**steps 1–4**) one more time.
6. Wash the wall fragments three times with excess ice-cold CWW buffer by centrifugation at  $400\times g$ , for 5 min at  $4^{\circ}\text{C}$ .
7. The final cell wall fraction can be stored at  $-20^{\circ}\text{C}$  (*see Note 7*).

### 3.2 Cell Wall Digestion Using Cellulase

1. Thaw 10 mL of the cell wall fraction from Subheading 3.1 and resuspend with excess volume of digestion buffer (without protease inhibitors). Centrifuge for 5 min at  $400\times g$  at  $4^{\circ}\text{C}$  in 50 mL Falcon tubes. Discard the supernatant and keep the 10 mL pellet on ice.
2. Dissolve the cellulase R-10 powder in 10 mL of digestion buffer at the final concentration of 1.4 % w/v.
3. Incubate the cellulase solution at  $55^{\circ}\text{C}$  for 5 min (*see Note 8*).
4. Filter the cellulase solution through a  $0.2\ \mu\text{m}$  filter (*see Note 9*).
5. Just before use, add the protease inhibitors (*see Subheading 2.3; see Note 10*) and mix 1 volume of the 1.4 % cellulase solution with 1 volume of the cell wall fraction from **step 1** (10 mL/10 mL). The final concentration of cellulase should be 0.7 %.

6. Incubate the mixture at 37 °C for 1.5 h with gentle shaking in a rotating incubator (50–100 rpm).
7. Remove undigested wall fragments by centrifugation at 5,850×*g* for 5 min at 4 °C in 30 mL Corex tubes.
8. Collect the supernatant for ultracentrifugation at 110,000×*g* for 40 min at 4 °C with a swing-out rotor.
9. Carefully discard the supernatant by inverting the tubes and resuspend the pellet, containing PD membranes, with an excess volume of cold TBS 1×.
10. Sediment the resuspended pellet again at 110,000×*g* for 40 min at 4 °C.
11. Resuspend the final pellet (the PD fraction) with 100 µL of TBS 1× containing protease inhibitors.
12. Store the PD fraction at –20 °C.

### 3.3 Quality Assessment of the PD Fraction

The purity level of the PD fraction should be determined by western blot analysis. Compared to total cell extract, the PD fraction should be enriched for PD markers while deprived for other subcellular compartments (Fig. 2; *see* **Note 11**).

1. Measure the protein concentration of the final PD fraction using a BCA Assay Kit (from 10 mL of pelleted walls you should recover approximately 100 µg of PD membrane protein equivalent; *see* **Note 12**).
2. Resuspend 1 volume of PD and total cell extract (*see* Subheading 3.1.1, **step 6**) with 1 volume of 2× Laemmli buffer and heat the samples for 30 min at 50 °C.
3. Load the same amount of proteins for each sample and separate proteins by 1D-SDS polyacrylamide gel electrophoresis. Subsequently, transfer to PVDF membranes using standard protocols.
4. Perform immunoblotting using the appropriate antisera (*see* Subheading 2.4 and **Note 11**) and visualize specific binding using standard techniques.

---

## 4 Notes

1. *Arabidopsis* cells grow in clumps of about 30–40 cells. Optimal culture condition with the appropriate hormonal balance is important for cell wall purification. In case of hormonal overdose cells divide faster, forming large clumps (liquid culture looks grainier). These clumps are more reluctant to disruption with the cell disruption device and could result in a wall fraction of insufficient quality.

2. In *Arabidopsis thaliana* suspension cells, PD are mostly present on the division walls. Cell walls are prepared from cultured cells in the middle of the linear growth phase (about 5 days after subculturing) in order to maximize the proportion of dividing walls containing PD.
3. Stirring will help to maintain cells in a uniform suspension in the N<sub>2</sub> cell disruption vessel. This will guarantee maximum cell disruption and accelerate the equilibrium step.
4. A pressure lower than 100 bars inside the vessel will reduce the efficiency of the disruption process and may lead to a contaminated cell wall fraction.
5. The actual disruption process does not take place while the cells are pressurized within the vessel. Cell disruption occurs at the instant of decompression as the sample goes from high-pressure environment to atmospheric pressure. Shearing of the cells as they pass through the discharging valve also participate in cell disruption. The valve is therefore opened gradually to leave as little space as possible for the liquid suspension cell to pass through.
6. Beware that the last 5 mL of solution may come at once and produce a splash.
7. The purity of the final cell wall fraction can be visually estimated, by looking at the color of the pelleted walls. The final pellet should be plain white and not yellowish. If it is not the case, additional grinding and washing steps may be necessary.
8. Do not exceed 5 min or the enzyme activity will diminish.
9. This step helps to remove any residual debris contained in the cellulase solution. It is recommended for electron microscopy studies.
10. It is necessary to use both PMSF and a complete inhibitor cocktail to avoid protein degradation during the incubation of the wall fragment with cellulase. PMSF is rapidly degraded upon light and water exposures. The stock solution should therefore be kept in a tube opaque to light. PMSF is very toxic and should be handled with appropriate care.
11. As PD membranes are continuous with the ER and the PM, these two compartments are likely to be a source of contamination and should therefore be tested for (using for instance PMA2 and BiP antisera; *see* Subheading 2.4). Contamination from any other subcellular compartments can also be investigated (for instance chloroplast and Golgi). Enrichment in PD membranes is monitored through the use of intrinsic PD protein markers (PDCB and PDLF; *see* Subheading 2.4).
12. The PD purification yield (assessed by protein quantification) can be affected by a decrease of the cellulase activity. This effect has been observed with the use of “old” cellulase (older than a year).

## References

1. Salmon MS, Bayer EM (2013) Dissecting plasmodesmata molecular composition by mass spectrometry-based proteomics. *Front Plant Sci* 3:307
2. Faulkner C, Maule A (2011) Opportunities and successes in the search for plasmodesmal proteins. *Protoplasma* 248:27–38
3. Sagi G, Katz A, Guenoune-Gelbart D et al (2005) Class I reversibly glycosylated polypeptides are plasmodesmal-associated proteins delivered to plasmodesmata via the golgi apparatus. *Plant Cell* 17:1788–1800
4. Lee JY, Taoka K, Yoo BC et al (2005) Plasmodesmal-associated protein kinase in tobacco and Arabidopsis recognizes a subset of non-cell-autonomous proteins. *Plant Cell* 17:2817–2831
5. Lee JY, Yoo BC, Rojas MR et al (2003) Selective trafficking of non-cell-autonomous proteins mediated by NtNCAPP1. *Science* 299:392–396
6. Simpson C, Thomas C, Findlay K et al (2009) An Arabidopsis GPI-anchor plasmodesmal neck protein with callose binding activity and potential to regulate cell-to-cell trafficking. *Plant Cell* 21:581–594
7. Thomas CL, Bayer EM, Ritzenthaler C et al (2008) Specific targeting of a plasmodesmal protein affecting cell-to-cell communication. *PLoS Biol* 6:e7
8. Jo Y, Cho WK, Rim Y et al (2011) Plasmodesmal receptor-like kinases identified through analysis of rice cell wall extracted proteins. *Protoplasma* 248:191–203
9. Levy A, Erlanger M, Rosenthal M et al (2007) A plasmodesmata-associated beta-1,3-glucanase in Arabidopsis. *Plant J* 49:669–682
10. Epel BL, Kuchuck B, Kotlizky G et al (1995) Isolation and characterization of plasmodesmata. *Methods Cell Biol* 50:237–253
11. Faulkner C, Petutschnig E, Benitez-Alfonso Y et al (2013) LYM2-dependent chitin perception limits molecular flux via plasmodesmata. *Proc Natl Acad Sci U S A* 110:9166–9170
12. Fernandez-Calvino L, Faulkner C, Walshaw J et al (2011) Arabidopsis plasmodesmal proteome. *PLoS One* 6:e18880
13. Benitez-Alfonso Y, Faulkner C, Pendle A et al (2013) Symplastic intercellular connectivity regulates lateral root patterning. *Dev Cell* 26:136–147
14. Bayer E, Thomas CL, Maule AJ (2004) Plasmodesmata in Arabidopsis thaliana suspension cells. *Protoplasma* 223:93–102
15. Hofte H, Chrispeels MJ (1992) Protein sorting to the vacuolar membrane. *Plant Cell* 4:995–1004
16. Vallon O, Wollman FA, Olive J (1986) Lateral distribution of the main protein complexes of the photosynthetic apparatus in *Chlamydomonas reinhardtii* and in spinach: an immunocytochemical study using intact thylakoid membranes and PS II enriched membrane preparation. *J Photobiophys Photobiophys* 12:203–220
17. Morsomme P, Dambly S, Maudoux O et al (1998) Single point mutations distributed in 10 soluble and membrane regions of the *Nicotiana plumbaginifolia* plasma membrane PMA2 H<sup>+</sup>-ATPase activate the enzyme and modify the structure of the C-terminal region. *J Biol Chem* 273:34837–34842



## Immunofluorescence Detection of Callose Deposition Around Plasmodesmata Sites

Ali Pendle and Yoselin Benitez-Alfonso

### Abstract

Accumulation of callose ( $\beta$ -1,3 glucans) at the plasmodesmata (PD) neck region dynamically regulates symplastic intercellular transport. Here we describe a 2–3-day immuno-labelling protocol to determine callose levels in the cell wall region at PD. The method relies on exposure of internal cell walls by hand-sectioning of the sample and digestion of the cell wall with enzymes in order to improve antibody penetration to deep tissue layers. By using this protocol, combined with high-resolution confocal imaging, we successfully detected PD-associated callose in *Arabidopsis* root apical meristem, vascular tissue, and developing lateral root primordia.

**Key words** Callose, Immuno-labelling, Immunolocalization, Cell wall, Plasmodesmata, *Arabidopsis* roots

---

### 1 Introduction

Plant cells are connected by channels embedded in the cell wall called plasmodesmata (PD). Molecular flux through these channels controls plant development and the ability of plants to respond to biotic and abiotic factors [1, 2]. The cell wall surrounding the PD dynamically regulates the size of the channel aperture, which, in turn, regulates intercellular molecular transport and turgor pressure during plant development [2–4]. These cell wall microdomains have special properties that play a role in both maintenance of channel structure and shape while allowing for modifications in PD architecture (twinning or branching) during development [5]. Not surprisingly, biochemical assays and ultrastructural characterization indicate that cell wall composition around PD varies from other cell wall regions, with an enrichment in both  $\beta$ -1,3 glucans (callose) and

in pectic polysaccharides that cross-react with antibodies raised against homogalacturonan epitopes (JIM5 and LM6) [6, 7].

Proteomic and genetic screens for PD-associated proteins led to the identification of cell wall-modifying enzymes, which were subsequently used to reveal the biological function of these specialized cell wall microdomains [8–11]. Changing the amount of callose, by altering its metabolism or regulation, leads to defects in PD transport and affects plant development and the response of plants to viral and fungal pathogens [4, 7, 10–12]. The function of pectins in PD cell wall micro-domains is less clear, but a recent study has shown that pectin methylesterases (which modify pectin esterification) co-localize to the PD and can interact with viral movement proteins to facilitate virus spreading [13].

Given that the cell wall around PD determines intercellular connectivity, methods to detect changes in cell wall composition, and especially in callose deposition, are used routinely in PD research. Two main approaches are used to directly probe for callose at PD sites: (1) staining callose with a fluorescent histochemical stain like aniline blue and (2) immuno-labelling using a commercially available antibody against callose. Both of these approaches have advantages and limitations. Staining with aniline blue is fast and inexpensive but, depending on the tissue type, certain cell wall regions may show uneven labelling and nonspecific staining can cause high background levels. Using immuno-localization techniques for callose is more sensitive and gives cleaner results when compared to aniline blue staining but tends to be more labor intensive. Immuno-labelled sections can be imaged by either electron or fluorescence microscopy. Analysis of immuno-labelled sections by electron microscopy (EM) provides greater localization accuracy and can be used to quantify the amount of callose at PD sites [11]. However the preparation techniques for EM are laborious, requiring expert technical knowledge and the preparation materials such as gold-labelled antibodies are expensive. Analysis of immuno-labelled sections using bright fluorescence probes (such as the Alexa Fluor dye series) for imaging by either confocal microscopy or one of the emerging super-resolution techniques can be faster, more cost effective, and similarly sensitive to changes in callose deposition [14].

One of the major challenges when using callose antibodies is poor tissue penetration. Treatment of the samples with cell wall-digesting enzymes using controlled conditions and/or thin sectioning of the sample can solve this issue. Both of these approaches require optimization, which is tissue dependant and very challenging at the whole-organ level. We have developed a fast immunofluorescence protocol (described here), which involves “hand shaving” of fixed plant material positioned on a multiwell microscope slide. This technique requires some practice but, in trained hands, exposure of cell walls in large regions of an organ can be accomplished. This technique overcomes the need for tissue embedding and thin

sectioning, thus allowing for fast detection and comparison of PD-associated callose in whole-tissue organs at different developmental stages. We found this method especially useful when studying processes occurring in deep tissue layers (such as vascular development or lateral root formation) where antibody penetration is usually restricted [15]. The method has been optimized for small volumes, which reduces the cost of primary and secondary antibodies. Although here we use as starting material *Arabidopsis thaliana* roots, this procedure was also successful in detecting PD callose in other plant species, such as *Medicago truncatula*. Finally, the protocol can be easily adapted for immuno-labelling of other cell wall components at PD using the appropriate antibodies.

---

## 2 Materials

### 2.1 Materials for Plant Growth and Tissue Preparation

1. Sterile square Petri dishes for plant growth media.
2. Murashige and Skoog basal salt medium without vitamins.
3. Sucrose.
4. Phytigel.
5. Bleach containing 5–10 % sodium hypochlorite.
6. Double-edge razor blades.
7. Tweezers.

### 2.2 Components for Slide Treatment and Mounting

1. Multiwell slides.
2. Decon90 cleaning agent.
3. Acetone (analytical reagent grade).
4. 3-Amino-propyl triethoxysilane (APTES).
5. Glutaraldehyde solution, grade II, 25 %.
6. Glass Coplin jars or similar.
7. Slide racks.
8. Phosphate-buffered saline (PBS) pH 7: 150 mM NaCl, 15 mM  $\text{NaH}_2\text{PO}_4$ , 15 mM  $\text{Na}_2\text{HPO}_4$ .
9. 2,2'-Thiodiethanol (TDE) solution: 97 % TDE in 3 % PBS pH 7. Store at 4 °C and protect from light.
10. Cover slips, No. 1.5.

### 2.3 Solutions for Immuno-Labelling

1. Fixative reagent: 4 % formaldehyde solution in PBS. To prepare:
  - (a) Add a measured amount of paraformaldehyde to  $\text{dH}_2\text{O}$  in a fume cupboard to obtain an 8 % (w/v) solution (*see Note 1*). Warm to approx. 60 °C on a heated stirrer and make the solution alkaline by the addition of few drops of 1 M NaOH (about ten drops/100 ml). Stir until dissolved.

- (b) Add an equal volume of 2× PBS pH 7 to obtain a final concentration of 4 % formaldehyde in PBS.
  - (c) Adjust the pH to 7 using very few drops of 10 % H<sub>2</sub>SO<sub>4</sub>; use Whatman pH 4.5–10 indicator strips for monitoring the pH level (*see Note 2*).
  - (d) Add Triton X-100 to a final concentration of 0.01 %.
2. Blocking solution: 3 % w/v bovine serum albumin (BSA) in PBS pH 7.0. Make fresh each time.
  3. Cell wall-degrading enzyme mix: 2 % pectinase (Sigma), 0.01 % pectolyase Y23 (Sigma) in PBS pH 7.0.
  4. Nuclear staining solution: 1 µg/ml 4',6-Diamidino-2-phenylindole (DAPI) in dH<sub>2</sub>O. Protect from light and store at 4 °C.

#### **2.4 Primary and Secondary Antibodies Used in This Protocol**

1. Monoclonal antibody to (1-3)-β-glucan (mouse IgG, kappa light) (Biosupplies, Australia PTY LTD).
2. Alexa Fluor® 488 Goat Anti-Mouse IgG (Invitrogen).

---

### **3 Methods**

Carry out all procedures at room temperature unless otherwise stated.

#### **3.1 Growth of Plant Material**

1. Prepare M&S media plates. Use 1× Murashige and Skoog medium supplemented with 0.5 % (w/v) phytigel and 1 % (w/v) sucrose; autoclave for 20 min at 120 °C; allow to cool to about 60 °C before adding any selection reagent and pour into square Petri dishes while still molten (*see Note 3*). Allow to cool and solidify before use.
2. Surface-sterilize *Arabidopsis thaliana* seeds with 10 % bleach for 10 min in a 1.5 ml microcentrifuge tube. Wash 3–5 times with sterile water to remove the bleach.
3. Plate out individual seeds at 2–3 mm spacing on M&S media plates, allowing space for root growth.
4. Stratify the seeds by incubating for 2 days at 4 °C (*see Note 4*).
5. Germinate and grow seedlings by placing plates vertically in a 25 °C growth chamber under constant illumination (*see Note 5*).

#### **3.2 Cleaning and Silanization of Microscope Slides**

This step is essential for the adhesion of the plant tissue to the glass surface. APTES-treated slides can be stored until use but activation with the glutaraldehyde solution must be carried out on the day of use.

1. Wash Multiwell slides in 3 % decon90 cleaning agent for 10–30 min.
2. Rinse well in dH<sub>2</sub>O and allow the slides to dry.

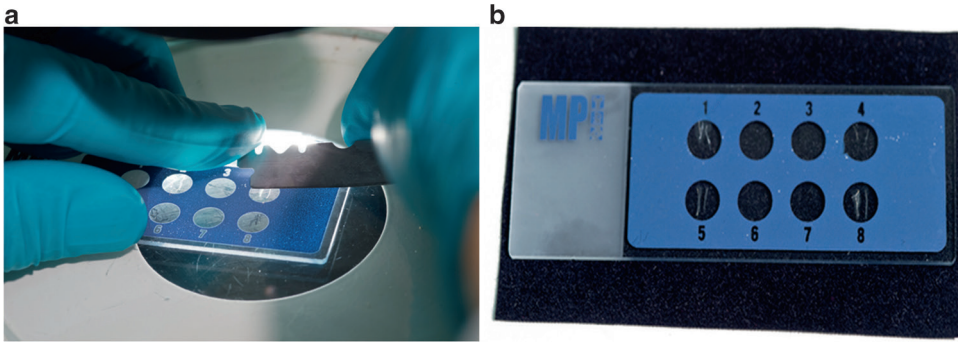


**Fig. 1** Fixed young (6 days old) *Arabidopsis* roots are hand-shaved with a razor blade under the dissecting microscope on an APTES-treated multiwell microscope slide (**a**). Root sections are allowed to dry on the slide before continuing with the following steps (**b**)

3. Prepare a fresh 2 % solution of APTES in acetone. Dip slides into the APTES solution for 10 s (*see Note 6*). Wash immediately in acetone and allow to air-dry.
4. Prepare a 2.5 % solution of glutaraldehyde in PBS pH 7 (*see Note 7*). Incubate the slides in this solution for 30 min and gently shake.
5. Remove the glutaraldehyde solution and wash thoroughly in dH<sub>2</sub>O.
6. Allow the slides to dry.

### 3.3 Fixation and Hand-Sectioning

The following procedure is also shown in Movie S1 ([see http://extras.springer.com/](http://extras.springer.com/)).

1. Place up to 20 seedlings (approx. 6 days old) in a 30 ml universal bottle containing about 20 ml of fixative reagent.
2. Vacuum infiltrate until the seedlings sink in the fixative solution in the absence of a vacuum. Normally complete infiltration is achieved in 2–3 min.
3. Incubate the seedlings in the fixative for 1 h with gentle agitation.
4. Wash the seedlings three times for 10 min each in PBS, pH 7.0.
5. Pick up an individual seedling with a pair of forceps and position the root tip and the first 3–4 mm of the root over a well of the APTES-treated multiwell slide (Fig. 1). While holding the seedling and root in place with the forceps, cut the root off at the top edge of the well with a razor blade. Lay the next 3–4 mm of the root parallel to the first portion and cut off again at the top of the well. Remove any excess liquid with a strip of filter paper.
6. Allow 30–60 s for root pieces to attach to the APTES-coated slide and to partially dry. Then, under a dissecting microscope,

using a high-quality razor blade, carefully shave off portions of the outer tissue to expose internal cell layers. This procedure will take some practice and requires a very steady hand (*see Note 8*).

7. Allow roots to dry completely on the slides for 1–2 h (*see Note 9*).

### **3.4 Cell Wall Digestion and Labelling**

1. Add a drop of the cell wall-degrading enzyme mix to each well and incubate at 37 °C for 30 min (*see Note 10*).

2. Remove the enzyme mix and wash the roots three times for 10 min each with PBS, pH 7.

3. Remove the PBS and add a drop of blocking solution. Incubate for 1 h.

4. Replace the blocking solution with blocking solution containing an appropriate dilution of primary antibody (for anti-callose we use a 1:400 dilution). Incubate overnight at 4 °C.

5. Wash the wells six times for 10 min each with PBS, pH 7.

6. Apply secondary antibody diluted in blocking solution (for Alexa Fluor® 488 anti-mouse we use 1:200). Incubate for 4 h at room temperature in light-tight boxes. From this step forward samples labeled with fluorescent conjugated antibodies should always be protected from the light.

7. Wash the wells six times for 10 min each with PBS, pH 7.

### **3.5 Counterstaining, Mounting, and Visualization of Immuno-Labelled Sections**

The sections can be counterstained with DAPI before mounting. This dye allows visualization of nuclei under UV light (fluorescence emission at 450–460 nm).

1. Cover the sections with a 1 µg/ml solution of DAPI and incubate for 30 min.

2. Wash with PBS, 2 × 10 min.

3. Remove all liquid, add 10–15 µl/well of a suitable mounting media (*see Note 11*), and cover with a glass cover slip (*see Note 12*).

4. Seal with nail varnish. Mounted slides can be stored at 4 °C in the dark.

5. Visualize the samples with a confocal microscope (*see Note 13*).

The protocol described here was successfully applied in the detection of callose at cell plates, sieve plates, and PD sites in *Arabidopsis* root meristems, differentiated vascular tissue, and non-emerged lateral root primordia (Fig. 2).

---

## **4 Notes**

1. We find it best to make fresh formaldehyde each time. Formaldehyde may cause cancer and should always be used in a fume cupboard. Weigh paraformaldehyde in the fume cupboard; wear

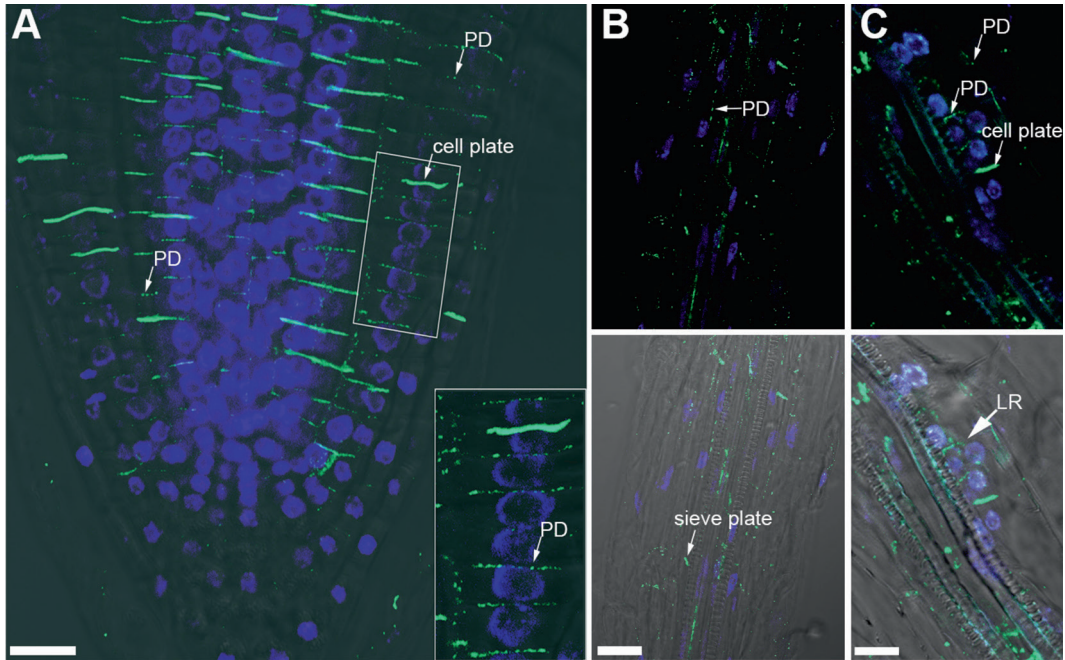


**Fig. 2** Confocal micrographs of *Arabidopsis* hand-shaved roots subjected to immunofluorescence labelling with callose antibody. Anti-mouse Alexa 488 was used as secondary (*green*) antibody and DAPI (nuclei, *blue*) was used for counterstaining. (a) Root apical meristem region showing callose accumulation in the cell plate (new cell wall formed during cell division) and at PD (punctate pattern at the cell periphery). (b) In the differentiation zone of the root the callose labelling is mainly found in the sieve plates of the vascular tissue and at PD. (c) Developing lateral root primordium showing callose deposition in the cell plate of dividing cells and at PD of nondividing walls. Lower panels in (b) and (c) show the bright-field channel superimposed. Scale bars, (a, b) 20  $\mu\text{m}$ , (c) 10  $\mu\text{m}$

appropriate safety clothing, lab coat, gloves, and eye protection. Do not allow the solution to boil as this will degrade the formaldehyde. We recommend using paraformaldehyde “prilled” rather than powder to avoid harmful dust. Paraformaldehyde dissolves best at alkaline pH; therefore make it in  $\text{H}_2\text{O}$  with a few drops of alkali (rather than in a buffer) and then add a 2 $\times$  buffer once the powder is dissolved. In this way, less acid is needed to bring the pH back to neutral. Paraformaldehyde should be kept dry at all times. It lasts longer at 4  $^{\circ}\text{C}$  than at room temperature, but should be allowed to warm to room temperature before opening the container to avoid condensation.

2. Prepare 10 % sulfuric acid solution by the careful dropwise addition of concentrated (98 %) sulfuric acid to  $\text{dH}_2\text{O}$ . To adjust the pH of the formaldehyde solution, do NOT use HCl, as reaction of formaldehyde and HCl produces the carcinogen Bis (chloromethyl) ether. Use pH strips to determine the pH rather than a pH electrode, as fixatives can degrade pH electrodes.

3. It is not possible to remelt phytigel, so allow the media to cool to a reasonable working temperature of about 60 °C before pouring the plates under sterile conditions.
4. Stratification of seeds by a cold treatment of 2 days will ensure an even germination rate.
5. By placing the plates vertically, the germinating roots will grow along the surface of the gel and can be removed easily without damage to the root structure. We use 25 °C and constant light as growth conditions to germinate our *Arabidopsis* seedlings. However, this procedure works equally well with seedlings grown at cooler temperatures with light/dark cycles. However, different conditions will need different times to reach a specific stage of seedling development.
6. Prepare the solution immediately before use. Make an appropriate volume of APTES solution depending on how many slides you wish to prepare. For a small number of slides prepare 50 ml of APTES solution in a glass Coplin jar, dip two slides at a time, then transfer to a jar containing the acetone only, and then return to a rack to air-dry. It is important to dip for just 10 s; otherwise, high backgrounds can occur during antibody labelling. Slide racks can be used to treat several slides at a time. Thus, a rack containing 25 slides can be dipped into a glass dish containing 400 ml of APTES solution, then washed in another glass dish of acetone, and then dried in the rack.
7. Use reagent-grade glutaraldehyde for treatment of slides. The solution can be reused many times, usually up to 6 months or until it begins to discolor, depending on how often it is used.
8. It is vital to use very-high-quality razor blades for this procedure. The single-edged razor blades used for many procedures are not sufficient. We use “Wilkinson Sword” double-edge razor blades which we break into half while in the protective paper sleeve, and then use one half of this being very careful to hold it so as not to cut ourselves! We use two hands to hold the razor and have best success with cutting towards ourselves with the razor edge at a shallow angle to the surface of the root. Rest one edge of the blade on the glass well to steady the blade and move the razor from the top of the well downwards shaving pieces of root epidermis as precisely as possible. It is rarely possible to shave the whole root; instead portions of the root are shaved and other pieces missed. This procedure does take some practice; thus, vary the amount of time the roots are allowed to dry before shaving as well as the angle for shaving. We manage about one in three roots shaved nicely on a good day!
9. Drying is essential for strong adherence of the tissue to the slide and it also aids penetration of antibodies into the material as the material physically “cracks open” as it dries.

10. Avoid freezing/thawing the enzyme solution. We make up a batch, aliquot it to 100  $\mu$ l, and store it at  $-20^{\circ}\text{C}$ . Typically, use about 20  $\mu$ l per well.
11. There are many mounting solutions available, but, as it is important for optimal image collection to match refractive indexes as closely as possible within your imaging setup, careful consideration of the mounting medium is critical. Ideally the refractive index of the immersion medium for the lens (we frequently use oil immersion lens), the glass cover slip, and the sample mounting medium should be the same. The mounting medium should also have good anti-fade properties and be able to limit the amount of fluorescence quenching through photo-bleaching. We have found that a solution of 97 % TDE in PBS pH 7.0 [16] meets these requirements optimally.
12. Most objectives designed for use in high-resolution biological imaging are calculated for a cover slip thickness of 170 nm (No. 1.5). For the highest quality imaging we recommend using high-precision cover slips such as Carl Zeiss high-performance cover slips, as these have a much smaller deviation from the nominal 170 nm than standard cover slips.
13. Confocal microscopy enables optical sectioning of thick samples and improves signal-to-noise ratio which reduces background fluorescence, thus improving contrast and definition of PD sites within the cell wall. We use a Zeiss LSM510 meta confocal microscope. The fluorescent dyes DAPI and Alexa 488 are excited using 405 nm and 488 nm laser lines and fluorescence emission is collected at 420–480 nm and 500–550 nm, respectively.

---

## Acknowledgments

We would like to thank Grant Calder and Prof. Peter Shaw for critical reading and editing of the manuscript and Andrew Davis for help with production of the video. Financial support for this research was provided by the UK Biotechnology and Biological Sciences Research Council (BBSRC).

## References

1. Maule AJ (2008) Plasmodesmata: structure, function and biogenesis. *Curr Opin Plant Biol* 11:680–686
2. Maule AJ, Benitez-Alfonso Y, Faulkner C (2011) Plasmodesmata - membrane tunnels with attitude. *Curr Opin Plant Biol* 14:683–690
3. Peret B, Li G, Zhao J, Band LR, Voss U, Postaire O, Luu DT, Da IO, Casimiro I, Lucas M et al (2012) Auxin regulates aquaporin function to facilitate lateral root emergence. *Nat Cell Biol* 14:991–998
4. Ruan YL, Xu SM, White R, Furbank RT (2004) Genotypic and developmental evidence for the role of plasmodesmatal regulation in cotton fiber elongation mediated by callose turnover. *Plant Physiol* 136:4104–4113

5. Burch-Smith TM, Stonebloom S, Xu M, Zambryski PC (2011) Plasmodesmata during development: re-examination of the importance of primary, secondary, and branched plasmodesmata structure versus function. *Protoplasma* 248:61–74
6. Orfila C, Knox JP (2000) Spatial regulation of pectic polysaccharides in relation to pit fields in cell walls of tomato fruit pericarp. *Plant Physiol* 122:775–781
7. Zavaliev R, Ueki S, Epel BL, Citovsky V (2011) Biology of callose (beta-1,3-glucan) turnover at plasmodesmata. *Protoplasma* 248:117–130
8. Faulkner C, Maule A (2011) Opportunities and successes in the search for plasmodesmal proteins. *Protoplasma* 248:27–38
9. Guseman JM, Lee JS, Bogenschutz NL, Peterson KM, Virata RE, Xie B, Kanaoka MM, Hong Z, Torii KU (2010) Dysregulation of cell-to-cell connectivity and stomatal patterning by loss-of-function mutation in *Arabidopsis* *chorus* (glucan synthase-like 8). *Development* 137:1731–1741
10. Levy A, Erlanger M, Rosenthal M, Epel BL (2007) A plasmodesmata-associated beta-1,3-glucanase in *Arabidopsis*. *Plant J* 49:669–682
11. Vaten A, Dettmer J, Wu S, Stierhof YD, Miyashima S, Yadav SR, Roberts CJ, Campilho A, Bulone V, Lichtenberger R et al (2011) Callose biosynthesis regulates symplastic trafficking during root development. *Dev Cell* 21:1144–1155
12. Benitez-Alfonso Y, Cilia M, San RA, Thomas C, Maule A, Hearn S, Jackson D (2009) Control of *Arabidopsis* meristem development by thioredoxin-dependent regulation of intercellular transport. *Proc Natl Acad Sci U S A* 106:3615–3620
13. Chen MH, Sheng J, Hind G, Handa AK, Citovsky V (2000) Interaction between the *Tobacco mosaic virus* movement protein and host cell pectin methylesterases is required for viral cell-to-cell movement. *EMBO J* 19: 913–920
14. Fitzgibbon J, Bell K, King E, Oparka K (2010) Super-resolution imaging of plasmodesmata using three-dimensional structured illumination microscopy. *Plant Physiol* 153: 1453–1463
15. Benitez-Alfonso Y, Faulkner C, Pendle A, Miyashima S, Helariutta Y, Maule A (2013) Symplastic intercellular connectivity regulates lateral root patterning. *Dev Cell* 26:136–147
16. Staudt T, Lang MC, Medda R, Engelhardt J, Hell SW (2007) 2,2'-thiodiethanol: a new water soluble mounting medium for high resolution optical microscopy. *Microsc Res Tech* 70:1–9

## Imaging Callose at Plasmodesmata Using Aniline Blue: Quantitative Confocal Microscopy

Raul Zavaliev and Bernard L. Epel

### Abstract

Callose ( $\beta$ -1,3-glucan) is both structural and functional component of plasmodesmata (Pd). The turnover of callose at Pd controls the cell-to-cell diffusion rate of molecules through Pd. An accurate assessment of changes in levels of Pd-associated callose has become a first-choice experimental approach in the research of intercellular communication in plants.

Here we describe a detailed and easy-to-perform procedure for imaging and quantification of Pd-associated callose using fixed plant tissue stained with aniline blue. We also introduce an automated image analysis protocol for non-biased quantification of callose levels at Pd from fluorescence images using ImageJ. Two experimental examples of Pd-callose quantification using the automated method are provided as well.

**Key words** Callose, Plasmodesmata, Aniline blue, Confocal microscopy, ImageJ

---

### 1 Introduction

Callose ( $\beta$ -1,3-glucan) is reversibly deposited at the neck region of plasmodesmata (Pd) and is involved in controlling Pd conductivity [1]. Recent works employing nondestructive high-resolution confocal microscopy have confirmed that the callose collar is a structural component of Pd in non-stressed cells [2, 3]. Aniline blue has long been employed as ultimate dye for callose staining in plant tissues [4] and has been widely used to detect callose associated with pollen tubes, microsporocytes, cell plate, phloem tissue, pathogen-associated molecular pattern (PAMP)-induced papillae, and Pd. The aniline blue interaction with the  $\beta$ -1,3-glucan induces yellow fluorescence [5, 6]. Commercial aniline blue is a heterogeneous mixture of various components, including a fluorochrome that has its excitation maximum at around 380 nm and a maximum emission at around 455 nm [5]. The callose-specific fluorochrome, sirofluor, has been isolated from aniline blue preparations [5, 7]. Fluorescence of both aniline blue and sirofluor is pH dependent

and is most efficient in highly alkaline solutions [7]. Aniline blue solution at acidic pH is used as a blue color stain for chromatin in human sperm cells [8]. In addition, acidic aniline blue can also be used as a fluorescent dye for the analysis of cellular architecture in plant embryos with 514 nm excitation and 550 nm emission maximums [9, 10].

Changes in levels of callose accumulation at Pd have significant impact on cell-to-cell diffusion of molecules in plant tissues [11]. Therefore callose staining and imaging is a valuable tool in assessing the changing callose levels at Pd and monitoring the permeability of Pd under different physiological conditions and developmental stages [12–14]. Aniline blue-based methods have been developed for efficient detection and quantification of callose in phloem tissue [15] and papillae in whole leaves [16] using confocal microscope images. However, in comparison to callose associated with these tissues, the physiological levels of callose at Pd are significantly low. Therefore, callose detection and quantification at Pd require higher resolution fluorescent images that contain high background signal. Furthermore, the presence of nonspecific fluorescence, particularly from stomata and chloroplasts, can also be a major obstacle in the subsequent image analysis.

Recent published methods in bio-image analysis provide algorithms able to combine specific image analysis functions for data extraction from fluorescent images of cells and tissues [16, 17]. These methods are specific in the kind of data they extract from images and they use the platform of commercial image analysis programs, like Volocity® and Acapella® for implementation. Most of the basic and advanced image analysis functions are available as individual open-source algorithms applied through ImageJ or Fiji platforms, which are noncommercial and publicly accessible programs that are continually updated with new tools and plug-ins, and widely used in bio-image analyses [18]. The correct use of these programs can oftentimes yield as good and satisfactory results as provided by more sophisticated commercial programs. By clearly defining the kind of specific information needed to be extracted from microscope images, one can correctly choose the appropriate function/s for the image analysis process.

A critical step in the bio-image analysis is image thresholding (segmentation). Thresholding is used to segment an image by assigning all the pixels with intensity values above a certain threshold value as foreground signal representing objects, and all the pixels below the threshold as a background signal. The foreground pixels forming the objects in the thresholded image are termed regions of interest (ROI) from which various information, such as area, pixel intensity, and circularity, can be automatically extracted. Conventional thresholding methods compute one global threshold value for all pixels using image histogram. Such *global thresholding* is not applicable in the analysis of images from aniline-blue-stained

tissue, which usually contains uneven background signal as well as large saturated objects like stomata. *Local*, or *adaptive*, thresholding methods overcome these problems by computing thresholds for each pixel in the image according to the pixel data within a user-defined radius  $r$  (in pixels) around it. An additional similar function, applied before image thresholding, is *background subtraction* in which uneven background signals are subtracted from areas defined by a user-defined radius around the brightest pixels.

We describe here a procedure for comparative callose staining and quantification at Pd in fixed plant tissue using aniline blue and confocal microscopy. Using ImageJ program we apply a series of specific image analysis functions to the microscope images for improved identification and measurement of fluorescence intensities from Pd-callose deposits. In the first phase, the analysis is performed on a randomly picked sample image from the collection of images containing both control and test groups (dataset). In this phase the optimal values are determined for radii of background and noise reduction and local thresholding, as well as for range of size and shape of the measured objects. In the second phase these optimal values are fed into a macro code developed in the ImageJ program for the automated analysis of the entire dataset. The applicability of the current image analysis procedure was shown previously [14], and is demonstrated here with two example experiments.

---

## 2 Materials

1. Plant material: The method described here has been validated with leaf tissues of *Arabidopsis thaliana*, *Nicotiana benthamiana*, and *N. tabacum*. It can also be applied for other organs and tissues, as well as other plant species. For quantification of callose levels at Pd, grow plants under controlled homogeneous conditions (light, humidity, temperature, soil/medium, etc.). Handle the plants as little as possible to avoid wounding as it will cause callose formation. Use plants at similar age, and use organs at similar developmental stage. If treatments are performed, choose correct appropriate controls.
2. Aniline blue solution: 0.01 % (w/v) aniline blue in 0.01 M  $K_3PO_4$  (pH=12) (*see Note 1*). Run the solution through a Millipore filter (0.45  $\mu m$ ) and store at room temperature (RT) in a container wrapped with aluminum foil. Freshly prepared aniline blue solution is blue/violet in color. Before use, incubate the mixture at RT for at least 48 h for complete decolorization until the solution reaches a bright yellow color (*see Note 2*).
3. 96 % ethanol.

4. Double-distilled water (DDW) with 0.01 % Tween-20.
5. Large-size (24×60 mm) microscope cover glasses.
6. Microscope wire loop.
7. Aluminum foil.
8. Parafilm.
9. Razor blades.
10. Plastic containers.
11. Glass tubes (25 ml).
12. Thin forceps.
13. Shaker.
14. Vacuum desiccator.
15. Confocal microscope equipped with a 405 nm laser for aniline blue excitation and with 475–525 or 420–480 nm band-pass emission filters for aniline blue fluorescence collection.
16. Image analysis software: For data analysis we will use the publicly available image analysis program ImageJ. Download and install ImageJ from the NIH website (<http://rsbweb.nih.gov/ij/>). Launch ImageJ, go to *Help>Update ImageJ*, and update the program into its latest version. The version 1.47a and later ones contain all functions and plug-ins required for the analysis described here.

---

### 3 Methods

#### 3.1 Tissue Staining and Sample Preparation

1. Cut the entire leaf by holding it at the petiole with forceps and submerge immediately in a plastic container containing a relatively large volume of 96 % ethanol. Take care not to touch or damage the leaf before inserting it into ethanol (*see Note 3*). Cover and seal the container with parafilm. Incubate at room temperature (RT) on a slow (30–40 rpm) shaker for 2–5 h, or until complete bleaching (*see Note 4*). To speed up the bleaching, change the ethanol after 1 h of incubation.
2. Remove the bleached leaf from ethanol while holding it by the petiole. Note that since the tissue is dehydrated it is very rigid and easily breakable. Place the leaf gently on a flat surface and cut strips of 5 mm wide using a razor blade (Fig. 1a). Be consistent in sampling the same regions of the leaf between control and test, as different regions of leaves may have different callose levels and/or respond differently to treatments.
3. Rehydrate tissue samples by placing the leaf strips into excess of DDW with 0.01 % Tween-20. Incubate at RT on a slow shaker for 1 h. Make sure that the strips do not float, but sink well into the water. Rehydration makes the subsequent dye penetration and staining more efficient and homogeneous.

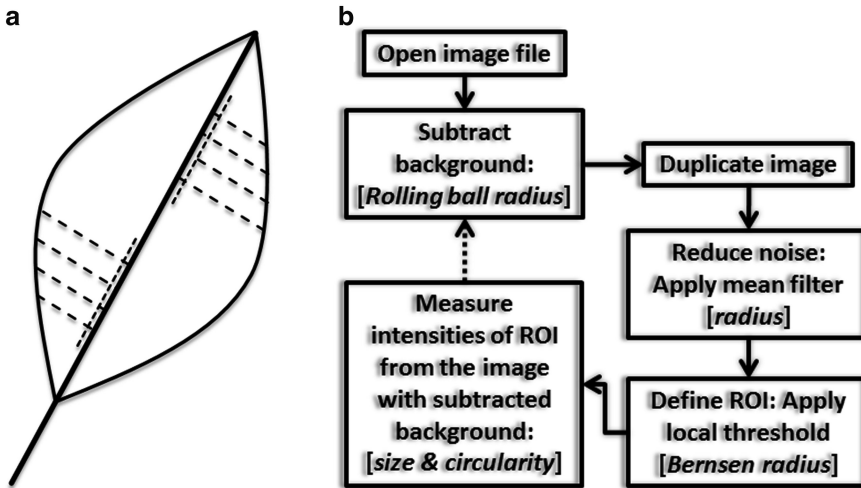


**Fig. 1** (a) A diagram of leaf exemplifying tissue sampling for in situ callose staining and quantification. *Dashed lines* show the directions of cut. (b) Image analysis workflow in the ImageJ program for detecting Pd-callose sites followed by the quantification of fluorescence intensities for those sites

- Using a wire loop, remove the strips from DDW and place in a 25 ml glass tube filled to 1/3 with aniline blue solution.
- Place the tubes in a vacuum desiccator and apply vacuum for 10 min followed by a slow release of the pressure. Good dye penetration is evident by a complete yellowing of the leaf strips.
- Wrap the tubes with aluminum foil and incubate at RT for 2 h on a 100 rpm shaker. The samples can now be used for microscopy directly from the aniline blue solution—there is no need for de-staining (*see Note 5*).

### 3.2 Confocal Microscope Settings and Data Collection

The following steps describe the image acquisition from the epidermis of leaf tissue samples stained with aniline blue.

- Begin the imaging with control samples (*see Note 6*). Place the leaf sample from aniline blue solution between the two large cover glasses. Do not use microscope slide. This way both sides of the sample can be observed by flipping the sample when needed. Use a 40× water immersion objective for observation.
- Since the tissue is transparent, the leaf side cannot be visually identified. Under transmitted light, determine the side of leaf you want to analyze. The adaxial side can easily be identified by observing the tightly packed round-shaped palisade mesophyll cells right under the epidermal layer. Flip the sample to observe the abaxial side. Always observe the same epidermis between control and test samples.
- Using transmitted light, focus on sample and position the objective at the upper-left corner of the specimen, two to three

cells away from the cut cells of the edge (*see Note 7*). Do not use the reflected light (UV) for focussing as it will bleach the observed area.

4. Build the configuration of the confocal microscope in single-track mode. Use the 405 nm diode laser for excitation and the 475–525 nm band-pass emission filter for aniline blue fluorescence (*see Note 8*). Choose white pseudo-color for aniline blue emission. Leave the channel of transmitted light switched off.
5. Set the scanning parameters as follows: frame scanning mode; frame size 1,024×1,024; scan speed 8; pixel depth 8 bit; line scanning; scan average 4; and zoom 1×.
6. Set the pinhole aperture to open state to detect as much Pd sites as possible (*see Note 9*).
7. Adjust the values of laser intensity, detector gain, amplifier offset, and amplifier gain to get the image that best shows specific Pd-related fluorescence against the background signal. Set the values such that you do not get oversaturated Pd-callose sites. Use *Profile display mode* from the image menu bar to view the histogram of pixel intensities along the line drawn over strongest Pd-callose deposits. Make sure that the peaks of intensities from brightest Pd sites do not reach saturation (255) but remain within the upper fifth section of the histogram (200–220). When adjusting the above parameters disregard the usually saturated intensities of the irrelevant objects like stomata (*see Note 10*).
8. After optimal scanning conditions for best image are found, take images with those conditions for the rest of the control and test samples. If test samples show many oversaturated Pd sites, reduce the laser intensity or amplifier gain such that you do not get oversaturation. Do the reverse with samples, in which Pd show very weak fluorescence intensity (below 200) (*see Note 11*). When taking images, use a systematic way of sampling by setting up a simple rule of sampling the area of the specimen. Stick to this rule in all your experiments. For example, after each image move the stage to the left to a defined distance, and upon reaching the end of specimen (two–three cells away from edge) move down and take images by moving to the right. Take 10–15 images per specimen (*see Note 12*).
9. The obtained raw microscope image files (\*.LSM files) are single-channel, 8-bit resolution, RGB files (with only one color channel). These files can be directly used for subsequent image analysis in ImageJ (*see Note 13*). Create a folder containing all image files you need to analyze (dataset). Because the analysis is comparative, the dataset folder must contain at least two groups of images, control and test. Name and number image files according to the experimental set (for example, “mock1,

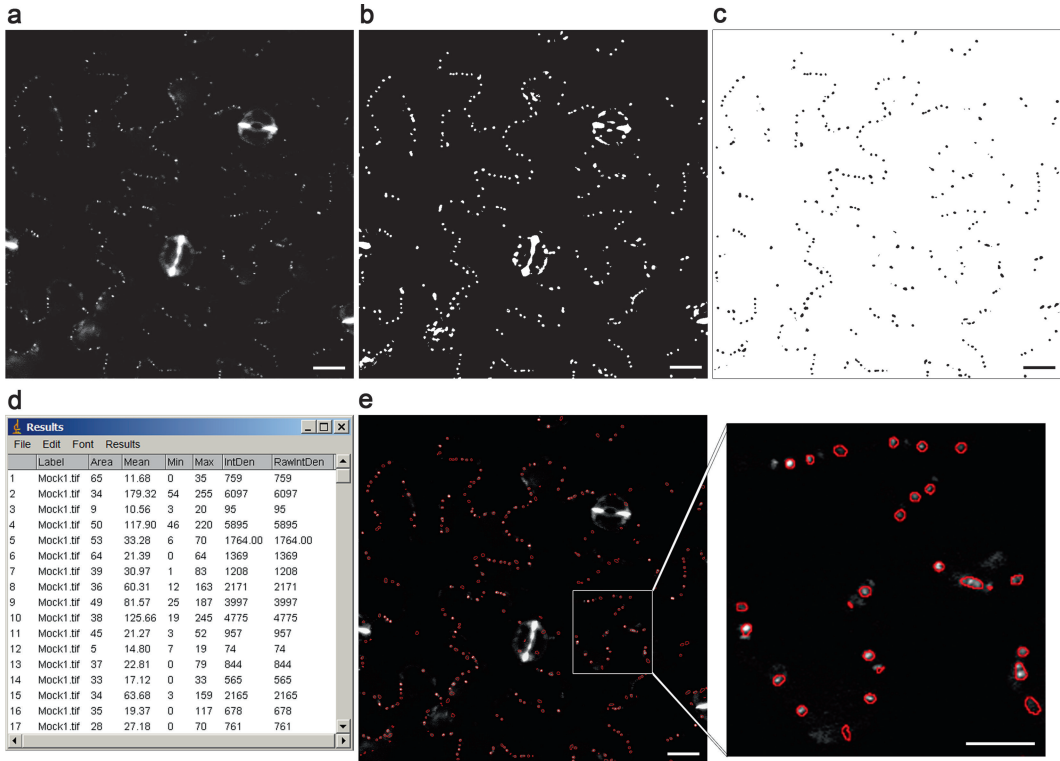


**Fig. 2** Key steps of the sample image analysis. **(a)** Original sample image is a  $1,024 \times 1,024$  size, 8-bit, single-channel image. **(b)** Masks of total ROI objects before particle analysis, created with background subtraction rolling ball radius [30]; mean filter radius [3]; auto-local threshold Bernsen radius [10]. **(c)** Masks of ROI objects (inverted image) after particle analysis with particle size [3–100 pixel<sup>2</sup>] and circularity [0.5–1]. **(d)** Results table of particle analysis (fragment). **(e)** An overlay of outlines of the analyzed ROI (red) with the original image. The *insert at left* shows the enlargement from the *marked area*. Bars: **(a)**, **(b)**, **(c)**, and **(e)** = 20  $\mu\text{m}$ ; enlargement in **(e)** = 10  $\mu\text{m}$

2, 3...” and “infection1, 2, 3...”). Make sure that the dataset folder contains no other files or file types except the image files needed for processing.

### 3.3 Data Analysis

The workflow of the image analysis for identification of sites of Pd-callose deposits and measuring the fluorescence intensities from those sites is shown in Fig. 1b. In order to determine optimal values for the parameters shown in square brackets (Fig. 1b), the analysis will first be run manually for a randomly picked sample image from a given experimental dataset. Once optimal values of parameters are determined, they will be used for batch mode analysis of the entire dataset using the ImageJ macro code developed for automated analysis of multiple images (*see below*). In the following steps we demonstrate the process of the analysis by using a dataset of images from salicylic acid (SA)-treated and mock-treated *N. benthamiana* plants. First, we demonstrate the analysis of a sample image titled *Mock1.tif* (Fig. 2a) from the dataset followed by the

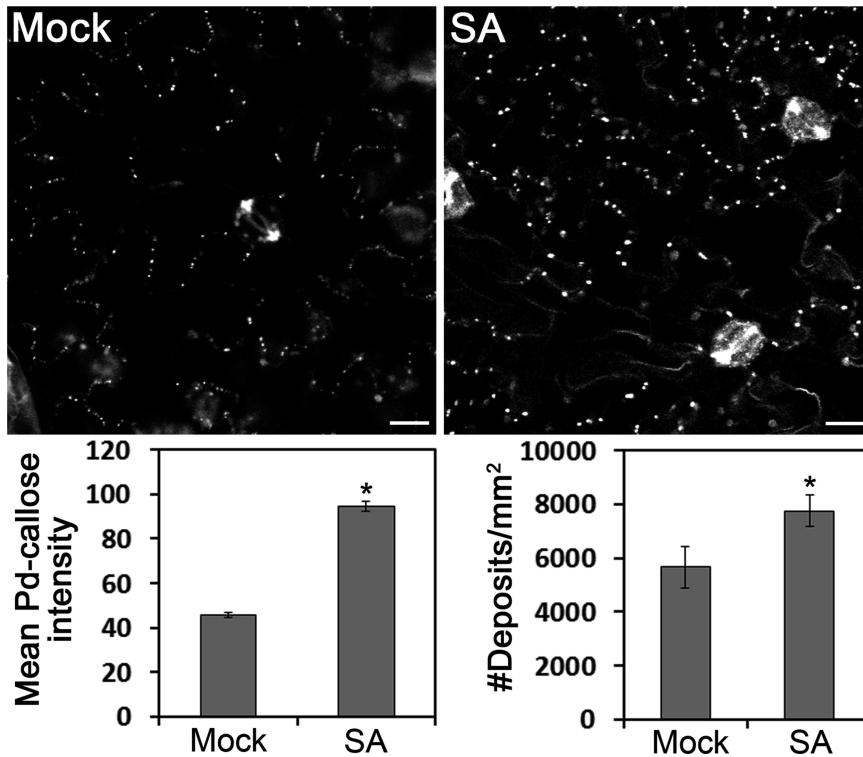


**Fig. 3** Callose levels at Pd and number of callose deposits per leaf area in *N. benthamiana* leaves sprayed either with water (mock) or 5 mM SA (SA) at 24 h after treatment. Asterisks indicate statistical significance of the mean ( $\pm$ SE) determined in independent groups *T*-test,  $P < 0.05$ . Bars = 20  $\mu$ m

automated analysis of the entire dataset. Figure 2 shows the key steps in the sample image analysis process, and Fig. 3 shows the result of automated analysis of the entire dataset.

1. Launch ImageJ program, go to *File > Open*, and open a randomly picked sample image file from the dataset folder.
2. Background subtraction: Go to *Process > Subtract Background*. In the pop-up menu enter a value for the *Rolling ball radius* (30 for our sample image). The value of rolling ball radius should always be greater than the radius of the average Pd-callose deposit (see Note 14). Check *Preview* to see the result. Make sure that all other options are unchecked and click *OK*. This modified image will be used later for measuring the intensities of Pd-callose deposits. Do not use too small values for rolling ball radius as it will subtract parts of large foreground objects, like stomata. Reducing such objects into smaller objects will increase the proportion of false positives during subsequent particle analysis.

3. Image duplication: Go to *Image>Duplicate*. A new title is automatically given for the duplicated image (*Mock1-1.tif* for our sample image). Click *OK* to agree. The duplicated image will appear and it will be now used for noise reduction and thresholding, which will define all the ROI. Leave the original image opened.
4. Noise reduction by mean filter application: Go to *Process>Filters>Mean*. In the pop-up menu enter the radius value (3 for our sample image) (*see Note 15*). Check *Preview* to see the result. Click *OK*.
5. Image thresholding: Go to *Image>Adjust>Auto Local Threshold*. In the pop-up menu choose method—"Bernsen," and enter value of radius (10 for our sample image). Leave *Parameter 1* and 2 as zero. Make sure that *White objects on black background* is checked. Click *OK*. By using *undo* command (Ctrl+Z) refine the radius of thresholding until you get fairly good representation of actual Pd-callose deposits by the recognized ROI against the background (*see Note 16*). Disregard the larger objects representing stomata (*see Note 10*). The obtained thresholded image is now binary and consists only of the ROI (both relevant and irrelevant), which appear as white (255) objects on the black (0) background (Fig. 2b).
6. Particle analysis: Before performing particle analysis, set the measurement parameters: go to *Analyze>Set Measurements*. In the pop-up menu make sure that the following options are checked: *Area*, *Min & max grey value*, *Integrated density*, *Mean grey value*, and *Display label*. In the *Redirect to* sub-menu select *Mock1.tif* (original image with the subtracted background). Click *OK*. Next, go to *Analyze>Analyze Particles*. In the pop-up menu enter the size range of ROI objects you want to analyze (3–100 pixel<sup>2</sup> for our sample image) (*see Note 14*). Set the range of circularity of the objects to 0.5–1 (*see Note 17*). In the *Show* sub-menu choose *Masks* (*see Note 18*). Check *Display results* and *Exclude on edges* (*see Note 19*). Uncheck all other options. Click *OK*. The output of this step is an inverted image (black objects on white background) of analyzed ROI masks (Fig. 2c) and a result table (Fig. 2d). In the results table you can view the number of analyzed objects and their measured parameters. Figure 2e shows the overlay of colored outlines of the analyzed ROI with the original image (*see Note 20*). This image is helpful in visually estimating the accuracy of the segmentation and particle analysis.
7. Write down the parameters (background subtraction rolling ball radius, mean filter radius, auto-local threshold Bernsen radius, particle size range, circularity range) evaluated from the sample image analysis and enter them into the macro code

provided below for batch mode analysis of the entire dataset. The following code contains the parameters from our sample image analysis (shaded) and the final result of the automated analysis of the entire dataset is shown in Fig. 3.

```
dir1=getDirectory("Get Directory");
list=getFileList(dir1);
setBatchMode(true);
for (i=0; i<list.length; i++) {
showProgress(i+1, list.length);
open(dir1+list[i]);
run("Subtract Background...", "rolling=30");
original_file_name=File.name;
duplicated_file_name = File.nameWithout
Extension+"-1";
run("Duplicate...", "title=&duplicated_file_name");
run("Mean...", "radius=3");
run("Auto Local Threshold", "method=Bernsen
radius=10 parameter_1=0 parameter_2=0 white");
setOption("BlackBackground", false);
run("Set Measurements...", "area mean min inte-
grated display redirect=[&original_file_name]
decimal=2");
run("Analyze Particles...", "size=3-100 circu-
larity=0.50-1.00 show=[Bare Outlines] dis-
play exclude");
close();}
```

8. Copy the above code (16 lines) into the clipboard and paste it into a new text file (\*.txt), and save the file in a specified directory (*see Note 21*). This macro code will serve as a generic code that can be modified by replacing the shaded values each time a new dataset is analyzed.
9. To modify and run the macro for the analysis of your dataset, launch ImageJ, and go to *Plugins>Macros>Edit*. In the pop-up menu navigate to- and open the previously saved macro code file. In the opened code replace the values of background subtraction rolling ball radius (line 7), mean filter radius (line 11), auto-local threshold Bernsen radius (line 12), particle size range, and circularity range (line 15) with those determined in your sample image analysis. Save the changes.
10. In the menu bar of the code window go to *Macros>Run Macro*. In the pop-up window navigate to the dataset folder and click *Select* (*see Note 22*). This will implement the code for

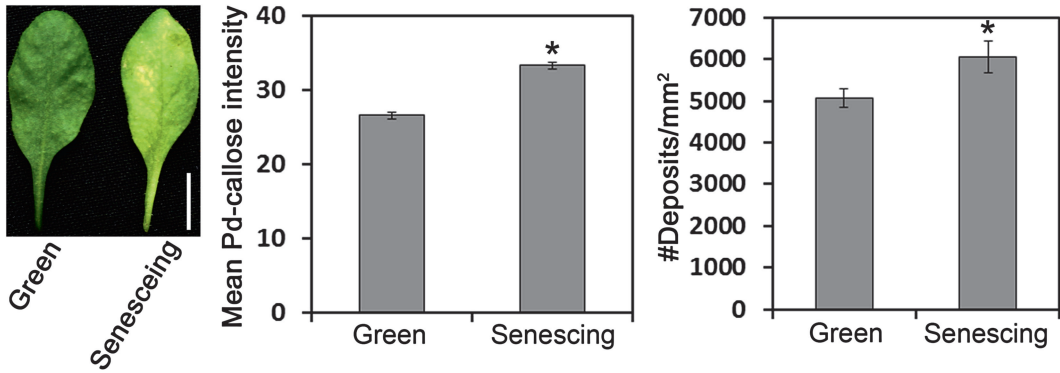


**Fig. 4** Callose levels at Pd and number of callose deposits per leaf area in green and senescing *Arabidopsis thaliana* (Col.) leaves. Asterisks indicate statistical significance of the mean ( $\pm$ SE) determined in independent groups *T*-test,  $P < 0.05$ . Bar = 1 cm

the entire dataset and output a combined result table that will contain measurements from all images of the selected dataset. Save the output results table in the Excel format.

11. In the result Excel table, the groups of control and test can easily be separated using file name (label). Use the mean grey value as the measure of the level of callose accumulation at Pd (Fig. 3). If many test groups are compared to control, present the mean intensity as percentage/fraction of control. By knowing the area of each image and the number of Pd objects per image it is possible to calculate the number of Pd-callose deposits per unit area of the leaf (Fig. 3). Group the variables and apply *t*-test statistics for independent samples (see **Note 23**). The rest of the variables—object area, min and max grey value, and integrated density (the sum of intensities within the area of the ROI)—can also be used for comparison between control and test groups.
12. An additional example of the application of the automated image analysis is shown in Fig. 4. Callose levels were determined from two kinds of *Arabidopsis* leaves—mature green leaves and leaves showing signs of senescence. Callose levels as well as the number of callose deposits were found to be higher in senescing compared to green leaves (Fig. 4).

## 4 Notes

1. Aniline blue, also called “water blue,” is commercially available from several manufacturers as a water-soluble sodium salt. In this work we use aniline blue from Sigma Aldrich (brand Fluka). Because variations between manufacturers are common, we advise to stick to one manufacturer and to the same batch of aniline blue in all your experiments.

2. The freshly prepared, blue-colored aniline blue solution will not stain callose; it must be decolorized first. Similarly, buffers with lower pH (below 8.5) used for aniline blue preparations will result in blue-colored solution that will not decolorize and thus will not be suitable for callose staining. The decolorized aniline blue solution can be stored in darkness and at RT for a long period and still can be usable; however do not use solutions older than 1 year.
3. The ethanol fixation of intact leaves, rather than leaf sections, prevents callose formation induced by subsequent handling and cutting of the leaf.
4. If large leaves or several leaves are fixed together the incubation time can be increased to overnight, or alternatively, fixation could be done at 37 °C.
5. Do not overstain the samples, as it will increase the proportion of nonspecific aniline blue fluorescence.
6. Because callose levels at Pd are quantified relative to control (wild type, mock treatment, etc.), the image acquisition should be started from control samples.
7. The cut cells and cells immediately adjacent to them usually are overstained and emit high background fluorescence compared to a more uniformly stained central area.
8. A 420–480 nm band-pass filter can also be used for aniline blue fluorescence collection. However, we noticed that aniline blue has a wide range of emission between 420 and 550 nm with higher peak at the red end, which is still specific for callose. Therefore the use of a more red-shifted filter slightly increases the fluorescence signal of aniline blue.
9. In order to collect as many Pd sites as possible use pinhole apertures between 650 and 850 (10–12 airy units). This would give a good Z-axis resolution (optical slice thickness of 7–10  $\mu\text{m}$ ) on one hand and reduce background signal on the other hand. Another way to avoid high background signal is to close pinhole and perform Z-sectioning with 7–10  $\mu\text{m}$  stack size, which would cover the thickness of the anticlinal wall, and collect maximum Pd sites.
10. Because the subsequent particle analysis is based on size and circularity range of the ROI, the large objects representing stomata and irregular amorphous objects representing background signal will be excluded from the analysis.
11. Both underexposed and overexposed images are not suitable for the subsequent image analysis. It is better to take all images (both control and test) such that intensities from brightest Pd-callose sites would be at the range of 200–220 of the histogram by adjusting the intensity of laser or amplifier gain.

The latter two parameters of the confocal microscope, unlike detector gain and amplifier offset, are roughly linear functions and therefore can be used for final data correction [19]. If adjustments have been made to laser or amplifier gain, correct the final values of mean intensity by multiplying them by the ratio of changed laser intensity or amplifier gain. For example, if control images have been taken with 10 % laser and test with 5 % laser, multiply the mean intensities measured from the test samples by factor of 2.

12. Taking too many images from the same specimen is unnecessary and erroneous. Instead, have more samples and take few images from each sample. Likewise, it is important to be consistent with the defined rules of random sampling when taking images.
13. Always use either the raw microscope images for analysis or the exported image files in formats that do not lose the pixel data (256 in 8-bit images), such as TIFF format. When exporting the single-channel images as TIFF files, make sure that the file is exported as *Raw data – single plane*. If raw data is exported as TIFF file in RGB format (three channels), it must be splitted before quantitative analysis. To split the RGB file in ImageJ, open the file and go to *Image > Color > Split Channels*. Pick the correct channel showing the relevant signal (in grayscale) and save it for further analysis. If raw microscope images are used for analysis, the ImageJ software will automatically set the scaling in  $\mu\text{m}$  rather than in pixels. To change to pixel scaling after opening the raw image file go to *Analyze > Set Scale*. In the pop-up menu click *Click to Remove Scale* and check the *Global* option to apply the pixel scaling to all subsequent files.
14. To find the approximate radius of the Pd-callose deposit in your image, first go to *Analyze > Set Measurements*. In the pop-up menu make sure that *Area* is checked. Next, using a *freehand selections* tool from the drawing control panel, circle a callose deposit on the image and click Ctrl + M (measure). In the result table, the area value (in  $\text{pixel}^2$ ) of the Pd-callose deposit will appear. Calculate the radius using area equation  $A = \pi r^2$ .
15. Mean filter is used to reduce the impact of noise during subsequent thresholding. The filter performs smoothing by replacing each pixel in the image by an average of the intensities within its neighborhood defined by the radius (in pixels). Run the filter with three different values (1–3) and compare the results. Do not use values greater than 3, as it will result in loss of the weak Pd-callose deposits.
16. Like in the case of background subtraction, the Bernsen radius should also be greater than the radius of average Pd-callose deposit. Try three values between 10 and 30 for Bernsen radius.

Keep in mind that a too small radius will over-segment the image, and a too large radius will miss many relevant ROI. Since this method of local segmentation binarizes the image pixel data (0 or 255), the thresholded image itself cannot be used for measuring the intensity values represented by the ROI. Therefore the measurements will be redirected to the original image with subtracted background.

17. The sites of Pd-callose deposits are mostly circular compared to other objects in the image, like stomata and large patches of irregular non-subtracted background. Therefore, the circularity range should always remain 0.5–1.
18. All the options of *Show* submenu are for demonstration only. Masks are chosen since it will show only those ROI that have been analyzed.
19. This will exclude the truncated Pd-callose deposits on image edges from the analysis.
20. To create color outlines of ROI go back to *Analyze>Analyze Particles* and in *Show* submenu choose *Bare Outlines* and click OK. An image with black outlines will appear. Next, invert the outline image by clicking *Edit>Invert*. Next, change the type of image to RGB color: go to *Image>Type>RGB Color*. Next, go to *Image>Adjust>Color Threshold*. In the pop-up menu select *Red* in the *Color Threshold* sub-menu, and check the *Dark background* option. An image with red outline will appear. Next, open the original image and also change its type to RGB color. To create an overlay image, select the outline image, and copy and paste into the original image. Next, go to *Edit>Paste Control*. In the pop-up menu choose *transparent zero*. Save the overlay image.
21. Copying into new file may break the lines of the macro code, which will disrupt the functioning of the macro. Make sure that in the new file the code is 16 lines and that each line ends with either of “;” or “{” or “}”.
22. The number of images that can be analyzed in the batch mode is limited only by the processing memory of ImageJ. To change the memory limit go to *Edit>Options>Memory & Threads* and change the default value of *Maximum Memory*.
23. As most biological data do not have normal distribution it is necessary first to apply the normality test of the variables before statistical analysis. If the variables do not have normal distribution, either transform the variables using log function and apply the independent samples *T*-test, or apply the nonparametric Mann–Whitney *U*-test suitable for data that do not have normal distribution.

## Acknowledgement

We thank Eran Bosis at Tel Aviv University (TAU) for editing the ImageJ macro script. This work was supported by the Israel Science Foundation grant 723/00-17.1 to BLE, and by the Manna Institute for Plant Biosciences at TAU. RZ is partially supported by the Constantiner Institute for Molecular Genetics at TAU.

## References

1. Radford JE, Vesk M, Overall RL (1998) Callose deposition at plasmodesmata. *Protoplasma* 201:30–37
2. Bell K, Oparka K (2011) Imaging plasmodesmata. *Protoplasma* 248:9–25
3. Fitzgibbon J, Bell K, King E, Oparka K (2010) Super-resolution imaging of plasmodesmata using three-dimensional structured illumination microscopy. *Plant Physiol* 153:1453–1463
4. Currier HB (1957) Callose substance in plant cells. *Am J Bot* 44:478–488
5. Smith MM, McCully ME (1978) A critical evaluation of the specificity of aniline blue induced fluorescence. *Protoplasma* 95:229–254
6. Wood PJ (1984) Specific interaction of aniline blue with (1,3)-beta-D-glucan. *Carbohydr Polym* 4:49–72
7. Stone BA, Evans NA, Bonig I, Clarke AE (1984) The application of sirofluor, a chemically defined fluorochrome from aniline blue for the histochemical detection of callose. *Protoplasma* 122:191–195
8. Sati L, Huszar G (2013) Methodology of aniline blue staining of chromatin and the assessment of the associated nuclear and cytoplasmic attributes in human sperm. *Methods Mol Biol* 927:425–436
9. Pernas M, Ryan E, Dolan L (2010) SCHIZORIZA controls tissue system complexity in plants. *Curr Biol* 20:818–823
10. Bougourd S, Marrison J, Haseloff J (2000) Technical advance: an aniline blue staining procedure for confocal microscopy and 3D imaging of normal and perturbed cellular phenotypes in mature *Arabidopsis* embryos. *Plant J* 24:543–550
11. Zavaliev R, Ueki S, Epel BL, Citovsky V (2011) Biology of callose (beta-1,3-glucan) turnover at plasmodesmata. *Protoplasma* 248:117–130
12. Benitez-Alfonso Y, Faulkner C, Pendle A et al (2013) Symplastic intercellular connectivity regulates lateral root patterning. *Dev Cell* 26:136–147
13. Wang X, Sager R, Cui W et al (2013) Salicylic acid regulates plasmodesmata closure during innate immune responses in *Arabidopsis*. *Plant Cell* 25:2315–2329
14. Zavaliev R, Levy A, Gera A, Epel BL (2013) Subcellular dynamics and role of *Arabidopsis* beta-1,3-glucanases in cell-to-cell movement of tobamoviruses. *Mol Plant Microbe Interact* 26:1016–1030
15. Furch AC, Hafke JB, Schulz A, van Bel AJ (2007) Ca<sup>2+</sup>-mediated remote control of reversible sieve tube occlusion in *Vicia faba*. *J Exp Bot* 58:2827–2838
16. Zhou J, Spallek T, Faulkner C, Robatzek S (2012) CalloseMeasurer: a novel software solution to measure callose deposition and recognize spreading callose patterns. *Plant Methods* 8:49
17. Fitzgibbon J, Beck M, Zhou J et al (2013) A developmental framework for complex plasmodesmata formation revealed by large-scale imaging of the *Arabidopsis* leaf epidermis. *Plant Cell* 25:57–70
18. Hartig SM (2013) Basic image analysis and manipulation in ImageJ. *Curr Protoc Mol Biol* Chapter 14, Unit 14.15
19. Liarzi O, Epel BL (2005) Development of a quantitative tool for measuring changes in the coefficient of conductivity of plasmodesmata induced by developmental, biotic, and abiotic signals. *Protoplasma* 225:67–76



## Localization of Fluorescently Tagged Protein to Plasmodesmata by Correlative Light and Electron Microscopy

Shannon Modla, Jeffrey L. Caplan, Kirk J. Czymmek, and Jung-Youn Lee

### Abstract

Plasmodesmata (PD) are intercellular communication channels that form long, membrane-lined cylinders across cellular junctions. A fluorescent-tagging approach is most commonly used for an initial assessment to address whether a protein of interest may localize or associate with PD domain. However, owing to the dimension of PD being at nanoscale, PD-associated fluorescent signals are detected only as small spots scattered at the cell periphery, hence requiring additional confirmatory evidence. Immunogold labeling provides such information, but suitable antibodies are not always available and morphological preservation is often compromised with this approach. Here we describe an alternative approach using a correlative light and electron microscopy (CLEM) technique, which combines fluorescent imaging and transmission electron microscopy. By employing this method, a clear correlation between fluorescent speckles and the presence of individual or clusters of PD is achieved.

**Key words** Correlative microscopy, Plasmodesmata, Fluorescent fusion proteins, Transmission electron microscopy, Confocal microscopy

---

### 1 Introduction

Plasmodesmata (PD) form thin membranous strips embedded in the cell wall. A single plasmodesmal channel, which is approximately 60 nm wide, is constituted by a cytoplasmic sleeve between endoplasmic reticulum (ER) membrane and plasma membrane (PM) as inner and external linings, respectively [1]. Many proteins are suggested to localize or associate with PD on the basis of fluorescent protein-tagging. However, only a few cases are confirmed to be bona fide PD-localized proteins by employing immunogold labeling studies [2–6]. Although the latter method provides direct evidence at the ultrastructural level, often the data inherently suffer from poor morphological resolution of PD. Moreover, antibodies

that are suitable for immunogold labeling of each candidate protein are not readily available.

In a recent study, we demonstrated PD localization of a fluorescently tagged protein using three independent approaches, i.e., colocalization with a known PD marker, immunogold labeling, and correlative light and electron microscopy (CLEM) [3]. CLEM provides a comprehensive view of a biological sample through the use of multiple imaging modalities but has been mainly applied to non-plant samples [7]. Confocal microscopy allows for a collection of large volumes of spatial, temporal, and chemical information from living or fixed samples, but the data are restricted to approximately 0.2  $\mu\text{m}$  lateral resolution. In contrast, while transmission electron microscopy (TEM) provides ultrastructural details at a much higher resolution, only a very small fraction of fixed, static specimens can be examined. And hence, TEM analysis becomes highly tedious when a cellular overview of small and rare structures, including PD, is desired. By combining these two microscopy platforms for imaging the same sample, CLEM complements their limitations and offers the advantages of both imaging systems.

Several correlative techniques have been developed to localize specific substructures by utilizing probe-based systems that can be visualized with both the light and electron microscopes. Examples of such bifunctional markers include quantum dots [8], HRP-conjugated antibodies [9], FluoroNanogold<sup>TM</sup> [10], and photooxidation of diaminobenzidine (DAB) [11]. However, with these methods, ultrastructure is often compromised in order to preserve antigenicity or to generate a reaction product. Moreover, the suitability of these methods to plant samples is limited or yet unknown. Other recent and promising probes developed for mammalian cell systems use genetically engineered plant-derived proteins such as mini Singlet Oxygen Generator (miniSOG) [12] and APEX [13] that in the presence of DAB produce a highly localized, osmium tetroxide-reactive, electron-dense precipitate. The engineered ascorbate peroxidase, APEX, is of particular note because it is compatible with osmium tetroxide fixation (which improves the preservation of cellular morphology) and does not require light to form the reaction product, making it potentially well suited for thick plant tissues. As protocols for focused ion beam scanning electron microscopy (FIB-SEM) [14], other forms of serial block-face imaging [15], and array tomography [16] become more broadly available, these approaches in conjunction with protein labeling techniques such as APEX may even allow for 3-dimensional CLEM studies.

Here, we present a CLEM approach that was used to correlate punctate fluorescent signals produced by a green fluorescent protein (GFP)-tagged PD protein with the presence of PD structures in *Arabidopsis* seedlings [3]. One clear benefit of applying CLEM technique for studying PD association of a protein is that

one can easily select any specific fluorescent signal produced by the fluorescently tagged protein of interest and examine whether the corresponding ultrastructure is indeed PD or not. Using this approach, unambiguous correlations between single or grouped fluorescent spots with individual or clusters of PD (or pit-field) along clonal or nonclonal walls of any cell type are achievable. The CLEM technique described here is designed to allow fluorescent signals within thick (40  $\mu\text{m}$ ) tissue sections to be first mapped by laser scanning confocal microscopy (LSCM) and then subsequently targeted and imaged by TEM [17]. In this way, the highly specific regions containing fluorescently tagged proteins are imaged at high resolution by EM, without requiring the use of electron-dense markers and risking the potential loss of ultrastructural integrity. Briefly, transgenic *Arabidopsis* seedlings that express GFP-tagged PD-Located Protein 5 (PDL5) [3] are first sucrose protected and then sectioned on a cryostat into manageable segments that are mapped by LSCM. Subsequently, the marked target sections are processed for TEM analysis and embedded in resin. Ultrathin serial sections of the resin block are prepared and imaged by TEM. Acquired TEM images are aligned and overlaid with LSCM images using suitable image software (Fig. 1).

---

## 2 Materials

### 2.1 Plant Material

1. Transgenic GFP-PDL5 *Arabidopsis* seedlings grown vertically on 1 % agar plates containing 0.5 $\times$  Murashige Skoog medium [18] for 5 days.

### 2.2 Cryostat Sectioning

Prepare all solutions fresh. All tissue fixation procedures should be performed in a fume hood while wearing safety glasses, lab coat, and gloves.

1. Primary fixative: 4 % paraformaldehyde and 0.1 % glutaraldehyde in 0.15 M Sorensen's phosphate buffer (SPB), pH 7.2 (*see Note 1*). To make 20 mL of primary fixative, combine 5 mL 16 % EM grade paraformaldehyde, 0.25 mL 8 % EM grade glutaraldehyde, and 14.75 mL 0.2 M Sorensen's phosphate buffer pH 7.2. SP wash buffer: 0.1 M SPB, pH 7.2.
2. Cryo-protectant: 2.3 M sucrose in 0.1 M SPB, pH 7.2. To make 100 mL of cryo-protectant, weigh 78.7 g sucrose and fill the volume to 100 mL with 0.1 M SPB, pH 7.2. Mix on a stir plate until sucrose has completely dissolved.
3. Tissue freezing medium, TFM<sup>TM</sup> or Tissue-Tek<sup>®</sup> O.C.T. Compound (*see Note 2*).
4. Disposable base molds.
5. Cryostat equipped with a CryoJane<sup>®</sup> Tape-Transfer System (Leica Microsystems, Buffalo Grove, IL).

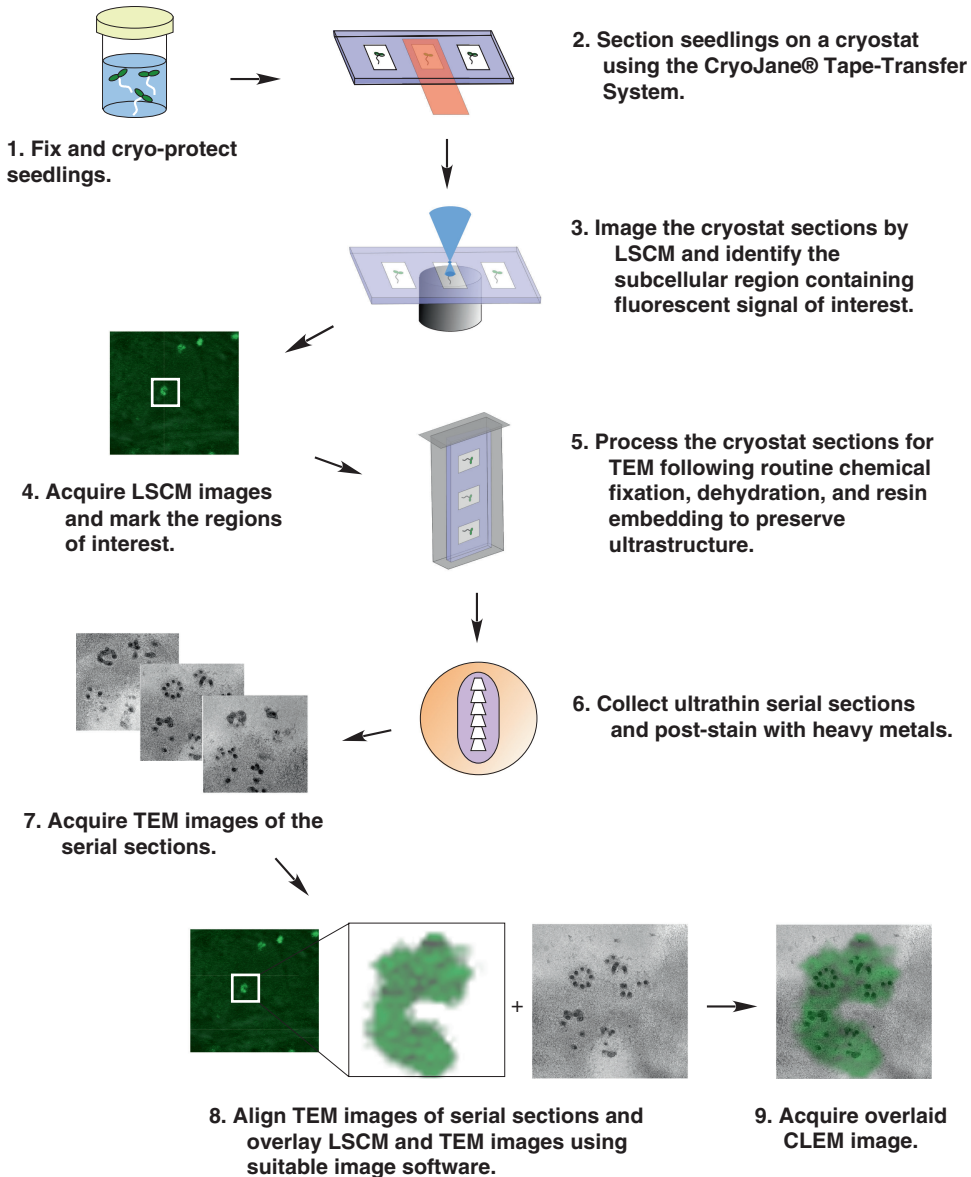


**Fig. 1** Major steps of the CLEM procedure

6. CryoJane® supplies: Adhesive tape windows, hand roller, and 1× adhesive Permanox™ slides (*see Note 3*).
7. Dissecting microscope. We use a Zeiss M<sup>2</sup>BIO dissecting microscope.

### 2.3 Laser Scanning Confocal Microscopy (LSCM)

1. *SlowFade*® Gold antifade reagent.
2. Rectangular coverslips, 20×40 mm, No. 1.5.
3. Laser scanning confocal microscope equipped with a 488 nm excitation laser and appropriate filter sets for imaging green fluorescent protein (GFP) fluorescence.

## **2.4 Processing Samples for Transmission Electron Microscopy (TEM)**

Prepare all solutions fresh. All tissue fixation procedures should be performed in a fume hood while wearing safety glasses, lab coat, and gloves.

1. Secondary fixative: 2 % paraformaldehyde and 2 % glutaraldehyde in 0.1 M sodium cacodylate buffer (SCB), pH 7.4. To prepare 20 mL of secondary fixative combine 5 mL 8 % EM grade glutaraldehyde, 2.5 mL 16 % EM grade paraformaldehyde, 10 mL 0.2 M sodium cacodylate buffer pH 7.4, and 2.5 mL deionized distilled water.
2. SC wash buffer: 0.1 M SCB, pH 7.4.
3. Tertiary fixative: 1 % osmium tetroxide in 0.1 M SCB, pH 7.4.
4. 100 % Ethanol (200 proof), anhydrous.
5. EMbed-812 resin, hard formulation without accelerator: Weigh 20 g EMbed 812, 9 g dodecenylsuccinic anhydride (DDSA), and 12 g nadic methyl anhydride (NMA) into a disposable specimen cup and mix on a stir plate with a magnetic stir bar for 10 min.
6. EMbed-812 resin, hard formulation with accelerator: Weigh 20 g EMbed 812, 9 g DDSA, 12 g NMA, and 0.7 g 2,4,6-[Tri (Dimethylaminoethylphenol)] (DMP-30) into a disposable specimen cup and mix on a stir plate with a magnetic stir bar for 10 min.
7. Slide duplicating mold.
8. Embedding oven.

## **2.5 Ultramicrotomy and Staining of Sections**

1. Jeweler's saw.
2. Cyanoacrylate glue (super glue).
3. Liquid nitrogen.
4. Resin blocks formed by polymerizing resin in polyethylene embedding capsules with a pyramid tip or flat bottom embedding capsules (*see Note 4*).
5. Ultramicrotome.
6. Diamond knife for ultrathin sections.
7. 2 × 1 slot grids.
8. Heat pen for flattening sections.
9. Methanolic uranyl acetate and Reynolds' lead citrate.

---

## **3 Methods**

See the schematic in Fig. 1 for an illustrative overview of the CLEM procedure.

### 3.1 Cryostat Sectioning

During the initial fixation and cryo-protection steps of the seedlings, it is necessary to protect the seedlings from light to prevent loss of GFP fluorescence.

1. Fix transgenic GFP-PDLP5 *Arabidopsis* seedlings overnight at 4 °C in primary fixative (*see Note 1*).
2. Wash seedlings 2 × 15 min each with SP wash buffer.
3. Infiltrate seedlings with an ascending series of cryo-protectant: SPB (1:3, 1:2, 1:1, 2:1, 3:1), 1 h each, and then with 100 % cryo-protectant for 1 h on a rotator at room temperature.
4. Infiltrate overnight in a fresh exchange of 100 % cryo-protectant at 4 °C.
5. Remove excess sucrose from the seedlings and place them into disposable base molds containing Tissue Freezing Medium or Tissue-Tek® O.C.T. Compound. Position them in desired orientation, and freeze seedlings with a chamber and object temperature set to -30 °C (*see Note 5*).
6. Mount the block on the sample mount in the cryostat with Tissue Freezing Medium or Tissue-Tek® O.C.T. Compound, and trim the block with a razor blade to remove excess Tissue Freezing Medium or Tissue-Tek® O.C.T. Compound.
7. Collect 40 µm thick sections onto adhesive tape windows using the hand roller at a chamber and object temperature of -30 °C.
8. Affix sections to adhesive-coated Permanox® slides using the hand roller, flash slides with UV light using the CryoJane® Tape-Transfer System, and carefully remove the adhesive tape window from the slide.
9. Store slides in SP wash buffer, protected from light.
10. Slides can be briefly screened with a dissecting microscope to determine if sections were collected from appropriate locations within the plant tissue before proceeding to LSCM.

### 3.2 Laser Scanning Confocal Microscopy (LSCM)

1. Mount sections in *SlowFade* Gold® using a 20 × 40 mm rectangular coverslip, No. 1.5 (*see Note 6*).
2. Image sections on a laser scanning confocal microscope configured for the detection of GFP fluorescence and transmitted light using a 40× C-Apochromat NA 1.2 water objective lens. Identify a cell of interest and acquire a Z-stack of images (Fig. 2a, e, i). Cells located closest to the coverslip will be easier to target for ultramicrotomy as less excess tissue will need to be removed before reaching the region of interest. Then acquire a tile scan that encompasses a large area of the tissue section (Fig. 3a). Acquiring images at intermediate magnifications between those used for the tile scan and Z-stack may be necessary depending on the size and type of tissue. The tile scan and additional images will provide an overview of the tissue and

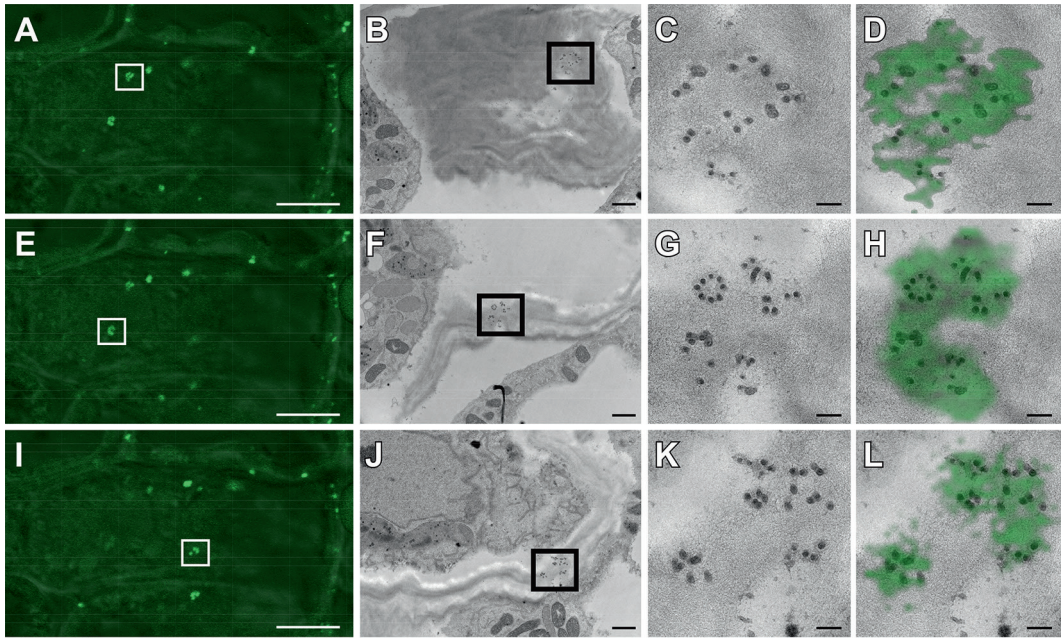


**Fig. 2** Confocal and TEM images correlating fluorescent signals produced by PDL5-GFP with PD pit fields across nonclonal cells in transgenic *Arabidopsis* hypocotyl. (a, e and i) Confocal Z-stack images showing fluorescent PD pit fields in a cell within a cryostat section collected from PDL5:GFP-expressing *Arabidopsis* hypocotyl. The *boxed areas* contain PD pit fields that were targeted for TEM. Scale bars in (a), (e), and (i), 10  $\mu\text{m}$ . (b, f, and j) Low magnification TEM images of the same PD pit fields *boxed* in (a), (e), and (i), respectively. Scale bars in (b), (f), and (j), 1  $\mu\text{m}$ . (c, g, and k) High magnification TEM images of the PD pit fields depicted in the *boxed* regions in (b), (f), and (j), respectively. Scale bars in (c), (g), and (k), 0.2  $\mu\text{m}$ . (d, h, and l) Overlay of the fluorescent confocal signal (a, e, and i) onto the TEM micrographs (c, g, and k) showing the close correspondence between the GFP signal of the PD marker (PDL5:GFP) and the arrangement of PD within the pit fields. Scale bars in (d), (h), and (l), 0.2  $\mu\text{m}$

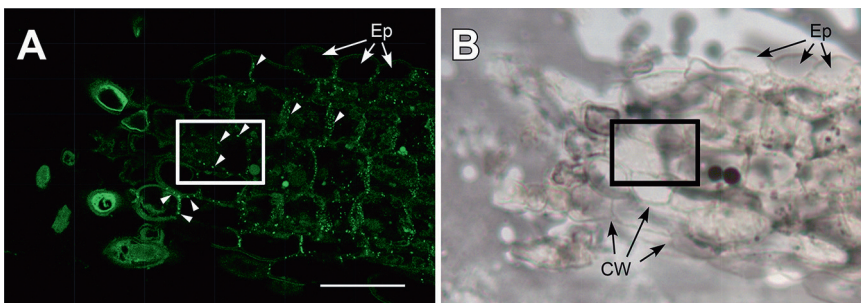


**Fig. 3** Confocal and transmitted light images of a tissue block before and after resin embedding and trimming. (a) A confocal tile scan showing an overview of the GFP signal within the cryostat tissue section that was targeted for ultrathin sectioning and TEM. Darts, PD labeled by PDL5-GFP. Note the punctate signals appear only at the intercellular cell wall (CW) junctions. Scale bar, 25  $\mu\text{m}$ . (b) Image of the resin block face showing the same tissue as in (a) but after being processed for TEM and trimmed in preparation of ultramicrotomy. Note the close correlation between the locations of epidermal cells Ep in (a) and (b), which helps to pinpoint the position of the cell of interest identified by LSCM in the resin-embedded tissue (*boxes*). The splotchy background pattern in (b) that interferes with clarity of the plant tissue is due to the transfer of adhesive from the Permanox<sup>®</sup> slide to the resin-embedded cryostat sections

allow unique landmarks to be selected for the re-identification of the cell from which the Z-stack was obtained once the section has been further processed for ultramicrotomy. If there are multiple sections on a single slide, be sure to note which section was imaged for correlative microscopy.

### **3.3 Processing the Cryostat Sections for Transmission Electron Microscopy (TEM)**

All steps should be carried out at room temperature unless otherwise noted. At this point, it is not necessary to protect the sample from light.

1. Gently remove the coverslip from the slide by floating it off in a petri dish containing SP wash buffer (*see Note 7*).
2. Fix the cryostat sections overnight at 4 °C in secondary fixative (*see Note 8*).
3. Wash with SCB for 3 × 15 min each.
4. Fix with tertiary fixative for 2 h.
5. Wash with SCB for 2 × 15 min each.
6. Wash with deionized distilled water for 2 × 15 min each.
7. Dehydrate the cryostat sections in an ascending ethanol series (25, 50, 75, 95 %; each for 15 min). Store samples in 95 % ethanol overnight at 4 °C.
8. Allow the cryostat sections to warm to room temperature, and dehydrate them in 100 % anhydrous ethanol for 2 × 15 min each.
9. Infiltrate with EMBED-812 resin (hard formulation without accelerator): 100 % anhydrous ethanol (1:3, 1:2, 1:1, 2:1, 3:1, for 1 h each).
10. Infiltrate with 100 % EMBED-812 (hard formulation without accelerator) for 1 h.
11. Infiltrate with 100 % EMBED-812 (hard formulation with accelerator) for 1 h followed by a fresh exchange of 100 % EMBED-812 (hard formulation with accelerator) overnight.
12. On the next day, infiltrate with another fresh exchange of 100 % EMBED-812 (hard formulation with accelerator) for 1 h.
13. Embed the Permanox® slide using a slide duplicating mold. First, dispense resin into the mold and then float the Permanox® slide, with the side containing the cryostat section facing down, on top of the resin in the slide duplicating mold. Polymerize at 60 °C for 48 h.

### **3.4 Sectioning the Embedded Cryostat Section by Ultramicrotomy and Staining Ultrathin Sections with Heavy Metals**

1. After polymerization of the resin, remove the Permanox® slide from the mold, and immerse the slide into liquid nitrogen. The layer of resin contained by the slide-duplicating mold, including the embedded cryostat sections, should then separate from the slide. Identify the specific section within the layer of resin that was imaged by LSCM, excise it from the resin using a jeweler's saw, and attach it using a cyanoacrylate glue to the flat

end of a resin block, which was created by polymerizing resin in a polyethylene embedding capsule (*see* **Notes 4 and 9**).

2. Trim the resin-embedded cryostat section with a razor blade to encompass the region imaged by LSCM. Use a glass knife to cut sections off the surface of the resin-embedded cryostat section to a depth just above the region of interest (*see* **Note 10**). Once a final trapezoid is made, it is useful to image the surface of the resin-embedded cryostat section with a dissecting microscope and overlay it with the overview image acquired by LSCM using imaging software (Fig. 3b). In this way, the cell previously imaged by LSCM can be re-identified.
3. Use an ultramicrotome equipped with a diamond knife to cut serial ultrathin (60–70 nm thick) sections. Collect enough serial sections until you are confident that you have sectioned through the same volume of tissue that contained the region of interest identified in the confocal Z-stack. Flatten the sections with a heat pen and collect ribbons onto 2 × 1 slot grids (*see* **Note 11**).
4. Stain the sections with methanolic uranyl acetate and Reynolds' lead citrate to provide contrast (*see* **Note 12**). Allow grids to air dry.

### **3.5 TEM Imaging and Image Analysis**

1. Pre-irradiate grids under low TEM magnification to help stabilize the ultrathin sections and to minimize the formation of burn marks at high magnification.
2. Under low TEM magnification, identify the cell of interest (*see* **Note 13**). Multiple grids may need to be examined before the section containing the cell previously imaged by LSCM is identified. Initially, it is useful to examine every third grid or so until the tissue region containing the cell of interest is found.
3. Once the tissue region of interest is found, image successive serial sections by TEM at high magnification (Fig. 4).
4. Optional: Once TEM data have been acquired, serial sections can be aligned using a program such as Reconstruct [19]. Since cell walls are never perfectly flat, multiple PD pit fields appearing within the region of interest mapped by LSCM will never come into view within a single ultrathin section. Therefore, aligning the serial sections will allow one to visualize multiple PD pit fields along the entirety of the cell wall. The positions of multiple PD pit fields relative to one another in addition to unique landmarks within the tissue itself (cell wall shape, etc.) allow PD pit fields imaged by TEM to be matched with the specific fluorescent signals (GFP-fused PDLp5 as PD marker) obtained by LSCM. The close correlation between confocal and TEM images can also be displayed by overlaying the fluorescent signal from confocal images onto corresponding TEM micrographs using Adobe Photoshop (*see* Fig. 2).

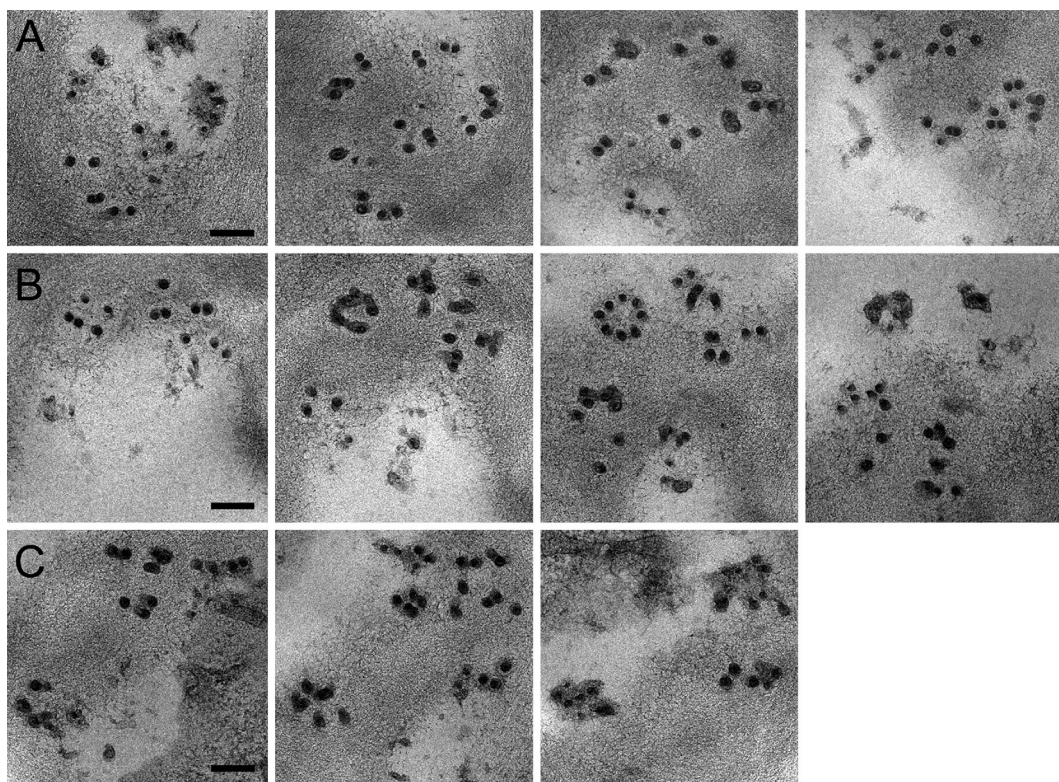


**Fig. 4** TEM of ultrathin serial sections of the PD pit fields captured in Fig. 2. Serial sections in rows (a), (b), and (c) correspond to PD pit fields in Fig. 2a–d, e–h, and i–l, respectively. Scale bars 0.2  $\mu\text{m}$

Briefly, the magic wand tool is used to select the GFP signal from the confocal images, which is then copied and pasted onto the corresponding TEM micrograph. The opacity of the layer corresponding to the fluorescent signal is reduced so that both the fluorescence and TEM ultrastructure can be visualized simultaneously. The free transform tool is then used to align the fluorescent signal with the ultrastructure.

## 4 Notes

1. The primary fixative and buffer must preserve tissue ultrastructure while maintaining the fluorescence of the specific fluorescent fusion protein of interest. The concentration of the fixative, type of fixative and buffer, and duration of fixation may need to be modified according to the tissue and fluorescent fusion protein under study. Sorensen's phosphate buffer (SPB) was prepared by mixing  $\text{NaH}_2\text{PO}_4$  and  $\text{Na}_2\text{HPO}_4$  stock solutions to desired final concentration and pH.
2. Tissue Freezing Medium, TFM<sup>TM</sup>, and Tissue-Tek<sup>®</sup> O.C.T. Compound are commercially available products consisting of

water-soluble glycols that provide a supportive embedding matrix around the tissue for cryostat sectioning. The tissue is placed in an embedding mold, surrounded by the embedding matrix, and then placed in the cryostat chamber, frozen, and sectioned.

3. Adhesive Permanox® slides were custom ordered from Instrumedics. Currently the CryoJane® tape-transfer system is owned by Leica Microsystems, and they do not provide custom coating services. As an alternative, slides can be coated by ordering a pretreatment solution (Solution A) and an Instrumedics Slide Adhesive (Solution B) from Leica Biosystems, Richmond, IL. In our experience, we have had the most success with coating Permanox® slides by omitting the pretreatment with Solution A and simply treating slides with Solution B. The glass adhesive slides (1× or 4× coating; Leica Biosystems, Richmond, IL or Electron Microscopy Sciences, Hatfield, PA) can also be used, but care must be taken to separate the resin from the glass prior to sectioning. This can be accomplished by heating the glass slide on a hot plate set to 60 °C for several minutes until the resin is soft and then carefully using a razor blade to excise the embedded tissue and separate it from the underlying glass slide, or an approach similar to that described in [20] can be used. Separating the resin from a glass slide is more difficult than using Permanox® and is more prone to complications.
4. A flat surface to affix embedded tissues can be easily generated by polymerizing EMBed-812 resin in polyethylene embedding capsules, which have a pyramidal tip at one end and flat end provided by the closed cap. First, cut off the pointed tip of the capsule using a single-edged razor blade, close the cap of the capsule, fill with resin, and allow the resin to polymerize at 60 °C for 24 h. Once the resin has been removed from the capsule, the resin that was against the cap provides a flat surface for gluing specimens.
5. For long-term storage of samples, frozen blocks can be placed in a Ziploc® bag containing a damp paper towel and frozen at -80 °C.
6. It may be necessary to attach a glass slide to the back of the Permanox® slide using a cyanoacrylate glue to prevent flexing of the sections during confocal image acquisition.
7. Avoid pushing the coverslip off the slide. The forces may damage the tissue or cause it to detach from the slide.
8. We have used plastic slide mailers with a flip top lid during the processing steps for easy exchange of solutions of multiple slides.
9. Be careful to position the embedded section in the same orientation that was used for LSCM imaging. Once separated from the slide, the side of the section with exposed tissue will correspond to the side in contact with the slide. This side would need to be glued to the end of a resin-filled polyethylene-embedding capsule.

10. To facilitate sectioning the resin-embedded cryostat section to approximately the correct depth, LSCM can be employed. To image through the resin-embedded cryostat section using LSCM, wrap double-sided sticky tape around the resin-filled embedding capsule, submerge the block face in a drop of water, and affix the resin-filled capsule to an interior wall of a Nunc® Lab-Tek™ chamber slide. Acquire a Z-stack of images from the surface of the resin to the cross-wall of interest, and use the z-interval to estimate the distance. Be sure to start collecting sections 2–3  $\mu\text{m}$  above the depth determined by LSCM to account for any discrepancies between the Z-step interval and the advance of the ultramicrotome cantilever arm.
11. For serial sectioning, we use  $2 \times 1$  slot grids that were dipped in 0.5 % formvar in ethylene dichloride and dried. Ribbons are picked up in the slot and then dried on a domino rack (Electron Microscopy Sciences, Hatfield, PA) coated with a film of 0.5 % formvar in ethylene dichloride [21]. The domino racks are dried for 1–2 h on a warm hot plate and the grids are “punched out” by using the head of a nail.
12. We stain sections using a commercially available Hiraoka plate, a flexible plastic plate with multiple slots that firmly hold grids. Grids are loaded into a Hiraoka plate, which is then relaxed on a hot plate and inverted onto a 35 mm  $\times$  10 mm suspension dish filled with 9 mL of filtered methanolic uranyl acetate. Grids are stained for 5 min and then washed in methanol and dried. Filter paper is used to remove liquid from around the base of the grids. The Hiraoka plate is then placed in a petri dish containing NaOH pellets, and the grids are stained with filtered Reynolds’ lead citrate for 5 min. Grids are washed with boiled, cooled, and filtered distilled water, and filter paper is used to remove excess liquid from around the grids.
13. The images acquired by TEM may have an orientation that is inverted relative to the images of cryostat sections collected by LSCM. This discrepancy may arise due to the orientation of the TEM grid when it was placed in the sample rod and whether the confocal microscope used to acquire the images was inverted or upright.

---

## Acknowledgements

The research pertinent to the development of this protocol was supported by grants provided by the National Science Foundation (IOB 0954931) and partially by the grants from the National Center for Research Resources (5P30RR031160-03) and the National Institute of General Medical Sciences (8 P30 GM103519-03) from the National Institutes of Health to J.-Y. L.

## References

1. Ding B, Turgeon R, Parthasarathy MV (1992) Substructure of freeze-substituted plasmodesmata. *Protoplasma* 169:28–41
2. Ding B, Haudenschild JS, Hull RJ, Wolf S, Beachy RN, Lucas WJ (1992) Secondary plasmodesmata are specific sites of localization of the tobacco mosaic virus movement protein in transgenic tobacco plants. *Plant Cell* 4:915–928
3. Lee JY, Wang X, Cui W, Sager R, Modla S, Czymmek K et al (2011) A plasmodesmata-localized protein mediates crosstalk between cell-to-cell communication and innate immunity in arabidopsis. *Plant Cell* 23:3353–3373
4. Simpson C, Thomas C, Findlay K, Bayer E, Maule AJ (2009) An arabidopsis gpi-anchor plasmodesmal neck protein with callose binding activity and potential to regulate cell-to-cell trafficking. *Plant Cell* 21:581–594
5. Blackman LM, Harper JDI, Overall RL (1999) Localization of a centrin-like protein to higher plant plasmodesmata. *Eur J Cell Biol* 78:297–304
6. Tian Q, Olsen L, Sun B, Lid SE, Brown RC, Lemmon BE et al (2007) Subcellular localization and functional domain studies of defective kernell in maize and arabidopsis suggest a model for aleurone cell fate specification involving crinkly4 and supernumerary aleurone layer1. *Plant Cell* 19:3127–3145
7. van Rijnsoever C, Oorschot V, Klumperman J (2008) Correlative light-electron microscopy (clem) combining live-cell imaging and immunolabeling of ultrathin cryosections. *Nat Methods* 5:973–980
8. Giepmans BN, Deerinck TJ, Smarr BL, Jones YZ, Ellisman MH (2005) Correlated light and electron microscopic imaging of multiple endogenous proteins using quantum dots. *Nat Methods* 2:743–749
9. Polishchuk RS, Polishchuk EV, Marra P, Alberti S, Buccione R, Luini A et al (2000) Correlative light-electron microscopy reveals the tubular-saccular ultrastructure of carriers operating between Golgi apparatus and plasma membrane. *J Cell Biol* 148:45–58
10. Robinson JM, Vandre DD (1997) Efficient immunocytochemical labeling of leukocyte microtubules with fluoronogold: an important tool for correlative microscopy. *J Histochem Cytochem* 45:631–642
11. Deerinck TJ, Martone ME, Lev-Ram V, Green DP, Tsien RY, Spector DL et al (1994) Fluorescence photooxidation with eosin: a method for high resolution immunolocalization and in situ hybridization detection for light and electron microscopy. *J Cell Biol* 126:901–910
12. Shu X, Lev-Ram V, Deerinck TJ, Qi Y, Ramko EB, Davidson MW et al (2011) A genetically encoded tag for correlated light and electron microscopy of intact cells, tissues, and organisms. *PLoS Biol* 9:e1001041
13. Martell JD, Deerinck TJ, Sancak Y, Poulos TL, Mootha VK, Sosinsky GE et al (2012) Engineered ascorbate peroxidase as a genetically encoded reporter for electron microscopy. *Nat Biotechnol* 30:1143–1148
14. Wei D, Jacobs S, Modla S, Zhang S, Young CL, Cirino R et al (2012) High-resolution three-dimensional reconstruction of a whole yeast cell using focused-ion beam scanning electron microscopy. *Biotechniques* 53:41–48
15. Denk W, Horstmann H (2004) Serial block-face scanning electron microscopy to reconstruct three-dimensional tissue nanostructure. *PLoS Biol* 2:e329
16. Micheva KD, Smith SJ (2007) Array tomography: a new tool for imaging the molecular architecture and ultrastructure of neural circuits. *Neuron* 55:25–36
17. Modla S, Mendonca J, Czymmek KJ, Akins RE (2010) Identification of neuromuscular junctions by correlative confocal and transmission electron microscopy. *J Neurosci Methods* 191:158–165
18. Murashige T, Skoog F (1962) A revised medium for rapid growth and bio-assays with tobacco tissue cultures. *Physiol Plant* 1:473–497
19. Fiala JC (2005) Reconstruct: a free editor for serial section microscopy. *J Microsc* 218:52–61
20. Hanson HH, Reilly JE, Lee R, Janssen WG, Phillips GR (2010) Streamlined embedding of cell monolayers on gridded glass-bottom imaging dishes for correlative light and electron microscopy. *Microsc Microanal* 16:747–754
21. Rowley JC, Moran DT (1975) A simple procedure for mounting wrinkle-free sections on formvar-coated slot grids. *Ultramicroscopy* 1:151–155



# **Part IV**

## **Analysis of Plasmodesmata Conductivity and Regulation**



## Quantification of Plant Cell Coupling with Live-Cell Microscopy

Johannes Liesche and Alexander Schulz

### Abstract

Movement of nutrients and signaling compounds from cell to cell is an essential process for plant growth and development. To understand processes such as carbon allocation, cell communication, and reaction to pathogen attack it is important to know a specific molecule's capacity to pass a specific cell wall interface. Transport through plasmodesmata, the cell wall channels that directly connect plant cells, is regulated not only by a fixed size exclusion limit, but also by physiological and pathological adaptation. The noninvasive approach described here offers the possibility of precisely determining the plasmodesmata-mediated cell wall permeability for small molecules in living cells.

The method is based on photoactivation of the fluorescent tracer caged fluorescein. Non-fluorescent caged fluorescein is applied to a target tissue, where it is taken up passively into all cells. Imaged by confocal microscopy, loaded tracer is activated by UV illumination in a target cell and its spread to neighboring cells monitored. When combined with high-speed acquisition by resonant scanning or spinning disc confocal microscopy, the high signal-to-noise ratio of photoactivation allows collection of three-dimensional (3D) time series. These contain all necessary functional and anatomical data to measure cell coupling in complex tissues noninvasively.

**Key words** Plasmodesmata, Live-cell microscopy, Fluorescent tracer, Diffusion, Fluorescein, Permeability

---

### 1 Introduction

Plant cells are directly connected by plasmodesmata (PD) that form channels through the cell wall and enable the intercellular movement of cytosolic solutes, membrane lipids, and signaling molecules [1]. Quantitative data on the intercellular movement of nutrients and signaling compounds is an essential factor for our understanding of plant growth and developmental processes, such as pattern formation in embryos [2], phloem loading and unloading [3–5], nutrient transport to growth centers [6], and hormone distribution patterns [7]. The PD that connect neighboring plant cells can have very different structures and, accordingly, very different transport properties [8, 4]. Intercellular transport through

PD has been investigated primarily by using fluorescent tracers. In contrast to natural compounds, their distribution can be monitored with high resolution in living tissue with a fluorescence microscope. In various cell and tissue types, fluorescent tracer molecules under a certain size-exclusion limit (SEL) were shown to diffuse freely between cells through the cytoplasmic sleeve of PD [9–11]. PD typically have a SEL of about 800 Da. A prerequisite for coupling experiments is that the tracer size is below this limit. Selective and facilitated transport through PD has been, so far, only described for intercellular movement of non-cell autonomous proteins [12, 13] and viruses [14].

The objective of the method described here is to quantify intercellular movement of small molecules. The importance of such data is highlighted by three publications: Rutschow et al. [7] could show that hydrogen peroxide has a concentration-dependent effect on PD permeability for hormones and nutrients in the *Arabidopsis* root. Liesche and Schulz [3] quantified cell coupling in the leaves of several plant species to identify bottlenecks in symplasmic transport related to different mechanisms of photoassimilate export. The same authors could subsequently experimentally determine the diffusion capacity of single PD in the *Cucurbita pepo* leaf and use the data to model the PD's substructure, which, as these PDs are narrower than "regular" PDs, cannot even be resolved with electron microscopy [4]. In general, electron microscopy can resolve structures with a resolution of a few nanometers and it has been used to produce images of PD on which our current knowledge of PD structure is based [15, 16]. Nevertheless, the harsh sample preparation that is required for electron microscopy is prone to artifacts. For example, preparation-induced callose synthesis can introduce uncertainty if spaces that appear empty, e.g., between plasma membrane and desmotubule, are actually available for transport in vivo. This can only be assessed in a noninvasive live-cell approach, in which all cell-specific influences and dynamic regulation are integrated to control the permeability of PD. Although the permeability of specific cell–cell interfaces has been studied for more than 25 years, absolute quantitative measurements based on the laws of diffusion were limited to one-dimensional cell-chains, like the staminal hairs of *Setcreasea purpurea* [17], or to uniform single-layer tissues, such as *Egeria densa* epidermis [10]. Moreover, methods relied on microinjection of tracers, which can cause artifacts [18, 19], and two-dimensional (2D) imaging, which can introduce mathematical errors due to uneven cell geometry [20]. Recent technical developments enable a less invasive and more precise measurement of cell coupling. Advanced confocal laser-scanning microscopes (CLSMs) offer the possibility of optical sectioning, thereby producing 3D image data of a living tissue at depths of up to 150  $\mu\text{m}$ . Lasers as light source enable noninvasive photoactivation and bleaching approaches that are less

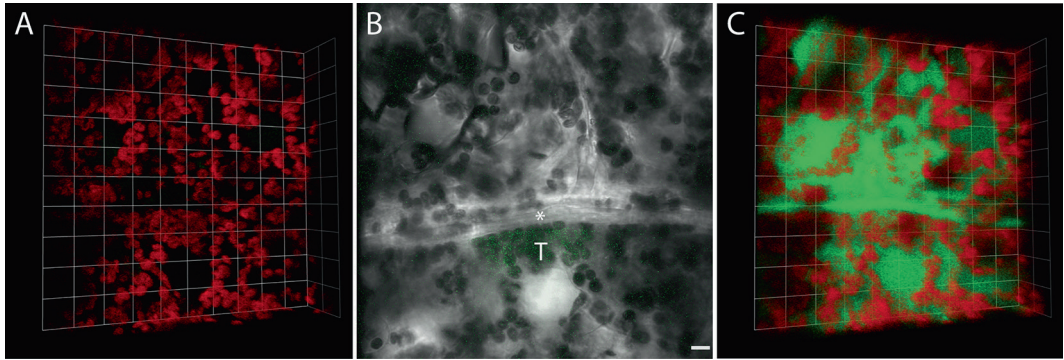


**Fig. 1** Example images from a photoactivation experiment to measure coupling between a bundle sheath cell (target cell T) and a phloem intermediary cell (*asterisk*) in the *Cucurbita pepo* leaf. **(a)** 3D projection of chlorophyll fluorescence. After passive uptake of the photoactivatable tracer in all cells, cells in the target area are identified with the help of bright field and chlorophyll fluorescence images. **(b)** Optical section during the 10 s photo-activation phase. Data is acquired before, during, and after photoactivation. **(c)** 3D projection of tracer (*green*) and chlorophyll (*red*) fluorescence after complete uncaging to determine the tracer-accessible volume of each cell, which is needed to calculate fluorescence concentrations. Scale bars: **(a)** and **(c)**, 1 Unit =  $12 \mu\text{m}^2$ , **(b)**  $10 \mu\text{m}$

prone to artifacts compared to the introduction of fluorescent tracers by microinjection. CLSMs equipped with a resonant scanner or spinning disc unit are especially suited for the determination of cell coupling, because of their high image acquisition rates of 15–35 frames per second. High image acquisition speed shortens the time period between pre-activation/pre-bleaching and post-activation/post-bleaching measurements and thereby decreases the error that tracer diffusion from neighbor cells into adjacent cells introduces if slower acquisition methods are applied [20].

The present protocol will focus on a photoactivation approach rather than on photobleaching. In fluorescence recovery after photobleaching (FRAP), a fluorescent tracer is loaded in all cells and subsequently bleached by strong laser illumination in one specific target cell, after which signal decrease in neighboring cells and signal recovery in the target cell can be followed. In photoactivation, a non-fluorescent tracer is loaded in all cells, which is then activated by UV-laser illumination in the target cell and signal spread to neighbor cells is monitored (Fig. 1). As activation rates are considerably higher than bleaching rates, methods based on photoactivation provide a higher signal-to-noise ratio, which allows for the shortest possible imaging protocol and, thereby, the most precise data. The method gives consistent results of intercellular tracer movement without relying on mathematical models. If rapid scanning methods are not available, cell coupling can also be derived from 2D data over time. However, in complex tissues the cell geometry of the target and neighboring cells has to be taken into account and compensated for in order to achieve a cell-coupling

factor (CCF) that can be compared between different tissue and plant species [3]. More elegantly, all necessary functional and anatomical data can be collected directly from 3D time series. In both methods, non-fluorescent “caged” fluorescein is applied to a target tissue, where it is taken up passively into all cells. Imaged by CLSM, loaded tracer is activated by UV illumination in a target cell and its spread to neighboring cells monitored. From flux  $J$  between the target cell and an adjacent cell, the concentration potential  $\Delta c$ , the diffusion distance  $d$ , and the diffusion coefficient  $D$  for the tracer molecule can be calculated with Fick’s law of diffusion:

$$D = \frac{J}{\Delta c} d \quad (1)$$

For most physiological questions, the net permeability of a whole cell wall interface is relevant, not the permeability of specific PD. This can be described as PD-mediated cell wall permeability:

$$P = J \times \Delta c \quad (2)$$

Flux  $J$  describes the flow rate  $Q$  per interface area  $A$  with  $J = \frac{Q}{A}$  and has the unit  $\text{mol/s}/\mu\text{m}^2$ . Determination of the concentration potential  $\Delta c$  (in  $\text{mol}/\mu\text{m}^3$ ) requires knowledge of the tracer abundance in the target cell  $N_0$  and the neighbor cell  $N_1$  and the tracer-accessible volume  $V$  of both cells with  $\Delta c = \frac{N_0}{V_0} - \frac{N_1}{V_1}$ . The parameters that have to be determined in order to be able to calculate the PD-mediated cell wall permeability  $P$  ( $\mu\text{m/s}$ ) are therefore: The flow rate  $Q$  ( $\text{mol/s}$ ), the interface area  $A$  ( $\mu\text{m}^2$ ), the tracer abundance  $N$  ( $\text{mol}$ ), and the tracer-accessible cell volume  $V$  ( $\mu\text{m}^3$ ).

---

## 2 Materials

### 2.1 Chemicals and Solutions

1. Phosphate buffered saline (PBS), pH 7.4: 137 mM NaCl, 2.7 mM KCl, 10 mM  $\text{Na}_2\text{HPO}_4 \cdot 2\text{H}_2\text{O}$ , 2 mM  $\text{KH}_2\text{PO}_4$ . Adjust the pH with 1 M KOH if necessary.
2. Tracer solution for uncaging: CMNB-caged fluorescein solution. For CMNB-caged fluorescein (Invitrogen, USA) stock solution, 1 mg powder is dissolved in 100  $\mu\text{l}$  DMSO, stored at  $-20^\circ\text{C}$  protected from light. Right before use, 1  $\mu\text{l}$  of stock solution is diluted with 500  $\mu\text{l}$  0.1 M PBS to a final concentration of 20  $\mu\text{g/ml}$  (*see Note 1*). Alternative caged probes are available or can be synthesized (*see Note 2*).
3. Propidium iodide (PI) solution: 10  $\mu\text{g/ml}$ , dissolved in 0.1 M PBS.

## 2.2 Imaging Equipment

1. CLSM capable of high-speed image acquisition (*see Note 3*).
2. Lasers: For uncaging, a UV-laser with wavelength between 340 and 365 nm is essential. A two-photon laser can be used as alternative in some instances (*see Note 4*). A 405 nm diode laser generally offers insufficient photoactivation efficiency.
3. Optical Objectives: A wide field of view is necessary to capture the cells of interest entirely. Therefore, 20× or 40× objectives should be used. Water-dipping lenses are preferable as they show less aberration when imaging deep inside the tissue and allow post-experiment viability tests.
4. Image processing software has to be capable of 3D rendering and 3D object detection. The commercial programs Volocity (PerkinElmer, USA) and Imaris (Andor, Ireland) are well suited, while the use of the open-source ImageJ software depends on different plug-ins that make image processing and analysis considerably more cumbersome (*see Note 5*).

---

## 3 Methods

### 3.1 Photoactivation of Caged Fluorescein with a Confocal Microscope

1. Some specimens require preparation to ensure efficient uptake of the tracer. Accessible tissues, such as leaf trichomes or epidermis, do not require any preparation procedures. For experiments with leaf mesophyll cells, it is usually necessary to remove the lower epidermis to enable tracer uptake in deeper tissue layers. Infiltration of the tracer through stomata is possible but does not allow efficient washing. Any tracer in the apoplast has impact on the precision of measurements. Roots require very careful handling to preserve cell viability (*see Note 6*).
2. Incubate the target tissue with caged fluorescein solution for 15–20 min. Immobilize the respective plant tissue on a slide and apply a drop of tracer solution to cover the area of interest. If the sample is small, it can be submerged in tracer solution in a staining jar and transferred to a slide after the following washing step.
3. Wash with 0.1 M PBS, 1–3 times for several minutes.
4. Transfer the specimen to the microscope (*see Note 7*).
5. Select the tissue target area by using bright field illumination and the green fluorescence channel (495–550 nm), where the fluorescein signal will be detected after photoactivation. Main criteria are cell integrity and the absence of background fluorescence before photoactivation in the green channel. Observing the red chlorophyll fluorescence (650–750 nm) can also help to identify a suitable area.

6. Calibrate the photoactivation parameters for the specific specimen. This involves finding the optimal length for the photoactivation step (*see Note 8*) and detection channel sensitivity of the green fluorescence detection channel (*see Note 9*). Test photoactivation by exciting several potential target cells with the UV-laser to find parameters that combine clearly visible signal increases with a minimal photoactivation period. The UV-laser should be set to close to 100 % laser power, while the 488 nm laser that is necessary to excite the activated fluorescein is used at normal imaging levels, typically about 15 %.
7. Define the upper and lower z-limit for image stack acquisition such that whole cells are included (*see Note 10*). It is important for the later image analysis that whole-cell data are available for every time point.
8. Define an imaging protocol for the photoactivation experiment (Fig. 2). The only factor that changes between steps is the UV illumination. The 488 nm laser and green-channel detection (495–550 nm) are active during the whole imaging phase. Ideally, xyz-image stacks are recorded for each time point (referred to as “stacks” in the following). If 3D imaging is not possible, xy-images of a single optical plane can be recorded instead, which limits the comparability of results to a certain extent (*see Note 11*).
  - (a) Pre-bleaching: Record two stacks as reference. Only the 488 nm laser is used to show any background in the fluorescein detection channel and potential stage drift between the two stacks. Readjust the specimen in case of stage drift.
  - (b) Photoactivation: Illuminate a region of interest (ROI) that corresponds to the target cell in two to five stacks (*see Note 12*) with close to maximal UV-laser power. Signal development can be followed in the green detection channel. Typically, the signal will be saturated due to the additional excitation of fluorescein by the UV-laser and can therefore not be used for quantification.
  - (c) Post-photoactivation: Monitor the activated fluorescein signal in one to ten stacks with the UV-laser turned off. While the first post-photoactivation stack is the most relevant for the determination of coupling between target and first neighbor cell, later time points can be used to investigate additional parameters of tracer diffusion (*see Note 13*).
  - (d) Field-of-view photoactivation: Activate caged fluorescein in the whole field of view in five to ten stacks with close to maximal UV-laser power. Data from this second photoactivation step will be used to determine the tracer-accessible volume in each cell.
  - (e) Post-photoactivation: Record one stack with the UV-laser turned off.

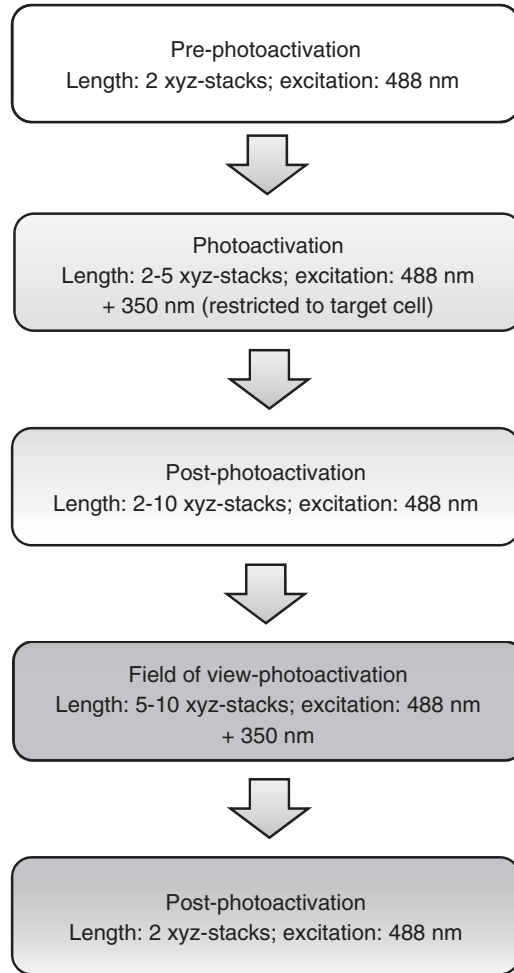


**Fig. 2** Flow diagram of imaging procedure

9. Define the imaging protocol to run as autonomously as possible to minimize delays between steps. Some acquisition programs might require manual change of parameters, which should be executed as quickly as possible.
10. Optionally, a test for cell viability can be performed at this point. For this, lower the microscope stage and replace the PBS with PI solution. After 5 min incubation replace the PI solution with 0.1 M PBS again and return the stage to imaging position. Red fluorescence (detection at 590–650 nm) should only show cell outlines. If the signal is also found inside the cells, especially in the nucleus, the cell membrane has been compromised and the experiment should be repeated with unaffected cells.

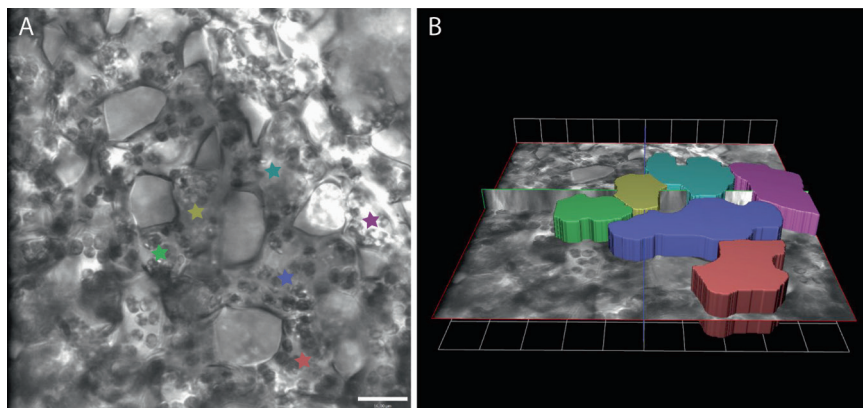


**Fig. 3** (a) Single bright field image from a z-stack of *Cucurbita maxima* leaf mesophyll cells. (b) The same image displayed in 3D view to illustrate the regions of interest that correspond to the target cell (*blue*) and the neighboring cells. Scale bars: (a) 16  $\mu\text{m}$ , (b) 1 Unit = 12  $\mu\text{m}^2$

### 3.2 Image Processing

1. Assess the interface area of the cell wall between the target cell and each neighbor cell using the three-dimensional image information of the z-stacks. In general, drawing the ROI on the bright field images results in the most accurate value for interface area.
2. Optional: If background signal is present before photoactivation, subtract it by using the image calculator function of the image processing software to subtract the signal from pre-photoactivation from the post-photoactivation images.
3. Determine the flux by drawing ROIs corresponding to each of the neighboring cells on the first post-photoactivation stack (Fig. 3). The signal in these ROIs represents all molecules that crossed the target-cell neighbor-cell interface.
4. Measure the tracer abundance, which is necessary to determine the concentration potential, by subtracting the signal in a ROI corresponding to the target cell from the signal in a ROI corresponding to a neighbor cell on the first post-photoactivation stack.
5. Measure the tracer-accessible volume by applying an object detection algorithm on ROIs that correspond to the target cell and neighbor cells using the first stack after the field-of-view photoactivation. In this stack, all the accessible compartments in a cell are populated by fluorescein and can be integrated into a single volume per cell by the algorithm.
6. Calculate the concentration potential between target and neighbor cell from tracer abundance and tracer-accessible cell volume as described in the introduction. Values should be integrated to reflect the potential at any one time point during

the experiment. Because data acquired during photoactivation is usually not usable due to signal saturation effects, pre- and post-photoactivation data is averaged.

7. Calculate the PD-mediated cell wall permeability with Eq. 2. Repeat the procedure described under Subheading 3.1 with equivalent specimens until enough data is collected for statistically sound calculations.

---

## 4 Notes

1. The concentration of caged fluorescein solution can be varied to ensure uniform uptake into all cells of the tissue. For most tissues, a concentration of 5  $\mu\text{g}/\text{ml}$  is sufficient. Concentrations higher than 20  $\mu\text{g}/\text{ml}$  are not useful, because if a tissue does not take up tracer efficiently, it is generally not a matter of concentration but tissue penetration, which can be compromised, e.g., by a wax layer covering the cells. In order to facilitate tissue penetration, caged fluorescein solution can be pressure infiltrated through stomata using a syringe or the outer cell layer carefully removed with forceps or very fine sand paper.
2. In addition to caged fluorescein, which fluoresces green after activation, caged tracers with other colors are available. Notably, there is a caged rhodamin (Aberrior GmbH, Germany), which is useful, for example when a GFP-tagged protein is expressed in the target tissue. Other caged compounds can be synthesized as described by Lee et al. [21].
3. As redistribution of fluorescent molecules inside cells happens within milliseconds, imaging with a high temporal resolution is essential. In conventional CLSMs the recording speed is limited by the scan mirror that controls the laser beam over the field of view. When the regular mirror is replaced with one that vibrates at resonant speed, acquisition speed increases 10–20 times. In spinning disc confocals, two discs, one with micro-lenses and one with pinholes, create a series of minibeams that swipe over the field of view as the discs rotate. The minibeams cover the field of view much faster than the single beam in a conventional confocal. The integration of the resonant scanner into a regular CLSM allows for the use of all excitation lasers, including multi-photon, and all detection channels. For spinning disc confocals only standard laser lines are available and simultaneous detection is limited by the number of cameras. In case the acquisition rate is considerably slower than expected diffusion rates, control experiments have to be performed and correction factors included in the calculations as described by Rutschow et al. [7].

4. A two-photon laser has been used for activation of caged fluorescein [22], but the photoactivation efficiency is usually too low at low magnifications, while at high magnifications, absorption of laser energy causes severe damage to the imaged cells in many plant tissues.
5. Future plug-ins for ImageJ might enable more convenient work with 3D-ROIs. Experienced users of ImageJ might be able to write their own plug-in. Similarly, image processing with Matlab (Mathworks, USA) might be possible for knowledgeable users.
6. Root cells are very sensitive and mounting on slides can compromise cell viability [23]. To prevent damage, plants should be grown in a microscopy-compatible root chamber [24] or root chip [25]. Roots from pot or plate-grown plants can also be carefully washed and embedded in a drop of agar on a slide [23].
7. Imaging conditions can be an important factor for the measurement of cell coupling, since PD have been shown to be sensitive to environmental conditions [26, 27]. Potential measures to counteract any influence are to keep the lights on in the microscope room and to use whole plants [3].
8. In general, the photoactivation phase should be as short as possible. The signal increases exponentially, but typically the first seconds can be described as linear, which makes the calculation of the average concentration potential between target and neighbor cell simpler [20]. Shorter photoactivation times also minimize the influence of diffusion from neighbor cells back into the target cell.
9. Signal saturation of the detection channel has to be prevented, as saturation would mean that signal intensity is no longer proportional to fluorophore abundance.
10. Increasing the confocal pinhole might be an option in case the cells of the target area are so large that the time it takes to record one z-stack becomes too long, as long as the z-resolution is high enough to enable accurate image analysis.
11. The accurate calculation of PD-mediated cell wall permeability requires three-dimensional anatomical information on the involved cells. Restricting imaging to a single optical plane can introduce a considerable error to the calculations, especially if cell shape and tracer-accessible volume are variable [20]. In uniform tissue or in cases where differences in cell geometry are accounted for, a factor equivalent to PD-mediated cell wall permeability can be derived [3, 7].
12. Most acquisition software is not capable of restricting the excitation light to a self-drawn three-dimensional ROI. In this case, it is the best option to draw two-dimensional free-hand ROIs and limit their extension in z.

13. In addition to the calculation of flux from the last pre-activation and the first post-activation time point, later post-activation data might also be useful. In some cases, this data can allow the calculation of the flux from first neighbor to second degree neighbor [20].

## References

1. Roberts AG, Oparka KJ (2003) Plasmodesmata and the control of symplastic transport. *Plant Cell Environ* 26:103–124
2. Kim I, Kobayashi K, Cho E, Zambryski PC (2005) Subdomains for transport via plasmodesmata corresponding to the apical-basal axis are established during Arabidopsis embryogenesis. *Proc Natl Acad Sci U S A* 102:11945–11950
3. Liesche J, Schulz A (2012) In vivo quantification of cell coupling in plants with different phloem-loading strategies. *Plant Physiol* 159:355–365
4. Liesche J, Schulz A (2013) Modeling the parameters for plasmodesmal sugar filtering in active symplastic phloem loaders. *Front Plant Sci* 4:207
5. Patrick JW (2013) Does Don Fisher's high-pressure manifold model account for phloem transport and resource partitioning? *Front Plant Sci* 4:184
6. Bret-Harte MS, Silk WK (1994) Nonvascular, symplastic diffusion of sucrose cannot satisfy the carbon demands of growth in the primary root tip of *Zea mays* L. *Plant Physiol* 105:19–33
7. Rutschow HL, Baskin TI, Kramer EM (2011) Regulation of solute flux through plasmodesmata in the root meristem. *Plant Physiol* 155:1817–1826
8. Schulz A (1995) Plasmodesmal widening accompanies the short-term increase in symplastic phloem unloading in pea root-tips under osmotic-stress. *Protoplasma* 188:22–37
9. Terry BR, Robards AW (1987) Hydrodynamic radius alone governs the mobility of molecules through plasmodesmata. *Planta* 171:145–157
10. Goodwin PB, Shepherd V, Erwee MG (1990) Compartmentation of fluorescent tracers injected into the epidermal-cells of *Egeria densa* leaves. *Planta* 181:129–136
11. Martens HJ, Hansen M, Schulz A (2004) Caged probes: a novel tool in studying symplastic transport in plant tissues. *Protoplasma* 223:63–66
12. Kim JY, Yuan Z, Cilia M, Khalfan-Jagani Z, Jackson D (2002) Intercellular trafficking of a KNOTTED1 green fluorescent protein fusion in the leaf and shoot meristem of Arabidopsis. *Proc Natl Acad Sci U S A* 99:4103–4108
13. Kurata T, Ishida T, Kawabata-Awai C, Noguchi M, Hattori S, Sano R et al (2005) Cell-to-cell movement of the CAPRICE protein in Arabidopsis root epidermal cell differentiation. *Development* 132:5387–5398
14. Itaya A, Ma F, Qi Y, Matsuda Y, Zhu Y, Liang G et al (2002) Plasmodesma-mediated selective protein traffic between “symplastically isolated” cells probed by a viral movement protein. *Plant Cell* 14:2071–2083
15. Ding B, Turgeon R, Parthasarathy MV (1992) Substructure of freeze-substituted plasmodesmata. *Protoplasma* 169:28–41
16. Brecknock S, Dibbayawan TP, Vesk M, Vesk PA, Faulkner C, Barton DA, Overall RL (2011) High resolution scanning electron microscopy of plasmodesmata. *Planta* 234:749–758
17. Tucker EB, Spanswick RM (1985) Translocation in the staminal hairs of *Setcreasea purpurea*. kinetics of intercellular transport. *Protoplasma* 128:167–172
18. Oparka KJ, Duckett CM, Prior DM, Fisher DB (1994) Real-time imaging of phloem unloading in the root-tip of Arabidopsis. *Plant J* 6:759–766
19. Turgeon R, Wolf S (2009) Phloem transport: cellular pathways and molecular trafficking. *Annu Rev Plant Biol* 60:207–221
20. Liesche J, Schulz A (2012) Quantification of plant cell coupling with three-dimensional photoactivation microscopy. *J Microsc* 247:2–9
21. Lee HM, Larson DR, Lawrence DS (2009) Illuminating the chemistry of life: design, synthesis, and applications of “caged” and related photoresponsive compounds. *ACS Chem Biol* 4:409–427
22. Sowinski at conference “PD 2010”, Sydney, Australia
23. Gjetting KS, Ytting CK, Schulz A, Fuglsang AT (2012) Live imaging of intra- and extracellular

- pH in plants using pHusion, a novel genetically encoded biosensor. *J Exp Bot* 63:3207–3218
24. Froelich DR, Mullendore DL, Jensen KH, Ross-Elliott TJ, Anstead JA, Thompson GA et al (2011) Phloem ultrastructure and pressure flow: sieve-element-occlusion-related agglomerations do not affect translocation. *Plant Cell* 23:4428–4445
  25. Grossmann G, Guo WJ, Ehrhardt DW, Frommer WB, Sit RV, Quake SR et al (2011) The RootChip: an integrated microfluidic chip for plant science. *Plant Cell* 23:4234–4240
  26. Schulz A (1994) Phloem transport and differential unloading in pea-seedlings after source and sink manipulations. *Planta* 192:239–248
  27. Liarzi O, Epel BL (2005) Development of a quantitative tool for measuring changes in the coefficient of conductivity of plasmodesmata induced by developmental, biotic, and abiotic signals. *Protoplasma* 225:67–76

# Chapter 10

## Drop-AND-See: A Simple, Real-Time, and Noninvasive Technique for Assaying Plasmodesmal Permeability

Weier Cui, Xu Wang, and Jung-Youn Lee

### Abstract

Gating of plasmodesmata (PD) is a highly dynamic cellular process spatiotemporally controlled by various physiological, developmental, and environmental conditions. Here, we describe a quantitative approach named Drop-AND-See (DANS), which allows for a real-time, in situ assessment of plasmodesmal permeability in an array of comparative studies. The power of the DANS assay lies in its simplicity: a membrane-permeable, non-fluorescent dye is loaded onto the adaxial epidermis of an intact leaf; the absorbed dye is cleaved by cellular esterases and become fluorescent yet membrane-impermeable; this symplasmic form then diffuses via PD through the mesophyll and into the abaxial epidermis, where the extent of fluorescent dye spreading can be imaged and quantified by confocal microscopy as a measure of cell-to-cell permeability. By employing this DANS assay, rapid changes in PD permeability upon chemical, biological, or environmental treatments can be easily analyzed. Furthermore, PD permeability as a phenotype or a trait of interest can be evaluated using various genetic backgrounds or mutants. We provide hereby an easy-to-follow visual guide of the DANS assay using *Arabidopsis* plants as an example along with a description of the step-by-step protocol.

**Key words** Plasmodesmata, Cell-to-cell permeability, Fluorescent probe, *Arabidopsis*

---

### 1 Introduction

Direct cell-to-cell coupling through plasmodesmata (PD) allows small, soluble molecules such as ions, photosynthates, amino acids, hormones, etc. to diffuse between neighboring cells. This capacity plays a crucial role in distributing nutrients and signaling molecules both locally and systemically throughout the whole plant. However, these symplastic passageways do not operate under a simple two state (open or closed) switch mechanism. Rather, additional levels of regulation exist such as changes in the size exclusion limits through active dilation and/or structural modifications of PD and changes in PD frequencies via de novo generation and degeneration. Furthermore, the spatiotemporal PD modulation, long recognized as the end result of certain physiological and developmental

responses, has recently been found to act as a signal itself influencing plant fitness and health [1–3]. For example, it was demonstrated that the loss of PD closure compromises innate immune responses and elevates plant susceptibility to microbial pathogens. Given the fundamental roles of PD in the plant, it would not be surprising to find more signaling pathways integrated into the regulation of PD. Hence, there is a greater than ever need for a method to measure symplastic connectivity *in situ* and in real time to facilitate such discoveries.

Conventionally, two popular approaches were taken to assess PD permeability in a given tissue: either a fluorescent protein (e.g., single or tandem GFP) that can move symplastically was used as a genetically-encoded reporter, or a fluorescent probe was microinjected into a target cell [4–8]. The advantage of using GFP is that it can be expressed in transgenic plants to monitor PD permeability in specific cell types during development. It can also be transiently expressed in epidermal cells via biolistic bombardment. However, GFP can only serve as a reporter for macromolecular diffusion in cells or tissues where the basal or induced size exclusion limit (SEL) allows for the movement of GFP, and is not suitable for monitoring rapid changes in PD permeability. On the other hand, microinjection allows for a real-time analysis of PD closure or dilation. A wide range of fluorescently labeled probes (e.g., chemicals, proteins, or nucleic acids) with various sizes can be injected individually or in combination into the cell. This technique is highly versatile in this regard but it requires extensive experimental system setups and it is inherently invasive due to the high pressure applied to the target cell, injury from tissue detachment or removal of the epidermal cell layer.

Small fluorescent tracers such as 5(6)-carboxyfluorescein (CF), 8-hydroxy-1,3,6-pyrenetrisulfonate, and Lucifer yellow, as well as larger tracers with multiple sizes (like F-dextran), have also been used to monitor symplastic movement in various plant tissues by perfusion of the dye through cuts or wounds. These tracers have been used for symplastic loading in various plant and tissue types [9–11]. Loading the dye into cuts allows it to move into the phloem, thus dispersing the reporter throughout the tissue or whole plant via the vasculature. This aspect is necessary for monitoring long-distance movement of the dye; however, the invasive nature of dye introduction and inability to consistently control the amount of dye uptake are disadvantages of this type of loading when it comes to comparative and quantitative analyses of PD permeability. Here, we describe a noninvasive dye loading approach using a membrane permeable form of CF to assess PD permeability *in situ* and in real time. CF diacetate (CFDA) is a non-fluorescent, membrane permeable dye of MW 460 Da; the acetyl groups of CFDA allow a rapid uptake of the dye into cells. Intracellular esterases

cleave CFDA, which generates the fluorescent but membrane-impermeable CF form of the dye in the cells; CF can then diffuse symplastically into the neighboring cells only through PD in plants. Our Drop-AND-See method capitalizes on these properties of CFDA/CF, and has proven to represent a simple and effective approach for assessing molecular diffusion through PD. Our method is also highly accessible, since a conventional confocal microscope is basically the only equipment it requires.

Briefly, the DANS assay is performed on intact rosette leaves (fourth and fifth) of 3-week-old *Arabidopsis* by loading CFDA onto the adaxial surface of a leaf and monitoring the extent of CF diffusion into the abaxial surface of the leaf (Fig. 1). Dye loading is achieved by placing a 1  $\mu$ L droplet of 1 mM CFDA onto the upper leaf surface. Subsequent dye diffusion occurs during a 5-min incubation, which was sufficient in our system to measure dye diffusion to the other surface of the leaf. Subsequently, the leaf is detached and mounted on a microscope slide with a cover glass or in a cover glass chamber. A laser scanning confocal microscope is used to scan the fluorescent signal from the abaxial surface and the extent of the CF diffusion is quantified by measuring the diameter of the fluorescent area. Epidermal loading of CFDA within the time frame used for diffusion lets the dye move from the adaxial epidermis into underlying mesophyll cell layers and finally into the abaxial epidermis but not into the vein, likely due to the symplastic isolation of the phloem in *Arabidopsis*. Moreover, dye loading on the upper surface allows dye absorption directly into the mature guard cells on that surface, yet in the lower side of the leaf, CF is excluded from mature guard cells, confirming the symplastic nature of the dye movement (Fig. 2).

The simple and highly reproducible characteristics of the DANS assay allow for complex, comparative analyses to be performed between different genetic backgrounds and/or between various treatments with chemical or biological agents that may effect overall PD permeability. When different genetic backgrounds are used to evaluate relative PD permeability, it is critical to perform appropriate control analyses. For example, it is necessary to confirm that the plants of interest are comparable in the dye uptake properties of their adaxial leaf surfaces, their epidermal cell sizes, and the number of cell layers in their leaves.

---

## 2 Materials

### 2.1 Plant Material

*Arabidopsis thaliana* plants grown at 22 °C and 60 % humidity under the 16 h/8 h light/dark cycle (120  $\mu$ mol/m<sup>2</sup>/s with mixed fluorescent and incandescent lights) for 3–3.5 weeks (*see* **Note 1**).

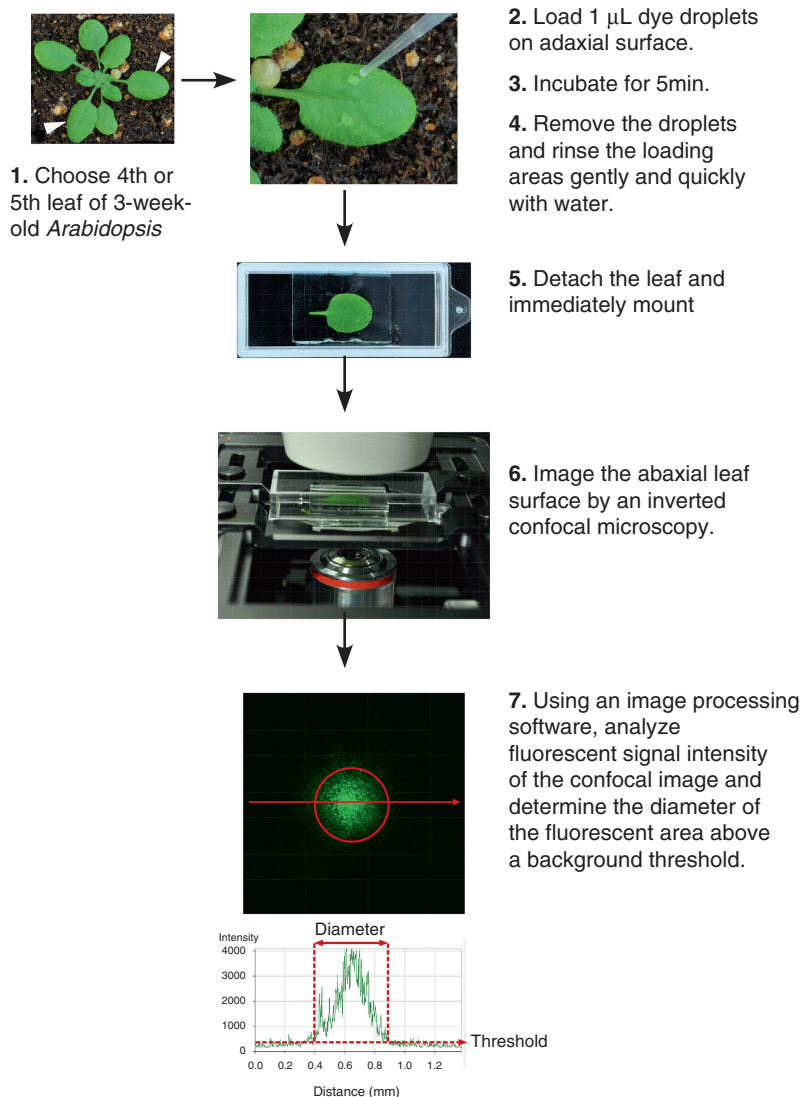


**Fig. 1** A visualized step-by-step DANS assay

## 2.2 Chemicals and Lab Wares

1. 5(6)-Carboxyfluorescein diacetate (CFDA). Dissolve 2.3 mg CFDA in 100  $\mu\text{L}$  of dimethyl sulfoxide to make a 50 mM stock and store it in the dark at  $-20\text{ }^{\circ}\text{C}$  for up to 6 months. Make a fresh working solution for each experiment by diluting the stock 1:50 in autoclaved nano-water (*see Note 2*).
2. Nano-water (or double distilled water) in a squirt bottle.
3. Pipettes and autoclaved pipette tips (*see Note 3*).
4. Fine forceps and sharp razor blades.

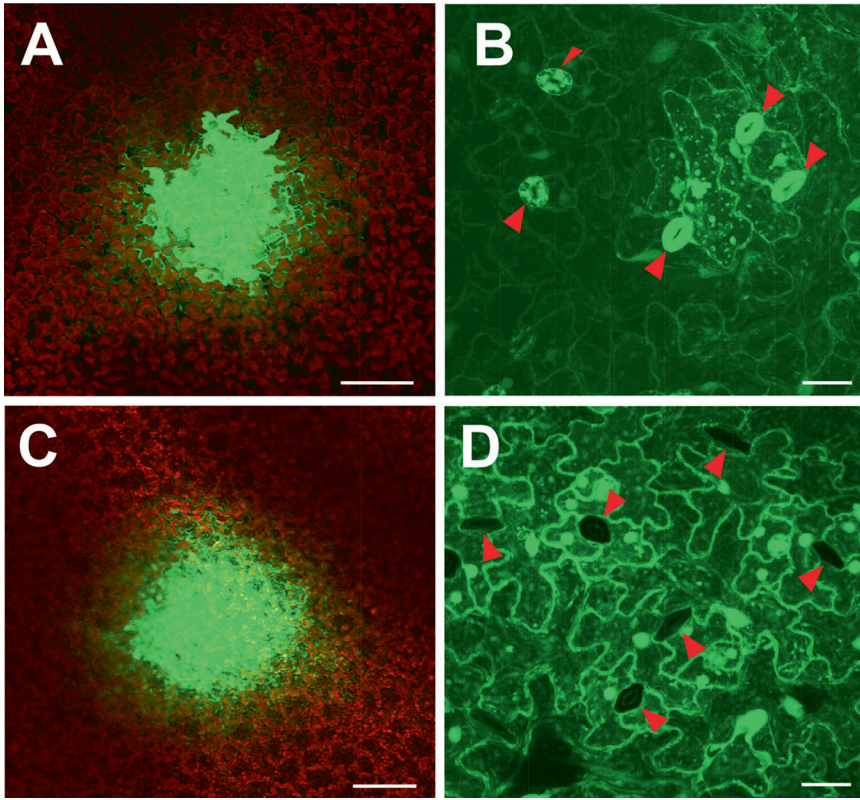


**Fig. 2** Images showing CFDA absorption into the adaxial leaf surface and symplastic movement of CF into the epidermal cells of the abaxial side. **(a)** A confocal image of the adaxial leaf surface demonstrating proper dye absorption after 5 min of loading. **(b)** A close-up confocal image showing dye absorption into mature guard cells as well as pavement cells. **(c)** A confocal image of the abaxial leaf surface showing proper dye diffusion into epidermal cells of the abaxial side of the leaf after 5 min of loading of CFDA on the adaxial leaf surface. **(d)** A close-up confocal image showing symplastic movement of CF in the abaxial leaf epidermis based on the lack of CF fluorescence in mature guard cells. **(a)** and **(c)** are merged images of *green* (for CF) and *red* (for chloroplast autofluorescence) channels. *Darts*, mature guard cells. Size bars = 20  $\mu\text{m}$  in **(a)** and **(c)** and 200  $\mu\text{m}$  in **(b)** and **(d)**. Images are adapted from Lee et al. [1] with permission from the authors

### 2.3 Microscopy and Image-Processing Software

1. Zeiss LSM 5 LIVE DUO confocal microscope with an LSM 510 META scanhead, or an equivalent confocal microscope.
2. Zeiss 5 $\times$ /0.25 Fluar objective lens.
3. Lab-Tek®II cover glass chamber (#1.5) or microscope slides with cover glasses (#1.5).
4. Zeiss LSM Image Examiner or Zen for processing the images or other software that can process fluorescent intensity distribution, such as ImageJ.

### 3 Methods

#### 3.1 Determining Proper Dye Absorption on the Adaxial Leaf Surface

1. Select healthy plants for dye loading and keep the plants under the required growth conditions until immediately before the dye loading starts (*see* Fig. 1, step 1 and **Note 4**).
2. Using the pipette tip, place 1  $\mu$ L of the CFDA solution onto the centers of the adaxial side of each half leaf blade (*see* Fig. 1, step 2).
3. Leave the droplets on the leaf for 5 min (*see* Fig. 1, step 3).
4. Remove the droplet by withdrawing it with the pipette, rinse the loading area briefly with a short and gentle stream of nano-water, and detach the leaf at the petiole with a razor blade (*see* Fig. 1, step 4).
5. Mount the detached leaf in a Lab-Tek®II coverglass chamber or on a glass slide with coverslip to image the adaxial side (*see* Fig. 1, step 5).
6. Adjust the sample stage so that the epidermal layer of the adaxial surface is on a focal plane (*see* Fig. 1, step 6).
7. Scan a single z-section image of the fluorescent area using a 5 $\times$  objective lens with appropriate laser and filter settings (*see* Fig. 2a and **Note 5**). Check the presence of bright fluorescent area to confirm the CFDA dye absorption is occurring properly on the adaxial leaf surface.
8. Zoom in on the fluorescent area using a 10 $\times$  objective lens and confirm direct dye absorption into both pavement and guard cells (*see* Fig. 2b and **Note 6**).

#### 3.2 Determining Symplastic Movement of CF in the Abaxial Surface

1. Perform **steps 1** through **4** as described in Subheading 3.1.
2. Mount the detached leaf in the chamber or on a glass slide with cover to image the abaxial side (*see* Fig. 1, step 5).
3. Scan a single z-section image of the fluorescent area with 5 $\times$  objective lens and check the presence of bright fluorescent area to confirm the CF dye movement into abaxial leaf epidermis (*see* Fig. 1, step 7 and Fig. 2c).
4. Zoom in on the fluorescent area using 10 $\times$  objective lens and confirm symplastic CF movement into the epidermal cells by checking that the CF fluorescence is excluded from mature guard cells (*see* Fig. 2d).

#### 3.3 Image Acquisition, Processing, and Quantification

1. Perform dye-loading assays as described in **steps 1** through **4** of Subheading 3.1.
2. Mount the detached leaf in the chamber or on a glass slide with coverslip to image the abaxial side (*see* Fig. 1, steps 5 and 6).

3. Scan a single 0.5  $\mu\text{m}$  z-section image of each fluorescent area with the  $\times 5$  objective (*see* Fig. 1, step 7 and Fig. 2c).
4. Repeat **steps 1–3** to acquire at least 20 images from 10 or more plants per set of DANS assay.
5. Open each image in Zen software or Image J and select the Intensity Distribution Profile.
6. Draw a line across the center of the fluorescent region (*see* Fig. 1, step 7 and **Note 7**).
7. Analyze the “Intensity-Distance” chart and select a threshold to determine the background level (*see* **Note 8**).
8. Calculate and record the base width of each fluorescent peak, i.e., the diameter of the fluorescent area based on the data from the distribution table in an Excel work sheet.
9. Repeat **steps 5–8** until all the images collected for a set of DANS assay are processed and the resulting data recorded.
10. Perform statistical analysis on each DANS assay data set and evaluate the result in terms of the statistical significance of the data sets.

---

## 4 Notes

1. Plants can be grown at different conditions. However, for each growth condition, the loading efficiency and the selection of rosette leaves most suitable for dye loading assays need to be established. Note also that plants that are grown with flatter leaves are easier to image.
2. The working stock needs to be wrapped in foil to keep it in the dark for the duration of the assay. If it needs to be used for several hours keep it on ice, however, do not store the working stock more than 24 h.
3. For a clean placement of a 1  $\mu\text{L}$  dye droplet, we find using low retention, extra-long tips with extra fine point is helpful.
4. Most suitable rosette leaves of the *Arabidopsis* grown under the conditions described above are the fourth and fifth true leaves based on our experience. However, it is advisable to establish an optimal experimental condition by empirically determining which leaves in what developmental stage of the plant under a given growth condition produce consistent results.
5. The images shown in Fig. 2a, c were produced by using 488-nm Argon laser line with a 500- to 550-nm band-pass emission filter for CF and 636- to 754-nm emission wave length with META detector for chloroplast autofluorescence.

6. The images shown in Fig. 2b, d were produced by using Zeiss 10 $\times$ /0.45 Plan-Apochromat objective.
7. The fluorescent area does not always form a perfect circle. If the area forms an oval shape, measure the long and short diameters and use the averaged value. Alternatively, measuring the area instead of diameter also works fine.
8. If using ImageJ to analyze the intensity profile, draw the line across the fluorescent area first, and then select “Plot Profile” under the “Analyze” menu to generate the “Intensity-Distance” chart.

---

## Acknowledgments

The research pertaining to the development of this protocol was supported by the grants provided by the National Science Foundation (IOS-0954931) and partially by the grants from the National Center for Research Resources (5P30RR031160-03) and the National Institute of General Medical Sciences (8 P30 GM103519-03) from the National Institutes of Health. We thank J. Caplan for helpful comments and edit.

## References

1. Lee J-Y, Wang X, Cui W et al (2011) A plasmodesmata-localized protein mediates crosstalk between cell-to-cell communication and innate immunity in Arabidopsis. *Plant Cell* 23:3353–3373
2. Faulkner C, Petutschnig E, Benitez-Alfonso Y et al (2013) Lym2-dependent chitin perception limits molecular flux via plasmodesmata. *Proc Natl Acad Sci U S A* 110:9166–9170
3. Wang X, Sager R, Cui W et al (2013) Salicylic acid regulates plasmodesmata closure during innate immune responses in Arabidopsis. *Plant Cell* 25:2325–2329
4. Crawford KM, Zambryski PC (2001) Non-targeted and targeted protein movement through plasmodesmata in leaves in different developmental and physiological states. *Plant Physiol* 125:1802–1812
5. Storms MMH, van der Schoot C, Prins M et al (1998) A comparison of two methods of microinjection for assessing altered plasmodesmal gating in tissues expressing viral movement proteins. *Plant J* 13:131–140
6. Barton DA, Cole L, Collings DA et al (2011) Cell-to-cell transport via the lumen of the endoplasmic reticulum. *Plant J* 66:806–817
7. Oparka KJ, Boevink P, SantaCruz S (1996) Studying the movement of plant viruses using green fluorescent protein. *Trends Plant Sci* 1:412–418
8. Wolf S, Lucas WJ (1994) Virus movement proteins and other molecular probes of plasmodesmal function. *Plant Cell Environ* 17: 573–585
9. Wang N, Fisher DB (1994) The use of fluorescent tracers to characterize the post-phloem transport pathway in maternal tissues of developing wheat grains. *Plant Physiol* 104:17–27
10. Duckett CM, Oparka KJ, Prior DAM et al (1994) Dye-coupling in the root epidermis of Arabidopsis is progressively reduced during development. *Development* 120:3247–3255
11. Wright KM, Oparka KJ (1996) The fluorescent probe HPTS as a phloem-mobile, symplastic tracer: an evaluation using confocal laser scanning microscopy. *J Exp Bot* 47:439–445

# Chapter 11

## Mapping Symplasmic Fields at the Shoot Apical Meristem Using Iontophoresis and Membrane Potential Measurements

Christiaan van der Schoot and Päivi L.H. Rinne

### Abstract

Microinjections of fluorescent dyes have revealed that the shoot apical meristem (SAM) is dynamically partitioned into symplasmic fields (SFs), implying that plasmodesmata (Pd) are held shut at specific locations in the proliferating cellular matrix. The SFs are integrated into a coherent morphogenetic unit by exchange of morphogens and transcription factors via gating Pd between adjacent SFs, and by ligand–receptor interactions that operate across the extracellular space. We describe a method for the real-time mapping of SF in the SAM by iontophoresis and membrane potential measurements.

**Key words** Shoot apical meristem, Cell communication, Plasmodesmata, Iontophoresis, Symplasmic field

---

## 1 Introduction

### 1.1 *The Symplasmic Organization of the SAM*

The SAM is the origin of the shoot system in higher plants [1, 2]. Major organizing principles of SAM behavior are cell–cell communication via Pd [3–6] and signaling via membrane-localized receptor kinases [7, 8]. These complementary forms of communication coordinate the differential growth of tunica and corpus and the positional expression of genes. Morphogenesis at the SAM is self-referential [2], and the SAM operates as a self-organizing system, which is characterized by extensive feedback [3–5, 7]. Despite its autonomous organization the SAM is sensitive to specific inputs from the shoot and the environment. These include signaling cascades that mediate phyllotactic patterning at the periphery of the SAM [9] as well as the transition to flowering [10, 11] and dormancy [11, 12]. The dynamic organization of the SAM is giving rise to a characteristic cellular network topology [4–6]. Typically the SAM has a duplex organization, with superimposed sets of initial cells (central stem cells) (Fig. 1a,b) the descendents of which give rise to a proliferating sheet (tunica) and a subjacent corpus.

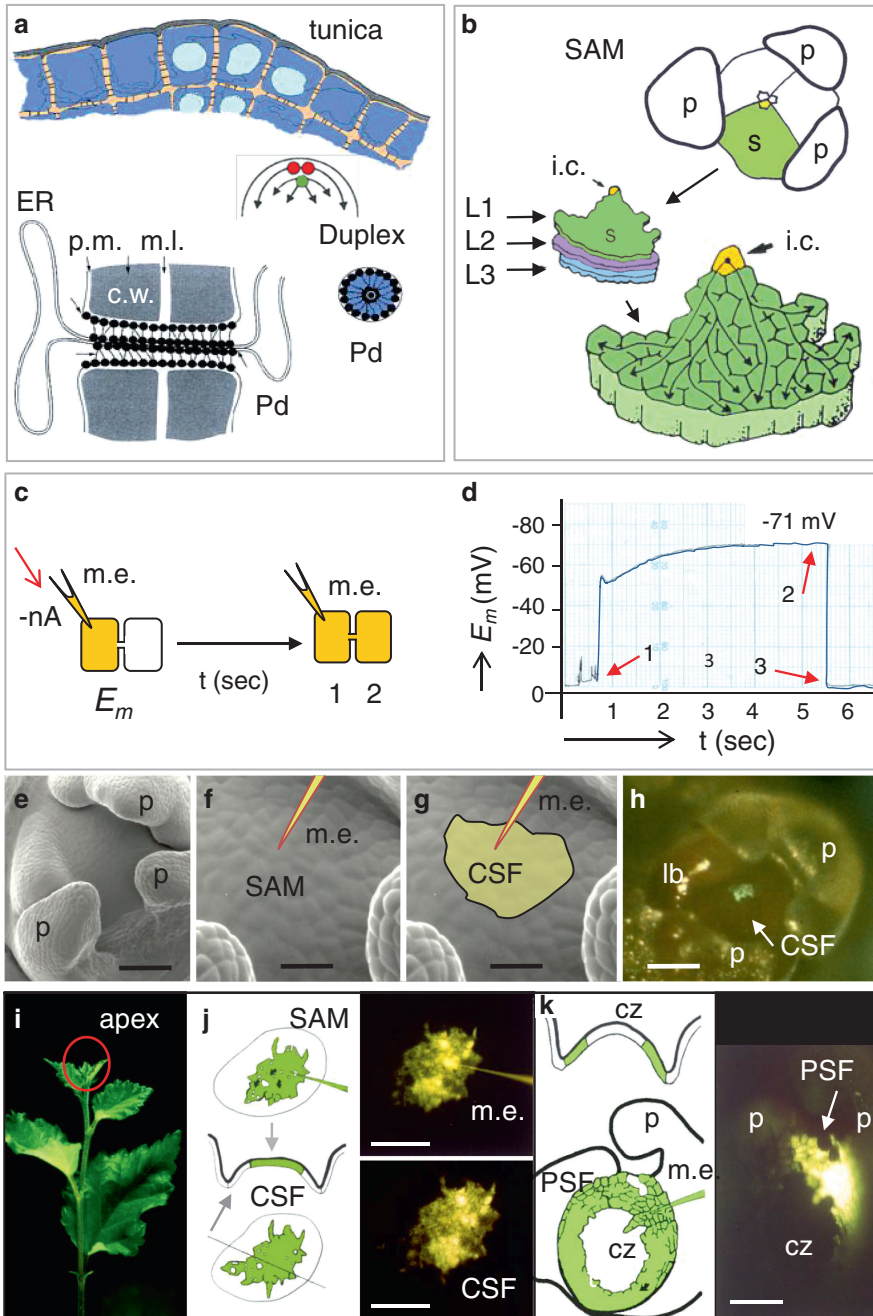


**Fig. 1** SAM structure and symplasmic organization. **(a)** The tunica is a sheet of proliferating cells, covering a three-dimensional corpus. Tunica and corpus originate from two superimposed sets of initial cells (or stem cells) thereby forming the so-called duplex SAM of angiosperms. All cells are symplasmically connected via plasmodesmata (Pd), formed either in cell plates or in existing walls. Schematic drawings show Pd in longitudinal and transverse views. ER endoplasmic reticulum, p.m. plasma membrane, m.l. middle lamella, c.w. cell wall. **(b)** Sector analysis has shown that often a SAM has three central stem cells or initial cells (i.c.). Each one gives rise to a branched cell lineage (green sector, s). Within a lineage cells are cytoplasmically continuous via Pd formed in the cell plate. Between lineage-branches within a sector and between adjacent and subjacent

Initial cells, by virtue of their position, are the origins of cell lineages which are cytoplasmically continuous via Pd that arise in the cell plate [3–6]. A symplasmic map (Fig. 1b) revealed that as a consequence tunica and corpus are subdivided into a number of sectors, each resembling a lineage tree [4–6, 13]. Cells of adjacent lineage trees and lineage branches become interconnected by secondary Pd, giving rise to a symplasmically integrated morphogenetic unit [4–6, 13]. Despite this, the SAM does not operate as a single symplasmic compartment. On the contrary, its cells are metabolically and electrically coupled into SFs, the borders of which are positionally maintained in a proliferating field of cells [4, 6, 14, 15]. SFs may represent morphogenetic fields in which cells share metabolism, electrical characteristics, and cell cycle properties. The activities of the adjacent SFs are integrated by the “gated” passage of morphogens and transcription through Pd between them [4, 6, 16, 17]. A consequence of the lineage patterns is that differential gating of primary and secondary Pd could dictate a corresponding pattern of signal flow within the SAM [4, 6]. Indeed, experiments confirmed this proposition, showing that some transcription factors move selectively and directionally within the SAM [18–21]. Classic models emphasized self-maintenance of the SAM [1, 2], and the distinct gene expression domains discovered by modern genetic analyses seemed to underpin this notion [7]. Currently, however, the attention for this paradigm is diminishing and the SAM is often referred to as a mere “population of stem cells.” Regardless, conceptualizing the SAM as a self-organizing system that interacts with the shoot system provides a useful framework for exploring its functioning [3–5]. Mapping its symplasmic organization is a step in that direction.

## 1.2 Why Use Microinjection?

The dynamic nature of the SAM complicates the mapping of its symplasmic organization. A number of approaches have been followed so far. Stem feeding of symplasmic tracers and transgenic

**Fig. 1** (continued) sectors (L1–L3) Pd are formed secondarily. p, primordia. **(c)** A microelectrode (m.e.) penetrates a SAM cell, a membrane potential ( $E_m$ ) is measured, and current injection (–nA) drives LYCH into the target cell (1), and via Pd to an adjacent cell (2). **(d)** Before the tip enters the cell small charges at the SAM surface may be recorded (arrow 1). Upon penetration, a stable potential difference is recorded (arrow 2), which after withdrawal of the tip returns to zero (arrow 3). **(e–g)** SEM photos of a poplar SAM. **(e)** Overarching primordia (p). **(f)** The central part of the SAM surface with a projection of a microelectrode (m.e.). **(g)** As f, but with an additional ad hoc central symplasmic field (CSF). **(h)** Poplar SAM with actual CSF, viewed with a mix of white and blue light. lb leaf buttress; p primordia. **(i–k)** Birch apex and SAM. **(i)** Young birch seedling with apex encircled. **(j)** Projection (left panel) of a real CSF (right panel) in the SAM. **(k)** Projection (left panel) of a real PSF (right panel) in the SAM. Size of bars is 75  $\mu$ m (**e** and **h**), 20  $\mu$ m (**f** and **g**), 50  $\mu$ m (**j** and **k**). m.e. microelectrode, p primordia, cz central zone. **a, b, d** and **h, j–k**, are modified from respectively [3, 13, 15, 4]

expression of GFP-tagged peptides in leaves have both been used to study the symplasmic delivery path to and into the SAM [22, 23]. The end-result is dependent on Pd status and behavior along the entire path, from application or production point to final destination. Similarly, expression of GFP or GFP-tagged transcription factors within areas of the SAM show where Pd have been either in an open state, or have facilitated gated passage of the molecules during the time frame of the experiment [24]. A further complication is that it takes time to express GFP to visible levels. So far, real-time detection of symplasmic coupling in the SAM appeared to be possible only by using microinjection, which led to the discovery of SFs. The mere presence of SFs implies that cell–cell trafficking of proteins through Pd between SFs is possible without compromising SF integrity, suggesting that they pass through transiently gating Pd [16, 17]. Both iontophoresis and pressure injection have been used to study cell-coupling [25, 26], lineage analysis [27], and fate mapping [28] in animals, and cell-coupling in plants [4, 14, 29, 30]. In plants, presence of a cell wall, vacuole, and turgor pose unique problems [31, 32].

### 1.3 Why Use Iontophoresis?

As SAM cells are often smaller than 10  $\mu\text{m}$ , the impact of an invasive microelectrode should be minimized by using a very fine tip. In case of pressure injection this dramatically increases the required pressure, and thereby the risk that the tip moves in the cell, killing it [32]. Apart from this, injection of a volume tends to disrupt tiny plant cells and break the membrane seal, particularly as the injection volume is difficult to control. Thus, for SAM cells iontophoresis has important advantages above pressure injection. A smaller tip can be used, no volume is injected into the cell, and the procedure can be combined with membrane potential ( $E_m$ ) measurements. The advantage of the latter is that it allows registration of tip entry and the monitoring of the cell state during and after the injection [4, 14, 15]. Microinjections that failed due to cell collapse can thus be discarded. A down-side of this method is that it is restricted to injection of small charged compounds. Here, a step-by-step description is given of an experiment in which a SAM of a model tree species is iontophoretically microinjected.

---

## 2 Materials

### 2.1 Plant Material

Poplar (*Populus tremula*  $\times$  *P. tremuloides*) or birch (*Betula pubescens* Ehrh.) seedlings (see **Note 1**).

### 2.2 Microscopes (See Note 2) and Ancillary Equipment

1. Stereo dissection microscope (see **Note 3**).
2. Upright microscope with epi-fluorescent attachment (see **Note 4**), equipped with a high-pressure mercury arc lamp and specific excitation/barrier filter sets (excitation 470–490/

barrier 515/dichroic mirror 510 and excitation 400–440/ barrier 470/dichroic mirror 455) (*see* **Note 5**).

3. Vibration-free table in a room with a solid concrete floor (*see* **Note 6**).
4. Two fiber optic illuminators (*see* **Note 7**).
5. Hydraulic micromanipulator (*see* **Note 8**); head stage MN-2 and 3-D controller MO-203, Narishige PN-3, Narishige Scientific Instruments Lab.
6. Microelectrode puller (*see* **Note 9**) Narishige PN-3.
7. Iontophoresis unit, WPI Duo 773 Dual Microprobe System, World Precision Instruments (WPI) (*see* **Note 10**), with head-stage and low-input impedance ( $10^{11} \Omega$ ) probe WPI-712P.
8. Single channel flatbed recorder (*see* **Note 11**).
9. Camera system (*see* **Note 12**).

### **2.3 Small Materials, Probes, Medium, and Electrolyte Solution**

1. Borosilicate glass microcapillaries with inner filament (*see* **Note 13**).
2. Half-cell microelectrode holders with Ag/AgCl bridge (pellet), female socket and screw-cap; e.g. MEH3F10, WPI (*see* **Note 14**).
3. Syringe and filter, e.g. WPI F02010H50S (0.02  $\mu\text{m}$ ) (*see* **Note 15**).
4. Flexible nonmetallic filling syringe for back-filling of micro-electrodes, MicroFil MF34G, WPI (*see* **Note 16**).
5. 1 % LYCH in distilled water [Lucifer Yellow CH (457 kDa)] (*see* **Note 17**).
6. 100 mM KCl and 1 M KCL solutions made with distilled water (*see* **Note 18**).
7. 10 mM 2-deoxy-D-glucose (*see* **Note 19**).
8. Medium: Distilled water, pH 6.5–7.0, pre-equilibrated to room temperature (ca. 20 °C).

---

## **3 Methods**

1. Study the manual of the microelectrode puller. Run a test series (*see* **Note 20**), and select settings that will give the desired tip shape and size.
2. Estimate the approximate outer tip size of the microelectrode using a calibrated ocular micrometer (*see* **Note 21**). An outer tip of 1.0 to 0.5  $\mu\text{m}$  is suitable (*see* **Note 22**).
3. Familiarize yourself with the operation of the microscope (*see* **Notes 23 and 40**).

4. Get to know the basics of the iontophoresis unit by studying the manual and testing some functions as described therein (*see Note 24*).
5. Prepare stock solutions of 100 mM and 1 M KCl in distilled water, and store in a fridge. Next prepare a 1 % LYCH solution in distilled water, and keep a few small aliquots in eppendorf tubes in a fridge. For immediate use keep one tube on ice (*see Note 25*).
6. Prepare the bathing chamber (*see Note 26*). Press a small clump of nontoxic modeling clay (*see Note 27*) firmly at the bottom and puncture a hole in it that can accommodate the stem-apex unit. Fill the small hole with medium using a Pasteur pipette.
7. Cut the upper part of a shoot (ca. 5 cm) (*see Note 28*) and remove with a scalpel all leaves larger than 0.5 cm. Use the dissection microscope to gently remove with forceps the small leaves around the apex except for the smallest. Cut the stem back to a few millimeters below the apex (3–4 mm), and fix it with the lower end in the pre-made hole of the modeling clay. Press the modeling clay tightly but gently around the stem to immobilize it.
8. Fill the bathing chamber half with the medium using a Pasteur pipette. Remove under the dissection microscope the remaining minute leaves around the SAM, except for those that directly border the SAM (Fig. 1e). Add more medium, just enough to cover the SAM surface (*see Note 29*), but avoid pipetting it directly on top of the SAM.
9. Inspect position and condition of the SAM under the dissection microscope using epi-illumination from a fiber optic lamp. Transfer the chamber to the stage of the fluorescence microscope. Position the arms of a second fiber optic lamp in such a way that the SAM surface is illuminated. Inspect with the 4× objective to make sure that the SAM is properly visible, located in the center, and ready for injection.
10. Place the reference electrode (*see Note 30*) carefully in the bathing medium at close proximity of the apex. Measure tip resistance by sending a –1 nA current pulse through the microelectrode, using the ETR button on the iontophoresis unit (*see Note 31*).
11. Pull a microelectrode with the desired tip properties (*see Notes 21–23*).
12. Backfill the tip by carefully placing the end of the microelectrode in an eppendorf tube filled with the probe (e.g. LYCH) solution. The tip fills by capillary force in about 15–20 s. If this doesn't happen the tip might have trapped air or become sealed during the pulling process (*see Note 32*). In such case make a new microelectrode.

13. Fill a syringe with the electrolyte 0.1 M KCL and back-fill the microelectrode completely via a flexible syringe needle (*see* **Notes 16** and **33**). Inspect the microelectrode under the dissection microscope, making sure that no air bubbles are trapped inside, as they will make it useless.
14. Fill the electrode holder (*see* **Note 34**) with 0.1 M KCl, using the flexible syringe. Insert the back of the microelectrode through the screw cap into the holder (*see* **Note 35**). Electrolyte that spills over should be removed with a Kleenex tissue (*see* **Note 36**).
15. Inspect the microelectrode holder with the inserted microelectrode one final time to make sure no air bubbles are present (*see* **Note 37**).
16. Clamp the red microamplifier probe (712P) to the micro-manipulator that is fixed to the microscope stage, and connect it to the  $10^{11} \Omega$  of channel B at the WPI Dual 773 amplifier for measurement of the  $E_m$ .
17. Connect the microelectrode holder (with the inserted microelectrode) to the 712P probe.
18. Position the microelectrode tip manually above the chamber (*see* **Notes 8** and **38**).
19. Use the control knobs at the microscope stage to position the tip approximately above the apex in the center of the field of vision, but above the focal plane (*see* **Note 39**).
20. Lower the apex (SAM) just below the focal plane, and move it sideways just outside the field of vision to avoid unnecessary exposure to excitation light. Now turn on the excitation light source (*see* **Note 40**) and dim/shut-off the fiber optics lamp. Find the tip of the microelectrode. This is not too difficult as the tip is strongly fluorescent when exposed to blue light. Position the tip exactly in the center of the field of view and lower it into the bathing medium, but with the tip just above the focal plane.
21. Close the shutter of the excitation light source, and turn up/on the fiber optics lamp. The tip is now visible in the center of the field of view, but slightly out of focus. Subsequently, move the apex back into position under the out-of-focus tip. Both will now be visible in the center of the field of vision, but the SAM surface is just below the focal plane and the tip just above. Then bring tip and surface together so that they are almost in the same focal plane. Select the target cell and adjust the tip (*see* **Note 41**).
22. The set up is now ready for iontophoresis. As the tip of the microelectrode is in the bathing medium and the reference electrode connected to earth, we have obtained a closed electrical circuit. This will result in a small reading on the voltmeter,

a few millivolts, which can be nullified by using the offset knob on the DUAL WPI 773. The tip resistance can now be measured using the built-in circuit of the DUAL WPI 773.

23. Gently lower the tip with the help of the remote fine control until an abrupt negative jump in the potential ( $E_m$ ) is recorded (*see Note 42*). If the  $E_m$  rapidly stabilizes the cell has made a seal around the tip of the microelectrode (*see Note 43*; Fig. 1c, d).
24. When the  $E_m$  is stabilized (*see Note 44*) apply current to the microelectrode. Current should be kept as low as possible (*see Note 45*) to avoid leakage, cell collapse, and occlusion of the tip (*see Note 46*). Start with  $-1$  nA and, if necessary, increase the current gradually. In poplar and birch SAM cells can handle intermittent currents of up to  $-5$  nA (*see Note 47*). After obtaining a dye-coupling result (Fig. 1c) the  $E_m$  can be measured again to see if the cell has survived (*see Note 48*). However, once a SF is established (*see Note 49*) survival of the impaled cell is less critical as SF boundaries are created by cells that are peripheral to the injected cell. Occasionally, current application is not necessary and dye flows out spontaneously [30] during  $E_m$  recording.
25. Once a SF is established record the  $E_m$  from as many cells as possible, both within the SF and at its immediate periphery. Score all stable  $E_m$  values (Fig. 1d) and calculate the average (and standard error) for a SF (*see Note 50*). In birch and poplar  $E_m$  values within the CSF are lower than those in the PSF, showing that cells in a SF are not only dye-coupled (Fig. 1i–k) but also electrically coupled.
26. To minimize the impact of blue light on the SAM cells it is necessary to monitor the outflow of LYCH only for very brief moments (seconds), and only photograph the pattern once it has been established and spreading has stopped (*see Note 51*).
27. In case it seems uncertain if the dye-coupling group represents a CSF or not, a second cell of the dye-coupling group (containing dye imported from the original microinjected cell) can be microinjected. If the dye-coupling group brightens as a whole without changing its boundary it can be considered a genuine SF [14].

---

## 4 Notes

1. Good results are obtained by using vigorously growing seedlings, height of 30–75 cm. The stem can be cut at approx. 3–4 mm below the apex without inflicting damage to the apex, and firmly fixed in place in the middle of a microscope bathing chamber using nontoxic laboratory modeling clay.

2. All major brands have suitable dissection microscopes and fluorescence microscopes.
3. A stereo dissection microscope is necessary to surgically isolate a stem apex unit, to properly fix it in the bathing chamber, to remove the larger leaf primordia that surround the SAM, and to inspect microelectrodes during and after backfilling (*see Note 33*).
4. The microscope should be modified. Firstly, the resistances of filter block change-over levers and other filters should be removed, otherwise simply sliding the filters during an experiment will trigger a movement that will send the tip of the microelectrode into vibration, which will kill the impaled cell. Secondly, the micromanipulator headstage should be attached mechanically to the microscope stage so that the microelectrode moves together with the microscope table during focusing. This modification has to be carried out by a fine-mechanic (the microscope company might assist to realize this). The numerical aperture (NA) of the objective lenses determines their light-gathering capacity. Preferentially it should be 1.0. However, a higher NA means a shorter working distance. In case of microinjection of apices a compromise has to be found as the microelectrode should fit with a certain angle between objective and apex.
5. These filter block combinations were selected for use with Lucifer Yellow CH (LYCH). Other suitable dyes may require the same filter block combinations.
6. SAM cells are so small ( $\leq 10\ \mu\text{m}$ ) that tiny vibrations of the microelectrode tip tend to kill the impaled cell. To reduce this risk the injection microscope should be placed on a vibration-free table. A cheap version can be made in-house as follows. The manually operated remote 3-D controller should be placed on a separate table, with a central “window” for the microscope, which is placed over the microscope table. This way the microscope, and thereby the attached microelectrode, is not mechanically perturbed by what happens on the upper table. The microscope table should have a very sturdy metal construction that can carry a heavy stone plate (200 kg or more) on isolating rubber patches. The metal legs of the table should be standing in metal holders on heavy rubber stops. The floor should not transmit any vibrations, and placement of the table on a concrete floor in a ground level room or basement is advisable. Similarly, air movement caused by air conditioners, open windows, and people passing through the room should be prevented. Sophisticated vibration-free tables are available commercially.
7. The substage halogen lamp of the microscope cannot be used in case of apices and epi-illumination by fiber optics must be used.

8. Hydraulically operated micromanipulators (controllers) serve to avoid mechanical perturbation of the microscope and microelectrode tip (*see Note 6*). Various types are commercially available. A suitable brand is Narishige which has 3D and 4D hydraulically operated controllers that remotely move the headstage with the microelectrode-holder, which is fastened to the stage of the microscope.
9. Various types are commercially available. There are horizontal and vertical pullers, some of which are programmable (*see Note 20*). Most pullers would be suitable, but it requires some exercise to find the right settings for the microelectrode that is desirable.
10. Iontophoresis units have a voltmeter for  $E_m$  measurements (in mV) and a current pump (in  $\pm$ nA), allowing the registration of tip entry into the target cell as well the current-driven injection of small charged probes.
11. A chart or pen recorder can be used to graphically display membrane potentials (Fig. 1d). Electrical signals can also be read digitally allowing downloading to a computer.
12. A camera is required to record the emerging dye-coupling pattern. Excellent recordings can be made with classic ISO400 high-speed slide films. Digital images can be made by using a slide-scanner and compatible software. Alternatively, digital (video) cameras that are suited for low light intensities can be used.
13. Thick- and thin-walled capillaries with various outside diameters are commercially available. The outer diameter of the microcapillaries should precisely match the size of the microelectrode holder (*see Note 14*). Thick-walled capillaries are sturdier but for the tiny cells of the SAM thin-walled capillaries are better as they have a smaller outer-inner tip diameter ratio [33]. Microcapillary tubing with a minute filament sealed onto the inner side is particularly useful. During the pulling process the inner filament is extended into the tip, which allows for easy back-filling. The volume that is drawn into the tip relates to the tip diameter, and is estimated to be around 100 nl in a 1  $\mu$ m tip [33], the maximum tip dimension that can be used for SAM cells. Borosilicate microcapillaries are available from, among others, WPI (USA) or Clark Medical instruments (UK). The same companies also sell different microelectrode holders. Storage jars for microelectrodes are commercially available, but it is recommended to make a fresh microelectrode each time one is needed.
14. Select the right microelectrode holder. Firstly, it should fit onto the WPI due 773 probe. Secondly, it should be matching the diameter of the microelectrode tubing. A convenient type is a female holder with screw cap. The latter minimizes sliding

of the microelectrode in the holder. This is important as any sliding could break the membrane seal around the tip, and dislocate the tip to the nucleus, vacuole, or endomembrane system.

15. It is recommended that dye solutions are filtered to remove possible impurities.
16. MicroFil is a syringe needle made of plastic and fused silica (quartz) that can be coupled to a syringe filter via its luer fitting. The long, flexible, and elastic needle allows easy filling of the microelectrode very close to the tip. MicroFil model MF34G has a length of 67 mm, an outer diameter of 0.164 mm and an inner diameter of 0.1 mm. The needle can be cut with a razor blade to an appropriate length if desired.
17. Two forms are commercially available, LYCH and LYVS [34]. LYCH is most often used. It is nontoxic and has a high quantum yield (i.e. it is highly fluorescent). It is charged at neutral pH and can be iontophored, it diffuses rapidly through the cytoplasm but not through the cell membrane (due to its charge at cytoplasmic pH), it easily passes through Pd due to its small size (MW 457), and it does not affect cytoplasmic pH or Pd permeability. Although it becomes bound to cytoplasmic components and can accumulate in nuclei, this does not occur immediately [4, 26]. A disadvantage is that it may precipitate during iontophoresis in the presence of KCl, especially at high concentrations, thereby blocking the tip. Other suitable dyes with comparable properties are available commercially, e.g. Cascade Blue.
18. The 100 mM solution is used to fill the microelectrode shanks once the tip is backfilled with LYCH solution. The 1 M KCl solution is used to fill the chamber of the holder.
19. 2-deoxy-D-glucose (2-DDG) can be used when dye-coupling is absent or erratic. This could be due to cell damage that is inflicted by the microelectrode tip, involving callose (1,3- $\beta$ -D-glucan) deposition at Pd. 2-DDG is a competitive inhibitor that minimizes callose formation, and using it might improve success rates. As 2-DDG is not cheap the stem-apex unit should be pre-incubated in 2-DDG for 30 min (1–5 mM solution in distilled water) prior to its fixation in the chamber.
20. The horizontal Narishige PN-3 puller uses a magnet that operates in a two-step pulling process. A current is sent through a platinum resistance strip (Platinum Board PN-3H) that is surrounding the capillary, which will start to glow and melt the glass. The capillary is then pulled into two halves by the force of the magnet. Three factors determine the tip properties: type and composition of the glass, the current that is sent through the platinum strip and the strength of the programmed double pull of the magnet. Although in principle both microelectrodes

can be used it is recommended to use only the one that is pulled away from the platinum strip by the puller.

21. It is good practice to pull and fill a microelectrode only after the tissue is prepared and positioned under the injection microscope (*see* 3.11-12) to prevent LYCH precipitation in the tip and dust collection at the outside. The tip can be long, slender, and flexible, or short and sturdy. For birch and poplar SAMs the tips should not be too flexible in order to successfully penetrate the outer cell walls. However, the tip should also not be too short in order to prevent that the shanks, the widening part of the tip, touches the smallest primordia that surround the dome of the SAM (Fig. 1e).
22. Important interrelated properties are tip size and tip resistance. Iontophoresis units, like the WPI DUAL 773, have a built-in circuit to determine tip resistance, a measure for tip opening. Tips with resistances in the  $20\text{--}30 \times 10^6 \Omega$  ranges are recommendable [35]. Tip properties are fairly reproducible, but vibrations and deformation of the heating element might cause deviations. Avoid hitting (and deforming) the platinum strip while installing the glass tube.
23. It pays off to spend time in familiarizing yourself with the equipment. In particular, it is challenging to master the positioning and the fine-movement of the microelectrode under the microscope objectives and to bring the tip of the microelectrode and the SAM surface together in the same focal plane. Experiment with the microelectrode angle. Repeat these exercises with a tissue that is submersed in water, and only start real experiments when you feel comfortable in carrying out the necessary movements with some routine.
24. See for example [http://www.wpiinc.com/pdf/Duo773\\_IM.pdf](http://www.wpiinc.com/pdf/Duo773_IM.pdf).
25. Keeping small aliquots of dye-solution in the fridge is fine during continuous experimentation, but with longer breaks make a fresh solution.
26. A microscope bathing chamber can be custom made from transparent Plexiglas. A cheap solution is to use a transparent microscope slide box.
27. It is also possible to use the removable adhesive Tack-it, commonly available from office stores.
28. The length of the isolated shoot top is not critical.
29. This prevents it from losing turgor. Submersion is also necessary to create a closed electrical circuit between the microelectrode tip and the reference electrode.
30. It is recommended to ground the microscope to avoid spurious electrical fields from interfering with  $E_m$  measurements.
31. The ETR button sends a  $-1 \text{ nA}$  current through the probe, and from the reading of the voltmeter the tip resistance can be

calculated using Ohms law,  $V = I \times R$ . For example, applying  $-1$  nA might give a reading of  $-30$  mV, giving a tip resistance of  $30 \times 10^6 \Omega$ .

32. Backfilling (*see* **Note 13**) is a convenient and safe way of loading the tip. Alternatively, the tip can be filled with a syringe with a flexible plastic needle (*see* **Note 16**). It can, however, result in the trapping of a small air bubble, making the microelectrode useless. The filling process can be monitored under the dissection microscope. In case an air bubble is trapped in the tip, it may be removed by gently tapping the microelectrode below the tip. If this doesn't help then discard the microelectrode and make a new one.
33. Alternatively, thin hollow needles can be pulled by hand from a disposable plastic pipette tip that is heated over a small flame. The thin plastic thread can be cut with a razor blade, and the base of the pipette tip can be placed on a syringe filled with electrolyte.
34. The microelectrode holder (WPI) contains an Ag/AgCl disc.
35. First insert the back-end of the microelectrode through the screw cap, move the screw cap up to half-way the microelectrode, and then place the back-end into the electrode holder. Lower the screw cap and fasten it slowly. It is important to do this carefully, not tightening the cap too much as it will pressurize the content of the microelectrode. The function of the screw cap is not to apply pressure, but to prevent the tip from sliding.
36. This is necessary to prevent leak currents on the outside of the holder.
37. Air bubbles would insulate the tip and prevent iontophoretic microinjection.
38. This should be done by inspection from the side, and it is a first approximation.
39. The tip will be visible out of focus as a "shadow."
40. The Hg-lamp needs some minutes to stabilize. Keep the shutter closed to avoid unnecessary exposure of the apex to excitation light.
41. This whole procedure requires some patience as well as steady hands. It is recommended to exercise this procedure in advance with spare apices to prevent the unnecessary frustration of dealing with broken tips and damaged apices during real experiments.
42. Often, a very small  $E_m$  of a few  $-mV$  is recorded when the tip is touching the SAM surface (Fig. 1d). A substantial jump indicates that the tip has entered the cytoplasm. Best is to sit back, gently lower the tip with the remote fine-controller and watch the reading on the voltmeter ( $-mV$ ). The  $E_m$  curve can be recorded on paper (Fig. 1d) or electronically.

43. If  $E_m$  drops to zero while the tip is still in the cytoplasm the cell did not to produce a proper seal around the tip and the procedure should be repeated with another cell.
44.  $E_m$  values vary within a SAM. In poplar and birch cells of the central zone have smaller  $E_m$  values (close to the diffusion potential) than those of the peripheral zone (which might have active proton pumps) (*see Note 50*).
45. A high current ( $\geq -5$  nA) hyperpolarises  $E_m$  beyond physiological values and will induce leakage and often cell collapse.
46. The cytoplasm and tip locally heat up due to current flow, leading to coagulation of protoplasmic components at the tip, obstructing the opening and blocking dye outflow. To avoid such situation current may be applied intermittently.
47. The tip might be blocked by LYCH deposits, visible as an orange deposit that contrast with the bright yellow of dissolved LYCH. In case of very tiny deposits brief pulses of reverse current might dissolve the orange deposit and unplug the tip. The tip might also collect cell wall material during penetration that obstructs the opening. If so, it is best to make a new microelectrode.
48.  $E_m$  is often somewhat more negative after iontophoresis than before.
49. SFs form very quickly. In birch, CSFs often form in a few seconds, whereas a complete symplasmic ring at the SAM periphery (PSF) may take longer, up to 30 s [4].
50. In birch the average  $E_m$  in the CSF was  $-52$  mV ( $\pm$ s.e. 2), whereas at the PSF it was  $-98$  mV ( $\pm$ s.e. 4) [4]. In poplar the corresponding values were  $-44$  mV ( $\pm$ s.e. 1.3) and  $-89$  mV ( $\pm$ s.e. 3.6) [15].
51. Results can be further analyzed on a CSLM with an upright microscope.

## References

1. Steeves TA, Sussex IM (1989) Patterns in plant development. Cambridge University Press, New York
2. Sussex IM (1989) Developmental programming of the shoot apical meristem. *Cell* 56: 225–229
3. Van der Schoot C (1996) Dormancy and symplasmic networking at the shoot apical meristem. In: Lang GA (ed) *Plant dormancy: physiology, biochemistry and molecular biology*. CAB International, Wallingford, pp 59–81
4. Rinne PLH, van der Schoot C (1998) Symplasmic fields in the tunica of the shoot apical meristem coordinate morphogenetic events. *Development* 125:1477–1485
5. Van der Schoot C, Rinne PLH (2011) Dormancy cycling at the shoot apical meristem: transitioning between self-organisation and self-arrest. *Plant Sci* 180:120–131
6. Van der Schoot C, Rinne P (1999) Networks for shoot design. *Trends Plant Sci* 4:31–37
7. Schoof H, Lenhard M, Haecker A et al (2000) The stem cell population of Arabidopsis shoot meristems is maintained by a regulatory loop between the *CLAVATA* and *WUSCHEL* genes. *Cell* 100:635–644

8. Becraft PW (2002) Receptor kinase signalling in plant development. *Annu Rev Cell Dev Biol* 18:163–192
9. Reinhardt D, Pesce ER, Steiger T et al (2003) Regulation of phyllotaxis by polar auxin transport. *Nature* 426:255–260
10. Yanovsky MJ, Kay SA (2002) Molecular basis of seasonal time measurement in *Arabidopsis*. *Nature* 419:308–312
11. Böhlenius H, Huang T, Charbonell-Campaa L et al (2006) CO/FT regulatory module controls timing of flowering and seasonal growth cessation in trees. *Science* 312:1040–1043
12. Rinne PLH, Kaikuranta PM, van der Schoot C (2001) The shoot apical meristem restores its symplasmic organization during chilling-induced release from dormancy. *Plant J* 26:249–264
13. Bergmans A, de Boer D, Derksen D et al (1997) The symplasmic coupling of L2 cells diminishes in early floral development of *Iris*. *Planta* 203:245–252
14. Ormenese S, Havelange A, Bernier G et al (2002) The shoot apical meristem of *Sinapis alba* L. expands its central symplasmic field during the floral transition. *Planta* 215:67–78
15. Ruonala R, Rinne P, Kangasjärvi J et al (2008) *CENLI* expression in the rib meristem affects stem elongation and the transition to dormancy in *Populus*. *Plant Cell* 20:59–74
16. Epel BL (1994) Plasmodesmata: composition, structure and trafficking. *Plant Mol Biol* 26:1343–1356
17. McLean BG, Hempel FD, Zambryski PC (1997) Plant intercellular communication via plasmodesmata. *Plant Cell* 9:1043–1054
18. Carpenter R, Coen ES (1995) Transposon induced chimeras show that *floricaula*, a meristem identity gene, acts non-autonomously between cell layers. *Development* 121:19–26
19. Perbal M-C, Haugh G, Seadler H et al (1996) Non-cell autonomous function of the Antirrhinum floral homeotic proteins DEFICIENS and GLOBOSA is exerted by their polar cell-to-cell trafficking. *Development* 122:3433–3441
20. Kim JY, Yuan Z, Jackson D (2003) Developmental regulation and significance of KNOX protein trafficking in *Arabidopsis*. *Development* 130:4351–4362
21. Urbanus SL, Martinelli AP, Dinh QD et al (2010) Intercellular transport of epidermis-expressed MADS domain transcription factors and their effect on plant morphology and floral transition. *Plant J* 63:60–72
22. Gisel A, Barella S, Hempel FD et al (1999) Temporal and spatial regulation of symplasmic trafficking during development in *Arabidopsis thaliana* apices. *Development* 126:1879–1889
23. Corbusier L, Vincent C, Jang S et al (2007) FT protein movement contributes to long-distance signalling in floral induction of *Arabidopsis*. *Science* 316:1030–1033
24. Wu X, Dinneny JR, Crawford KM et al (2003) Modes of intercellular transcription factor movement in the *Arabidopsis* apex. *Development* 130:3735–3745
25. Stewart WW (1978) Functional coupling between cells as revealed by dye-coupling with a highly fluorescent naphthalamide tracer. *Cell* 14:741–759
26. De Laat SW, Tertoolen LGJ, Dorrestein AWG et al (1980) Intercellular communication patterns are involved in cell determination in early molluscan development. *Nature* 287:546–548
27. Weisblat DA, Sawyer RT, Stent G (1978) Cell lineage analysis by intracellular injection of a tracer enzyme. *Science* 202:1295–1298
28. Technau GM, Campos Ortega JA (1985) Fate mapping in wild type *Drosophila melanogaster*. II. Injections of horse radish peroxidase in cells of the early gastrula. *Roux Arch Dev Biol* 194:196–212
29. Erwee MG, Goodwin PB (1985) Characterisation of the *Egeria densa* Planch. leaf symplast. Symplast domains in extrastelar tissues of *Egeria densa*. *Planta* 163:9–19
30. Tucker EB (1990) Analytical studies of dye-coupling between plant cells. In: Robards AW, Lucas WJ, Pitts JD et al (eds) *Parallels in cell to cell junctions in plants and animals*, vol 46, NATO ASI series, Series H: cell biology. Springer, Berlin, pp 239–248
31. Brownlee C (1994) Microelectrode techniques in plant cells and microorganisms. In: Ogden D (ed) *Microelectrode techniques: the Plymouth Workshop Handbook*. Company of Biologists Limited, Cambridge, pp 347–359
32. Storms MMH, van der Schoot C, Prins M et al (1998) A comparison of two methods of microinjection for assessing altered plasmodesmal gating in tissues expressing viral movement proteins. *Plant J* 13:131–140
33. Mobbs P, Becker D, Williamson R et al (1994) Techniques for dye injection and cell labelling. In: Ogden D (ed) *Microelectrode techniques: the Plymouth Workshop Handbook*. Company of Biologists, Cambridge, pp 361–387
34. Stewart WW (1981) Lucifer dyes: highly fluorescent dyes for biological tracing. *Nature* 292:17–21
35. Halliwell JV, Whitaker MJ, Ogden D (1994) Using microelectrodes. In: Ogden D (ed) *Microelectrode techniques: the Plymouth Workshop Handbook*. Company of Biologists, Cambridge, pp 1–15



## Analysis of the Conductivity of Plasmodesmata by Microinjection

Friedrich Kragler

### Abstract

Pressure microinjection can be used to introduce fluorescent dyes and labeled macromolecules into single cells. The method allows measuring transport activity of macromolecules such as proteins and RNA molecules within and between cells. Routinely, plant mesophyll cells are injected with fluorescent dextran molecules of specific sizes to measure an increase of the size exclusion limit of plasmodesmata in the presence of a co-injected or expressed protein. The mobility of a macromolecule can also be addressed directly by injecting a recombinant protein that itself is labeled with fluorescent dye and following its transport to neighboring cells. This chapter describes a pressure microinjection protocol successfully applied to *Nicotiana* leaves. This protocol requires basic skills and experience in handling a microscope equipped with an imaging system, a micromanipulator, and a microinjection system attached to an upright microscope. Using this equipment, a trained person can inject approximately 10–20 mesophyll cells per hour.

**Key words** Microinjection, Single-cell manipulation, Intercellular transport, Plasmodesmata

---

### 1 Introduction

Microinjection into plant cells is a way to test symplasmic conductivity between individual cells and tissues established by the intercellular pores named plasmodesmata [1–5]. The methods applied here are relatively simple given that the right equipment is available and the user is experienced in microscopy and micromanipulation. Various fluorescent probes ranging from large labeled RNAs and proteins to small tracer molecules are microinjected into a single cell and tested for their capacity to move into adjacent cells. Distribution of the dye within and between neighboring cells is followed under an epifluorescence microscope or a confocal laser scanning microscope (CLSM) equipped with appropriate fluorescence filters and a sensitive detection and imaging system. Injection of fluorescent tracers and macromolecules of various sizes and compositions into single living cells allows to (1) measure the size exclusion limit (SEL), and thus the open, dilated, or closed state of plasmodesmata,

which reflects the potential symplasmic connectivity between cells, and (2) the intercellular transport capacity of proteins and RNA-protein complexes. An open state of plasmodesmata allows the diffusion of small symplasmic tracers (<1 kDa) from cell to cell. A dilated state of plasmodesmata is indicated by intercellular movement of fluorescent tracers, i.e., large fluorescent dextrans (>10 kDa) that normally do not move [3]. The observation of such a dilated (or increased) SEL upon injection of large fluorescent tracers (>10 kDa) in the presence of specific co-injected proteins or protein-RNA complexes indicates the capacity of the specific macromolecular probe to interact with plasmodesmata and to increase their SEL. By opening the plasmodesmata, the injected macromolecular probe may itself move between cells. Thus, another application of microinjection is to inject labeled RNAs and proteins in order to follow their intra- and intercellular transport routes.

In general two types of microinjection procedures, iontophoretic injection or pressure injection, are employed and each of these has its individual advantages and disadvantages [6]. Iontophoretic injection systems apply a high electrical current to drive a charged dye out of the micropipette tip into a cell. This method has the advantage that transmembrane electrical potentials can be measured simultaneously [7], which allows to monitor the integrity of the injected cell. However, necessary currents driving a charged dye or a protein/RNA from a loaded micropipette into a targeted cell might not be applicable to a number of dyes as the applied current depends on the isoelectric point of the injected molecules. In addition, interfering with the electro-potential of a cell or tissue might irreversibly disrupt cytoplasmic streaming [2, 6], potentially render tonoplasts leaky [7], and change the redox status and, thus, the metabolism of the probed cell or tissue. In addition the redox status shift can result in opening or closing of plasmodesmatal pores [1]. In contrast to iontophoresis, the pressure injection system applies a physical force (air pressure) to propel the probe into the target cell. To achieve expulsion of the probe into a cell, the hydrostatic pressure in the microcapillary (=injection needle) is raised above that of the turgor pressure of the injected cell compartment [4, 6]. In general, it is thought that sudden pressure changes are less harmful to plant cells than changes in the electro-potential of cells as plants evolved to tolerate turgor pressure changes. Here we describe the pressure injection technique used by a number of independent laboratories to investigate intercellular mobility of specific proteins and, thus, the transport activity in living tissues.

---

## 2 Materials

### 2.1 Microinjection Buffer

1. Sterile 5× injection buffer (5× IB): 50 % glycerol, 500 mM NaCl, 50 mM Tris base pH 7.5, 5 mM EDTA. Dilute and add 1 mM DTT to 1× IB prior to use (*see* **Note 1**).

## 2.2 *Fluorescent Tracers*

Prepare 10× stocks (20 mM, dissolved in 1× IB) of the following fluorescent dyes and store protected from light at 4 °C for short-term storage or at –80 °C for long-term storage. The fluorescent probes used in microinjection assays should have a final concentration of 0.5–2 mM in 1× IB (*see Note 2*).

1. Fluorescent dyes to measure plasmodesmatal SEL:
  - (a) 1 kDa Dextran (fluorescein isothiocyanate or rhodamine labeled; Sigma).
  - (b) 10–12 kDa Dextran (fluorescein isothiocyanate or rhodamine labeled; Sigma).
  - (c) 20–25 kDa Dextran (fluorescein isothiocyanate or rhodamine labeled; Sigma).
2. Fluorescent dyes to stain the cytoplasm and to control tissue integrity and intercellular connectivity (sympasmic tracer):
  - (a) Lucifer Yellow (Sigma); green fluorescent.
  - (b) Fluorescein; green fluorescent.
  - (c) Acridine Orange (Molecular Probes/Sigma); green and red fluorescent; binds to RNA/DNA and cell wall material; good indicator for leakage of injections and for training. Store at 4 °C protected from light.
3. Osmotic pressure equilibration solutions:
  - (a) 100 mM Mannitol.
  - (b) 50 mM Mannitol.
  - (c) 10 mM Mannitol.Prepare in sterile water and store at room temperature.

## 2.3 *Microscope and Microinjection Equipment*

1. Upright epi-fluorescence microscope equipped with appropriate filters such as green (GFP, fluorescein) and red (RFP, Texas Red) band-pass filters that block the visualization of chloroplast auto-fluorescence, and a sensitive imaging system, or an upright confocal laser scanning microscope (e.g., SP5, Leica) (*see Note 3*). Either system is suitable for microinjection assays and should be equipped with a long-distance 20× air objective and a micropipette holder attached to the microscope stage to allow focusing the microscope to the needle by z-axis movement of the stage (Fig. 1). To avoid damage of the microinjected cells during microinjection the microscope with the attached needle holder has to be placed on a suitable vibration-free table (e.g., an air floating table). For additional information on a suitable setup, *see ref. 4*.
2. Micropipette holder (e.g., from Eppendorf) attached to a movement manipulator hydraulically connected to a 3-D controller with additional forward movement (e.g., from Narishige Scientific Instruments): The holder together with 3-D hydraulic

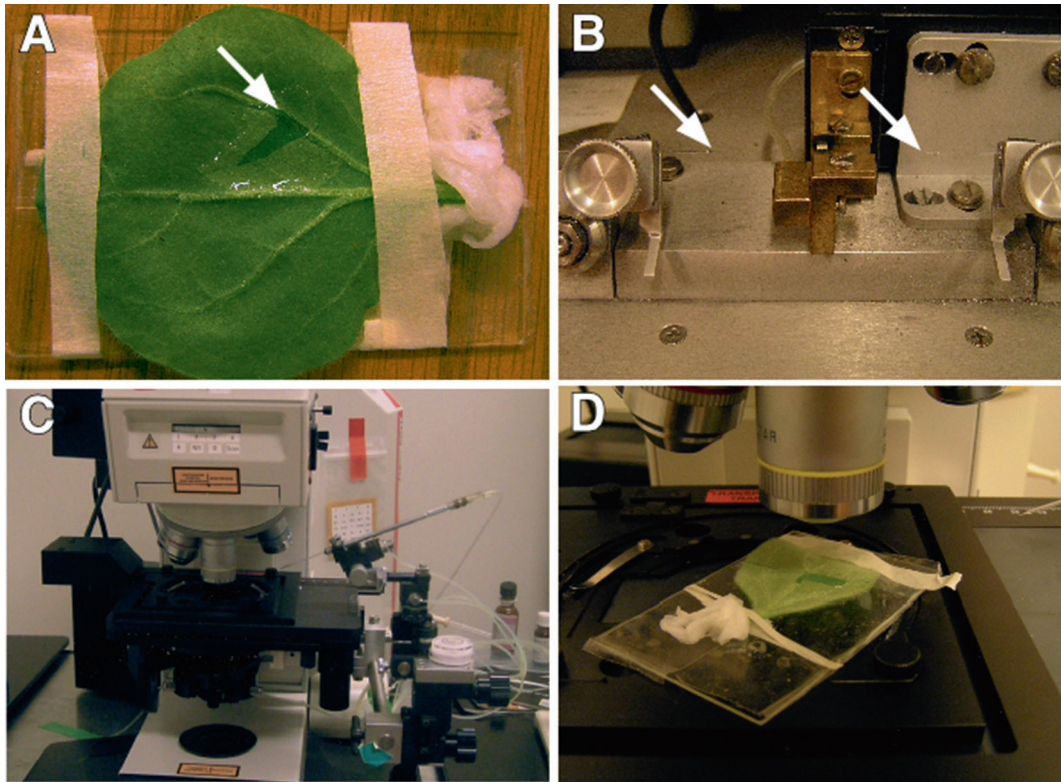


**Fig. 1** (a) Example of a detached *N. benthamiana* leaf used for microinjection of mesophyll cells. The dark green area (arrow) shows tissue where the epidermis was peeled of and incubated with water. (b) A pair of microinjection needles made from a microfilament. (c) Setup of a confocal laser scanning microscope placed on an airflow table and equipped with a micromanipulator and a microinjection needle holder attached to the stage. (d) Object holder with a prepared leaf under a 20 $\times$  long-working-distance objective

movement system should be tightly connected to the stage of the upright microscope (Fig. 1). The back of the micropipette holder must be connected by plastic tubing to the outlet of an air pressure supply system controlled by a manual valve (up to 10 bar) or by a pressure injector controller (Eppendorf) connected to a pressure source (N<sub>2</sub>, He, or air bottle).

3. Pressure injection regulation unit (e.g., from Eppendorf, or a manual valve): This unit is required for applying a controlled injection pressure of approximately 1.5–10 bar during pressure injection. Air pressure sources can be a pneumatic pump or any air pressure supply such as N or He bottles with suitable pressure regulators, or compressed air from the house supply (see **Note 4**).
4. Needle puller (e.g., Narishige micropipette puller or Sutter Instruments micropipette puller) for controlled microinjection needle production from glass tubes.

5. Filamented borosilicate glass tubes (e.g., BF100-50-10, Sutter Instrument; or GC 150F-10, Clark Electromedical) with an outside diameter of 1 mm, an inside diameter of 0.5 mm, and an overall length of 10 cm.
6. Large glass slides (e.g., 76.2×50.8 mm) and adhesive textile tape (double sided).

#### 2.4 Plant Material

1. Mature leaves from 3 to 5-week-old nonflowering and healthy *Nicotiana* sp. plants grown in the green house or environmental chamber.

---

### 3 Methods

To test the capacity of a macromolecule to move from cell to cell and dilate plasmodesmatal pores it should be fluorescently labeled or co-injected with large fluorescent dextrans, respectively. For both assays the macromolecule has to be isolated and purified.

#### 3.1 Optional Preparation of Proteins or RNA for Microinjection and Fluorescent Labeling

1. Prepare purified protein (>1 µg/µl, >95 % purity) or RNA using a suitable expression or isolation system. Proteins can be easily purified by tagging and purification techniques such as GST- or His-tag systems. RNA can be synthesized by in vitro transcription using available systems such as the T7-based transcription systems (*see Note 5*).
2. Produce fluorescently tagged proteins. Use standard protein labeling kits that attach amine- or sulfhydryl-reactive fluorophores to purified proteins. These kits are available from several companies (Pierce or Sigma-Aldrich). Following the labeling reaction, separate the protein from non-incorporated fluorophores and also change the buffer to 1× IB by stepwise dialysis or by using a size-exclusion chromatography system (e.g., Bio-spin columns, BioRad).
3. Label RNA with fluorescence. In vitro transcribe RNA in the presence of modified fluorescent nucleotides (for example, by using the Atto Labeling Kit from Jena Bioscience), or label RNA after in vitro transcription by chemical coupling of a fluorophore (e.g., Ulysis Nucleic Acid Labeling Kit, Molecular Probes). Use a size-exclusion chromatography system (e.g., Bio-spin columns, BioRad) to separate labeled RNA from non-bound fluorophores and change the buffer system to 1× IB.

#### 3.2 Preparation of Plant Material for Microinjection

1. Place a fully expanded *Nicotiana* sp. source leaf (nonflowering plant) either detached at the petiole or attached to the plant with its adaxial side (upper leaf surface) onto a large microscope slide. Use double-sided tape or small stripes of a textile tape for fixation (Fig. 1). When using detached leaves, wrap a paper tissue soaked with water around the petiole.

2. Apply water onto the leaf surface (1–2 ml over an area of 1–2 cm<sup>2</sup>) to ensure that the leaf tissue will not dry after removing the epidermis by peeling (*see Note 6*).
3. Use aligned straight or bend precision forceps to grip the epidermal tissue at a vascular strand and remove slowly the epidermis in the water-covered area.
4. Cover the exposed subepidermal tissue again with water and wash 2–3 times within 1 min by taking off the water with a tissue paper and reapplying water with a pipette. After washing, the water is replaced twice by a mannitol solution (normally 20–50 mM) for osmotic pressure adjustment (*see Note 7*). Take care that the exposed tissue is covered with liquid during all steps.
5. Use the peeled leave area for injection of your probes after 5-min incubation at room temperature. A detached leaf prepared for microinjection is shown in Fig. 1a.

### **3.3 Preparation of the Microinjection Needle and Probe Loading**

1. Prepare a microinjection needle by placing a filamented glass tube into the needle puller and use the settings recommended by the supplier to pull appropriately shaped injection needles. The needles should have an opening of 1 µm or smaller (*see Note 8*).
2. Load the glass needle with a fluorescent probe (*see Note 9*) by immersing the rear end in 5–10 µl of the probe in a 0.5 ml Eppendorf tube for >2 min. Check the presence of the loaded probe in the needle tip by exposing the needle to a fluorescent light source, e.g., by holding it under the microscope fluorescent light source (e.g., under the 10× objective).
3. Move the rear end of the needle into the needle holder and make sure that the end is airtightly sealed (Fig. 1).
4. Adjust the loaded needle at an angle of about 30° in the needle holder, center the tip under the objective (20×, long working distance) above the peeled tissue, and focus on the needle tip.

### **3.4 Microinjection**

1. Use the normal-phase contrast setting of the microscope and avoid exposure to fluorescent light to limit bleaching of your fluorescent probe. Use a long-distance 20× objective.
2. Move the needle tip in the center of your field of view and above the peeled tissue covered by mannitol.
3. While focusing the view through the microscope onto the needle tip, move the needle using the micromanipulator slowly down along the z-axis towards the peeled tissue surface until the needle is submerged into the mannitol solution (*see Note 10*).
4. Proceed with downward movement until mesophyll cells can be distantly recognized.
5. Without changing the position of the needle, now focus the view on the tissue and move the stage until you identify a specific mesophyll cell for injection (*see Note 11*).

6. Center the tissue or move the needle in such a way that the needle orifice resides over the aerial space between the mesophyll cells (*see Note 12*).
7. Lower the stage until the needle is again in focus.
8. Lower the needle and the focus until both the target cell and the needle are in focus.
9. Use the  $x$ - and  $y$ -axes of the micromanipulator to position the needle tip in the mesophyll air space close to the target mesophyll cell.
10. Use the micromanipulator to move the needle tip slowly towards the edge of the cell wall of the targeted cell without touching it.
11. Move the needle, if possible, in parallel to the micro-needle angle, through the cell wall. The cell wall/membrane will slightly bend as the needle pushes against the cell surface.
12. Interrupt the movement of the needle when a sudden slight movement of the cell wall towards the tip of the needle is observed. This observation marks the penetration of the needle tip into the cytosol.
13. Switch the microscope to fluorescent light emission and detection.
14. Inject the probe by opening the pressure valve until the injected dye is loaded into the target cell (*see Note 13*).
15. Use the micromanipulator to remove the needle as fast as possible from the cell and out of the mannitol solution covering the tissue.
16. Use a paper towel to remove the mannitol solution, which might be contaminated by the fluorescent probe, and apply new mannitol solution onto the tissue with a pipette.
17. Readjust the microscope focus to visualize the injected cell and observe the distribution of the injected fluorescent probe through the ocular or the digital imaging system. If a symplasmic tracer probe was used, the fluorescent dye will appear in the neighboring (attached) cells within several seconds (*see Fig. 2* for illustration of successful and failed injection experiments); if a non-moving labeled control protein (e.g., BSA or GST) or a large fluorescent dextran molecule (>10 kDa) was used, the fluorescent probe will remain in the cytosol of the injected cell (*see Note 14*).
18. Record the distribution of the injected probe using the appropriate fluorescent filter settings available with your imaging system (*see Note 15*).
19. For a new injection, change the needle (*see Note 16*).

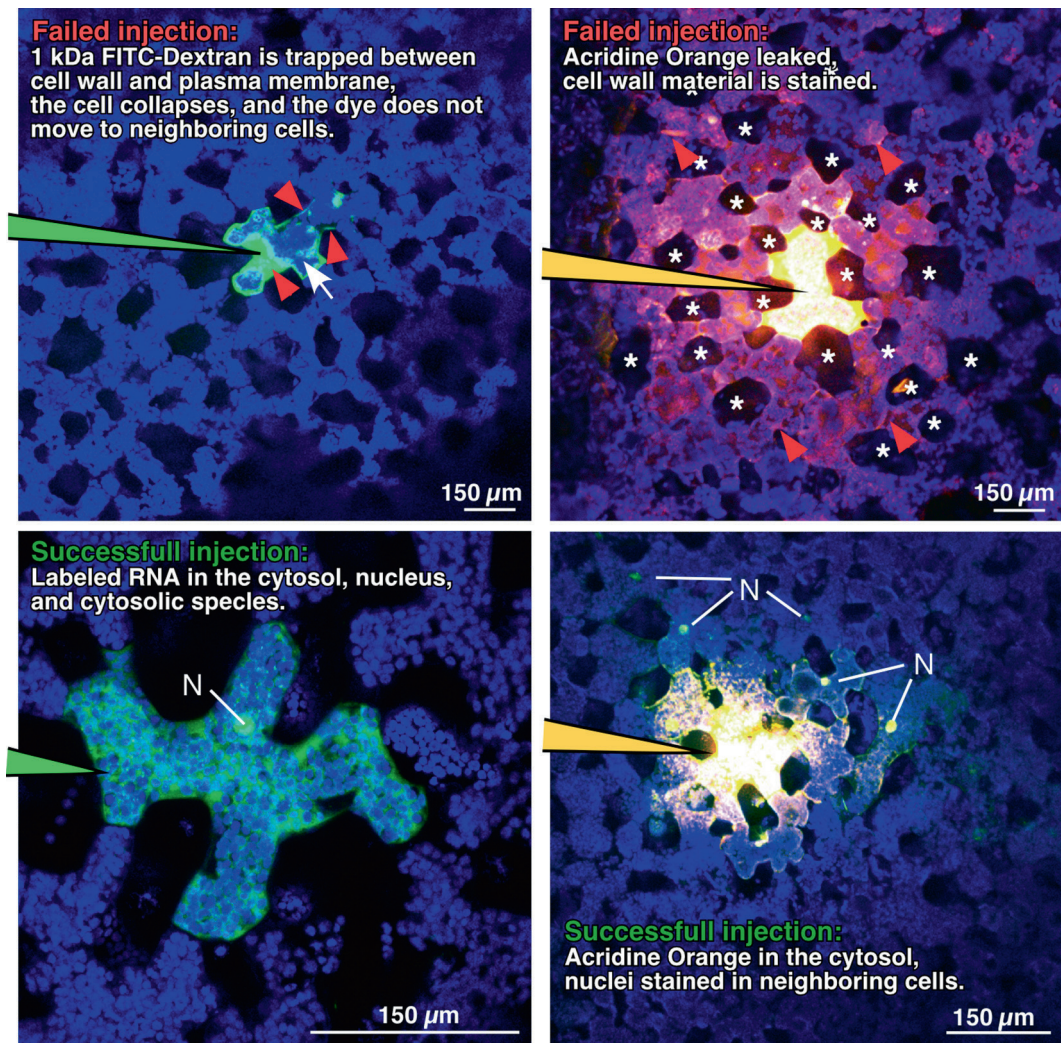


**Fig. 2** Confocal images showing failed and successful microinjections of mesophyll cells. *Upper panel:* Failed injections; *red arrowheads* indicate the region where the fluorescent dyes were located in cellular areas that do not resemble the cytoplasm. *Stars* indicate the areal space between mesophyll cells. *Lower panel:* Successful injections. *Left:* The subcellular distribution of labeled RNA appears normal in the cytosol and in the nucleus. *Right:* Microinjection of the small symplasmic tracer dye Acridine Orange, which binds to RNA, DNA, and cell wall material. Note that the injection was successful as the nuclei (N), but not the cell walls, are stained in adjacent cells (compared to *upper panel*)

## 4 Notes

1. The 50 mM Tris buffer in the 5× IB can be replaced by a 50 mM phosphate buffer pH 7.5.
2. Depending on the sensitivity of the microscopic detection/filter system the concentration of the fluorescent dyes can be increased or decreased. The final concentration of the IB in a mixed probe, e.g., 10 kDa dextran mixed with a recombinant produced protein, should be 1×.

3. Both systems are suitable for microinjection assays. However, a confocal system has several advantages as leakage of the probe during microinjection and subcellular as well as intercellular transport can be evaluated at a higher cellular resolution compared to a conventional microscopic system. The disadvantage of a high-resolution confocal system is that it takes some time (30 s to 2 min) to adjust the focus (z stacks), start the detection system, and make a high-resolution scan of the tissue after injection. Thus, the initial dynamics of the probes, e.g., pace of movement into neighboring cells, and intracellular dynamics might not be documented properly.
4. The pressure necessary for injection depends on the plant species, the age of the plants, and also the cell type used as different cells have their specific turgor pressure and volume. Accordingly, the duration of injection and required pressure can vary significantly.
5. *E. coli*-expressed proteins lack eukaryotic modifications and, thus, when such activities are expected to be necessary for movement, the protein should be purified from a eukaryotic expression system or from plant cells using a suitable transient expression system (e.g., expression and purification after leaf agro-infiltration).
6. The epidermis has to be peeled to gain access to the mesophyll cells. Alternatively, epidermal cells can be injected directly without wounding of the tissue. However, this needs some adaptation to the protocol as the turgor pressure is higher in the intact epidermal cell and the evaluation of the transport of injected probes might be difficult without prior training and experience in microinjection of mesophyll cells.
7. Osmotic pressure adjustment with mannitol is necessary to avoid collapsing of the cells or expulsion of cytoplasmic content when the microinjection needle is inserted. Thus, the turgor pressure of the liquid covering the tissue has to be adjusted by increasing or decreasing the mannitol concentration accordingly.
8. Micropipette pullers are very diverse in their making depending on the product generation and the type of heater filaments used. Refer to the manual of the supplier for a guideline and optimal parameters to produce a suitable injection needle. The following settings were used with a Sutter Instruments P-97 Micropipette Puller and may serve as a guideline:
  - Airflow set to 540
  - Loop 1: Heat 670, Pull 15, Vel. 16, Time 8 (determines the neck of the needle)
  - Loop 2: Heat 670, Pull 22, Vel. 12, Time 1 (determines the length and diameter of the orifice)
  - Loop 3: Heat 670, Pull 150, Vel. 100, Time 200 (produces the orifices)

9. Use first small symplasmic tracer probes such as Lucifer Yellow, Acridine Orange, or small fluorescent dextrans (<1 kDa) to test the integrity and connectivity of the injected tissue. When you confirmed intercellular movement of one of these tracers and that large dextrans (>10 kDa) remain in the injected cells, use the labeled protein/RNA probe or a mixture of non-labelled protein/RNA probe with larger dextrans (>10 kDa) to test their movement capacity or effect on plasmodesmatal SEL. Note that concentrated RNA or protein probes (>5 µg/µl) might precipitate prior to loading or during the capillary surface tension transfer along the filament in the needle and, thus, will not be present in the tip. To avoid precipitation, you may dilute your probe, sonicate your probe in a water bath sonicator for 5 s, or test dilutions, or an alternative microinjection buffer system.
10. If an excess of liquid (mannitol solution) was used to cover and wash the peeled area, it might be difficult to keep the needle in focus as the needle approaches the tissue surface and enters the liquid. In this case, take off some liquid with a paper towel, but make sure that the tissue is still covered with the mannitol solution.
11. The choice of a suitable cell is based on the integrity of the target cell and its neighboring cells (e.g., the cells should not be collapsed or otherwise damaged). The injection should not be in cells too close to the epidermal peeling border or in proximity of cells above veins. Keep a distance of at least four cells from damaged cells or veins.
12. The placement of the needle in the aerial space between the mesophyll cells and close to the same *z* level (focus point) as the cell wall of the injected cell provides room for needle movement in all three dimensions without touching and wounding cells and to choose the best injection point.
13. Note that leakage of the dye might appear at the position where the needle penetrates the cell. This should be avoided. If leakage does not stop after releasing the pressure and after retraction of the needle, a new injection in a distant cell should be performed. Alternatively, the needle orifice might be broken or too large and a new needle with different settings should be produced. If the probe does not leave the needle upon applying pressure, the microcapillary might be plugged by cell wall material or by precipitation of the probe. Use a new needle and inspect the probe in the loaded needle for uneven fluorescence such as the presence of fluorescent bodies appearing in the loaded solution or of a fluorescent gradient along the loading filament.

14. If the injected probe disperses rapidly within the whole lumen of the cell and does not show a dynamic distribution within the injected cell, or if a small symplasmic dye such as Lucifer Yellow does not move as expected to neighboring cells, the needle most likely pierced through the cytoplasm and the injection occurred into the vacuole. If a symplasmic tracer dye such as Lucifer Yellow or small dextran (1 kDa) does not move to the neighboring cells within seconds, the cell or tissue used for microinjection has closed plasmodesmatal connections and is not suitable for probing protein/RNA movement. Try another cell. If injection of other cells also fails to indicate transport of the dye to neighboring cells, prepare a new leaf from a different plant for microinjection. Note that a detached *N. benthamiana* leaf should not be used for longer than 30 min for microinjection and make sure that the petiole is properly wrapped with a paper towel soaked with water during all stages of manipulation.
15. Once it is confirmed that a symplasmic tracer dye such as Lucifer Yellow or small dextran (1 kDa) moves between cells whereas larger dextrans (>10 kDa) do not, begin as soon as possible (within minutes) with the injection of your probe of interest such as fluorescent protein or protein/RNA or a protein or protein/RNA sample mixed with large fluorescent dextran (>10 kDa). The evaluation of movement is based on the number of events of dye movement into neighboring cells observed in at least three different leaves from independent plants. Approximately 20 injections of each probe should be made, and all tissues should be controlled for the ability to support Lucifer Yellow movement between cells. A protein probe which moves between cells and dilates the plasmodesmatal pore has normally a movement rate of >50 % (e.g., 10 of 20 microinjections show movement of the probe out of the injected cell) whereas large dextran (>10 kDa) has a movement rate well below 10 % (e.g., 2 of 20 injections could indicate some limited movement activity). Also the extent of movement indicated by the number of cells receiving the fluorescent probes and are not in direct contact to the injected cell should be evaluated. For example, proteins that are co-injected with large fluorescent dextran (>10 kDa) might be able to dilate plasmodesmata in the injected cell but not move from cell to cell and thus not dilate the plasmodesmata of the adjoining cells. In such a case the fluorescence associated with the fluorescently tagged dextran probe would not move beyond the adjoining cells.
16. The orifice of a needle is normally plugged by cell wall material or broken after two injections. Thus, change the needle after injection to ensure that you can microinject another cell.

## References

1. Benitez-Alfonso Y, Jackson D, Maule A (2011) Redox regulation of intercellular transport. *Protoplasma* 248:131–140
2. Goodwin PB, Shepherd V, Erwee MG (1990) Compartmentation of fluorescent tracers injected into the epidermal cells of *Egeria densa* leaves. *Planta* 181:129–136
3. Haywood V, Kragler F, Lucas WJ (2002) Plasmodesmata: pathways for protein and ribonucleoprotein signaling. *Plant Cell* 14(Suppl): S303–S325
4. Komarova Y, Peloquin J, Borisy G (2011) Components of a microinjection system. *Cold Spring Harb Protoc* 2011:935–939
5. Lucas WJ, Ham BK, Kim JY (2009) Plasmodesmata—bridging the gap between neighboring plant cells. *Trends Cell Biol* 19: 495–503
6. Oparka KJ, Murphy R, Derrick PM et al (1991) Modification of the pressure-probe technique permits controlled intracellular microinjection of fluorescent probes. *J Cell Sci* 98:539–544
7. Van der Schoot C, Bel AJE (1989) Glass micro-electrode measurements of sieve tube membrane potentials in internode discs and petiole strips of tomato (*Solanum lycopersicum* L.). *Protoplasma* 149:144–154

## Investigating Plasmodesmata Genetics with Virus-Induced Gene Silencing and an *Agrobacterium*-Mediated GFP Movement Assay

Jacob O. Brunkard, Tessa M. Burch-Smith, Anne M. Runkel,  
and Patricia Zambryski

### Abstract

Plasmodesmata (PD) are channels that connect the cytoplasm of adjacent plant cells, permitting intercellular transport and communication. PD function and formation are essential to plant growth and development, but we still know very little about the genetic pathways regulating PD transport. Here, we present a method for assaying changes in the rate of PD transport following genetic manipulation. Gene expression in leaves is modified by virus-induced gene silencing. Seven to ten days after infection with *Tobacco rattle virus* carrying a silencing trigger, the gene(s) of interest is silenced in newly arising leaves. In these new leaves, individual cells are then transformed with *Agrobacterium* to express GFP, and the rate of GFP diffusion via PD is measured. By measuring GFP diffusion both within the epidermis and between the epidermis and mesophyll, the assay can be used to study the effects of silencing a gene(s) on PD transport in general, or transport through secondary PD specifically. Plant biologists working in several fields will find this assay useful, since PD transport impacts plant physiology, development, and defense.

**Key words** Plasmodesmata, Virus-induced gene silencing, Plant transformation, Transient gene expression, Agroinfiltration, *Agrobacterium*

---

### 1 Introduction

Plasmodesmata (PD) are small, membrane-bound channels that cross the cell wall, connecting the cytoplasm of adjacent cells. Small molecules (e.g., water, ions, sugars, and signaling compounds) and large biomolecules (e.g., proteins, RNAs, and viruses) move between cells via PD. PD are essential conduits for intercellular communication and resource allocation in plants: all land plants have PD, and no mutant lacking PD has ever been recovered [1, 2].

Classically, PD transport was assessed by the “size exclusion limit” of PD: the size of the largest molecule capable of transporting from one cell to the next via PD. While the size exclusion limit is a useful measure of changes in PD transport over developmental

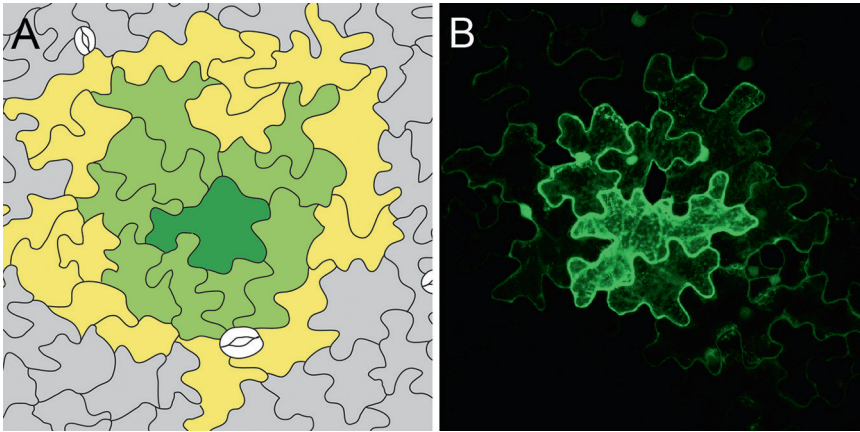


**Fig. 1** GFP diffusion in the leaf epidermis. **(a)** After a cell is transformed by *Agrobacterium* carrying  $35S_{pro}::GFP$  T-DNA, GFP expresses most strongly in that cell (dark green). Over the course of 2–3 days, GFP may diffuse via PD to neighboring cells; here, GFP has spread two cells from the transformed cell (light green and yellow). GFP is not found in more distant cells, nor in stomatal guard cells (which lack PD; white). **(b)** Using confocal microscopy, the pattern of GFP expression can be visualized; here, GFP has spread two cells from the transformed cell two days after agroinfiltration. The transformed cell is usually easily distinguished by its bright cytoplasmic fluorescence (center). Adjacent cells also show cytoplasmic fluorescence, but nuclear GFP is most prominent. Cells two rings out from the transformed cell show fluorescence in the nucleus, but cytoplasmic fluorescence is nearly undetectable

time scales—for example, during the source-sink transition, or as PD transport becomes restricted during embryogenesis—we now know that PD transport is highly dynamic over shorter, physiological time scales [3, 4]. Thus, PD transport is better described by the *rate* of transport of molecules between cells via PD.

Here, we present methods to measure the rate of PD transport by assaying GFP diffusion via PD in leaves. *Nicotiana benthamiana* leaves are infiltrated with *Agrobacterium tumefaciens* carrying  $35S_{pro}::GFP$  transfer DNA (T-DNA). By infiltrating with a low concentration of *Agrobacterium*, a handful of well-isolated individual epidermal cells are transformed to express GFP. Using confocal microscopy, the degree of GFP spread from one of these individual transformed cells can be visualized 2–3 days after agroinfiltration. In a typical *N. benthamiana* leaf, for example, GFP often spreads two or three cells away from the transformed cell after 48 h (Fig. 1).

This GFP movement assay has several advantages over other approaches to measuring PD transport. PD are very sensitive to mechanical manipulation, such that microinjection and high-pressure biolistics induce severe PD closure [5]. Low-pressure biolistics do not induce such severe PD closure, but do cause some mechanical damage and require cutting the leaf off the plant before conducting the movement assay, triggering various defense responses and physiological changes. *Agrobacterium*-mediated transient gene expression, on the other hand, involves almost no physical manipulation

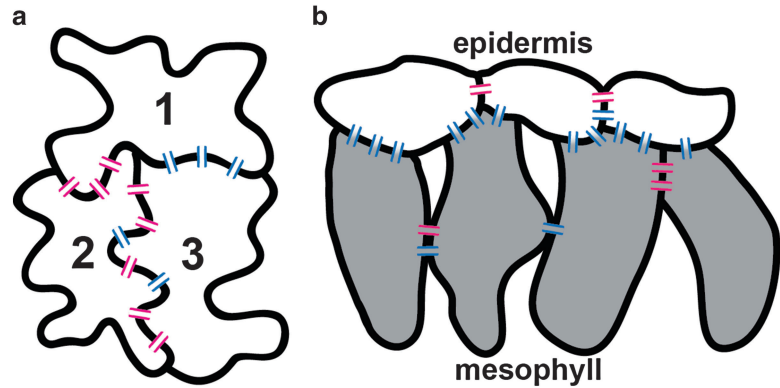


**Fig. 2** Primary PD (*pink*) form at the cell plate during cell division by distinct mechanisms from secondary PD (*blue*), which form in the cell wall at some time after cell division. (a) An epidermal pavement cell divided to form cells 1 and 2, which are therefore connected by primary PD. Cell 2 then divided to form cells 2 and 3, which are also connected by primary PD. After cell division, additional, secondary PD may form, as shown here between cells 2 and 3. In this example, all PD directly connecting cells 1 and 3 formed after cell division, and are therefore secondary. (b) Epidermal cells almost always derive from division of other epidermal cells, not from the underlying ground tissue (*grey*). Thus, while epidermal cells may be connected to each other by either primary or secondary PD, and mesophyll cells may also be linked by either primary or secondary PD, effectively all connections between the epidermis and the ground tissue are only secondary PD

of the leaf and induces minimal defense responses [6], so that PD transport rates under relatively normal conditions can be observed.

Another advantage of the GFP movement assay is that it can also be used to specifically measure changes in transport via secondary PD. In the epidermis, pavement cells are connected to each other with both primary PD (which form at the cell plate during division) and secondary PD (which form at some time after division through unknown mechanisms; Fig. 2a). The epidermis and underlying mesophyll are connected only by secondary PD, as epidermal cells almost always derive from the division of other epidermal cells—not from the ground tissue (Fig. 2b). Thus, by determining the frequency of GFP movement from transformed pavement cells to mesophyll cells, transport through secondary PD can be measured separately from PD transport in general [7–9].

Virus-induced gene silencing (VIGS) is a powerful tool to study PD genetics. Due to the critical importance of PD to plant growth, mutants with strong defects in PD transport are unable to develop into mature plants [10]. By drastically lowering gene expression in young leaves after plants have reached maturity, the acute effects of loss of a gene(s) on PD function and formation can be investigated while keeping the rest of the plant alive and healthy. Infection with *Tobacco rattle virus* (TRV) does not have a significant

impact on intercellular transport (based on many experiments in our lab), making this TRV-based VIGS method especially appealing. VIGS can also target several genes simultaneously, for example to silence whole gene families, which is a much more rapid approach than generating multiple mutation lines through crosses [11].

The approach presented in this method is versatile and can be adjusted to address any number of questions regarding PD transport. In addition to VIGS, other techniques to alter gene expression in *N. benthamiana*, such as *Agrobacterium*-mediated transient gene expression or generation of stable transgenic lines, could be coupled with the GFP movement assay to test the effects of overexpression or ectopic expression of genes on PD transport. Apart from exploring the effects of direct genetic manipulation, the GFP movement assay can also be used to test for differences in PD transport under various physiological conditions, stresses, or chemical treatments (e.g., application of phytohormones or metabolic inhibitors).

For studies focusing specifically on viral movement protein dynamics, GFP-tagged movement proteins can be used instead of GFP for the movement assay. *Tobacco mosaic virus* P30-2×GFP, for example, has been used to assay changes in PD transport following VIGS [7, 12, 13]. Similarly, these methods can be adapted for studies endeavoring to identify factors that promote facilitated PD transport; for instance, the intercellular movement of some transcription factors is likely facilitated by unknown proteins [14]. Instead of assaying GFP spread, a gene of interest (e.g., a transcription factor) can be fused with a fluorescent tag and then the movement of this fusion protein can be assayed following *Agrobacterium*-mediated transformation. Mutant screens for factors facilitating PD transport of the KNOTTED1 transcription factor have used a comparable approach (assaying activity of a KNOTTED1-GLABRA1-GFP fusion) [15], but since the movement of some transcription factors is essential for early developmental patterning in plant embryos, mutant screens are unlikely to reveal many key factors that promote facilitated PD transport. By acute silencing of gene expression with VIGS and tracking movement of transcription factor-GFP fusion proteins using the methods described below, greater insight into how specific proteins move from cell to cell can be obtained.

To exemplify our approach, we offer methods for a single experiment with one silencing construct (against a gene or genes of interest) along with appropriate controls (overview in Fig. 3). The experiment should be replicated at least three times under the same conditions, both to ensure that results are reproducible and to increase the sample size for stronger statistical analysis of movement assay results. We recommend staggering experiments if the effects of several different silencing constructs will be studied, because the final step of this method, confocal microscopy to visualize GFP diffusion, is both time-consuming and time-sensitive.

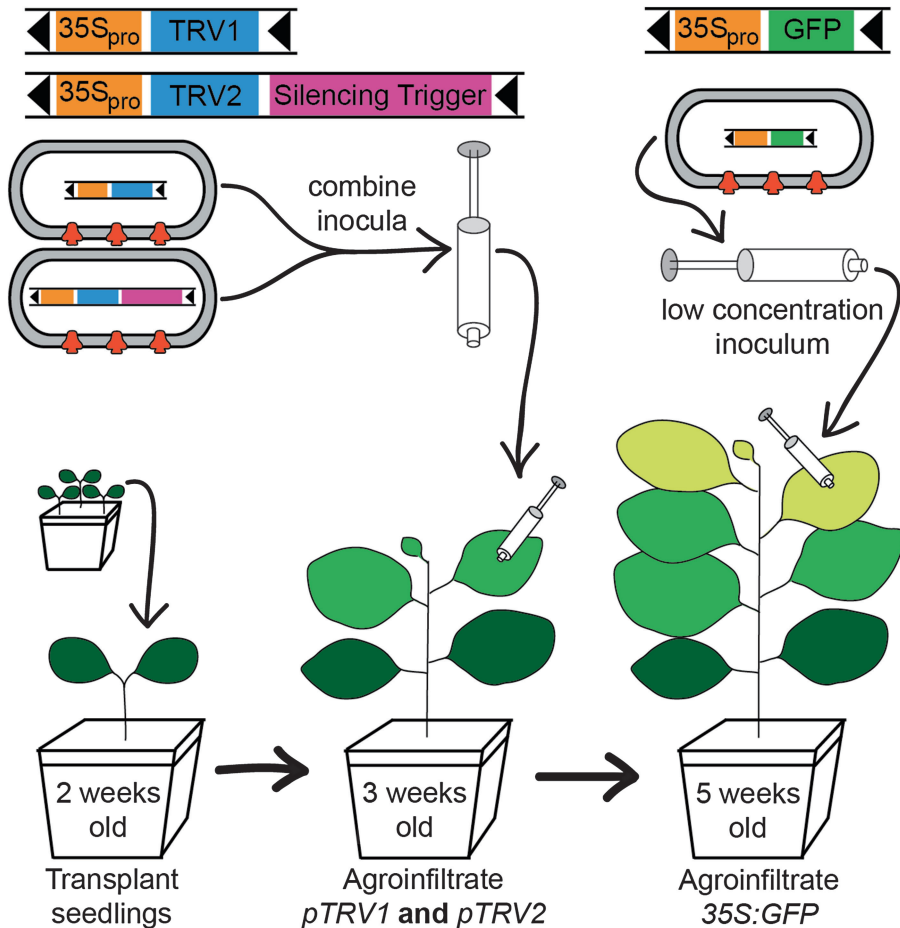


**Fig. 3** Overview of *Nicotiana benthamiana* growth and agroinfiltration methods. *Top left:* For virus-induced gene silencing, two strains of *Agrobacterium* are used to infect plants with *Tobacco rattle virus* (TRV). pTRV1 and pTRV2 are binary vectors that contain T-DNA encoding either the TRV1 RNA (blue) or the TRV2 RNA (blue) along with the silencing trigger (magenta), respectively, under the strong CaMV 35S promoter (orange). *Top right:* Another *Agrobacterium* strain carrying a binary vector that contains T-DNA encoding GFP under the 35S promoter is used for transient GFP expression. *Agrobacterium* cells (outlined in grey) are induced for virulence, infiltrated into leaves, and then transfer DNA into plant cells through the virulence type IV secretion system (T4SS) (red). (For simplicity only 3 T4SS are shown, but in reality there are 10–14 T4SS around the entire circumference of virulence-induced bacterial cells [25].) *Bottom:* *N. benthamiana* seedlings (dark green) are transplanted into individual pots 2 weeks after germination. One week later, both TRV1 and TRV2 (carrying the VIGS silencing trigger) are introduced into young leaves (green) by agroinfiltration with a syringe. After infection with TRV, expression of the targeted gene(s) is dramatically reduced in all newly emerging leaves, which should first be visible within 7–10 days (light green leaves, 5 weeks old). About 14 days after TRV infection, *Agrobacterium* carrying a binary vector with 35S<sub>pro</sub>:GFP T-DNA is infiltrated (by syringe) at low concentration into these young leaves (light green) with silenced gene expression. PD transport can then be assayed by the rate of GFP diffusion from a transformed epidermal cell using confocal microscopy (Fig. 1)

---

## 2 Materials

### 2.1 Plants

1. *Nicotiana benthamiana* seeds (*see Note 1*): We recommend using accession Nb-1, which was used to generate the draft genome [16].
2. Soil (any standard professional soil mix providing good drainage and aeration, such as Sun-Gro Sunshine® MVP).
3. 4" pots (clean and sterilized).
4. Flats (clean and sterilized).
5. Clear plastic domes.
6. Light source (photosynthetic flux density ~100  $\mu\text{mol photons/m}^2/\text{s}$ ).
7. Miracle-Gro® Liquid All-Purpose Plant Food (8-7-6) or comparable fertilizer.

### 2.2 Plasmids for *Agrobacterium*-Mediated Transformation

1. *Agrobacterium tumefaciens* cells competent for transformation [17] (*see Note 2*).
2. For VIGS: pTRV1, pTRV2::*NbPDS*, pTRV2::*GUS*, pTRV2::*TARGET GENE* (*see Notes 3 and 4*).
3. For the movement assay: An *Agrobacterium* binary vector with T-DNA borders surrounding a sequence encoding a monomeric GFP derivative (such as mGFP5 or EGFP) under the *Cauliflower mosaic virus* (CaMV) 35S promoter (*see Note 5*).

### 2.3 Media

1. Infiltration medium: 10 mM MES, 10 mM  $\text{MgCl}_2$ , 200  $\mu\text{M}$  acetosyringone; adjust pH to 5.5 with NaOH (*see Note 6*).
2. LB agar plates containing 50 mg/L kanamycin, 50 mg/L rifampicin, 50 mg/L gentamicin (*see Note 7*).
3. LB containing 50 mg/L kanamycin, 50 mg/L rifampicin, 50 mg/L gentamicin (*see Note 7*).

### 2.4 Agroinfiltration

1. *Agrobacterium* cultures (on fresh LB agar plates; *see Note 8*).
2. Needleless syringes (1 mL).

### 2.5 Microscopy

1. Confocal laser scanning microscope equipped with a 488 nm laser and GFP emission filters. We use an LSM 710 confocal microscope (Carl Zeiss AG) and collect GFP emission with wavelengths between 500 and 530 nm.
2. Needleless syringe (5 mL).
3. Glass microscope slides.
4. Glass cover slips (#1).
5. Single-edged razor blades.
6. Image processing software (such as ImageJ, <http://rsbweb.nih.gov/ij/>).

### 3 Methods

#### 3.1 Plant Growth

1. Spread 30–50 *N. benthamiana* seeds in one pot filled with wet soil, and place the pot in a tray containing water. For optimal germination and growth, cover the pot and tray with plastic wrap or a clear plastic dome to create a small vivarium.
2. Grow plants under a regular diurnal cycle (we typically use 16-h light/8-h dark) in a growth cart.
3. Once the seedlings are ~14 days old, carefully transplant the healthiest seedlings into 4" pots (one plant per pot) placed in flats containing water. Cover seedlings with a clear plastic dome for 3 days, and then slowly remove the cover over the course of 1–2 days. Fertilize the seedlings by half-filling the flat with water containing 150  $\mu$ L of Miracle-Gro per liter of water (approximately 2 L of water per flat with ten pots).
4. Continue watering plants from the bottom (in the flat) throughout the experiment.

#### 3.2 Preparing *Agrobacterium* for Infiltration into *N. Benthamiana*

1. From stocks (such as frozen glycerol stocks), streak *Agrobacterium* strains containing binary vectors on LB agar plates containing antibiotics for selection and grow in an incubator at 28 °C for 2 days.
2. Inoculate LB containing antibiotics for selection with *Agrobacterium* and grow in a 28 °C rotary shaker (250 rpm) overnight.
3. In the morning, centrifuge *Agrobacterium* culture at 3,000  $\times g$  for 10 min at room temperature.
4. In the morning, prepare fresh infiltration medium (*see Note 6*).
5. Resuspend the *Agrobacterium* pellet in infiltration medium and bring to desired optical density (*see below*, Subheading 3.3, **step 1**, and Subheading 3.4, **step 1**). Leave cultures on shaker (60 rpm) at room temperature for 2–4 h to induce virulence, i.e., to induce expression of the virulence genes required for T-DNA transfer.

#### 3.3 Virus-Induced Gene Silencing

1. Prepare *Agrobacterium* for infiltration as in Subheading 3.2. For a typical experiment with 24 plants, prepare the following *Agrobacterium* cultures: 12 mL carrying pTRV1, 5 mL carrying pTRV2::*TARGET GENE*, 5 mL carrying pTRV2::*GUS* (negative control for movement assay), and 2 mL carrying pTRV2::*NbPDS* (positive control for silencing; *see Note 3*). All resuspended bacteria should be adjusted to a final optical density at 600 nm (OD<sub>600</sub>) of 1.0 in infiltration medium.
2. TRV has a bipartite RNA genome; both TRV1 and TRV2 must be introduced into the plant for VIGS (*see Note 3*).

Combine equal volumes of virulence-induced *Agrobacterium* inocula carrying pTRV1 and pTRV2 into a 15 mL tube immediately before infiltrating leaves.

3. Infiltrate the induced *Agrobacterium* inoculum through the abaxial surface of the two youngest fully emerged leaves of 3-week-old plants (usually the third and fourth leaves) using a needleless 1 mL syringe. Again, assuming a typical experiment with 24 plants, infiltrate 10 plants with pTRV1 and pTRV2::GUS, 10 plants with pTRV1 and pTRV2::TARGET GENE, and 4 plants with pTRV1 and pTRV2::NbPDS.
4. Silencing should be visible in the upper leaves of TRV-infected plants about 7–10 days after agroinfiltration (Fig. 3). If silencing your target gene(s) does not lead to a visible phenotype, monitor the plants infected with pTRV2::NbPDS to track when gene silencing begins. After silencing is detected, movement assays should only be conducted in comparable, newly emerged leaves infected with TRV2::TARGET GENE or TRV2::GUS (control).

### 3.4 Transformation with Fluorescent Tracer

Once leaves with silenced gene expression have emerged, typically ~14 days after agroinfiltration of TRV constructs, begin the movement assay by transforming leaves using *Agrobacterium* carrying a construct to express the fluorescent tracer (GFP).

1. Prepare *Agrobacterium* carrying a 35S::GFP binary vector for agroinfiltration as in Subheading 3.2, growing a 5 mL overnight culture. First resuspend and dilute bacteria in infiltration medium to OD<sub>600</sub>=0.1. Then, make a 1:100 or 1:1,000 dilution of this inoculum with infiltration medium, so that the final OD<sub>600</sub> of the inoculum is 0.001 or 0.0001 (determine the appropriate dilution for your experiment with a preliminary trial).
2. Infiltrate the induced *Agrobacterium* culture through the abaxial surface of the newly emerged leaves with silenced gene expression using a needleless 1 mL syringe.
3. Two days after agroinfiltration, image GFP movement using confocal microscopy as described in Subheading 3.5 (see Note 9).

### 3.5 Assaying Transport: Microscopy

#### 3.5.1 Tissue Preparation

PD transport varies dramatically during development, for example, during the sink-source transition in leaves. Hence, for this assay, it is extremely important to always use leaves of the same age and size, and to always select the same region of a leaf for comparison. For most experiments, we use the basal region of the leaf.

1. Cut an ~1 cm square section of the leaf using a sharp razor blade. Be sure that this section does not include any area damaged by the syringe during agroinfiltration.
2. Remove air from the leaf to obtain the best images. To do this, place the leaf section into a 5 mL needleless syringe filled with

water and squeeze out all air from the syringe with the plunger. Then, create a vacuum by covering the syringe orifice with a finger and pulling the plunger, which will remove air from the leaf section, followed by releasing the finger to allow water to fill the leaf. Repeat until most of the air has been removed. When the air is removed, the leaf becomes a deeper green.

3. Add a drop of water to a slide, and then place the leaf section on the slide. Add another drop of water to the leaf surface, and cover with the cover slip. Gently tap the cover slip to remove air bubbles. Either the adaxial or abaxial surface may be visualized, but the same surface must be used throughout the experiment.

### 3.5.2 Visualizing GFP Spread Within the Epidermis

1. At low magnification, search for a cell that is expressing GFP. The transformed cell will have bright fluorescence in the nucleus and cytoplasm when visualized with GFP filters (*see* **Note 10**).
2. Increase magnification to 100× (usually the 10× objective) and adjust laser power, excitation and emission filters, and electronic gain to clearly visualize any GFP fluorescence in the nuclei of cells near the transformed cell. Once settings that permit visualization of GFP spread have been determined, keep the same settings for the rest of the experiment.
3. Since the leaf surface is not flat, and the epidermal layer is three-dimensional, take a z stack of images through the epidermis. Collect both GFP fluorescence and transmitted light images (ideally with a contrast-enhancing technique, such as phase contrast microscopy or differential interference contrast) for the entire z stack.

### 3.5.3 Visualizing GFP Spread from the Epidermis to the Mesophyll

1. Repeat **steps 1** and **2** above (Subheading 3.5.2).
2. Use bright-field microscopy to determine the depth of the underlying mesophyll cell(s), to ensure that the entire mesophyll cell will be visualized (since the nucleus, where GFP fluorescence will be brightest, may be in any z plane of the cell).
3. Take a z stack of images from the transformed epidermal cell through the entire underlying mesophyll cell(s). If GFP has spread to the mesophyll cell, it should be visible in the nucleus (*see* **Notes 10** and **11**).
4. For this assay, only count whether or not GFP has spread into the immediately connected mesophyll cell. This is the only pathway that is *exclusively* reliant on transport through secondary PD.

### 3.5.4 Analyzing GFP Movement Results

1. Use image processing software, such as ImageJ, to scan through z stacks. Count the maximal spread of GFP (in number of cells) from the transformed cell in the epidermis (Fig. 1). Note that GFP spread is not always even on all sides of the

transformed cell, and that epidermal cells are often irregularly shaped, occasionally making it difficult to determine how many cells are present (Fig. 1b). Regularly refer to transmitted light images to determine cell boundaries and accurately assay GFP spread; GFP will be most easily visible in the nucleus (Fig. 1b, *see Note 8*).

2. If also specifically assaying intercellular transport via secondary PD, tally the number of times that GFP is observed in mesophyll cells directly underlying the transformed epidermal cell. Report the frequency of GFP movement from the epidermis to the mesophyll.
3. Compare movement in leaves with silenced target gene expression (infected with TRV2::*TARGET GENE*) versus negative controls (infected with TRV2::*GUS*). Statistical significance should be determined with a Mann-Whitney *U* test [4, 7]. Report the sample size (typically >30 independent observations in total derived from three replications of the experiment), *U* value, and *P* value, as well as a table showing the frequencies of maximal GFP movement.

---

## 4 Notes

1. The GFP movement assay can also be performed in *Arabidopsis thaliana*, but mature *A. thaliana* leaves are more resistant to *Agrobacterium*-mediated transformation for transient gene expression (in this case, GFP expression). If the assay must be conducted in *Arabidopsis*, ecotypes or mutants that are more susceptible to *Agrobacterium* transformation (such as the *Ler* ecotype or *efr* mutants) may yield more consistent results [18]. For details on VIGS methods in *Arabidopsis*, *see refs.* 19, 20.
2. Any laboratory strain of *Agrobacterium* can be used for these methods, because *N. benthamiana* is a highly permissive host for *Agrobacterium*-mediated transformation. The efficiency of transformation does vary, however, because of differences in the virulence of *Agrobacterium* strains. While this caveat is not critical for the introduction of TRV1 and TRV2 for VIGS (since the precise rate of transformation is not critical, and they are introduced with fairly high concentrations of *Agrobacterium* to ensure high overall transformation rates), the GFP movement assay depends on a very specific rate of transformation so that only isolated, individual cells express GFP. Thus, if using different strains of *Agrobacterium*, the bacterial concentration and virulence-induction conditions may need to be adjusted for optimal results.

We use *Agrobacterium* GV3101, a C58 strain carrying a disarmed (T-DNA deletion) derivative of the nopaline C58 Ti

plasmid, pMP90 [21]. GV3101 is highly efficient at transformation of both *N. benthamiana* and *A. thaliana*. Some labs report improved transformation with GV2260, a C58 strain that instead carries a disarmed Ti plasmid (pGV2260) derived from an octopine strain (B6S3) [21]. pGV2260 encodes an additional virulence factor, VirF, that is not encoded by pMP90, but can improve *Agrobacterium* infection in most plants [22, 23]. Similarly, transformation efficiency may improve with the so-called hypervirulent strains that overexpress virulence factors, such as AGL1 (a C58 strain with the disarmed pTiBo542 from genome A281 that overexpresses the virulence-inducing two-component *virA/virG* system) [21]. On the other hand, some strains are notably less efficient at transforming *N. benthamiana* than GV3101, such as LBA4404 (pAL4404), a disarmed Ach5 strain.

3. *Tobacco rattle virus* (TRV) is a positive-sense single-stranded RNA virus. The TRV genome is bipartite, composed of two RNAs: TRV1 and TRV2. In this VIGS system, TRV1 and TRV2 were cloned and inserted in separate *Agrobacterium* binary vectors (derived from pCambia0390) so that each is flanked by T-DNA borders. These plasmids are called pYL192 and pYL156; for simplicity, we will call them pTRV1 and pTRV2, respectively. Agroinfiltration of both of these constructs is required for viral spread and silencing (Fig. 3).
4. Three pTRV2-derived vectors are used in every silencing experiment. TRV2::*NbPDS* efficiently silences expression of *PHYTOENE DESATURASE* (*PDS*) that encodes an enzyme required for carotenoid biosynthesis in leaves. Newly emerged leaves in *PDS*-silenced plants are white, a striking visual phenotype. Thus, silencing with TRV2::*NbPDS* serves as a positive control to demonstrate VIGS efficiency and to determine when leaves with silenced gene expression begin to emerge (typically ~7–10 days, but this can vary), if silencing your gene of interest does not cause a visible phenotype.

As a negative control, we infect plants with TRV2::*GUS*, which contains a silencing trigger against  $\beta$ -glucuronidase (*GUS*), which encodes an enzyme that is absent from plants. Plants infected with TRV2::*GUS* should not exhibit any VIGS phenotypes, but are an important negative control to account for any effects of agroinfiltration and TRV infection. It should be noted, however, that under our growth conditions, we have not observed any difference in PD transport between uninfectected plants and plants infected with TRV2::*GUS*.

To silence a gene(s) of interest, a short portion (~300–700 bp) of the 5' UTR, 3' UTR, or coding sequence of the gene is cloned into TRV2. Several pTRV2 vectors are available from the Arabidopsis Biological Resource Center (ABRC) at Ohio

State University (abrc.osu.edu and arabidopsis.org), including pYL156 (for traditional, restriction digest-based cloning) and pYL279 (for gateway cloning). A draft genome of *Nicotiana benthamiana* is now available at the Sol Genomics Network (solgenomics.net) to facilitate design of silencing triggers and cloning [16]. Since *N. benthamiana* is an allotetraploid, there are often two highly similar homoeologous copies of each gene in the genome; thus, it is critical to design silencing triggers that target both copies of the gene for efficient silencing. Several closely related or redundant genes may be silenced simultaneously by designing triggers that are complementary to highly conserved sequences of these genes. Always use quantitative or semiquantitative RT-PCR to confirm that expression of your gene(s) of interest is reduced [24]. For detailed methods on cloning silencing triggers into pTRV2, *see ref. 20*.

5. A fusion of two tandem copies of GFP, 2×GFP, may be used instead of 1×GFP, depending on the experiment. 2×GFP diffuses much more slowly than 1×GFP, which is useful in cases where PD transport is very rapid (such as in very young leaves).
6. Acetosyringone (3',5'-dimethoxy-4'-hydroxyacetophenone), which induces *Agrobacterium* virulence, is not stable in aqueous solution, so the infiltration medium should always be prepared fresh. Acetosyringone should be prepared in small aliquots as a 1,000× stock solution (200 mM) in DMSO, and can be stored for at most a few months at −20 °C.
7. These antibiotics are appropriate for GV3101(pMP90) (resistant to rifampicin and gentamicin) carrying the binary vectors listed here (resistant to kanamycin); adjust antibiotic selection to match the strain of *Agrobacterium* and binary vectors being used.
8. *Agrobacterium* should always be used from fresh cultures on plates that have not been stored in the cold.
9. In some cases, the movement assay may be more sensitive 3 days after agroinfiltration [7]. Thus, to optimize the movement assay for a given experiment, it may be useful to conduct a preliminary experiment to check both time points, and then replicate the experiment using one or both time points, depending on preliminary results. After 3 days, GFP has often diffused too far beyond the individual transformed cell for accurate measurement, or in many cases, transient expression of GFP has been silenced by endogenous plant mechanisms. Thus, the assay should never be conducted more than 3 days after agroinfiltration.
10. As seen in Fig. 1b, in cells surrounding the transformed cell, GFP fluorescence is strongest in the nucleus. Most of the volume of plant epidermal pavement cells is occupied by a large

central vacuole, with much of the remainder occupied by organelles; thus, cytoplasmic GFP fluorescence is diffuse and challenging to visualize. Since fluorescence intensity is proportional to the concentration of the fluorophore, and GFP is present at a much higher concentrations in the original transformed cells, you may need to increase excitation power and electronic gain to high levels in order to detect GFP spread.

11. In general, the adaxial epidermis is in direct contact with palisade mesophyll cells, and the abaxial epidermis is in direct contact with spongy mesophyll cells. In some cases, however, the epidermis is not adjacent to a true mesophyll cell (for example, near vascular bundles). Check for the presence of many chloroplasts (using bright-field microscopy or fluorescence microscopy with lasers and emission filters to detect chlorophyll fluorescence) to guarantee that the adjacent cells are mesophyll.

---

## Acknowledgments

J.O.B. and A.M.R. are supported by National Science Foundation predoctoral fellowships and by National Institutes of Health Grant GM45244 to P.Z. T.M.B.S. is supported by start-up funds from the University of Tennessee.

## References

1. Burch-Smith TM, Zambryski PC (2012) Plasmodesmata paradigm shift: regulation from without versus within. *Annu Rev Plant Biol* 63:1–22
2. Raven J (2005) Evolution of plasmodesmata. In: Oparka K (ed) *Plasmodesmata*. Blackwell Publishing Ltd, Ames, IA, pp 33–52
3. Rutschow HL, Baskin TI, Kramer EM (2011) Regulation of solute flux through plasmodesmata in the root meristem. *Plant Physiol* 155:1817–1826
4. Stonebloom S, Brunkard JO, Cheung AC et al (2012) Redox states of plastids and mitochondria differentially regulate intercellular transport via plasmodesmata. *Plant Physiol* 158:190–199
5. Liarzi O, Epel BL (2005) Development of a quantitative tool for measuring changes in the coefficient of conductivity of plasmodesmata induced by developmental, biotic, and abiotic signals. *Protoplasma* 225:67–76
6. Baron C, Zambryski PC (1995) The plant response in pathogenesis, symbiosis, and wounding: variations on a common theme? *Annu Rev Genet* 29:107–129
7. Burch-Smith TM, Zambryski PC (2010) Loss of INCREASED SIZE EXCLUSION LIMIT (ISE)1 or ISE2 increases the formation of secondary plasmodesmata. *Curr Biol* 20:989–993
8. Burch-Smith TM, Stonebloom S, Xu M, Zambryski P (2011) Plasmodesmata during development: re-examination of the importance of primary, secondary, and branched plasmodesmata structure versus function. *Protoplasma* 248:61–74
9. Zambryski PC, Xu M, Stonebloom S, Burch-Smith TM (2012) Embryogenesis as a model system to dissect the genetic and developmental regulation of cell-to-cell transport via plasmodesmata. In: Hülskamp M, Kragler F (eds) *Short and long distance signaling*. Springer, New York, NY, pp 45–60
10. Kim I, Hempel FD, Sha K, Pfluger J, Zambryski P (2002) Identification of a developmental transition in plasmodesmatal function during embryogenesis in *Arabidopsis thaliana*. *Development* 129:1261–1272
11. Baulcombe DC (1999) Fast forward genetics based on virus-induced gene silencing. *Curr Opin Plant Biol* 2:109–113

12. Stonebloom S, Burch-Smith TM, Kim I et al (2009) Loss of the plant DEAD-box protein ISE1 leads to defective mitochondria and increased cell-to-cell transport via plasmodesmata. *Proc Natl Acad Sci U S A* 106: 17229–17234
13. Xu M, Cho E, Burch-Smith TM, Zambryski PC (2012) Plasmodesmata formation and cell-to-cell transport function are reduced in *decreased size exclusion limit 1* during embryogenesis in *Arabidopsis*. *Proc Natl Acad Sci U S A* 109:5098–5103
14. Wu S, Gallagher KL (2012) Transcription factors on the move. *Curr Opin Plant Biol* 15: 645–651
15. Xu XM, Wang J, Xuan Z et al (2011) Chaperonins facilitate KNOTTED1 cell-to-cell trafficking and stem cell function. *Science* 333:1141–1144
16. Bombarely A, Rosli HG, Vrebalov J et al (2012) A draft genome sequence of *Nicotiana benthamiana* to enhance molecular plant-microbe biology research. *Mol Plant Microbe Interact* 25:1523–1530
17. Wise AA, Liu Z, Binns AN (2006) Three methods for the introduction of foreign DNA into *Agrobacterium*. *Methods Mol Biol* 343:43–53
18. Zipfel C, Robatzek S, Navarro L et al (2004) Bacterial disease resistance in *Arabidopsis* through flagellin perception. *Nature* 428: 764–767
19. Burch-Smith TM, Schiff M, Liu Y, Dinesh-Kumar SP (2006) Efficient virus-induced gene silencing in *Arabidopsis*. *Plant Physiol* 142: 21–27
20. Hayward A, Padmanabhan M, Dinesh-Kumar SP (2011) Virus induced silencing in *Nicotiana benthamiana* and other plant species. *Methods Mol Biol* 678:55–63
21. Hellens R, Mullineaux P, Klee H (2000) A guide to *Agrobacterium* binary Ti vectors. *Trends Plant Sci* 5:446–451
22. Magori S, Citovsky V (2011) *Agrobacterium* counteracts host-induced degradation of its effector F-box protein. *Sci Signal* 4:ra69
23. Magori S, Citovsky V (2012) The role of the ubiquitin-proteasome system in *Agrobacterium tumefaciens*-mediated genetic transformation of plants. *Plant Physiol* 160:65–71
24. Liu D, Shi L, Han C et al (2012) Validation of reference genes for gene expression studies in virus-infected *Nicotiana benthamiana* using quantitative real-time PCR. *PLoS One* 7:e46451
25. Aguilar J, Zupan J, Cameron TA, Zambryski PC (2010) *Agrobacterium* type IV secretion system and its substrates form helical arrays around the circumference of virulence induced cells. *Proc Natl Acad Sci U S A* 107:3758–3763

## Probing Plasmodesmata Function with Biochemical Inhibitors

Rosemary G. White

### Abstract

To investigate plasmodesmata (PD) function, a useful technique is to monitor the effect on cell-to-cell transport of applying an inhibitor of a physiological process, protein, or other cell component of interest. Changes in PD transport can then be monitored in one of several ways, most commonly by measuring the cell-to-cell movement of fluorescent tracer dyes or of free fluorescent proteins. Effects on PD structure can be detected in thin sections of embedded tissue observed using an electron microscope, most commonly a Transmission Electron Microscope (TEM). This chapter outlines commonly used inhibitors, methods for treating different tissues, how to detect altered cell-to-cell transport and PD structure, and important caveats.

**Key words** *Arabidopsis thaliana*, Cell-to-cell transport, Fluorescence microscopy, Fluorescent tracer dyes, Green fluorescent protein, Microinjection, Transmission electron microscopy

---

### 1 Introduction

Plasmodesmata play a key role in transmission of cytoplasmic signals from cell to cell, yet there are large gaps in our knowledge of their composition, function, and regulation. Proteomic analyses have identified a large suite of proteins potentially located within or associated with PD, but most of these await experimental confirmation of both their location and function (e.g. [1, 2], reviewed in ref. 3). Mutant analyses are beginning to reveal an additional set of proteins not located at PD but which are essential to regulate PD behavior (e.g. [4–6]). For example, mutations in the thioredoxin GAT1, a plastid-located regulator of redox status essential in PD function, tissue viability, and embryo development, cause reduced cell–cell transport [4] and mutations in ISE1, a mitochondrial DEAD-box RNA helicase [5] or ISE2, a DEVH box RNA helicase [6], cause increased cell–cell transport. Such analyses can demonstrate the role of a single gene by knockout and subsequent complementation studies, but this is difficult if the RNA or protein

product is vital to cell function since mutants may be lethal at the embryo or young seedling stage (e.g. [7]). Even for proteins known to be PD components, such as myosin, analysis of nonlethal mutants or green fluorescent protein- (GFP-) tagged lines has been less informative than expected (e.g. [8–10]).

For these reasons, it is still common to use well-characterized chemical inhibitors of biological processes to probe PD function. For example, the role of microtubules in cell-to-cell movement of transcription factors was shown using a combination of microtubule mutants with moderate phenotypes together with chemical treatments [11]. This approach is based on the assumption that the chosen inhibitors are specific, in that they target a single enzyme or small class of enzymes, or target a specific molecular substructure within a class of proteins, lipids, or carbohydrates. For example, inhibitors of ATP activity or energy metabolism have been used to show that regulation of PD requires energy from the cell (e.g. [12–14]). Herbicides, such as alloxan, that induce callose ( $\beta$ -1,3 glucan) synthesis were used to show that additional callose restricts transport via PD [4], and treatment with the callose synthesis inhibitor, 2-deoxy-D-glucose (DDG; [15, 16]) showed that reducing callose causes PD opening [17, 18]. Furthermore, new, more targeted inhibitors of specific proteins are constantly under development (e.g. small molecule inhibitors of actin; [19–21]), and could be used in plants after suitable testing. Finally, the phenotypic effects of inhibitors can be compared with similar effects of partial inhibition or knockout of proteins to suggest a role for the inhibited protein in the cell process under study.

This chapter summarizes current methods for using biochemical inhibitors, proteins, and antibodies to alter PD permeability, with considerations about how to detect effects on PD, which will affect the type of plant material to use, together with known artifacts and how to avoid or ameliorate them.

### **1.1 Monitoring Effects on Plasmodesmata**

The effects of biochemicals on PD can be examined either by functional analyses or by detecting structural changes. To elucidate the role of a putative PD regulator in transport dynamics, effects on cell-to-cell transport need to be monitored, and for this, both the appropriate type of plant material and assessment protocol must be chosen (Subheading 1.2). Most experiments involve monitoring the spread of fluorescent tracer molecules from the cytoplasm of one cell into the cytoplasm of an adjacent cell or cells. These observations require a fluorescence microscope, in which shorter wavelengths of light (excitation light) are projected onto the tissue, causing emission of fluorescence from the tracer molecules at somewhat longer wavelengths of light. The appropriate optical filters must be used to select excitation and emission wavelengths for detection of specific tracer molecules, whether dyes or fluorescent proteins. In some cases, a dissecting microscope equipped for fluorescence imaging can provide sufficient resolution to discriminate

effects of biochemical modulators on cell-to-cell transport via PD. More often, either a regular fluorescence compound microscope or a confocal laser scanning microscope (CLSM) is required to provide sufficient detail, intensity of excitation light and sensitivity of detectors to the fluorescence emission in order to locate low levels of tracers that have moved from the source cell into neighboring cells.

Assessment of changes in structure generally requires imaging at sufficient magnification to resolve the small size of PD, which have cross-section diameters of the order of 40–50 nm. This can be obtained using an electron microscope, usually a Transmission Electron Microscope (TEM). The tissue must be prepared to withstand observation under an electron beam in a vacuum, and this necessitates fixation (chemically cross-linking proteins to lock them in place) of the plant material, dehydration in solvent to enable penetration of water-immiscible resins, infiltration with liquid resin, polymerization of the resin (usually by heat or UV light), ultrathin sectioning, and staining with electron-dense heavy metals. Both short- and long-term structural effects can be monitored which may require slightly different fixation protocols. Tissue processing also varies depending on the specific tissue to be examined and whether external (in the cell wall) or internal (within the cytoplasmic sleeve) details of PD structure are of interest. Instantaneous, rapid structural changes are best seen in rapidly frozen and freeze-substituted material. However, ultrastructural details within larger tissue pieces are usually poorly preserved by rapid freezing techniques, and more conventional chemical fixation can often reveal changes caused by biochemical treatments. For example, reduction in callose synthesis after treatment with the callose synthesis inhibitor DDG is easily seen in chemically fixed tissues [17, 18].

In some cases, structural modifications associated with PD maturation, e.g. in *Arabidopsis* leaves, can be detected by their ability to incorporate fluorescently tagged viral proteins [22].

## **1.2 Choice of Plant Material**

### **1.2.1 Studying PD Dynamic Behavior**

The key requirement for studying PD dynamics is usually that a fluorescent tracer can be detected moving from one cell or tissue to the next. These tracers (listed in Table 1) include fluorescent dyes, such as carboxyfluorescein diacetate (CFDA), which can be ester-loaded into cells without injection (e.g. [23–26]), or loaded into the phloem via application to source tissue (e.g. [24, 27, 28]), to follow movement via PD into surrounding tissue. More conventionally, we can follow the movement of fluorescent tracers into neighboring cells after they have been microinjected or bombarded into single cells (e.g. [29, 30] and references therein [31, 32]). The latter techniques do involve some cell damage and such wound responses will affect cell–cell transport [18, 33], and quantitation is not straightforward (e.g. [34]). For application of chemical inhibitors, tissues ideally need to have external cell walls that allow

**Table 1**  
**Properties of fluorescent tracers used for tracking cell-to-cell transport via plasmodesmata<sup>a</sup>**

Tracer	mw (kDa) <sup>b</sup>	Fluorescence <sup>c</sup>	Reference <sup>d</sup>	Reference
		Ex, Em	Use in inhibitor studies	Use in other analyses
Small fluorescent probes				
Fluorescein <sup>c</sup>	0.332	494, 521	[30, 38, 60]	
Carboxyfluorescein (CF)	0.376	492, 517	[34, 45–47, 65]	[23–25, 27, 31, 37, 66–68]
Lucifer yellow carbohydrazide (LYCH)	0.443	425, 528	[12, 13, 18, 38, 69, 70]	[23, 25, 33, 42]
8-Hydroxypyrene-1,3,6-trisulfonic acid (HPTS)	0.524	403, 454		[7, 26, 27, 67]
Sulforhodamine 101, sulforhodamine G, lissamine rhodamine B	0.547	578, 594	[13, 18, 38]	[26, 31]
Fluorescent-tagged amino acids <sup>f</sup>				
FITC-single amino acid	0.464–0.594	490, 525 <sup>g</sup>	[45, 47, 66, 71]	[30]
FITC-amino acid polymers	0.639–1.678	490, 525 <sup>g</sup>	[45, 47, 66, 71]	[30]
Fluorescent dextrans (dextran mw without fluorescent tag)	1–40	<sup>h</sup>	[12, 13, 18, 67, 70, 72, 73]	[4, 5, 7, 31, 33]
Fluorescent proteins, tagged proteins				
GFP (or photoactivatable GFP) or RFP	27	488, 509	[4, 14, 38]	[6, 7, 32, 68, 74, 75]
SHR-GFP	86	488, 509	[11]	

<sup>a</sup>Fluorescent proteins are included here since they can be expressed in specific tissues, for example in phloem companion cells, and spread into adjacent cells if PD are open (e.g. spread into the root tips of *Arabidopsis thaliana*; [70])

<sup>b</sup>mw = molecular weight of free dye in cell cytoplasm, whether injected as dye or derived from acetate conjugate

<sup>c</sup>Fluorescence excitation (Ex) and emission (Em) maxima from company catalogues

<sup>d</sup>Selected references in which fluorescent probes were used together with inhibitors to analyze PD transport. Other references using injected, bombarded, or expressed fluorescent probes may be found with a literature search

<sup>e</sup>From injected FITC (fluorescein isothiocyanate) or caged fluorescein (fluorescein bis-[5-carboxymethoxy-2-nitrobenzyl] ether)

<sup>f</sup>Properties (charge, polarity, hydrodynamic radius) of amino acid and other probes are given in refs. 30, 31, 45; details of synthesis in ref. 76

<sup>g</sup>Ex and Em will depend on the attached fluorochrome, in this case, FITC

<sup>h</sup>Ex and Em will depend on the attached fluorochrome

penetration of the inhibitor, which then must be able to cross the plasma membrane if a protein in the cytoplasmic sleeve of PD is the target. Some way of assessing inhibitor penetration into cells is essential, for example, being able to see the slowing or cessation of cytoplasmic streaming. If streaming is not affected, a method of assessing treatment effects is critical and may require preliminary experiments to work out the minimum inhibitor concentration and duration of treatment needed to affect the tissue, as with any chemical treatment. For example, a dye with similar chemical

properties to the inhibitor may be used to assess penetration in preliminary experiments, or a transgenic line expressing a visible reporter protein responsive to inhibitor-generated changes in calcium, pH, or membrane potential may be used.

Since in most cases effects on transport are monitored by cell-to-cell movement of visible tracers, the tissue used must be transparent enough to see the earliest signs of the tracer in adjacent cells. The roots of *Arabidopsis thaliana* and other small plants are useful as they are fairly transparent and cytoplasmic streaming can be monitored in root hairs. They are also very sensitive to growing conditions and uniformity of growth is essential for reasonable quantitation of transport in treated and control tissues. Examples of quantitative comparisons of *Arabidopsis* root growth after application of different metabolic and cytoskeleton inhibitors are shown in [35, 36]. In addition, ref. 34 presents an elegant method to rapidly quantify tracer dye flux and show dynamic behavior in timeframes similar to that measured by electrophysiological techniques (*see below*). Although the method is limited somewhat by currently available image capture speeds, this will be more amenable as more sensitive and faster instruments become more routinely available.

Plants expressing GFP or other fluorescent protein in just one or a few cell types are very useful as they can give insights into PD regulation between developmental domains. Least traumatic to the plant and the experimental system are expressed fluorescent proteins, such as GFP (e.g. [37]). GFP is relatively large (27 kDa) compared to many signals that move through PD, although the photoconvertable forms of GFP eliminate the physical trauma of microinjection (e.g. [38, 39]). There is now a selection of smaller expressed proteins, such as iLOV (10 kDa), engineered from the light, oxygen, and voltage-sensing (LOV) domain of the blue light receptor phototropin [40] and other small flavin-based fluorescent proteins [41]. Whether monitoring injected tracers or spread of expressed proteins, in all cases, maintenance of rapid growth by optimal growing conditions is essential. Before and after application of inhibitors, cell viability should be monitored by observing cytoplasmic streaming and membrane integrity (exclusion of propidium iodide, for example).

Epidermal peels, especially from *Allium* species, are commonly used for PD transport studies (e.g. [42–44] and references therein), because the epidermal layer is readily detached from underlying tissue for imaging. For repeatability, elongating tissue from leaves, e.g. from *Allium porrum* (leek), is best (e.g. [44]) since the growth and storage history of *Allium cepa* (onion) bulbs purchased at the supermarket is usually unknown. Alternative two-dimensional tissues are the fronds of water plants, such as *Elodea canadensis* [31] or *Egeria densa* [45] with highly permeable outer cell walls which usually lack a hydrophobic cuticle.

Detection of fluorescent tracer movement is most straightforward in single cell files, as found in stamen hairs of *Tradescantia virginiana* ([13, 29] and references therein) or *Setcreasea purpurea* (e.g. [30, 46, 47]), which requires maintenance of these plants in a warm greenhouse with long daylength. The multicellular trichomes of *Nicotiana* species are also useful (e.g. *N. tabacum*, [38]) since their tip cells can be loaded with tracer dye, or alternatively, they can be readily transformed to express fluorescent protein tracers, either by transient or constitutive expression. In all of these tissues, the permeability of the cell walls may be an issue and young tissues are desirable for chemical treatments.

One aspect of PD behavior that is hard to monitor by following the movement of tracer dyes or proteins is their very fast dynamic behavior in response to certain stimuli or inhibitors. For example, application of calcium causes rapid closure of PD within 5 s, followed by reopening within a further 5–10 s, and the sharp opening and closing profiles can be detected only by monitoring electrical signals [48]. Here, considerable skill is required to insert microelectrodes into adjacent cells with the least cell damage or effects on PD. If a series of cells is to be studied, electrodes must be inserted into each cell of the series (e.g. [49, 50]). We assume that there is less PD damage than when tracer dyes are injected since cell membrane voltage is monitored, the electrodes are small, and there is no addition of a relatively undefined volume of tracer dye to a small volume of cytoplasm. Electrophysiology appears rarely in recent PD methods, but will be needed in future studies to understand subtle details of PD protein function.

### 1.2.2 Analysis of PD Structure

A much greater range of tissues is used to analyze effects on PD structure. As for dynamic studies, penetration of the inhibitor must be assessed to ensure that it is affecting the tissue under study. Often, this involves baseline analysis of all cell structures, including PD, likely to be modified by inhibitor treatment, for example, noting loss of actin microfilaments in tissue treated with an actin inhibitor (e.g. [51, 52]) or loss of microtubules in tissue treated with a microtubule inhibitor (e.g. [11, 53]). A further requirement is development of a fixation, embedding, staining, and imaging protocol that allows both qualitative and quantitative assessment of inhibitor effects. Short-term treatments may affect the usual range of PD morphologies seen within a given tissue (e.g. effects of cytochalasin on young PD, [54]), and somewhat longer-term treatments (similar to effects of genetic mutations) may affect the usual change in PD morphologies seen during maturation of the tissue, or tissue interface [22]. Because the distribution, density, branching, and cell wall structures are likely to be different at each cell wall interface, and will vary with growing conditions, baseline PD structural information must be collected in each case.

### **1.3 Recognizing Artifacts of Treatment or Handling**

A major caveat to the use of chemical inhibitors is that they are often applied to the entire tissue under study, and will affect all targeted proteins in the tissue, not just those in PD. A second reservation is that inhibitors commonly are less specific than claimed and may interfere with a number of other cell processes. With these caveats in mind, additional artifacts are common to all chemical treatments, and involve the numerous steps required to incubate tissue in the inhibitor, introduce a tracer dye into the cells, either before or after treatment, then observe the tissue for some time under fluorescence illumination.

Apart from chemical side-effects, tissue preparation generally requires transfer of the tissue into the test solution in a chamber for observation or microinjection or placement onto the test agar for treatment followed by a second transfer for microinjection. Controls must be carefully monitored to quantify the effects on and/or allow for any inhibition of PD caused by handling during the experiment. Plants are surprisingly sensitive to mechanical handling, which will generate callose at PD and affect assessment of cell-to-cell transport ([17] and references therein), which can be ameliorated by treatment with DDG [17, 18, 33]. DDG is added to block callose synthesis, and does this by trapping nucleotides, here UDP, into a metabolically unusable form [55]. Inside the cell, DDG is phosphorylated to DDG-6-phosphate and then converted into UDP-2-DDG, which competes with UDP-glucose for dolichol phosphate forming dolichol-phosphate-DDG, which cannot be incorporated into  $\beta$ -glucans, such as callose [15, 56–58]. The experimental tissue needs to be carefully monitored to ensure that, although specific functions are inhibited or blocked by each treatment chemical, the cells examined are still alive and relatively healthy.

### **1.4 Selection of Biochemical Inhibitors**

A wide range of chemical agents, antibodies, and injected proteins has been used to modify PD function, outlined in Table 2. Also shown are references in which each inhibitor has been used, the range of concentrations applied and length of treatments. Selection of inhibitor depends upon the process under investigation, background information about the tissue and inhibitor and their interactions, and experience of the investigator.

Many of these agents are not readily soluble in aqueous solutions and are first prepared and then stored as stock solutions in the appropriate nonaqueous solvent, which is often dimethylsulfoxide (DMSO). Each needs to be monitored when diluted to working concentration in aqueous solution to ensure they do not precipitate out of solution. Furthermore, since some of these nonaqueous solvents have unanticipated effects on either the action of the inhibitor, the activities of cell enzymes, or the integrity of membranes, constant monitoring of membrane integrity is

Table 2

Application of biochemical inhibitors and their reported effects on cell–cell transport or PD structure

Compound, mode of action, stock solution	Concentration (in bathing solution unless stated otherwise)	Effects on transport or PD structure; specific tissue tested	Detection method	Reference
Cytochalasin B: Actin inhibitor 4.2 or 42 mM in DMSO at –20 °C	21, 42 or 104 μM for up to 90 min	Reduced transport due to reduced cytoplasmic streaming; <i>Chara sp.</i>	Chloride transport	[77]
	42 μM for 20 min	No effect (non-sig. reduction in transport); <i>Egeria densa</i> leaf tissues	Transport of 5 FITC-tagged amino acid conjugates	[45]
	0.21 mM in 1 % DMSO for 60 min	Widening of PD neck region; <i>Nephtrolepis exaltata</i> rhizomes	TEM analysis	[54]
	0.63, 6.3 or 63 μM for up to 30 min	No effect on PD structure; <i>Hordeum vulgare</i> roots, <i>Azolla pinnata</i> roots	Cell–cell electrical conductance	[78]
Cytochalasin D: Actin inhibitor 0.5–42 mM in DMSO at –20 °C	53 mM plus 0.5 % DMSO in buffer	No effect on transport, <i>Setcreasea purpurina</i> stamen hairs	CF dye transport monitored for 5 min	[65]
	10 μM in 2 % DMSO	Increased transport, <i>Nicotiana tabacum</i> mesophyll	FITC-dextran transport	[72]
	2 μM co-injected with dye	Increased transport, <i>Nicotiana tabacum</i> mesophyll	FITC-dextran transport	[73]
	2 μM for 22 days in growth medium	No effect on spread of silencing signal in <i>Arabidopsis</i>	Small RNA transport	[68]
	20 μM for 24 h in growth medium	Little effect on transport; <i>Arabidopsis</i> roots	SHR-GFP movement between stele and endodermis	[11]
	1 mM for 1 or 6 h in growth medium	No effect on transport; <i>Arabidopsis</i> root tissues	Transport of injected dyes, GFP export from phloem	<sup>a</sup>

Latrunculin A: Actin polymerization inhibitor 1 or 2 mM in DMSO at -20 °C	0.1 µM for 30 min prior to injection of virus movement protein ± dye	Increased transport, <i>Nicotiana tabacum</i> mesophyll	FITC-dextran transport	[73]
Latrunculin B: Actin polymerization inhibitor 1 or 2 mM in DMSO at -20 °C	10 µM for 2 h, 6 h or 3 days 25 µM in 0.5 % DMSO for 15 min 50 nM for 60 min 1 µM for 22 days in growth medium 50 nM for 24 h in growth medium 25 µM in 0.5 % DMSO for 15 min	Reduced transport (smaller diameter virus spread), <i>N. tabacum</i> mesophyll No effect on transport; <i>N. tabacum</i> leaf trichomes No effect on transport; <i>Tradescantia virginiana</i> stamen hairs No effect on spread of silencing signal in <i>Arabidopsis</i> Little effect on transport; <i>Arabidopsis</i> roots No effect on transport; <i>Arabidopsis</i> root tissues	Virus transport LYCH transport Transport of injected dyes Small RNA transport SHR-GFP movement between stele and endodermis Transport of injected dyes, GFP export from phloem <sup>a</sup>	[79] [38] [13] [68] [11] <sup>a</sup>
Phalloidin: Actin filament stabilizer 10 µM in methanol at -20 °C	6.6 µM co-injected with dye 2 µM co-injected with dye	No effect on transport; <i>N. tabacum</i> mesophyll Prevented increased transport due to virus movement protein, <i>N. tabacum</i> mesophyll	FITC dextran transport FITC-dextran transport	[72] [73]
Jasplakinolide: Actin filament stabilizer 1 mM in DMSO at -20 °C	1 µM for 22 days in growth medium 25 µM in 0.5 % DMSO for 15 min	No effect on spread of silencing signal in <i>Arabidopsis</i> No effect; <i>Arabidopsis</i> root tissues	RNA transport GFP export from phloem <sup>a</sup>	[68] <sup>a</sup>
Profilin: Sequesters actin monomers maintained in 20 mM Tris-HCl, pH 7.4, 150 mM KCl, 0.2 mM DTT	60 µM co-injected with dye	Increased transport; <i>N. tabacum</i> mesophyll	FITC-dextran transport	[72]

(continued)

Table 2  
(continued)

Compound, mode of action, stock solution	Concentration (in bathing solution unless stated otherwise)	Effects on transport or PD structure; specific tissue tested	Detection method	Reference
2,3 Butanedione 2-monoxime (BDM); Myosin inhibitor 300–500 mM aqueous (made fresh)	0.1–30 mM for 1 h	Narrowing of PD neck region; <i>Zea mays</i> roots	TEM analysis	[80]
	1 mM for 2 h, 6 h, 3 days	No effect on transport; <i>N. tabacum</i> mesophyll	Virus transport	[79]
	1 and 30 mM for 60 min	Increased transport; <i>T. virginiana</i> stamen hairs	Dye transport	[13]
	2.5 mM for 22 days in growth medium	No effect on spread of silencing signal in <i>Arabidopsis</i>	Small RNA transport	[68]
	1 and 30 mM for 60 min	Reduced transport; <i>Arabidopsis</i> root tissues, <i>Elodea canadensis</i> leaf epidermis	Transport of injected dyes, GFP export from phloem	<sup>a</sup>
<i>N</i> -Ethyl maleimide (NEM); Myosin inhibitor 50–100 mM aqueous (made fresh)	0.1 mM for up to 50 min	Irreversible cessation of transport; <i>Nitella translucens</i>	<sup>11</sup> C and <sup>14</sup> C transport	[81]
	1 mM in for 60 min	Reduced transport; <i>T. virginiana</i> stamen hairs	Dye transport	[13]
	50 $\mu$ M for 22 days in growth medium	Increased movement of silencing signal in <i>Arabidopsis</i>	Small RNA transport	[68]
	0.1–10 mM for 1–2 h in bathing solution or growth medium	Increased transport; <i>Arabidopsis</i> root tissues, <i>E. canadensis</i> leaf epidermis	Dye transport, GFP transport	<sup>a</sup>
Myosin antibodies: Block myosin function	0.2 mg/ $\mu$ l coinjected with dye	Increased transport; <i>Arabidopsis</i> root epidermis, <i>N. tabacum</i> mesophyll	LYCH or FITC-dextran transport, respectively	[70]
	0.5 mg/ml aqueous coinjected with dye	Increased transport; <i>T. virginiana</i> stamen hairs	Dye transport	[13]
	0.5 mg/ml aqueous coinjected with dye	Reduced transport; <i>Arabidopsis</i> root epidermis	Dye transport	<sup>a</sup>

Colchicine: Microtubule inhibitor Aqueous (made fresh)	0.05 mM for 20 min	No effect on transport; <i>Nitella translucens</i>	$^{11}\text{C}$ and $^{14}\text{C}$ transport	[81]
Oryzalin: Microtubule inhibitor 20 mM in DMSO	0.3–3.0 $\mu\text{M}$ for 12 h, 1.0 $\mu\text{M}$ for 6 h in growth medium	Reduced transport; <i>Arabidopsis</i> roots	SHR-GFP movement between stele and endodermis	[11]
Tamoxifen: Microtubule stabilizer 10 mM in DMSO	1.0 $\mu\text{M}$ for 12 h, or 10 $\mu\text{M}$ for 6 h in growth medium	No effect on transport; <i>Arabidopsis</i> roots	SHR-GFP movement between stele and endodermis	[11]
Alloxan, paraquat: Herbicides inducing $\text{H}_2\text{O}_2$ or $\text{O}_2^-$ respectively Aqueous (made fresh)	1.5 mM or 1 $\mu\text{M}$ , respectively, for 7 days in growth medium	Reduced transport; <i>Arabidopsis</i> roots	GFP export from root phloem	[4]
$\text{H}_2\text{O}_2$ : Metabolic inhibitor 60 mM aqueous (made fresh each day)	0.6 mM for 2 h in growth medium  6 mM for 2 h in growth medium	Increased transport; <i>Arabidopsis</i> root tissue  Completely blocked transport; <i>Arabidopsis</i> root tissue	Dye transport  Dye transport	[34]  [34]
$\text{NaN}_3$ : Metabolic poison 50 mM or 10 % aqueous (made fresh)	1 mM for 5 min  10 mM added to bathing solution immediately after dye injection  10 mM co-injected	Reduced transport in oat coleoptile parenchyma  No effect, <i>S. purpurea</i> stamen hairs  Increased transport, <i>S. purpurea</i> stamen hairs	Electrical coupling  CF dye transport  Transport of FITC-tagged amino acids	[82]  [65]  [47]
	1–10 mM in bathing solution  3 mM for 20 min  1 mM for 60 min	Increased transport, wheat root epidermal cells  Increased transport, <i>N. tabacum</i> leaf trichomes  Increased transport; <i>T. virginiana</i> stamen hairs	Transport of fluorescent dextrans  LYCH transport  Dye transport	[12]  [38]  [13]

(continued)

Table 2  
(continued)

Compound, mode of action, stock solution	Concentration (in bathing solution unless stated otherwise)	Effects on transport or PD structure; specific tissue tested	Detection method	Reference
KCN: Metabolic poison 50 mM aqueous	1 mM for 5 min	Reduced transport in oat coleoptile parenchyma	Electrical coupling	[82]
	1 mM added to bathing solution immediately after dye injection	No effect on transport, <i>S. purpurea</i> stamen hairs	CF dye transport	[65]
Carbonyl CN trifluoromethoxyphenyl hydrazone: Metabolic poison	1 $\mu$ M for 60 min	Increased transport, <i>Egeria densa</i> leaf tissues	Dye transport	[45]
Amiprophosmethyl: Metabolic poison	50 $\mu$ M for 2 h, 6 h, 3 days	No effect on transport; <i>N. tabacum</i> mesophyll	Virus transport	[78]
2-Dioxy-D-glucose (DDG); Callose synthesis inhibitor 10 mM aqueous	0.1 mM for 60 min	Increased transport; <i>T. virginiana</i> stamen hairs	Dye transport	[13]
Adenosine 5'-( $\beta$ , $\gamma$ -imido) triphosphate (AMP- PNP); blocks Energy metabolism	1 mM for 2 h, 6 h, 3 days	No effect on transport; <i>N. tabacum</i> mesophyll	Virus transport	[79]
ATP $\gamma$ S: Blocks processes requiring ATP	12.5 mM co-injected with dye 0.5 mg/ml in water coinjected with dye	Blocked transport; <i>T. virginiana</i> stamen hairs Reduced transport; <i>Arabidopsis</i> root epidermis	Dye transport Dye transport	[13] a

Adenosine triphosphate; ATP: alters energy balance	12.5 mM coinjected with dye	Transient inhibition of transport; <i>T. virginiana</i> stamen hairs	Dye transport	[13]
Ca-BAPTA: Calcium buffer	100 mM plus 50 mM Ca in buffer plus dye; co-injected with dye	Reduced transport, <i>S. purpurea</i> stamen hairs	CF dye transport	[45]
A23187: Calcium ionophore	100 $\mu$ M for 10 min	Reduced transport, <i>Egeria densa</i> leaf tissues	Fluorescent amino acid transport	[45]
Trifluralin: Calcium ionophore	100 $\mu$ M for 10 min	Reduced transport, <i>Egeria densa</i> leaf tissues	Fluorescent amino acid transport	[45]
Trifluoperazine: Calmodulin inhibitor	5 $\mu$ M for 60 min	Slight reduction in transport, <i>Egeria densa</i> leaf tissues	Fluorescent amino acid transport	[45]
Metal cations: $\text{Ca}^{2+}$ , $\text{Mg}^{2+}$ , $\text{Sr}^{2+}$ Concentrated aqueous solutions: modulate processes requiring divalent cations	Co-injected with dye	Slight reduction in transport, <i>Egeria densa</i> leaf tissues	Fluorescent amino acid transport	[45]

<sup>a</sup>RG White et al., unpublished data

essential to ensure the cell-to-cell movement is via PD rather than across the intervening plasma membranes and cell walls. Propidium iodide (PI) is a useful monitor of membrane integrity as it can be included in the bathing medium at very low concentrations (0.01  $\mu\text{g/ml}$ ) and is not fluorescent unless it binds to cell wall pectins or to DNA and other components within cells (e.g. [44]). If nuclei are fluorescent in the presence of PI, cell membrane integrity has been compromised.

Although plant tissues may tolerate up to 1 % concentration of many of these solvents, it is advisable to use the lowest concentration possible (e.g. [35, 44]), and as with all other applied treatments, this must be tested with the particular tissue under study. Some tissues will tolerate up to 1 % solvent for a short time but will eventually show compromised membranes. Therefore as long as the chemical agent does not precipitate out of solution, the solvent concentration should be kept as low as possible.

A literature search will show a wide range of inhibitor concentrations used on different tissues by different groups; it is best to use the lowest concentration to start with and constantly monitor cell viability. Some chemicals penetrate poorly and are best applied at a lower concentration for longer times. For example, the cytochalasins (actin inhibitors) diffuse relatively slowly into tissue and when used at moderate concentrations it can take more than 15 min for cytoplasmic streaming to cease, indicating disruption of actin filaments. By contrast, applications of cyanides or peroxides generally have immediate effects, indicating ready permeation of these small molecules throughout the tissue.

### **1.5 Application of Inhibitors to Different Tissues**

Readily water-soluble inhibitors can be dissolved in agar growth medium for treatment of *Arabidopsis* or other roots, or simply applied as drops of solution onto the tissue on a slide ready for imaging, or prepared for immersion of tissue in the treatment solution. Depending on the aim of the experiment, in our experience, a short treatment at relatively high concentration is preferable to a long treatment at low concentration. PD should respond rapidly, and a short treatment should reduce the chance of secondary effects via long-term inhibition of essential metabolic processes.

For application to a local zone of tissue or to just a few cells, the inhibitor can be added to molten agarose, which is allowed to set as a thin sheet, and cut into 1 mm<sup>3</sup> (or smaller/larger) cubes, which are then placed on the tissue of interest. Targeting of very few cells can be achieved by soaking resin beads with the inhibitor, as done for local application of pectin methyl esterase to *Arabidopsis* shoot apical meristems [59], followed by co-loading with a fluorescent tracer. Or the inhibitor can be loaded into one end of a trichome via a microinjection needle as for loading of fluorescent tracers [38].

Wounding artifacts can be ameliorated by co-incubation in DDG, but this can block other cell functions requiring UDP-glucose, and a short treatment is preferable over a long treatment [17, 18]. This is especially true for microinjection experiments, in which application of DDG is useful to separate treatment effects from wound artifacts [17, 18, 33].

A little-used alternative to application of inhibitors to the entire tissue under study is uncaging of a caged inhibitor within a column of cells with single-photon or within a single cell using multiphoton confocal illumination of the appropriate wavelength, usually short UV (*see* Chapter 9). The inhibitor is only activated within a single cell and a caged dye, such as caged fluorescein (e.g. fluorescein bis-(5-carboxymethoxy-2-nitrobenzyl) ether [CMNB-fluorescein], [38, 60]), can be included to confirm the localisation of uncaging. Most chemicals can be caged, but there are relatively few publications in which caged compounds have been used as this usually requires the collaboration of a specialist organic chemistry lab to create the caged compound of interest (e.g. caged IP<sub>3</sub> [61], caged hormones [62–64]). Several caged compounds are now available commercially and this will increase with future demand.

This chapter outlines protocols for treatment of plant tissues with compounds known to alter PD permeability, together with methods for prior propagation and subsequent analysis of two species and tissues examined in the literature. Shown here are materials and protocols used by the author, but they can be modified for use with other plant tissues, and more recent protocols (e.g. Chapters 9, 16 and 17) can be substituted.

---

## 2 Materials

### 2.1 Materials for Plant Growth

#### 2.1.1 MS Agar Plates

Add 10 g agar to 900 ml distilled water. Add nutrients, usually Murashige and Skoog (MS) mixture (available commercially), as per supplier's recommendation. Adjust nutrient type and strength as required for specific plant material. Autoclave. For *Arabidopsis*, add 20 g sucrose and 0.5 g MES, pH 6.5, dissolved in 100 ml distilled water, filter sterilize, and add to molten agar. Maintain agar at 60 °C in a waterbath until ready to dispense into 9 cm (or other) diameter petri dishes. Add inhibitors to the agar before dispensing into petri dishes (*see* **Note 1**).

1. Agar (final concentration 1 %).
2. Murashige and Skoog nutrient mix (available commercially).
3. Sucrose (final concentration 1–3 %).
4. 2-(*N*-Morpholino)ethanesulfonic acid (MES).
5. pH meter.

6. Autoclave.
7. Sterile petri dishes, 9 cm diameter.
8. Laminar flow cabinet.
9. Household bleach (approx. 4 % NaOCl).
10. Micropore tape (1/2 or 1 in. wide).
11. Sterile distilled water.

## **2.2 Fluorescent Tracers and Dyes**

Fluorescent tracers, their molecular weights and fluorescence excitation and emission maxima are listed in Table 1.

1. Propidium iodide solution: 16 nM working solution, prepared from 16  $\mu$ M stock solution in water (store in darkness at 4 °C).

## **2.3 Materials for Microinjection**

Make up all solutions using distilled water unless specified otherwise. Precise details of bathing solutions, dye loading solutions, and microinjection equipment may be varied according to the tissue under study and microinjection facilities available.

1. 0.05 % Triton X-100.
2. Incubation buffer: 0.5 mM HEPES ((N[2-hydroxyethyl] piperazine-*N'*-[2-ethanesulfonic acid])), 0.1 mM KCl, 0.1 mM  $\text{CaCl}_2$ , 0.5 mM NaCl, pH 7.0.
3. Chamber slides for microinjection: for each slide, attach a coverslip (with a nontoxic, flexible compound that remains adhesive under water and is easy to remove; we find Kemdent sticky dental wax useful for this purpose), over a 25 mm diameter hole drilled in a 75  $\times$  50 mm glass slide, 1 mm thick.
4. Double-edged sharp razor blades.
5. Fine forceps (no. 5 or no. 7).
6. Pink dental wax.
7. 1 % ultra low temperature gelling agar (gel point approx. 37 °C).
8. Ice pack.
9. 2-Deoxy-D-glucose: 10 mM stock solution in distilled water.
10. Polydisperse 4 kDa FITC-dextran (*see Note 2*).
11. 3 kDa cutoff microconcentrator (e.g. microcon 3, Amicon) (*see Note 2*).
12. Quix-sep separator (e.g. Membrane Filtration Products) or similar to separate polydisperse fluorescent dextrans into different size classes—use according to manufacturer's instructions (*see Note 2*).
13. 1 kDa dialysis membrane (*see Note 2*).
14. Kieselgel 60F thin layer chromatography sheets.

15. Running solution: 150:30:100:120 *n*-butanol:acetic acid:pyridine: water.
16. Microcapillary tubes; 1.2 mm OD borosilicate glass with inner filament.
17. Very fine micropipettes for backfilling microinjection needles (e.g. MicroFil 28 gauge syringe, World Precision Instruments [WPI]).
18. 100 mM KCl.
19. Silver/silver chloride reference electrode (e.g. Sigma).
20. Micropipette holder that will fit into the hydraulic micromanipulator.
21. 1 mM aqueous solution of dye to be injected, prepared immediately before use.
22. Aniline blue stain: 0.05 % aniline blue in 0.067 M phosphate buffer, pH 8.5.

## **2.4 Materials for TEM**

Precise details of fixative, buffer, dehydration solvent, resin, and method of polymerization will need to be adjusted depending on the tissue under study and availability of materials and preparation facilities.

1. Sharp double-edged razor blades.
2. Fine forceps (no. 5 or no. 7).
3. Pink dental wax.
4. Fixative: 2.5 % glutaraldehyde in 0.025 M phosphate buffer, pH 7.2.
5. Buffer: 0.025 M phosphate buffer, pH 7.2.
6. 1 % aqueous osmium tetroxide.
7. 10, 20, 30, 50, 70, 90, 95 % acetone solutions.
8. 100 % dry acetone (dried over molecular sieve).
9. Spurr's resin—prepare liquid resin according to supplier's instructions (*see* **Note 3**).
10. LRWhite resin—prepare liquid resin according to supplier's instructions (*see* **Note 4**).
11. Ultramicrotome, e.g. Leica Ultracut 6.
12. Knife glass for sectioning.
13. Knifemaker to make glass knives.
14. Diamond knife, e.g. Diatome.
15. TEM copper grids, 3.5 mm 400 mesh, coated or uncoated (*see* **Note 5**).

16. Ethanolic uranyl acetate: 1.2 % uranyl acetate in ethanol (*see* **Notes 6** and **7**).
17. Reynolds lead citrate (*see* **Notes 6** and **7**).
18. Propane (*see* **Note 8**).
19. Plunge-freezing apparatus.
20. Freeze-substitution apparatus or  $-80$  and  $-20$  °C freezers plus 4 °C refrigerator.
21. 100 % dry ethanol or acetone (dried over molecular sieve) maintained at  $-80$  °C.

## **2.5 Imaging Hardware (See Note 9)**

In each case, the appropriate excitation and emission filters for fluorescent tracers must be identified, sourced, and installed, if not already available on the instrument.

1. Dissecting microscope equipped for fluorescence imaging.
2. Fluorescence compound microscope.
3. Confocal laser scanning microscope.

## **2.6 Microinjection Hardware (See Note 10)**

1. Fluorescence inverted microscope or upright microscope.
2. Hydraulic micromanipulator, e.g. Narashige OR-60.
3. Flaming/Brown type electrode puller, e.g. Sutter P67.
4. Iontophoresis apparatus, comprising Electrometer (e.g. S7071A, WPI) plus miniMainframe (WPI).
5. Multimeter to monitor membrane potential.

## **2.7 Plant Material (See Note 11)**

1. *Arabidopsis thaliana* L. plants. Grow on standard MS agar plates (*see* Subheading 2.1.1).
2. *Tradescantia virginiana* L. Maintain under long daylength at 25 °C with minimal fertilization, and regular watering and pruning for vigorous growth and continued flowering.

## **2.8 Biochemical Inhibitors (See Note 12)**

Biochemicals that target different known or putative components or regulators of plasmodesmata are listed in Table 2.

1. Treatment solution 1 for *Arabidopsis thaliana* root epidermal cells: working concentration of the selected biochemical inhibitor as defined in Table 2 in MS nutrient mix made according to manufacturer's recommendation, 2.5 mM MES, pH 6.5.
2. Treatment solution 2 for *Tradescantia virginiana* stamen hairs: working concentration of the selected biochemical inhibitor as defined in Table 2 in 0.5 mM HEPES, 0.1 mM KCl, 0.1 mM  $\text{CaCl}_2$ , 0.1 mM  $\text{MgCl}_2$ , 0.5 mM NaCl pH 7.

### 3 Methods

#### 3.1 Selection, Growth, and Chemical Treatment of Plant Material (See Note 12)

The treatments of two types of tissue, i.e. three-dimensional roots, and one-dimensional filaments, are detailed below (see Note 13).

##### 3.1.1 *Arabidopsis* *thaliana* Roots

1. Prepare MS agar plates (see Subheading 2.1.1).
2. Seed sterilization:
  - (a) Place 30–100 *Arabidopsis* seeds in a 1.5–2.0 ml microfuge tube. Place tube in a vacuum desiccator in a fume hood.
  - (b) Place 100 ml household bleach in a 250 ml beaker next to the *Arabidopsis* seeds in the desiccator. Add 3 ml concentrated HCl to the bleach. Immediately place the lid on the desiccator.
  - (c) After 3.0–3.5 h, remove seeds from desiccator and transfer immediately into a laminar flow cabinet. Allow to sit for 5–10 min to ensure that residual Cl<sub>2</sub> gas dissipates.
  - (d) Scatter seeds sparsely on MS agar plates, seal with micropore tape. Place in the dark at 4 °C for 24–48 h to stratify.
3. Alternatively, in a laminar flow cabinet, surface sterilize *Arabidopsis* seeds in 30 % bleach containing 0.1 % Triton X-100 for 10 min followed by 4×10 min rinses in sterile distilled water. Dispense seeds individually onto agar using wide sterile pipette tips. Seal plates with micropore tape and place in the dark at 4 °C for 24–48 h to stratify.
4. After stratification, place plates on their sides in 22 °C growth room in constant light (or other light regime) so roots will grow vertically down along the agar surface. Roots can be used 5–7 days after germination.
5. Prepare agar plates containing inhibitor(s) (see Note 1). Either a) transfer *Arabidopsis* seedlings onto this agar or b) place a small cube, no greater than 1 mm on each side, of this agar onto each *Arabidopsis* root while still on MS agar (see Note 14).
6. Alternatively, incubate roots in treatment solution 1 with or without inhibitor for 1 h. Pretreatment with 1 mM DDG for 1 h will reveal whether the inhibitor stimulates production of wound-induced callose (also see Note 15).

##### 3.1.2 *Tradescantia* *virginiana* L. Stamen Hairs

1. Selection of the appropriate size of flower bud is trial and error at first. The stamen hairs need to be young, or the outer walls become hydrophobic, virtually impervious to inhibitors and difficult to microinject. However, they need to be sufficiently mature to show vigorous cytoplasmic streaming (see Note 16).

2. Remove an appropriately sized bud from the plant. Place into a drop of distilled water on a piece of dental wax. Slice off the pedicel, cutting through the base of the ovary.
3. Press gently on the top of the bud to squeeze out the remainder of the ovary and the two young stamens.
4. Carefully remove the pollen sacs from the filament, using a sharp razor blade. Dip each filament with attached stamen hairs into 0.05 % Triton X-100 for 1–2 s. This treatment greatly enhances penetration of treatment chemicals without apparent damage to the cells.
5. Transfer the filament with attached stamen hairs into treatment solution 2 for the length of time desired, less 15 min. With a 45 min incubation the tissue is allowed to recover for 15 min on the microscope before imaging and microinjection, giving a total of 1 h treatment. Bathe control filaments and hairs in the treatment solution 2 without inhibitor for an equivalent period of time (*see* **Note 15**).

### 3.2 Assessing PD Permeability

This section outlines procedures for microinjection of dyes, imaging cell–cell dye transport, and methods to quantify transport (*see* **Note 17**).

#### 3.2.1 Microinjection of Tracer Dyes

##### *Arabidopsis thaliana* Root Epidermal Cells (*See* **Note 11**)

1. Cut *Arabidopsis* seedlings with supporting agar from the Petri dish and place vertically in treatment solution 1 (with or without inhibitor, *see* **Note 15**). Submerge just the tips of the roots in solution. Avoid disturbance to the roots by handling the supporting agar rather than the seedlings themselves.
2. If using dissected tissues, cut *Arabidopsis* roots from the cotyledons at least 10 mm away from the planned injection site.
3. After incubation in treatment solution 1, mount the roots horizontally in the well of a chamber slide
4. Hold roots in place by embedding in a thin layer of cool but still-molten 1 % ultra low temperature gelling agar (Type IX, Sigma), and set it by placing on ice (or use an ice-pack) for 5–10 s.
5. Immediately add treatment solution 1 (with or without inhibitor) to the well and allow the tissues to rest for 15 min prior to injection (*see* **Note 15**).
6. Prepare 1 mM dye solution for injection. If not using FITC-dextran, go to **step 13**.
7. Prepare FITC-dextran from polydisperse 4 kDa FITC-dextran dissolved in water to a concentration of 20 mM and separated using a 3 kDa cutoff microconcentrator (*see* **Note 2**).

8. Dilute the solution remaining in the filter to approximately 1 mM. This is the fraction larger than 3 kDa.
9. Dialyse the filtered solution (<3 kDa) in a separator using a 1 kDa dialysis membrane to give the 1–3 kDa fraction.
10. If required, check that free FITC has been removed from the purified dextrans by thin layer chromatography (TLC) using the protocol of [31].
11. For TLC, separate the FITC-dextran solution on Kieselgel 60 F thin layer chromatography sheets using a running solution of 150:30:100:120 *n*-butanol:acetic acid:pyridine:water. Visualize the purified dextran with UV illumination; it should be seen as a single fluorescent spot.
12. Pull microinjection needles on a Flaming/Brown micropipette puller (or equivalent) (*see* **Note 18**).
13. Fill the tips of the needles with dye by capillary action using a very fine filament syringe (e.g. Microfil syringe, 28 gauge) that fits easily into the injection needle.
14. Back-fill the needles with 100 mM KCl.
15. Mount the needle on a silver chloride half-cell connected to an electrometer to detect membrane potential (e.g. Electrometer module with miniMainframe; WPI).
16. Use a return electrode filled with 3 mM KCl connected via a silver chloride half-cell.
17. Bring the tip of the injection needle up to a selected cell and tap the microscope gently so that the needle penetrates the cell wall.
18. Monitor cell membrane potential using a multimeter connected to the electrometer. A drop in this reading indicates penetration into the cytoplasm, but a substantial drop indicates that the needle has penetrated through into the vacuole or injury to the cell. Discard cells with vacuolar penetration or injury.
19. Inject dye by applying a brief, small (approx. 1 nA for 1–5 s, longer if required) current to the microinjection needle. Use a negative current for lucifer yellow and sulforhodamine 101. Use a positive current for the FITC-dextrans.
20. Test the viability of the injected tissue by releasing a small amount of dye into the microinjection buffer surrounding the tissue. If tissue is damaged it will take up dye from the medium, showing that the membranes have become leaky.
21. If assessing callose deposition, stain tissue with 0.05 % aniline blue in 0.067 M phosphate buffer, pH 8.5. Apply the stain immediately before observation on a fluorescence microscope.

*Tradescantia virginiana* Stamen Hairs

1. Prepare chamber slides by first attaching a coverslip over a 25 mm diameter hole drilled in a 75 × 50 mm glass slide.
2. Prepare and incubate stamen hairs in treatment solution 2 (*see* **Note 15**).
3. After incubation in treatment solution 2, mount the hairs in the well of a chamber slide.
4. Hold hairs in place by embedding in a thin layer of cool but still molten 1 % ultra low temperature gelling agar, and set the agar by placing on ice (or on an ice pack) for 5–10 s.
5. Immediately add fresh treatment solution 2 to the well and allow the tissues to rest for 15 min prior to injection.
6. Continue as described in **steps 6–21** above for *Arabidopsis* roots.

### 3.3 Assessing Changes in PD Structure

Because tissue handling and noncryo fixation procedures will generate additional callose at the PD neck, either pretreatment with DDG, or its addition to the treatment solution, is very useful to separate fixation-induced changes in PD structure from treatment-induced changes (e.g. [17, 18]).

#### 3.3.1 PD Structure in Roots: Conventional Chemical Fixation

1. Incubate live germinated seeds with root attached in 0.1 mM DDG for 1 h to prevent fixation-induced formation of callose (*see* **Note 15**).
2. Incubate live tissues in inhibitor in water (*see* Table 2), with or without 0.1 mM DDG, for 1 h.
3. Fix specimens in 2.5 % glutaraldehyde in 0.025 M phosphate buffer, pH 7.2, for 2 h.
4. Rinse in phosphate buffer, three times, 10 min each time.
5. Incubate in 1 % aqueous osmium tetroxide for 2 h.
6. Rinse in distilled water, two times, 10 min each time.
7. Dehydrate in a progressive acetone or ethanol series, 20 min each step (*see* **Note 19**).
8. Infiltrate slowly in liquid Spurr's resin (*see* **Notes 3, 4, and 20**) over 2 days.
9. Polymerise at 50 °C overnight (*see* **Note 21**).
10. Collect ultrathin sections 80–90 nm thick on uncoated or coated copper grids.
11. Stain with 1.2 % ethanolic uranyl acetate for 10 min (*see* **Note 6**).
12. Rinse briefly in distilled water.
13. Stain with Reynold's lead citrate for 8–12 min (*see* **Note 6**).
14. Rinse briefly with warm (approx. 30 °C) distilled water.
15. View on a TEM according to the manufacturer's instructions.

16. Take measurements of the neck regions of PD directly from negatives (or on-screen images) (*see* **Note 22**).
17. In most cases, comparison using the Student's *t*-test ( $p < 0.01$ ) is sufficient to assess the statistical significance of differences in PD dimensions [17].

### 3.3.2 PD Structure in Roots: Cryofixation

In general, cryofixation followed by freeze-substitution is optimal for faithful preservation of PD architecture. Even here, prior incubation in DDG will show the significance of tissue handling in generation of artefactual callose (*see* **Note 15**).

1. Incubate live germinated seeds with root attached in 0.1 mM DDG for 1 h to prevent handling-induced formation of callose.
2. Incubate in water 1 with or without inhibitor (*see* Table 2) for 1 h.
3. Immediately plunge-freeze in liquid propane, in a rapid-freezing apparatus, according to the manufacturer's recommendations.
4. Freeze-substitute in a commercial freeze-substitution apparatus according to the manufacturer's recommendations, or if this is unavailable, continue **steps 5–9** below.
5. Transfer to dry ethanol or acetone (dried over molecular sieve) at  $-80^{\circ}\text{C}$ .
6. Allow to freeze-substitute for 1–3 days at  $-80^{\circ}\text{C}$ , change solvent once after the first 12 h.
7. Transfer to  $-20^{\circ}\text{C}$  freezer for 24 h.
8. Transfer to  $4^{\circ}\text{C}$  refrigerator for 24 h.
9. Bring to room temperature and proceed as in **steps 8–17** of Subheading 3.3.1.

---

## 4 Notes

1. Add the inhibitor to the agar before dispensing into petri dishes but after the agar has been autoclaved. In most cases the treatment agar does not need to be sterile since treatments are short. If sterility is essential, filter the drug solution through a  $0.22\ \mu\text{m}$  filter. Make a stock solution of ten times the final concentration and add 3 ml of this to 27 ml of agar solution to cover the base of one 9 cm diameter petri dish.
2. This protocol uses a 4 kDa polydisperse FITC-dextran mixture as starting material to prepare dextrans of different molecular size classes. For dextrans of larger size class, use a larger polydisperse fluorescent dextran mixture as starting material, with dialysis membranes of the required size cutoff to prepare dextrans of specific size-classes. Dextrans with different fluorescent tags, e.g. rhodamine, Texas Red, can be used also. Separate

the polydisperse dextrans into different size classes using a separator and dialysis membranes according to the manufacturers' instructions.

3. The original formulation of Spurr's resin is no longer available, and the new formulation, available from several suppliers, should be tested before use to ascertain the best component ratios, and infiltration and polymerization regimes for each plant tissue under study.
4. Although London Resin White (LR White) resin is somewhat less stable than Spurr's resin under the electron beam, it is perfectly satisfactory if used with coated grids. LR White is considerably less viscous and generally requires shorter infiltration times. LR White Medium Grade is appropriate for most tissues.
5. Those experienced in TEM preparation techniques may prepare their own coated grids, but perfectly satisfactory ones are available from a number of suppliers.
6. Different TEM laboratories have different preferences for uranyl acetate and Reynolds lead citrate [83] staining which may differ from the formulations and staining times suggested here. Use the formulations recommended on-site and only modify if needed.
7. Spurr's and LR White resin sections require somewhat different staining times with uranyl acetate and lead citrate, and these must be determined empirically.
8. A small (D-size) cylinder of propane gas will be required whether using a home-made liquid propane freezing device or a commercially available device.
9. Most research facilities will have one or more options for fluorescence imaging. Instruction in use of the instruments should be obtained on site.
10. The microinjection hardware currently available is highly integrated, such that microiontophoresis current generators and micropressure systems require no prior assembly from separate components. Both types of systems have built-in current detection for monitoring membrane potential during microneedle insertion and injection of tracers. In each case, instruction in use of specific instruments should be obtained on site.
11. Plant materials listed here have been used by the author. The protocols will need to be modified for application to other plant tissues, for example, seedling roots of other species, epidermal peels from *Allium* species (onion—*A. cepa* or leek—*A. porrum*), or fronds from aquatic plants such as *Egeria densa* or *Elodea canadensis*.
12. These protocols are appropriate for treatments with small molecules that can permeate throughout plant tissues. In addition,

proteins and antibodies may be pressure-injected to assess their potential effects on PD.

13. For quantitative comparison of inhibitor effects, it is essential that plants can repeatedly be grown very uniformly. Rapid growth is another key criterion, as is membrane integrity during chemical treatment. Healthy cells with undamaged walls and membranes are essential. This can be tested by daily growth measurement of roots, and by incubation in dyes that are membrane impermeant, such as propidium iodide—entry of dye into the cells indicates that the plasma membrane has reduced integrity. Membrane integrity is critical to interpretation of results in which altered cell–cell transport via PD rather than altered cell–cell membrane transport is desired.
14. For treatment, transfer plants to agar containing the inhibitor. Protect the shoots from treatment by first placing a narrow strip of parafilm on the agar and ensuring the shoots lie on this strip. For treatment of a small section of tissue, place small inhibitor-soaked agar cubes or resin beads onto the tissue.
15. Manipulation of tissues during experiments and insertion of microinjection needles induces callose [18, 33] as does chemical fixation [17]. Pretreatment with 0.1 mM DDG in water or treatment solution with or without inhibitor is a useful additional control treatment.
16. A general rule is that the flower buds should be no more than 2–3 mm long and about 2–3 days before anthesis (*see* refs. 13, 18 and references therein).
17. It is essential to learn microinjection in a laboratory with proven success in using this technique. Each laboratory has their own set of instruments and protocols, and it is impossible to pick up essential technical skills without hands-on training. Dye flux can be quantitated using fluorescence recovery after photobleaching (FRAP) of a small tracer, CF, ester-loaded into root cells by incubating in CFDA [34]. Other quantification techniques for measuring very rapid changes in flux have generally involved measuring changes in electrical coupling (e.g. [48–50]). Although the latter technique has fallen from favor, it is indispensable for detecting fast changes in PD permeability, and to identify rapid PD opening and closing events. In unpublished observations, we have observed interactions between tracer dyes and certain inhibitors that alters their fluorescence intensity. This should be checked, for example, by applying dye to agar pre-soaked with either water or inhibitor.
18. Preparation of the correct-sized microinjection needle is determined empirically on the individual electrode puller. The needles

must be sharp enough to penetrate through the cell wall, but strong enough to penetrate without breaking. In most cases, needles can be used only once, because the tip breaks off as it traverses the cell wall, and after entry, wound responses in the cytoplasm block the tip, preventing further injection of dye or other components.

19. Both Spurr's and LR White resins are soluble in either ethanol or acetone. While acetone often produces superior results when used as infiltration solvent, ethanol is less toxic and may be preferred for safety reasons.
20. Slow infiltration is critical to excellent preservation, and infiltration times must be longer for denser, larger tissues.
21. LR White resin requires polymerization in the absence of oxygen, either in an oven or under UV light. The capsules containing resin to be polymerised must either be sealed, to prevent entry of oxygen, or must be maintained in a nitrogen gas atmosphere during polymerization.
22. Measure the outer diameter at the narrower section of PD deep within the cell wall, from the outer layer of the plasma membrane on each side as reference. Then measure at the neck region, where PD open to the cell cytoplasm, also from the outer layer of the plasma membrane on each side. Differences may be obvious (e.g. [54]) or more subtle (e.g. [17, 80]).

---

## Acknowledgements

Thanks to Janine Radford at Monash University; Robyn Overall, Terena Holdaway-Clarke, Debbie Barton, and other Sydney University colleagues; Mark Talbot, summer students, and others in my lab at CSIRO Plant Industry for tips, tricks, comments, and assistance along the way.

## References

1. Faulkner CR, Blackman LM, Cordwell SJ, Overall RL (2005) Proteomic identification of putative plasmodesmatal proteins from *Chara corallina*. *Proteomics* 5:2866–2875
2. Bayer EM, Bottrill AR, Walshaw J et al (2006) *Arabidopsis* cell wall proteome defined using multidimensional protein identification technology. *Proteomics* 6:301–311
3. Faulkner C, Maule A (2011) Opportunities and successes in the search for plasmodesmal proteins. *Protoplasma* 248:27–38
4. Benitez-Alfonso Y, Cilia M, San RA et al (2009) Control of Arabidopsis meristem development by thioredoxin-dependent regulation of intercellular transport. *Proc Natl Acad Sci U S A* 106:3615–3620
5. Stonebloom S, Burch-Smith T, Kim I et al (2009) Loss of the plant DEAD-box protein ISE1 leads to defective mitochondria and increased cell-to-cell transport via plasmodesmata. *Proc Natl Acad Sci U S A* 106:17229–17234
6. Kobayashi K, Otegui MS, Krishnakumar S et al (2007) *INCREASED SIZE EXCLUSION LIMIT2* encodes a putative DEVH box RNA helicase involved in plasmodesmata function

- during *Arabidopsis* embryogenesis. *Plant Cell* 19:1885–1897
7. Kim I, Hempel FD, Sha K et al (2002) Identification of a developmental transition in plasmodesmatal function during embryogenesis in *Arabidopsis thaliana*. *Development* 129: 1261–1272
8. Avisar D, Prokhnevsky AI, Dolja VV (2008) Class VIII myosins are required for plasmodesmatal localization of a closterovirus hsp70 homolog. *J Virol* 82:2836–2843
9. Golomb L, Abu-Abied M, Belausov E, Sadot E (2008) Different subcellular localizations and functions of *Arabidopsis* myosin VIII. *BMC Plant Biol* 8:3
10. Yokota E, Ueda S, Tamura K et al (2009) An isoform of myosin XI is responsible for the translocation of endoplasmic reticulum in tobacco cultured BY-2 cells. *J Exp Bot* 60: 197–212
11. Wu S, Gallagher KL (2013) Intact microtubules are required for the intercellular movement of the SHORTROOT transcription factor. *Plant J* 74:148–159
12. Cleland RE, Fujiwara T, Lucas WJ (1994) Plasmodesmal-mediated cell-to-cell transport in wheat roots is modulated by anaerobic stress. *Protoplasma* 178:81–85
13. Radford JE, White RG (2011) Inhibitors of myosin, but not actin, alter transport through *Tradescantia* plasmodesmata. *Protoplasma* 248: 205–216
14. Stonebloom S, Brunkard JO, Cheung AC et al (2012) Redox states of plastids and mitochondria differentially regulate intercellular transport via plasmodesmata. *Plant Physiol* 158: 190–199
15. Gale EF, Wayman F, Orlean PA (1984) The action of 2-deoxy-D-glucose on the incorporation of glucose into (1-3)- $\beta$ -glucan in stationary phase cultures of *Candida albicans*. *J Gen Microbiol* 130:3303–3311
16. Jaffe MJ, Leopold AC (1984) Callose deposition during gravitropism of *Zea mays* and *Pisum sativum* and its inhibition by 2-deoxy-D-glucose. *Planta* 161:20–26
17. Radford JE, Vesik M, Overall RL (1998) Callose deposition at plasmodesmata. *Protoplasma* 201:30–37
18. Radford JE, White RG (2001) Effects of tissue-preparation-induced callose synthesis on estimates of plasmodesma size exclusion limits. *Protoplasma* 216:47–55
19. Fenteany G, Zhu S (2003) Small-molecule inhibitors of actin dynamics and cell motility. *Curr Top Med Chem* 3:593–616
20. Baggett AW, Cournia Z, Han MS et al (2012) Structural characterization and computer-aided optimization of a small-molecule inhibitor of the Arp2/3 complex, a key regulator of the actin cytoskeleton. *ChemMedChem* 7: 1286–1294
21. Bonello T, Coombes J, Schevzov G et al (2012) Therapeutic targeting of the actin cytoskeleton in cancer. In: *Cytoskeleton and human disease*. Humana, Totowa, NJ, pp 181–200
22. Fitzgibbon J, Beck M, Zhou J et al (2013) A developmental framework for complex plasmodesmata formation revealed by large-scale imaging of the *Arabidopsis* leaf epidermis. *Plant Cell* 25:57–70
23. Duckett CM, Oparka KJ, Prior DAM et al (1994) Dye-coupling in the root epidermis of *Arabidopsis* is progressively reduced during development. *Development* 120:3247–3255
24. Oparka KJ, Duckett CM, Prior DAM, Fisher DB (1994) Realtime imaging of phloem unloading in the root tip of *Arabidopsis*. *Plant J* 6:759–766
25. Wang N, Fisher DB (1994) The use of fluorescent tracers to characterize the post-phloem transport pathway in maternal tissues of developing wheat grains. *Plant Physiol* 104:17–27
26. Wang HL, Offler CE, Patrick JW, Ugalde TD (1994) The cellular pathway of photosynthate transfer in the developing wheat grain. I. Delineation of a potential transfer pathway using fluorescent dyes. *Plant Cell Environ* 17: 257–266
27. Wright KM, Oparka KJ (1996) The fluorescent probe HPTS as a phloem-mobile, symplastic tracer, an evaluation using confocal laser scanning microscopy. *J Exp Bot* 47:439–445
28. Wang X, Sager R, Cui W et al (2013) Salicylic acid regulates plasmodesmata closure during innate immune responses in *Arabidopsis*. *Plant Cell* 35:2315–2329
29. Tyree MT, Tammes PML (1975) Translocation of uranin in the symplasm of staminal hairs of *Tradescantia*. *Can J Bot* 53:2038–2046
30. Tucker EB (1982) Translocation in the staminal hairs of *Setcreasea purpurea*. I. A study of cell ultrastructure and cell-to-cell passage of molecular probes. *Protoplasma* 113: 193–201
31. Goodwin PB (1983) Molecular size limit for movement in the symplast of the *Elodea* leaf. *Planta* 157:124–130
32. Faulkner C, Petutschnig E, Benitez-Alfonso Y et al (2013) LYM2-dependent chitin perception limits molecular flux via plasmodesmata. *Proc Natl Acad Sci U S A* 110:9166–9170
33. Storms MHM, van der Schoot C, Prins M et al (1998) A comparison of two methods of

- microinjection for assessing altered plasmodesmal gating in tissues expressing viral movement proteins. *Plant J* 13:131–140
34. Rutschow HL, Baskin TI, Kramer EM (2011) Regulation of solute flux through plasmodesmata in the root meristem. *Plant Physiol* 155: 1817–1826
  35. Baskin TI, Bivens NJ (1995) Stimulation of radial expansion in arabidopsis roots by inhibitors of actomyosin and vesicle secretion but not by various inhibitors of metabolism. *Planta* 197:514–521
  36. Baskin TI, Wilson JE (1997) Inhibitors of protein kinases and phosphatases alter root morphology and disorganize cortical microtubules. *Plant Physiol* 113:493–502
  37. Roberts AG, Cruz SS, Roberts IM et al (1997) Phloem unloading in sink leaves of *Nicotiana benthamiana*, comparison of a fluorescent solute with a fluorescent virus. *Plant Cell* 9:1381–1396
  38. Christensen NM, Faulkner C, Oparka K (2009) Evidence for unidirectional flow through plasmodesmata. *Plant Physiol* 150:96–104
  39. Urbanus SL, Dinh QK, Angenent GC, Immink RGH (2010) Investigation of MADS domain transcription factor dynamics in the floral meristem. *Plant Signal Behav* 5:1260–1262
  40. Chapman S, Faulkner C, Kaiserli E et al (2008) The photoreversible fluorescent protein iLOV outperforms GFP as a reporter of plant virus infection. *Proc Natl Acad Sci U S A* 105: 20038–20043
  41. Mukherjee A, Walker J, Weyant KB, Schroeder CM (2013) Characterization of flavin-based fluorescent proteins: an emerging class of fluorescent reporters. *PLoS One* 8(5):e64753
  42. Palevitz BA, Hepler PK (1985) Changes in dye coupling of stomatal cells of *Allium* and *Commelina* demonstrated by microinjection of Lucifer yellow. *Planta* 164:473–479
  43. Scott AS, Wyatt S, Tsou P-L et al (1999) Model system for plant cell biology: GFP imaging in living onion epidermal cells. *Biotechniques* 26:1125–1132
  44. Collings DA (2013) Subcellular localization of transiently expressed fluorescent fusion proteins. In: Chapter 16 in *Legume genomics: methods and protocols*. *Methods in molecular biology*, vol 1069. doi:10.1007/978-1-62703-613-9\_16
  45. Erwee MG, Goodwin PB (1983) Characterisation of the *Egeria densa* Planch. leaf symplast. Inhibition of the intercellular movement of fluorescent probes by group II ions. *Planta* 158(320):328
  46. Tucker EB (1990) Calcium-loaded 1,2-bis(2-aminophenoxy)ethane-N, N, N', N'-tetraacetic acid blocks cell-to-cell diffusion of carboxyfluorescein in staminal hairs of *Setcreasea purpurea*. *Planta* 182:34–38
  47. Tucker EB (1993) Azide treatment enhances cell-to-cell diffusion in staminal hairs of *Setcreasea purpurea*. *Protoplasma* 174:45–49
  48. Holdaway-Clarke TL, Walker NA, Hepler PK, Overall RL (2000) Physiological elevations in cytoplasmic free calcium by cold or ion injection result in transient closure of higher plant plasmodesmata. *Planta* 210: 329–335
  49. Spanswick RM (1972) Electrical coupling between cells of higher plants: a direct demonstration of intercellular communication. *Planta* 102:215–227
  50. Overall RL, Gunning BES (1982) Intercellular communication in *Azolla* roots: II. Electrical coupling. *Protoplasma* 111:151–160
  51. Staiger CJ (2000) Signaling to the cytoskeleton in plants. *Annu Rev Plant Physiol Plant Mol Biol* 51:257–288
  52. Collings DA (2008) Crossed wires: interactions and cross-talk between the microtubule and microfilament networks in plants. In: Nick P (ed) *Plant cell monographs: plant microtubules, development, and flexibility*. Springer, Berlin, pp 47–82
  53. Heinlein M, Padgett HS, Gens JS et al (1998) Changing patterns of localization of the Tobacco Mosaic Virus movement protein and replicase to the endoplasmic reticulum and microtubules during infection. *Plant Cell* 10: 1107–1120
  54. White RG, Badelt K, Overall RL, Vesik M (1994) Actin associated with plasmodesmata. *Protoplasma* 180:169–184
  55. Mooré D (1980) Effects of hexose analogues on fungi: mechanisms of inhibition and of resistance. *New Phytol* 87:487–515
  56. Breier A, Crane AM, Kennedy C, Sokoloff L (1993) The effects of pharmacologic doses of 2-deoxy-D-glucose on local cerebral blood flow in the awake, unrestrained rat. *Brain Res* 618:277–282
  57. Datema R, Schwartz RT, Rivas LA, Pont-Lezica R (1983) Inhibition of  $\beta$ -1,4-glucan biosynthesis by deoxyglucose. *Plant Physiol* 71:76–81
  58. Stone BA, Clarke AE (1992) *Chemistry and biology of (1 $\rightarrow$ 3)- $\beta$ -glucans*. La Trobe University Press, Bundoora, VIC
  59. Peucelle A, Louvet R, Johansen JN et al (2008) *Arabidopsis* phyllotaxis is controlled by the methyl-esterification status of cell-wall pectins. *Curr Biol* 18:1943–1948
  60. Martens HJ, Hansen M, Schulz A (2004) Caged probes: a novel tool in studying

- symplasmic transport in plant tissues. *Protoplasma* 223:63–66
61. Gilroy S, Read N, Trewavas AJ (1990) Elevation of cytoplasmic calcium by caged calcium or caged inositol trisphosphate initiates stomatal closure. *Nature* 346:769–771
62. Ward JL, Beale MH (1995) Caged plant hormones. *Phytochemistry* 38:811–816
63. Allan AC, Ward JL, Beale MH, Trewavas AJ (1998) Caged plant growth regulators. *Methods Enzymol* 291:474–483
64. Kusaka N, Maisch J, Nick P et al (2009) Manipulation of intracellular auxin in a single cell by light with esterase-resistant caged auxins. *ChemBioChem* 10:2195–2202
65. Tucker EB (1987) Cytoplasmic streaming does not drive intercellular passage in staminal hairs of *Setcreasea purpurea*. *Protoplasma* 137: 140–144
66. Tucker EB, Tucker JE (1993) Cell-to-cell diffusion selectivity in staminal hairs of *Setcreasea purpurea*. *Protoplasma* 174:36–44
67. Zhu T, Lucas WJ, Rost TL (1998) Directional cell-to-cell communication in the *Arabidopsis* root apical meristem. I. An ultrastructural and functional analysis. *Protoplasma* 203:35–47
68. Liang DC, White RG, Waterhouse PM (2012) Gene silencing in *Arabidopsis* spreads from the root to the shoot, through a gating barrier, by template-dependent, non-vascular, cell to cell movement. *Plant Physiol* 159:984–1000
69. Oparka KJ, Prior DAM (1988) Movement of lucifer yellow CH in potato tuber storage tissue: a comparison of symplastic and apoplastic transport. *Planta* 176:533–540
70. Volkmann D, Mori T, Tirlapur UK et al (2003) Unconventional myosins of the plant-specific class VIII: endocytosis, cytokinesis, plasmodesmata/pit-fields, and cell-to-cell coupling. *Cell Biol Int* 27:289–291
71. Erwee MG, Goodwin PB (1984) Characterisation of the *Egeria densa* leaf symplast: response to plasmolysis, deplasmolysis and to aromatic amino acids. *Protoplasma* 122: 162–168
72. Ding B, Kwon M-O, Warnberg L (1996) Evidence that actin filaments are involved in controlling the permeability of plasmodesmata in tobacco mesophyll. *Plant J* 10:157–164
73. Su S, Liu Z, Chen C et al (2010) Cucumber Mosaic Virus movement protein severs actin filaments to increase the plasmodesmal size exclusion limit in tobacco. *Plant Cell* 22: 1373–1387
74. Stadler R, Wright KM, Lauterbach C et al (2005) Expression of GFP-fusions in *Arabidopsis* companion cells reveals non-specific protein trafficking into sieve elements and identifies a novel post-phloem domain in roots. *Plant J* 41:319–331
75. Imlau A, Truernit E, Sauer N (1999) Cell-to-cell and long distance trafficking of the green fluorescent protein in the phloem and symplastic unloading of the protein into sink tissues. *Plant Cell* 11:309–322
76. Simpson I (1978) Labelling of small molecules with fluorescein. *Anal Biochem* 89: 304–305
77. Bostrom TE, Walker NA (1975) Intercellular transport in plants I. The flux of chloride and the electric resistance in Chara. *J Exp Bot* 26: 767–782
78. Krasavina MS, Ktitorova IN, Burmistrova NA (2001) Electrical conductance of cell-to-cell junctions and the cytoskeleton of plant cells. *Russ J Plant Physiol* 48:741–748
79. Kawakami S, Watanabe Y, Beachy RN (2004) Tobacco mosaic virus infection spreads cell to cell as intact replication complexes. *Proc Natl Acad Sci U S A* 20:6291–6296
80. Radford JE, White RG (1998) Localization of a myosin-like protein to plasmodesmata. *Plant J* 14:743–750
81. Dale N, Lunn G, Fensom DS, Williams EJ (1983) Rates of axial transport of  $^{11}\text{C}$  and  $^{14}\text{C}$  in Characean cells: faster than visible streaming? *J Exp Bot* 34:130–143
82. Drake G (1979) Electrical coupling, potentials, and resistances in oat coleoptiles: effects of azide and cyanide. *J Exp Bot* 30:719–725
83. Reynolds ES (1963) Electron-opaque stain in electron microscopy. *J Cell Biol* 17:208–212



# **Part V**

## **Studying Macromolecular Trafficking**



## GAL4 Transactivation-Based Assay for the Detection of Selective Intercellular Protein Movement

Dhinesh Kumar, Huan Chen, Yeonggil Rim, and Jae-Yean Kim

### Abstract

Several plant proteins function as intercellular messenger to specify cell fate and coordinate plant development. Such intercellular communication can be achieved by direct, selective, or nonselective (diffusion-based) trafficking through plasmodesmata (PD), the symplasmic membrane-lined nanochannels adjoining two cells. A trichome rescue trafficking assay was reported to allow the detection of protein movement in *Arabidopsis* leaf tissue using transgenic gene expression. Here, we provide a protocol to dissect the mode of intercellular protein movement in *Arabidopsis* root. This assay system involves a root ground tissue-specific GAL4/UAS transactivation expression system in combination with fluorescent reporter proteins. In this system, mCherry, a red fluorescent protein, can move cell to cell via diffusion, while mCherry-H2B is tightly cell autonomous. Thus, a protein fused to mCherry-H2B that can move out from the site of synthesis likely contains a selective trafficking signal to impart a cell-to-cell gain-of-trafficking function to the cell-autonomous mCherry-H2B. This approach can be adapted to investigate the cell-to-cell trafficking properties of any protein of interest.

**Key words** GAL4 transactivation, Non-cell-autonomous protein, Plasmodesmata, Selective intercellular trafficking, Transcription factors

---

### 1 Introduction

The plant kingdom is distinctive with respect to the coordination of development by the intercellular trafficking of regulatory proteins and mRNAs through plasmodesmata (PD) [1–3]. PD-mediated protein trafficking can either be nonselective or selective. While nonselective movement is achieved by simple diffusion through PD as proposed for the LEAFY (LFY) transcription factor (TF) [4] and for GFP movement between adjoining cells [1], selective movement is achieved through the induced dilation of the PD size exclusion limit (PD-SEL). The latter involves specific protein-protein interactions and/or protein unfolding/folding by chaperone proteins, as was shown for the non-cell-autonomous movement of the KNOTTED1 (KN1) TF required for maize

shoot meristem development [5–9]. Other well-characterized non-cell-autonomous TFs are the floral homeotic proteins from *Antirrhinum*, DEFICIENS and GLOBOSA [10], and *Arabidopsis* TFs involved in root development, such as the GRAS family member SHORT ROOT (SHR) [11] and the Myb-like DNA-binding domain protein CAPRICE [12, 13].

Over the years, several in vivo assay methods have been developed to study non-cell-autonomous protein trafficking in plants. First, a trichome rescue assay system was established to determine the selective trafficking motif of KN1. When expressed subepidermally in *gll* glabrous mutant plants, GLABROUS1 (GL1), an Myb-family TF, failed to rescue trichome development; however, GL1 fused to a selectively trafficking protein or peptide functionally rescued the *gll* glabrous phenotype, indicating its intercellular trafficking. In our recent study, we developed a high-throughput system to screen for non-cell-autonomous TFs [14–16]. This approach utilizes a tissue-specific GAL4/UAS transactivation system for the detection of non-cell-autonomous movement of TFs-mCherry fusions following expression in root endodermis and cortex cells marked with a cell-autonomous GFP (green fluorescent protein). This cell-specific, trans-inducible system has been successfully used for the analysis of *Arabidopsis* Dof family TFs and led to the identification of AtDof4.1, or INTERCELLULAR TRAFFICKING DOF1 (ITD1), as a non-cell-autonomous protein (NCAP). An intercellular trafficking motif (ITM) containing a zinc-finger motif was shown to be necessary and sufficient for intercellular trafficking in this assay [17]. More recently, we refined the root-based selective trafficking system by using the cell-specific GAL4/UAS transactivation expression system in combination with mCherry fused to histone 2b (H2B), a chromatin-binding protein with a strong nuclear localization signal (NLS). The fusion of H2B can mediate the sequestration of a fusion protein within the nucleus, thus preventing them from diffusing out through PD into the surrounding cells. However, it cannot fully block PD-mediated selective trafficking pathways and, thus, can be used to distinguish nonselective from selective pathways. In this chapter, we describe the design and construction of plasmids required to develop the H2B-based system, the transformation of these plasmids into *Arabidopsis* GAL4/UAS reporter plants (J0571), and the application of the H2B-based system for the detection of NCAPs and the analysis of their selective intercellular trafficking.

### **1.1 Intercellular Protein Movement Assay Using the GAL4/UAS System**

As shown in Fig. 1, the enhancer trap cassette in *Arabidopsis* line J0571 encodes the chimeric GAL4/VP16 transcriptional activator under the control of a specific enhancer leading to expression in root endodermis and cortex cells. The same cassette encodes GFP<sub>ER</sub> (green fluorescent protein carrying an endoplasmic reticulum (ER) retention signal) flanked by an upstream activating sequence (UAS).

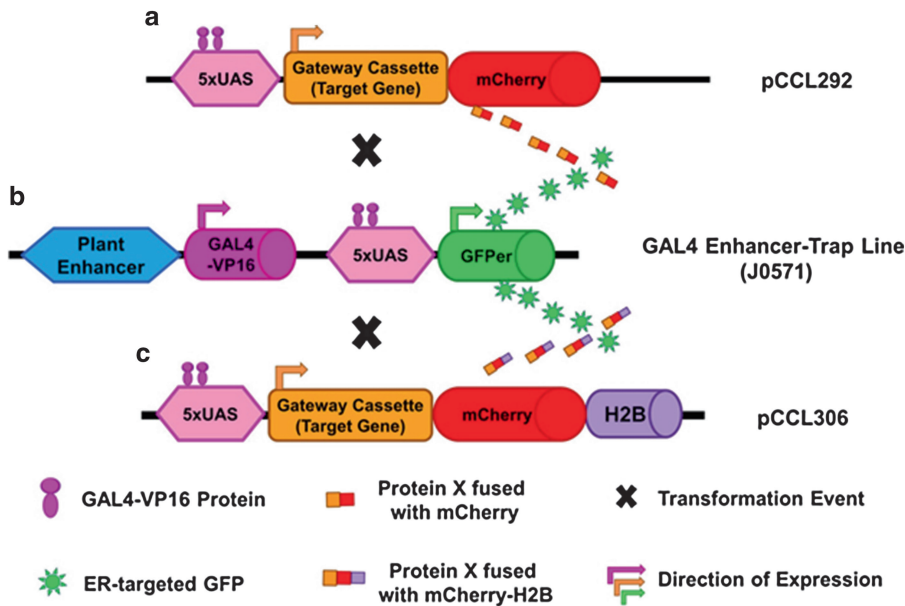


**Fig. 1** Schematic representation of the GAL4/UAS-based systems for transgene expression. The J0571 plant cassette (**b**) consists of the chimeric coding regions of GAL4/VP16 (a potential plant enhancer shown upstream) and endoplasmic reticulum-targeted green fluorescent protein (GFP<sub>ER</sub>) flanked by an upstream activating sequence (5xUAS). Upon transformation of J0571 plants with Gateway vectors that encode a TF-mCherry fusion (**a**) or a TF-mCherry-H2B fusion (**c**) under control of the 5xUAS, expression of the respective fusion proteins is activated in trans only in the GFP-marked cells of the endodermis and cortex

Thus, expression of GAL4/VP16 in root endodermis and cortex cells leads to the expression of GFP<sub>ER</sub> in the same tissue (Fig. 1b) (*see Note 1*) [14]. The UAS is also present in the expression plasmids pCCL292 and pCCL306, which allow expression of proteins of interest in fusion to mCherry or to mCherry fused to H2B, respectively (Fig. 1a, c; *see Subheadings 3.1 and 3.2*). H2B, a chromatin-binding protein with a strong nuclear localization signal (NLS), mediates the sequestration of the mCherry fusion protein within the nucleus and thus provides strong cell autonomy to this protein [18]. Therefore, this protein will exit the cell of expression only if fused to a non-cell-autonomous TF. The UAS-containing expression vectors introduced in line J0571 allow expression of mCherry, mCherry-H2B, a TF of interest fused to mCherry (TF-mCherry), or a TF of interest fused to mCherry-H2B (TF-mCherry-H2B) in the cortex and endodermal cells. The same cells will be highlighted by UAS-directed expression of GFP<sub>ER</sub>. Fluorescent signals for GFP and mCherry can be readily seen with a confocal laser scanning microscope as shown in Figs. 2 and 3. Any TF-mCherry or its H2B fusion able to exit the expression domain and move beyond the cortical and endodermal cells is defined as a non-cell-autonomous TF in this experimental system.

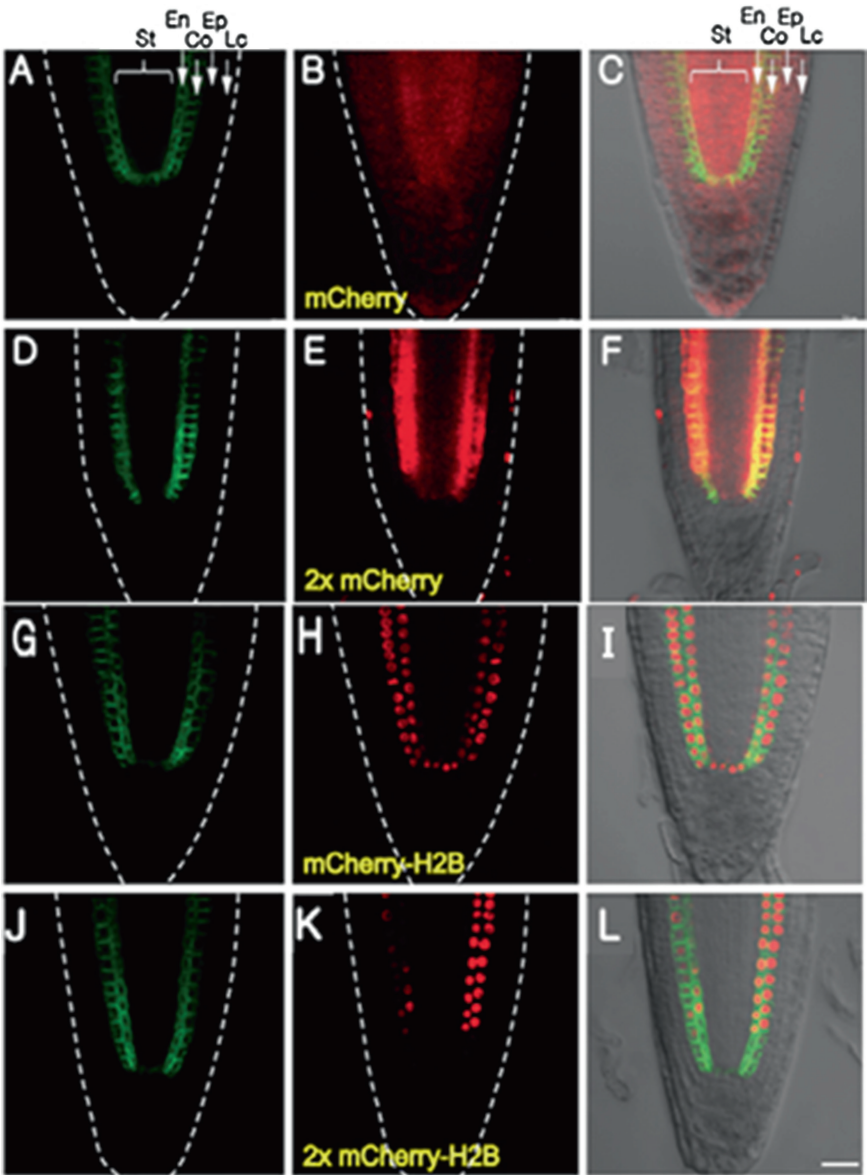


**Fig. 2** Fusion of H2B affects intercellular movement of mCherry. Capacity of mCherry to move symplasmically within the root apex is reduced by the sequestration of H2B to the nucleus. (a–c) mCherry, (d–f) 2xmCherry, (g–i) mCherry-H2B, and (j–l) 2xmCherry-H2B. Images in panels (c), (f), (i), and (l) are overlays with bright-field DIC images. *St* stele, *En* endodermis, *Co* cortex, *Ep* epidermis, *Lc* lateral cap cell. Bar in (l) is common to all images and equals 20  $\mu$ m. Reprinted with permission from [14]

**Fig. 3** (continued) root for mCherry-H2B fused to the indicated Dof motif. (d–f) The Dof5.4<sub>44–93</sub>-mCherry-H2B fusion remained confined to cortical and endodermal cells. (g–i) The ITD1\_ΔITM-mCherry-H2B signal was confined to nuclei in cortex/endodermal cells. (j–l) ITD1\_ΔITM-mCherry-H2B showed multicell layer movement into the stele. All images are overlays with bright-field DIC images. *St* stele, *En* endodermis, *Co* cortex, *Ep* epidermis, *Lc* lateral cap cell. Bar = 20  $\mu$ m. Reprinted with permission from [17]

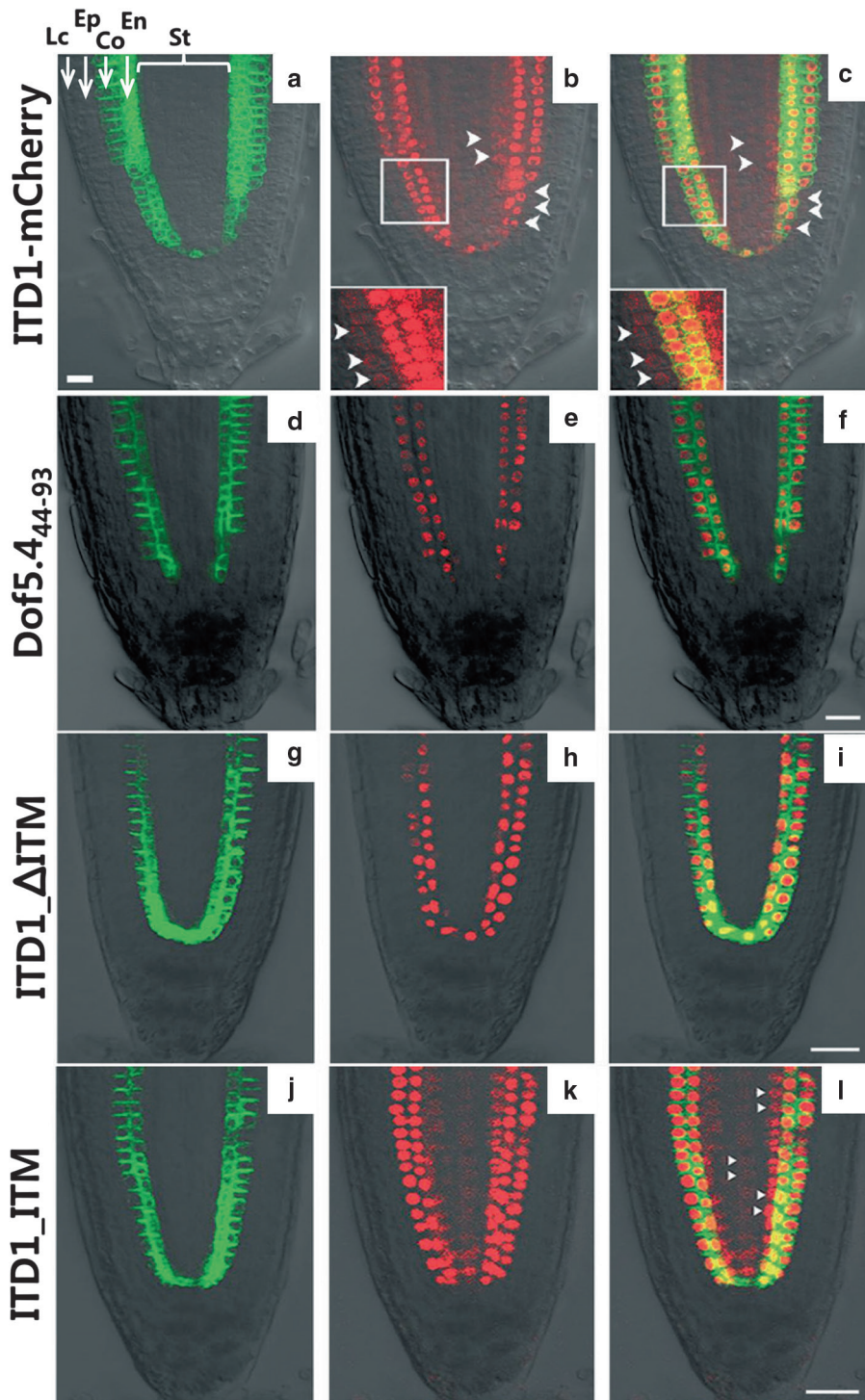


**Fig. 3** ITD1 or ITM confers a gain-of-trafficking function to the cell-autonomous mCherry-H2B. The capacity of mCherry-H2B to move symplasmically within the root apex of J0571 enhancer line is recovered upon fusion with either full-length ITD1 or its intercellular trafficking motif (ITM). (a–c) ITD1-mCherry showed one cell layer outward and multicell layer inward movement (arrowheads). (d–l) Cellular patterns observed in *Arabidopsis*

## 1.2 ITD1 Traffics by a Selective Non-Cell-Autonomous Pathway

The application of the GAL4-based transactivation assay is illustrated in Fig. 2. The J0571 *Arabidopsis* line carrying an UAS::mCherry reporter construct shows green fluorescence in the endodermis and cortex cells as expected. However, red fluorescent signals occur throughout the entire root tip (Fig. 2a–c) [14], indicating that root tip cells have a PD-SEL of larger than 27 kDa allowing mCherry to freely diffuse throughout the tissue. However, the movement of UAS::2xmCherry (increased molecular mass) is limited to stele and epidermis, indicating that PD impose limits to the movement of proteins of this molecular size (Fig. 2d–f). Anchoring mCherry and 2xmCherry to H2B causes strong cell autonomy with exclusive fluorescent signals in nuclei, suggesting that the functional fusion to H2B reduces the level of mCherry within the cytoplasm to such an extent that movement is prevented (Fig. 2g–i). Upon fusion of ITD1 to mCherry, ITD1-mCherry (61.7 kDa), being larger than 2xmCherry (54 kDa), displayed inward and outward movement from the cells of synthesis (Fig. 3a–c). The H2B system was then used to analyze the distribution pattern of ITD1\_ITM, truncated ITD1\_ΔITM, and an equivalent region of ITD1\_ITM from *AtDof5.4* (*AtDof5.4*<sub>44–93</sub>) fused to mCherry-H2B. While *AtDof5.4*<sub>44–93</sub> (Fig. 3d–f) and truncated ITD1\_ΔITM (Fig. 3g–i) fusion proteins showed little movement from the endodermis into the stele, the ITD1\_ITM fusion protein moved extensively from the endodermis into the stele, where it accumulated in nuclei (Fig. 3j–l). These studies provided corroborative evidence for the role of ITD1\_ITM in imparting cell-to-cell gain-of-trafficking function to the otherwise cell-autonomous mCherry-H2B protein. This system has been invaluable to the screening of a range of non-cell-autonomous TFs being capable of selective trafficking via PD. For example, this system was successfully employed for the screening of Dof TFs from other species as well as for domain deletion analysis to identify the protein motifs that impart cell-to-cell trafficking capacity [17]. Here, the cloning protocol and technical tips for generating cell-autonomous and non-cell-autonomous H2B fusions are thoroughly described using *Arabidopsis* ITD1 as a model. In addition, the protocols for stable expression of these constructs in *Arabidopsis* GAL4/UAS reporter plants (J0571) and for scoring intercellular movement of proteins are also described. The simplicity and universality of the H2B-based intercellular trafficking assay system undoubtedly reinforce its utility in investigating plant TFs for their selective trafficking ability.

## 2 Materials

### 2.1 Plant Materials

1. Seedlings of *Arabidopsis thaliana* ecotype *Col-0*.
2. J0571 enhancer trap plant line (GAL4/UAS::GFP<sub>er</sub>, *A. thaliana* ecotype C24). Available from the Arabidopsis Biological Information Resource Center.

## 2.2 Vectors and Primers

1. Gateway pENTR/D-TOPO vector (Invitrogen) and modified Gateway destination vectors pCCL276, pCCL284, pCCL292, pCCL306, pZY375, pEarlyGate103 and pRSetB-mCherry (available upon request).
2. Custom synthetic oligonucleotides

mCherry- <i>SalI</i> -d1	AAATGTCGACATGGTGAGCAAGGGCG
mCherry-SacKA <sub>vr</sub> -r3	GGGCCCTAGGTCCGGTACCTTAGAGCTC CTTGACAGCTCGTCCATG
H2B- <i>AvrII</i> -d1	GGGCCCTAGGATGGCGAAG GCAGATAAGAA
H2B- <i>HpaK</i> -r1	GGGCGGTACCTCAGTTAACAGAA
<i>AvrII</i> -mCherry-d4	GGGGCCTAGGATGGTGAGCA AGGGCGAG
mCherry-SacKA <sub>vr</sub> -r3	GGGCCCTAGGTCCGGTACCTTAGAG CTCCTTGACAGCTCGTCCATG
Dof4.1_F	CACCATGG ACCATCATCAGTATCATCATC
Dof4.1_R	GTTACCATGTTGGTCCACCACTATCA
Dof5.4_F	CACCATGGCTATGCAAGATATTC ATGATTTCTC
Dof5.4_R	AGGAAGGTAGAGACCACTCTG
Dof4.1_ZFM_F	CACCATGGCTAGCACTAGGCCGCAAGAACC
Dof4.1_ZFM_R	GTTACGGAGAGAGCCACCTTC
Dof4.1_ΔZFM_F	TTGATGACGACAATGGTCCCCGTAG GCGGAGGTTC
Dof4.1_ΔZFM_R	CATTGTCGTCATCAACTTCTTC
Dof5.4_ZFM_F	CACCATGGCTATACTTAACCATCA TCAATCTC
Dof5.4_ZFM_R	GTTACGGAGAACACCACTT

## 2.3 Generation of the H2B Fusion Constructs

1. Genomic DNA extraction kit. Store at room temperature.
2. Total RNA extraction kit. Store at room temperature.
3. SuperScript III First-Strand Synthesis System (Invitrogen). Store at -20 °C.
4. *Pfu* DNA polymerase and buffer. Store at -20 °C.
5. dNTPs: 10 mM stock solution containing 2.5 mM of each dNTPs. Store at -20 °C.
6. Restriction enzymes for molecular cloning. Store at -20 °C.

7. T4 DNA ligase. Store at  $-20^{\circ}\text{C}$ .
8. Gateway pENTR/D-TOPO Cloning Kit (Invitrogen). Store at  $-20^{\circ}\text{C}$ .
9. Gateway LR Clonase II enzyme mix (Invitrogen). Store at  $-20^{\circ}\text{C}$ .
10. Gel and PCR DNA Purification System.
11. 5 $\times$  Tris-borate-EDTA (TBE) buffer: 0.45 M Tris-borate, 10 mM EDTA, pH 8.0. Store at room temperature. Prepare a diluted 0.5 $\times$  TBE buffer in double-distilled water before use.
12. 5 mg/mL ethidium bromide (EtBr) in double-distilled water. Wear gloves while handling.
13. Agarose gel electrophoresis kit.
14. Gel imaging and analysis system.
15. Cultures of *Escherichia coli* (*E. coli*) strain DH10B and of *Agrobacterium tumefaciens* GV3101.
16. Plasmid isolation Mini Prep Kit.
17. NanoDrop 2000c UV-Vis Spectrophotometer.
18. Electroporator and electroporation cuvettes (400  $\mu\text{L}$ ; 2 mm gap).

## **2.4 Media for Bacterial Culture and Plant Growth**

1. Luria-Bertani (LB) media: 10 g/L Bacto tryptone, 5 g/L yeast extract, and 10 g/L NaCl. Autoclave at  $121^{\circ}\text{C}$ , 15 psi for 20 min.
2. Yeast extract peptone (YEP) media: 10 g/L yeast extract, 10 g/L peptone from meat, and 5 g/L NaCl. Autoclave at  $121^{\circ}\text{C}$ , 15 psi for 20 min.
3. Murashige and Skoog (MS) medium: 4.4 g/L MS salt powder (with vitamins), 0.5 g/L 2-(N-morpholino)ethanesulfonic acid (MES), and pH 5.7. Adjust pH with 1.0 M KOH. Add 6 g of plant agar. Autoclave at  $121^{\circ}\text{C}$ , 15 psi for 20 min. Add hygromycin (50 mg/mL) to autoclaved media if needed.
4. Peat mix was used for plant growth.

## **2.5 Antibiotics and Screening**

1. Rifampicin: 50 mg/L rifampicin in both liquid and solidified agar LB or YEP plates.
2. Gentamicin: 25 mg/L gentamicin sulfate salt in both liquid and solidified agar LB or YEP plates.
3. Kanamycin: 50 mg/L kanamycin sulfate in both liquid and solidified agar LB or YEP plates.
4. Hygromycin B: 50 mg/L hygromycin B in MS media plates (*see* Subheading 3.5).

## **2.6 Plant Transformation**

1. Sucrose: 150 g sucrose/500 mL secondary culture before floral dip.
2. Silwet L-77: 200  $\mu\text{L}$  Silwet L-77/500 mL secondary culture before floral dip.

**2.7 Seed Sterilization**

1. 0.2× domestic bleach solution (final 1.1 % sodium hypochlorite solution).
2. Double-distilled water.

**2.8 Imaging**

1. Confocal laser scanning microscope.

---

**3 Methods****3.1 Cloning of Constructs for the Cell-Autonomous H2B Protein Fusions**

1. Amplify an mCherry fragment from pRsetB-mCherry vector by *Pfu*-PCR with the primer set mCherry-*SalI*-d1/mCherry-SacKAvr-r3 and digest with *SalI* and *SacI*. Ligate this fragment with *SalI*/*SacI*-digested pZY375 (available from David Jackson's lab, Cold Spring Harbor Laboratory, NY, USA) to yield the Gateway destination vector, pCCL276 (UAS::mCherry).
2. Amplify a histone 2B (H2B) fragment from genomic DNA by *Pfu*-PCR with the primer set H2B-*AvrII*-d1/H2B-*HpaK*-r1 and then digest with *AvrII* and *KpnI*. Ligate this fragment with *AvrII*/*KpnI*-digested pCCL276 to yield pCCL284 (UAS::mCherry-H2B).
3. Amplify an mCherry fragment from pRsetB-mCherry vector by *Pfu*-PCR using the primer set *AvrII*-mCherry-d4/mCherry-SacKAvr-r3 and digest with *AvrII* and *SacI*. Ligate this fragment with *AvrII*/*SacI*-digested pCCL276 to construct pRYG237 (UAS::2XmCherry).

**3.2 Cloning of Constructs for the Non-Cell-Autonomous H2B Protein Fusions**

1. Digest the vector pEarlyGate103 with *XhoI* to obtain a gateway fragment.
2. Ligate this fragment with the *SalI*-digested pCCL276 to get pCCL292 (UAS::GW-mCherry) (*see Note 2*).
3. Then digest both pCCL292 and PCR-amplified H2B fragment with *AvrII* and *KpnI*. Mix both in the ligation mixture to clone pCCL306 (UAS::GW-mCherry-H2B).
4. Isolate total RNA from *Arabidopsis* plants using total RNA extraction kit according to the manufacturer's instructions.
5. Reverse-transcribe this total RNA into cDNA using the SuperScript III First-Strand Synthesis System according to the manufacturer's instructions and respective gene-specific and gateway sites – added forward and reverse primers.
6. From cDNA, amplify the full-length coding regions of ITD1 and Dof5.4 using the primer sets Dof4.1\_F/Dof4.1\_R and Dof5.4\_F/Dof5.4\_R, respectively, and also their respective truncated regions *ITD1\_ITM*, *ITD1\_ΔITM*, and *Dof5.4<sub>44-93</sub>* using the primer sets Dof4.1\_ZFM\_F/Dof4.1\_ZFM\_R, Dof4.1\_ΔZFM\_F/Dof4.1\_ΔZFM\_R, and Dof5.4\_ZFM\_F/Dof5.4\_ZFM\_R.

7. Perform gateway reactions to clone PCR amplicons into pENTR/D-TOPO vector using the Gateway TOPO cloning method (Invitrogen), according to the manufacturer's instructions.
8. Perform the gateway LR reaction using Gateway LR Clonase II enzyme mix (Invitrogen) according to the manufacturer's instructions to transfer the target chimeric fragments cloned in pENTR/D-TOPO vectors to the desired destination vectors. This will lead to the generation of the final expression vectors to be transformed in plants.

### **3.3 *Agrobacterium* Transformation**

1. Thaw electro-competent *A. tumefaciens* GV3101 on ice. Add 0.1 µg to 1 µg of the respective expression vectors.
2. Transfer competent cells into a clean and dried electroporation cuvette.
3. Keep the cuvette on ice. After wiping moisture off the cuvette, expose it to an electric pulse (2.5 kV) using an electroporator.
4. Immediately add 1 mL of YEP medium and shake the cells at 28 °C for 2 h.
5. Spread 100–200 µL of the culture on YEP agar plates supplemented with rifampicin (50 mg/L), gentamicin (25 mg/L), and kanamycin (50 mg/L) and incubate the plates at 28 °C for 48 h.

### **3.4 Plant Transformation**

1. Inoculate a single colony of *Agrobacterium* harboring the target expression clone in 3 mL YEP media containing antibiotics (rifampicin, kanamycin, and gentamicin).
2. Shake the culture at 28 °C for 48 h until OD<sub>600nm</sub> reaches 1.0.
3. Add 500 µL of this primary culture to 500 mL of YEP media containing antibiotics (kanamycin and gentamicin). Shake at 28 °C overnight.
4. Add 100 mL of 30 % sucrose and 200 µL of Silwet L-77 to the 500 mL overnight secondary culture.
5. Prepare the enhancer trap plants, J0571, grown on pots (*see* **Notes 3** and **4**).
6. Dip the inflorescence shoots of the enhancer trap plants into the *Agrobacterium* culture for 15–20 s (*see* **Note 5**).
7. Place the plants back into the culture room in such a way that they are laid on their sides in a growth chamber for 24 h.
8. Grow the plants under normal conditions (*see* **Note 6**) until siliques are fully matured and dried.
9. After maturity and proper drying, cut the inflorescence. Harvest the seeds in paper bags after removing tissue debris using sieves.
10. Store the paper bags at 10 % relative humidity conditions.

### 3.5 Selection of Transgenic *Arabidopsis*

1. Transfer primary transformed seeds (T1) into 50 mL Falcon tube and surface-sterilize the seeds by adding 1/4th the volume of 0.2× bleach solution for 5 min.
2. Rinse the seeds three to five times with 30 mL of autoclaved double-distilled water.
3. Pour the seeds on petri dishes with plant growth media supplemented with hygromycin.
4. Keep the plates for moist chilling at 4 °C for 5 days in the dark and then move to a growth chamber (*see* **Notes 6** and **7**).
5. Pick the seedlings that are visibly resistant to hygromycin within 2 weeks and transfer to soil pots kept in a greenhouse.
6. Harvest the seeds separately from each plant as mentioned in Subheading 3.4.

### 3.6 Scoring Intercellular Protein Movement

1. Select about 7–10-day-old transgenic plants for observation with a confocal laser scanning microscope.
2. In one channel, set the wavelengths to 488 nm and 510–540 nm for specific excitation and imaging of GFP fluorescence.
3. In another channel, set the wavelengths to 543 nm and 587–625 nm for specific excitation and imaging of mCherry fluorescence.
4. Transfer individual seedlings to clean microscope slides (*see* **Note 8**). Cover with a cover slide after adding double-distilled water and then move to the stage of confocal microscope setup for fluorescence microscopy.
5. Bring the roots into focus (with a 20× or 40× objective) using bright-field (white light) illumination. Then switch on filtered light and scan the slides for fluorescence (*see* **Notes 9** and **10**).

---

## 4 Notes

1. The targeting of GFP to the endoplasmic reticulum ensures that the GFP does not move cell to cell and remains in the cells where the gene is transcribed and translated. This also marks the cells where the TF-mCherry is produced.
2. *XhoI* and *SaII* produce compatible cohesive DNA ends.
3. Five- to six-week-old *Arabidopsis* plants carrying young floral buds should be transformed using *Agrobacterium*.
4. Before floral dipping, the already formed siliques from the flowering shoots should be removed.
5. Additional protocols and guidelines for the growth and transformation of *Arabidopsis* plants can be obtained from the Arabidopsis Biological Information Resource Center (<http://www.biosci.ohio-state.edu/~plantbio/Facilities/abrc/handling.htm>).

6. Grow *Arabidopsis* plants at 22 °C under 3-wave fluorescent light with cycles of 16 h light/8 h dark regimes either on soil or on MS plates in growth chamber.
7. *Arabidopsis* C24 ecotype needs a minimum 4-day stratification to improve germination rate and synchrony.
8. From the different transgenic lines, select plants that are in the same stage of growth during the time of imaging.
9. Make sure that the fluorescence settings are same to all samples while taking images since higher/lower gain settings of such signals can misinterpret the results.
10. Control imaging in the setting condition should not show any GFP or mCherry signal from non-transgenic plants.

---

## Acknowledgments

We thank Roger Tsien for providing the mCherry construct and Jim Haseloff for seeds of the J0571 plant line. This research was supported by Basic Science Research Program through the National Research Foundation of Korea (NRF) funded by the Ministry of Education (NRF-2013R1A1A2007230) and by a grant from the Next-Generation BioGreen 21 Program (SSAC, grant PJ009495), Rural Development Administration, Republic of Korea.

## References

1. Crawford KM, Zambryski PC (2000) Subcellular localization determines the availability of non-targeted proteins to plasmodesmatal transport. *Curr Biol* 10:1032–1040
2. Lucas WJ, Lee JY (2004) Plasmodesmata as a supracellular control network in plants. *Nat Rev Mol Cell Biol* 5:712–726
3. Oparka KJ (2004) Getting the message across: how do plant cells exchange macromolecular complexes? *Trends Plant Sci* 9:33–41
4. Wu X, Dinneny JR, Crawford KM, Rhee Y, Citovsky V, Zambryski PC (2003) Modes of intercellular transcription factor movement in the *Arabidopsis* apex. *Development* 130: 3735–3745
5. Parcy F, Nilsson O, Busch MA, Lee I, Weigel D (1998) A genetic framework for floral patterning. *Nature* 395:561–566
6. Lucas WJ, Bouche-Pillon S, Jackson DP, Nguyen L, Baker L, Ding B, Hake S (1995) Selective trafficking of KNOTTED1 homeodomain protein and its mRNA through plasmodesmata. *Science* 270:1980–1983
7. Sessions A, Yanofsky MF, Weigel D (2000) Cell-cell signaling and movement by the floral transcription factors LEAFY and APETALA1. *Science* 289:779–782
8. Kim JY, Yuan Z, Cilia M, Khalfan-Jagani Z, Jackson D (2002) Intercellular trafficking of a KNOTTED1 green fluorescent protein fusion in the leaf and shoot meristem of *Arabidopsis*. *Proc Natl Acad Sci U S A* 99:4103–4108
9. Xu XM, Wang J, Xuan Z, Goldshmidt A, Borrell PG, Hariharan N, Kim JY, Jackson D (2011) Chaperonins facilitate KNOTTED1 cell-to-cell trafficking and stem cell function. *Science* 333: 1141–1144
10. Perbal MC, Haughn G, Saedler H, Schwarz-Sommer Z (1996) Non-cell-autonomous function of the Antirrhinum floral homeotic

- proteins DEFICIENS and GLOBOSA is exerted by their polar cell-to-cell trafficking. *Development* 122:3433–3441
11. Nakajima K, Sena G, Nawy T, Benfey PN (2001) Intercellular movement of the putative transcription factor SHR in root patterning. *Nature* 413:307–311
  12. Wada T, Kurata T, Tominaga R, Koshino-Kimura Y, Tachibana T, Goto K, Marks MD, Shimura Y, Okada K (2002) Role of a positive regulator of root hair development, CAPRICE, in Arabidopsis root epidermal cell differentiation. *Development* 129:5409–5419
  13. Kurata T, Ishida T, Kawabata-Awai C, Noguchi M, Hattori S, Sano R, Nagasaka R, Tominaga R, Koshino-Kimura Y, Kato T, Sato S, Tabata S, Okada K, Wada T (2005) Cell-to-cell movement of the CAPRICE protein in Arabidopsis root epidermal cell differentiation. *Development* 132:5387–5398
  14. Rim Y, Huang L, Chu H, Han X, Cho WK, Lucas WJ, Kim JY (2011) Analysis of Arabidopsis transcription factor families revealed extensive capacity for cell-to-cell movement as well as discrete trafficking patterns. *Mol Cells* 32:519–526
  15. Kim JY, Rim Y, Wang J, Jackson D (2005) A novel cell-to-cell trafficking assay indicates that the KNOX homeodomain is necessary and sufficient for intercellular protein and mRNA trafficking. *Genes Dev* 19:788–793
  16. Ahmad M, Cho WK, Rim Y, Huang L, Kim JY (2011) How to assess the intercellular trafficking of transcription factors. In: Yuan L, Perry ES (eds) *Methods in molecular biology*. Humana Press, New York, p 235
  17. Chen H, Ahmad M, Rim Y, Lucas WJ, Kim JY (2013) Evolutionary and molecular analysis of Dof transcription factors identified a conserved motif for intercellular protein trafficking. *New Phytol* 198:1250–1260
  18. Boissnard-Lorig C, Colon-Carmona A, Bauch M, Hodge S, Doerner P, Bancharel E, Dumas C, Haseloff J, Berger F (2001) Dynamic analyses of the expression of the HISTONE:YFP fusion protein in Arabidopsis show that syncytial endosperm is divided in mitotic domains. *Plant Cell* 13:495–509



## Techniques for Assessing the Effects of Pharmacological Inhibitors on Intercellular Protein Movement

Shuang Wu and Kimberly L. Gallagher

### Abstract

Intercellular protein movement is an important mechanism in plant development. Here we present an integrated protocol that utilizes an inducible system to block plasmodesmata-dependent movement and assessment of fluorescent recovery after photobleaching (FRAP) to identify compounds that influence intercellular protein movement.

**Key words** Plasmodesmata, FRAP, Protein movement, SHORT-ROOT, Live cell imaging, Callose

---

### 1 Introduction

The understanding of complex biological processes, like the intercellular movement of proteins between plant cells, requires the establishment of reliable and unbiased tools. Pharmacological inhibitors have been extremely useful in plants and animals in understanding the functions of the cytoskeleton, the endomembrane, and the process of secretion [1–7]. However, similar approaches to study plasmodesmata dependent movement have been confounded by the secondary effects of long-term drug treatments on the cell, and short-term treatments have been hampered by the stability of the mobile protein in the target cells, which makes subtle decreases in protein movement difficult to detect and quantify [8, 9]. Here we describe protocols that we have devised for measuring the effects of pharmacological inhibitors on the movement of the SHORT-ROOT (SHR) protein in the *Arabidopsis* root [9]. While these methods were devised to study SHR movement, they are applicable to other proteins that show short-range, cell-specific movement, for example, CAPRICE in the root epidermis or the mobile proteins involved in trichome specification in the *Arabidopsis* leaf [10–14]. These assays are probably not suitable for studying the long-range trafficking of proteins like FLOWERING

LOCUS T from the leaf to the shoot apical meristem as there are too many different cell types and presumably multiple different movement processes involved [15].

The protein that we use as a model for examining intercellular movement is SHR. Therefore, we provide here a brief description of SHR expression and movement so that the following assays described in the methods can be viewed in a biologically relevant context. In the *Arabidopsis* root, SHR is expressed exclusively in the stele cells (the central cylinder of vascular cells, procambium, and pericycle). The SHR protein then moves via plasmodesmata (PD) out of the stele into the neighboring cell layers; these cells include the quiescent center cells, the ground tissue progenitor cells, and the endodermis [16, 17]. SHR is found in both the nuclei and cytoplasm of stele cells; in the endodermis, SHR is restricted to nuclei [17, 18]. PD-dependent movement into the endodermis was demonstrated using an estradiol-inducible system that expresses a synthetic, semidominant allele of CALLOSE SYNTHASE 3 (*icals3m*) that when activated produces PD-localized callose that reliably blocks symplastic protein movement. In our system, the *icals3m* transgene is expressed in the stele from the *WOODENLEG* promoter (*pWOL*, also known as the *CRE1* promoter). Application of estradiol leads to the accumulation of callose at PD in the stele, which consequently reduces the PD aperture. As a result, the movement of SHR is reduced as evidenced by a loss of SHR-GFP signal in the endodermis [16]. However, this block to SHR movement is reversible. The removal of the treated seedlings from estradiol allows the recovery of SHR trafficking as indicated by SHR-GFP fluorescence in the endodermis. Therefore, the movement of SHR-GFP is blocked, essentially reducing the SHR-GFP signal in the endodermis to background, and then recovery is monitored in the endodermis in the presence or absence of a potential inhibitor of protein movement [9, 16]. We have adapted the *icals3m* system to use it as a tool for assessing the effects of inhibitors of the cytoskeleton on the recovery of SHR movement [9]. This system provides some advantages over direct inhibitor treatment. A common problem with the use of inhibitors to study protein movement is the long half-life of the protein in the target cells. In instances where the mobile protein has a long half-life, long-term treatment with an inhibitor becomes necessary in order to see an effect on protein levels in the recipient cell (e.g., in the case of SHR, the endodermis). This may confound interpretation of data if extended contact with the drug induces secondary effects in the plant. As an alternative to long-term treatment with an inhibitor, the *icals3m* system allows blocking SHR movement [16] and then monitoring recovery in the presence of a chemical inhibitor within a relatively short time frame.

We have found the *icals3m* system to be a reliable and sensitive tool for detecting defects in protein movement that can be verified

by assessing fluorescent recovery after photobleaching (FRAP), which we have optimized for the analysis of protein movement in the root. Here, we provide step-by-step protocols for use of the *icals3m* system and FRAP to study cell-to-cell trafficking of SHR. However, these assays are applicable to a wide range of mobile proteins. Also, since these protocols are optimized for live cell imaging, they can conceivably be adapted for use in the long-term imaging of other processes such as the monitoring cell division or intracellular movement *in vivo*.

---

## 2 Materials

1. Microcentrifuge tubes.
2. 50 mL polypropylene centrifuge tubes.
3. Forceps.
4. 90 mm and 55 mm sterile Petri plates.
5. Sterile water.
6. Household bleach.
7. Triton X-100.
8. Transparent tape.
9. MS salts.
10. MES (w/v; 2-(N-morpholino)ethanesulfonic acid).
11. Sucrose.
12. Granulated agar.
13. Estradiol dissolved in DMSO or ethanol.
14. 75 × 25 mm glass microscope slides.
15. 44 mm × 25.5 mm × 2.0 mm silicone gaskets.
16. 22 × 50 mm and 22 × 22 mm #1 glass coverslips.
17. Kimwipes®.
18. Parafilm®.
19. Bleach solution: 50 % household bleach (6.15 % sodium hypochlorite diluted with water to a concentration of 3.075 %) and 0.01 % Triton X-100.
20. Liquid ½ strength MS: same recipe as **item 21** below without the agar.
21. ½ strength MS agar plates: ½ of the amount of MS salts suggested by the manufacturer, 1 % (w/v) sucrose, 0.05 % MES, 1 % (w/v) granulated agar, and pH 5.7. Autoclave the medium for 30 min on a standard liquid cycle (*see Note 1*). Once cooled, pour the ½ strength MS into 90 mm sterile Petri plates in a sterile tissue culture hood. These plates are used for seedling growth.

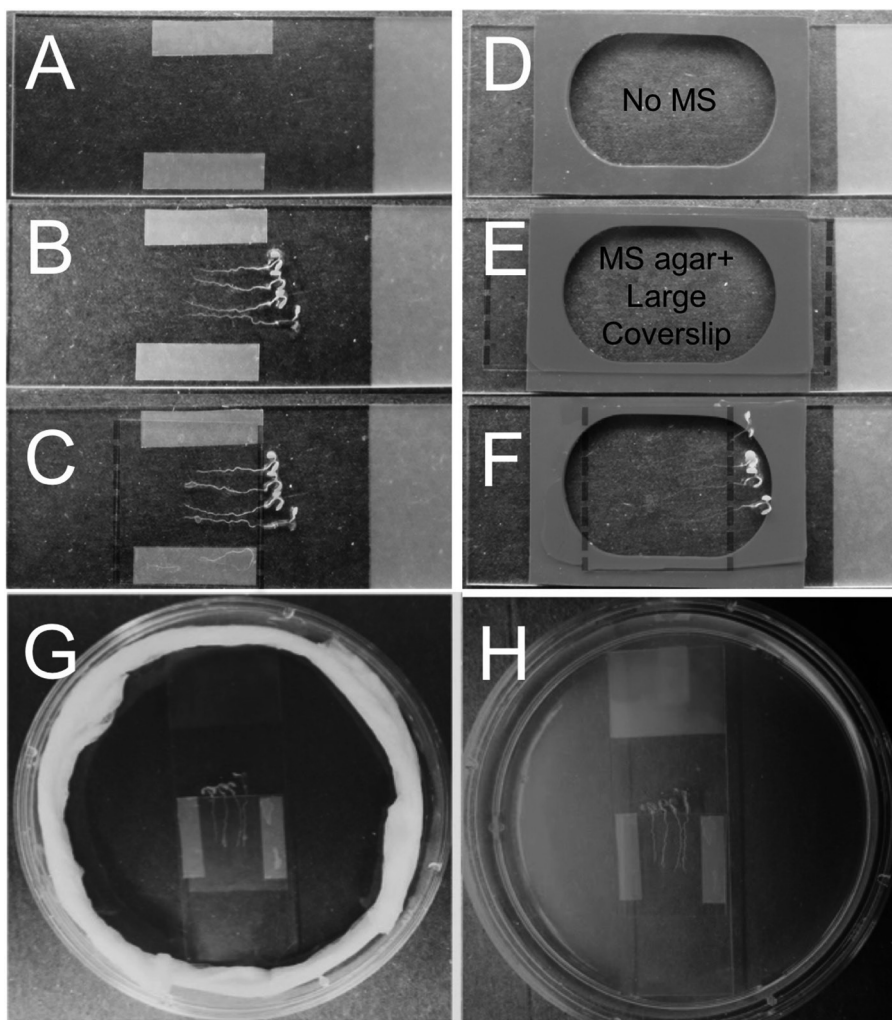


**Fig. 1** Mounting of seedlings for imaging. (a–c) Seedlings are mounted on taped slides in a drop of  $\frac{1}{2}$  strength MS medium. (d, e) Assembly of the agar pad and mounting of the seedlings on the slide. The *dotted lines* indicate the approximate edges of the coverslips. (g) A slide properly oriented in a moisture chamber created with water moistened Kimwipes. (h) A slide incubated on the surface of an MS plate

22.  $\frac{1}{2}$  strength MS agar plates containing 1  $\mu$ M estradiol with and without inhibitors (*see* **Notes 1** and **2**).
23.  $\frac{1}{2}$  MS agar plates containing only the estradiol and/or specific inhibitor solvents (e.g., DMSO or ethanol) (*see* **Note 1**).
24. Taped glass slides: put two pieces of clear adhesive tape onto the two long sides of a glass slide (as shown in Fig. 1a–c) to create a chamber for the roots. The tape provides a space between the slide and the coverslip to reduce mechanical stress to the roots during the imaging process.

25. Glass slides with agar pad: place a silicone gasket (*see above item 15*) onto a glass slide (Fig. 1d). Pour ~0.5 mL liquefied ½ strength MS agar into the well created by the silicone gasket. Immediately cover the MS medium with a 22 mm × 50 mm coverslip and allow the agar to thoroughly solidify (Fig. 1e). Then gently remove the coverslip (*see Note 3*) and mount the seedlings onto the surface of the agar (Fig. 1f; details on aligning roots given below).
26. Moisture chamber: in a 90 mm sterile Petri plate, surround the slide setup containing the seedlings with water-soaked Kimwipes (Fig. 1g). As an alternative, one may use a normal ½ MS agar plate and place the glass slides directly on the agar surface. The slide sticks tightly to the agar surface, which makes it possible to incubate the slide vertically (Fig. 1h).

---

### 3 Methods

#### 3.1 Using a Semidominant Inducible Allele of *CAL3* to Assay Intercellular Protein Movement

1. Surface sterilize the seeds expressing *pSHR-SHR-YFP* and the *pWol:icals3m* transgene by placing them for 3 min into a 1.5 mL microcentrifuge tube containing 500 µL bleach solution. Subsequently, wash three times with sterile water. Keep seeds at 4 °C in sterile water for 1–5 days.
2. Germinate 20–30 seeds individually on 90 mm Petri plates containing ½ strength MS medium, sealed with Parafilm and kept vertically for 5–6 days in a growth chamber at 23 °C and under 16 h light/8 h dark cycle. 100–120 seeds are recommended for each experiment.
3. Five days after plating (dap), aseptically transfer three-quarters of the seedlings to ½ strength MS agar plates containing 1 µM estradiol (Fig. 2; *see Note 4*) and one-quarter of the seedlings to ½ MS agar plates containing the estradiol solvent (i.e., DMSO or ethanol) as controls (Fig. 2). Return the seedlings to the growth chamber and incubate vertically for 8 h (*see Note 5*).
4. From the estradiol-containing plates, gently rinse in water and transfer one-third of the seedlings to ½ strength MS agar plates without estradiol (Fig. 2). The second third of the seedlings should be transferred in the same way onto ½ strength MS agar plates containing the putative inhibitor (*see Note 2*). Return the plates to the growth chambers and incubate vertically for 6 h before imaging. Use the remaining third of the seedlings on the estradiol plates and also the seedlings previously transferred to ½ strength MS agar plates for a first imaging experiment (below).
5. Place the seedlings for imaging on a standard glass slide in a drop of water. Dissect the roots with a scalpel and cover them

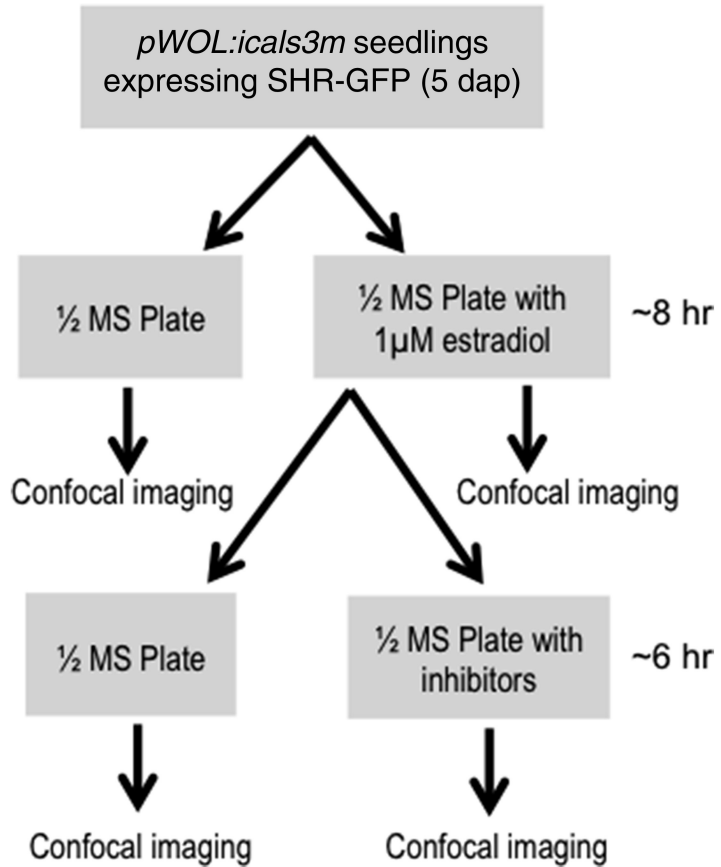


**Fig. 2** Flow diagram showing the key steps of the assays that utilize the *icals3m* transgene as a tool to assess protein movement in the presence of an inhibitor (dap = days after plating)

with a (22 mm × 22 mm) coverslip. Alternatively, leave the seedling intact and just place the coverslip over the roots (*see Note 6*). Generally, 6–8 roots can be examined per slide.

6. Use a standard laser scanning confocal microscope for imaging. Scanning with a 4× zoom in 512 × 512 pixel format is recommended. Set the laser power, offset, and gain to capture the full dynamic range of fluorescence (with less than 10 % saturated pixels) while minimizing bleaching. Since during image analysis the endodermal levels will be normalized to the stele, take several confocal images for each root in order to capture a medial optical section of the stele and of the endodermis. Often, both sides of the root will not be in focus at the same time so three or more images may need to be captured.
7. Use ImageJ software to measure the level of fluorescence in medial sections through the stele and in the nuclei of the endodermal cells immediately adjacent to the stele cells.

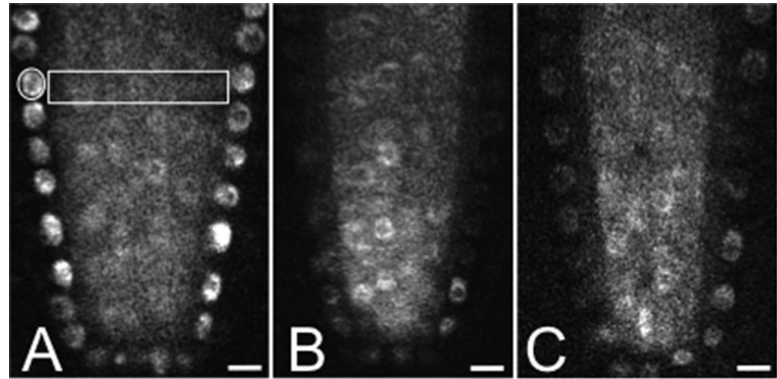


**Fig. 3** Typical effects of the *icals3m* transgene on the movement of SHR-GFP. (a) In the absence of estradiol, the movement of SHR-GFP is normal in the *icals3m*-containing seedlings. The endodermal-to-stele (E:S) ratio is calculated by measuring the fluorescence intensity in the endodermis (*circle*) and dividing this number by the intensity of fluorescence in the corresponding region of the stele (*rectangle*). (b) After 8 h on 1  $\mu$ M estradiol, the SHR-GFP signal in the endodermis is significantly reduced. (c) Six hours after removal from estradiol, the movement of SHR-GFP into the endodermis has begun to recover. The images in (a–c) show typical roots. Scale bars = 20  $\mu$ M

Since the stele and endodermis may not be in the same focal plane in the same field, multiple images may be required for the calculations. Since the stele is the source of the SHR-GFP signal that moves into the endodermis, the endodermal-to-stele (E:S) ratio reflects protein movement [9, 19, 20]. In wild-type or uninduced *icals3m* roots (Fig. 3), this ratio is reproducibly between 1.2 and 1.3. The use of the E:S ratio controls for root-to-root variability in expression and for any effects caused by photobleaching. The average E:S ratio should be calculated for all roots before estradiol induction (Fig. 3a) and after estradiol induction (Fig. 3b). The difference between these two ratios represents the total potential for recovery after removal from estradiol (*see Note 7*).

8. Measure the E:S ratio in roots treated with inhibitors. Compare this E:S ratio to the E:S ratio of roots recovered on  $\frac{1}{2}$  strength MS medium without estradiol (Fig. 3c). Any significant change is attributed to the presence of the inhibitor (*see Note 7*).

### 3.2 Using FRAP to Assay Protein Intercellular Movement

When using the *icals3m* system to assess the effects of inhibitors on protein movement, there is always the possibility that the inhibitor is not affecting movement per se, but instead the ability of the cells to recover from estradiol treatment. Since the recovery of movement requires the breakdown of callose and the reopening of the PD, the inhibitor could affect either of these processes. To specifically address the effects of inhibitors on SHR-GFP movement and

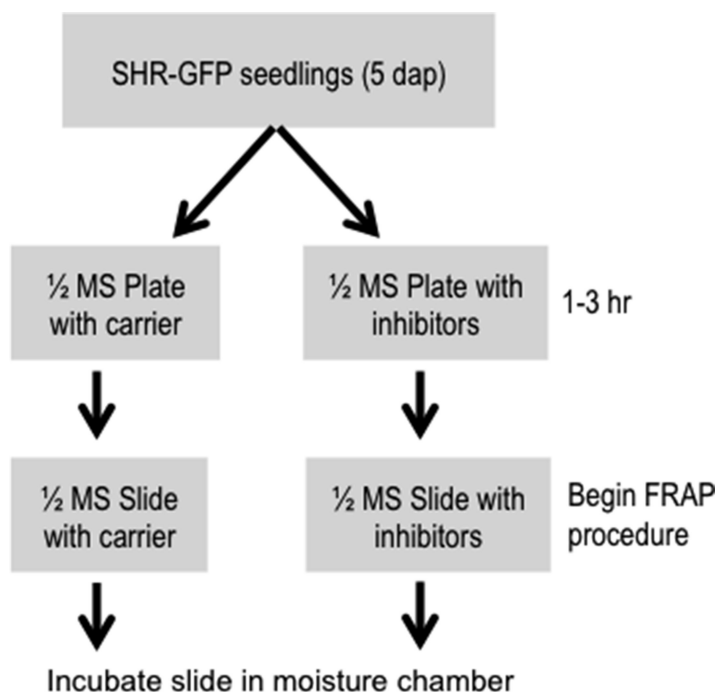


**Fig. 4** Flow diagram showing the initial steps to prepare the seedlings for analysis of FRAP

to exclude effects of the inhibitors on callose levels and PD conductance as the origin of a change in the E:S ratio in the presence of inhibitor, FRAP should be used. Assessing FRAP of SHR-YFP is more time consuming and technically challenging than assessing the effect of *icals3m* system alone. Nevertheless, prescreening the effect of inhibitors greatly reduces effort and the number of compounds to be tested using FRAP:

1. Prepare seeds expressing *pSHR-SHR-YFP* and the *pWol:icals3m* transgene as in Subheading 3.1, **steps 1** and **2** above (Fig. 4).
2. Aseptically transfer 5-day-old seedlings from the  $\frac{1}{2}$  strength MS agar plates onto 90 mm  $\frac{1}{2}$  strength MS agar plates containing the inhibitor or (as a control) containing just the carrier (*see Note 2*). Seal the plates with Parafilm and return all seedlings back to the growth chamber to incubate vertically for 1–3 h.
3. While the seedlings from **step 2** are incubating, prepare glass slides for imaging. The seedlings can either be placed on a taped glass slide in a few drops of  $\frac{1}{2}$  strength MS liquid or be placed on a  $\frac{1}{2}$  strength MS agar pad (directions in the materials section, Fig. 1c, f). One slide should contain the inhibitor and the other the carrier/solvent to be used as a control.

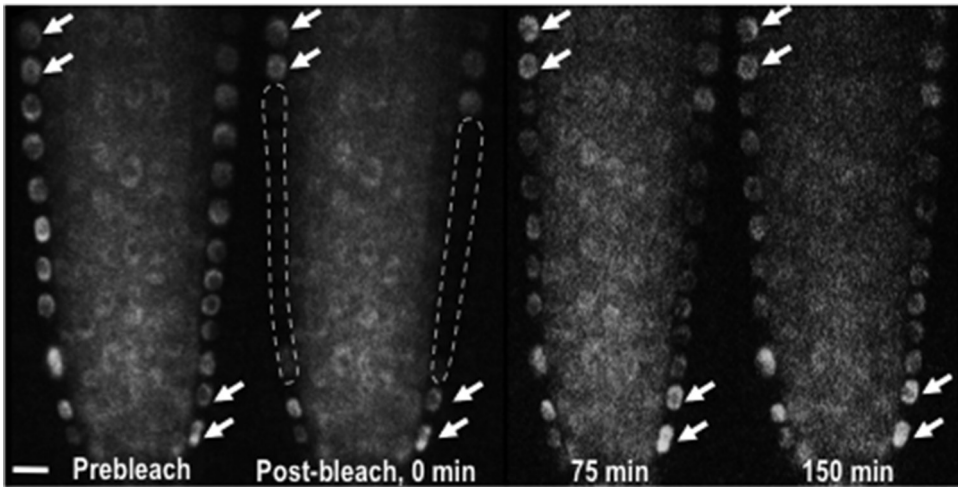


**Fig. 5** FRAP of SHR-GFP. Typical images of a root expressing SHR-GFP before and after photobleaching. The bleached regions are *encircled by the dotted lines*. Times are indicated on the images. The *arrows* point out fluorescent landmarks that were useful in identifying the region of interest. Scale bar = 20  $\mu$ M

4. Place 3–4 seedlings onto either the taped glass slide with liquid  $\frac{1}{2}$  strength MS or onto a  $\frac{1}{2}$  strength MS agar pad (with and without the inhibitor). Add a drop of liquid  $\frac{1}{2}$  strength MS to the agar pad and then gently align the roots (*see Note 8*). When aligning the roots, it is often easiest to grasp the leaves or stem with fine forceps and gently pull the root across the agar pad and through the liquid  $\frac{1}{2}$  strength MS medium. Once the roots are aligned, cover with a cover glass as shown in Fig. 1c, f (*see Note 9*).
5. Place the slide sets in a moisture container. To prevent the seedlings from drying out during the incubation, the slide sets containing the seedlings should be kept in a moisture container or a  $\frac{1}{2}$  strength MS agar plate as described in Subheading 2 (Fig. 1g, h; *see Note 10*). The container should be transparent to allow light in and handling should be gentle. The roots are easily damaged by any pressure applied to the coverslip.
6. Use a standard laser scanning confocal microscope to take one or two images of the region of interest (Fig. 5). Laser power should be set to avoid bleaching (on our system, a Leica TCS SL microscope, generally 10–30 % power for GFP/YFP is appropriate). Adjust the zoom to include the region of interest and tune the gain and offset to capture the full dynamic range of fluorescence while avoiding pixel saturation, as the fluorescence intensity will be quantified after image collection.
7. Use the confocal microscope to bleach the reason of interest. In bleaching mode of the software of the confocal microscope, set the laser to full power (100 %); GFP or YFP can be bleached

using a 488 nm laser (400 Hz,  $512 \times 512$ ). To study the inter-cellular movement of SHR-GFP, select the endodermis as the region of interest (ROI). Bleach the ROI repeatedly with 488 nm light at 100 % laser power. Five iterations (2–3 s duration for each iteration) lead to around 70–80 % reduction in the fluorescence of SHR-GFP in the endodermis (*see Note 11*). Multiple cells can be bleached at the same time for each root.

8. Immediately following the bleaching series, take an image of the bleached region using the same confocal settings as in Fig. 5.
9. Acquire recovery images. Recovery of fluorescence in the bleached region can be monitored over time. The time of recovery should be empirically determined for individual proteins. In our system, the SHR-YFP signal in endodermis recovers to around 80 % of the prebleach levels after 150 min (Fig. 5). The same focal plane for each bleached area needs to be found when the recovery images are taken. As there may be slight movement of the samples, opening the prebleached and postbleached images side by side with the live scanning windows can help to verify that imaging is in the same focal plane. Details about finding the ROI are described in **Notes 12** and **13**.
10. As SHR is not directly expressed in the endodermis, any recovery in fluorescent signal in the endodermis represents the movement of the SHR-GFP protein from the stele. Use the same endodermal-to-stele (E:S) ratio measurement as in the *icals3m* method to evaluate the recovery of SHR and to control for root-to-root variations in SHR expression. Calculate the E:S ratio before bleach, after bleach, and after recovery in Excel according to  $(FA-FB)/(FP-FB)$ , where FA is the E:S ratio of fluorescence after recovery, FB is the E:S ratio of fluorescence after bleaching, and FP is the E:S ratio of fluorescence prebleaching (*see Notes 7* and **14**).

---

## 4 Notes

1. We find that *Arabidopsis* root growth is very sensitive to growth conditions. Media that have been autoclaved for more than 30 min or that show signs of caramelization may inhibit root growth and should not be used. For MS plates containing estradiol or inhibitors, add the compounds after autoclaving and cooling to approximately 60 °C. The solution is then mixed well and poured into 90 mm Petri plates (*see Note 2*) in a sterile hood. The plates and slides containing estradiol or inhibitor should be made fresh the day of use. Therefore, as an alternative to pouring plates daily,  $\frac{1}{2}$  strength MS medium can be made in advance, autoclaved, aliquoted into sterile 50 mL polypropylene tubes (about 30 mL/tube), and allowed to cool.

When the medium is ready to use, it can be microwaved at 50 % power in the 50 mL Falcon tube, in a beaker of water until melted. Once sufficiently cooled, the estradiol or inhibitor can then be added.

2. We have used both oryzalin and cytochalasin D treatment in the root to disrupt the microtubule and actin cytoskeletons, respectively. Oryzalin was dissolved in 100 % DMSO to make a 10 mM stock solution and then added directly to the cooled  $\frac{1}{2}$  MS medium to a final concentration of 1  $\mu$ M. Cytochalasin D was also dissolved in 100 % DMSO to make a 10 mM stock and then diluted to a concentration of 20  $\mu$ M in the  $\frac{1}{2}$  MS plates. Both of these inhibitors decrease SHR movement as assayed using the *icals3m* system and analysis of FRAP [9]. Media containing the same amount of the solvent (e.g., ethanol or DMSO) used to dissolve the inhibitor should be prepared for use as a control. As above, the  $\frac{1}{2}$  strength MS solution is mixed well and poured into Petri plates in a sterile hood. Some inhibitors can be cost prohibitive to use in large volumes. For these, we generally use 55 mm Petri plates and approximately 3 mL of total media volume.
3. The removal of the coverslip is best done with forceps using a sliding motion. Attempts to pull the coverslip directly upwards may result in breaking the coverslip and damaging the agar pad.
4. The response of different *icals3m* lines to estradiol will vary. It is important that the lines are homozygous for both the *icals3m* transgene and the fluorescent marker. In order to select the appropriate lines for these assays, we did extensive controls to show that there is a minimal effect of the *icals3m* transgene on the movement of SHR-GFP in the absence of estradiol and that SHR-GFP movement could reliably recover upon the removal of estradiol.
5. Incubation time in estradiol should be empirically determined based on the turnover rate of the fluorescent-tagged protein in the destination cells. We previously showed that SHR-GFP levels in endodermis are significantly reduced after 7 h in 10  $\mu$ M estradiol [16]. For recovery experiments, we use 1  $\mu$ M estradiol, which is efficient at blocking SHR movement. Higher concentrations of estradiol (e.g., 10  $\mu$ M) showed a more rapid response but often retarded the recovery process. After 1  $\mu$ M treatment and then 6 h incubation in  $\frac{1}{2}$  strength MS, SHR-GFP levels in the endodermis reliably recovered to ~70 % of preinduction.
6. Leaving the aerial portions intact works well if one is imaging structures at the root apex. However, if imaging is done closer to the root-shoot junction, the leaves may come in contact with the microscope objective and cause the roots to be damaged.

7. The average E:S ratio of SHR-GFP prior to induction with estradiol is typically 1.2. After 7–8 h on estradiol, the average E:S ratio of the treated plants falls to about 0.5 (a drop of 0.7). After 5–6 h on estradiol-free medium, the E:S typically recovers to around 1.0 (an increase of 0.5). This then represents a 71 % (0.5/0.7) recovery. For statistical significance, a sufficient number of roots and technical replicates should be included for each treatment. Normally, three plates for each treatment and 8–10 roots for each plate are used.
8. Do not apply too much liquid to the agar pad or the slide chamber. An excess of liquid will cause the roots to float during incubation, which alters the focal plane. If you find that the coverslip is floating, the edge of a Kimwipes can often be used to gently and judiciously wick out some of the media until the coverslip is stable. The roots, however, should be completely surrounded by liquid.
9. Avoid mechanical stress as much as possible. Once the coverslip is placed over the roots, do not try to move or readjust the position of the coverslip. This will damage the roots. One frequently encountered problem is the pressure from the glass coverslip during its placement on the slide or from the objective on the roots during the imaging. One way to overcome this issue is to grow the seedlings in a 35 mm sterile culture dish (e.g., FluoroDish). Although this permits one to grow and observe the roots in the same plate without transferring the seedlings, it has several disadvantages. First, it only accommodates seedlings less than 6 days old. Second, the roots that grow into the agar often become twisted or bent, making it difficult for consistent observation by confocal microscopy. Third, it is not convenient for controlled pharmacological assays as the inhibitor would have to be added to the top of the medium and allowed to diffuse throughout. Also, the concentration of the inhibitor will not be exact, as there is some water loss from the culture dishes as the roots grow.
10. To avoid desiccation during the intervals between imaging, the seedlings should be immediately returned back to the moisture chambers. The slides should be incubated vertically to reduce bending in response to gravity.
11. The number of iterations to achieve sufficient bleaching should be empirically determined. The first time trying this protocol, it is useful to counterstain the roots with propidium iodide (PI). The PI localization can be used as a marker, as overbleaching (phototoxicity) often results in an accumulation of PI in the nuclei of the bleached cells.
12. We capture the images of the bleached areas every 30–40 min to reduce the possibility of additional bleaching from frequent

scanning; however, more frequent imaging may be required for rapidly moving proteins. Several methods can be used to facilitate the identification of the same region of interest. First, the *X*, *Y*, and *Z* position of the initial images and bleaching steps are noted. Second, the cells expressing the fluorescent protein often form recognizable patterns that can be used as landmarks to identify the same region of interest. For example, when we bleach SHR-YFP in the endodermis, not all endodermal cells are bleached; the non-bleached cells can serve as “markers” that can be identified later (Fig. 5, arrowheads). Occasionally, such markers are lost due to cell division and cell expansion or growth; the use of the *X*, *Y*, and *Z* coordinates along with several “landmarks” is sufficient to identify the region of interest. To further increase the precision, one can capture a brief *Z*-stack series of sections with short interval (several micrometers) around the region of interest. In this way, the same region should be included in the series of images and can be retracked later for analysis.

13. One concern is cell division can affect the pattern of “markers” during the incubation, making it difficult to find exactly the same cells of interest at different time points. However, we found that cell division does not occur frequently and can be solved by increasing the numbers of the samples. Previous cell flux assays demonstrated that cell production for a single cortex cell file is around 40 cells/day in a 7-day-old root [21]. This means the average rate is only 1.7 cells/h for one cortex cell file. So if the sample number is sufficient, it is very likely to observe cells that stay in the G0 stage during the incubation.
14. To obtain statistically reliable results, a minimum of 6–8 roots from three experiments and 6–8 cells for each root should be analyzed.

---

## Acknowledgments

The *icals3m* construct was part of the collaboration with the Y. Helariutta lab. S. Wu is supported by a grant from NSF (award # 1243945) to K. Gallagher.

## References

1. Drakakaki G, Dandekar A (2013) Protein secretion: how many secretory routes does a plant cell have? *Plant Sci* 203–204:74–78
2. Drakakaki G, Robert S, Raikhel NV, Hicks GR (2009) Chemical dissection of endosomal pathways. *Plant Signal Behav* 4:57–62
3. Drakakaki G, Robert S, Szatmari AM et al (2011) Clusters of bioactive compounds target dynamic endomembrane networks in vivo. *Proc Natl Acad Sci U S A* 108:17850–17855
4. Hicks GR, Raikhel NV (2010) Advances in dissecting endomembrane trafficking with small molecules. *Curr Opin Plant Biol* 13:706–713
5. Mishev K, Dejonghe W, Russinova E (2013) Small molecules for dissecting endomembrane

- trafficking: a cross-systems view. *Chem Biol* 20: 475–486
6. Peterson JR, Mitchison TJ (2002) Small molecules, big impact: a history of chemical inhibitors and the cytoskeleton. *Chem Biol* 9:1275–1285
7. Zabolina O, Malm E, Drakakaki G et al (2008) Identification and preliminary characterization of a new chemical affecting glucosyltransferase activities involved in plant cell wall biosynthesis. *Mol Plant* 1:977–989
8. Harries PA, Schoelz JE, Nelson RS (2010) Intracellular transport of viruses and their components: utilizing the cytoskeleton and membrane highways. *Mol Plant Microbe Interact* 23:1381–1393
9. Wu S, Gallagher KL (2013) Intact microtubules are required for the intercellular movement of the SHORT-ROOT transcription factor. *Plant J* 74:148–159
10. Kurata T, Ishida T, Kawabata-Awai C et al (2005) Cell-to-cell movement of the CAPRICE protein in Arabidopsis root epidermal cell differentiation. *Development* 132:5387–5398
11. Pesch M, Hulskamp M (2011) Role of TRIPTYCHON in trichome patterning in Arabidopsis. *BMC Plant Biol* 11:130–145
12. Savage NS, Walker T, Wieckowski Y et al (2008) A mutual support mechanism through intercellular movement of CAPRICE and GLABRA3 can pattern the Arabidopsis root epidermis. *PLoS Biol* 6:e235
13. Wang S, Kwak SH, Zeng Q et al (2007) TRICHOMELESS1 regulates trichome patterning by suppressing GLABRA1 in Arabidopsis. *Development* 134:3873–3882
14. Wester K, Digiuni S, Geier F et al (2009) Functional diversity of R3 single-repeat genes in trichome development. *Development* 136: 1487–1496
15. Liu L, Liu C, Hou XL et al (2012) FTIP1 is an essential regulator required for florigen transport. *PLoS Biol* 10:e1001313
16. Vaten A, Dettmer J, Wu S et al (2011) Callose biosynthesis regulates symplastic trafficking during root development. *Dev Cell* 21: 1144–1155
17. Nakajima K, Sena G, Nawy T, Benfey PN (2001) Intercellular movement of the putative transcription factor SHR in root patterning. *Nature* 413:307–311
18. Gallagher KL, Paquette AJ, Nakajima K, Benfey PN (2004) Mechanisms regulating SHORT-ROOT intercellular movement. *Curr Biol* 14:1847–1851
19. Koizumi K, Hayashi T, Wu S, Gallagher KL (2012) The SHORT-ROOT protein acts as a mobile, dose-dependent signal in patterning the ground tissue. *Proc Natl Acad Sci U S A* 109:13010–13015
20. Koizumi K, Wu S, MacRae-Crerar A, Gallagher KL (2011) An essential protein that interacts with endosomes and promotes movement of the SHORT-ROOT transcription factor. *Curr Biol* 21:1559–1564
21. Wu S, Scheible WR, Schindelasch D, Van Den Daele H, De Veylder L, Baskin TI (2010) A conditional mutation in *Arabidopsis thaliana* separase induces chromosome non-disjunction, aberrant morphogenesis and cyclin B1;1 stability. *Development* 137:953–961

## Probing Protein Targeting to Plasmodesmata Using Fluorescence Recovery After Photo-Bleaching

Kathryn M. Wright and Katrin M. MacKenzie

### Abstract

Fluorescence recovery after photo-bleaching (FRAP) involves the irreversible bleaching of a fluorescent protein within a specific area of the cell using a high-intensity laser. The recovery of fluorescence represents the movement of new protein into this area and can therefore be used to investigate factors involved in this movement. Here we describe a FRAP method to investigate the effect of a range of pharmacological agents on the targeting of *Tobacco mosaic virus* movement protein to plasmodesmata.

**Key words** *Tobacco mosaic virus*, Movement protein, Plasmodesmata, Fluorescence recovery after photo-bleaching

---

### 1 Introduction

Plant viruses use plasmodesmata (PD) to move from cell to cell, apparently “hijacking” host macromolecular transport pathways in the process. As such, study of their movement provides valuable insight into normal host processes. *Tobacco mosaic virus* (TMV), the type member of the tobamoviruses, is a rod-shaped, positive-strand RNA virus, encoding 126 kDa and 183 kDa replicase subunits, a 17.5 kDa coat protein and a 30 kDa movement protein (MP). The MP is required for the movement of viral replication complexes to and through PD and during this process accumulates in the branched PD of source leaves [1–5].

During the course of cell infection, MP associates with the endoplasmic reticulum (ER) and components of the cytoskeleton, actin, and microtubules (MTs) (for review *see* ref. 6), leading to speculation regarding the mechanism by which the protein is targeted to PD. The fluorescence recovery after photo-bleaching (FRAP) method described in this chapter was developed in an attempt to identify the intracellular route involved [7]. The method involves the selective photo-bleaching of MP-GFP-labeled PD at the leading edge of an infection site and the subsequent imaging of

the recovery of fluorescence within the PD, this reflecting the movement of new fluorescent MP to the PD. The response of this fluorescence recovery to a range of pharmacological agents, that disrupt the ER or cytoskeleton components, was used to identify cell components involved in this transport of MP.

As a FRAP investigation, the study of the recovery of MP fluorescence into PD [7] is unusual in that it occurs over a much longer period of time (many minutes) than many processes investigated previously, including the recovery of photo-bleached Golgi bodies [8], intraluminal diffusion in the ER [9], or the remodeling and diffusion of plant ER membranes [10]. This may be due to the lower amount of MP available to accumulate at PD at the leading edge of an infection front.

Our results obtained using FRAP indicated an important role for the cortical ER/actin network in MP trafficking [7]. Subsequent results, recently reviewed in a number of papers [6, 11, 12] have supported the requirement of an intact ER network for trafficking of MP within the cell, with a role for actin and associated motor proteins in accelerating lateral diffusion along the ER and the involvement of MTs in the attachment and release of movement-competent viral replication complexes.

In addition to the FRAP method, protocols are included to test the effectiveness of the inhibitors used to disrupt the cell components. These include observation of various cell components labeled with fluorescent protein either in stable transgenic plants or in transient expression systems. However, due to the anomalous behavior of some of these labeling systems, this chapter also includes details of methods for the fluorescent labeling of actin with phalloidin and of MTs with antibodies.

---

## 2 Materials

Prepare all solutions using distilled water. A number of the chemicals used in these procedures are hazardous or toxic. Therefore note and observe all details provided in material safety data sheets, wear suitable protective clothing, and diligently follow all waste disposal regulations when disposing of waste materials and genetically modified organisms.

### 2.1 Plant Growth Conditions and Material

1. All plants can be grown from seed in a compost mix and maintained under glasshouse conditions with a day-length of 16.5 h, minimum daytime temperature of 28 °C and minimum night-time temperature of 22 °C. Supplementary lighting should be provided below a daytime threshold of 250 W/m<sup>2</sup>, and sun screening used above 400 W/m<sup>2</sup> (*see Note 1*). Plants are used for experiments when they are 30–35 days old with expanded leaves that are around 7 cm long.
2. Nontransgenic plants: *Nicotiana benthamiana* (*see Note 2*).

3. Transgenic plant lines expressing cellular markers fused to GFP.
  - (a) ER-GFP: *N. benthamiana* plants expressing m-gfp5-ER as a marker for the endoplasmic reticulum, provided by Baulcombe [13].
  - (b) TUA-GFP: *N. benthamiana* plants expressing a fusion of GFP to the Arabidopsis  $\alpha$ -tubulin, marking MTs, constructed as described previously [14].
  - (c) STtmd-GFP: *N. tabacum* plants expressing the sialyl-transferase transmembrane domain fused to GFP as a Golgi body marker, created in a similar way to STtmd-mRFP plants [15] provided by Hawes and Andreeva.
  - (d) GFP-fABD2: *N. tabacum* plants expressing a fusion between GFP and the second actin-binding domain of Arabidopsis fimbrin provided by David McCurdy [16].

## 2.2 Infectious Transcript and Plant Inoculation

1. 0.1 M phosphate buffer, pH 7.0: 57.7 mL of 1 M  $\text{Na}_2\text{HPO}_4$  (dissolve 141.96 g in 1 L water) and 42.3 mL 1 M  $\text{NaH}_2\text{PO}_4$  (dissolve 119.48 g in 1 L water) diluted to 1 L.
2. Coat protein monomers at 25 mg/mL in phosphate buffer (*see Note 3*).
3. T7 transcription kit (e.g. Ambion mMessage mMachine, Austin, TX).
4. Aluminum oxide powder. Grit size F4000 WP, mean particle size tolerance 16.3–18.3  $\mu\text{m}$ .

## 2.3 Inhibitors

All stock solutions should be stored at  $-20^\circ\text{C}$  except sodium azide which can be maintained at room temperature (*see Note 4*).

1. 10  $\mu\text{g}/\text{mL}$  Brefeldin A: Weigh around 10 mg brefeldin A (BFA) and dissolve in dry methanol (*see Note 5*) to a concentration of 10  $\text{mg}/\text{mL}$  (*see Note 6*). Dilute 1  $\mu\text{L}$  of stock solution into 0.999 mL of distilled water (1  $\mu\text{L}/\text{mL}$  of working solution).
2. 100  $\mu\text{g}/\text{mL}$  Brefeldin A: Dilute the 10  $\text{mg}/\text{mL}$  BFA stock solution above 10  $\mu\text{L}/\text{mL}$  of working solution.
3. 25  $\mu\text{M}$  Latrunculin B: Weigh around 1 mg latrunculin B and dissolve in dry dimethyl sulphoxide (DMSO) to a concentration of 1  $\text{mg}/\text{mL}$  (2.53 mM). Dilute 9.89  $\mu\text{L}/\text{mL}$  of working solution.
4. 200  $\mu\text{M}$  Cytochalasin B: Weigh around 10 mg cytochalasin B and dissolve in dry DMSO to a concentration of 10  $\text{mg}/\text{mL}$  ( $\approx 20$  mM). Dilute 10  $\mu\text{L}/\text{mL}$  of working solution.
5. 500  $\mu\text{M}$  Colchicine: Weigh around 5 mg colchicine and dissolve in sterile distilled water to a concentration of 19.97  $\text{mg}/\text{mL}$  (50 mM). Dilute 10  $\mu\text{L}/\text{mL}$  of working solution.
6. 20  $\mu\text{g}/\text{mL}$  Oryzalin: Weigh around 20 mg oryzalin and dissolve in dry acetone to a concentration of 50  $\text{mg}/\text{mL}$ . Dilute 5  $\mu\text{L}$  ethanol, plus 2.4  $\mu\text{L}$  stock oryzalin, in 6 mL water as a working solution.

7. 0.02 % sodium azide: Weigh around 10 mg sodium azide and dissolve in sterile distilled water to a concentration of 10 % w/v (i.e. 10 mg/100  $\mu$ L). Dilute 2  $\mu$ L/mL of working solution.

## **2.4 Labeling of Actin with Phalloidin**

1. 100 mM PIPES (*see Note 7*): Add 3.024 g PIPES to 80 mL water. With stirring, add 2 M KOH until the PIPES dissolves and adjust volume to 100 mL.
2. 50 mM EGTA (*see Note 8*): To 35 mL water, add 0.9508 g EGTA and 2 M KOH until dissolved. Adjust volume to 50 mL.
3. 1 M  $\text{MgSO}_4$ : Dissolve 1.204 g of anhydrous  $\text{MgSO}_4$  in water and adjust total volume to 10 mL.
4. 0.1 M 3-Maleimidobenzoic acid-N-hydroxysuccinimide ester (MBS): Dissolve 25 mg in 795  $\mu$ L DMSO. Store in the fridge after dilution and discard if it becomes very pink in color.
5. 10 % Igepal (*see Note 9*): Dilute 1 mL Igepal with 9 mL of water and warm gently to dissolve.
6. Alexa Fluor<sup>®</sup> 488 phalloidin: Dilute 300 units in 1.5 mL dry methanol and store in the freezer.
7. Base buffer: 50 mM PIPES, 5 mM EGTA, 5 mM  $\text{MgSO}_4$ , 0.05 % Igepal. Mix together 25 mL of 100 mM PIPES, 5 mL of 50 mM EGTA, 250  $\mu$ L of 1 M  $\text{MgSO}_4$ . Adjust the pH to 6.9 using 2 M KOH, add 250  $\mu$ L 10 % Igepal and adjust the volume to 50 mL.
8. MBS buffer: Make up 10 mL of base buffer as above but add 30  $\mu$ L of 0.1 M MBS using a fume cupboard/bench before adjusting the final volume.

## **2.5 Immunolabeling of $\beta$ -Tubulin**

1. 1 M  $\text{MgSO}_4$ : *see* Subheading 2.4, **item 3**.
2. 5 $\times$  stock PEMT buffer: 0.5 M PIPES, 25 mM EGTA, 10 mM  $\text{MgSO}_4$ , 0.25 % Triton X-100. To approximately 16 mL water in a beaker, add 3.02 g PIPES, 0.19 g EGTA, 200  $\mu$ L of 1 M  $\text{MgSO}_4$ . Whilst stirring add 5 M KOH dropwise until PIPES dissolves. Adjust the pH to 6.8 and then add 50  $\mu$ L Triton X-100. Finally, adjust volume to 20 mL.
3. Fixative (*see Note 10*): 4 % formaldehyde, 0.1 % glutaraldehyde in 1 $\times$  PEMT. To 10.92 mL water add 4 mL of 5 $\times$  PEMT stock, 5 mL formaldehyde (purchased as 16 % aqueous solution) and 80  $\mu$ L glutaraldehyde (purchased as 25 % aqueous solution).
4. 10 $\times$  stock Phosphate buffered saline (PBS): To 800 mL water add 80 g NaCl, 2 g KCl, 2 g  $\text{KH}_2\text{PO}_4$  and 29 g  $\text{Na}_2\text{HPO}_4 \cdot 12\text{H}_2\text{O}$  and adjust the volume to 1 L. When diluted to 1 $\times$  PBS this has a pH of 7.4.
5. PBS+50 mM glycine: To 10 mL of 10 $\times$  PBS solution, add 0.375 g glycine and adjust the volume to 100 mL.

6. Antibody: Monoclonal Anti- $\beta$ -Tubulin, Cy3 conjugate, purified mouse immunoglobulin clone TUB2.1. Dilute 1  $\mu$ L/100  $\mu$ L PBS + 50 mM glycine.

---

### 3 Methods

#### **3.1 Preparation and Reassembly of Infectious Transcript, Inoculation of Plants, and Lesion Growth**

1. Under sterile conditions, mix together 113  $\mu$ L 0.1 M phosphate buffer and 7  $\mu$ L coat protein monomers and incubate at 25 °C for at least 5 h or overnight.
2. Using a T7 transcription kit, add the following in order to a 1.5 mL microfuge tube: 2xNTP-CAP 5  $\mu$ L; DNA Template of TMV.MP-EGFP.CP 3  $\mu$ L (*see Note 11*); Buffer 1  $\mu$ L; Enzyme 1  $\mu$ L. Incubate at 37 °C for 2 h.
3. Add the coat protein monomers to the transcription reaction mixture and incubate overnight at 25 °C. The reassembled transcript is stable for about 6 weeks if stored in the fridge (*see Note 3*).
4. Dust a small amount of aluminum oxide powder on to the upper (adaxial) surface of 2 leaves of a *N. benthamiana* plant and place a 5  $\mu$ L drop of reassembled transcript on each leaf. Spread this drop over the surface of the leaf with gentle rubbing.
5. Maintain the plants in a glasshouse for 4 days with a day length of 16.5 h, minimum daytime temperature of 33 °C and minimum night-time temperature of 28 °C to allow lesion growth (*see Note 12*).

#### **3.2 Fluorescence Recovery After Photo-Bleaching (FRAP) of PD**

1. Remove an infected leaf from a plant and infiltrate the apoplastic space by making a small hole in the abaxial epidermis with a scalpel blade, placing a 1 mL syringe (without a needle) filled with water to the hole and applying gentle pressure against a finger held on the adaxial side of the leaf. Float the leaf on water in a petri dish for between 1 and 2 h (this acts as a control for leaves infiltrated with inhibitor). Cut the leaf in half, dry the adaxial surface with a paper towel and attach it to a microscope slide with double-sided tape.
2. Using a 5 $\times$  or 10 $\times$  objective and fluorescent illumination (*see Note 13*) locate the leading edge of an infection site (Fig. 2a). Change to a 63 $\times$  objective (*see Note 14*) and using confocal imaging (*see Note 15*) with excitation of 488 nm and 500–535 nm emission locate at least 2 PD in the same focal plane, within 2 cells of the visible leading edge of the lesion. Note there should be at least two PD visible, one to be treated and another to act as the control for changes in fluorescence, either due to imaging or as a result of movement of the sample, and therefore distinguishing features should also be identified to aid realignment where necessary (*see Note 16*).

3. Adjust the laser intensity and gain setting to ensure there is no saturation of signal, and the offset so that the black-level is correctly set. Record these settings and use them for all subsequent measurements.
4. Collect a single image at 1× zoom using these settings without any averaging. This is the pre-bleached image or time  $t=0$ .
5. Immediately zoom in to the maximum setting (32×) on the selected PD to be treated, increase the laser intensity to 100 % and scan three times at medium speed. This bleaching should result in the disappearance of the PD. Immediately reduce the zoom to 1× and collect a single image using the defined conditions and note the time.
6. At times  $t=10, 20, 30$ , and 40 min, scan using continuous mode to realign the designated PD and markers and then collect a single image using the defined conditions (Fig. 1).
7. After collecting similar images from at least ten pairs of PD, measure the fluorescence intensities associated with the selected

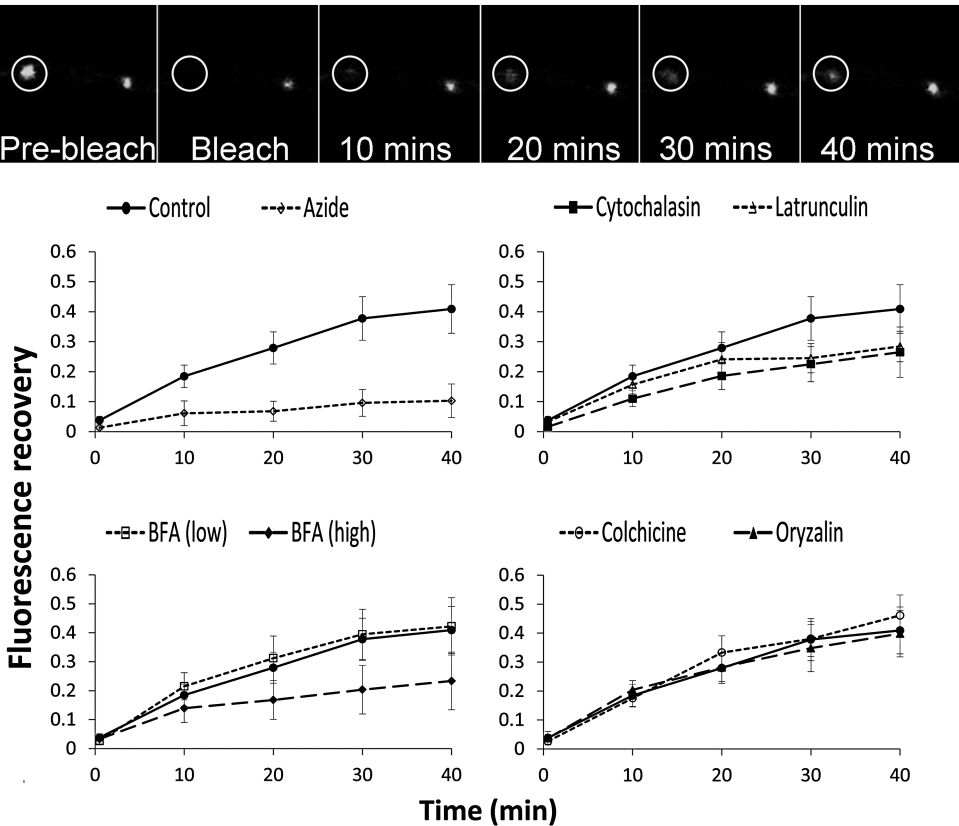


**Fig. 1** Images collected under control conditions of a pair of PD, prior to bleaching (see Subheading 3.2, step 4), immediately following (see Subheading 3.2, step 5), and at 10–40 min after bleaching (see Subheading 3.2, step 6). Graphs are presented of time versus fluorescence recovery as a proportion of the pre-bleached value following treatment with the various inhibitors, the bars representing 95 % confidence intervals

**Table 1**

**Spreadsheet describing the calculations to convert measured fluorescence intensities to corrected intensities expressed as a proportion of the pre-bleached value**

A	B	C	D	E	F	G	1
Time	0	0.2	10	20	30	40	2
Intensity bleached PD	3,500	50	1,000	990	1,600	2,300	3
Intensity control PD	2,990	2,400	3,330	2,340	3,330	3,790	4
For the control samples divide each value by the time 0 value <sup>a</sup>							5
	=B4/B4	=C4/B4	=D4/B4	=E4/B4	=F4/B4	=G4/B4	6
Intensity	1.0	0.8	1.1	0.8	1.1	1.3	7
Multiply each bleached value by this factor <sup>b</sup>							8
	=B3×B7	=C3×C7	=D3×D7	=E3×E7	=F3×F7	=G3×G7	9
Intensity	3,500.0	40.1	1,113.7	774.8	1,781.9	2,915.4	10
Divide each bleached value by the pre-bleached value <sup>c</sup>							11
	=B10/B10	=C10/B10	=D10/B10	=E10/B10	=F10/B10	=G10/B10	12
Intensity <sup>d</sup>	1	0.011467	0.318204	0.221366	0.509126	0.832967	13

<sup>a</sup>This adjusts for any change in intensity due to bleaching during imaging or change in sample position

<sup>b</sup>To correct the treated sample for any changes in intensity due to imaging

<sup>c</sup>Allows PDs of different initial intensities to be compared

<sup>d</sup>Final fluorescence intensity as a proportion of the pre-bleached value

photo-bleached PD and the neighboring nonbleached PD using the software provided with the confocal system. In order to allow for changes in the focal plane, or additional photo-bleaching during imaging, the fluorescence intensity of the bleached PD is adjusted by the factor of change in fluorescence of the nonbleached PD (*see* Table 1 for details). Express the corrected fluorescence intensities as a proportion of the pre-bleached value.

8. Determine the optimal inhibitor treatment conditions (*see* **Note 17** and Subheadings 3.3–3.6). Repeat the FRAP experiments on lesions pretreated with inhibitor, mounted on double sided tape and using the appropriate inhibitor solution to immerse the dipping lens.
9. After collecting data from between 10 and 20 replicates for each treatment fit a curve of the form  $I = ax^b$  and calculate the value of this curve for  $x = 40$  (*see* **Note 18**). Use the variance of the results of this calculation, an appropriate significance threshold, usually 5 %, and an effect equal to a 20 % difference between the control and each treatment and a power to detect a difference of this size of 80 % to determine the number of samples required. The number of samples is determined by the size of the difference to be detected, the smaller the difference,

**Table 2**  
**Sample results**

Inhibitor	Proportion FRAP	Significance threshold	Number of replicates required	Number of replicates measured
Control	0.41 ± 0.08	–		22
BFA (10 µg/mL)	0.42 ± 0.10	ns	9	24
BFA (100 µg/mL)	0.23 ± 0.10	0.01	9	16
Latrunculin	0.28 ± 0.05	0.05	9	16
Cytochalasin	0.27 ± 0.08	0.05	8	16
Colchicine	0.46 ± 0.07	ns	14	21
Oryzalin	0.40 ± 0.08	ns	10	16
Azide	0.10 ± 0.06	0.01	6	22

The proportion FRAP represents the fluorescence intensity, expressed as a proportion of the pre-bleached value (mean ± 95 % confidence interval) of PD for a range of inhibitors 40 min after bleaching. Significant differences between inhibitor treatments and control, based on analysis of variance of  $\log(a)$  are presented (similar results were obtained for analysis of variance  $\log(b)$ ). The number of treatment replicates required to have a 95 % probability of detecting a 20 % difference in  $\log(a)$  and the actual number of replicates measured are shown [7]

the larger the sample size required. A statistical package such as Genstat [17], can be used to derive the sample size. Collect sufficient data replicates to exceed this value.

10. Fit an exponential curve of the form;  $i = a + bc^t$  to each set of data, where  $i$  = fluorescence intensity as a proportion of the pre-bleached value and  $t$  is time in minutes. A natural log transformation of  $i$  is usually required because the variance in intensity tends to increase with the mean. Perform an Analysis of Variance [18] on parameters  $a$ ,  $b$ , and  $c$ , under appropriate transformations as necessary, in order to identify treatments that resulted in significant differences from the control. For example results see Table 2.

**3.3 Effectiveness of Inhibitors to Disrupt the Endomembrane System**

1. Infiltrate a leaf of *N. benthamiana* expressing STtmd-GFP (Golgi) (Fig. 2b) with 10 µg/mL BFA and float in a petri dish containing the same solution. At designated intervals (see Note 19) remove a sample of leaf, mount on a microscope slide

**Fig. 2** (continued) *N. benthamiana* under control conditions showing actin filaments (g) and their fragmentation after treatment with 200 µM cytochalasin B (h) (see Subheading 3.4, **step 9**). GFP-fABD2 expressing *N. tabacum* plant (i) treated with 25 µM latrunculin showing the disruption of the actin network (see Subheading 3.4, **step 2**). Anti-β-tubulin Cy3 conjugate labeling of *N. benthamiana* under control conditions showing intact MT (j), and after treatment with 500 µM colchicine with a fragmented network (k) (see Subheading 3.5, **step 9**). TUA-GFP expressing *N. benthamiana* plant showing disruption of the MT network after treatment with 20 µg/mL oryzalin (l) (see Subheading 3.5, **step 2**). All images are maximum-intensity projections of z-stacks of epidermal cells with the position of chloroplasts (ch) being indicated where appropriate and all scale bars representing 25 µm

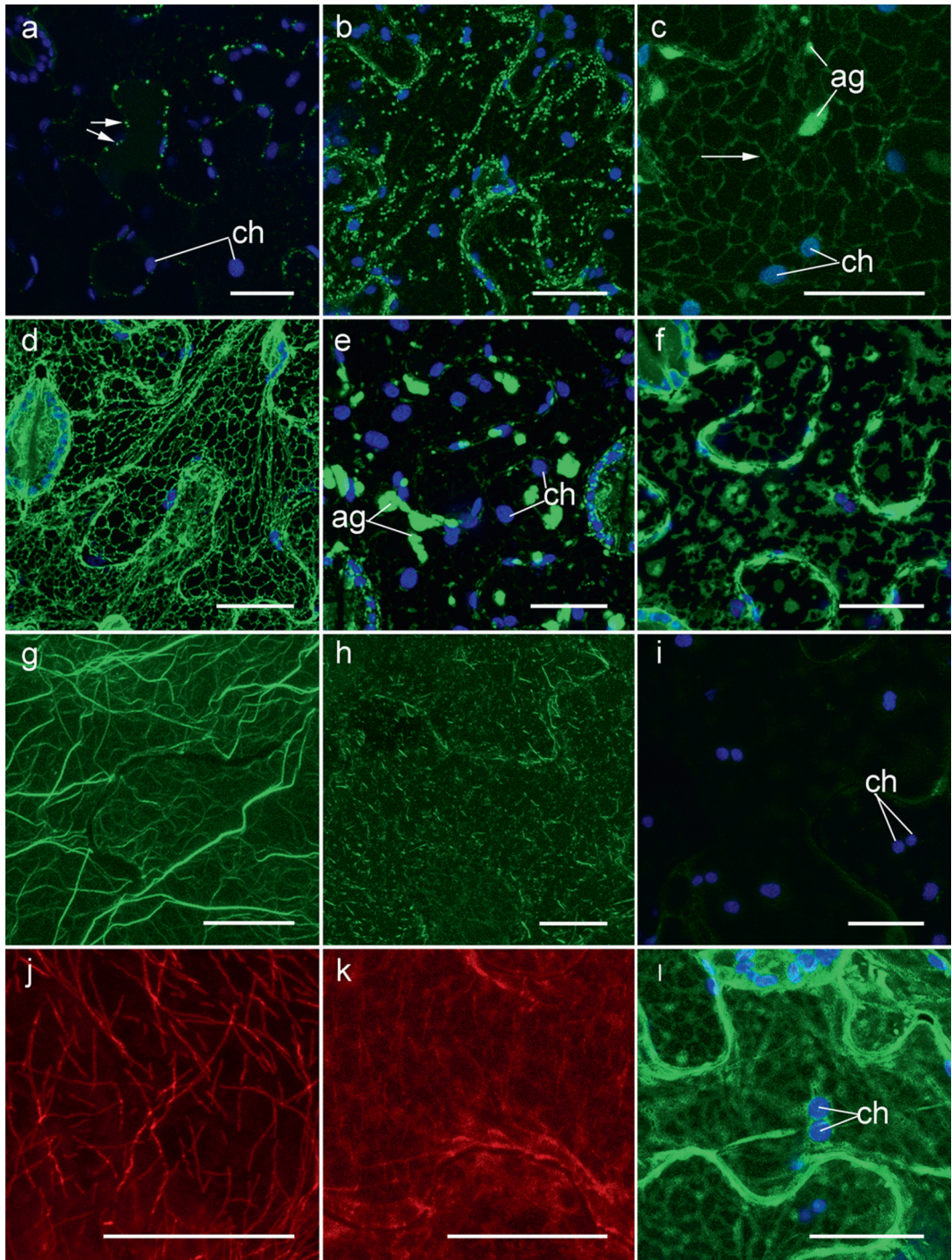


**Fig. 2** Confocal laser scanning micrographs showing the appearance of *Nicotiana* cells. The leading edge of a TMV.MP-EGFP.CP lesion on *N. benthamiana* (**a**) showing the targeting of MP to PD (arrows) and the punctate labeling of intracellular structures under control conditions (see Subheading 3.2, **step 2**). STtmd-GFP *N. tabacum* plants under control conditions showing dispersed Golgi stacks (**b**), and following treatment with 10  $\mu$ g/mL BFA (**c**) showing a faint ER network (arrow) and fluorescent aggregates (ag) due to the absorption of the Golgi bodies into the ER (see Subheading 3.3, **step 1**). ER-GFP expressing *N. benthamiana* plants under control conditions with a reticulate network (**d**), showing complete disruption of the ER network and the formation of aggregates (ag) after treatment with 100  $\mu$ g/mL BFA (**e**) (see Subheading 3.3, **step 3**), or alteration and immobilization of the network in the presence of latrunculin B (**f**) (see Subheading 3.4, **step 2**). Alexa 488 phalloidin staining of actin in

(see Subheading 3.2, **step 8.**) and observe using either fluorescent (see **Note 13**) or confocal imaging (see **Note 20**) until the green fluorescence of the Golgi is reabsorbed into the ER (around 1 h) (Fig. 2c).

2. Infiltrate a leaf from an ER-GFP plant with 10 µg/mL BFA for the same length of time, mount and observe. The ER should not be disrupted.
3. Infiltrate an ER-GFP leaf (Fig. 2d) with 100 µg/mL BFA and observe at regular intervals. After treatment for around 2 h the ER should be severely disrupted (Fig. 2e).

### **3.4 Effectiveness of Inhibitors to Disrupt Actin**

1. Infiltrate a leaf of *N. benthamiana* expressing ER-GFP (see **Note 21**), or a leaf of *N. tabacum* expressing GFP-fABD2 (actin) (see **Note 22**) with either 25 µM latrunculin B or 200 µM cytochalasin B.
2. Observe at designated intervals using either fluorescent or confocal imaging. The ER will show signs of disruption (Fig. 2f) and will cease movement once the actin becomes disrupted. The GFP-labeled actin network should disappear from the GFP-fABD2 plants (Fig. 2i).
3. To prepare tissue for phalloidin staining of actin, treat leaves of *N. benthamiana* with either latrunculin B or cytochalasin B for the time determined above (see **Note 23**). Also infiltrate tissue with 10 µL/mL DMSO and incubate for the same length of time as a control.
4. Coat a small plastic sheet (1 cm×2 cm×1 mm) with double sided tape. Remove the center portion of the tape, leaving a border about 3 mm wide.
5. Blot the leaf tissue and place the mount on the target leaf with the upper epidermis (adaxial surface) against the plastic and trim around the mount. Abrade the leaf tissue under water, using a piece of fine abrasive paper to leave only the adaxial epidermis. Float this on base buffer (Subheading 2.4, **item 7**) until all segments are prepared (see **Note 24**).
6. Add sufficient MBS buffer to cover the base of a 9 cm petri dish and transfer the mounted leaf samples. Incubate on a gently swirling flatbed shaker for 1½–2 h. For leaf tissue treated with inhibitor, float the samples in MBS buffer plus the appropriate concentration of inhibitor.
7. Transfer the leaf segments to a 9 cm petri dish containing 8 mL MBS buffer plus 200 µL Alexa Fluor® 488 phalloidin (without inhibitor) (see **Note 25**). Incubate in the dark for 45 min.
8. Transfer the mounted leaves to a dish containing base buffer. Using a scalpel, cut around the inner area of each leaf holder to

release the epidermal tissue and, by floating the tissue on a coverslip, mount on a microscope slide in base buffer under a coverslip.

9. Examine the samples by confocal microscopy (*see Note 20*). An intact network of actin microfilaments should be seen in control tissues (Fig. 2g) whilst a fragmented or disrupted network is observed in tissue treated with inhibitor (Fig. 2h).

### **3.5 Effectiveness of Inhibitors to Disrupt Microtubules**

1. Infiltrate a leaf of *N. benthamiana* expressing *tua*-GFP (MT) with either 500  $\mu$ M colchicine or 20  $\mu$ g/mL oryzalin and incubate in a petri dish floating on the same solution.
2. Observe at designated intervals using either fluorescent or confocal imaging. The GFP-tagged microtubules will become disrupted and disappear (Fig. 2l).
3. To prepare tissue for staining with antibodies, treat leaves of *N. benthamiana* with either colchicine or oryzalin for the time determined above (*see Note 26*). Also infiltrate control tissue with either water (as colchicine control) or 2.4  $\mu$ L acetone, plus 5  $\mu$ L ethanol in 6 mL water (as oryzalin control) and incubate for the same length of time.
4. Cut leaf tissue from the test areas into 4 mm  $\times$  1 mm sections and add to fixative (Subheading 2.5, **item 3**) in a bijou bottle. Vacuum infiltrate the tissue (*see Note 27*) and incubate overnight with gentle rotation.
5. Remove the fixative solution and rinse the leaf segments three times with 5 mL of 1 $\times$  PEMT buffer for 30 min each wash.
6. Prechill two metal blocks to  $-80^{\circ}\text{C}$ . Blot the leaf tissue slightly and place between two microscope slides. Freeze these by dipping in liquid nitrogen and then squash them between the chilled blocks. Rinse the tissue off the slide into a petri dish with PBS + 1 % Triton X100 and incubate for 3 h.
7. Rinse the leaf tissue with PBS, two immediate washes followed by 1 wash of 30 min and then an overnight wash.
8. Transfer the tissue to 1.5 mL microfuge tubes and incubate for 30 min in PBS + 50 mM glycine. Remove the buffer and replace it with antibody (*see Note 28*) diluted in PBS glycine and incubate for 3 h at  $37^{\circ}\text{C}$ .
9. Rinse the tissue in 1 $\times$  PBS and mount between a microscope slide and coverslip in PBS + 50 % w/v glycerol and observe by confocal microscopy (*see Notes 20 and 29*). An intact network of MT should be observed in control tissue (Fig. 2j) with a disrupted network in tissue treated with inhibitor (Fig. 2k).

### 3.6 Effectiveness of Sodium Azide for Energy-Depletion

1. Infiltrate a leaf of *N. benthamiana* expressing ER-GFP with 0.02 % sodium azide and incubate in a petri dish floating on the same solution (*see* **Note 30**).
2. Observe at designated intervals using either fluorescent or confocal imaging. The ER will become severely disrupted after about 2 h.

---

## 4 Notes

1. The plant growth conditions described are provided as standard for the *Nicotiana* plant material grown at our facility. We have not tested whether different growth conditions have any significant effect on these investigations.
2. *Nicotiana benthamiana* Domin. [19] was grown from seed stocks maintained at the James Hutton Institute (previously the Scottish Crop Research Institute). Other laboratories specializing in virus studies may also maintain their own seed stocks.
3. For details of virus reassembly *see* Sleat et al. [20]. Whilst reassembled transcript is more stable, if coat protein monomers are not readily available, infection can be achieved by inoculating the leaf with freshly prepared transcript.
4. Working solutions are prepared fresh just before use. The inhibitors are diluted in a petri dish by adding the required amount of stock solution to distilled water. To avoid precipitation of the inhibitor it is advisable to gently swirl the liquid as the stock is added.
5. Acetone, DMSO and methanol are maintained as dry solutions by storing them over Molecular sieve type 3A.
6. Since it is difficult to weigh out defined quantities in the milligram range, attempt to get as close as possible, note the weight achieved, and calculate the volume of solvent required to dilute the substance to the given concentration.
7. PIPES: 1,4-Piperazinediethanesulfonic acid, as free acid.
8. EGTA: Ethylene glycol-bis(2-aminoethylether)-*N,N,N',N'*-tetraacetic acid.
9. Igepal CA-630 is the nonionic detergent octylphenoxy-polyethoxyethanol.
10. All procedures involving fixative should be carried out in a fume cupboard/bench.
11. The viral vector, TMV.MP-EGFP.CP, used in this study was produced as described previously [7, 14]. This employs the EGFP variant rather than cycle 3 GFP, which resists photo-bleaching.
12. Maintenance of plants at a higher temperature increases the replication and spread of the virus and, at the leading edge of

the infection, influences the distribution and size of inclusion bodies containing MP and its association with MTs [21].

13. To locate GFP fluorescence use either a designed GFP filter block or one appropriate for FITC. In the present case a dual wavelength FITC/Rhodamine block was used with, for FITC, an excitation filter BP 490/15, a dichroic mirror 500 and a suppression filter BP 525/20. Due to the presence of chloroplasts it is advisable to use a suppression filter that limits the fluorescence emitted by chlorophyll.
14. For example a Leica HCX APO 63× water dipping lens.
15. The experiments described were conducted using a Leica TCS-SP1 confocal laser scanning microscope (CLSM) with an argon laser supplying excitation at 488 nm. However any CLSM fitted with a laser capable of exciting and imaging GFP and bleaching EGFP using the zoom function would be suitable for this work.
16. Two PD are selected in each field of view, one to be bleached and a second to act as the control. In many confocal systems it is difficult to produce identical imaging conditions either throughout the day, and particularly from day to day, since laser output will vary dependent on the laser temperature. Many systems do not allow this output to be measured or accurately controlled. Therefore the second PD acts as an internal standard. Change in fluorescence of the treated PD is expressed in relation to change in fluorescence of the control PD caused either by photo-bleaching or due to changes in the focal plane of the Fig. resulting from the extended time course (*see* calculation Table 1 for details).
17. For each inhibitor used, it is necessary to determine the concentration of inhibitor and the duration of treatment required, and demonstrate that the treatment has effectively disrupted the organelle or structure required. Under our experimental conditions, leaf tissue was treated with each inhibitor for 2 h to ensure disruption, apart from the treatment for 1 h with low concentrations of BFA to disrupt the Golgi.
18. In this term, “*a*” is the mean value reached as time increases and “*b*” is the difference between the starting value and “*a*”.
19. Designated time intervals: for example, every 15 or 30 min.
20. Confocal imaging conditions. GFP is excited at 488 nm with the emission collected at 500–535 nm. If appropriate, the autofluorescence signal from chlorophyll can be collected at 600–650 nm. Alexa Fluor® 488 conjugates can be imaged using the same conditions as GFP. An excitation of 561 nm is used for fluorescent proteins labeled with RFP (emission 590–630 nm) or for Cy3 antibody (emission 570–590 nm)

21. Since the movement of the ER network depends on an intact actin network, the treatment of the ER-GFP plant and disruption of the ER network gives an indication of the time required for effective inhibition.
22. Data obtained using transgenic lines or transient expression systems expressing actin associated proteins fused to fluorescent protein may need to be treated with caution. Whilst GFP-fABD2 appears to label the whole actin network, expression of a GFP-mTalin fusion (GFP tagged to the carboxy-terminal actin-binding domain of mouse talin) in *Arabidopsis* causes increased bundling of filaments, did not label all the actin filaments and adversely affected plant morphology [16]. The treatment of GFP-fABD2 plants with either latrunculin B or cytochalasin B results in disappearance of the actin network and therefore provides a direct indication of the length of time required for its disruption. However since these plants are *N. tabacum* the time or conditions may vary from that required for *N. benthamiana*.

Whilst labeling with tagRFP-Lifeact does not appear to affect actin dynamics or plant morphology [22], preliminary results suggest that the actin filaments may be less sensitive to treatment with either latrunculin B or cytochalasin B since some remain intact after 2 h treatment (K.M. Wright unpublished data).

23. In order to confirm that disruption of actin by either latrunculin B or cytochalasin B occurs under similar conditions in wild-type *N. benthamiana* as in fluorescent protein tagged tissue, it is advisable to label the actin with phalloidin according to the method of Goodbody and Lloyd [23].
24. This procedure requires patient, gentle abrasion to remove the majority of the leaf tissue to leave only the epidermis tissue thus allowing penetration of the phalloidin stain. The layer of epidermis should remain intact and should not be ripped.
25. A range of fluorescent conjugates are available in addition to Alexa Fluor® 488 phalloidin used in this protocol. Selection of a suitable conjugate should include consideration of the laser line available for excitation and the brightness and photostability of the conjugate.
26. To ensure that MTs from wild-type *N. benthamiana* respond to treatment with inhibitors in the same way as fluorescently labeled MTs, it is advisable to confirm their disruption using the antibody staining method, e.g. the one developed by Wasteney and coworkers [24].
27. The vacuum can be produced using a hand-held vacuum pump attached to a bijou bottle. Alternatively a vacuum desiccator can be used but the procedure must ensure that air is removed from the internal air spaces in the leaf and the tissue segments become submerged in the fixative.

28. As with phalloidin, the choice of fluorescent conjugate for the anti-tubulin antibody depends on the laser line available for excitation and the brightness and photostability of the conjugate. In the present study an anti- $\beta$ -Cy3 conjugate was used.
29. The best labeling with antibody is found near the shattered edges of the tissue.
30. Since the movement of the ER is energy-dependent, observation of plants expressing ER-GFP can be used to indicate the effect of sodium azide. Cytoplasmic streaming will also cease in response to energy depletion.

---

## Acknowledgements

This work was funded by the Scottish Government Rural and Environmental Science and Analytical Services Division (RESAS). We thank D.A. Elston and P.J. Wright for critical review and helpful comments.

## References

1. Atkins D, Hull R, Wells B et al (1991) The *Tobacco mosaic virus* 30K movement protein in transgenic tobacco plants is localized to plasmodesmata. *J Gen Virol* 72:209–211
2. Ding B, Haudenschild JS, Hull RJ et al (1992) Secondary plasmodesmata are specific sites of localization of the *Tobacco mosaic virus* movement protein in transgenic tobacco plants. *Plant Cell* 4:915–928
3. Itaya A, Hickman H, Bao Y et al (1997) Cell-to-cell trafficking of *Cucumber mosaic virus* movement protein: green fluorescent protein fusion produced by biolistic gene bombardment in tobacco. *Plant J* 12:1223–1230
4. Itaya A, Woo Y-M, Masuta C et al (1998) Developmental regulation of intercellular protein trafficking through plasmodesmata in tobacco leaf epidermis. *Plant Physiol* 118:373–385
5. Roberts IM, Boevink P, Roberts AG et al (2001) Dynamic changes in the frequency and architecture of plasmodesmata during the sink-source transition in tobacco leaves. *Protoplasma* 218:31–44
6. Liu C, Nelson RS (2013) The cell biology of *Tobacco mosaic virus* replication and movement. *Front Plant Sci* 4:12. doi:10.3389/fpls.2013.00012
7. Wright KM, Wood NT, Roberts AG et al (2007) Targeting of TMV movement protein to plasmodesmata requires the actin/ER network; evidence from FRAP. *Traffic* 8:21–31
8. Brandizzi F, Snapp EL, Roberts AG et al (2002) Membrane protein transport between the endoplasmic reticulum and the Golgi in tobacco leaves is energy dependent but cytoskeleton independent: evidence from selective photobleaching. *Plant Cell* 14:1293–1309
9. Nehls S, Snapp EL, Cole NB et al (2000) Dynamics and retention of misfolded proteins in native ER membranes. *Nat Cell Biol* 2:288–295
10. Runions J, Brach T, Kuhner S et al (2006) Photoactivation of GFP reveals protein dynamics within the endoplasmic reticulum membrane. *J Exp Bot* 57:43–50
11. Peña EJ, Heinlein M (2012) RNA transport during TMV cell-to-cell movement. *Front Plant Sci* 3:193. doi:10.3389/fpls.2012.00193
12. Niehl A, Peña EJ, Amari K et al (2013) Microtubules in viral replication and transport. *Plant J* 75:290–308
13. Ruiz MT, Voinnet O, Baulcombe DC (1998) Initiation and maintenance of virus-induced gene silencing. *Plant Cell* 10:937–946
14. Gillespie T, Boevink P, Haupt S et al (2002) Functional analysis of a DNA-shuffled movement protein reveals that microtubules are dispensable for the cell-to-cell movement of *Tobacco mosaic virus*. *Plant Cell* 14:1207–1222
15. Latijnhouwers M, Hawes C, Carvalho C et al (2005) An Arabidopsis GRIP domain protein locates to the *trans*-Golgi and binds the small GTPase ARL1. *Plant J* 44:459–470

16. Sheahan MB, Staiger CJ, Rose RJ et al (2004) A green fluorescent protein fusion to actin-binding domain 2 of *Arabidopsis* fimbrin highlights new features of a dynamic actin cytoskeleton in live plant cells. *Plant Physiol* 136:3968–3978
17. Genstat (2012) Genstat for Windows release 15.1. VSM International Ltd, Hemel Hempstead, Hertfordshire
18. Lyalin OO, Lukyanova SA (1993) Effects of kinetin and ABA on parameters of root exudation. *Fiziol Rast* 40:368–374
19. Goodin MM, Zaitlin D, Naidu RA et al (2008) *Nicotiana benthamiana*: its history and future as a model for plant-pathogen interactions. *Mol Plant Microbe Interact* 21: 1015–1026
20. Sleat DE, Turner PC, Finch JT et al (1986) Packaging of recombinant RNA molecules into pseudovirus particles directed by the origin-of-assembly sequence from tobacco mosaic virus RNA. *Virology* 155:299–308
21. Boyko V, Ferralli J, Heinlein M (2000) Cell-to-cell movement of TMV RNA is temperature-dependent and corresponds to the association of movement protein with microtubules. *Plant J* 22:315–325
22. Vidali L, Rounds CM, Hepler PK et al (2009) Lifeact-mEGFP reveals a dynamic apical F-actin network in tip growing plant cells. *PLoS One* 4:e5744. doi:10.1371/journal.pone.0005744
23. Goodbody K, Lloyd CW (1990) Actin filaments line up across *Tradescantia* epidermal cells, anticipating wound-induced division planes. *Protoplasma* 157:92–101
24. Wasteneys GO, Willingale-Theune J, Menzel D (1997) Freeze shattering: a simple and effective method for permeabilizing higher plant cell walls. *J Microsc* 188:51–61

## The Tracking of Intercellular Small RNA Movement

Christophe Himber and Patrice Dunoyer

### Abstract

RNA silencing is a regulatory mechanism that controls the expression of endogenous genes and exogenous molecular parasites such as viruses, transgenes, and transposable elements. The sequence specificity of these processes relies on small noncoding RNA (sRNA) molecules. In plants, one of the most fascinating aspects of RNA silencing is its mobile nature, in other words its ability to spread from the cell where it has been initiated to neighboring cells, through movement of sRNA molecules. To study this process, a key step is to directly monitor the spread of these nucleic acid species. Here we describe how this can be achieved through biolistic delivery of fluorescently labeled siRNA.

**Key words** RNA silencing, Small RNA, Intercellular movement, Biolistic

---

### 1 Introduction

RNA silencing is a fundamental regulator of gene expression, heterochromatin formation, suppression of transposable elements and defense against viruses. This evolutionarily conserved mechanism is triggered by double-stranded RNA that is processed, by RNaseIII-like enzymes called Dicers, into 21–24-nt small interfering (si)RNA or micro (mi)RNA which provide the sequence specificity of the silencing effects [1]. In plants, one of the most fascinating aspects of RNA silencing is its ability to move locally and/or systemically, to orchestrate developmental and stress responses non-cell-autonomously. During these processes, the nucleic acid components of the silencing signal have been ascribed to siRNAs [2–4]. Whereas their systemic movement occurs through the phloem, their cell-to-cell movement likely occurs through plasmodesmata (the pores interconnecting plant cells), based on the resistance to mobile silencing of mature stomata guard cells that are symplastically isolated from neighboring cells due to the loss of their plasmodesmal connections [5].

In order to follow the intercellular movement of siRNA and to determine if a given mutation impairs non-cell autonomous silencing

through inhibition of siRNA movement, a key step is to directly monitor the spread of these nucleic acid species. Next, we will cover the key points of biolistic delivery of fluorescently labeled siRNA that allowed us to follow their movement in planta.

---

## 2 Materials

### 2.1 Material

1. Biolistic® PDS-1000/He™ particle delivery system (Biorad).
2. Tank of pressurized Helium (grade 4.5 or 5).
3. Vacuum source with a pumping speed of 90–150 L/min (*see Note 1*).
4. The 500 Optimization Kit (Biorad). This kit provides the consumables needed for 500 bombardments and contains three different sizes of gold microcarriers (0.6, 1.0, and 1.6  $\mu\text{m}$ ), different rupture disks (ranging from 450 to 2,200 psi), macrocarriers, and stopping screens (*see Note 2*).
5. A Thermomixer.
6. A microtube centrifuge.
7. Petri dishes (50 mm diameter).
8. An on-axis macro-documentation system coupled to epifluorescence illumination.

### 2.2 Media

1. Sterile MS Medium: 4.4 g/L Murashige & Skoog (MS) Basal Medium (SIGMA), 2.3 mM MES Sodium salt, 1 % Sucrose. Dissolved all components in millipore water, adjust pH to 5.8 with KOH and add 0.8 % Agar. Sterilize using standard procedure (121 °C; 0.8 bar; 20 min) and store in the dark at room temperature.
2. Freshly prepared 70 % ethanol.
3. Sterile 50 % glycerol.
4. Fluorescently labeled siRNA duplex (5  $\mu\text{g}/\mu\text{l}$ ) (*see Note 3*).
5. 2.5 M  $\text{CaCl}_2$ .
6. 0.1 M spermidine.
7. 100 % ethanol.

---

## 3 Methods

### 3.1 Design of Specific and Optimal siRNA

Various software has been designed to determine the best siRNA sequence in order to induce efficient silencing of a given target (i.e. [http://www.rnaiweb.com/RNAi/siRNA\\_Design/index.html](http://www.rnaiweb.com/RNAi/siRNA_Design/index.html); <http://www.protocol-online.org/prot/Protocols/Rules-of-siRNA-design-for-RNA-interferenc--NA--210.html>). However, if the purpose of the biolistic delivery of siRNA is solely to score for

movement, the target accessibility of the siRNA is not of prime importance. Nevertheless, we recommend to choose an siRNA duplex where the guide strand sequence starts with a 5'-U in order to optimize loading into AGO1, the cognate effector of RNAi in plants [6].

In order to monitor directly siRNA movement in planta, one of the two strands of the siRNA duplex has to be covalently labeled at its 3'-end with the fluorophore ALEXA555 (e.g. Life Technologies). This dye can be detected using standard filter sets designed for Alexa Fluor® 555, Cy®3, DsRed, Texas Red®, or rhodamine fluorophores. We recommend labeling the passenger strand rather than the guide strand. Although this is not mandatory to score siRNA movement, as it most likely occurs under its duplexed form, this considerably increases the efficiency of the siRNA-triggered silencing, presumably because the ALEXA555 dye prevents optimal loading of guide-strands into AGOs. Annealing of the siRNA passenger strand to the guide strand is performed by the company to which they are purchased.

Fluorescently labeled siRNA duplexes (*see Note 3*) should be resuspended at a final concentration of 5 µg/µl in sterile millipore water and stored at -20 °C.

### **3.2 Preparation of Microcarriers**

This part of the protocol details the preparation of gold microparticles for 140 bombardments using 500 µg of 1.0 µm gold particles per bombardment, based on the method of Sanford and colleagues [7].

1. Weigh out 70 mg of 1.0 µm gold microparticles and transfer into a 1.5 ml microcentrifuge tube.
2. Add 1 ml of freshly prepared 70 % ethanol (v/v) and vortex the tube continuously for 3–5 min at room temperature (RT) on a ThermoMixer at 1,400 revolutions per minute (rpm).
3. Incubate the particles for 15 min in 70 % ethanol.
4. Pellet the microparticles by spinning for 30 s at 1,000 rpm (100 relative centrifugal force, rcf).
5. Remove and discard the supernatant.
6. Repeat the following steps three times:
  - (a) Add 1 ml of sterile millipore water and vortex at RT for 1 min on a Thermomixer (1,400 rpm).
  - (b) Allow the microparticles to settle for 1 min.
  - (c) Pellet the microparticles by spinning for 30 s at 1,000 rpm.
  - (d) Remove and discard the supernatant.
7. After the third wash, add sterile 50 % glycerol to bring the microparticle concentration to 120 mg/ml and store the particles at -20 °C. At this temperature, the microparticles can be stored for up to 2 years.

### **3.3 Coating Microcarriers with siRNA Duplex and Preparing Macrocarriers**

This part of the protocol details the procedure to prepare microcarriers for six bombardments. If fewer or more bombardments are needed, reduce or increase all volumes proportionally.

1. Vortex the microcarriers prepared in 50 % glycerol continuously for 3–5 min at RT on a ThermoMixer at 1,400 rpm, to maximize uniform sampling and disrupt agglomerated particles (*see Note 4*).
2. Remove 25  $\mu$ l (3 mg) of microcarriers and transfer to a 1.5 ml microcentrifuge tube.
3. While vortexing continuously on a ThermoMixer (*see Note 5*), add in order to the aliquots of microcarriers:
  - (a) 6  $\mu$ l of fluorescently labeled siRNA duplex (5  $\mu$ g/ $\mu$ l).
  - (b) 25  $\mu$ l 2.5 M  $\text{CaCl}_2$ .
  - (c) 10  $\mu$ l 0.1 M spermidine.
4. When all components are added, continue vortexing for 3–5 min.
5. Allow the microcarriers to settle for 1 min.
6. Pellet the microcarriers by spinning for 30 s at 100 rcf.
7. Remove and discard the supernatant.
8. Add 300  $\mu$ l of freshly prepared 70 % ethanol without disturbing the pellet of microcarriers.
9. Remove the liquid and discard.
10. Add 300  $\mu$ l of 100 % ethanol without disturbing the pellet.
11. Remove the liquid and discard.
12. Add 48  $\mu$ l of 100 % ethanol.
13. Gently resuspend the pellet by tapping the side of the tube several times or by pipetting up and down.
14. Remove 8  $\mu$ l aliquots of microcarriers (approximately 500  $\mu$ g) and spread evenly over the central 1 cm of the macrocarrier using the pipette tip (*see Note 6*).
15. Air dry for 10 min to evaporate the ethanol and leave the siRNA-coated microcarriers adhering to the macrocarrier. Alternatively, use a small desiccating chamber (containing  $\text{CaCl}_2$  as desiccant). The macrocarriers must be used within the 6 h following their preparation.

### **3.4 Sowing the Biological Material for Bombardment**

1. Pour 8 ml of MS medium in 50 mm petri dishes.
2. Plate around 50 seeds of *Arabidopsis thaliana* per dish, after classical sterilization procedure (*see Note 7*). We recommend sowing the seeds in the gray ring depicted in Fig. 1 (*see Note 8*).
3. Leave the seedlings to grow in vitro for at least 12–15 days after germination before using them for bombardment.

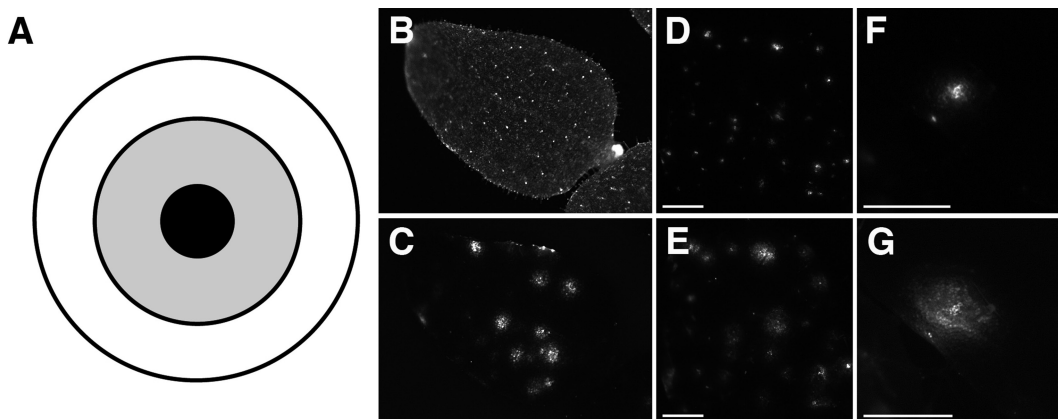


**Fig. 1** (a) Cartoon target for 50 mm petri dishes. Plants in the *central dark zone* are usually highly damaged due to the high velocity of the microparticles in this area. Plants in the *gray zone* display a high number of transformation events. Plants in the *white zone* display rare and more isolated transformation events. (b and c) Leaf of GFP-expressing *Nicotiana benthamiana* line bombarded with ALEXA555-labeled siRNA duplex and visualized using either the GFP (b) or the Alexa555 (c) filter set at 20 h post-bombardment (hpb). (d and e) *Arabidopsis* Col-0 leaf bombarded with ALEXA555-labeled siRNA duplex at 1 hpb (d) and 20 hpb (e). Reproduced from [2]. (f and g) Same as in (d) and (e) but at higher magnification. Reproduced from [3]. Scale bars: 500  $\mu\text{m}$  for (d) and (e); 200  $\mu\text{m}$  for (f) and (g)

### 3.5 Biolistic Transformation and Observation

1. Load sterile rupture disk, macrocarrier, and stopping screen into microcarrier launch assembly of the PDS-1000/He<sup>TM</sup> particle delivery system (*see Note 9*).
2. Place microcarrier launch assembly and petri dish into the chamber (*see Note 10*) and close the door.
3. Establish vacuum at desired level (*see Note 1*).
4. Press Fire button continuously until rupture disk bursts to bombard sample.
5. Release Fire button and release slowly vacuum from chamber (*see Note 11*).
6. Shortly after bombardment, place the seedlings under an on-axis macro-documentation system coupled to epifluorescence illumination for imaging of initially bombarded cells. In order to have enough time for proper imaging of 5–10 independent events, we recommend performing each bombardment with at least 30 min intervals.
7. Put back the bombarded plates to the same in vitro growth conditions until the next time point. We usually monitor spreading of siRNA after 3 h, 6 h and 20 h post bombardment (Fig. 1).

## 4 Notes

1. This pumping speed is required in order to minimize the time target cells are exposed to vacuum and to provide a vacuum level of 0.3 Bar.
2. After optimal conditions are determined, Standard Pressure Kits may be used.
3. Fluorescently labeled siRNA duplexes can be obtained directly from companies such as Life Technologies, ThermoScientific, or Qiagen.
4. When removing aliquots of microcarriers, it is important to vortex the tube containing the microcarriers continuously in order to maximize uniform sampling. To do so, hold the microcentrifuge tube firmly at the top while constantly vortexing the base of the tube.
5. Continuous agitation of the microcarriers is needed for uniform siRNA precipitation onto microcarriers. Alternatively, the various component can be quickly added to an aliquot of non-vortexed microcarriers if the aliquot is continuously vortexed for 1 min before and after each addition.
6. Pipet from a continuously vortexed tube and rapidly apply suspended microcarriers to the macrocarrier, as microcarriers quickly settle out from the ethanol solution in the tube or even in the pipette tip.
7. For sterilization, immerse the seeds in 70 % Ethanol for 2 min. After removing the Ethanol, add 4 % hypochlorite and put on a rotator for 15 min. Remove hypochlorite and wash the seeds four times with sterile water. Plate the seeds on Petri dishes.
8. We recommend sowing the seeds in the gray area depicted in Fig. 1, where the optimal number of transformation events occurs. Plants presents in the central dark zone are usually either damaged by the higher velocity of the microcarriers in this area, or present too many transformation events such that spreading of siRNA from an initially bombarded cell to the neighboring cells is almost impossible to score. Plants grown in the white area (or leaves present in this white area from plants grown in the gray area) usually display much less transformation events which can be useful to identify clearly isolated bombarded cells.
9. The day of the bombardment, sterilize with 70 % ethanol all components of the PDS-1000/He<sup>TM</sup> particle delivery system followed by drying, just prior to use.
10. For 12–15-days-old *Arabidopsis thaliana* seedlings, preliminary experiments had revealed that the optimal starting conditions are the following: Helium pressure of 1,300 psi,

1.0  $\mu\text{m}$  diameter gold particles, 1,350 psi rupture disks, target plate shelf at position 3 from the bottom of the PDS-1000/He<sup>TM</sup> particle delivery system. However, it should be noted that if the bombardment has to be performed on a different type of plant material, further optimization might be required.

11. A detailed protocol to perform a bombardment using the PDS-1000/He<sup>TM</sup> particle delivery system can be found at the following URL: <http://www.bio-rad.com/webroot/web/pdf/lsr/literature/M1652249LEASE.pdf>.

---

## Acknowledgments

This work was supported by a research grant from the Agence Nationale pour la Recherche (ANR-10-LABX-36) and the Bettencourt-Schueller foundation.

## References

1. Baulcombe DC (2004) RNA silencing in plants. *Nature* 431:356–363
2. Dunoyer P, Schott G, Himber C et al (2010) Small RNA duplexes function as mobile silencing signals between plant cells. *Science* 328:912–916
3. Dunoyer P, Brosnan CA, Schott G et al (2010) An endogenous, systemic RNAi pathway in plants. *EMBO J* 29:1699–1712
4. Molnar A, Melnyk CW, Bassett A et al (2010) Small silencing RNAs in plants are mobile and direct epigenetic modification in recipient cells. *Science* 328:872–875
5. Voinnet O, Vain P, Angell S, Baulcombe DC (1998) Systemic spread of sequence-specific transgene RNA degradation in plants is initiated by localized introduction of ectopic promoter-less DNA. *Cell* 95:177–187
6. Kim VN (2008) Sorting out small RNAs. *Cell* 133:25–26
7. Sanford JC, Smith FD, Russell JA (1993) Optimizing the biolistic process for different biological applications. *Methods Enzymol* 217: 483–509



## Analysis of the Role of Myosins in Targeting Proteins to Plasmodesmata

Martin Di Donato and Khalid Amari

### Abstract

Plasmodesmata (PD) are dynamic cell wall microchannels that facilitate the intercellular trafficking of RNA and protein macromolecules playing cell nonautonomous roles in the orchestration of plant development, growth, and plant defense. The trafficking of macromolecules and organelles within cells depends on cytoskeletal components and their associated motor proteins. Plant viruses evolved to hijack this transport system to move their infectious genomes to PD. Current efforts concentrate on dissecting the role of specific myosin motors in transporting plant or viral proteins to the channels. Here we describe a method that addresses the role of specific myosins by expression of myosin tails that cause the repression of myosin activity in a dominant-negative manner. As an example, we explain the use of myosin tails from *Nicotiana benthamiana* to address the role of *N. benthamiana* myosins in the targeting of PLASMODESMATA-LOCATED PROTEIN 1 (PDLPI) to PD.

**Key words** Plasmodesmata, Myosin, Dominant-negative inhibition, Myosin tails, *Nicotiana benthamiana*, PLASMODESMATA LOCATED PROTEIN 1

---

### 1 Introduction

Plasmodesmata (PD) are dynamic, highly organized, plasma membrane (PM)-lined microchannels that connect adjacent cells through the plant cell walls. The PD channel is spanned by the desmotubule, which connects the ER network of adjacent cells [1]. Actin and myosin are detected along the length of PD and may be involved in maintenance of the curvature of the desmotubular ER membrane and in tethering the desmotubule to the plasma membrane (PM) [2–7]. Transport through PD involves the passive diffusion of water and solutes, and also includes the selective trafficking of endogenous macromolecules such as non-cell-autonomous proteins (NCAPs), short RNAs (sRNAs), and mRNAs, playing an important role as intercellular signaling messengers during plant development and pathogen defense [8–11]. Thus, studying the trafficking of host and pathogen proteins and RNAs to and through

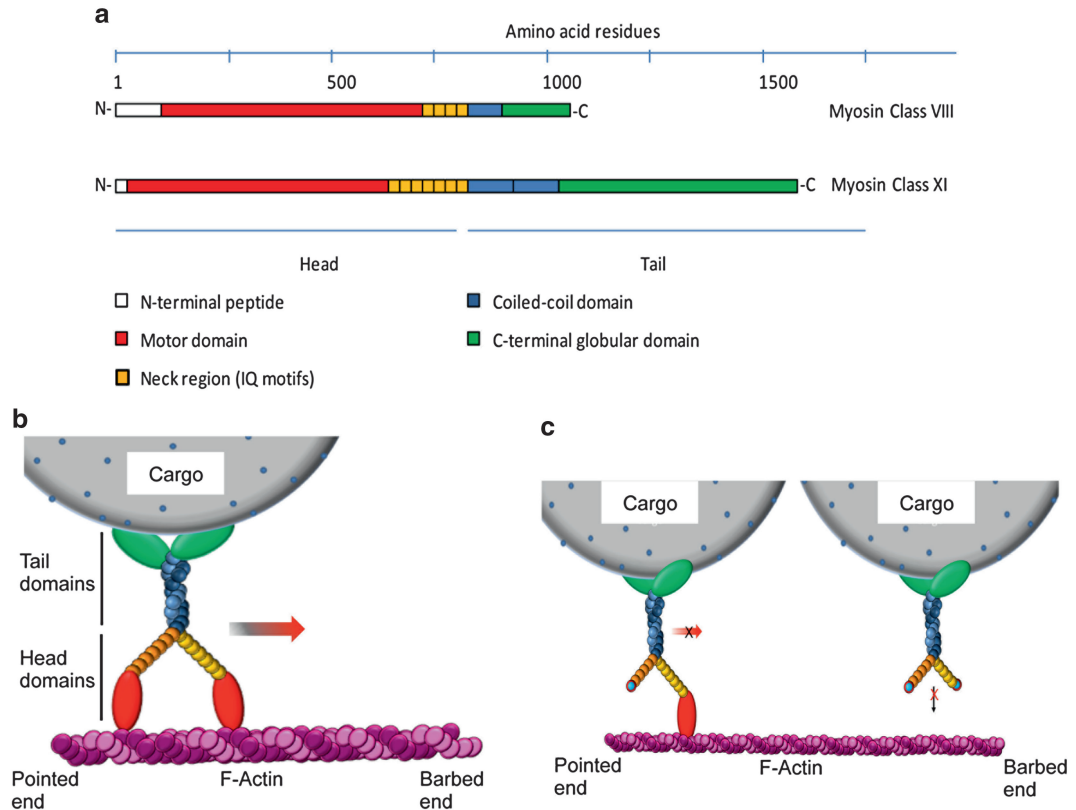


**Fig. 1** (a) Schematic domain structure of plant class VIII and XI myosins. Myosin head domains: N-terminal peptide containing a PEST motif in case of myosins VIII and a SH-3-like domain in case of myosins XI; Motor domain with ATPase activity; Neck region with IQ motifs. Myosin tail domains:  $\alpha$ -helical coiled-coil domain; C-terminal globular domain containing a DILUTE motif in class XI myosins. (b) Myosins dimerize and transport cargo along F-actin filaments in direction towards the barbed (+) end. (c) Dominant-negative repression of myosin action by expression of myosin tails. The molecular mechanism by which myosin tails repress the action of endogenous myosins is not known. The proposed model predicts the formation of heterodimers with endogenous myosins, thus inhibiting the trafficking of cargo along F-actin (*left*), and the formation of tail homodimers competing with endogenous myosins for cargo-binding and sequestering cargo away from F-actin (*right*) [34]

PD is central to our understanding of intercellular communication. The mechanisms used by proteins and viral pathogens to target PD involve the actomyosin system, which is known to play important roles in the intracellular transport of vesicles and organelles as well as in endocytosis [12–18]. Myosins consist of an N-terminal motor domain, a neck region containing several IQ tandem repeats, and C-terminal coiled-coil and globular domains (Fig. 1a). The N-terminal motor domain and adjacent neck region are referred to as myosin head, whereas the C-terminal domains form the myosin tail (Fig. 1b). The myosin motor domain has ATPase activity and is responsible for binding to and translocation along actin filaments.

The neck region is the site of interaction with myosin light chains (e.g. calmodulin) that have a regulatory function [19, 20]. The tail domains are responsible for dimerization of myosins and cargo binding. The *Arabidopsis* genome encodes 17 myosins that are clustered into 4 class VIII myosins and 13 class XI myosins [21–24]. Class VIII myosins are involved in cell plate formation, endocytosis, and intercellular trafficking of plant viruses through PD [5, 25–28], whereas class XI myosins have been suggested to be involved in cytokinesis, organelle, and vesicle trafficking, normal ER shape and dynamics, cytoplasmic streaming and virus movement [23, 29–41]. To study the role of myosins in the intra- and intercellular transport of molecules, the myosin inhibitor BDM (2,3-butanedione 2-monoxime), which inhibits myosin ATPase activity, has been used [42, 43]. However, the inhibitory effect of BDM is not specific to individual myosins or a specific class of myosins, and could affect also other cellular activities requiring ATPase activity. Thus, to investigate the role of myosins in trafficking by more specific methods, silencing of individual myosins by virus-induced gene silencing or the analysis of myosin-specific knockout mutants have been used [31, 44]. However, due to the functional redundancy of myosins [32, 34, 45–47] the effects of silencing or knock-out of specific members of the myosin families may be complemented by other myosins fulfilling the same function and therefore may fail to reveal the potential involvement of myosins with such redundant roles. A method that avoids this redundancy problem is dominant-negative inhibition. In contrast to the inhibition of specific myosins by silencing or mutation, dominant-negative myosin inhibition occurs upon expression of myosin tails, which are still able to interact with cargo but lack the actin-interacting motor domain [26, 40] (Fig. 1c). Myosin tails compete with the functional myosins for cargo binding and thus inhibit myosins sharing the same cargo transport specificity. Moreover, dominant inhibition is thought to occur also by formation of nonfunctional heterodimers with the respective functional myosins [26]. Because of these dominant inhibitory effects, the expression of myosin tails is the method of choice for inhibition of myosins that share redundant functions in a specific biological process.

The present protocol describes the use of myosin tails for the dominant-negative repression of myosins and for identifying the role of myosins in the targeting of a protein to PD. As an example for a PD-targeted protein we use the *Arabidopsis* PLASMODESMATA LOCATED PROTEIN 1 (PDLPI) [48] fused to the green fluorescent protein (GFP) [39, 40]. The protocol can be used to study the role of myosins in the PD-targeting of any protein.

---

## 2 Materials

### 2.1 Transient Expression of PDL1:GFP, RFP and Myosin Tails in *N. benthamiana*

1. Five-weeks-old *N. benthamiana* plants (*see* **Note 1**).
2. *Agrobacterium tumefaciens* strain LBA4404 (Life Technologies) carrying a plasmid for expression of PDL1:GFP (or your protein of interest fused to a fluorescent protein).
3. *Agrobacterium tumefaciens* strain C58 GV2260 cells carrying plasmids for expression of different *N. benthamiana* class VIII and class XI myosin tails tagged with hemagglutinin (HA) [26].
4. *Agrobacterium tumefaciens* strain LBA4404 (Life Technologies) carrying a plasmid for expression of RFP or GFP (for control experiments).
5. LB medium: 10 g/l tryptone, 5 g/l yeast extract, 10 g/l NaCl. Adjust the pH to 7. Before use, add appropriate antibiotics for selective growth of the agrobacteria (*see* **Note 2**).
6. Syringes (2 ml).
7. Rotary shaker.
8. Table-top centrifuge.
9. Spectrophotometer.

### 2.2 Confocal Laser Scanning Microscopy

1. Desiccator connected to a vacuum pump (optional).
2. Microscope slides and cover slips.
3. Sticky tape.
4. Confocal microscope.

### 2.3 Immunoblot Analysis

1. Protein extraction buffer: 10 % glycerol, 5 % 2-mercaptoethanol, and 2 % SDS in 75 mM Tris-HCl, pH 6.8.
2. 2× sample buffer: 4 % SDS, 10 % 2-mercaptoethanol, 20 % glycerol, 125 mM Tris-HCl, pH 6.8, 0.005 % bromophenol blue. Adjust the pH to 6.8.
3. Immobilon-P PVDF-membrane (Millipore).
4. TBS: 50 mM Tris-HCl pH 7.4, 150 mM NaCl.
5. TBS-Tween: TBS containing 0.1 % Tween-20.
6. Blocking buffer: TBS-Tween containing 5 % skimmed milk powder.
7. Primary antibodies: rat-monoclonal anti-HA (Roche).
8. Secondary antibodies: peroxidase-labeled anti-mouse IgG developed in goat (Invitrogen).
9. Lumi-Light<sup>Plus</sup> Western blotting substrate (Roche).
10. Water bath.
11. BioRad mini-protean system.

12. BioRad mini-trans-blot electrophoretic transfer cell.
13. Power supply system (BioRad).
14. Film-developing machine or chemiluminescence detection system.

---

### 3 Methods

#### **3.1 Transient Agrobacterium-Mediated Expression of PDLP1:GFP, RFP and Myosin Tails in *N. benthamiana***

1. Inoculate liquid cultures of Agrobacteria carrying plasmids for the expression of myosin tails, PDLP1:GFP and RFP control, respectively, in 5 ml LB medium containing the appropriate antibiotics and grow the cultures overnight at 28 °C on a rotary shaker at 180 rpm.
2. Centrifuge the cultures for 5 min at  $4,000 \times g$  and resuspend the pelleted cells in 5 ml sterile, double distilled water (*see Note 3*). Measure the OD<sub>600</sub> and dilute the cells with sterile, double distilled water to an OD<sub>600</sub> of 0.3 for PDLP1:GFP- and RFP-expressing bacteria, and to an OD<sub>600</sub> of 0.4–0.5 for bacteria expressing myosin tails (*see Note 4*).
3. Mix the diluted Agrobacterium suspension for PDLP1:GFP at a ratio of 1:1 with the diluted Agrobacterium suspensions for the myosin tail to be tested or RFP control, respectively.
4. For each agroinfiltration experiment, use a yellow Eppendorf micropipette tip or a needle to pierce a *N. benthamiana* leaf from the abaxial side (*see Note 5*).
5. Place a 2 ml syringe (without needle) filled with the respective bacterial suspension on top of the pierced leaf surface and carefully inject the bacterial suspension into the abaxial air space of the leaves (*see Note 6*).
6. After infiltration, keep the plants in a growth chamber or in a greenhouse with 16/8 h day/night illumination, a temperature of approximately 22/18 °C, and approximately 70 % humidity.

#### **3.2 Confocal Laser Scanning Microscopy to Study the Subcellular Localization of PDLP1:GFP in the Presence of RFP or Myosin Tails**

Leaf samples expressing PDLP1:GFP together with RFP or myosin tails should be prepared for confocal microscopy at 24–48 h post infiltration (*see Note 7*).

1. Mount leaf disc samples (*see Note 8*) on a microscope slide with the adaxial side facing the glass and cover with a cover slip.
2. Fix the cover slip to the microscope slide with sticky tape.
3. Use a pipet to fill the space between the glass slide and the cover slip with double-distilled water, so that the leaf disc is fully immersed in water.

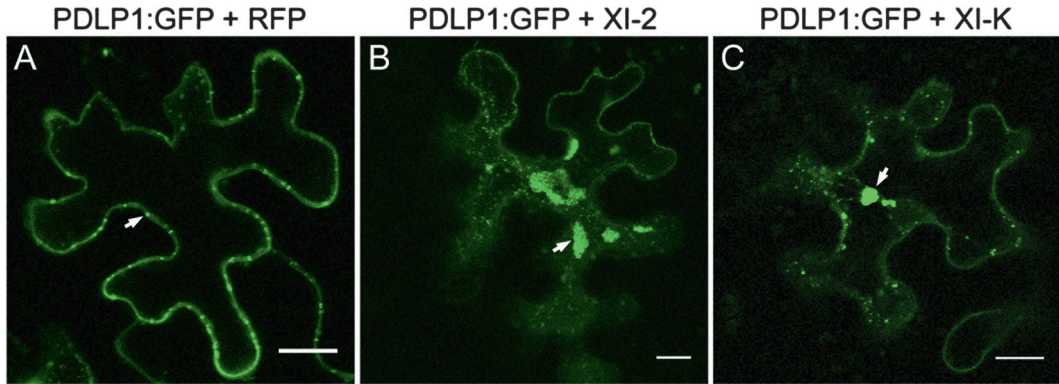


**Fig. 2** Effect of the expression of myosin tails on the targeting of PDL1:GFP to PD. (a) Coexpression of PDL1:GFP together with RFP displays normal PD localization of PDL1:GFP (arrow). A similar result was observed upon expression of PDL1:GFP together with myosins XI-F, VIII-1, VIII-2, or VIII-B tails. (b and c) Coexpression of PDL1:GFP with myosin XI-2 tails (b) or myosin XI-K tails (c) disrupts the PD localization of PDL1:GFP leading to the formation of PDL1:GFP-containing aggregates (arrows). Scale bars, 20  $\mu$ m

4. Place the microscope slide into a vacuum desiccator connected to a vacuum pump to replace the air within intercellular spaces with water (*see Note 9*).
5. Observe PD-localization of PDL1:GFP in the presence of RFP or myosin tails, in epidermal cells using a confocal microscope (*see Note 10* and Fig. 2).

### 3.3 Immunoblot Analysis to Verify Expression of Myosin Tails

To confirm that the observed effects on PD-localization of PDL1:GFP are indeed due to myosin tail expression, an immunoblot analysis with anti-HA antibodies should be performed (Fig. 3). Leaf material for immunoblot analysis must be taken from the same half leaves that were also used for confocal microscopy.

1. Homogenize 100 mg of plant material with Mortar and Pestle in 150  $\mu$ l protein extraction buffer.
2. Add 150  $\mu$ l 2 $\times$  sample buffer, vortex for 10 s and centrifuge at 12,000 rpm 13,400 $\times g$  for 3 min at 4  $^{\circ}$ C.
3. Transfer the supernatant into a new tube and boil for 5 min at 95  $^{\circ}$ C in a water bath.
4. Separate 20  $\mu$ l of protein extract by SDS-PAGE using a 12.5 % polyacrylamide gel.
5. Use the electrophoretic transfer cell to transfer the proteins from the gel onto a PVDF membrane for 1.5 h at 80 V at 4  $^{\circ}$ C.
6. Incubate the membrane at room temperature for 2–3 h in blocking buffer with continuous shaking on a rotary shaker at room temperature.
7. Discard the blocking buffer and incubate the membrane over night at 4  $^{\circ}$ C in TBS-Tween containing primary anti-HA antibody (1:1,000).

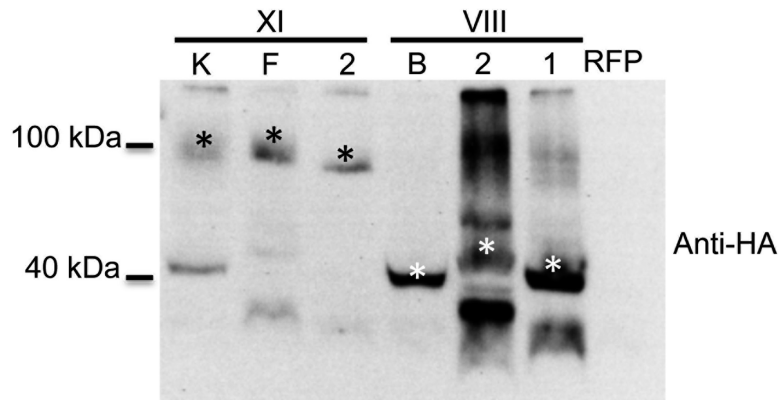


**Fig. 3** Example of an immunoblot analysis of myosin tail accumulation using anti-HA antibodies. In agreement with the calculated size of myosin XI tails, extracts from half leaves infiltrated with PDLP1:GFP and myosin XI tails (XI-K, XI-F, XI-2) contained immunoreactive bands corresponding to protein sizes of approximately 100 kDa (*black asterisks*). Similarly, bands reflecting proteins of around 40 kDa correspond to the expected size of myosin VIII-B, VIII-2, and VIII-1 tails were detected in extracts of half leaves expressing PDLP1:GFP together with these respective proteins (*white asterisks*). No myosin tail-specific signal was detected in half leaves expressing PDLP1:GFP together with RFP

8. Remove the primary antibody and wash the membrane four times for 5 min with TBS-Tween at room temperature.
9. Incubate the membrane for 1 h at room temperature with the secondary antibody (1:10,000) in TBS-Tween containing 2.5 % skimmed milk powder.
10. Remove the secondary antibody and wash the membrane four times for 5 min with TBS-Tween at room temperature.
11. Bath the membrane in western blotting substrate and observe the protein bands after exposing of an X-ray film or other bioilluminescent detection system.

## 4 Notes

1. Use 5-weeks-old plants of similar size, grown and maintained under identical conditions.
2. Prepare Stock solutions of the antibiotics at 100 mg/ml in the solvent indicated on the antibiotics bottle. Dilute Rifampicin 1:1,000 into the LB-medium to a final concentration of 100 µg/ml. Dilute Spectinomycin (PDLP1:GFP) and Kanamycin (Myosin tails, RFP) 1:2,000 into the LB-medium to a final concentration of 50 µg/ml.
3. For accurate measurement of the bacterial titer by spectrophotometry ( $OD_{600nm}$ ) and to facilitate the injection of the bacteria

into plant tissues, it is important to resuspend the bacteria pellet by careful pipetting until all bacterial aggregates are dissolved.

4. Since myosin tails are not highly expressed, the use of a high concentration of agrobacteria for tissue infiltration ( $OD_{600nm}$  of 0.5) improves the myosin tail expression level required to obtain the dominant-negative effect.
5. Leaves of approximately 5-weeks-old *N. benthamiana* plants that are about to be fully expanded are best suited for agroinfiltration. Younger, expanding leaves usually do not permit easy infiltration of the whole leaf area and older leaves yield only low protein expression levels.
6. To avoid the outcome to be influenced by leaf size or the position of leaf infiltration, infiltrate halves of the same leaf, i.e. one half leaf with PDLP1:GFP and RFP and the other half with PDLP1:GFP and the specific myosin tail. In each respective case, avoid the spreading of the agrobacteria across the midrib and the contamination of the other leaf half. To avoid the spreading across the midrib, inject the bacteria close to the leaf borders and allow the solution with bacteria to slowly spread to near the midrib.
7. In the case of PDLP1:GFP, expression and localization of the protein is observable at 24 h post infiltration. In the case of myosin tails, immunoblot analysis indicates that these proteins reach a maximum expression level after 48 h. Thus, studying the subcellular localization of your protein of interest in the presence of myosin tails must be accomplished within 48 h after infiltration of the myosin tails, and should be initiated at 24 h after infiltration, depending on the expression level of your protein. In the case that the expression of your protein requires longer than 48 h, the agroinfiltrations for expression of myosin tails could be performed separately, thus some time after infiltration of the bacteria expressing your protein. In any case, it should be taken into account that myosin tails inhibit myosins most efficiently between 24 h and 48 h post infiltration.
8. Leaf disks must not be harvested from the region close to the midrib to avoid cross contaminations.
9. Water-infiltration of the leaf disc before microscopy is optional and optimized for water-immersion lenses. It reduces the diffraction index of the light when passing through the different media (objective—water—cover slip glass—water) before it reaches the sample. For infiltration, switch on the vacuum pump, open the valve to generate a vacuum inside the desiccator until air exits from intercellular spaces and air bubbles are observed. The time for infiltration may vary and depends on the strength of the vacuum pump and the size of the desiccator used. Once no more air bubbles are formed, close the

valve, switch off the vacuum pump, disconnect the pump from the desiccator and slowly open the valve to release the vacuum. You will see that water enters the previously air-filled spaces in the leaf disc.

10. We used a Zeiss LSM780 laser scanning confocal microscope under multitrack mode and with excitation/emission wavelengths of 488 nm/505–545 nm for GFP and 543 nm/585–615 nm for RFP.

---

## Acknowledgements

Our work was supported by a postdoctoral fellowship grant from the Zurich-Basel Plant Science Center and a grant from the Swiss National science Foundation (SNF 31003A\_140694) to Manfred Heinlein. We thank Manfred Heinlein for supporting us in contributing this chapter and for his critical comments on the manuscript. We also thank Annette Niehl for critical reading of the manuscript. We thank Valerian Dolja for provision of binary expression vectors encoding HA-tagged *N. benthamiana* myosin tails.

## References

1. Ding B, Turgeon R, Parthasarathy MV (1992) Substructure of freeze-substituted plasmodesmata. *Protoplasma* 169:28–41
2. Radford JE, White RG (1998) Localization of a myosin-like protein to plasmodesmata. *Plant J* 14:743–750
3. Blackman LM, Overall RL (1998) Immunolocalisation of the cytoskeleton to plasmodesmata of *Chara corallina*. *Plant J* 14:733–741
4. White RG, Badelt K, Overall RL et al (1994) Actin associated with plasmodesmata. *Protoplasma* 180:169–184
5. Reichelt S, Knight AE, Hodge TP et al (1999) Characterization of the unconventional myosin VIII in plant cells and its localization at the post-cytokinetic cell wall. *Plant J* 19:555–567
6. White RG, Barton DA (2011) The cytoskeleton in plasmodesmata: a role in intercellular transport? *J Exp Bot* 62:5249–5266
7. Tilsner J, Amari K, Torrance L (2011) Plasmodesmata viewed as specialized membrane adhesion sites. *Protoplasma* 248:39–60
8. Heinlein M, Epel BL (2004) Macromolecular transport and signaling through plasmodesmata. *Int Rev Cytol* 235:93–164
9. Cilia ML, Jackson D (2004) Plasmodesmata form and function. *Curr Opin Cell Biol* 16:500–506
10. Vionnet O (2005) Non-cell autonomous RNA silencing. *FEBS Lett* 579:5858–5871
11. Maule AJ, Benitez-Alfonso Y, Faulkner C (2011) Plasmodesmata-membrane tunnels with attitude. *Curr Opin Plant Biol* 14:683–690
12. Mollenhauer HH, Morre DJ (1976) Cytochalasin B, but not colchicine, inhibits migration of secretory vesicles in root tips of maize. *Protoplasma* 87:39–48
13. Picton JM, Steer MW (1981) Determination of secretory vesicle production rates by dictyosomes in pollen tubes of *Tradescantia* using cytochalasin D. *J Cell Sci* 49:261–272
14. Picton JM, Steer MW (1983) Membrane recycling and the control of secretory activity in pollen tubes. *J Cell Sci* 63:303–310
15. Nebenführ A, Staehelin LA (2001) Mobile factories: Golgi dynamics in plant cells. *Trends Plant Sci* 6:160–167
16. Waller F, Riemann M, Nick P (2002) A role for actin-driven secretion in auxin-induced growth. *Protoplasma* 219:72–81
17. Grebe M, Xu J, Mobius W et al (2003) Arabidopsis sterol endocytosis involves actin-mediated trafficking via ARA6-positive early endosomes. *Curr Biol* 13(16):1378–1387
18. Baluska F, Samaj J, Hlavacka A et al (2004) Actin-dependent fluid-phase endocytosis in

- inner cortex cells of maize root apices. *J Exp Bot* 55:463–473
19. Yokota E, Muto S, Shimmen T (1999) Inhibitory regulation of higher-plant myosin by  $\text{Ca}^{2+}$  ions. *Plant Physiol* 119:231–239
  20. Awata J, Saito K, Shimada K et al (2001) Effects of  $\text{Ca}^{2+}$  and calmodulin on the motile activity of characean myosin in vitro. *Plant Cell Physiol* 42:828–834
  21. Reddy AS, Day IS (2001) Analysis of the myosins encoded in the recently completed *Arabidopsis thaliana* genome sequence. *Genome Biol* 2(7):research0024.1–research0024.17
  22. Foth BJ, Goedecke MC, Soldati D (2006) New insights into myosin evolution and classification. *Proc Natl Acad Sci U S A* 103:3681–3686
  23. Avisar D, Prokhnevsky AI, Makarova KS et al (2008) Myosin XI-K is required for rapid trafficking of Golgi stacks, peroxisomes, and mitochondria in leaf cells of *Nicotiana benthamiana*. *Plant Physiol* 146:1098–1108
  24. Peremyslov VV, Mockler TC, Filichkin SA et al (2011) Expression, splicing, and evolution of the myosin gene family in plants. *Plant Physiol* 155:1191–1204
  25. Baluska F, Cvrckova F, Kendrick-Jones J et al (2001) Sink plasmodesmata as gateways for phloem unloading. Myosin VIII and calreticulin as molecular determinants of sink strength? *Plant Physiol* 126:39–46
  26. Avisar D, Prokhnevsky AI, Dolja VV (2008) Class VIII myosins are required for plasmodesmal localization of a closterovirus Hsp70 homolog. *J Virol* 82:2836–2843
  27. Golomb L, Abu-Abied M, Belausov E et al (2008) Different subcellular localizations and functions of *Arabidopsis* myosin VIII. *BMC Plant Biol* 8:1–13
  28. Sattarzadeh A, Franzen R, Schmelzer E (2008) The *Arabidopsis* class VIII myosin ATM2 is involved in endocytosis. *Cell Motil Cytoskeleton* 65:457–468
  29. Sparkes IA, Teanby NA, Hawes C (2008) Truncated myosin XI tail fusions inhibit peroxisome, Golgi, and mitochondrial movement in tobacco leaf epidermal cells: a genetic tool for the next generation. *J Exp Bot* 59:2499–2512
  30. Prokhnevsky AI, Permyslov VV, Dolja VV (2008) Overlapping functions of the four class XI myosins in *Arabidopsis* growth, root hair elongation, and organelle motility. *Proc Natl Acad Sci U S A* 105:19744–19749
  31. Peremyslov VV, Prokhnevsky AI, Avisar D et al (2008) Two class XI myosins function in organelle trafficking and root hair development in *Arabidopsis*. *Plant Physiol* 146:1109–1116
  32. Peremyslov VV, Prokhnevsky AI, Dolja VV (2010) Class XI myosins are required for development, cell expansion, and F-actin organization in *Arabidopsis*. *Plant Cell* 22:1881–1897
  33. Yokota Y, Ueda H, Hashimoto K et al (2011) Myosin XI-dependent formation of tubular structures from endoplasmic reticulum isolated from tobacco cultured BY-2 cells. *Plant Physiol* 156:129–143
  34. Avisar D, Abu-Abied M, Belausov E et al (2009) A comparative study of the involvement of 17 *Arabidopsis* myosin family members on the motility of Golgi and other organelles. *Plant Physiol* 150:700–709
  35. Avisar D, Abu-Abied M, Belausov E et al (2012) Myosin XIX is a major player in cytoplasm dynamics and is regulated by two amino acids in its tail. *J Exp Bot* 63:241–249
  36. Ueda H, Yokota E, Kutsuna N et al (2010) Myosin dependent endoplasmic reticulum motility and F-actin organization in plant cells. *Proc Natl Acad Sci U S A* 107:6894–6899
  37. Ojangu EL, Jarve K, Paves H et al (2007) *Arabidopsis thaliana* myosin XI-K is involved in root hair as well as trichome morphogenesis on stems and leaves. *Protoplasma* 230:193–202
  38. Sattarzadeh A, Krahmer J, Germain A et al (2009) A myosin XI tail domain homologous to the yeast myosin vacuole-binding domain interacts with plastids and stromules in *Nicotiana benthamiana*. *Mol Plant* 2:1351–1358
  39. Amari K, Boutant E, Hofmann C et al (2010) A family of plasmodesmal proteins with receptor-like properties for plant viral movement proteins. *PLoS Pathog* 6:e1001119. doi:10.1371/journal.ppat.1001119
  40. Amari K, Lerich A, Schmitt-Keichinger C et al (2011) Tubule-guided cell-to-cell movement of a plant virus requires class XI myosin motors. *PLoS Pathog* 7:e1002327. doi:10.1371/journal.ppat.1002327
  41. Feng Z, Chen X, Bao Y et al (2013) Nucleocapsid of *Tomato spotted wilt tospovirus* forms mobile particles that traffic on an actin/endoplasmic reticulum network driven by myosin XI-K. *New Phytol* 200(4):1212–1224. doi:10.1111/nph.12447
  42. Tominaga M, Yokota E, Sonobe S et al (2000) Mechanism of inhibition of cytoplasmic streaming by a myosin inhibitor, 2,3-butanedione monoxime. *Protoplasma* 213:46–54
  43. Funaki K, Nagata A, Akimoto Y et al (2004) The motility of *Chara corallina* myosin was

- inhibited reversibly by 2,3-butanedione monoxime (BDM). *Plant Cell Physiol* 45:1342–1345
44. Harries PA, Park JW, Sasaki N et al (2009) Differing requirements for actin and myosin by plant viruses for sustained intercellular movement. *Proc Natl Acad Sci U S A* 106: 17594–17599
45. Vidali L, Burkart GM, Augustine RC et al (2010) Myosin XI is essential for tip growth in *Physcomitrella patens*. *Plant Cell* 22(6):1868–1882. doi:10.1105/tpc.109.073288
46. Ojangu EL, Tanner K, Pata P et al (2012) Myosins XI-K, XI-1, and XI-2 are required for development of pavement cells, trichomes, and stigmatic papillae in *Arabidopsis*. *BMC Plant Biol* 12:81. doi:10.1186/1471-2229-12-81
47. Park E, Nebenführ A (2013) Myosin XIK of *Arabidopsis thaliana* accumulates at the root hair tip and is required for fast root hair growth. *PLoS One* 8(10):e76745. doi:10.1371/journal.pone.0076745
48. Thomas CL, Bayer EM, Ritzenthaler C et al (2008) Specific targeting of a plasmodesmal protein affecting cell-to-cell communication. *PLoS Biol* 6(1):e7. doi:10.1371/journal.pbio.0060007



## Pumilio-Based RNA In Vivo Imaging

Jens Tilsner

### Abstract

Subcellular, sequence-specific detection of RNA in vivo is a powerful tool to study the macromolecular transport that occurs through plasmodesmata. The RNA-binding domain of Pumilio proteins can be engineered to bind RNA sequences of choice and fused to fluorescent proteins for RNA imaging. This chapter describes the construction of a Pumilio-based imaging system to track the RNA of *Tobacco mosaic virus* in vivo, and practical aspects of RNA live-cell imaging.

**Key words** RNA imaging, Pumilio homology domain, RNA-binding protein, Fluorescence complementation, Protein engineering, Fluorescent protein, Fluorescence microscopy, *Tobacco mosaic virus*

---

### 1 Introduction

Plasmodesmata serve as intercellular conduits for different species of RNA between plant cells, including siRNAs mediating systemic posttranscriptional silencing [1], miRNAs involved in developmental control [2], the infectious genomes of RNA viruses and viroids [3, 4], and cellular mRNAs [5, 6]. Therefore, techniques which permit the sequence-specific, dynamic localization of RNAs in live cells are a valuable tool to study plasmodesmata function. A number of such techniques are now available (reviewed in refs. 7, 8), but in walled plant cells, noninvasive, genetically encoded reporters are most easily applicable. Such systems use sequence-specific RNA-binding proteins (RBPs) fused to fluorescent proteins (FPs), and are best suited to the detection of large RNA species such as viruses and mRNAs. Two classes of RBPs have been employed for generally applicable RNA imaging: bacteriophage-derived peptides that recognize the secondary structure of specific RNA stem-loops (*see* Chapter 21), and the RNA-binding domain of Pumilio proteins.

Pumilio/FBF family (PUF) proteins are a group of sequence-specific RBPs that are ubiquitous in eukaryotes (26 genes in the *Arabidopsis* genome) and often function as translational repressors [9–13]. Their RNA-binding domain, the Pumilio homology

domain (PUMHD), has a modular structure consisting of eight tandem repeats of a trihelical, 36 amino acid Puf motif. Each of these Puf repeats binds one nucleotide (Nt) in an eight-Nt binding motif that has no stable secondary structure. All contacts between the PUMHD and RNA are mediated by three amino acid side chains per Puf repeat, and the RNA bases. Amino acid side chains in positions 12 and 16 of each repeat form hydrogen bonds or van der Waals interactions with the Watson-Crick edge of the RNA base whilst the side chain of amino acid 13 forms a stacking interaction [14]. Because only the interactions at position 12 and 16 are base-specific, the sequence specificity of the PUMHD can be modified with just two amino acid modifications per repeat to bind to an RNA sequence of choice [14–19].

To date, only the PUMHD of human Pumilio1 (HsPUM1-HD) has been used for RNA imaging, but in the future, PUMHDs derived from other PUF proteins may emerge as valuable alternatives and broaden the range of imaging possibilities. Pumilio-based RNA imaging has enabled subcellular detection of the mRNAs of mitochondrial NADH dehydrogenase and  $\beta$ -actin, as well as retroviral RNA in mammalian cultured cells [20–23], and of the genomes of *Tobacco mosaic virus*, *Potato virus X*, and *Turnip mosaic virus* in live plant tissue [24–27]. Of particular relevance to the topic of this volume, Pumilio-based RNA imaging has recently shown that *Potato virus X* is present in membrane structures at the entrances of plasmodesmata that also contain the viral replicase [27].

The advantages of using modified PUMHDs for RNA imaging are (1) untagged, native RNA species expressed from their native genomic context can be localized [20, 21, 24], avoiding both the need to modify the RNA and to introduce expression constructs into the genome; (2) if instead PUMHD recognition sequences are engineered into an RNA as a tag, no extensive secondary structures are introduced which might affect RNA function and localization (though the PUMHD can actually access substantially structured target motifs [18]); (3) PUMHD variants can have 10- to 100-fold higher RNA affinities than stem-loop binding peptides used in alternative RNA imaging systems, thus PUMHD-based imaging is potentially more sensitive.

On the other hand, PUMHD RNA recognition has a degree of promiscuity [28, 29], and eukaryotic cells contain mRNA targets of native Pumilio proteins. Therefore, all Pumilio-based RNA imaging approaches use two PUMHD variants binding to the same target RNA to increase overall specificity and RNA affinity [20, 30]. In the future, artificial PUMHDs with more than eight repeats that recognize longer target sequences may further improve the specificity of Pumilio-based RNA imaging [18, 30].

The adjustable sequence specificity of the PUMHD requires redesign and optimization of Pumilio-based RNA imaging systems for any RNA of interest. Therefore, in the following paragraphs the

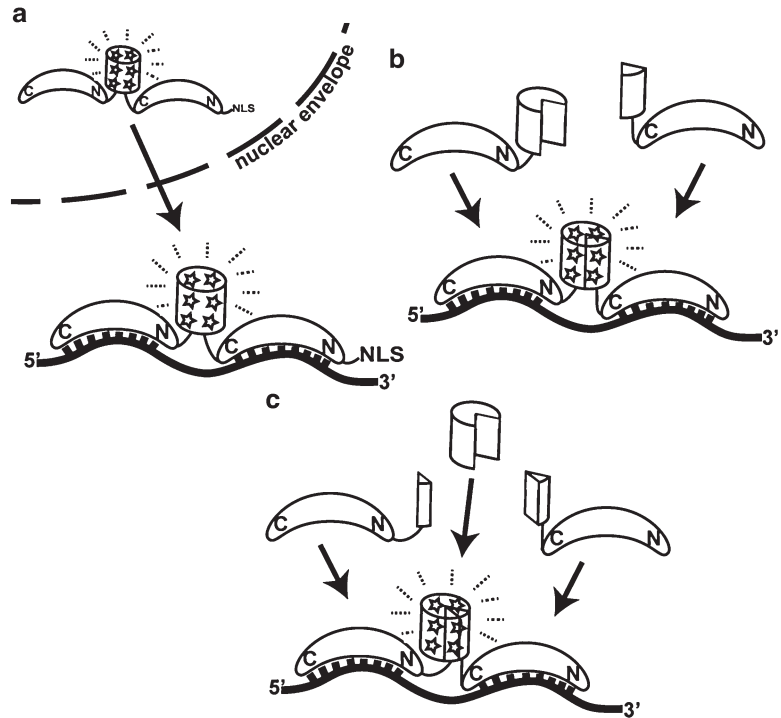


**Fig. 1** Methods to distinguish RNA-bound and unbound PUMHD reporters. (a) Relocalization of a nuclear-targeted, permanently fluorescent double-PUMHD fusion to the cytoplasm in the presence of target RNA [23]. (b) Assembly of a bimolecular fluorescence complementation complex on the target RNA (PUM-BiFC) [20]. This is the approach described in this protocol. (c) Assembly of a tetramolecular fluorescence complementation complex on the target RNA (PUM-TetFC) [33]

considerations that have to be made when designing a PUMHD-based reporter system for a new RNA of interest are discussed, before providing a detailed protocol for imaging a specific RNA, that of *Tobacco mosaic virus* (TMV).

### 1.1 Choice of Reporter System

When using any RBP-FP fusion for RNA imaging, it is necessary to distinguish between the RNA-bound and free states of the reporter, i.e., RNA-dependent signal and RNA-independent background. For PUMHD-based reporters, three different approaches have been used to identify RNA-bound fluorescence (Fig. 1). All systems use two PUMHD variants.

Nuclear targeting of a permanently fluorescent pair of fused PUMHDs (Fig. 1a) leads to confinement of fluorescence in the nucleus in the absence of target RNA. If the reporter is co-exported from the nucleus with a bound RNA, or binds to cytoplasmic RNA after translation, cytoplasmic fluorescence reveals the RNA's location. This approach is routinely used in RNA imaging with stem-loop binding bacteriophage peptides (*see* Chapter 21). Attempts to apply the

same principle to PUMHD-based imaging with two directly coupled PUMHDs fused to an FP and nuclear localization signal (NLS) at their N-terminus (NLS-FP-PUMHD-PUMHD) proved unfeasible in plant cells because the reporter aggregated in the nucleus (unpublished data). However, a fusion with the FP inserted between the PUMHDs (NLS-PUMHD-FP-PUMHD) was recently used in mammalian cells [23] and may also work in plants.

Alternatively, the two PUMHD variants can be fused separately to two halves of a split FP, so that when both fusion proteins bind to the same target RNA, the split FP halves come into close proximity and refold into the complete FP, resulting in bimolecular fluorescence complementation (PUM-BiFC) at the location of the RNA [20, 24] (Fig. 1b). This principle is the only form of Pumilio-based RNA imaging so far applied in plants [24–27].

Unfortunately, PUM-BiFC is not background-free. In BiFC, the fluorescent complex of N- and C-terminal split FP halves is extremely stable [31]. As the BiFC constructs accumulate in a cell, the increasing frequency of random collisions will result in the formation of low levels of reassembled FP, independent of interactions of fused PUMHDs with their cognate RNA. Additionally, due to their stability, PUM-BiFC complexes formed on the target RNA can dissociate from the RNA without “switching off.” Both of these processes lead to the gradual accumulation of false-positive signal and thus reduce the signal-to-noise ratio. RNA-dependent PUM-BiFC signal has to be distinguished from this background by relative fluorescence levels and localization (*see* Subheading 3.3). An additional side effect of RNA-independent formation of PUM-BiFC complexes is that these pre-formed complexes can be recruited to the target RNA by the interaction of only one of the two PUMHDs. Thus, RNAs can be imaged with only a single binding site [24, 25] or when the orientation of PUMHD fusions would be expected to prevent proximity of split FP halves after RNA binding (*see* below) [22]. Whilst this may sometimes be useful, it is not generally desirable, as it reduces the overall specificity of the PUM-BiFC system and eliminates the benefits of using two RNA-binding domains.

Several recently developed approaches that improve the signal-to-noise ratio of BiFC by introducing further modifications into the split FP fragments [31, 32] are still unexplored for PUM-BiFC applications. Also, a tetramolecular fluorescence complementation system for Pumilio-based RNA detection was recently introduced (PUM-TetFC) [33] (Fig. 1c) which has a very high signal-to-noise ratio *in vitro*, but is still untested *in vivo*. In PUM-TetFC, superfolder GFP is split into three fragments, the main  $\beta$ -barrel containing  $\beta$ -sheets 1–9, and the isolated  $\beta$ -sheets 10 and 11, which are fused to the two PUMHD variants (the fourth component of TetFC is the RNA).

In the protocol below, I describe the construction of a PUM-BiFC system as this is the only Pumilio-based approach so far used successfully in plants. However, as fluorescence complementation techniques are being continuously improved, it is recommended to consult relevant recent literature before constructing a novel PUM-BiFC system.

### 1.1.1 Choice of FP

BiFC can be performed with various derivatives of both GFP and red FPs [31, 34–39]. This allows selection of an FP that will facilitate co-localizing the RNA of interest with other fluorescent markers that may already be available. In practice, only the GFP derivatives EGFP, Venus, and mCitrine have so far been used for PUM-BiFC, and of these, only PUMHD-split-mCitrine fusions in plants [20, 24]. PUMHD fusions with split-mRFP1(Q66T) [40] failed to produce fluorescence in preliminary experiments (unpublished data).

### 1.1.2 Choice of FP Splitting Position

Commonly, FPs are split either between  $\beta$ -sheets 7 and 8 (amino acids 154/155 or 157/158) or between  $\beta$ -sheets 8 and 9 (amino acids 172/173) [31, 34]. Both have been employed in PUM-BiFC (EGFP, Venus split at 157/158 [20], mCitrine split at 172/173 [24]). As it is the only PUM-BiFC system used in plants so far, fusions with mCitrine split between amino acids 172/173 are recommended until other split FPs have been tested.

### 1.1.3 Orientation of PUMHD-Split FP Fusions

The PUMHD interacts with RNA in an antiparallel orientation, i.e., the N terminus is oriented towards the 3' and the C terminus towards the 5' end of the target sequence (Fig. 2). This means that the *N terminus of the upstream* and the *C terminus of the downstream* binding PUMHD will be in proximity to each other and have to be fused to the split FP halves. Fusing FP fragments at the opposite ends (C terminus of upstream and N terminus of downstream PUMHD) prevents fluorescence complementation [33]. This leaves two possible choices of fusion orientations: if PUMHDs are fused to the N terminus of the FPN and the C terminus of the FPC fragment, they are attached to the natural termini of the FP. If PUMHDs are fused to the C terminus of FPN and the N terminus of FPC, they are attached to the rim of the FP  $\beta$ -barrel, with splitting positions between  $\beta$ -sheets 7 and 8 or 8 and 9 resulting in fusions to opposite rims of the  $\beta$ -barrel. Both configurations are possible and allow fluorescence complementation. Thus, the constraints imposed by the structures of both the PUMHD and the FP allow for two possible fusion combinations: FPC-PUMHD<sub>upstream</sub> + PUMHD<sub>downstream</sub>-FPN, or FPN-PUMHD<sub>upstream</sub> + PUMHD<sub>downstream</sub>-FPC. Only the latter combination has so far been used in RNA imaging and is therefore the recommended option [20, 21, 24, 33].

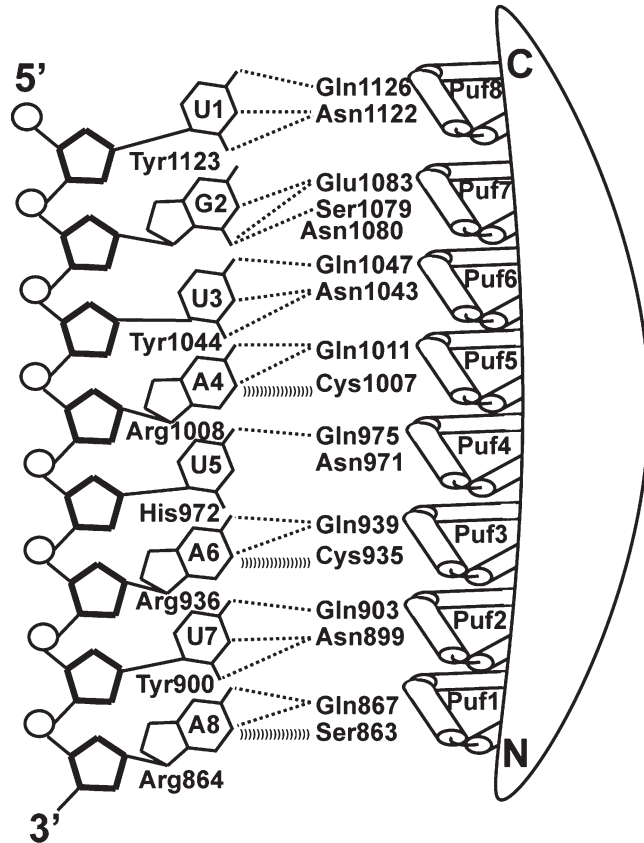


**Fig. 2** Base-specific interactions between the HsPUM1-HD and its target sequence. *Dotted lines* represent hydrogen bonds and *parentheses* represent van der Waals contacts. Modified from [14, 15]

## 1.2 Choice of Target Sequences and PUMHD Variants

PUM-BiFC imaging can be used in two different modes: PUMHDs can be modified to bind to the native RNA of interest [20, 21, 23–25], or the RNA can be tagged with recognition motifs of previously characterized PUMHD variants [22, 24, 26, 27, 33] (Table 1). As described in the introduction, leaving the RNA unmodified has the advantage of avoiding potential RNA processing and localization artifacts that could be caused by a tag, and by the expression of the tagged construct from an artificial genomic context. The latter is mainly a concern with nuclear mRNAs, not viruses. On the other hand, suitable binding sites that can be easily targeted with a limited number of PUMHD modifications may not be present in the RNA of interest, and whilst the binding specificity of modified PUMHDs can be predicted, it is harder to predict effects of modifications on RNA affinity, binding promiscuity, and protein solubility and stability [15]. Such potential problems can be avoided by using an RNA tag recognized by previously characterized PUMHD variants (Table 1), which can also increase specificity. For instance, Kellermann et al. [33] used a combination of

**Table 1**  
**Modified HsPUM1-HD variants**

PUMHD	Puf8	Puf7	Puf6	Puf5	Puf4	Puf3	Puf2	Puf1	References
wild-type	Q112	E108	Q104	Q101					[14,22,24,25,33,52]
	6	3	7	1	Q975	Q939	Q903	Q867	
	Y112	N108	Y104	R100					
	3	0	4	8	H972	R936	Y900	R864	
	N112	S107	N104	C100					
	2	9	3	7	N971	C935	N899	S863	
k <sub>D</sub> = 0.5 nM	U	G	U	A	U/C	A	U	A	
U1C	R112	E108	Q104	Q101					[18]
	6	3	7	1	Q975	Q939	Q903	Q867	
	Y112	N108	Y104	R100					
	3	0	4	8	H972	R936	Y900	R864	
	G11	S107	N104	C100					
	22	9	3	7	N971	C935	N899	S863	
k <sub>D</sub> n.d.	C	G	U	A	U/C	A	U	A	
PUF#2	R112	Q10	E104	Q101					[19]
	6	83	7	1	Q975	Q939	R903	Q867	
	Y112	N108	Y104	R100					
	3	0	4	8	H972	R936	Y900	R864	
	S112	N107	S104	C100					
	2	9	3	7	N971	C935	S899	S863	
k <sub>D</sub> n.d.	C	U	G	A	U/C	A	C	A	

(continued)

**Table 1**  
**(continued)**

<b>PUF-E</b>	<b>E112</b>	<b>R108</b>	Q104	<b>E101</b>				[19]
	<b>6</b>	<b>3</b>	7	<b>1</b>	Q975	Q939	<b>E903</b>	<b>R867</b>
	Y112	<b>Y108</b>	Y104	R100				
	3	<b>0</b>	4	8	H972	R936	Y900	<b>Y864</b>
<b>k<sub>D</sub> n.d.</b>	<b>S112</b>	S107	N104	<b>S100</b>				
	<b>2</b>	9	3	<b>7</b>	<i>N971</i>	<b>N935</b>	<b>S899</b>	S863
	<b>G</b>	<b>C</b>	U	<b>G</b>	U/C	<b>U</b>	<b>G</b>	<b>C</b>
<b>PUF#1</b>	<b>E112</b>	<b>R108</b>	<b>E104</b>	<b>E101</b>				[19]
	<b>6</b>	<b>3</b>	<b>7</b>	<b>1</b>	Q975	<b>E939</b>	Q903	<b>E867</b>
	Y112	<b>Y108</b>	Y104	R100				
	3	<b>0</b>	4	8	H972	R936	Y900	R864
<b>k<sub>D</sub> n.d.</b>	<b>S112</b>	S107	<b>S104</b>	<b>S100</b>			<b>C/S</b>	
	<b>2</b>	9	<b>3</b>	<b>7</b>	<i>N971</i>	<b>S935</b>	<b>899</b>	S863
	<b>G</b>	<b>C</b>	<b>G</b>	<b>G</b>	U/C	<b>G</b>	<b>A</b>	<b>G</b>
<b>Mut7-2</b>	Q112	<b>Q10</b>	Q104	Q101				[15]
	6	<b>83</b>	7	1	Q975	Q939	Q903	Q867
	Y112	N108	Y104	R100				
	3	0	4	8	H972	R936	Y900	R864
<b>k<sub>D</sub> = 6.0 nM</b>	N112	<b>N107</b>	N104	C100				
	2	<b>9</b>	3	7	<i>N971</i>	C935	N899	S863
	U	<b>U</b>	U	A	U/C	A	U	A

(continued)

Table 1  
(continued)

<b>R7(S<sup>N</sup>/<sub>YXX</sub></b>	Q112	<b>R108</b>	Q104	Q101				[19]
<b>R)</b>	6	<b>3</b>	7	1	Q975	Q939	Q903	Q867
	Y112	N/Y	Y104	R100				
	3	1080	4	8	H972	R936	Y900	R864
	N112	S107	N104	C100				
	2	9	3	7	<i>N971</i>	C935	N899	S863
$k_D$ n.d.	U	<b>C</b>	U	A	U/C	A	U	A

<b>G2C</b>	Q112	<b>R108</b>	Q104	Q101				[18]
	6	<b>3</b>	7	1	Q975	Q939	Q903	Q867
	Y112	N108	Y104	R100				
	3	0	4	8	H972	R936	Y900	R864
	N112	<b>G10</b>	N104	C100				
	2	<b>79</b>	3	7	<i>N971</i>	C935	N899	S863
$k_D$ n.d.	U	<b>C</b>	U	A	U/C	A	U	A

<b>Mut6-2/7-2</b>	Q112	<b>Q10</b>	<b>E104</b>	Q101				[15,33,52]
<b>= Var1</b>	6	<b>83</b>	<b>7</b>	1	Q975	Q939	Q903	Q867
	Y112	N108	Y104	R100				
	3	0	4	8	H972	R936	Y900	R864
	N112	<b>N107</b>	<b>S104</b>	C100				
	2	<b>9</b>	<b>3</b>	7	<i>N971</i>	C935	N899	S863
$k_D = 18$ nM	U	<b>U</b>	<b>G</b>	A	U/C	A	U	A

(continued)

**Table 1**  
**(continued)**

<b>Mut7-2/3-1</b>	Q112	<b>Q10</b>	Q104	Q101				[15]
	6	<b>83</b>	7	1	Q975	Q939	Q903	Q867
	Y112	N108	Y104	R100				
	3	0	4	8	H972	R936	Y900	R864
	N112	<b>N107</b>	N104	C100				
	2	<b>9</b>	3	7	<i>N971</i>	<b>N935</b>	N899	S863
	U	<b>U</b>	U	A	U/C	<b>U</b>	U	A
	$k_D = 0.6 \text{ nM}$							
<b>U3A</b>	Q112	E108	Q104	Q101				[18]
	6	3	7	1	Q975	Q939	Q903	Q867
	Y112	N108	Y104	R100				
	3	0	4	8	H972	R936	Y900	R864
	N112	S107	<b>C104</b>	C100				
	2	9	<b>3</b>	7	<i>N971</i>	C935	N899	S863
	U	G	<b>A</b>	A	U/C	A	U	A
	$k_D \text{ n.d.}$							
<b>U3G</b>	Q112	E108	<b>E104</b>	Q101				[18]
	6	3	<b>7</b>	1	Q975	Q939	Q903	Q867
	Y112	N108	Y104	R100				
	3	0	4	8	H972	R936	Y900	R864
	N112	S107	<b>S104</b>	C100				
	2	9	<b>3</b>	7	<i>N971</i>	C935	N899	S863
	U	G	<b>G</b>	A	U/C	A	U	A
	$k_D \text{ n.d.}$							

(continued)

**Table 1**  
**(continued)**

<b>mPum2</b>	Q112	E108	<b>E104</b>	Q101				[14, 20]
	6	3	7	1	Q975	Q939	Q903	Q867
	Y112	N108	<b>N104</b>	R100				
	3	0	4	8	H972	R936	Y900	R864
	N112	S107	<b>S104</b>	C100				
$k_D = 92 \text{ nM}$	2	9	3	7	<i>N971</i>	C935	N899	S863
	U	G	<b>G</b>	A	U/C	A	U	A
<b>R6(S<sup>Y</sup>/<sub>HXX</sub> R)</b>	Q112	E108	<b>R104</b>	Q101				[19]
	6	3	7	1	Q975	Q939	Q903	Q867
	Y112	N108	<b>Y/H</b>	R100				
	3	0	1044	8	H972	R936	Y900	R864
	N112	S107	<b>S104</b>	C100				
$k_D \text{ n.d.}$	2	9	3	7	<i>N971</i>	C935	N899	S863
	U	G	<b>C</b>	A	U/C	A	U	A
<b>U3C</b>	Q112	E108	<b>R104</b>	Q101				[18]
	6	3	7	1	Q975	Q939	Q903	Q867
	Y112	N108	Y104	R100				
	3	0	4	8	H972	R936	Y900	R864
	N112	S107	<b>C</b>	C100				
$k_D \text{ n.d.}$	2	9	<b>1043</b>	7	<i>N971</i>	C935	N899	S863
	U	G	<b>C</b>	A	U/C	A	U	A

(continued)

Table 1  
(continued)

PUF-B	Q112	E108	<b>R104</b>	Q101				[19]
	6	3	7	1	Q975	Q939	Q903	
	Y112	N108	Y104	R100				
	3	0	4	8	H972	R936	Y900	
k <sub>D</sub> n.d.	N112	S107	<b>S104</b>	<b>N100</b>				
	2	9	3	7	<i>N971</i>	C935	N899	
	U	G	<b>C</b>	<b>U</b>	U/C	A	U	
PUF-C	Q112	E108	<b>R104</b>	Q101				[19]
	6	3	7	1	Q975	<b>R939</b>	Q903	
	Y112	N108	Y104	R100				
	3	0	4	8	H972	<b>Y936</b>	Y900	
k <sub>D</sub> n.d.	N112	S107	<b>S104</b>	<b>N100</b>				
	2	9	3	7	<i>N971</i>	<b>S935</b>	N899	
	U	G	<b>C</b>	<b>U</b>	U/C	<b>C</b>	U	
mPum1	Q112	E108	Q104	Q101				[20]
	6	3	7	1	<b>S975</b>	<b>E939</b>	Q903	
	Y112	N108	<b>N104</b>	R100				
	3	0	4	8	H972	R936	Y900	
k <sub>D</sub> = 163	N112	S107	<b>C104</b>	<b>N100</b>				
	2	9	3	7	<i>N971</i>	<b>S935</b>	N899	
nM	U	G	<b>A</b>	<b>U</b>	<b>G</b>	<b>G</b>	U	<b>U</b>

(continued)

Table 1  
(continued)

T3809	Q112	E108	Q104	Q101				[24,26,27]
	6	3	7	1	Q975	E939	Q903	Q867
	Y112	N108	Y104	R100				
	3	0	4	8	H972	R936	Y900	R864
	N112	S107	C104	N100				
	2	9	3	7	C971	S935	N899	N863
k <sub>D</sub> n.d.	U	G	A	U	A	G	U	U

PUF-D	Q112	E108	R104	Q101				[19]
	6	3	7	1	E975	R939	Q903	E867
	Y112	N108	Y104	R100				
	3	0	4	8	Y972	Y936	Y900	R864
	N112	S107	S104	N100				
	2	9	3	7	S971	S935	N899	S863
k <sub>D</sub> n.d.	U	G	C	U	G	C	U	G

R6/R2(SYx xR)	Q112	E108	R104	Q101				[19]
	6	3	7	1	Q975	Q939	R903	Q867
	Y112	N108	Y104	R100				
	3	0	4	8	H972	R936	Y900	R864
	N112	S107	S104	C100				
	2	9	3	7	N971	C935	S899	S863
	U	G	C	A	U/C	A	C	A

(continued)

**Table 1**  
**(continued)**

PUF-A	Q112	E108	<b>R104</b>	Q101				[19]
	6	3	7	1	Q975	Q939	Q903	
	Y112	N108	Y104	R100				
	3	0	4	8	H972	R936	Y900	R864
	N112	S107	<b>S104</b>	C100				
	2	9	3	7	<i>N971</i>	C935	N899	S863
k <sub>D</sub> n.d.	U	G	<b>C</b>	A	U/C	A	U	<b>G</b>
R5(S <sup>R</sup> / <sub>YXX</sub>	Q112	E108	Q104	<b>R101</b>				[19]
	6	3	7	1	Q975	Q939	Q903	
	Y112	N108	Y104	R/Y				
R)	3	0	4	1008	H972	R936	Y900	R864
	N112	S107	N104	<b>S100</b>				
	2	9	3	7	<i>N971</i>	C935	N899	S863
k <sub>D</sub> n.d.	U	G	U	<b>C</b>	U/C	A	U	A
A4C	Q112	E108	Q104	<b>R101</b>				[18]
	6	3	7	1	Q975	Q939	Q903	
	Y112	N108	Y104	R100				
	3	0	4	8	H972	R936	Y900	R864
	N112	S107	N104	<b>G10</b>				
	2	9	3	07	<i>N971</i>	C935	N899	S863
k <sub>D</sub> n.d.	U	G	U	<b>C</b>	U/C	A	U	A

(continued)

**Table 1**  
**(continued)**

<b>actPUM2</b>	Q112	E108	Q104	<b>E101</b>				[23]
	6	3	7	<b>1</b>	Q975	Q939	<b>E903</b>	Q867
	Y112	N108	Y104	R100				
	3	0	4	8	H972	R936	Y900	R864
	N112	S107	C104	<b>S100</b>				
<b>k<sub>D</sub> n.d.</b>	2	9	3	<b>7</b>	<i>N971</i>	<b>N935</b>	<b>S899</b>	<b>N863</b>
	U	G	U	<b>G</b>	U/C	<b>U</b>	<b>G</b>	<b>U</b>
<b>mPUM4</b>	Q112	E108	Q104	<b>E101</b>				[21]
	6	3	7	<b>1</b>	Q975	<b>E939</b>	<b>E903</b>	Q867
	Y112	N108	Y104	R100				
	3	0	4	8	H972	R936	Y900	R864
	N112	S107	C104	<b>S100</b>				
<b>k<sub>D</sub> n.d.</b>	2	9	3	<b>7</b>	<i>N971</i>	<b>N935</b>	<b>S899</b>	<b>N863</b>
	U	G	U	<b>G</b>	U/C	<b>U</b>	<b>G</b>	<b>U</b>
<b>T3794</b>	Q112	E108	Q104	Q101				[22, 24, 26, 27]
	6	3	7	1	<b>E975</b>	Q939	Q903	Q867
	Y112	N108	Y104	R100				
	3	0	4	8	<b>N972</b>	R936	Y900	R864
	N112	S107	N104	C100				
<b>k<sub>D</sub> n.d.</b>	2	9	3	7	<b>S971</b>	C935	N899	S863
	U	G	U	A	<b>G</b>	A	U	A

(continued)

**Table 1**  
**(continued)**

<b>U5C</b>	Q112	E108	Q104	Q101				[18]
	6	3	7	1	<b>R975</b>	Q939	Q903	Q867
	Y112	N108	Y104	R100				
	3	0	4	8	H972	R936	Y900	R864
<b>k<sub>D</sub> n.d.</b>	N112	S107	N104	C100	<b>G97</b>			
	2	9	3	7	<b>1</b>	C935	N899	S863
	U	G	U	A	<b>C</b>	A	U	A
<b>Mut3-1</b>	Q112	E108	Q104	Q101				[15]
	6	3	7	1	Q975	Q939	Q903	Q867
	Y112	N108	Y104	R100				
	3	0	4	8	H972	R936	Y900	R864
<b>k<sub>D</sub> = 0.5 nM</b>	N112	S107	N104	C100				
	2	9	3	7	N971	<b>N935</b>	N899	S863
	U	G	U	A	U/C	<b>U</b>	U	A
<b>Mut3-2 = mPUM3</b>	Q112	E108	Q104	Q101				[15,21,52]
	6	3	7	1	Q975	<b>E939</b>	Q903	Q867
	Y112	N108	Y104	R100				
	3	0	4	8	H972	R936	Y900	R864
<b>k<sub>D</sub> = 0.05 nM</b>	N112	S107	N104	C100				
	2	9	3	7	N971	<b>S935</b>	N899	S863
	U	G	U	A	U/C	<b>G</b>	U	A

(continued)

**Table 1**  
**(continued)**

<b>A6C</b>	Q112	E108	Q104	Q101				[18]
	6	3	7	1	Q975	<b>R939</b>	Q903	Q867
	Y112	N108	Y104	R100				
	3	0	4	8	H972	R936	Y900	R864
<b>k<sub>D</sub> n.d.</b>	N112	S107	N104	C100		<b>G93</b>		
	2	9	3	7	<i>N971</i>	<b>5</b>	N899	S863
	U	G	U	A	U/C	<b>C</b>	U	A

<b>R3(SYxxR)</b> <b>-Y972</b>	Q112	E108	Q104	Q101				[19]
	6	3	7	1	Q975	<b>R939</b>	Q903	Q867
	Y112	N108	Y104	R100		R/Y9		
	3	0	4	8	<b>Y972</b>	36	Y900	R864
<b>k<sub>D</sub> n.d.</b>	N112	S107	N104	C100				
	2	9	3	7	<i>N971</i>	<b>S935</b>	N899	S863
	U	G	U	A	U/C	<b>C</b>	U	A

<b>actPUM1</b>	Q112	E108	Q104	Q101				[23]
	6	3	7	1	Q975	<b>E939</b>	Q903	<b>E867</b>
	Y112	N108	Y104	R100				
	3	0	4	8	H972	R936	Y900	R864
<b>k<sub>D</sub> n.d.</b>	N112	S107	N104	C100				
	2	9	3	7	<i>N971</i>	<b>S935</b>	N899	S863
	U	G	U	A	U/C	<b>G</b>	U	<b>G</b>

(continued)

**Table 1**  
**(continued)**

<b>R2(SYxxR)</b>	Q112	E108	Q104	Q101				[19]
	6	3	7	1	Q975	Q939	<b>R903</b>	Q867
	Y112	N108	Y104	R100				
	3	0	4	8	H972	R936	Y900	R864
<b>k<sub>D</sub> n.d.</b>	N112	S107	N104	C100				
	2	9	3	7	<i>N971</i>	C935	<b>S899</b>	S863
	U	G	U	A	U/C	A	<b>C</b>	A
<b>U7C</b>	Q112	E108	Q104	Q101				[18]
	6	3	7	1	Q975	Q939	<b>R903</b>	Q867
	Y112	N108	Y104	R100				
	3	0	4	8	H972	R936	Y900	R864
<b>k<sub>D</sub> n.d.</b>	N112	S107	N104	C100			<b>G89</b>	
	2	9	3	7	<i>N971</i>	C935	<b>9</b>	S863
	U	G	U	A	U/C	A	<b>C</b>	A
<b>Mut1-1</b>	Q112	E108	Q104	Q101				[15]
	6	3	7	1	Q975	Q939	Q903	<b>E867</b>
	Y112	N108	Y104	R100				
	3	0	4	8	H972	R936	Y900	R864
<b>k<sub>D</sub> = 1.3 nM</b>	N112	S107	N104	C100				
	2	9	3	7	<i>N971</i>	C935	N899	S863
	U	G	U	A	U/C	A	U	<b>G</b>

(continued)

**Table 1**  
(continued)

<b>A8C</b>	Q112	E108	Q104	Q101					[18]
	6	3	7	1	Q975	Q939	Q903	<b>R867</b>	
	Y112	N108	Y104	R100					
	3	0	4	8	H972	R936	Y900	R864	
<b>k<sub>D</sub> n.d.</b>	N112	S107	N104	C100				<b>G86</b>	
	2	9	3	7	<i>N971</i>	C935	N899	<b>3</b>	
	U	G	U	A	U/C	A	U	<b>C</b>	

RNA-contacting amino acid residues and cognate targets of HsPUM1-HD variants. For each variant, Puf repeats from Puf8 to Puf1 (C- to N-terminal direction) and RNA sequences in 5′–3′ orientation are shown from left to right in each row; amino acid residues 16, 13, and 12 are shown from top to bottom in each column. PUMHD variants are listed in order of changes to the target sequence specificity in 5′–3′ direction. Changes in amino acids and RNA targets are highlighted in bold and shaded. Italicized N971 does not contribute to RNA contacts in HsPUM1-HD. Where absolute dissociation constants have been determined for the shown target sequence, these are listed (*n.d.* not determined). Note that dissociation constants for promiscuously bound alternate target sequences are not shown. These are always higher than for the main target, but may well be in a range suitable for RNA imaging purposes (refer to original publications for alternative *k<sub>D</sub>*’s and relative binding activities of individual PUMHD variants, in particular [15])

wild-type PUMHD and Mut6-2/7-2 because these bind to their cognate targets with high affinities, but have low affinities for the binding sites of the respective other variant [15]. The choice between modifying PUMHD variants or tagging the RNA will thus depend on considerations of the available target sequences and the suitability of previously characterized PUMHD variants for any given RNA.

Analyze the RNA of interest for the presence of sequences with similarity to native Pumilio binding sites. The target sequence of wild-type HsPUM1-HD is UGUANAUA (N=A, U, or C) [29, 41] (Fig. 2) and most PUMHDs bind to sequences starting with a 5′UGU triplet [29]. This sequence motif is thus a good starting point for the identification of suitable target sequences. However, PUMHD variants with altered specificity of Puf repeats 6–8 (Table 1), which bind to the triplet, have also been used for RNA imaging and detection [20, 24, 33]. Plant RNA virus genomes often contain native Pumilio binding sites that can be exploited for PUM-BiFC imaging (and may be targets of native Pumilio proteins involved in host defense responses) [24, 25, 42, 43].

The two target sites should be closely adjacent, but separated by a short linker region to prevent steric hindrance of two simultaneously binding PUMHD fusions. With PUM-BiFC, dual target sites separated by linkers between 5 and 11 nucleotides long have been successfully imaged [20–22, 24] (but *see* **Note 1**).

So far, modified PUMHD variants with up to five altered base specificities have been used for RNA imaging [20, 24], and with up to seven modified Puf repeats in engineered splicing factors [19]. However, with increasing numbers of amino acid changes, effects on overall RNA affinity and protein folding become more unpredictable.

If no suitable binding sites can be identified or very extensive PUMHD modifications would be required, and if no disadvantages from tagging the RNA are expected, select suitable previously described PUMHD variants, e.g., wild-type and mut6-2/7-2 PUMHD [33], to design an RNA tag. In order to not disrupt open reading frames, RNA tags have to be inserted into untranslated regions. A good starting point is to introduce the tag directly downstream of an ORF immediately after the stop codon. Tagging upstream of the start codon may also work, and in some cases, several options may have to be tested [24, 44].

Table 1 lists previously characterized modified PUMHD variants ordered by alterations in their recognition sites from 5' to 3', to facilitate easier selection of RNA target sites or tags. After selection of target sites or tags, the wild-type HsPUM1-HD needs to be modified into two different variants to bind the selected sequences. The molecular code for base specificity of Puf repeats is as follows [15, 16, 18, 19, 30, 45]:

$$\begin{aligned} \text{C/sXXXXQ} &= \text{A} \\ \text{NXXXXQ} &= \text{U} \\ \text{SXXXE} &= \text{G} \\ \text{s/T/G/C/AXXXR} &= \text{C} \end{aligned}$$

where the letters represent amino acids 12–16 of each Puf repeat, and X in positions 13–15 are amino acids not involved in base specificity. In the HsPUM1 ORF, the relevant amino acids corresponding to residues 12 and 16 in each repeat, respectively, are: Puf1 [863, 867]; Puf2 [899, 903]; Puf3 [935, 939]; Puf4 [971, 975]; Puf5 [1007, 1011]; Puf6 [1043, 1047]; Puf7 [1079, 1083]; Puf8 [1122, 1126] (Table 1). The italicized residue 971 in Puf4 does not actually participate in RNA interactions [14, 15]. The amino acids in position 13, which contribute stacking interactions to RNA binding, are left unchanged (*see* **Note 2**). Avoid using Puf4/Nt5 modifications as a main specificity determinant (*see* **Note 3**).

### 1.3 Choice of Expression System

In principle, PUM-BiFC reporter constructs can be stably expressed, but so far all *Pumilio*-based RNA imaging in plants has been done with transient expression systems (agroinfiltration

or microprojectile bombardment) [24–27]. Since nonspecific background fluorescence increases with the accumulation of the PUM-BiFC fusions, transient expression may be preferable as it permits limiting background fluorescence by reducing the expression time (*see* Subheading 3.3).

Agroinfiltration is generally preferable to biolistic bombardment, as it leads to reporter expression in large tissue areas, and makes it easier to assess cell-to-cell variability of PUM-BiFC signal and find optimal imaging conditions (*see* Subheading 3.3). It is therefore recommended to use agroinfiltration as the first choice of expression system. However, when viral RNAs are imaged, co-expression of agrobacterium-delivered plasmids and virus can be problematic and in that case, bombardment provides a useful alternative means of delivering reporter constructs.

After these general considerations, the following protocol describes the construction of a PUM-BiFC system to image the untagged, genomic RNA of *Tobacco mosaic virus* (TMV) [24, 26].

---

## 2 Materials

1. A plasmid containing an *HsPUM1-HD* ORF (encoding amino acids Gly828-Gly1176 of the full-length HsPUM1 protein) as a PCR template (available from [www.openbiosystems.com](http://www.openbiosystems.com)).
2. A plasmid containing a *Citrine* fluorescent protein ORF as a PCR template, e.g., pSAT6-Citrine-N1 (GeneBank acc. AY818369) [46].
3. Primers (*see* Table 2).
4. Standard molecular cloning materials: Commercial kits for high-fidelity PCR amplification, PCR clean up, DNA gel extraction, and plasmid minipreps; PCR machine; gel chamber and power supply for running horizontal agarose gels; benchtop centrifuges; electrocompetent *E. coli* cells, e.g., strain DH5 $\alpha$ , and electroporator; LB media (liquid and agar plates) containing either 15  $\mu$ g/ml gentamicin or 100  $\mu$ g/ml spectinomycin; 37 °C shaking and non-shaking incubators.
5. Gateway™ vectors pDONR207 (Life Technologies) and pGWB402 $\Omega$  [47].
6. Gateway™ BP and LR Clonase (Life Technologies).
7. Electrocompetent *Agrobacterium tumefaciens* cells, strain AGL1; LB media (liquid and agar plates) containing 100  $\mu$ g/ml spectinomycin and 50  $\mu$ g/ml rifampicin; 28 °C shaking and non-shaking incubators.
8. Infiltration medium: 10 mM MES pH 5.6, 10 mM MgCl<sub>2</sub>, 15  $\mu$ M acetosyringone.

**Table 2**  
**Oligonucleotide primers for constructing a PUM-BiFC system to image TMV RNA**

Primer name	Sequence (5'→3')
attB- PUMfor	AAAAAGCAGGCTCTAGATGGGCAGGAGCAGGCTTTTGG
attB- PUMrev	AGAAAGCTGGGTCTCGAGTTATCCCTAAGTCAACACCGTTCT TCATG
link- PUMfor	GGAGGTGGTGGATCTAGAGGCAGGAGCAGGCTTTTGG
link- PUMrev	AGATCCACCACCTCCCTCGAGTCCCTAAGTCAACACCGTTCT TCATG
A8U_095for	ACCAGCATGGGAAACAGATTCATTCAG
A8U_119re v	TGAATGAATCTGTTCCCATGCTGGTC
A6G_323for	GCCGTGTTATCGAGAAAGCTCTTGAG
A6G_333re v1	GATAACACGGCTGCCATACATCTGTAG
A6G_333re v2	TCAAGAGCTTTCTCGATAACACGGCTGCCATACATCTGTAG
U5G_425for	ATGGCAGTAACGTGGTTGAGAAATG
U5G_434for	ACGTGGTTGAGAAATGCATTGAATGTG
U5G_441re v	AACCACGTTACTGCCATTCTGATCTTTCAC
U5G_449re v	CATTTCTCAACCACGTTACTGCCATTCTGATCTT

(continued)

**Table 2**  
**(continued)**

U5A_416for	AAGATCAGAATGGCT <b>TC</b> GCACGTGGTTC
U5A_440re v	ACCACGTGAC <b>CAG</b> CCATTCTGATCTTTC
A4U_527for	ATCCTTATGGCA <b>AA</b> CCGAGTGATTCAG
A4U_549re v	AATCACTCGG <b>TT</b> GCCATAAGGATGTG
U3A_625for	CTTGTACAGGATCAATATGGAT <b>TC</b> TTATGTAATCC
U3A_658re v	GGATTACATAA <b>CA</b> TCCATATTGATCCTGTACAAG
attB-Citfor	AAAAAGCAGGCTATGGTGAGCAAGGGCGAGG
attB-Citrev	AGAAAGCTGGGTTTACTTGTACAGCTCGTCCATGCCG
link-CitNrev	<u>TCTAGAT</u> CCACCACCTCCGTCCTCGATGTTGTGGCGGATC
link-CitCfor	<u>CTCGAGG</u> GAGGTGGTGGATCTGGCAGCGTGCAGCTCGC
Citmonofor	CTACCAGTCC <b>AA</b> ACTGAGCAAAGAC
Citmonorev	GTCTTTGCTCAG <b>TTT</b> GGACTGGTAG
attB1- adapter	GGGGACAAGTTTGTACAAAAAAGCAGGCT
attB2- adapter	GGGGACCACTTTGTACAAGAAAGCTGGGT

Primers required for construction of a PUM-BiFC system to image untagged TMV RNA in vivo. *Xba*I and *Xho*I restriction sites are underlined; mutagenic nucleotides highlighted by boldface font and shading

9. Spectrophotometer for measuring optical density at 600 nm ( $OD_{600}$ ).
10. Gauge 25 needles.
11. 1 ml syringes.
12. 3–4 weeks old *Nicotiana benthamiana* plants.

13. An infectious clone of TMV which must contain nucleotides 3794–3816 (within the 183 k RNA polymerase domain), e.g., TMV.DsRed [24].
14. A commercial kit for RNA in vitro transcription with an RNA polymerase matching the infectious TMV construct (T7 for TMV.DsRed).
15. Aluminum oxide powder.
16. A confocal laser-scanning microscope equipped with 514 and 561 nm excitation light sources and suitable detection systems for mCitrine and mRFP. An upright microscope equipped with water-dipping lenses is the preferable setup for imaging intact plant tissue in vivo.

---

### 3 Methods

#### 3.1 Modification of PUMHDs

To direct one PUMHD variant (PUMHD3794) to bind to the sequence UGUAGUA (nucleotides 3794–3801 of the TMV genome), the specificity of Puf4 needs to be modified (U5G: N971S/H972N/Q975E). A second PUMHD variant (PUMHD3809) is engineered to bind the sequence UGAUAGUU (nucleotides 3809–3816 of TMV) by altering the specificities of Puf1 (A8U: S863N), 3 (A6G: C935S/Q939E), 4 (U5A: N971C), 5 (A4U: C1007N), and 6 (U3A: N1043C).

- 1 PUMHD3794 (*see* Fig. 3a for schematic of the construction process and finished fusion construct):

PCR#1: Amplify an N-terminal fragment of PUMHD3794 from a wild-type PUMHD template using primer pair link-PUMfor/U5G\_441rev (*see* Table 1 for all primer sequences used in this protocol. All primers are designed for annealing at 55 °C). Use a proof-reading, high-fidelity polymerase according to manufacturer's instructions, but amplify for only 10 cycles to minimize the likelihood of PCR errors. The link-PUMfor primer adds the flexible GGGGS linker that will connect the PUMHD to the N-terminal mCitrine fragment (*see* below) and a unique *Xba*I site for easy exchange of PUMHD variants.

- 2 Gel-purify the ~0.4 kb PCR product on a 2 % agarose gel using a commercial gel extraction kit. The PCR product will serve as the template in the next PCR reaction and gel purification removes the wild-type PUMHD template that would otherwise be amplified in the next PCR.
- 3 PCR#2: Amplify the purified N-terminal PUMHD fragment again, this time with primers link-PUMfor/U5G\_449rev and again using only 10 PCR cycles.
- 4 PCR#3: From the wild-type PUMHD template, amplify a ~0.6 kb C-terminal fragment of PUMHD3794 using primers

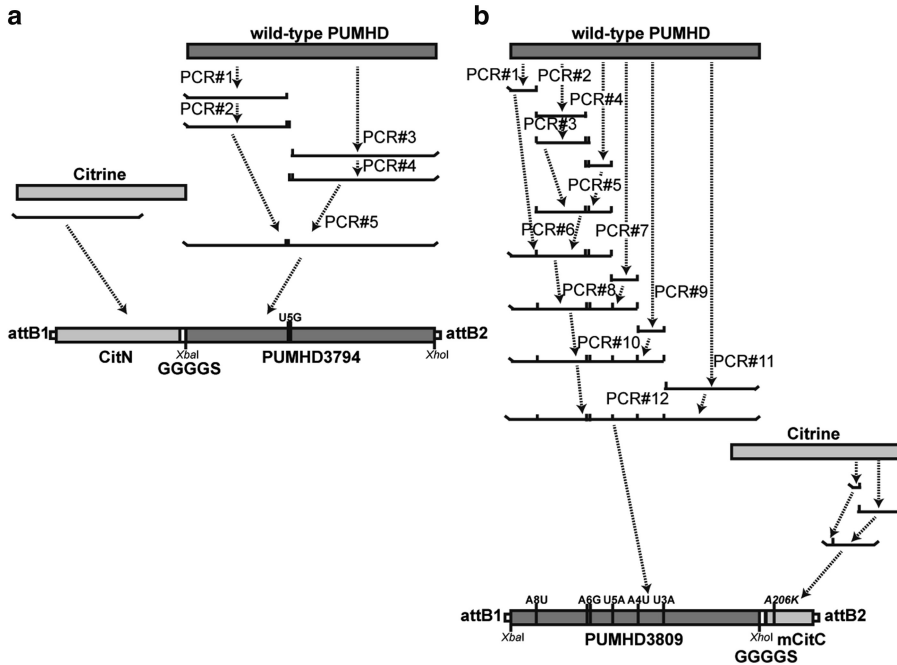


**Fig. 3** Construction schematics and finished PUMHD-split mCitrine fusions for TMV imaging. **(a)** CitN-PUMHD3794. **(b)** PUMHD3809-mCitC

U5G\_434for/attB-PUMrev (10 cycles only). Gel-purify the product as above. The attB-PUMrev primer adds a Gateway attB2 anchor as well as a unique *XhoI* site for easy exchange of PUMHD variants.

5 PCR#4: Amplify the C-terminal fragment again using primers U5G\_425for/attB-PUMrev (10 cycles).

6 PCR#5 (overlap PCR of full-length PUMHD3794): The four U5G primers have introduced all three required point mutations and also created a 25 bp overlap between the N- and C-terminal fragments. Using the products of PCR#2 and #4 as templates, amplify the ~1.05 kb full-length PUMHD3794 using primers link-PUMfor/attB-PUMrev with 10 PCR cycles.

7 PUMHD3809 (*see* Fig. 3b):

The multiple mutations introduced in this PUMHD variant require a multistep overlap PCR. As above, use a high-fidelity polymerase and only 10 PCR cycles for each PUMHD fragment. All PCR products amplified from wild-type template need to be gel-purified before proceeding to subsequent overlap PCR steps.

8. PCR#1: Amplify an N-terminal 0.12 kb fragment of PUMHD3809 using primers attB-PUMfor/A8U\_119rev. Gel-purify. The attB-PUMfor primer adds a Gateway attB1

anchor, as well as a unique *Xba*I site for easy exchange of PUMHD variants.

9. PCR#2: Amplify a ~0.2 kb fragment from bp 95 to 333 of PUMHD3809 using primers A8U\_095for/A6G\_333rev1. Gel-purify.
10. PCR#3: Extend PCR#2 product by amplification with primers A8U\_095for/A6G\_333rev2.
11. PCR#4: Amplify a 0.12 kb fragment from bp 323 to 440 of PUMHD3809 using primers A6G\_323for/U5A\_440rev. Gel-purify.
12. PCR#5: Amplify a 0.32 kb overlap product from bp 95 to 440 of PUMHD3809 using both PCR#3 and PCR#4 products as templates and primers A8U\_095for/U5A\_440rev.
13. PCR#6: Amplify a 0.44 kb overlap product from bp 1 to 440 of PUMHD3809 using both PCR#1 and PCR#5 products as templates, and primers attB-PUMfor/U5A\_440rev.
14. PCR#7: Amplify a ~0.13 kb fragment from bp 416 to 549 of PUMHD3809 using primers U5A\_416for/A4U\_549rev. Gel-purify.
15. PCR#8: Amplify a 0.55 kb overlap product from bp 1 to 549 of PUMHD3809 using both PCR#6 and PCR#7 products as templates, and primers attB-PUMfor/A4U\_549rev.
16. PCR#9: Amplify a ~0.13 kb fragment from bp 527 to 658 of PUMHD3809 using primers A4U\_527for/U3A\_658rev. Gel-purify.
17. PCR#10: Amplify a 0.66 kb overlap product from bp 1 to 658 of PUMHD3809 using both PCR#8 and PCR#9 products as templates, and primers attB-PUMfor/U3A\_658rev.
18. PCR#11: Amplify a ~0.43 kb C-terminal fragment of PUMHD3809 using primers U3A\_625for/link-PUMrev. Gel-purify. The link-PUMrev primer extends the PUMHD with the flexible GGGGS linker that will connect it to the C-terminal fragment of mCitrine (*see* below) and also adds a unique *Xho*I site for easy exchange of PUMHD variants.
19. PCR#12 (overlap PCR of full-length PUMHD3809): Amplify ~1.05 kb full-length PUMHD3809 using both PCR#10 and PCR#11 products as templates, and primers attB-PUMfor/link-PUMrev.

### **3.2 Construction of PUMHD-Split mCitrine Fusions**

1. Amplify the 0.52 kb N-terminal fragment of Citrine fluorescent protein (CitN; amino acids 1–172) using a plasmid encoding Citrine (e.g., pSAT-Citrine-N1 [46]) as the template, and primers attB-Citfor/link-CitNrev (high-fidelity polymerase, 10 PCR cycles). The attB-Citfor primer adds a Gateway attB1 anchor, while the link-CitNrev primer adds the GGGGS linker for connection to PUMHD3794.

2. Amplify a C-terminal fragment of Citrine (mCitC; amino acids 173–239) in an overlap PCR that introduces the A206K mutation which prevents dimerization of GFP and its derivatives [48, 49]: Amplify two ~0.1 kb fragments in separate PCRs using primers link-CitCfor/Citmonorev and Citmonofor/attB-Citrev, respectively, from a Citrine-encoding plasmid (high-fidelity polymerase, 10 cycles). The link-CitCfor primer adds the GGGGS linker that will connect to PUMHD3809. The attB-Citrev primer adds a Gateway attB2 anchor. After gel-purification, amplify the complete C-terminal fragment of monomerized Citrine (mCitC) using both partial PCR products as templates, and primers link-CitCfor/attB-Citrev (10 cycles).
3. Amplify the complete CitN-PUMHD3794 fusion using CitN and full-length PUMHD3794 PCR products as templates, and primers attB1-adapter/attB2-adapter. Use a high-fidelity polymerase and 20 PCR cycles. Run a 5 µl aliquot of the PCR reaction on a 1 % agarose gel. If there is a single, 1.6 kb product, remove remnants of the PCR reaction using a commercial PCR clean up kit. If more than one PCR product was obtained, run the rest of the PCR out on the gel, and excise and gel-purify the 1.6 kb band using a commercial kit.
4. Amplify the complete PUMHD3809-mCitC fusion using full-length PUMHD3809 and mCitC PCR products as templates, and primers attB1-adapter/attB2-adapter. Use a high-fidelity polymerase and 20 PCR cycles. Run a 5 µl aliquot of the PCR reaction on a 1 % agarose gel. If there is a single, 1.3 kb product, remove remnants of the PCR reaction using a commercial PCR clean up kit. If more than one PCR product was obtained, run the rest of the PCR out on the gel, and excise and gel-purify the 1.3 kb band using a commercial kit.
5. Recombine both CitN-PUMHD3795 and PUMHD3809-mCitC products into a Gateway DONR vector, e.g., pDONR207 (Gent<sup>R</sup>), using Gateway<sup>TM</sup> BP recombinase (Life Technologies) according to manufacturer's instructions. Transform the BP recombination into *E. coli* competent cells and plate on LB agar containing 15 µg/ml gentamicin. On the next day, pick several colonies for overnight culture in LB liquid media containing gentamicin, then isolate the plasmids using a commercial kit. Verify that the mCitN-PUMHD3794 and PUMHD3809-CitC fusions have no PCR errors by sequencing the DONR vector inserts.
6. Recombine error-free fusion constructs into a Gateway destination binary vector for plant expression, e.g., pGWB402Ω (Spec<sup>R</sup>; [46]), using Gateway<sup>TM</sup> LR Clonase (Life Technologies) according to manufacturer's instructions. Transform the LR reaction into *E. coli* competent cells and plate on LB agar containing 100 µg/ml spectinomycin. On the next day, pick

several colonies for overnight culture in LB liquid media containing spectinomycin, then isolate the plasmids using a commercial kit. Check that correct expression constructs were obtained by diagnostic restriction digest (e.g., excising the ~1.05 kb PUMHD using *XbaI/XhoI*).

### 3.3 PUM-BiFC In Vivo Imaging

1. Transform CitN-PUMHD3794 and PUMHD3809-mCitC binary expression vectors separately into electrocompetent *Agrobacterium tumefaciens* cells strain AGL1 (other strains are also suitable). Plate the transformed agrobacteria on LB agar containing 100 µg/ml spectinomycin to select for transformants, and 50 µg/ml rifampicin to suppress growth of other bacteria. Grow plates at 28 °C for 2 days.
2. Transcribe TMV.DsRed [24] RNA in vitro, using a commercial T7 polymerase kit according to manufacturer's instructions. Keep the RNA on ice after transcription. Infect 3–4 weeks old *N. benthamiana* plants by dusting the leaves thinly with aluminum oxide powder and then gently rub-inoculating 5–10 µl transcript with a gloved hand (see Note 4). Incubate plants at 33 °C after infection.
3. Two days after infection, pick single colonies into 4 ml liquid LB media containing spectinomycin and rifampicin and grow in a shaking incubator at 28 °C for 2 days (see Note 5).
4. Pellet the bacterial cultures, then resuspend each pellet into 2 ml infiltration medium.
5. Incubate the resuspended agrobacteria at room temperature in the dark for about 1 h, then measure the OD<sub>600</sub>.
6. Mix and dilute CitN-PUMHD3794 and PUMHD3809-mCitC containing agrobacteria with infiltration medium so that both are present at OD<sub>600</sub>=0.25 in the final mixture (i.e., total combined OD<sub>600</sub>=0.5).
7. With the tip of a needle, create small incisions on the abaxial (lower) side of uninfected and TMV-infected *N. benthamiana* leaves by gently touching the leaf surface with the needle so that a dark point is just visible.
8. Carefully infiltrate the agrobacterium mixture into these incisions using a 1 ml syringe without a needle pressed on the incision site (see Note 6). Ca. 1–2 ml of suspension is required to cover a leaf. Agrobacteria can be infiltrated in patches, e.g., overlapping with virus-infected issue areas, or into the entire leaf lamina, depending on experimental requirements.
9. For imaging, place whole or half leaves or ~2 × 2 cm leaf pieces under a microscope lens by fixing them to a microscope slide using double-sided sticky tape, with the lower epidermis facing up. An upright microscope with water-dipping lenses, which can be directly immersed in a drop of water placed on the leaf

with no cover glass in between, is ideal for plant imaging. Excite mCitrine BiFC at 514 nm and detect mCitrine fluorescence at 520–550 nm. Excite DsRed at 561 nm and detect DsRed fluorescence at 570–600 nm.

10. Begin imaging by monitoring the level and localization of background fluorescence in uninfected tissue every day from 1 to 4 days post-infiltration (dpi) (*see Note 7*). Expect false-positive BiFC fluorescence to be distributed fairly homogeneously throughout the nucleoplasm and cytoplasm. The nucleus tends to be brighter than the cytoplasm. At very high expression levels or in small cells, PUM-BiFC may aggregate.
11. In parallel to uninfected control plants, image the PUM-BiFC reporter constructs in TMV-infected tissue, also daily from 1 to 4 dpi (corresponding to 5–8 days after TMV infection). Compared to the negative control, expect increased fluorescence intensity (*see Note 8*), and also a relocalization. In particular, nucleoplasmic signal usually disappears in the presence of target RNA and instead of general cytoplasmic fluorescence, the PUM-BiFC signal is expected to be concentrated in granular viral replication sites which can be small and dispersed in the cytoplasm, or aggregated into a large perinuclear inclusion body [24, 25] (Fig. 4).
12. Monitoring BiFC for several days after infiltration and comparing the signal intensity and localization in uninfected and infected tissue establishes a suitable time window for obtaining

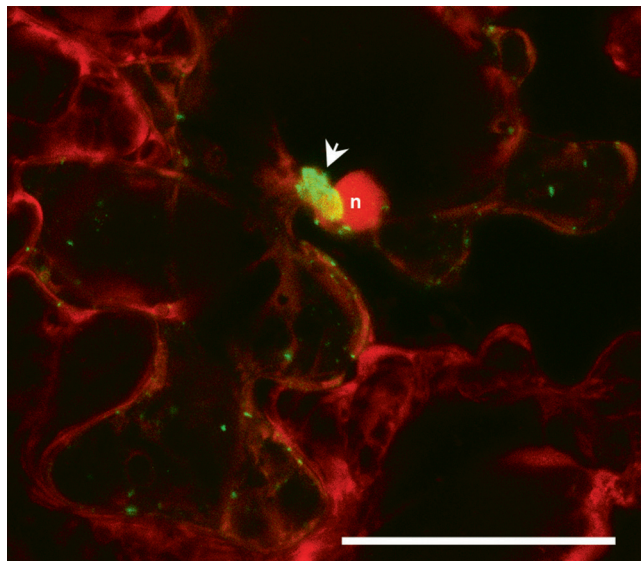


**Fig. 4** Example of TMV RNA imaged with the PUM-BiFC system. Viral RNA is visible in small punctae dispersed throughout the cytoplasm and a large perinuclear inclusion body (*arrow*). *N* nucleus. Scale bar: 50  $\mu\text{m}$

a good signal-to-noise ratio (*see* **Note 9**). Once this has been accomplished, the time span separating infection and reporter infiltration can be varied (*see* **step 3** above) to follow the TMV RNA localization throughout the infection cycle (*see* **Note 10**).

---

## 4 Notes

1. Kellermann et al. [33] found that a 7 nucleotides long linker between PUMHD binding sites was optimal for PUM-TetFC, and decreasing or increasing it to 5 or 9 nucleotides, respectively, significantly reduced the fluorescent signal. The length of a suitable linker will depend on the length and flexibility of the protein linker between PUMHD and FP fragment, but it should be kept in mind that the greater tolerance of PUM-BiFC for different linker lengths may actually be due to recruitment of pre-formed PUM-BiFC complexes to the RNA by just one of the two PUMHDs (*see* Subheading 1.1). In PUM-BiFC systems with improved signal-to-noise ratio, linker length may become more critical and may have to be empirically optimized.
2. Amino acid residues that participate in stacking interactions with the RNA bases can also contribute to base specificity, and their modification can either increase or decrease binding promiscuity [19, 50]. However, modifying these residues can also negatively affect overall RNA affinity and protein solubility [15, 50]. Therefore, until a systematic investigation has led to a detailed understanding of stacking interactions in HsPUM1-HD, it is recommended that amino acids at position 13 of the Puf repeats are not modified.
3. Note that Puf4 in the wild-type PUMHD can promiscuously bind any base at position 5 [29]. Puf4 differs slightly from the other Puf repeats in that its Asn971 in position 12 does not contact the RNA base, whereas Gln975 can interact either with the Watson-Crick edge of U, the Hoogsteen edge of A or G, or not contact the base at all when a C is in position 5. Whilst binding specificity of Puf4 can be modified, the fifth base of target sequences should therefore not be used as a critical specificity determinant, e.g., as the only difference between two target sites.

Position 8, bound by Puf1, also shows some promiscuity and can accept G instead of A [15], whilst other promiscuous binding modes of Puf3 and 7 have lower affinities for non-cognate bases but these may still be in a range that permits binding during RNA imaging in vivo [15, 20]. Lastly HsPUM1-HD can bind 9 nucleotide sequences by flipping one base out away from the protein surface [28]. It is useful to be aware of these alternative binding modes when choosing target sites for imaging and creating modified PUMHD variants.

4. The infectious TMV clone does not have to express a fluorescent protein, but this helps to identify infected leaf areas. Encapsidating transcribed RNA into TMV capsid protein *in vitro*, passaging TMV from infectious lesions, or expressing the TMV genome in plants from a CaMV 35S promoter (e.g., pTRBO; [51]) following either DNA rub-inoculation, microprojectile bombardment, or agroinfiltration are also suitable methods of infection.
5. It is useful to make glycerol stocks of transformed agrobacteria to save time when repeatedly growing liquid cultures for imaging.
6. Young leaves are easier to infiltrate as they have larger air spaces. Avoid pressing the opening on the syringe too hard onto the leaf surface as this will cause extensive damage. Also, if air spaces in the mesophyll are tight causing a high resistance to the infiltration, increasing the injection pressure is more likely to cause agrobacterium mixture to squirt out sideways from under the rim of the syringe than to improve infiltration.
7. Since folding and stability of split FP fragments are influenced by fusion partners such as the PUMHD variants (which may themselves differ in their respective *in vivo* folding efficiency and stability), unfused split FP halves are no suitable negative control in BiFC. Ideal BiFC controls are fusions with noninteracting variants of the proteins used in the actual experiments [31]. In the case of PUM-BiFC this corresponds to either the absence of the target RNA as described here, or PUMHD fusions that do not bind the target RNA [24, 33]. Background fluorescence due to random collisions should be the same for both types of controls. However, the ability to bind cellular RNAs promiscuously, as well as the folding efficiency and stability of the PUMHD-split FP fusions may differ for different pairs of PUMHDs. Therefore, expressing the target RNA-specific reporter constructs in the absence of the target provides the best negative control.
8. Make sure not to oversaturate images during acquisition. Differences in fluorescence intensity between infected cells and uninfected controls are only apparent when images are not overexposed. Try to work at the lowest possible gain settings to maximize the contrast.
9. A direct comparison between nonspecific and TMV-dependent BiFC levels may be difficult because viruses often suppress other ectopic expression constructs to a considerable degree. It may be necessary to increase OD<sub>600</sub> and expression time for infected tissue compared with the negative control.
10. PUM-BiFC expression levels may need to be re-optimized when imaging different infection stages. In strongly infected tissue at late infection stages, expression of the RNA reporter

constructs may be too strongly suppressed to produce sufficient PUM-BiFC signal for imaging. Conversely at early infection stages, if PUM-BiFC accumulates too much compared to viral RNA levels, the signal-to-noise ratio will be too low to clearly localize the viral RNA over the background.

To compensate for such effects, PUMHD fusion constructs can be agroinfiltrated at an OD<sub>600</sub> between ~0.1 and 1.0 each (at a 1:1 ratio). It may also be worth experimenting with unequal expression ratios to optimize the signal-to-noise ratio and minimize aggregation [24].

Even after optimization of imaging conditions, expression levels are usually very heterogeneous throughout the tissue and across viral lesions. The number of cells that have an optimal virus/PUM-BiFC ratio at a specific viral infection stage may be very small in a single experiment. It is therefore important to observe large areas of tissue and repeat experiments to both find suitable imaging conditions and ensure their reproducibility.

## References

1. Dunoyer P, Schott G, Himber C et al (2010) Small RNA duplexes function as mobile silencing signals between plant cells. *Science* 328:912–916
2. Carlsbecker A, Lee JY, Roberts CJ et al (2010) Cell signalling by microRNA165/6 directs gene dose-dependent root cell fate. *Nature* 465:316–321
3. Wang Y, Ding B (2010) Viroids: small probes for exploring the vast universe of RNA trafficking in plants. *J Integr Plant Biol* 52:28–39
4. Niehl A, Heinlein M (2011) Cellular pathways for viral transport through plasmodesmata. *Protoplasma* 248:75–99
5. Lucas WJ, Bouché-Pillon S, Jackson DP et al (1995) Selective trafficking of KNOTTED1 homeodomain protein and its mRNA through plasmodesmata. *Science* 270:1980–1983
6. Kim JY, Rim Y, Wang J et al (2005) A novel cell-to-cell trafficking assay indicates that the KNOX homeodomain is necessary and sufficient for intercellular protein and mRNA trafficking. *Genes Dev* 19:788–793
7. Tyagi S (2009) Imaging intracellular RNA distribution and dynamics in living cells. *Nat Methods* 6:331–338
8. Christensen NM, Oparka KJ, Tilsner J (2010) Advances in imaging RNA in plants. *Trends Plant Sci* 15:196–203
9. Wickens M, Bernstein DS, Kimble J et al (2002) A PUF family portrait: 3'UTR regulation as a way of life. *Trends Genet* 18:150–157
10. Francischini CW, Quaggio RB (2009) Molecular characterization of *Arabidopsis thaliana* PUF proteins—binding specificity and target candidates. *FEBS J* 276:5456–5470
11. Tam P, Barrette-Ng I, Simon D et al (2010) The Puf family of RNA-binding proteins in plants: phylogeny, structural modeling, activity and subcellular localization. *BMC Plant Biol* 10:44
12. Abbasi N, Park YI, Choi SB (2011) Pumilio Puf domain RNA-binding proteins in *Arabidopsis*. *Plant Signal Behav* 6:364–368
13. Quenault T, Lithgow T, Traven A (2011) PUF proteins: repression, activation and mRNA localization. *Trends Cell Biol* 21:104–112
14. Wang X, McLachlan J, Zamore PD et al (2002) Modular recognition of RNA by a human Pumilio-homology domain. *Cell* 110:501–512
15. Cheong CG, Tanaka Hall TM (2006) Engineering RNA sequence specificity of Pumilio repeats. *Proc Natl Acad Sci U S A* 103:13635–13639
16. Lu G, Dolgner SJ, Tanaka Hall TM (2009) Understanding and engineering RNA sequence specificity of PUF proteins. *Curr Opin Struct Biol* 19:110–115
17. Mackay JP, Font J, Segal DJ (2011) The prospects for designer single-stranded RNA-binding proteins. *Nat Struct Mol Biol* 18:256–261
18. Filipovska A, Razif MFM, Nygård KKA et al (2011) A universal code for RNA recognition by PUF proteins. *Nat Chem Biol* 7:425–427

19. Dong S, Wang Y, Cassidy-Amstutz C et al (2011) Specific and modular binding code for cytosine recognition in Pumilio/FBF (PUF) RNA-binding domains. *J Biol Chem* 286: 26732–26742
20. Ozawa T, Natori Y, Sato M et al (2007) Imaging dynamics of endogenous mitochondrial RNA in single living cells. *Nat Methods* 4:413–419
21. Yamada T, Yoshimura H, Inaguma A et al (2011) Visualization of nonengineered single mRNAs in living cells using genetically encoded fluorescent probes. *Anal Chem* 83:5708–5714
22. Yu SF, Lujan P, Jackson DL et al (2011) The DEAD-box RNA helicase DDX6 is required for efficient encapsidation of a retroviral genome. *PLoS Pathog* 7:e1002303
23. Yoshimura H, Inaguma A, Yamada T et al (2012) Fluorescent probes for imaging endogenous  $\beta$ -actin mRNA in living cells using fluorescent protein-tagged Pumilio. *ACS Chem Biol* 7:999–1005
24. Tilsner J, Linnik O, Christensen NM et al (2009) Live-cell imaging of viral RNA genomes using a Pumilio-based reporter. *Plant J* 57: 758–770
25. Wei T, Huang TS, McNeil J et al (2010) Sequential recruitment of the endoplasmic reticulum and chloroplasts for plant potyvirus replication. *J Virol* 84:799–809
26. Tilsner J, Linnik O, Wright KM et al (2012) The TGB1 movement protein of potato virus X re-organises actin and endomembranes into the ‘X-body’ a viral replication factory. *Plant Physiol* 158:1359–1370
27. Tilsner J, Linnik O, Louveaux M et al (2013) Replication and trafficking of a plant virus are coupled at the entrances of plasmodesmata. *J Cell Biol* 201:981–995
28. Gupta YK, Nair DT, Wharton RP et al (2008) Structures of human Pumilio with noncognate RNAs reveal molecular mechanisms for binding promiscuity. *Structure* 16:549–557
29. Lu G, Tanaka Hall TM (2011) Alternate modes of cognate RNA recognition by human PUMILIO proteins. *Structure* 19:361–367
30. Wang Y, Wang Z, Tanaka Hall TM (2013) Engineered proteins with Pumilio/fem-3 mRNA binding factor scaffold to manipulate RNA metabolism. *FEBS J*. doi:10.1111/febs.12367
31. Kodama Y, Hu C-D (2012) Bimolecular fluorescence complementation (BiFC): a 5-year update and future perspectives. *Biotechniques* 53:285–298
32. Li M, Doll J, Weckermann K et al (2010) Detection of in vivo interactions between Arabidopsis class A-HSFs, using a novel BiFC fragment, and identification of novel class B-HSF interacting proteins. *Eur J Cell Biol* 89:126–132
33. Kellermann SJ, Rath AK, Rentmeister A (2013) Tetramolecular fluorescence complementation for detection of specific RNAs in vitro. *Chembiochem* 14:200–204
34. Hu CD, Kerppola TK (2003) Simultaneous visualization of multiple protein interactions in living cells using multicolor fluorescence complementation analysis. *Nat Biotechnol* 21:539–545
35. Lee LY, Fang MJ, Kuang LY et al (2008) Vectors for multi-color bimolecular fluorescence complementation to investigate protein-protein interactions in living plant cells. *Plant Methods* 4:24
36. Waadt R, Schmidt LK, Lohse M et al (2008) Multicolor bimolecular fluorescence complementation reveals simultaneous formation of alternative CBL/CIPK complexes in planta. *Plant J* 56:505–516
37. Gehl C, Waadt R, Kudla J et al (2009) New GATEWAY vectors for high throughput analyses of protein-protein interactions by bimolecular fluorescence complementation. *Mol Plant* 2:1051–1058
38. Qin L, Chu J, Zheng Y et al (2009) A new red bimolecular fluorescence complementation based on TagRFP. *Proc SPIE* 7191:71910G
39. Zilian E, Maiss E (2011) An optimized mRFP-based bimolecular fluorescence complementation system for the detection of protein-protein interactions in planta. *J Virol Methods* 174:158–165
40. Jach G, Pesch M, Richter K et al (2006) An improved mRFP1 adds red to bimolecular fluorescence complementation. *Nat Methods* 3:597–600
41. Morris AR, Mukherjee N, Keene JD (2008) Ribonomic analysis of human PumI reveals cis-trans conservation across species despite evolution of diverse mRNA target sets. *Mol Cell Biol* 28:4093–4103
42. Huh SU, Kim MJ, Paek KH (2013) Arabidopsis Pumilio protein APUM5 suppresses Cucumber mosaic virus infection via direct binding of viral RNAs. *Proc Natl Acad Sci U S A* 110:779–784
43. Huh SU, Paek KH (2013) Role of Arabidopsis Pumilio RNA binding protein 5 in virus infection. *Plant Signal Behav* 8:e23975
44. Lange S, Katayama Y, Schmid M et al (2008) Simultaneous transport of different localized mRNA species revealed by live-cell imaging. *Traffic* 9:1256–1267
45. Filipovska A, Rackham O (2011) Designer RNA-binding proteins: new tools for manipulating the transcriptome. *RNA Biol* 8: 978–983

46. Tzfira T, Tian G-W, Lacroix B et al (2005) pSAT vectors: a modular series of plasmids for autofluorescent protein tagging and expression of multiple genes in plants. *Plant Mol Biol* 57:503–516
47. Nakagawa T, Suzuki T, Murata S et al (2007) Improved Gateway binary vectors: high-performance vectors for creation of fusion constructs in transgenic analysis of plants. *Biosci Biotechnol Biochem* 71:2095–2100
48. Zacharias DA, Violin JD, Newton AC et al (2002) Partitioning of lipid-modified monomeric GFPs into membrane microdomains of live cells. *Science* 296:913–916
49. Shaner NC, Steinbach PA, Tsien RY (2005) A guide to choosing fluorescent proteins. *Nat Methods* 2:905–909
50. Koh YY, Wang Y, Qiu C et al (2011) Stacking interactions in PUF-RNA complexes. *RNA* 17:718–727
51. Lindbo JA (2007) TRBO: a high-efficiency Tobacco mosaic virus RNA-based overexpression vector. *Plant Physiol* 145:1232–1240
52. Wang Y, Cheong CG, Tanaka Hall TM et al (2009) Engineering splicing factors with designed specificities. *Nat Methods* 6: 825–830

## In Vivo RNA Labeling Using MS2

Eduardo Peña, Manfred Heinlein, and Adrian Sambade

### Abstract

The trafficking and asymmetric distribution of cytoplasmic RNA is a fundamental process during development and signaling across phyla. Plants support the intercellular trafficking of RNA molecules such as gene transcripts, small RNAs, and viral RNA genomes by targeting these RNA molecules to plasmodesmata (PD). Intercellular transport of RNA molecules through PD has fundamental implications in the cell-to-cell and systemic signaling during plant development and in the systemic spread of viral disease. Recent advances in time-lapse microscopy allow researchers to approach dynamic biological processes at the molecular level in living cells and tissues. These advances include the ability to label RNA molecules in vivo and thus to monitor their distribution and trafficking. In a broadly used RNA labeling approach, the MS2 method, the RNA of interest is tagged with a specific stem-loop (SL) RNA sequence derived from the origin of assembly region of the bacteriophage MS2 genome that binds to the bacteriophage coat protein (CP) and which, if fused to a fluorescent protein, allows the visualization of the tagged RNA by fluorescence microscopy. Here we describe a protocol for the in vivo visualization of transiently expressed SL-tagged RNA and discuss key aspects to study RNA localization and trafficking to and through plasmodesmata in *Nicotiana benthamiana* plants.

**Key words** RNA trafficking, RNA localization, RNA visualization, Time-lapse microscopy, MS2

---

### 1 Introduction

RNA transport and localization is a widely used cellular strategy to spatially control protein translation and determine cell polarity [1–3]. Several mRNAs with specific subcellular localization patterns are known to play important roles in developmental processes [4]. High-throughput in situ hybridization in *Drosophila* embryos showed spatially distinct localization patterns of more than 70 % of the analyzed RNA species [5]. There is evidence that also plants employ intracellular RNA localization as an important feature for the spatiotemporal control of gene expression [6, 7]. In addition, plants support the intercellular transport of RNA molecules through plasmodesmata (PD), membranous cell wall pores that interconnect the cytoplasm of adjoining cells and control the spread of informational molecules (proteins and RNA) between cells [8–10]. A wide range of mRNAs, such as *stBEL1* or *KN1*

mRNAs [11, 12] and small RNAs (sRNAs) [13], have been shown to move from cell to cell and over long distances. The cellular mechanisms governing RNA localization and movement are under intense study, particularly by using the spread of viral RNA as a model [14].

Advances in microscopy technologies allow researchers to approach dynamic biological processes at the molecular level *in vivo*. However, unlike proteins that can be easily imaged as genetically encoded translational fusions to fluorescent markers, RNA molecules need to be either *in vitro* labeled and then introduced into the cell for their direct visualization [15] or detected using indirect methods, either through hybridization with fluorescently tagged probes (e.g., molecular beacons) or by the sequence-specific recognition of co-expressed RNA-binding proteins. Among these last methods, the Pumilio system can be engineered to allow protein binding to an unmodified RNA sequence [16, 17] (*see* Chapter 20), whereas other methods require the incorporation of specific protein-binding RNA sequences into the target RNA, e.g., the broadly used MS2 [18],  $\lambda$ N [19], or BglG [20] “stem-loops” (SL). In these methods, the incorporated RNA sequence is specifically recognized and bound by the corresponding RNA-binding protein that when co-expressed in fusion to a fluorescent protein allows the *in vivo* observation of the target RNA.

Here we describe a protocol for the *in vivo* labeling of RNA molecules using the MS2 method, which was successfully implemented in cells from yeast to neurons [21] and plants [22, 23]. The method was optimized for the visualization of transiently expressed messenger RNA encoding the movement protein (MP) of *Tobacco mosaic virus* (TMV) [23]. TMV spreads its RNA genome between cells through PD in a non-encapsidated form and, therefore, represents a model for studying the cellular mechanisms involved in intercellular ribonucleoprotein transport in plants. The targeting of viral RNA and its transport through PD depends on MP and is associated with the occurrence of mobile, MP-containing granules. These granules form at junctions of microtubules with the cortical endoplasmic reticulum (ER):actin network (microtubule-associated ER sites or “c-MERs”) and exhibit stop-and-go movements between c-MERs [23–26]. Upon ectopic expression of the MP mRNA and protein, cytoplasmic MP-containing mobile particles, which resemble the MP-containing granules observed during infection, are formed. Using the bacteriophage MS2-derived system, it was shown that these MP particles contain MP mRNA and that the MP mRNA co-localizes with MP at PD [23]. These observations are in agreement with the ability of MP to bind single-stranded nucleic acids *in vitro* [27] and to interact with membranes and microtubules [28–32].

The MS2 method to *in vivo* label RNA molecules requires the co-expression of the RNA under investigation (in our case MP mRNA) tagged with MS2 bacteriophage stem-loops (SLs) together with the MS2 coat protein (MCP) fused to a fluorescent reporter protein (MCP:FP). The addition of SLs to the RNA of interest needs to be properly designed. For example, transcripts may contain specific “ZIP-code” elements (usually in their 3′ untranslated region) that actively participate in RNA maturation, regulation of translation, and subcellular localization by interacting with elements of the cytoskeleton and specific RNA-binding proteins. The activity of these *cis*-acting elements can be altered by the addition of the SLs, which in turn may cause aberrant mRNA localization or decay. Another consideration is to apply multiple SL copies to enhance the signal-to-background ratio as each SL is able to bind an MCP:FP dimer. However, while it has been shown that 24 SLs are sufficient for the detection of single mRNA molecules [33], a high number of repetitive sequences can affect RNA maturation and may also increase the risk of recombination and loss of SL copies during cloning procedures. Due to these reasons, it is advisable to create clones of RNA molecules that differ with respect to the location and number of SL repeats (e.g., 6–12 tandem repeats at different positions) and to verify the expected size of the mature mRNA as well as the functionality of the encoded protein upon expression. With respect to the RNA-binding protein, it is advisable to fuse the MCP:FP with a nuclear localization signal (NLS) since this will decrease the background of MCP:FP fluorescence in the cytoplasm and therefore increase the signal-to-noise ratio for the detection of MCP:FP-labeled RNAs. In addition, the high concentration of MCP:FP in the nucleus may enhance signal strength also by allowing the binding of the nuclear transcribed SL-tagged RNA already in the nucleus [18].

To obtain faithful information about the location of the RNA under study, multiple experimental controls are essential during the live-cell imaging. Expression of the NLS:MCP:FP in cells in the absence of target RNA and also in the presence of non-tagged RNA (target RNA without SLs) is an essential experiment to control for nonspecific fluorescence background of the system. Indeed, reliable information about the localization of target RNA molecules depends on the experimental confirmation that the expressed NLS:MCP:FP does not aggregate, form visible particles, or label cellular structures (except nucleus) in the absence of the specific SL-tagged target RNA. Expression of NLS:MCP:FP can produce a strong cytoplasmic signal even if targeted to the nucleus. Such strong overexpressing conditions must be avoided to prevent unspecific NLS:MCP:FP aggregation and/or localization that may be misinterpreted if applied in the presence of SL-tagged target RNA. Therefore, the expressing conditions must be rigorously

tested and optimized to obtain no signal in the absence of SLs, and a clear and significant signal in the presence of the SLs.

The MS2 method is compatible with both transient and stable gene expression. Thus, for labeling of MP mRNA, we took advantage of *Agrobacterium tumefaciens*-mediated transient expression (by agroinfiltration), which avoids the time-consuming generation of transgenic plants. It is usually recommended to express the SL-tagged target RNA from its native promoter as this may prevent over-expression and, thus, the risk of mislocalization due to the saturation of RNA-binding proteins and trafficking factors. Moreover, rather weak promoters should be used for expression of MCP:FP so that the risk of unspecific background and the formation of aberrant RNA clusters is reduced [22, 34]. However, in our approach we choose the strong *Cauliflower mosaic virus* 35S promoter, which is widely used for transient expression upon agroinfiltration in plant cells [35–37]. Desired expression levels can be obtained by carefully selecting the incubation time after agroinfiltration of leaf tissues as well as by adjusting the amount of infiltrated bacteria and thus the number of T-DNA copies transferred per cell.

In the protocol described here, we summarize key steps and considerations to achieve in vivo RNA visualization in plants by combining the simple and reliable use of *A. tumefaciens*-mediated transient expression in *N. benthamiana* epidermal cells with Gateway® (Life Technologies) cloning. The method was successfully used for the visualization of TMV MP mRNA [23] and can be generally applied for in vivo mRNA localization and trafficking studies.

---

## 2 Materials

### 2.1 Cloning of SL-Tagged RNA and NLS:MCP:FP into Plant Expression Vectors

1. Standard equipment and reagents for high-fidelity PCR amplification, agarose electrophoresis, and subsequent gel purification of the amplified DNA fragment (e.g., NucleoSpin® Gel and PCR Clean-up, Macherey-Nagel).
2. Reagents and plasmids for cloning PCR products (e.g., pGem®-T Easy, Promega) and for the isolation of plasmid DNA (e.g., NucleoSpin® Plasmid kit, Macherey-Nagel).
3. Shaking and non-shaking incubators set to 37 °C.
4. LB medium: 10 g/l bacto-tryptone, 5 g/l yeast extract, 85.6 mM NaCl, pH 7.0.
5. LB agar plates: LB medium with 15 g/l bacto-agar.
6. Antibiotic stock solutions (1,000×, filtered through a 0.22 µm filter to sterilize):

- (a) Zeocin: 20 mg/ml in distilled water.
- (b) Ampicillin: 100 mg/ml in distilled water.
- (c) Kanamycin: 50 mg/ml in distilled water.
- (d) Spectinomycin: 50 mg/ml in distilled water.
- (e) Chloramphenicol: 34 mg/ml in 100 % ethanol.
- 7. DNA restriction enzymes *PacI* and *SacI*.
- 8. Plasmids with the MCP gene and/or containing MS2 SL sequences (tandem of 6, 12, or 24 SLs; original plasmids can be requested from the laboratory of Robert Singer at [http://www.addgene.org/Robert\\_Singer](http://www.addgene.org/Robert_Singer)).
- 9. Gateway® pDONR™/Zeo Vector (Life Technologies).
- 10. Gateway® BP™ and LR™ clonase enzymes (Life Technologies).
- 11. Binary destination vector pMDC32 for *A. tumefaciens*-mediated transient expression. Plant destination vectors compatible with Gateway® cloning can be requested at [http://www.arabidopsis.org/abrc/catalog/vector\\_1.html](http://www.arabidopsis.org/abrc/catalog/vector_1.html) or <http://gateway.psb.ugent.be/>.
- 12. *E. coli* strain with genetic modifications to minimize genetic recombination of unstable sequences (e.g., Stb12™, Life Technologies).
- 13. *E. coli* strain for the amplification of Gateway® vectors (DB3.1™, Life Technologies).

## 2.2 Transient Expression in *N. benthamiana* Leaves

- 1. *A. tumefaciens* strain GV3101 [38].
- 2. Shaking and non-shaking incubators set to 28 °C and 180–200 rpm.
- 3. 50 ml Falcon tubes.
- 4. LB agar and liquid media (*see* Subheading 2.1).
- 5. Antibiotic stock solutions (*see* Subheading 2.1); in addition:
  - (a) Rifampicin: 50 mg/ml in DMSO.
  - (b) Gentamicin: 50 mg/ml in distilled water.
- 6. Spectrophotometer.
- 7. Centrifuge for 50 ml tubes.
- 8. Sterile distilled water.
- 9. Chamber or greenhouse for the cultivation of *N. benthamiana* plants (16/8-h light/dark, 24–22 °C).
- 10. 4–5-week-old *N. benthamiana* plants.
- 11. 1.0–2.5 ml syringes for tissue infiltration.
- 12. Transgenic plants or transformed *A. tumefaciens* lines for stable or transient expression of fluorescent subcellular markers (*see* **Note 1**).

### 2.3 Imaging and Time-Lapse Image Acquisition

1. Glass slides (75 mm × 25 mm) and cover slips (50 mm × 24 mm, 0.14 mm thick).
2. Cork borer (0.7–1.0 cm diameter).
3. Vacuum pump with vacuum desiccator.
4. Confocal or epifluorescence microscope equipped for time-lapse image acquisition and with high numerical aperture objectives (*see Note 2*).
5. Computer with ImageJ software (<http://rsbweb.nih.gov/ij/>).

## 3 Methods

### 3.1 Plasmid Constructs

To track an RNA using the MS2 system, plasmids encoding the target RNA of interest fused (and not fused) to SLs as well as plasmids for expression of fluorescent protein-tagged MCP need to be generated. Here we describe the construction of a pMDC32 [39]-derived, Gateway® cloning-compatible destination vector for the tagging of target RNA with 12 SLs. The construction of the plasmid for the expression of eGFP- and NLS-fused MCP (pB7-NLS:MCP:GFP) has been previously described and information is available upon request [23].

#### 3.1.1 Construction of pMDC32-3'-MS2-12xSL Destination Vector

1. Use the plasmid pSL-MS2-12 (<http://www.addgene.org/27119/>, [18]) and the primers MS2-12SLfw (5' ttaattaacgggcctatatatggtcc) and MS2-12SLrev (5' gagctcgcgtgatcgcgcgcgc) to PCR-amplify a 708 bp long DNA fragment encoding the 12xSL tandem repeat (*see Note 3*). The forward and reverse primers contain *PacI* and *SacI* restriction sites (underlined), respectively.
2. Gel-purify and clone the DNA fragment into a PCR cloning vector. Transform competent *E. coli* Stbl2™ cells (*see Note 4*) and grow colonies overnight (ON) on LB agar plates containing the appropriate antibiotic compound (100 µg/ml ampicillin for pGem®-T Easy), at 37 °C.
3. Pick colonies and grow bacteria ON in 2–5 ml liquid LB medium at 37 °C with agitation (180–200 rpm), under antibiotic selection (100 µg/ml ampicillin for pGem®-T Easy).
4. Harvest bacteria, isolate plasmid DNA, and verify the insert DNA sequence (T7 and SP6 universal primers for pGem®-T Easy).
5. Use restriction enzymes to release the *PacI/SacI* DNA fragment, purify the DNA fragment after agarose gel electrophoresis, and ligate the fragment into a previously *PacI/SacI*-digested pMDC32 vector.

6. Transform competent *E. coli* DB3.1™ cells and grow ON at 37 °C on LB agar plates containing 50 µg/ml kanamycin and 34 µg/ml chloramphenicol.
7. Grow bacterial cultures from several individual colonies at 37 °C and 180–200 rpm and under antibiotic selection (50 µg/ml kanamycin and 34 µg/ml chloramphenicol), isolate plasmid DNA and verify the plasmid insert sequence by DNA sequencing.

**3.1.2 Generation  
of an Entry Vector  
Containing the Sequence  
of Your Target RNA  
of Interest**

1. Design primers for the amplification of the DNA sequence encoding your RNA of interest and add *attB* sequences (required for BP™ Gateway® reaction) following the manufacturer's instructions (<http://tools.lifetechnologies.com/content/sfs/manuals/gatewayman.pdf>) (*see Note 5*).
2. Use the primers to amplify the DNA encoding your RNA of interest by PCR using the appropriate source DNA as template, purify the product after agarose gel electrophoresis, and insert the product into the plasmid pDONR™/Zeo by recombination using BP™ clonase according to the manufacturer's instructions. Transform competent *E. coli* and select ON at 37 °C on LB agar plates containing 20 µg/ml of zeocin.
3. Grow liquid cultures from several bacterial colonies, isolate plasmid DNA, and verify the insert by DNA sequencing.

**3.1.3 Generation  
of the Vector for Expression  
of SL-Tagged RNA**

1. Perform LR reactions between the entry vector and (a) the destination plasmid pMDC32 and (b) the destination plasmid pMDC32-3'-MS2-12xSL. Recombination with pMDC32 creates pMDC32-RNA, a vector for expression of the RNA of interest without SLs (for control experiments), whereas the recombination with pMDC32-3'-MS2-12xSL creates pMDC32-RNA-SL, thus a vector for expression of the RNA of interest fused to 12 SL repeats.
2. Transform competent *E. coli* Stbl2™ cells and select the cells on LB agar plates containing 50 µg/ml of kanamycin.
3. Grow liquid bacterial cultures from several colonies under antibiotic selection (50 µg/ml of kanamycin) and at 180–200 rpm, isolate plasmid DNA, and verify the constructs by DNA sequencing.

**3.2 Agroinfiltration  
for Transient  
Expression  
of the SL-Tagged RNA  
of Interest and GFP-  
Tagged RNA-Binding  
Protein in Plant Tissues**

1. Transform competent *A. tumefaciens* GV3101 with (1) pMDC32-RNA, (2) pMDC32-RNA-SL, and (3) pB7-NLS:MCP:GFP and select each of the, respectively, transformed bacteria on LB agar plates containing 50 µg/ml of rifampicin and 50 µg/ml of gentamicin, as well as either 50 µg/ml kanamycin for the pMDC32 vectors or 50 µg/ml spectinomycin for pB7-NLS:MS2CP:GFP. Incubate the plates at 28 °C for 48 h (*see Note 6*).

2. Select colonies and grow liquid cultures under respective antibiotic selection at 28 °C on a shaker set to 180–200 rpm.
3. Harvest the bacteria by centrifugation at room temperature (10 min at  $4,000\times g$ ), resuspend the bacterial pellets in sterile distilled water, and determine the concentration by absorbance at 600 nm ( $OD_{600}$ ).
4. Set up mixtures of the different bacteria for agroinfiltration. The final concentration of each bacterial clone in the infiltration mixture should correspond to the desired expression level for each plasmid. High levels of expression of the SL-tagged RNA will increase the efficiency of RNA detection and a low expression of NLS:MCP:GFP may be required to avoid the occurrence of nonspecific signal. For the labeling of the mRNA encoding the MP of TMV, we use a mixture of agrobacteria with pMDC32-RNA-SL (or pMDC32-RNA, as control) at  $OD_{600}=0.5$  and agrobacteria with pNLS:MCP:GFP at  $OD_{600}=0.1$  (see Note 7).
5. Use a 1.0–2.5 ml syringe without needle to infiltrate the fifth to seventh leaves of 4–5-week-old *N. benthamiana* plants. Use a needle or scalpel to make small holes into the abaxial side of the plant leaf and then press the syringe tip to the incision for injection of the bacterial solution into the leaf air space with gentle pressure. Inject the bacterial mixture for expression of pNLS:MCP:GFP together with pMDC32-RNA-SL into one half of the leaf and the bacterial mixture for expression of pNLS:MCP:GFP together with pMDC32-RNA (control without SL) into the other half of the leaf.
6. Incubate the infiltrated plants at 22–18 °C in 16-h/8-h light/dark for 1–4 days post-infiltration before microscopical analysis. The time of incubation after agroinfiltration required for achieving the best possible signal-to-noise ratio for fluorescence imaging must be empirically determined.

### 3.3 Sample Preparation, Imaging, and Time-Lapse Image Acquisition

1. Use a cork borer to excise leaf discs from the infiltrated leaf areas of interest.
2. Place leaf discs on microscope slides with the adaxial side facing the glass, cover the leaf disks with a cover slip, and use sticky tape for fixation. Fill the free space between glasses with sterile water.
3. Remove air from intercellular spaces in the leaf discs by placing the prepared samples into a vacuum desiccator and by evacuating the air up to  $-0.8$  bar. Release the vacuum slowly. The air spaces should now be filled with water, which gives the leaf discs a dark green appearance.
4. Compare the samples with a fluorescence microscope (see Note 8). Use a low-magnification objective (e.g.,  $20\times$ ) to

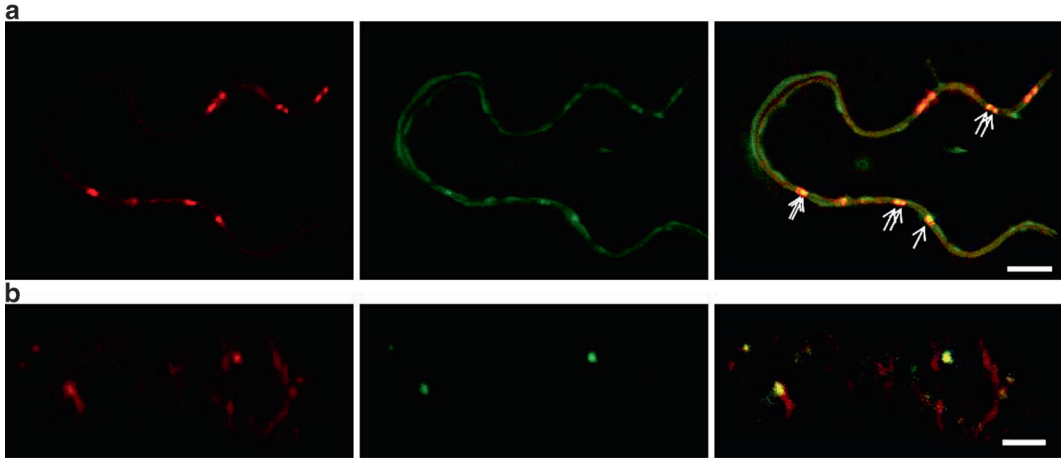


**Fig. 1** Visualization of TMV MP:mRFP mRNA using NLS:MCP:GFP in *N. benthamiana* epidermal cells. **(a)** MP:mRFP (red) and MP:mRFP mRNA (labeled with NLS:MS2CP:GFP, green) coincide at small dots located along the cell wall (presumably PD, white arrows in the merged image on the right). Size bar, 10  $\mu$ m. **(b)** Example of a video frame showing the colocalization of MP:mRFP (red) and MP:mRFP mRNA (labeled by NLS:MS2CP:GFP, green) in mobile particles present in the cortical cytoplasm. Red and green channel images are merged in the image on the right. Size bar, 5  $\mu$ m

verify that tissues expressing the SL-tagged RNA and the tissues expressing non-tagged RNA express similar levels of NLS:MCP:GFP (see Note 9).

5. Use a high-magnification objective (63–100 $\times$ ) to record time-lapse image series at high sampling rates in different focal planes (cortical and central views) of the cells (see examples shown in Fig. 1 a, b) (see Note 10).
6. Use ImageJ (<http://rsbweb.nih.gov/ij/>) or similar software for image analysis (see Note 11).

## 4 Notes

1. The determination of RNA subcellular localization may require the co-expression of specific cellular markers. This can be achieved either by using stably transformed plant lines, such as *N. benthamiana* expressing *tua::GFP* for visualization of microtubules [40] or GFP targeted to the ER (line 16c) [41], or by the simultaneous transient expression of fluorescent markers. Several markers for the specific labeling of microtubules, actin filaments, endoplasmic reticulum, PD, etc. are available (e.g., [42, 43]).
2. MCP:FP tracking depends on time-lapse imaging and the detection of the selected fluorescent tag. Therefore, some imaging systems are better adapted to this task than others

according to their light sources, filter set, acquisition rate, resolution, etc. In our experience, it is possible to use either a standard epifluorescence microscope or a confocal laser-scanning microscope. The higher resolution and removal of out-of-focus light provided by confocal microscopes could be an asset. Usually, an epifluorescence microscope equipped with a high-speed cooled charge-coupled device (CCD) camera, a wide-spectrum light source, and appropriate emission/excitation filter sets (usually for green and red fluorescent proteins) would provide the fastest acquisition setup. We use a Nikon TE2000 inverted fluorescence microscope equipped with a Roper CoolSnap CCD camera, piezo-driven Z-focus, and a 60× 1.45 aperture TIRF objective (excitation/emission wavelengths are 460–500/510–560 nm for GFP and 550–600/615–665 nm for RFP). In addition, a Dual-View beam splitter (Optical Insights) could be used to acquire images through two fluorescence channels at the same time. For image acquisition, we use MetaMorph<sup>®</sup> software that allows custom integration with various microscopes and image analysis. Light source intensity in epifluorescence microscopes can lead to rapid bleaching of samples, which compromises the length of time-course acquisition. If available, the use of a spinning disc confocal microscope could be an alternative that allows probes with low fluorescence yield to be imaged with reduced bleaching. However, although spinning disc microscopes are superior in sensitivity, the pinholes on the spinning disc are of a fixed size, which limits flexibility to optimize image quality. Point-scanning confocal microscopes, in contrast, have adjustable pinholes and allow full control over the scanning beam. We use a Zeiss LSM510 laser-scanning microscope equipped with a C-Apochromat (63× v1.2W Korr) water objective lens, excitation/emission wavelengths 488/505–545 nm for GFP and 561/575–615 nm for RFP, and LSM software (<http://www.zeiss.com/>) or a Zeiss LSM780 laser-scanning microscope equipped with a plan-apochromat ×63/1.4 oil-immersion objective, 488 and 561 nm excitation lasers, and a detection system optimized for eGFP and mRFP, respectively, and with Zen Imaging Software (<http://www.zeiss.com/>).

3. Use enzymes for high-fidelity DNA polymerization (e.g., Phusion<sup>®</sup> High-Fidelity PCR Master Mix, New England Biolabs), and apply a low number of amplification cycles (10–15), to minimize the incorporation of PCR errors.
4. To avoid the loss of the SL repeats during plasmid propagation, the use of bacterial strains with reduced recombination frequency, e.g., *E. coli* Stbl2<sup>™</sup>, is recommended.
5. If the target RNA of interest encodes a protein fused to fluorescent protein, the cells in which the RNA is expressed can be easily identified during microscopy.

6. To co-express these plasmids together with plasmids expressing fluorescent subcellular marker proteins, plasmid-carrying bacteria can be either mixed before infiltration or bacteria can be sequentially transformed with more than one plasmid by using compatible antibiotic resistances (e.g., for the expression of NLS:MCP:GFP together with an ER marker fused to mRFP) [44].
7. If required, increase expression levels by resuspending the harvested agrobacteria in infiltration medium (10 mM MES pH 5.6, 10 mM MgCl<sub>2</sub>) supplemented with 150  $\mu$ M aceto-syringone and incubate at room temperature for at least 2 h to allow the induction of *A. tumefaciens vir* genes [45]. Another strategy to enhance expression levels is by co-expression of an RNA silencing suppressor protein (e.g., P19 from *Tomato bushy stunt virus*) [46].
8. Microscopical observations should finish within 30–40 min after leaf discs were taken. After this time a new sample should be prepared to continue.
9. At low magnification (e.g., 20 $\times$  objective) it might already be possible to detect differences in the distribution of NLS:MCP:GFP between the two types of tissues.
10. RNA forms particles that move either by diffusion or by specific transport in association with molecular motors. To monitor the fast intracellular dynamics of the labeled RNA, short-term movies at high sampling rate should be acquired. Exposure times should be short and frame rates fast enough to register the movements of RNA particles over multiple frames. Similar to other intracellular dynamics studies, several considerations should be taken into account to ensure dataset quality, multicolor labeling, and acquisition speed [47]. Imaging sample size and the resolution of the acquisition system will directly influence lens selection (typically 63–100 $\times$  objectives with water or oil immersion and high numerical aperture are preferred). Time-lapse imaging may be compromised by photobleaching, which may depend on the biological system (e.g., the specific fluorophore used, the number of SL repetitions, and the expression levels of the RNA and the SL-binding protein) as well as on the microscope hardware used (e.g., excitation source and detection sensitivity, filters), and will restrict the time available for data acquisition. Although the acquisition of Z stacks might be needed to track mobile objects, Z-stack acquisition also strongly increases the length of acquisition time at each time point and thus the risk of photobleaching due to the prolonged exposure to excitation light.
11. ImageJ is a broadly used open-source software [48] that is capable of handling multidimensional data in most of the microscopy imaging file formats. A multitude of plug-ins/macros are available at the software website. Some of the

plug-ins are particularly useful for particle tracking, such as “StackReg/TurboReg” [49] for recursive alignment of a stack of images, “Reslice” for the illustration of dynamic trafficking events by kymographing (integrated in ImageJ), and “Spot tracker” [50] for the tracking of individual particles across time-lapse or Z-stack image sequences.

## Acknowledgement

Work of E.P. was supported by a grant from the Agence National de la Recherche (ANR, grant ANR-08-BLAN-244) to M.H.

## References

1. St Johnston D (2005) Moving messages: the intracellular localization of mRNAs. *Nat Rev Mol Cell Biol* 6:363–375
2. Holt CE, Bullock SL (2009) Subcellular mRNA localization in animal cells and why it matters. *Science* 326:1212–1216
3. Nevo-Dinur K, Nussbaum-Shochat A, Ben-Yehuda S, Amster-Choder O (2011) Translation-independent localization of mRNA in *E. coli*. *Science* 331:1081–1084
4. Martin KC, Ephrussi A (2009) mRNA localization: gene expression in the spatial dimension. *Cell* 136:719–730
5. Lecuyer E, Yoshida H, Parthasarathy N et al (2007) Global analysis of mRNA localization reveals a prominent role in organizing cellular architecture and function. *Cell* 131:174–187
6. Okita TW, Choi SB (2002) mRNA localization in plants: targeting to the cell’s cortical region and beyond. *Curr Opin Plant Biol* 5:553–559
7. Chuong SD, Good AG, Taylor GJ et al (2004) Large-scale identification of tubulin-binding proteins provides insight on subcellular trafficking, metabolic channeling, and signaling in plant cells. *Mol Cell Proteomics* 3:970–983
8. Ruiz-Medrano R, Xoconostle-Cazares B, Lucas WJ (1999) Phloem long-distance transport of CmNACP mRNA: implications for supracellular regulation in plants. *Development* 126:4405–4419
9. Kim M, Canio W, Kessler S, Sinha N (2001) Developmental changes due to long-distance movement of a homeobox fusion transcript in tomato. *Science* 293:287–289
10. Lucas WJ, Lee JY (2004) Plasmodesmata as a supracellular control network in plants. *Nat Rev Mol Cell Biol* 5:712–726
11. Banerjee AK, Chatterjee M, Yu Y et al (2006) Dynamics of a mobile RNA of potato involved in a long-distance signaling pathway. *Plant Cell* 18:3443–3457
12. Lucas WJ, Bouche-Pillon S, Jackson DP et al (1995) Selective trafficking of KNOTTED1 homeodomain protein and its mRNA through plasmodesmata. *Science* 270:1980–1983
13. Melnyk CW, Molnar A, Baulcombe DC (2005) Intercellular and systemic movement of RNA silencing signals. *EMBO J* 30:3553–3563
14. Peña EJ, Heinlein M (2012) RNA transport during TMV cell-to-cell movement. *Front Plant Sci* 3:193
15. Christensen N, Tilsner J, Bell K et al (2009) The 5' cap of *Tobacco mosaic virus* (TMV) is required for virion attachment to the actin/endoplasmic reticulum network during early infection. *Traffic* 10:536–551
16. Wang Y, Opperman L, Wickens M, Hall TM (2009) Structural basis for specific recognition of multiple mRNA targets by a PUF regulatory protein. *Proc Natl Acad Sci U S A* 106:20186–20191
17. Tilsner J, Linnik O, Christensen NM et al (2009) Live-cell imaging of viral RNA genomes using a Pumilio-based reporter. *Plant J* 57:758–770
18. Bertrand E, Chartrand P, Schaefer M et al (1998) Localization of ASH1 mRNA particles in living yeast. *Mol Cell* 2:437–445
19. Schönberger J, Hammes UZ, Dresselhaus T (2012) *In vivo* visualization of RNA in plants cells using the  $\lambda$ N<sub>22</sub> system and a GATEWAY-compatible vector series for candidate RNAs. *Plant J* 71:173–181
20. Chen J, Nikolaitchik O, Singh J et al (2009) High efficiency of HIV-1 genomic RNA packaging and heterozygote formation revealed by single virion analysis. *Proc Natl Acad Sci U S A* 106:13535–13540

21. Park HY, Buxbaum AR, Singer RH (2010) Single mRNA tracking in live cells. *Methods Enzymol* 472:387–406
22. Hamada S, Ishiyama K, Choi SB et al (2003) The transport of prolamine RNAs to prolamine protein bodies in living rice endosperm cells. *Plant Cell* 15:2253–2264
23. Sambade A, Brandner K, Hofmann C et al (2008) Transport of TMV movement protein particles associated with the targeting of RNA to plasmodesmata. *Traffic* 9:2073–2088
24. Boyko V, Hu Q, Seemanpillai M et al (2007) Validation of microtubule-associated *Tobacco mosaic virus* RNA movement and involvement of microtubule-aligned particle trafficking. *Plant J* 51:589–603
25. Niehl A, Peña EJ, Amari K, Heinlein M (2013) Microtubules in viral replication and transport. *Plant J* 75:290–308
26. Peña EJ, Heinlein M (2013) Cortical microtubule-associated ER sites: organization centers of cell polarity and communication. *Curr Opin Plant Biol* 16:764–773
27. Citovsky V, Knorr D, Schuster G, Zambryski P (1990) The P30 movement protein of *Tobacco mosaic virus* is a single-strand nucleic acid binding protein. *Cell* 60:637–647
28. Heinlein M, Epel BL, Padgett HS, Beachy RN (1995) Interaction of tobamovirus movement proteins with the plant cytoskeleton. *Science* 270:1983–1985
29. Heinlein M, Padgett HS, Gens JS et al (1998) Changing patterns of localization of the *Tobacco mosaic virus* movement protein and replicase to the endoplasmic reticulum and microtubules during infection. *Plant Cell* 10:1107–1120
30. Boyko V, Ferralli J, Ashby J et al (2000) Function of microtubules in intercellular transport of plant virus RNA. *Nat Cell Biol* 2:826–832
31. Ashby J, Boutant E, Seemanpillai M et al (2006) *Tobacco mosaic virus* movement protein functions as a structural microtubule-associated protein. *J Virol* 80:8329–8344
32. Peiro A, Martinez-Gil L, Tamborero S et al (2014) The *Tobacco mosaic virus* movement protein associates with but does not integrate into biological membranes. *J Virol* 88:3016–3026
33. Fusco D, Accornero N, Lavoie B et al (2003) Single mRNA molecules demonstrate probabilistic movement in living mammalian cells. *Curr Biol* 13:161–167
34. Dahm R, Zeitelhofer M, Gotze B et al (2008) Visualizing mRNA localization and local protein translation in neurons. *Methods Cell Biol* 85:293–327
35. Karimi M, Inze D, Depicker A (2002) GATEWAY vectors for *Agrobacterium*-mediated plant transformation. *Trends Plant Sci* 7:193–195
36. Karimi M, Bleys A, Vanderhaeghen R, Hilson P (2007) Building blocks for plant gene assembly. *Plant Physiol* 145:1183–1191
37. Karimi M, Depicker A, Hilson P (2007) Recombinational cloning with plant gateway vectors. *Plant Physiol* 145:1144–1154
38. Hellens R, Mullineaux P, Klee H (2000) Technical focus: a guide to *Agrobacterium* binary Ti vectors. *Trends Plant Sci* 5: 446–451
39. Curtis MD, Grossniklaus U (2003) A gateway cloning vector set for high-throughput functional analysis of genes in planta. *Plant Physiol* 133:462–469
40. Gillespie T, Boevink P, Haupt S et al (2002) Functional analysis of a DNA-shuffled movement protein reveals that microtubules are dispensable for the cell-to-cell movement of *Tobacco mosaic virus*. *Plant Cell* 14:1207–1222
41. Ruiz MT, Voinnet O, Baulcombe DC (1998) Initiation and maintenance of virus-induced gene silencing. *Plant Cell* 10:937–946
42. Mathur J (2007) The illuminated plant cell. *Trends Plant Sci* 12:506–513
43. Martin K, Kopperud K, Chakrabarty R et al (2009) Transient expression in *Nicotiana benthamiana* fluorescent marker lines provides enhanced definition of protein localization, movement and interactions in planta. *Plant J* 59:150–162
44. Buschmann H, Green P, Sambade A et al (2011) Cytoskeletal dynamics in interphase, mitosis and cytokinesis analysed through *Agrobacterium*-mediated transient transformation of tobacco BY-2 cells. *New Phytol* 190:258–267
45. Rogowsky PM, Close TJ, Chimera JA et al (1987) Regulation of the vir genes of *Agrobacterium tumefaciens* plasmid pTiC58. *J Bacteriol* 169:5101–5112
46. Voinnet O, Rivas S, Mestre P, Baulcombe D (2003) An enhanced transient expression system in plants based on suppression of gene silencing by the p19 protein of *Tomato bushy stunt virus*. *Plant J* 33:949–956
47. Buschmann H, Sambade A, Pesquet E et al (2010) Microtubule dynamics in plant cells. *Methods Cell Biol* 97:373–400
48. Collins TJ (2007) ImageJ for microscopy. *Biotechniques* 43(Suppl 1):S25–S30
49. Thevenaz P, Ruttimann UE, Unser M (1998) A pyramid approach to subpixel registration based on intensity. *IEEE Trans Image Process* 7:27–41
50. Sage D, Neumann FR, Hediger F et al (2005) Automatic tracking of individual fluorescence particles: application to the study of chromosome dynamics. *IEEE Trans Image Process* 14: 1372–1383



# INDEX

## A

- ACR4. *See* ARABIDOPSIS CRINKLY4 (ACR4)  
 Actin..... 39–40, 206, 207, 262, 268–269, 283  
 AGAMOUS (AG).....10, 190  
*Agrobacterium tumefaciens*..... 186, 190, 238,  
 286, 315, 322, 332  
 Agroinfiltration ..... 26, 186, 189, 190,  
 192, 195, 196, 287, 290, 314, 315, 325, 332, 335–336  
 Amyloplasts .....11  
 Aniline blue ..... 96, 105–118, 215, 219  
 Ankyrin-repeat containing protein (ANK) .....40  
 ARABIDOPSIS CRINKLY4 (ACR4) ..... 8, 11, 12  
*Arabidopsis* suspension cells.....83–92  
*Arabidopsis thaliana* .....84, 85, 92, 97, 98,  
 107, 115, 151, 194, 202, 203, 216–218, 236, 278, 280  
*Arabidopsis mosaic virus* (ArMV) .....28

## B

- Bacteriophage MS2.....330  
 BAK1 .....43  
*Bamboo mosaic virus* (BaMV) .....36, 37  
 BDM. *See* 2,3 Butanedione monoxime (BDM)  
*Bean common mosaic necrotic potyvirus* (BCMNV) .....32  
 Beta-1,3-glucanase ..... 13, 14, 40  
 Beta-1,3-glucan synthase (callose synthase) .....13, 40  
 BFA .....29, 261, 266–268, 271  
 Bimolecular fluorescence complementation  
 (BiFC) ..... 43, 297–299, 323, 325  
 Biolistic transformation .....279  
 Birch..... 9, 13, 159, 160, 164, 168, 170  
*Botrytis cinerea* .....42  
 BRASSINOSTEROID INSENSITIVE1  
 (BRI1)-ASSOCIATED RECEPTOR  
 KINASE1 (BAK1) .....43  
 Brefeldin A (BFA)..... 29, 261, 266–268, 271  
*Brome mosaic virus* (BMV).....33  
 2,3 Butanedione monoxime (BDM) .....29, 208, 285

## C

- Caged fluorescein ..... 140–146, 202, 213  
 Callose..... 4, 5, 13–17,  
 28, 31, 40–43, 55, 56, 60–61, 71, 77, 95–103,  
 105–118, 138, 167, 200, 201, 205, 210, 217,  
 219–221, 223, 246, 251, 252  
 Callose synthase .....13, 40

- CALLOSE SYNTHASE 3 (*icals3m*) ..... 14, 246, 247,  
 250–252, 254, 255  
 CaMV .....28, 71, 189, 190, 325, 332  
 CAPRICE (CPC)..... 9, 18, 19, 232, 245  
 Carboxyfluorescein diacetate (CFDA) ..... 150–154, 201, 223  
*Cauliflower mosaic virus* (CaMV) ..28, 71, 189, 190, 325, 332  
 CCT8..... 18, 19, 42  
 CDC48 .....34  
 Cell-coupling factor (CCF).....139, 140  
 Cell disruption..... 84–86, 88–92  
 Cell-to-cell coupling.....149  
 Cellulase ..... 84–87, 90–92  
 Cell wall purification .....88–91  
 CFDA. *See* Carboxyfluorescein diacetate (CFDA)  
 Chaperonin complex (CCT8) ..... 18, 19, 42  
 CLAVATA .....7  
 CLEM. *See* Correlative light and electron microscopy  
 (CLEM)  
 Closteroviruses .....31  
 c-MERs. *See* Microtubule-associated ER sites (c-MERs)  
 CmPP16.....41  
 CMV. *See* Cucumber mosaic virus (CMV)  
 Colchicine .....38, 209, 266, 269, 361  
 Concentration potential..... 140, 144, 146  
 Confocal laser scanning microscopy (CSLM) .....67, 68,  
 170, 286–288  
 Correlative light and electron microscopy  
 (CLEM) .....121–132  
*Cowpea mosaic virus* (CPMV) .....27–29  
 CPC. *See* CAPRICE (CPC)  
 CPMV. *See* Cowpea mosaic virus (CPMV)  
 Cryofixation .....221  
 Cryo-protectant.....123, 126  
 Cryostat sectioning..... 123–124, 126, 131  
 CSLM. *See* Confocal laser scanning microscopy (CSLM)  
*Cucumber mosaic virus* (CMV) .....33, 39  
 Cytochalasin ..... 204, 206, 212, 255, 261, 266, 268, 272

## D

- DANS. *See* Drop-ANd-See (DANS)  
 2-DDG ..... 161, 167, 200  
 Decreased size exclusion limit1 (*dse1*) .....17  
 DEFICIENS (DEF).....10, 232  
 2-Deoxy-D-glucose (2-DDG)..... 161, 167, 200  
 Desmotubule (DT)..... 4, 5, 27, 28, 37, 39, 43, 83, 283  
 Dominant-negative inhibition.....43, 285

Drop-AND-. See (DANS) .....149–156  
DSE1. See Decreased size exclusion limit1 (*dse1*)  
3D structured illumination microscopy  
    (3D-SIM) ..... 68–71, 73–75, 78  
DT. See Desmotubule (DT)  
Dye-coupling ..... 164, 166, 167

## E

EB1 .....33  
EGL3 ..... 8, 9  
 $E_{m1}$  ..... 57–170, 202, 203, 216, 219, 222  
Embryogenesis ..... 6, 10, 17, 186  
Endoplasmic reticulum (ER) ..... 4, 5, 28–40,  
    43, 83, 87, 92, 121, 158, 232, 233, 241, 259–261, 267,  
    268, 270, 272, 273, 283, 285, 330, 337, 339  
Energy depletion .....270, 273  
ENHANCER OF GLABRA3 (EGL3) .....8, 9  
ER. See Endoplasmic reticulum (ER)  
ER-actin network .....31, 33, 34, 36–39, 43

## F

Fick's law of diffusion .....140  
Field emission scanning electron microscope .....57, 61–63  
Fixation .....56–61, 63, 64, 75, 77,  
    99–100, 116, 122, 123, 125, 126, 130, 167, 177, 201,  
    204, 220–221, 223, 336  
FLIM-FRET .....43  
FLOWERING LOCUS T (FT) .....9  
Fluorescence .....55, 69–78, 96, 100, 103,  
    105–111, 116, 124, 126, 130, 138, 139, 141–143,  
    153, 154, 162, 165, 173, 175, 177, 182, 183, 186, 193,  
    196, 197, 200, 201, 205, 214, 216, 219, 222, 223, 236,  
    241, 242, 246, 250, 251, 253, 254, 259–273,  
    297–299, 315, 323, 325, 331, 336, 338  
Fluorescence recovery after photobleaching  
    (FRAP) ..... 39, 139, 223, 247, 251–255, 259–273  
Fluorescent dextran .....174, 177, 179, 182,  
    183, 202, 209, 214, 221  
Fluorescent tracer ..... 138, 139, 150,  
    173–175, 192, 200–202, 204, 212, 214, 216  
FRAP. See Fluorescence recovery after photobleaching  
    (FRAP)  
Freeze-cracking .....56, 58  
Freeze-substitution .....216, 221  
FT .....9

## G

GAL4/UAS reporter plants (J0571) ..... 5, 232, 233,  
    235, 236, 240  
GAT1. See GFP ARRESTED TRAFFICKING1 (GAT1)  
Gateway ..... 196, 233, 237–240,  
    315, 319–321, 332–335  
GFLV. See *Grapevine fanleaf nepovirus* (GFLV)

GFP ARRESTED TRAFFICKING1 (GAT1) .....16, 199  
GLABRA (GL2, GL3) .....7–9  
GLOBOSA (GLO) .....10, 232  
*Grapevine fanleaf nepovirus* (GFLV) .....28–30

## H

Hand-sectioning .....99–100  
High resolution scanning electron microscopy  
    (HRSEM) .....55–64  
Hordeivirus .....36, 41

## I

*icals3m* ..... 14, 246, 247, 250–252, 254, 255  
ImageJ .....106–112, 114, 117, 118,  
    141, 146, 153, 156, 190, 193, 250, 334, 337, 339, 340  
Image thresholding ..... 106, 107, 113  
Immunoblot analysis .....286–290  
Immuno-labelling .....56, 58–60, 96–98, 100, 262–263  
INCREASED SIZE EXCLUSION LIMIT (ISE) .....16  
Intercellular protein movement ..... 231–242, 245–257  
INTERCELLULAR TRAFFICKING  
    DOF1 (ITD1) ..... 232, 234–236, 239  
Iontophoresis ..... 157–170, 174, 216  
ISE. See INCREASED SIZE EXCLUSION  
    LIMIT (ISE)  
ITD1. See INTERCELLULAR TRAFFICKING DOF1  
    (ITD1)

## J

J0571 ..... 5, 232, 233, 235, 236, 240  
JACKDAW (JKD) .....12

## K

Katanin .....34  
KNOTTED ..... 7, 18, 42, 188, 231  
KOBITO1 (KOB1) .....17

## L

Laser scanning confocal microscopy (LSCM) ..... 123, 124,  
    126–129, 131, 132, 151, 250, 253, 291  
Latrunculin B .....29, 207, 261, 267, 268, 272  
LEAFY (LFY) ..... 9, 17, 18, 231  
*Lettuce mosaic potyvirus* (LMV) .....32  
Lipidomic analyses .....83  
London resin (LR) ..... 69–73, 75–78, 222,  
    224, 238, 240, 315, 321, 335  
LRWhite resin .....215  
LSCM. See Laser scanning confocal microscopy (LSCM)  
Lucifer Yellow ..... 150, 161, 165, 175, 182, 183, 202, 219  
LYSIN MOTIF DOMAIN-CONTAINING  
    GLYCOSYLPHOSPHATIDYLINO  
    SITOL-ANCHORED PROTEIN 2  
    (LYM2) .....17

## M

- Membrane potential ( $E_m$ )..... 157–170, 202, 203, 216, 219, 222
- Microcarrier.....276–280
- Microinjection..... 9, 26, 32, 36, 138, 139, 150, 159–160, 165, 169, 173–183, 186, 203, 205, 212–216, 218–220, 222, 223
- Micromanipulator .....161, 163, 165, 166, 176, 178, 179, 215, 216
- Micropipette puller..... 176, 181, 219
- MicroRNA (miRNA)..... 12, 13, 15, 296
- Microtubule..... 18, 19, 28, 29, 31, 33–35, 37, 38, 41, 43, 56, 63, 200, 204, 209, 255, 259, 269, 330, 337
- Microtubule-associated ER sites (c-MERs).....31, 33, 34, 38, 43, 330
- Microtubule END-BINDING 1 (EB1) .....33
- miRNA. *See* MicroRNA (miRNA)
- MONOPTEROS .....10
- Morphogen.....159
- Movement  
    non-targeted .....17  
    targeted .....16–19  
    virus ..... 25–44, 71, 207, 285
- Movement protein (MP)..... 10, 11, 18, 25–29, 31–36, 38–42, 71, 96, 188, 207, 259, 260, 267, 271, 330–332, 336
- MPBP2C .....42
- MS2 method .....330–332
- Myosin ..... 4, 5, 29, 31, 32, 34, 39, 55, 200, 208, 283–291  
    tail.....284–290

## N

- NCAPP1. *See* NON-CELL AUTONOMOUS PATHWAY PROTEIN 1 (NCAPP1)
- NCAPs. *See* Non-cell-autonomous proteins (NCAPs)
- Nicotiana benthamiana*.....40, 107, 186, 189, 190, 196, 260, 270, 279, 317
- Nicotiana tabacum*..... 206, 207
- NLS. *See* Nuclear localisation signal (NLS)
- NON-CELL AUTONOMOUS PATHWAY PROTEIN 1 (NCAPP1).....41
- Non-cell-autonomous proteins (NCAPs)..... 5, 41, 232, 283
- Nuclear localisation signal (NLS)..... 232, 233, 298, 331

## O

- Oryzalin .....209, 255, 261, 266, 269

## P

- PAMP. *See* Pathogen-associated molecular pattern (PAMP)
- PAMP-triggered immunity (PTI).....43
- PAPK. *See* Plasmodesmal-associated kinase (PAPK)

- Pathogen-associated molecular pattern (PAMP).....43, 105
- Pathogen recognition receptor (PRR) .....17, 42
- PD callose-binding (PDCB)..... 4, 5, 15, 87, 92
- PD fraction..... 83, 84, 87–88, 91
- PD-localized proteins (PDLp).....5, 28, 29, 31, 92, 121
- Pericycle..... 11, 12, 14, 246
- PHABULOSA (PHB) .....12
- PHLOEM PROTEIN 16 (CmPP16).....41
- Photoactivation ..... 138, 139, 141–146
- PI.....73, 76, 140, 143, 203, 212, 214, 223, 256
- Plant Transformation.....238, 240
- Plasmodesmal-associated kinase (PAPK).....27
- Plasmodesmata  
    aperture (open, closed, dilated) ..... 4, 6, 17, 25, 26, 39–41, 246  
    conductivity ..... 44, 105, 173–183  
    regulation.....203  
    size exclusion limit (SEL).....16, 17, 25, 28, 33, 36, 39, 41–43, 138, 149, 150, 173, 175, 185, 231, 236  
    structure, simple, branched ..... 19, 25, 28, 31, 122, 138, 201, 204, 206, 208, 210, 220–221
- Plum pox virus* (PPV) .....32
- P3N-PIPO .....31, 32
- Poplar ..... 9, 13, 159, 160, 164, 168, 170
- Potato virus A* (PVA).....32, 36
- Potato virus X* (PVX) ..... 36–38, 40, 42, 296
- Potexviruses .....33, 35–37
- PPV. *See* *Plum pox virus* (PPV)
- Pressure injection..... 160, 174, 176
- Propidium iodide (PI) ..... 73, 76, 140, 143, 203, 212, 214, 223, 256
- Protein movement ..... 231–242, 245–257
- Proteomic analyses ..... 4, 84, 199
- PRR. *See* Pathogen recognition receptor (PRR)
- PTI. *See* PAMP-triggered immunity (PTI)
- Pumilio .....295–326, 330  
    complementation .....297–299
- PVA. *See* *Potato virus A* (PVA)
- PVX. *See* *Potato virus X* (PVX)

## Q

- Quiescent center (QC) ..... 5, 8, 10, 11, 246

## R

- Reactive oxygen species (ROS).....16
- Remorin ..... 4, 5, 37
- Reversibly glycosylated polypeptides (RGPs) .....15, 16
- RNA  
    binding protein ..... 330–332, 335–336  
    growth .....10, 11, 98, 203, 254  
    imaging.....295–326  
    silencing..... 42, 275, 339  
    transport .....206–208, 329
- ROS. *See* Reactive oxygen species (ROS)

## S

Salicylic acid (SA) ..... 40, 42, 111, 112  
 SAM. *See* Shoot apical meristem (SAM)  
 SCARECROW (SCR) ..... 8, 10–13  
 Secretory pathway ..... 29–32, 34  
 Shoot apical meristem (SAM) ..... 7–9, 11, 13,  
 157–170, 212, 246  
 SHORT-ROOT (SHR) ..... 8, 10–13, 15, 18, 19,  
 232, 245–247, 254, 255  
 SHORT-ROOT INTERACTING EMBRYONIC  
 LETHAL (SIEL) ..... 18  
 Silanization ..... 98–99  
 Silencing suppressor ..... 42, 339  
 siRNA ..... 275–280, 295  
 Small RNA ..... 5, 41, 42, 206–208, 275–281, 330  
 SPEECHLESS (SPCH) ..... 15, 17  
 Spurr's resin ..... 215, 220, 222  
 Superresolution microscopy ..... 43  
 Symplasmic tracer ..... 159, 174, 175, 179, 180, 182, 183  
 Symplasmic domain ..... 6, 9, 14, 16

## T

TARGET OF MONOPTEROS (TMO7) ..... 10, 18  
 TEM. *See* Transmission electron microscopy (TEM)  
 TEV. *See* Tobacco etch virus (TEV)  
 Time-lapse image acquisition ..... 334, 336–337  
 Time-lapse microscopy ..... 334, 336–337, 339  
 TMO7. *See* TARGET OF MONOPTEROS (TMO7)  
 Tobacco etch virus (TEV) ..... 32  
 Tobacco mosaic virus (TMV) ..... 26, 27, 29, 31–36,  
 38–43, 71, 188, 259, 296, 297, 315–319, 322–325,  
 330, 332, 336, 337  
 Tobacco rattle virus (TRV) ..... 187, 189, 191, 192, 195  
 Tomato bushy stunt virus ..... 339  
 Tradescantia virginiana ..... 207, 216–218, 220  
 Transient expression ..... 26, 181, 196, 260,  
 272, 286, 314, 315, 332, 333, 335–337

Transmission electron microscopy (TEM) ..... 55, 56,  
 69–71, 75–78, 122, 123, 125, 127–130, 132, 201,  
 206, 208, 215–216, 220, 222  
 TRANSPARENT TESTA GLABRA 1 (TTG1) ..... 7–9  
 Trichome patterning ..... 9  
 Trichome rescue trafficking assay ..... 232  
 Triple-gene-block ..... 35–38  
 TRV ..... 187, 189, 191, 192, 195  
 TRYPTICHON (TRY) ..... 9  
 TTG1. *See* TRANSPARENT TESTA GLABRA 1  
 (TTG1)  
 Turnip mosaic virus (TuMV) ..... 31, 32, 296  
 Turnip vein clearing virus (TVCV) ..... 40

## U

Ultramicrotomy ..... 75, 125–129, 132, 215

## V

Vibrating microtome ..... 70–72, 74–75  
 VIGS. *See* Virus-induced gene silencing (VIGS)  
 Viral replication complex (VRC) ..... 31–35, 37,  
 40, 41, 259, 260  
 Viral ribonucleoprotein complex (vRNP) ..... 27, 28, 33–38  
 Virus-induced gene silencing (VIGS) ..... 32, 185–197, 285  
 Velocity ..... 106, 141  
 VRC. *See* Viral replication complex (VRC)  
 vRNP. *See* Viral ribonucleoprotein complex (vRNP)

## W

WUSCHEL (WUS) ..... 7, 8, 11  
 WUSCHEL-RELATED HOMEBOX 5  
 (WOX5) ..... 11, 12

## X

X-bodies ..... 34, 37  
 Xylem ..... 11, 13, 14, 74, 75